ACTA UNIVERSITATIS UPSALIENSIS
Uppsala Dissertations from the Faculty of Science and Technology
108

Mojtaba Soltanalian

Signal Design for Active Sensing and Communications

UPPSALA
UNIVERSITET

Dissertation presented at Uppsala University to be publicly examined in 2347, Building 2, Lägerhyddsvägen 2, Uppsala, Tuesday, 14 October 2014 at 13:15 for the degree of Doctor of Philosophy. The examination will be conducted in English. Faculty examiner: Bo Wahlberg (KTH Royal Institute of Technology).

Abstract

Soltanalian, M. 2014. Signal Design for Active Sensing and Communications. *Uppsala Dissertations from the Faculty of Science and Technology* 108. 346 pp. Uppsala: Acta Universitatis Upsaliensis. ISBN 978-91-554-9017-1.

Man-made active sensing systems such as active radar and sonar have been a vital part of our civilization's advancement in navigation, defense, meteorology, and space exploration. Modern active sensing systems rely heavily on the significant progress in the science and technology of communications made within the last century. Not surprising, the fast growing communications technology has changed each and every aspect of our everyday lives. This thesis is concerned with signal design for improving the performance of active sensing and communication systems: The target detection and estimation performance of the active sensing systems can be considerably improved by a judicious design of the probing signals. Similarly, signal design has a crucial role in the implementation and efficiency of communication systems.

Signal optimization for active sensing and communications usually deals with various measures of quality. This thesis focuses on several quality measures including (i) correlation and spectral metrics, (ii) signal-to-noise ratio (SNR) and mean-square error (MSE) performance metrics, (iii) information-theoretic criteria, (iv) sparsity-related metrics, and (v) beam-pattern matching metrics. The associated problems are studied and several novel algorithms are proposed to tackle the generally difficult arising problems.

Mojtaba Soltanalian, Department of Information Technology, Division of Systems and Control, Box 337, Uppsala University, SE-75105 Uppsala, Sweden.

ISSN 1104-2516
ISBN 978-91-554-9017-1
urn:nbn:se:uu:diva-230655 (http://urn.kb.se/resolve?urn=urn:nbn:se:uu:diva-230655)

Printed by Elanders Sverige AB, 2014

Contents

Acknowledgments

– We never get to where we are just by ourselves. I would like to express my deepest appreciation and admiration to my supervisor Prof. Petre Stoica for sharing his knowledge, experience, wisdom, and enthusiasm. Thank you for being a superstar supervisor!

– I would like to thank all my co-authors, and all those who reviewed, commented, or presented stimulating discussions on my works— a list of such contributions will be extensive, and many will be forgotten.

– I'm grateful to Prof. Jian Li and Prof. Antonio De Maio for all their support and guidance during my studies.

– Special thanks go to all my present and former colleagues at Syscon.

– I would like to thank Prof. Bo Wahlberg for serving as my faculty opponent, and also Prof. Angelia Nedic, Prof. Håkan Hjalmarsson, and Prof. Di Yuan for accepting to act as the defense committee members.

– Finally, very special thanks go to my family, my parents, and my wife, Azadeh, for all the sacrifices that they have made to help me. Azadeh has been the source of unconditional love and support. Without her kind patience, writing this thesis would have been impossible.

1. Introduction

Unveiled your love shines everywhere, wise man,
You who have a keen insight to see and scan;

Aims to point at the signals and the hidden—
Sometimes by allusion, sometimes boldly written.
If you happen to decode these signals you'll descry
That here one answer to all these codes does lie:
That there is one only, and none but the one,
It is the sole being– there is no beloved but one.

-Hatef Esfehani (18^{th} century)

The desire for interaction with the environment, and others of our kind lies within the human nature— a key bottleneck to such an interaction is posed by our information collection or *sensing* capabilities. Throughout history, we have been trying to come up with smart ways to sense our environment. The modern sensing systems can be categorized as

- Active systems, i.e. sensory systems that work based on probing the environment with their self-generated energy.
- Passive systems, i.e. sensory systems that rely on detecting the naturally occurring energy within the environment.

Man-made active sensing systems such as active radar and sonar have been a vital part of our civilization's advancement in navigation, defense, meteorology, and space exploration. In the animal world, active sensing schemes are used by bats and dolphins for positioning purposes. Interestingly, man-made systems employ a set of techniques similar to those used by bats and dolphins for collecting information (e.g. location and speed) of the targets. An active radar emits radio waves (referred to as *radar signals*) toward the targets. A portion of the transmitted energy is reflected by the targets and is received by the radar receiver antenna. Thanks to the known speed of electromagnetic wave, the radar system can estimate the location of the targets simply by measuring the time difference between the radar signal transmission and the reception of the reflected signal.

Modern active sensing systems rely heavily on the significant progress in the science and technology of communications made within the last century. Not surprising, the fast growing communications technology has changed each and every aspect of our everyday lives. This thesis is concerned with signal

design for improving the performance of active sensing and communication systems: The target detection and estimation performance of the active sensing systems can be considerably improved by a judicious design of the probing signals. Similarly, signal design has a crucial role in the implementation and efficiency of communication systems.

The theoretical and computational results in the field of signal design have been of interest to both engineers and mathematicians in the last decades. A signal design problem in active sensing or communications, in most cases, boils down to the optimization of a signal quality measure. Indeed, signal optimization for active sensing and communications usually deals with various measures of quality, namely:

- *Correlation and Spectral Metrics*
- *Signal-to-Noise Ratio (SNR) and Mean-Square Error (MSE) Performance Metrics*
- *Information-Theoretic Criteria*
- *Sparsity-Related Metrics*
- *Beam-Pattern Matching Metrics*

This thesis is organized in five parts each devoted to one of the above metric categories. Moreover, we consider the design problems that include a set of signal constraints, a challenge that arises in practical transmission scenarios. Typical examples of practical signal constraints include a limited energy, limited alphabet, or peak-to-average-power ratio constraints. Such a diversity in design metrics and problems leads to many challenging research works in signal design— up to this date, there are quite a few open problems in this research field which are pretty easy to describe but deemed to be very difficult to tackle!

1.1 Thesis Contributions

A summary of the thesis contributions will be provided in the following.

Part I: Correlation and Spectral Metrics
Chapter 2
Chapter 2 introduces a novel computational framework and a set of associated algorithms to design (sets of) sequences with given autocorrelation properties. As constrained (e.g. finite) alphabets are of interest in many applications, we introduce a modified version of our general framework that can be useful in these cases. The material in this chapter is based on the journal article

- M. Soltanalian and P. Stoica, "Computational Design of Sequences with Good Correlation Properties," *IEEE Transactions on Signal Processing*, vol. 60, no. 5, pp. 2180-2193, 2012.

Chapter 3
In Chapter 3, a fast frequency-domain optimization approach for designing complementary sequences is proposed. This chapter is based on the journal publication

- M. Soltanalian, M. M. Naghsh, and P. Stoica, "A Fast Algorithm for Designing Complementary Sets of Sequences," *Signal Processing*, vol. 93, no. 7, pp. 2096-2102, 2013.

Chapter 4
In this chapter, we study the problem of meeting peak periodic or aperiodic correlation bounds for complex-valued sets of sequences. A theoretical improvement upon the well-known Welch bound in the aperiodic correlation case is proposed. Moreover, a computational framework for meeting peak correlation bounds is devised. The chapter is based on the journal article

- M. Soltanalian, M. M. Naghsh, and P. Stoica,"On Meeting the Peak Correlation Bounds," *IEEE Transactions on Signal Processing*, vol. 62, no. 5, pp. 1210-1220, 2014.

and its conference version published as

- M. Soltanalian, M. M. Naghsh, and P. Stoica,"Approaching Peak Correlation Bounds Via Alternating Projections," *IEEE International Conference on Acoustics, Speech and Signal Processing (ICASSP)*, Florence, Italy, 2014.

Chapter 5
Chapter 5 presents a theoretical study of root-of-unity sequences with perfect periodic correlation. Using the tools developed in this chapter, several contributions are made to the current state-of-knowledge regarding the existence of such sequences. The material in this chapter is based on the journal publication

- M. Soltanalian and P. Stoica, "On Prime Root-of-Unity Sequences with Perfect Periodic Correlation," *IEEE Transactions on Signal Processing*, In press, 2014.

and a conference version published as

- M. Soltanalian and P. Stoica, "Perfect Root-of-Unity Codes with Prime Size Alphabet," in *IEEE International Conference on Acoustics, Speech*

and Signal Processing (ICASSP). Prague, Czech Republic: IEEE, 2011, pp. 3136-3139.

Chapter 6

Chapter 6 proposes a computational approach for designing polyphase sequences with two key properties; (i) a phase argument which is piecewise linear, and (ii) an impulse-like autocorrelation. The proposed approach relies on fast Fourier transform (FFT) operations and thus can be used efficiently to design sequences with a large length or alphabet size. Chapter 6 is based on the conference publication

- M. Soltanalian, P. Stoica, M. M. Naghsh and A. De Maio, "Design of Piecewise Linear Polyphase Sequences with Good Correlation Properties," *22nd European Signal Processing Conference (EUSIPCO)*, Lisbon, Portugal, 2014.

Part II: SNR and MSE Performance Metrics

Chapter 7

In this chapter, we have studied quadratic programming over unimodular (i.e. constant-modulus) vector sets. Such an NP-hard formulation [1] arises quite frequently in communications and active sensing[1]— particularly so, in the optimization of SNR and MSE performance metrics. A monotonically error-bound improving technique (MERIT) was developed that can seek for the global optimum, or the local optimum of the quadratic objective with good sub-optimality guarantees (that are easily available at each iteration). The provided sub-optimality guarantees are case-dependent and may outperform the $\pi/4$-approximation guarantee of semidefinite relaxation. As a result, the new method may have the potential to become an alternative to semidefinite relaxation. The chapter is based on the publications

- M. Soltanalian and P. Stoica, "Designing Unimodular Codes Via Quadratic Optimization," *IEEE Transactions on Signal Processing*, vol. 62, no. 5, pp. 1221-1234, 2014.
- M. Soltanalian and P. Stoica, "MERIT: A Monotonically Error-Bound Improving Technique for Unimodular Quadratic Programming," *IEEE International Conference on Acoustics, Speech and Signal Processing (ICASSP)*, Florence, Italy, 2014.

Chapter 8

Chapter 8 presents a SNR-based design of Doppler robust radar codes in the presence of clutter. To this end, we approach the problem with both average and worst-case metric alternatives. We propose several algorithms under

[1]Please see [2] for several examples.

two novel frameworks to solve the highly non-convex design problems. This chapter is based on the publications

- M. M. Naghsh, M. Soltanalian, P. Stoica and M. Hashemi, "Radar Code Design for Detection of Moving Targets," *IEEE Transactions on Aerospace and Electronic Systems*, In press, 2014.
- M. M. Naghsh, M. Soltanalian, P. Stoica and M. Hashemi, "Radar Code Optimization for Moving Target Detection," *21st European Signal Processing Conference (EUSIPCO)*, Marrakech, Morocco, 2013.

Chapter 9
An efficient joint design of transmit and receive codes of active sensing was proposed. Chapter 9 is based on the journal article

- M. Soltanalian, B. Tang, J. Li, and P. Stoica, "Joint Design of the Receive Filter and Transmit Sequence for Active Sensing," *IEEE Signal Processing Letters*, vol. 20, no. 5, pp. 423-426, 2013.

Chapter 10
Chapter 10 extends the design problem in Chapter 9 by further considering a robustness objective with respect to unknown speed of the target (i.e. Doppler robustness) in the presence of clutter. The chapter is based on the results from

- M. M. Naghsh, M. Soltanalian, P. Stoica, M. Hashemi, A. De Maio and A. Aubry, "A Doppler Robust Design of Transmit Sequence and Receive Filter in the Presence of Signal-Dependent Interference," *IEEE Transactions on Signal Processing*, vol. 62, no. 4, pp. 772-785, 2014.
- M. M. Naghsh, M. Soltanalian, P. Stoica, M. Hashemi, A. De Maio and A. Aubry, "A Max-Min Design of Transmit Sequence and Receive Filter," *IEEE International Conference on Acoustics, Speech and Signal Processing (ICASSP)*, Florence, Italy, 2014.

Part III: Information-Theoretic Criteria
Chapter 11
A unified framework to handle signal optimization based on several information-theoretic criteria is proposed in this chapter, which is based on the publications

- M. M. Naghsh, M. Hashemi, S. Shahbazpanahi, M. Soltanalian and P. Stoica, "Unified Optimization Framework for Multi-Static Radar Code Design using Information-Theoretic Criteria," *IEEE Transactions on Signal Processing*, vol. 61, no. 21, pp. 5401-5416, 2013.

- M. M. Naghsh, M. Hashemi, S. Shahbazpanahi, M. Soltanalian and P. Stoica, "Majorization-Minimization Technique for Multi-Static Radar Code Design", *21st European Signal Processing Conference (EUSIPCO)*, Marrakech, Morocco, 2013.

Part IV: Sparsity-Related Metrics
Chapter 12
In this chapter, a novel approach to the design of Costas arrays (a certain type of optimized time-frequency coding pattern for sonar and radar) is devised by employing sparse representations. Chapter 12 is based on the publication

- M. Soltanalian, P. Stoica and J. Li, "Search for Costas Arrays Via Sparse Representation," *22nd European Signal Processing Conference (EUSIPCO)*, Lisbon, Portugal, 2014.

Chapter 13
In Chapter 13, the fast techniques for the design of sequence sets with good correlation properties are successfully used for a sparsity-aware design of radar waveforms. This chapter is based on the conference publication

- H. Hu, M. Soltanalian, P. Stoica and X. Zhu, "Sparsity-Aided Radar Waveform Synthesis," *22nd European Signal Processing Conference (EUSIPCO)*, Lisbon, Portugal, 2014.

Part V: Beam-Pattern Matching Metrics
Chapter 14
In this chapter, a computationally efficient transmit beam pattern design for MIMO antennas is discussed. Chapter 14 is based on the journal article

- M. Soltanalian, H. Hu and P. Stoica, "Single-Stage Transmit Beamforming Design for MIMO Radar," *Signal Processing*, vol. 102, pp. 132-138, Sep. 2014.

1.2 Other Contributions

In addition to the articles listed above, the author has had the following publications during the Ph.D. studies:

[J]: Journal, [C]: Conference, [T]: Technical Report

[J] L. Dai, M. Soltanalian and K. Pelckmans, "On the Randomized Kaczmarz Algorithm", *IEEE Signal Processing Letters*, vol. 21, no. 3, pp. 330-333, 2014.

[C] E. Hidayat, M. Soltanalian, A. Medvedev and K. Nordström, "Stimuli Design for Identification of Spatially Distributed Motion Detectors in

Biological Vision Systems," *13th International Conference on Control, Automation, Robotics and Vision (ICARCV)*, Marina Bay Sands, Singapore, 2014.

[C] M. M. Naghsh, M. Hashemi, A. Sheikhi, M. Soltanalian and P. Stoica, "Unimodular Code Design for MIMO Radar Using Bhattacharyya Distance," *IEEE International Conference on Acoustics, Speech and Signal Processing (ICASSP)*, Florence, Italy, 2014.

[C] A. Aubry, A. De Maio, M. Piezzo, M. M. Naghsh, M. Soltanalian and P. Stoica, "Cognitive Radar Waveform Design for Spectral Coexistence in Signal-Dependent Interference," *IEEE Radar Conference (RADARCON)*, Cincinnati, OH, USA, 2014.

[C] M. Soltanalian and P. Stoica, "Design of Perfect Phase-Quantized Sequences with Low Peak-to-Average-Power Ratio," *European Signal Processing Conference (EUSIPCO)*, Bucharest, Romania, August 2012.

[T] M. Soltanalian and P. Stoica, "A Recursive Method for Enumeration of Costas Arrays," available at *arXiv*:1404.0173, 2014.

Part I:
Correlation and Spectral Metrics

2. Design of Sequences with Good Correlation Properties

Abstract
In this chpater, we introduce a computational framework based on an **i**terative **t**wisted app**rox**imation (ITROX) and a set of associated algorithms for various sequence design problems. The proposed computational framework can be used to obtain sequences (or complementary sets of sequences) possessing good periodic or aperiodic correlation properties and, in an extended form, to construct zero (or low) correlation zone sequences. Furthermore, as constrained (e.g. finite) alphabets are of interest in many applications, we introduce a modified version of our general framework that can be useful in these cases. Several applications of ITROX are studied and numerical examples (focusing on the construction of real-valued and binary sequences) are provided to illustrate the performance of ITROX for each application.

Keywords: Sequence design, finite alphabet, binary sequences, complementary sets, autocorrelation, zero correlation zone (ZCZ).

2.1 Introduction

Sequences with good correlation properties (used in the formulation of both discrete and continuous-time waveforms) lie at the core of many active sensing and communication schemes. Therefore, it is no surprise that the literature on the topic is extensive (e.g., see [3]-[22], [30]-[38] and the references therein). The alphabets (Ω) used in the literature are chosen to fit the application. The most common alphabets are binary, ternary, root-of-unity, unimodular and also the sets of real-valued or complex-valued numbers.

Let $\mathbf{x} = (\mathbf{x}(1), \mathbf{x}(2), \cdots, \mathbf{x}(n))$ denote a sequence where $\mathbf{x}(k) \in \Omega$. The periodic (c_k) and aperiodic (r_k) autocorrelations of $\mathbf{x}$ are defined as

$$c_k = \sum_{l=1}^{n} \mathbf{x}(l)\mathbf{x}^*(l+k)_{mod\ n}, \ \ 0 \leq k \leq (n-1) \tag{2.1}$$

$$r_k = \sum_{l=1}^{n-k} \mathbf{x}(l)\mathbf{x}^*(l+k) = r_{-k}^*, \ 0 \leq k \leq (n-1) \tag{2.2}$$

The in-phase lag (i.e. $k = 0$) of both autocorrelations represents the energy component E of the sequence. The problem of sequence design for good correlation properties usually arises when small out-of-phase (i.e. $k \neq 0$) autocorrelation lags are required. Several metrics can be defined to measure the goodness of such sequences, for example (considering the aperiodic autocorrelations), the *peak sidelobe level*

$$\text{PSL} = \max\{|r_k|\}_{k=1}^{n-1}, \tag{2.3}$$

the *integrated sidelobe level*

$$\text{ISL} = \sum_{k=1}^{n-1} |r_k|^2, \tag{2.4}$$

or the related *merit factor*,

$$\mathrm{MF} = \frac{|r_0|^2}{2\sum_{k=1}^{n-1}|r_k|^2} = \frac{E^2}{2\ \mathrm{ISL}}. \tag{2.5}$$

Note that such metrics can be defined for both aperiodic and periodic autocorrelations, and also when only a specific subset of lags are to be small.

Sequences with impulse-like periodic correlation (called perfect sequences) have found interest in pulse compression and wireless communications [8]. They are required in typical code-division multiple-access (CDMA) systems to handle the multiple access interference and are also used in the synthesis of orthogonal matrices for source coding as well as complementary coding [10]. While sequences with good periodic and aperiodic correlations have a considerable set of applications, there are also some cases in which solely good aperiodic correlation properties are of interest. For example, in synchronization applications, while sequences with good periodic correlation are used when the sequence can be transmitted several times in succession, sequences with good aperiodic correlation are required when the sequence can be used only once [11]. We note that finding and studying sequences with good aperiodic correlation properties is usually a harder task than that corresponding to sequences with good periodic correlation. In particular, unlike the case of periodic correlations, it is not possible to construct sequences with exact impulsive aperiodic autocorrelation.

Several variations on the theme of designing sequences with low correlation lags can be considered. For example, in some CDMA applications such as quasi-synchronous CDMA (QS-CDMA), the time delay among different users is restricted and, as a result, zero correlation zone (ZCZ) sequences (with zero correlations over a smaller range e.g. $k \leq T$ for some maximal time lag T) can be used as spreading sequences [12]. Another example is complementary sets of sequences. A set $S = \{\mathbf{x}_1, \mathbf{x}_2, \cdots, \mathbf{x}_m\}$ containing m sequences of length n is called a set of (periodically) complementary sequences when the (periodic) autocorrelation values of $\{\mathbf{x}_k\}_{k=1}^{m}$ sum up to zero at any out-of-phase lag. This property can be formulated as

$$\sum_{l=1}^{m} c_{l,k} = 0, \quad 1 \leq k \leq (n-1) \tag{2.6}$$

where $c_{l,k}$ represents the k^{th} (periodic) autocorrelation lag of $\mathbf{x}_l$. Sets of complementary sequences play an important role in applications such as radar pulse compression [13], CDMA communications [14], data hiding [15], aperture imaging [16], channel estimation [17], ultra-sonic ranging and ultra wideband (UWB) communications [18]. They are also of theoretical importance in the construction of sequences with zero correlation zone (ZCZ) [19]. The sets S containing two such sequences are usually referred as complementary pairs. The case of binary complementary pairs was first considered by Golay

in [20] [21]. Golay complementary pairs exist for lengths $n = 2^a 10^b 26^c$ where $a,b,c \in \mathbb{N} \cup \{0\}$ [22]. Some non-existence results for Golay complementary pairs can be found in [23].

In many cases (but not in all) there exist analytical construction methods for optimal or near-optimal sequences. However, even in such cases, it may be useful to have computational methods that can yield additional good sequences. For example, in multiple access channels (MACs) having more sequences with good correlation properties expands the capacity of the communication system. In addition, active sensing and communication systems working in hostile environments need hidden spreading sequences that are hard to find by the adversary (to avoid detection or jamming). Note that the sequences obtained with known construction methods are rather restricted in number and usually have a small number of unknown parameters which makes them easy to guess.

Stochastic search and other optimization design algorithms have been studied in the literature . However, these algorithms are generally hard to use when the size of the search space grows large. To avoid this problem, in [5]- [8] several cyclic algorithms have been proposed to generate unimodular sequences with good periodic or aperiodic properties. In this chapter, a general computational framework based on an **i**terative **t**wisted app**rox**imation (ITROX), to be defined shortly, and a set of associated algorithms are introduced that can be used to design sequences from a desired alphabet. We believe that the techniques introduced in this chapter can be adopted in new applications of sequence design where new alphabets are desired. Note that there is almost no prior information available to a foe about the sequences constructed by computational methods such as ITROX. Furthermore, ITROX does not impose any restrictions on the sequence size in contrast to most known analytical construction schemes.

The rest of this work is organized as follows. Section 2.2 provides several mathematical tools and definitions that are used in Section 2.3 to derive a general algorithmic form of ITROX. The convergence and the performance of ITROX with respect to the design metrics are also studied in Section 2.3. Section 2.4 is devoted to using ITROX for constrained sequence design. Several numerical examples are provided in Section 2.5. Finally, Section 2.6 concludes the chapter.

Notation: We use bold lowercase letters for vectors and bold uppercase letters for matrices. $(.)^T$, $(.)^*$ and $(.)^H$ denote the vector/matrix transpose, the complex conjugate, and the Hermitian transpose, respectively. $\mathbf{1}$ and $\mathbf{0}$ are the all-one and all-zero vectors/matrices. $\boldsymbol{e}_k$ is the k^{th} standard basis vector in $\mathbb{R}^n$. $\|.\|$ denotes an arbitrary norm. $\|\mathbf{x}\|_n$ or the l_n-norm of the vector $\mathbf{x}$ is defined as $(\sum_k |\mathbf{x}(k)|^n)^{\frac{1}{n}}$ where $\{\mathbf{x}(k)\}$ are the entries of $\mathbf{x}$. $\|.\|_{\max}$ represents the max-norm of a matrix that is equal to the maximum absolute value of the entries of the matrix. The Frobenius norm of a matrix $\boldsymbol{X}$ (denoted by $\|\boldsymbol{X}\|_F$) with

entries $\{\boldsymbol{X}(k,l)\}$ is equal to $\left(\sum_{k,l}|\boldsymbol{X}(k,l)|^2\right)^{\frac{1}{2}}$. The symbol $\odot$ stands for the Hadamard element-wise product of matrices. tr(.) is the trace of the square matrix argument. $vec(\boldsymbol{X})$ is a vector obtained by stacking the columns of $\boldsymbol{X}$ successively. **Diag**(.) denotes the diagonal matrix formed by the entries of the vector argument. Sets are designated via uppercase letters while lowercase letters are used for their elements. $\mathbb{N}$, $\mathbb{Z}$, $\mathbb{R}$ and $\mathbb{C}$ represent the set of natural, integer, real and complex numbers, respectively. For any real number x, the function $[x]$ yields the closest integer to x (the largest is chosen when this integer is not unique) and $\{x\} = x - [x]$. $\lceil x \rceil$ is the smallest integer greater than or equal to x. Finally, δ_k is the Kronecker delta function which is equal to one when $k = 0$ and to zero otherwise.

2.2 ITROX: The Problem Formulation

In this section, the necessary mathematical tools for the computational framework of ITROX are provided. We begin with the concept of twisted product and then discuss some useful connections of this vector product with the sequence design problem.

Definition 1. *The **twisted product** of two vectors* $\mathbf{x}$ *and* $\boldsymbol{y}$ *(both in* $\mathbb{C}^{n\times 1}$*) is defined as*

$$\mathbf{x} \circlearrowleft \boldsymbol{y}^H = \begin{pmatrix} \mathbf{x}(1)\boldsymbol{y}^*(1) & \mathbf{x}(2)\boldsymbol{y}^*(2) & \cdots & \mathbf{x}(n)\boldsymbol{y}^*(n) \\ \mathbf{x}(1)\boldsymbol{y}^*(2) & \mathbf{x}(2)\boldsymbol{y}^*(3) & \cdots & \mathbf{x}(n)\boldsymbol{y}^*(1) \\ \vdots & \vdots & \ddots & \vdots \\ \mathbf{x}(1)\boldsymbol{y}^*(n) & \mathbf{x}(2)\boldsymbol{y}^*(1) & \cdots & \mathbf{x}(n)\boldsymbol{y}^*(n-1) \end{pmatrix} \tag{2.7}$$

where $\mathbf{x}(k)$ *and* $\boldsymbol{y}(k)$ *are the* k^{th} *entries of* $\mathbf{x}$ *and* $\boldsymbol{y}$ *respectively. The **twisted rank-one approximation** of* $\boldsymbol{Z} \in \mathbb{C}^{n\times n}$ *is equal to* $\mathbf{x} \circlearrowleft \boldsymbol{y}^H$ *if and only if* $\mathbf{x}$ *and* $\boldsymbol{y}$ *are the solution of the optimization problem:*

$$\min_{\mathbf{x},\boldsymbol{y}\in\mathbb{C}^{n\times 1}} \|\boldsymbol{Z} - \mathbf{x} \circlearrowleft \boldsymbol{y}^H\|_F \tag{2.8}$$

Note that there exists a known permutation matrix $P \in \mathbb{C}^{n^2\times n^2}$ for which

$$\begin{aligned} \|\boldsymbol{Z} - \mathbf{x} \circlearrowleft \boldsymbol{y}^H\|_F &= \|vec(\boldsymbol{Z}) - vec(\mathbf{x} \circlearrowleft \boldsymbol{y}^H)\|_2 \\ &= \|vec(\boldsymbol{Z}) - P\, vec(\mathbf{x}\boldsymbol{y}^H)\|_2 \\ &= \|P^T vec(\boldsymbol{Z}) - vec(\mathbf{x}\boldsymbol{y}^H)\|_2 \\ &= \|\boldsymbol{Z}' - \mathbf{x}\boldsymbol{y}^H\|_F \end{aligned} \tag{2.9}$$

Therefore, the solution to the optimization problem in (2.8) is given by the dominant singular pair of a matrix $\boldsymbol{Z}'$ obtained by a specific re-ordering of the entries of $\boldsymbol{Z}$. In the sequel, we denote this re-ordering by the function $\mathscr{F}(\cdot)$ over the matrices in $\mathbb{C}^{n\times n}$; particularly, in Eq. (2.9) we have $\boldsymbol{Z}' = \mathscr{F}(\boldsymbol{Z})$.

We formulate the problem of finding sequences with good periodic or aperiodic correlation properties using the twisted product.

2.2.1 The Periodic Autocorrelation

A special case of twisted product is that of $\boldsymbol{y} = \mathbf{x}$. Interestingly, the periodic autocorrelation of a vector $\mathbf{x}$ can be written as $(\mathbf{x} \circlearrowleft \mathbf{x}^H)\mathbf{1}$. $\mathbf{x}$ is called a perfect sequence with energy E if and only if

$$(\mathbf{x} \circlearrowleft \mathbf{x}^H)\mathbf{1} = \mathbf{E}\boldsymbol{e_1}. \tag{2.10}$$

Remark 1: Due to practical considerations, sequences with low peak-to-average ratio (PAR),

$$\text{PAR} = \frac{\|\mathbf{x}\|_\infty^2}{\frac{1}{n}\|\mathbf{x}\|_2^2}, \tag{2.11}$$

are often required. Note that in order to obtain low PAR sequences from Eq. (2.10) one should avoid in particular its trivial solutions $\mathbf{x} \in \{\sqrt{E}\,\boldsymbol{e}_k\}_{k=1}^n$ which indeed have the highest possible PAR (i.e. PAR $= n$) in the set of obtainable sequences. ■

Next, let $S = \{\mathbf{x}_1, \mathbf{x}_2, \cdots, \mathbf{x}_m\}$ be a a set of periodically complementary sequences containing m sequences of length n. We have that

$$\sum_{k=1}^{m} (\mathbf{x}_k \circlearrowleft \mathbf{x}_k^H)\mathbf{1} = \mathbf{E}\boldsymbol{e_1} \tag{2.12}$$

where E represents the total energy of $\{\mathbf{x}_k\}_{k=1}^m$.

Suppose $\boldsymbol{X} \in \mathbb{C}^{n\times n}$ is such that the sum of the entries of its rows is E for the first row and zero otherwise. Let us suppose that $\mathscr{F}(\boldsymbol{X})$ has $m \leq n$ nonzero positive eigenvalues and therefore that $\mathscr{F}(\boldsymbol{X})$ can be written as (for $\mathbf{x}_k \neq \mathbf{0}$):

$$\mathscr{F}(\boldsymbol{X}) = \sum_{k=1}^{m} \mathbf{x}_k \mathbf{x}_k^H \tag{2.13}$$

It follows from (2.13) that $\boldsymbol{X} = \sum_{k=1}^m \mathbf{x}_k \circlearrowleft \mathbf{x}_k^H$ and as a result

$$\boldsymbol{X}\mathbf{1} = \sum_{\mathbf{k=1}}^{\mathbf{m}} (\mathbf{x_k} \circlearrowleft \mathbf{x_k^H})\mathbf{1} = \mathbf{E}\boldsymbol{e_1} \tag{2.14}$$

which implies that the total energy E is distributed over m sequences $\{\mathbf{x}_k\}_{k=1}^m$ that are complementary. Note that the energy of $\{\mathbf{x}_k\}_{k=1}^m$ is determined by the

corresponding eigenvalues of $\mathscr{F}(\boldsymbol{X})$ in (2.13). In particular, if $\mathbf{x}_1 \circlearrowright \mathbf{x}_1^H$ is the twisted rank-one eigen (i.e. with $\boldsymbol{y} = \mathbf{x}$) approximation of $\boldsymbol{X}$ and the energy of $\mathbf{x}_1$ is almost equal to E, one could regard $\mathbf{x}_1$ as an almost-perfect sequence.

We will study the problem of designing sets of (periodically) complementary sequences when the desired energy for each sequence is given. It can be easily seen that designing a single perfect sequence is just a special case of the latter problem corresponding to choosing only one nonzero energy component. As mentioned above, the energy components of the sequences dictate the eigenvalues of $\mathscr{F}(\boldsymbol{X})$. Consider the convex set $\Gamma_{\mathscr{P}}(E)$ ($\mathscr{P}$ *stands for Periodic*) of all matrices $\mathscr{F}(\boldsymbol{X}_0)$ such that $\boldsymbol{X}_0\mathbf{1} = \mathbf{E}\boldsymbol{e_1}$. Also, suppose the energies of the sequences are given via the vector $\boldsymbol{\rho} \in (\mathbb{R}^+ \cup \{0\})^{n\times 1}$ (whose entries sum up to E) and consider the set $\Lambda_{\mathscr{P}}(\boldsymbol{\rho})$ of all Hermitian matrices with the given vector of eigenvalues $\boldsymbol{\rho}$. Using this formulation, Eqs. (2.13) and (2.14) establish an one-to-one mapping between the solutions of the design problem and the elements (if any) lying in the intersection of the two sets $\Gamma_{\mathscr{P}}(E)$ and $\Lambda_{\mathscr{P}}(\boldsymbol{\rho})$.

2.2.2 The Aperiodic Autocorrelation

The proposed computational framework can be extended to the problem of designing sequences with good aperiodic properties. The extension is based on the simple idea that for a sequence $\mathbf{x}$ of length n, the periodic autocorrelation lags of

$$\mathbf{x}' = \begin{pmatrix} \mathbf{x} \\ \mathbf{0}_{(n-1)\times 1} \end{pmatrix} \tag{2.15}$$

are equal to the aperiodic autocorrelation lags of $\mathbf{x}$ for $0 \le k \le n-1$. Remember that we defined $\Gamma_{\mathscr{P}}(E)$ as the set of all matrices $\mathscr{F}(\boldsymbol{X}_0)$ such that $\boldsymbol{X}_0\mathbf{1} = \mathbf{E}\boldsymbol{e_1}$. For the aperiodic case, we replace $\Gamma_{\mathscr{P}}(E)$ with a new set $\Gamma_{\mathscr{A}\mathscr{P}}(E)$ ($\mathscr{A}\mathscr{P}$ *stands for Aperiodic*) which contains all matrices $\mathscr{F}(\boldsymbol{X}_0)$ such that

$$\begin{cases} \boldsymbol{X}_0 \in \mathbb{C}^{(2n-1)\times(2n-1)} \\ \boldsymbol{X}_0\mathbf{1} = \mathbf{E}\boldsymbol{e_1} \\ \mathscr{F}(\boldsymbol{X}_0) \odot \mathscr{M} = \mathscr{F}(\boldsymbol{X}_0) \end{cases} \tag{2.16}$$

where $\mathscr{M}$ is a masking matrix defined as

$$\mathscr{M} = \begin{pmatrix} \mathbf{1}_{\mathbf{n}\times\mathbf{n}} & \mathbf{0}_{n\times(n-1)} \\ \mathbf{0}_{(n-1)\times n} & \mathbf{0}_{(n-1)\times(n-1)} \end{pmatrix} \tag{2.17}$$

Let us also replace $\Lambda_{\mathscr{P}}(\boldsymbol{\rho})$ with $\Lambda_{\mathscr{A}\mathscr{P}}(\boldsymbol{\rho}) = \Lambda_{\mathscr{P}}(\boldsymbol{\rho}')$ where

$$\boldsymbol{\rho}' = \begin{pmatrix} \boldsymbol{\rho} \\ \mathbf{0}_{(n-1)\times 1} \end{pmatrix} \tag{2.18}$$

With the above definitions, the intersection of the two sets $\Gamma_{\mathscr{A}\mathscr{P}}(E)$ and $\Lambda_{\mathscr{A}\mathscr{P}}(\boldsymbol{\rho})$ yields sets of vectors of length $2n-1$ whose last $n-1$ entries are zero and whose first n entries form sequences with good aperiodic correlation properties.

2.2.3 Zero Correlation Zone (ZCZ)

Zero correlation zone properties can be defined for both periodic and aperiodic correlations. For ZCZ sequences zero (or low) correlation values at some specific lags are required. The proposed framework can be adapted to the ZCZ requirements by noting that only a given set of specific elements of $\boldsymbol{X}_0\mathbf{1}$ (corresponding to the zero correlation zone) should be equal to their corresponding positions in $E\boldsymbol{e}_1$. Let $\{p_1, p_2, \cdots, p_u\}$ be the set of ZCZ lags. Let

$$\boldsymbol{S} = \mathbf{Diag}\left(\sum_{k=1}^{u} \boldsymbol{e}_{p_k}\right) \tag{2.19}$$

In lieu of $\Gamma_{\mathscr{P}}(E)$ and $\Gamma_{\mathscr{A}\mathscr{P}}(E)$ we form the new sets $\Gamma^{\mathscr{Z}}_{\mathscr{P}}(E)$ and $\Gamma^{\mathscr{Z}}_{\mathscr{A}\mathscr{P}}(E)$ by employing the constraint

$$\boldsymbol{S}(\boldsymbol{X}_0\mathbf{1}) = \boldsymbol{S}(\mathbf{E}\boldsymbol{e}_\mathbf{1}) \tag{2.20}$$

As a result, the intersection of the sets $(\Gamma^{\mathscr{Z}}_{\mathscr{P}}(E), \Lambda_{\mathscr{P}}(\boldsymbol{\rho}))$ or $(\Gamma^{\mathscr{Z}}_{\mathscr{A}\mathscr{P}}(E), \Lambda_{\mathscr{A}\mathscr{P}}(\boldsymbol{\rho}))$ can be used to form (sets of) sequences with zero periodic or aperiodic correlation zone, respectively.

2.3 ITROX: The Algorithms

Using the problem formulation of Section 2.2, we propose a general iterative algorithm that can be used to design sequences with good correlation properties. The main challenge of such an algorithm is to tune the energy distribution over the sequences in each iteration while trying to preserve the mutual property of complementarity. This goal can be achieved using the idea of alternating projections which will be discussed in the following.

2.3.1 The Proposed Algorithms

Let $\Gamma(E)$ and $\Lambda(\boldsymbol{\rho})$ denote any of the set pairs defined in Section 2.2. Starting from an element $\boldsymbol{X}_1$ in $\Gamma(E)$, we find the closest element to $\boldsymbol{X}_1$ (for the $\|.\|_F$ norm) in $\Lambda(\boldsymbol{\rho})$ denoted by $\boldsymbol{Y}_1$ which we call the optimal projection of $\boldsymbol{X}_1$ on $\Lambda(\boldsymbol{\rho})$. Next, we find the optimal projection of $\boldsymbol{Y}_1$ on $\Gamma(E)$ denoted by $\boldsymbol{X}_2$. Repeating these projections leads to a method known as *alternating projections*. We refer the interested reader to the survey of the rich literature on alternating

projections in [26]. Note that, as the distance between the chosen points in the two sets is decreasing at each iteration, the convergence of the method is guaranteed. However, as $\Lambda(\boldsymbol{\rho})$ is non-convex, the alternating projections of ITROX may converge to different points depending on the initialization; this behavior is related to the multi-modality of the integrated sidelobe level (or the merit factor) metrics which are regularly used in the design of sequences with good correlation properties [6]- [9]. Further discussions regarding the convergence of ITROX are deferred to sub-section 2.3.2.

* Designing Periodically Complementary Sets of Sequences

We begin with finding the orthogonal projection of an element of $\Lambda_{\mathscr{P}}(\boldsymbol{\rho})$ on $\Gamma_{\mathscr{P}}(E)$.

Theorem 1. *Let $\boldsymbol{X} = \boldsymbol{Y}^{\perp}$ be the optimal projection (for the matrix Frobenius norm) of $\boldsymbol{Y} \in \mathbb{C}^{n\times n}$ on $\Gamma_{\mathscr{P}}(E)$. Then $\mathscr{F}^{-1}(\boldsymbol{X})$ can be obtained from $\mathscr{F}^{-1}(\boldsymbol{Y})$ by adding a fixed value to each row of $\mathscr{F}^{-1}(\boldsymbol{Y})$ such that $\mathscr{F}^{-1}(\boldsymbol{Y})\mathbf{1} = \mathbf{E}\boldsymbol{e_1}$; more precisely,*

$$\begin{aligned} \left[\mathscr{F}^{-1}(\boldsymbol{X})\right]_{k,l} &= \left[\mathscr{F}^{-1}(\boldsymbol{Y})\right]_{k,l} \\ &+ \frac{1}{n}\left(E\delta_{k-1} - \sum_{l'=1}^{n}\left[\mathscr{F}^{-1}(\boldsymbol{Y})\right]_{k,l'}\right). \end{aligned} \tag{2.21}$$

Proof: Let $\boldsymbol{\alpha} = (\alpha_1, \alpha_2, \cdots, \alpha_n)^T$ be a complex-valued vector with a fixed sum. Using the Cauchy-Schwarz inequality we have that

$$\|\boldsymbol{\alpha}\|_2^2 \geq \frac{(\mathbf{1^T}\boldsymbol{\alpha})^2}{n} \tag{2.22}$$

The equality condition for (2.22) implies that from all the vectors whose elements have a constant sum, the one with equal entries attains the minimum l_2-norm. Now let $\mathscr{F}^{-1}(\boldsymbol{X}) = \boldsymbol{X}_0$ and $\mathscr{F}^{-1}(\boldsymbol{Y}) = \boldsymbol{X}_0 + \Delta\boldsymbol{X}_0$. We have

$$\begin{aligned} \|\boldsymbol{Y} - \boldsymbol{X}\|_F &= \|\mathscr{F}^{-1}(\boldsymbol{Y}) - \mathscr{F}^{-1}(\boldsymbol{X})\|_F \\ &= \|\Delta\boldsymbol{X}_0\|_F \end{aligned} \tag{2.23}$$

which implies that $\|\Delta\boldsymbol{X}_0\|_F$ should be minimized to find the desired projection. Note that

$$\begin{aligned} \Delta\boldsymbol{X}_0\mathbf{1} &= \mathscr{F}^{-1}(\boldsymbol{Y})\mathbf{1} - \boldsymbol{X_0}\mathbf{1} \\ &= \mathscr{F}^{-1}(\boldsymbol{Y})\mathbf{1} - \mathbf{E}\boldsymbol{e_1}. \end{aligned} \tag{2.24}$$

Therefore, for any given $\boldsymbol{Y}$, the sum of the entries in each row of $\Delta\boldsymbol{X}_0$ is fixed. This fact implies that for the optimal $\Delta\boldsymbol{X}_0$, all the rows have identical entries (as given in (2.21)) which completes the proof. ■

Next, we study the orthogonal projection of an element of $\Gamma_{\mathscr{P}}(E)$ on $\Lambda_{\mathscr{P}}(\boldsymbol{\rho})$. Let $\boldsymbol{X}^{\perp}$ be the orthogonal projection (for the matrix Frobenius norm) of a Her-

mitian matrix $\boldsymbol{X} \in \mathbb{C}^{n\times n}$ on $\Lambda_{\mathscr{P}}(\boldsymbol{\rho})$. Then $\boldsymbol{X}^{\perp}$ can be represented as

$$\boldsymbol{X}^{\perp} = \boldsymbol{U}\boldsymbol{D}\boldsymbol{U}^{H} \tag{2.25}$$

where $\boldsymbol{D} = \mathbf{Diag}(\boldsymbol{\rho})$ and $\boldsymbol{U}$ is a unitary matrix. Suppose $\boldsymbol{X}$ has the eigenvalue decomposition

$$\boldsymbol{X} = \boldsymbol{V}\boldsymbol{D}'\boldsymbol{V}^{H} \tag{2.26}$$

Therefore, the problem of finding $\boldsymbol{X}^{\perp}$ is equivalent to

$$\begin{aligned} \min_{\boldsymbol{U}} \quad & \|\boldsymbol{V}\boldsymbol{D}'\boldsymbol{V}^{H} - \boldsymbol{U}\boldsymbol{D}\boldsymbol{U}^{H}\|_F^2 \\ \text{s.t.} \quad & \boldsymbol{U}\boldsymbol{U}^{H} = \boldsymbol{I} \end{aligned} \tag{2.27}$$

The following two theorems present a matrix inequality (due to von Neumann [27]) and an inequality for the inner product of re-ordered vectors (due to Hardy, Littlewood and Polya [28]) that pave the way for finding the closed-form solution of (2.27).

Theorem 2. *Let $\boldsymbol{A}, \boldsymbol{B} \in \mathbb{C}^{m\times n}$ have the singular value decompositions $\boldsymbol{J}\boldsymbol{\Delta}_1\boldsymbol{K}^{H}$ and $\boldsymbol{L}\boldsymbol{\Delta}_2\boldsymbol{M}^{H}$. Then*

$$\mathrm{tr}(\boldsymbol{A}\boldsymbol{G}\boldsymbol{B}^{H}\boldsymbol{H}) \leq \mathrm{tr}(\boldsymbol{\Delta}_1\boldsymbol{\Delta}_2) \tag{2.28}$$

where $\boldsymbol{G} \in \mathbb{C}^{n\times n}$ and $\boldsymbol{H} \in \mathbb{C}^{m\times m}$ are unitary matrices, and the equality is attained when $\boldsymbol{G} = \boldsymbol{K}\boldsymbol{M}^{H}$ and $\boldsymbol{H} = \boldsymbol{L}\boldsymbol{J}^{H}$.

Theorem 3. *Let $\boldsymbol{\alpha}$ and $\boldsymbol{\beta}$ be two real-valued vectors which are such that*

$$\begin{aligned} \boldsymbol{\alpha}(1) \geq \boldsymbol{\alpha}(2) \geq \cdots \geq \boldsymbol{\alpha}(n)\ , \\ \boldsymbol{\beta}(1) \geq \boldsymbol{\beta}(2) \geq \cdots \geq \boldsymbol{\beta}(n)\ . \end{aligned} \tag{2.29}$$

For any permutation $\pi_k : \{1,2,\cdots,n\} \to \{1,2,\cdots,n\}$,

$$\sum_{k=1}^{n} \boldsymbol{\alpha}(k)\boldsymbol{\beta}(n-k+1) \leq \sum_{k=1}^{n} \boldsymbol{\alpha}(k)\boldsymbol{\beta}(\pi_k) \leq \sum_{k=1}^{n} \boldsymbol{\alpha}(k)\boldsymbol{\beta}(k). \tag{2.30}$$

Suppose that the eigenvalues of $\boldsymbol{X}^{\perp}$ and $\boldsymbol{X}$ are sorted in the same order. The next theorem follows from the above results:

Theorem 4. *Let $\boldsymbol{X} \in \mathbb{C}^{n\times n}$ be a Hermitian matrix with the eigenvalue decomposition $\boldsymbol{V}\boldsymbol{D}'\boldsymbol{V}^{H}$. Then the orthogonal projection of $\boldsymbol{X}$ (for the matrix Frobenius norm) on $\Lambda_{\mathscr{P}}(\boldsymbol{\rho})$ denoted by $\boldsymbol{Y} = \boldsymbol{X}^{\perp}$ can be obtained from $\boldsymbol{X}$ by replacing $\boldsymbol{D}'$ with $\boldsymbol{D}$ (defined in Eq. (2.25)).*

Proof: Note that the objective function in (2.27) can be written as

$$\begin{aligned} Q(\boldsymbol{U}) &= \|\boldsymbol{V}\boldsymbol{D}'\boldsymbol{V}^H - \boldsymbol{U}\boldsymbol{D}\boldsymbol{U}^H\|_F^2 \\ &= \operatorname{tr}\left((\boldsymbol{V}\boldsymbol{D}'\boldsymbol{V}^H - \boldsymbol{U}\boldsymbol{D}\boldsymbol{U}^H)^2\right) \\ &= \operatorname{tr}\left(\boldsymbol{V}\boldsymbol{D}'^2\boldsymbol{V}^H + \boldsymbol{U}\boldsymbol{D}^2\boldsymbol{U}^H\right) \\ &- \operatorname{tr}\left(\boldsymbol{U}\boldsymbol{D}\boldsymbol{U}^H\boldsymbol{V}\boldsymbol{D}'\boldsymbol{V}^H + \boldsymbol{V}\boldsymbol{D}'\boldsymbol{V}^H\boldsymbol{U}\boldsymbol{D}\boldsymbol{U}^H\right) \\ &= \text{const} - 2\operatorname{tr}(\boldsymbol{D}\boldsymbol{U}^H\boldsymbol{V}\boldsymbol{D}'\boldsymbol{V}^H\boldsymbol{U}). \end{aligned} \tag{2.31}$$

Therefore, in order to minimize $Q(\boldsymbol{U})$, one can maximize $\operatorname{tr}(\boldsymbol{D}\boldsymbol{U}^H\boldsymbol{V}\boldsymbol{D}'\boldsymbol{V}^H\boldsymbol{U})$. Using Theorem 2,

$$\operatorname{tr}(\boldsymbol{D}\boldsymbol{U}^H\boldsymbol{V}\boldsymbol{D}'\boldsymbol{V}^H\boldsymbol{U}) \leq \operatorname{tr}(\boldsymbol{D}\boldsymbol{D}') \tag{2.32}$$

where equality is attained for $\boldsymbol{U}^H\boldsymbol{V} = \boldsymbol{V}^H\boldsymbol{U} = \boldsymbol{I}$ which implies $\boldsymbol{U} = \boldsymbol{V}$. In addition, Theorem 3 implies that $\operatorname{tr}(\boldsymbol{D}\boldsymbol{D}')$ attains its maximum when the diagonal entries of $\boldsymbol{D}$ and $\boldsymbol{D}'$ are sorted in the same order. With this observation, the proof is concluded. ■

The proposed alternating projection approach for designing periodically complementary sets of sequences with a given energy distribution ($\boldsymbol{\rho}$) is summarized in Table 2.1.

Table 2.1. *The ITROX-$\mathscr{P}$ Algorithm (for designing periodically complementary sets of sequences)*

Step 0: Consider an initial point $\boldsymbol{X} = \mathscr{F}(\boldsymbol{X}_0) \in \Gamma_{\mathscr{P}}(E)$ for some $\boldsymbol{X}_0$ that satisfies $\boldsymbol{X}_0\mathbf{1} = \mathbf{E}\boldsymbol{e_1}$.
Step 1: Compute the eigenvalue decomposition $\boldsymbol{X} = \boldsymbol{V}\boldsymbol{D}'\boldsymbol{V}^H$ and find $\boldsymbol{Y} = \boldsymbol{X}^{\perp}$ (the orthogonal projection of $\boldsymbol{X}$ on $\Lambda_{\mathscr{P}}(\boldsymbol{\rho})$) by replacing $\boldsymbol{D}'$ with $\boldsymbol{D}$ (i.e. $\boldsymbol{Y} = \boldsymbol{V}\boldsymbol{D}\boldsymbol{V}^H$) as described in Theorem 4.
Step 2: Compute $\boldsymbol{X} = \boldsymbol{Y}^{\perp}$ by adding a fixed value to each row of $\mathscr{F}^{-1}(\boldsymbol{Y})$ such that $\mathscr{F}^{-1}(\boldsymbol{Y}^{\perp})\mathbf{1} = \mathbf{E}\boldsymbol{e_1}$ according to Theorem 1.
Step 3: Repeat the projections in steps 1 and 2 until a stop criterion is satisfied, e.g. $\|\boldsymbol{X} - \boldsymbol{Y}\|_F < \varepsilon$ for some given $\varepsilon > 0$.

• Designing Aperiodically Complementary Sets of Sequences:

The projection on $\Gamma_{\mathscr{A}\mathscr{P}}(E)$ must have zero entries in known positions (given by the masking matrix $\mathscr{M}$) and its nonzero entries must be chosen such that they minimize the Frobenius norm of the difference between the given $Y \in \mathbb{C}^{(2n-1)\times(2n-1)}$ and its projection on $\Gamma_{\mathscr{A}\mathscr{P}}(E)$. This optimal projection can be obtained via a result similar to Theorem 1.

Theorem 5. *Let $\boldsymbol{X} = \boldsymbol{Y}^{\perp}$ be the optimal projection (for the matrix Frobenius norm) of $\boldsymbol{Y} \in \mathbb{C}^{(2n-1)\times(2n-1)}$ on $\Gamma_{\mathscr{A}\mathscr{P}}(E)$. Let w_k denote the number of ones in the k^{th} row of $\mathscr{F}^{-1}(\mathscr{M})$. Then*

$$w_k = \sum_{l'=1}^{2n-1} \left[\mathscr{F}^{-1}(\mathscr{M})\right]_{k,l'} = \begin{cases} n-k+1, & k \leq n \\ k-n, & k > n \end{cases} \tag{2.33}$$

and the entries of $\mathscr{F}^{-1}(\boldsymbol{X})$ are given by

$$\begin{aligned} \left[\mathscr{F}^{-1}(\boldsymbol{X})\right]_{k,l} &= \left[\mathscr{F}^{-1}(\boldsymbol{Y})\right]_{k,l} \\ &+ \frac{1}{w_k}\left(E\delta_{k-1} - \sum_{l'=1}^{2n-1}\left[\mathscr{F}^{-1}(\mathscr{M}\odot\boldsymbol{Y})\right]_{k,l'}\right). \end{aligned} \tag{2.34}$$

for all (k,l) such that $\left[\mathscr{F}^{-1}(\mathscr{M})\right]_{k,l} = 1$ and zero otherwise.

Proof: As $\boldsymbol{X} \in \Gamma_{\mathscr{A}\mathscr{P}}(E)$, the positions of nonzero entries of $\mathscr{F}^{-1}(\boldsymbol{X})$ are given by $\mathscr{F}^{-1}(\mathscr{M})$. Using the same observations as in Theorem 1, fixed values must be added to the nonzero entries of $\mathscr{F}^{-1}(\mathscr{M}) \odot \mathscr{F}^{-1}(\boldsymbol{Y}) = \mathscr{F}^{-1}(\mathscr{M} \odot \boldsymbol{Y})$ such that its rows sum up to E for the first row and zero otherwise. Therefore, for any (k,l) such that $\left[\mathscr{F}^{-1}(\mathscr{M})\right]_{k,l} = 1$, these fixed values are given by

$$\frac{1}{w_k}\left(E\delta_{k-1} - \sum_{l'=1}^{2n-1}\left[\mathscr{F}^{-1}(\mathscr{M}\odot\boldsymbol{Y})\right]_{k,l'}\right). \tag{2.35}$$

Considering $\mathscr{F}^{-1}(\mathscr{M})$, the numerical values of $\{w_k\}$ can be easily derived. ■
Next note that, for any matrix $\boldsymbol{X} \in \Gamma_{\mathscr{A}\mathscr{P}}(E)$, its eigenvalue decomposition has the form

$$\begin{aligned} \boldsymbol{X} = &\begin{pmatrix} \boldsymbol{V}_{n\times n} & \boldsymbol{0}_{n\times(n-1)} \\ \boldsymbol{0}_{(n-1)\times n} & \boldsymbol{I}_{n-1} \end{pmatrix} \begin{pmatrix} \boldsymbol{D}'_{n\times n} & \boldsymbol{0}_{n\times(n-1)} \\ \boldsymbol{0}_{(n-1)\times n} & \boldsymbol{0}_{(n-1)\times(n-1)} \end{pmatrix} \\ &\begin{pmatrix} \boldsymbol{V}^{*}_{n\times n} & \boldsymbol{0}_{n\times(n-1)} \\ \boldsymbol{0}_{(n-1)\times n} & \boldsymbol{I}_{n-1} \end{pmatrix} \end{aligned} \tag{2.36}$$

where $\boldsymbol{V}\boldsymbol{D}'\boldsymbol{V}^{*}$ is the eigenvalue decomposition of the $n \times n$ upper-left submatrix of $\boldsymbol{X}$. This implies that the projection on $\Lambda_{\mathscr{A}\mathscr{P}}(\boldsymbol{\rho})$ can be obtained as before by imposing the desired energy distribution over the n sequences i.e. replacing the diagonal matrix $\boldsymbol{D}'$ with $\boldsymbol{D}$.

The general form of ITROX for designing complementary sets of sequences with good aperiodic correlation properties is summarized in Table 2.2.

Table 2.2. *The ITROX-$\mathscr{A}\mathscr{P}$ algorithm (for designing complementary sets of sequences with good aperiodic correlation)*

Step 0: Consider an initial point $\boldsymbol{X} = \mathscr{F}(\boldsymbol{X}_0) \in \Gamma_{\mathscr{A}\mathscr{P}}(E)$ with nonzero entries only in its $n \times n$ upper-left sub-matrix and for which $\boldsymbol{X}_0$ that satisfies $\boldsymbol{X}_0\mathbf{1} = \mathbf{E}\boldsymbol{e_1}$.
Step 1: Compute the eigenvalue decomposition of $\boldsymbol{X}$ as in (2.36) and find $\boldsymbol{Y} = \boldsymbol{X}^{\perp}$ (the orthogonal projection of $\boldsymbol{X}$ on $\Lambda(\boldsymbol{\rho})$) by replacing $\boldsymbol{D}'$ with $\boldsymbol{D}$.
Step 2: Compute $\boldsymbol{X} = \boldsymbol{Y}^{\perp}$ by adding certain fixed values to some entires of $\boldsymbol{Y}$ and by making the others zero, according to Theorem 5.
Step 3: Repeat the projections in steps 1 and 2 until a stop criterion is satisfied, e.g. $\|\boldsymbol{X} - \boldsymbol{Y}\|_F < \varepsilon$ for some given $\varepsilon > 0$.

• Designing Complementary Sets of Sequences with Zero Correlation Zone:

In order to obtain sequences (or complementary sets of sequences) with zero correlation zone, the same approach as given in Theorem 1 or 5 can be used. The only difference is that since now some autocorrelation lags are not of interest, there is no need to change their corresponding rows in $\mathscr{F}^{-1}(\boldsymbol{Y})$.

Theorem 6. *Let $S = \{p_1, p_2, \cdots, p_u\}$ be the set of ZCZ lags.*

1. *Projection on $\Gamma^{\mathscr{Z}}_{\mathscr{P}}(E)$: if $\boldsymbol{X} = \boldsymbol{Y}^{\perp}$ denotes the optimal projection (for the matrix Frobenius norm) of a matrix $\boldsymbol{Y}$ on $\Gamma^{\mathscr{Z}}_{\mathscr{P}}(E)$ then $\left[\mathscr{F}^{-1}(\boldsymbol{X})\right]_{k,l}$ is given by (2.21) for every $k \in S$ and by $\left[\mathscr{F}^{-1}(\boldsymbol{Y})\right]_{k,l}$ for all $k \notin S$.*
2. *Projection on $\Gamma^{\mathscr{Z}}_{\mathscr{A}\mathscr{P}}(E)$: similarly, if $\boldsymbol{X} = \boldsymbol{Y}^{\perp}$ represents the optimal projection (for the matrix Frobenius norm) of a matrix $\boldsymbol{Y}$ on $\Gamma^{\mathscr{Z}}_{\mathscr{A}\mathscr{P}}(E)$, the entries $\left[\mathscr{F}^{-1}(\boldsymbol{X})\right]_{k,l}$ are given by (2.34) for every (k,l) such that $\left[\mathscr{F}^{-1}(\mathscr{M})\right]_{k,l} = 1$ and $k \in S$, by $\left[\mathscr{F}^{-1}(\boldsymbol{Y})\right]_{k,l}$ for every (k,l) such that $\left[\mathscr{F}^{-1}(\mathscr{M})\right]_{k,l} = 1$ and $k \notin S$, and by zero otherwise.*

Let

$$(\Gamma^{\mathscr{Z}}(E), \Lambda(\boldsymbol{\rho})) \in \{(\Gamma^{\mathscr{Z}}_{\mathscr{P}}(E), \Lambda_{\mathscr{P}}(\boldsymbol{\rho})), (\Gamma^{\mathscr{Z}}_{\mathscr{A}\mathscr{P}}(E), \Lambda_{\mathscr{A}\mathscr{P}}(\boldsymbol{\rho}))\} \tag{2.37}$$

Complementary sets of sequences for any given zero correlation zone can be generated by the ITROX-$\mathscr{Z}$ algorithm in Table 2.3.

Remark 2: If only one sequence is needed, the computational burden of the proposed algorithms can be reduced significantly. In this case, the Hermitian matrix $\boldsymbol{X} \in \Gamma(E)$ must attain rank-one and therefore a complete eigenvalue decomposition is not needed. Instead, one can compute the orthogonal projection on $\Lambda(\boldsymbol{\rho})$ (for $\boldsymbol{\rho} = E\boldsymbol{e}_1$) using the power method (note that the convergence of

Table 2.3. *The ITROX-$\mathscr{Z}$ algorithm (for designing sets of complementary ZCZ sequences)*

Step 0: Consider an initial point $\boldsymbol{X} = \mathscr{F}(\boldsymbol{X}_0) \in \Gamma^{\mathscr{Z}}(E)$ for some $\boldsymbol{X}_0$ such that $\boldsymbol{X}_0\mathbf{1}$ is equal to $E\boldsymbol{e}_1$ for the desired lags.
Step 1: Compute the eigenvalue decomposition $\boldsymbol{X} = \boldsymbol{V}\boldsymbol{D}'\boldsymbol{V}^H$ and find $\boldsymbol{Y} = \boldsymbol{X}^{\perp}$ (the orthogonal projection of $\boldsymbol{X}$ on $\Lambda(\boldsymbol{\rho})$) by replacing $\boldsymbol{D}'$ with $\boldsymbol{D}$.
Step 2: Compute $\boldsymbol{X} = \boldsymbol{Y}^{\perp}$ (the orthogonal projection of $\boldsymbol{Y}$ onto $\Gamma^{\mathscr{Z}}(E)$) as described in Theorem 6.
Step 3: Repeat the projections in steps 1 and 2 until a stop criterion is satisfied, e.g. $\|\boldsymbol{X} - \boldsymbol{Y}\|_F < \varepsilon$ for some given $\varepsilon > 0$.

$\boldsymbol{X}$ to a rank-one matrix also leads to faster convergence of the power method). ■

2.3.2 Convergence and Design Metrics

As indicated earlier, in any alternating projection-based algorithm, the distance between the two sets is decreasing. Because the distance is non-negative (thus lower bounded) and decreasing, it can be concluded that the projections are convergent in the sense of distance. We also note that as the projections provided for all $(\Gamma(E), \Lambda(\boldsymbol{\rho}))$ are unique, the latter conclusion can be extended to the convergence of solutions on the two sets.

Definition 2. *Consider a pair of sets (T_1, T_2). A pair of sets (C_1, C_2) where $C_1 \subseteq T_1$ and $C_2 \subseteq T_2$ is called an **attraction landscape** of (T_1, T_2) iff starting from any point in C_1 or C_2, the alternating projections on T_1 and T_2 end up in the same element pair (c_1, c_2) ($c_1 \in C_1$, $c_2 \in C_2$). Furthermore, for a pair of sets (T_1, T_2), an attraction landscape (C_1, C_2) is said to be **complete** iff for any attraction landscape (C_1', C_2') such that $C_1 \subseteq C_1'$ and $C_2 \subseteq C_2'$, we have $C_1 = C_1'$ and $C_2 = C_2'$.*

In terms of Definition 2, the aim of the alternating projections on $\Gamma(E)$ and $\Lambda(\boldsymbol{\rho})$ is to find the closest points in an attraction landscape of $(\Gamma(E), \Lambda(\boldsymbol{\rho}))$; particularly, the number of solutions is characterized by the number of complete attraction landscapes of $(\Gamma(E), \Lambda(\boldsymbol{\rho}))$. When it comes to constrained alphabets (which will be studied in Section 2.4), it is common that the solutions on the two sets $\boldsymbol{X} \in \Gamma(E)$ and $\boldsymbol{Y} \in \Lambda(\boldsymbol{\rho})$ are not identical. Clearly, $\boldsymbol{X}$ and $\boldsymbol{Y}$ are the closest points in an attraction landscape of $(\Gamma(E), \Lambda(\boldsymbol{\rho}))$ but the two sets may not intersect in the attraction landscape encompassing $\boldsymbol{X}$ and $\boldsymbol{Y}$. In these cases, $\boldsymbol{X}$ represents an optimal solution in the sense of the desired

correlation properties which, however, does not satisfy exactly the alphabet restriction and energy distribution while $\boldsymbol{Y}$ represents a solution that satisfies the energy distribution and alphabet restriction but has sub-optimal correlation properties.

In the following we study the goodness of the sequences obtained by ITROX for the ISL and PSL metrics. Interestingly, ITROX can be viewed as an ISL minimization scheme. Indeed, we note that the distance between the two sets $(\Gamma(E),\Lambda(\boldsymbol{\rho}))$ defined using the matrix Frobenius norm is nothing but the ISL metric. Let us suppose that at the s^{th} iteration of ITROX, the projection on $\Lambda(\boldsymbol{\rho})$ gives some sequences such that the sums of their autocorrelations for the first n lags are $\left\{c_k^{(s)}\right\}_{k=0}^{n-1}$ (for notational simplicity, $\{c_k\}$ are used here to represent both periodic and aperiodic correlation lags). We let S be the set of all lags that ITROX tries to make small. Considering S provides a unified approach for both ZCZ and all correlation lag cases (note that $S=\{1,2,\cdots,n-1\}$ represents the case for which all correlation lags are desired to be small). Let $\boldsymbol{X}$ be the optimal projection of $\boldsymbol{Y}\in\Lambda(\boldsymbol{\rho})$ on $\Gamma(E)$ and $\Delta\boldsymbol{X}_0=\mathscr{F}^{-1}(\boldsymbol{Y})-\mathscr{F}^{-1}(\boldsymbol{X})$ (as introduced in Theorem 1). We have

$$\|\Delta\boldsymbol{X}_0^{(s)}\|_F^2=\sum_{k\in\, S\cup\{0\}} n\left|\frac{c_k^{(s)}-\delta_k E}{n}\right|^2 \tag{2.38}$$

Taking into consideration that any projection on $\Lambda(\boldsymbol{\rho})$ must satisfy the total energy constraint (which must be equal to E), we obtain

$$\|\Delta\boldsymbol{X}_0^{(s)}\|_F^2=\sum_{k\in S} n\left|\frac{c_k^{(s)}}{n}\right|^2=\frac{1}{n}\,\mathrm{ISL}^{(s)} \tag{2.39}$$

This shows that *the ISL metric is decreasing through the iterations of ITROX for a non-constrained alphabet.*

Sequences obtained by ITROX also have a good performance with respect to the PSL metric. To explain why this is so, we show that there is an "*almost equivalency*" between the projections needed for optimization of the ISL and the PSL metrics. Note that

$$\begin{aligned}\mathrm{PSL}^{(s)} &= \max\left\{\left|c_k^{(s)}\right|\right\}_{k\in S}\\ &\leq \sqrt{\sum_{k\in S}\left|c_k^{(s)}\right|^2}=\sqrt{\mathrm{ISL}^{(s)}}\end{aligned} \tag{2.40}$$

which implies that if an algorithm makes the ISL metric small (for ITROX the ISL metric usually achieves practically zero values), it also makes the PSL metric small. To strengthen the above observation we prove that the projections that minimize the two metrics are related.

Lemma 1. *Among all complex-valued vectors $\boldsymbol{\alpha} = (\alpha_1, \alpha_2, \cdots, \alpha_n)^T$ with a fixed sum of entries, the one with equal entries has the minimum l_∞-norm.*

Proof: Let $\boldsymbol{\alpha}$ be the vector with minimum l_∞-norm for some fixed sum of entries. If $\{\alpha_k\}_{k=1}^n$ are not equal, we consider the vector $\boldsymbol{\alpha}' = (\alpha_1', \alpha_2', \cdots, \alpha_n')^T$ with identical entries

$$\alpha_k' = \frac{1}{n}\sum_{k=1}^{n} \alpha_k \tag{2.41}$$

It is straightforward to verify that $\|\boldsymbol{\alpha}'\|_\infty < \|\boldsymbol{\alpha}\|_\infty$ which is a contradiction. ■

Once again, we draw the attention of the reader to the projections in subsection 2.3.1. As explained above, choosing the Frobenius norm to obtain the optimal projections on the two sets $(\Gamma(E), \Lambda(\boldsymbol{\rho}))$ leads to the minimization of ISL. However, in light of Lemma 1, one observes that using the max-norm instead of the Frobenius norm leads to the minimization of PSL. Interestingly, the projection on $\Gamma(E)$ is exactly the same for both norms. Furthermore, for $\Delta\boldsymbol{X}_0 = \mathscr{F}^{-1}(\boldsymbol{Y}) - \mathscr{F}^{-1}(\boldsymbol{X})$ we have:

$$\begin{aligned} \|\Delta\boldsymbol{X}_0^{(s)}\|_{\max} &= \max\left\{\left|\frac{c_k^{(s)} - \delta_k E}{n}\right|\right\}_{k\in\, S\cup\{0\}} \\ &= \max\left\{\left|\frac{c_k^{(s)}}{n}\right|\right\}_{k\in S} \\ &= \frac{1}{n}\,\mathrm{PSL}^{(s)} \end{aligned} \tag{2.42}$$

On the other hand, the projection on $\Lambda(\boldsymbol{\rho})$ for the max-norm appears to be more complicated in general. Therefore, we end this section by showing that at least for a special case of (2.27) the max-norm and Frobenius norm projections on $\Lambda(\boldsymbol{\rho})$ are close to one another. We consider the rank-one form of (2.27),

$$\begin{aligned} \min_{\boldsymbol{u}} \quad & \|d'\boldsymbol{v}\boldsymbol{v}^H - d\boldsymbol{u}\boldsymbol{u}^H\|_{\max} \\ \text{s.t.} \quad & \|\boldsymbol{u}\|_2 = 1 \end{aligned} \tag{2.43}$$

where d, d' and $\boldsymbol{v}$ are given such that $d, d' > 0$ and $\|\boldsymbol{v}\|_2 = 1$.

Lemma 2. *For two n-length real-valued vectors $\boldsymbol{\alpha}$ and $\boldsymbol{\beta}$ whose entries can be re-arranged as desired, $\|\boldsymbol{\alpha} - \boldsymbol{\beta}\|_\infty$ is minimal when the entries of $\boldsymbol{\alpha}$ and $\boldsymbol{\beta}$ are sorted in the same order.*

Proof: Let

$$\begin{aligned} &\boldsymbol{\alpha}(1) \geq \boldsymbol{\alpha}(2) \geq \cdots \geq \boldsymbol{\alpha}(n)\,, \\ &\boldsymbol{\beta}(1) \geq \boldsymbol{\beta}(2) \geq \cdots \geq \boldsymbol{\beta}(n)\,. \end{aligned} \tag{2.44}$$

We want to determine the minimal value of $\max\{|\boldsymbol{\alpha}(k)-\boldsymbol{\beta}(\pi_k)|\}_{k=1}^n$ over all possible permutations $\pi_k : \{1,2,\cdots,n\} \to \{1,2,\cdots,n\}$. Let $\boldsymbol{\alpha}(k) > \boldsymbol{\alpha}(l)$ and $\boldsymbol{\beta}(\pi_k) < \boldsymbol{\beta}(\pi_l)$; then it can be easily verified that

$$\begin{aligned} & \max\{|\boldsymbol{\alpha}(k)-\boldsymbol{\beta}(\pi_l)|, |\boldsymbol{\alpha}(l)-\boldsymbol{\beta}(\pi_k)|\} \\ < \quad & \max\{|\boldsymbol{\alpha}(k)-\boldsymbol{\beta}(\pi_k)|, |\boldsymbol{\alpha}(l)-\boldsymbol{\beta}(\pi_l)|\} \quad . \end{aligned} \tag{2.45}$$

Therefore, replacing $\boldsymbol{\beta}(\pi_k)$ by $\boldsymbol{\beta}(\pi_l)$ leads to a smaller l_∞-norm for $\boldsymbol{\alpha}-\boldsymbol{\beta}$. We conclude that to attain the minimal $\|\boldsymbol{\alpha}-\boldsymbol{\beta}\|_\infty$ we can sort $\boldsymbol{\beta}$ in the same order as $\boldsymbol{\alpha}$. As an aside remark, note that there exist examples for which no other arrangement of the entries of $\boldsymbol{\beta}$ can lead to the optimal $\|\boldsymbol{\alpha}-\boldsymbol{\beta}\|_\infty$ (e.g. let $\boldsymbol{\beta}(k) = \boldsymbol{\alpha}(k)+t$ where $t \in \mathbb{R}$). ■

The optimization problem (2.43) can be studied using the above result. Suppose that $\boldsymbol{u}$ and $\boldsymbol{v}$ are real-valued. We note that for any given $\boldsymbol{u}$ and any re-arrangement of its entries, we obtain the same set of entries in the matrix $d\boldsymbol{u}\boldsymbol{u}^H$. Lemma 2 implies that for all arrangements of the entries in $d\boldsymbol{u}\boldsymbol{u}^H$, the one sorted in the same order as $d'\boldsymbol{v}\boldsymbol{v}^H$ yields the minimal max-norm. But this arrangement of entries in $d\boldsymbol{u}\boldsymbol{u}^H$ is obtainable if and only if we sort $\boldsymbol{u}$ in the same order as $\boldsymbol{v}$. This implies that there exist a global optimizer of (2.43) such that it has the same order of entries as $\boldsymbol{v}$. Therefore, $\boldsymbol{v}$ lies in a neighborhood of an optimal solution of (2.43); clearly, the neighborhood is defined by the difference of sorted entries of $\boldsymbol{v}$ and the constraint $\|\boldsymbol{u}\|_2 = 1$. Note that while $\boldsymbol{u} = \boldsymbol{v}$ yields the optimal solution of (2.43) for the Frobenius norm, the above discussion implies that $\boldsymbol{u} = \boldsymbol{v}$ can be expected to be a good (but probably not optimal) solution to (2.43).

2.4 Constrained Sequence Design

Besides complex-valued sequences, sequences with real-valued alphabets can be obtained directly via ITROX as the eigenvalue decomposition is well-defined in $\mathbb{R}$. However, in some design applications the sequence entries are constrained. In particular, due to implementation issues, it can be desirable that the entries of sequences be restricted to a specific subset of $\mathbb{C}$, a finite or discrete alphabet. In these cases, one generally needs to perform an exhaustive search to find good sequences. Our goal here is to adapt the ITROX algorithms such that they can handle constrained alphabets. Namely, we are particularly interested in binary $\{-1,+1\}$, integer $\mathbb{Z}$, unimodular $\{\zeta \in \mathbb{C} \mid |\zeta| = 1\}$ and root-of-unity $\{\zeta \in \mathbb{C} \mid \zeta^m = 1\}$ (for $m \geq 3$) alphabets. To tackle such sequence design problems, we introduce a method which uses the idea of alternating projections but on a sequence of converging sets:

Definition 3. *Consider a function $f(t,s) : \mathbb{C} \times (\mathbb{N} \cup \{0\}) \to \mathbb{C}$; as an extension, for every matrix $\boldsymbol{X}$ let $f(\boldsymbol{X},s)$ be a matrix such that $[f(\boldsymbol{X},s)]_{k,l} = f(\boldsymbol{X}(k,l),s)$.*

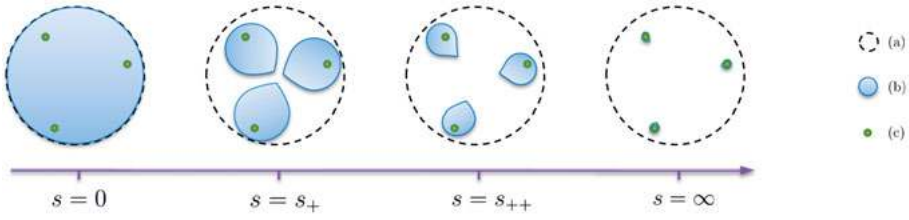

Figure 2.1. An example of a converging set. (a-c) show a (non-constrained) compact set T, the sets $T^{(s)}$, and entries of a (constrained) finite set $T^\dagger$ respectively for $0 < s_+ < s_{++} < \infty$.

We say that: ***(i)*** *f is* ***element-wisely monotonic*** *iff for any $t \in \mathbb{C}$, both $|f(t,s)|$ and $\arg(f(t,s))$ are monotonic in s.* ***(ii)*** *A set T is* ***converging*** *to a set $T^\dagger$ under a function f iff for every $t \in T$,*

$$\begin{cases} f(t,0) = t\ , \\ \lim_{s\to\infty} f(t,s) \in T^\dagger \end{cases} \tag{2.46}$$

and for every $t^\dagger \in T^\dagger$, there exists an element $t \in T$ such that

$$\lim_{s\to\infty} f(t,s) = t^\dagger. \tag{2.47}$$

(iii) *The function f is* ***identity*** *iff for any $t \in T$ and $t^\dagger \in T^\dagger$ satisfying (2.47), $t^\dagger$ is the closest element of $T^\dagger$ to t, and* ***(iv)*** *the sequence of sets $\{T^{(s)}\}_{s=0}^{\infty}$ where $T^{(s)} = \{f(t,s) \mid t \in T\}$ is a* ***sequence of converging sets****.*

An example of a converging set is depicted in Fig. 2.1. Note that in this example, while T is a compact set, $T^\dagger$ is a finite subset of T with 3 elements. Generally, we need to know both T and $T^\dagger$ to propose a suitable identity function f.

Example. *We present examples of f for some constrained alphabets commonly used in sequence design:*

(a) $T = \mathbb{R} - \{0\},\ T^\dagger = \{-1,1\}$:

$$f(t,s) = \operatorname{sgn}(t) \cdot |t|^{e^{-\nu s}} \tag{2.48}$$

(b) $T = \mathbb{R},\ T^\dagger = \mathbb{Z}$:

$$f(t,s) = [t] + \{t\} \cdot e^{-\nu s} \tag{2.49}$$

(c) $T = \mathbb{C} - \{0\},\ T^\dagger = \{\zeta \in \mathbb{C} \mid |\zeta| = 1\}$:

$$f(t,s) = |t|^{e^{-\nu s}} \cdot e^{j \arg(t)} \tag{2.50}$$

(d) $T = \mathbb{C} - \{0\}$, $T^{\dagger} = \{\zeta \in \mathbb{C} \mid \zeta^m = 1\}$:

$$f(t,s) = |t|^{e^{-\nu s}} \cdot e^{j\frac{2\pi}{m}\left(\left[\frac{m\arg(t)}{2\pi}\right] + \left\{\frac{m\arg(t)}{2\pi}\right\} \cdot e^{-\nu s}\right)} \tag{2.51}$$

where ν *is a positive real number. In all cases, the monotonic function* $e^{-\nu s}$ *is used to construct the desirable functions which are both element-wisely monotonic and identity. Note that* ν *tunes the speed of convergence (as well as the accuracy of the method described in the following).*

Consider the alternating projections on two compact sets T_1 and T_2. Suppose T_1 is converging to a constrained set $T_1^{\dagger} \subseteq T_1$ under some element-wisely monotonic identity function f. As discussed before, the aim of the alternating projections on T_1 and T_2 is to find the closest two points in an attraction landscape of (T_1, T_2); the closer the obtained points, the better the solution. We assume that the alternating projections (in an attraction landscape of (T_1, T_2)) end up at (t_1, t_2) and that $\lim_{s\to\infty} f(t_1, s) = t_1^{\dagger} \in T_1^{\dagger}$. The key idea is that $t_1^{\dagger} \in T_1^{\dagger}$ is a good solution if it has the properties below:

a) Its corresponding projection $t_1 \in T_1$ is a good solution in T_1.

b) $t_1^{\dagger}$ is close to t_1.

Typical alternating projections can provide good solutions $t_1 \in T_1$ and thus a) is satisfied. To satisfy b) as well, we consider the following modification: at the s^{th} step of the alternating projections, let $t_1^{(s)} \in T_1$ be the orthogonal projection of $t_2^{(s)} \in T_2$ on T_1 and let ${t'}_1^{(s)} = f(t_1^{(s)}, s) \in T_1^{(s)}$. Now, instead of projecting $t_1^{(s)}$ on T_2, we project ${t'}_1^{(s)}$ on T_2 to obtain $t_2^{(s+1)}$.

Fig. 2.2 illustrates the alternating projections with the proposed modification. Supposing that $\lim_{s'\to\infty} f(t_1^{(s)}, s') = {t^{\dagger}}_1^{(s)}$, we comment on two cases for the goodness of solutions in the constrained set $T_1^{\dagger}$ in connection with the modified projections:

- ${t^{\dagger}}_1^{(s)}$ *is close to* $t_1^{(s)}$: As f is element-wisely monotonic, $t_1^{(s)}$ is element-wisely closer to ${t'}_1^{(s)}$ than to ${t^{\dagger}}_1^{(s)}$ which implies that $\|t_1^{(s)} - {t'}_1^{(s)}\| < \|t_1^{(s)} - {t^{\dagger}}_1^{(s)}\|$. Therefore, if ${t^{\dagger}}_1^{(s)}$ is close to $t_1^{(s)}$ we can assume that ${t'}_1^{(s)}$ is also close to $t_1^{(s)}$. In this case, the modified projections approximate well the typical alternating projections which tend to improve the goodness of $t_1^{(s)} \in T_1$.
- ${t^{\dagger}}_1^{(s)}$ *is far from* $t_1^{(s)}$: One could then expect that ${t'}_1^{(s)}$ is also far from $t_1^{(s)}$; particularly so as s increases. Note that considering ${t'}_1^{(s)}$ instead of $t_1^{(s)}$ can change the complete attraction landscape. More important, when the algorithm is converging to a poor solution in $T_1^{\dagger}$, where ${t'}_1^{(s)}$ is far from $t_1^{(s)}$, it tries to replace complete attraction landscapes more often than in the case of good solutions (when ${t^{\dagger}}_1^{(s)}$ is close to $t_1^{(s)}$).

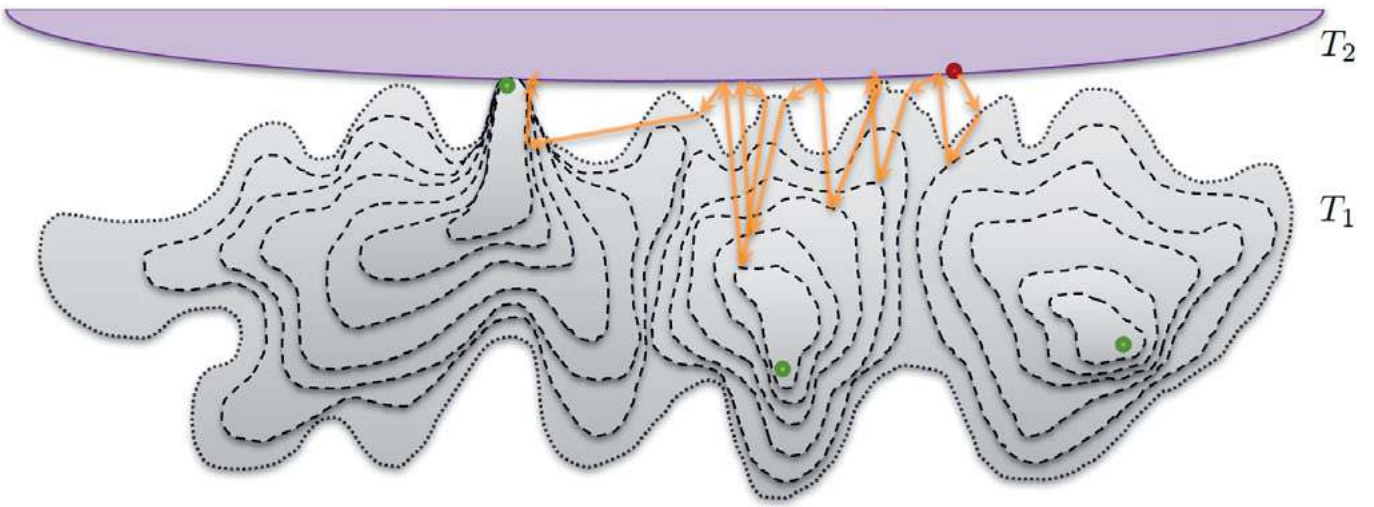

Figure 2.2. An illustration of the proposed modified alternating projections in which the algorithm converges to a good solution. The dashed-lines are used to represent the sets $T_1^{(s)}$ converging to $T_1^{\dagger} \subseteq T_1$ with 3 elements.

In sum, knowing the sets T_1 and $T_1^{\dagger}$ we design a convenient function f as described in Definition 3. The function f, and as a result, the sets $\{T_1^{(s)}\}_{s=0}^{\infty}$ provide information about the goodness (or closeness) of elements of $T_1^{\dagger}$ at the boundary of the compact set T_1. This information can be used to keep the good solutions and continue looking for other solutions when the obtained solution is not desirable. In the sequel, we consider the benefits of the proposed modification for alternating projections on some particular sets.

To use the above general ideas in the context of ITROX, suppose that the entries of sequences $\{\mathbf{x}_k\}$ are constrained to an alphabet Ω_x. Let

$$\Omega_{\boldsymbol{X}} = \left\{ \boldsymbol{X} \mid \boldsymbol{X} = \sum_k \mathbf{x}_k \mathbf{x}_k^H;\ \mathbf{x}_k(l) \in \Omega_x \right\} \tag{2.52}$$

The set $\Lambda(\boldsymbol{\rho})$ in the alternating projections of ITROX will be replaced by $\Omega_{\boldsymbol{X}}$ imposing that the projections must have some special structure. Clearly, $\Omega_{\boldsymbol{X}} \subseteq \Lambda(\boldsymbol{\rho})$ for some feasible power arrangement $\boldsymbol{\rho}$. Let us suppose that $\Lambda(\boldsymbol{\rho})$ is converging to $\Omega_{\boldsymbol{X}}$ under some identity function f. In this case, the general form of the modified ITROX algorithms can be summarized as in Table 2.4.

Table 2.4. *The general form of the ITROX algorithm for constrained sequence design*

Step 0: Consider an initial point $\boldsymbol{X} = \mathscr{F}(\boldsymbol{X}_0) \in \Gamma(E)$. Set the iteration counter (s) to zero.
Step 1: Compute the eigenvalue decomposition $\boldsymbol{X} = \boldsymbol{V}\boldsymbol{D}'\boldsymbol{V}^H$ and find $\boldsymbol{Y} = \boldsymbol{X}^{\perp}$ (the optimal projection of $\boldsymbol{X}$ on $\Lambda(\boldsymbol{\rho})$) by replacing $\boldsymbol{D}'$ with $\boldsymbol{D}$ (i.e. $\boldsymbol{Y} = \boldsymbol{V}\boldsymbol{D}\boldsymbol{V}^H$).
Step 2: Let $\Lambda(\boldsymbol{\rho})$ converge to $\Omega_{\boldsymbol{X}}$ under some convenient function f as described in Definition 3 (a set of examples are provided after the definition). Compute $\widetilde{\boldsymbol{Y}} = f(\boldsymbol{Y}, s)$.
Step 3: Compute $\boldsymbol{X} = \widetilde{\boldsymbol{Y}}^{\perp}$ by adding some fixed value to some given entries of $\widetilde{\boldsymbol{Y}}$, make certain of them zero and leave the others unchanged (depending on the application, see sub-section 2.3.1).
Step 4: Increase the iteration counter (s) by one. Repeat the modified alternating projections (steps 1-3) if the stop criterion (e.g. either $\|\widetilde{\boldsymbol{Y}} - \boldsymbol{X}\|_F < \varepsilon$ for some given $\varepsilon > 0$ or $\widetilde{\boldsymbol{Y}}$ is sufficiently close to an element of $\Omega_{\boldsymbol{X}}$) is not satisfied.

It is worthwile to note that the proposed modifications do not disturb the general convergence guarantee of ITROX. To justify this claim, it is sufficient to show that

$$\lim_{s\to\infty} \underbrace{\|f(\boldsymbol{Y}^{(s)}, s) - f(\boldsymbol{Y}^{(s+1)}, s+1)\|}_{Q_1(s)} = 0 \tag{2.53}$$

Using the triangle inequlity,

$$\begin{aligned} Q_1(s) &\leq \|f(\boldsymbol{Y}^{(s+1)},s)-f(\boldsymbol{Y}^{(s+1)},s+1)\| \\ &+ \underbrace{\|f(\boldsymbol{Y}^{(s)},s)-f(\boldsymbol{Y}^{(s+1)},s)\|}_{Q_2(s)} \end{aligned} \tag{2.54}$$

The first term on the right-hand side of (2.54) is vanishing as s increases. For the second term we have:

$$\begin{aligned} Q_2(s) &\leq \|\boldsymbol{Y}^{\dagger\,(s)}-f(\boldsymbol{Y}^{(s)},s)\| \\ &+ \|\boldsymbol{Y}^{\dagger\,(s+1)}-f(\boldsymbol{Y}^{(s+1)},s)\| \\ &+ \underbrace{\|\boldsymbol{Y}^{\dagger\,(s)}-\boldsymbol{Y}^{\dagger\,(s+1)}\|}_{Q_3(s)} \end{aligned} \tag{2.55}$$

where $\boldsymbol{Y}^{\dagger\,(s)} \triangleq \lim_{s'\to\infty} f(\boldsymbol{Y}^{(s)},s')$ for every $s \in \mathbb{N}\cup\{0\}$. Similar to the previous inequality, the first and second term in the right-hand side of (2.55) are vanishing in the limit. Therefore, we only need to show that

$$\lim_{s\to\infty} Q_3(s) = 0 \tag{2.56}$$

As f is identity, $\boldsymbol{Y}^{\dagger\,(s)}$ can be viewed as the optimal projection of $\boldsymbol{Y}^{(s)} \in \Lambda(\boldsymbol{\rho})$ on $\Omega_{\boldsymbol{X}}$. Therefore, the above calculations imply that the convergence of ITROX in the modified case is guaranteed by the convergence of projections in the following scenario: we compute the sequence of successive projections (SOSP) for the triple of sets $(\Gamma(E),\Lambda(\boldsymbol{\rho}),\Omega_{\boldsymbol{X}})$; i.e. starting from an element in the 1^{st} set we found its projection on the 2^{nd} set, then the projection of the 2^{nd} point on the 3^{rd} set and next we obtain the projection of the 3^{rd} point on the 1^{st} set. Performing these projections cyclically, a sequence of projections is obtained. The convergence of these projections has been shown and studied in [30] and [31].

2.5 Numerical Examples

In order to show the potential of ITROX to tackle different sequence design problems, several applications will be considered and numerical examples will be provided. Due to ease of implementation and optimal PAR, binary sequences have been commonly used in many applications. Therefore, sequences with binary entries are chosen to examine the performance of ITROX when dealing with constrained alphabets. Real-valued sequences are considered to illustrate the ITROX performance in the non-constrained case. In all cases, the algorithms are initialized with a random real-valued sequence.

2.5.1 Sequences with Good Periodic Correlation

Using the suggestion in Remark 2 we can employ a simplified version of ITROX-$\mathscr{P}$ to find single sequences with good periodic autocorrelation. An ITROX-$\mathscr{P}$ real-valued sequence of length $n = 64$ and its autocorrelation levels are shown in Fig. 2.3. The computational time for designing the sequence was about 18 seconds on a standard PC. The autocorrelation levels are normalized and expressed in dB:

$$\text{autocorrelation level (dB)} = 20\log_{10}\left|\frac{c_k}{c_0}\right| \tag{2.57}$$

We note that the out-of-phase autocorrelation lags of the generated sequence reach levels which are virtually zero.

Next, we consider the case of binary sequences. Unlike the real-valued sequences, no perfect binary sequence has been found for lengths $n > 4$ and it is widely conjectured that such a sequence does not exist [34]. In addition, it can be shown that the autocorrelation levels of a binary sequence are congruent to the sequence length (mod 4) [35] and as a result autocorrelation levels appear with a successive distance of 4. An ITROX binary sequence of length $n = 64$ with good periodic correlations is depicted in Fig. 2.4. We have let the function in (2.48) with $\nu = 0.0001$ operate on the entries of the sequence. The constructed sequence is optimal with out-of-phase autocorrelation levels of 0 and 4 [36]. A computational time of 13 seconds was required on a standard PC to accomplish the task.

2.5.2 Periodically Complementary Sets of Sequences

As discussed in Section 2.2, ITROX can be used to construct complementary sets of sequences for which the number of sequences is at most equal to their length.

We design a real-valued periodically complementary pair $\{\mathbf{x}_1, \mathbf{x}_2\}$ using ITROX-$\mathscr{P}$. The resultant sequences and the levels of their autocorrelation sum are shown in Fig. 2.5. On the other hand, Fig. 2.6 shows a periodically complementary pair of binary sequences along with their correlation sum. In the latter case, we have let the function f in (2.48) with $\nu = 0.0001$ operate on the entries of both sequences $\mathbf{x}_1$ and $\mathbf{x}_2$ through the iterations. The computational time for designing the two sequence pairs were 23 and 16 seconds on a standard PC, respectively.

2.5.3 Sequences with Good Aperiodic Correlation

We use ITROX-$\mathscr{A}\mathscr{P}$ to design single real-valued or binary sequences of length $n = 64$. The resultant sequences and their autocorrelations are shown in Fig. 2.7 and Fig. 2.8 respectively. The autocorrelation levels of the real-valued

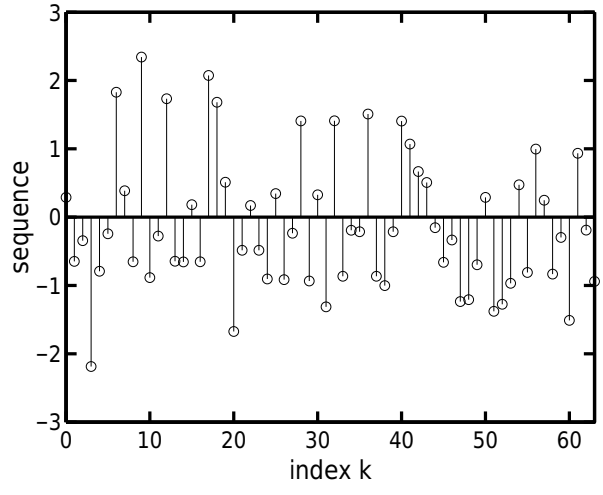

(a)

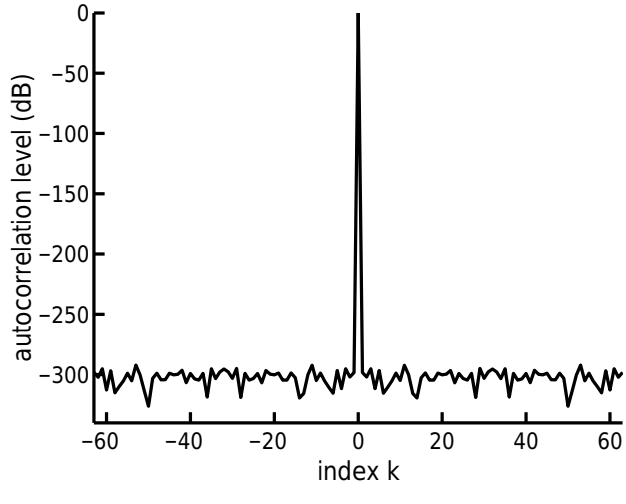

(b)

Figure 2.3. Design of a real-valued sequence of length 64 with good periodic autocorrelation. (a) and (b) depict the entries and the autocorrelation levels (in dB) of the sequence respectively.

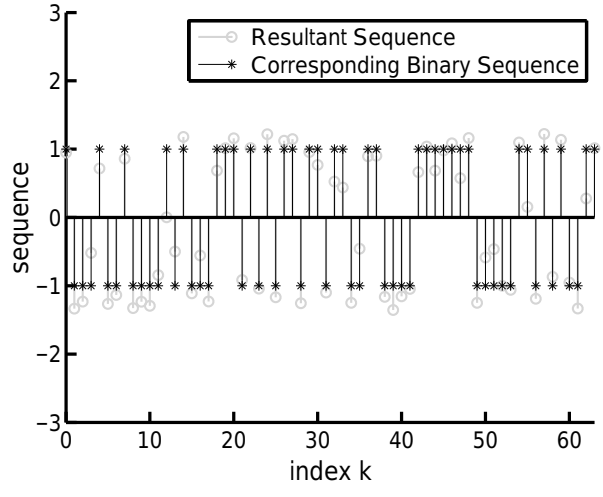

(a)

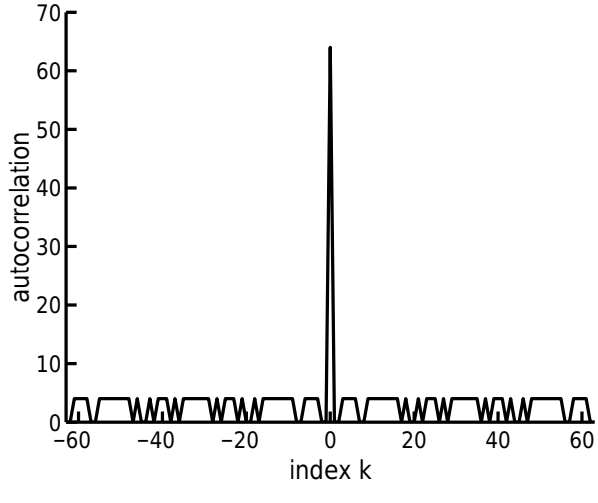

(b)

Figure 2.4. Design of a binary sequence of length 64 with good periodic autocorrelation. (a) shows the entries of the resultant sequence (i.e. the sequence provided by ITROX when stopped) along with the corresponding binary sequence (obtained by clipping the resultant sequence). The autocorrelation of the binary sequence is shown in (b).

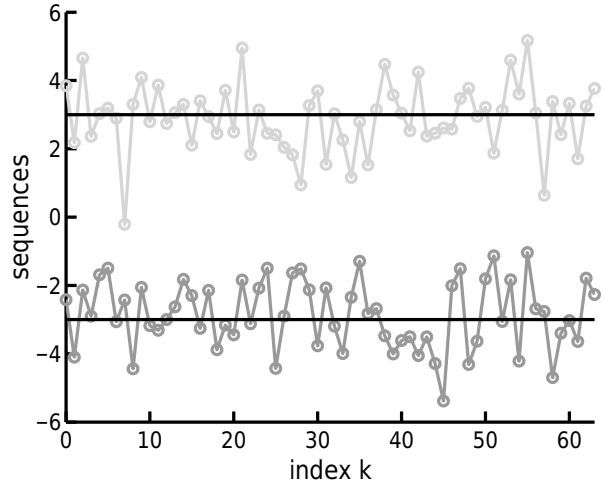

(a)

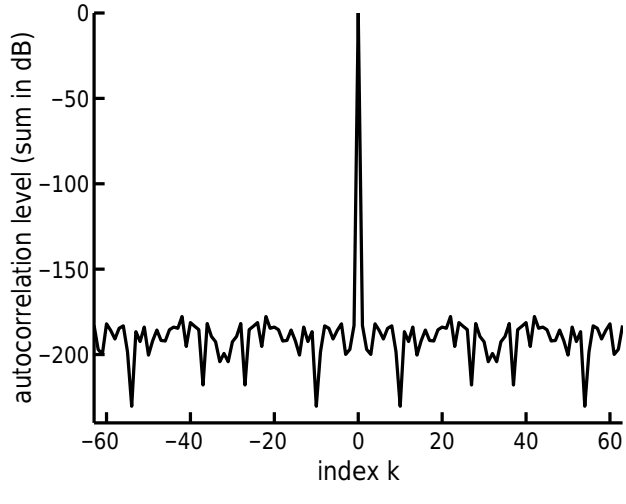

(b)

Figure 2.5. Design of a real-valued periodically complementary pair of sequences (both of length 64) using ITROX-$\mathscr{P}$. (a) plots of the sequences with a bias of $+3$ and -3 to distinguish the two sequences. (b) plot of the autocorrelation sum levels.

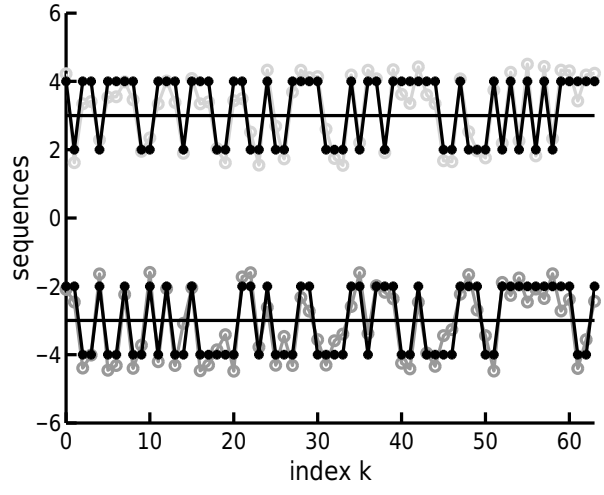

(a)

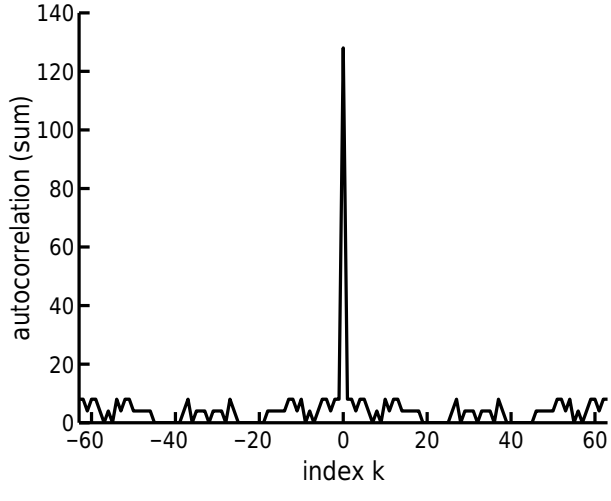

(b)

Figure 2.6. Design of a binary periodically complementary pair of sequences (both of length 64). (a) plots of the resultant sequences (i.e the sequences provided by ITROX when stopped) along with their corresponding binary sequences (obtained by clipping). A bias of $+3$ and -3 is used to distinguish the sequences. (b) plot of the autocorrelation sum.

sequence are normalized as in (2.57). The required time for designing the real-valued sequence of Fig. 2.7 was about 26 seconds on a standard PC, whereas it took 16 seconds to design the binary sequence of Fig. 2.8 on the same PC.

Under the binary constraint, Barker sequences have the lowest achievable PSL (i.e. PSL= 1). However, the longest known Barker sequence is of length 13. Moreover, finding sequences with optimal PSL requires exhaustive search. To design binary sequences, we use the function in (2.48) with $\nu = 0.0001$ as in the previous sub-sections. In this example, the binary sequence achieves a PSL value of 6 and a MF of 4.67. These values are comparable to those obtained by stochastic search algorithms [9]. The PSL and the MF of the sequence are depicted in Fig. 2.9 with respect to the iteration number.

It is shown in [37] that for any function $g(n) = o(\sqrt{n})$, the proportion of binary sequences of length n which have PSL values larger than $g(n)$ approaches 1 as n increases. Yet, no sequence families are known whose PSL grows like $o(\sqrt{n})$ or even $\Theta(\sqrt{n})$ [38]. We used ITROX-$\mathscr{A}\mathscr{P}$ to design binary sequences of length $5 \leq n \leq 69$. For each length, we run ITROX-$\mathscr{A}\mathscr{P}$ 5 times and save the best PSL. Fig. 2.10 compares our results with the optimal PSL values [39] and the square root of length.

2.5.4 Sequences With Zero Correlation Zone (ZCZ)

Considering the difficulty of finding sequences with good aperiodic correlation, we generate single real-valued or binary sequences (of length $n = 64$) with low aperiodic correlation zone. These sequences are shown in Fig. 2.11 and Fig. 2.12 respectively. In both cases, the lags $1 \leq |k| \leq 23$ (out of $0 \leq |k| \leq 63$) define the zone with low correlation. Furthermore, as in the previous sub-sections, the function f in (2.48) with $\nu = 0.0001$ was used in the binary case. The computational time for designing the real-valued and binary sequences were 85 and 57 seconds on a standard PC, respectively.

2.6 Concluding Remarks

A computational approach to the problem of sequence design for good correlation properties has been proposed. A general framework (called ITROX; to be pronounced “itrocks") and a set of associated algorithms were introduced to tackle several sequence design problems. The results can be summarized as follows:

- Using the concept of twisted product (see Definition 1) some basic formulations were provided that led to an alternating projection algorithm as the core of ITROX.
- Several specialized algorithms were proposed for different applications of sequence design, namely: (i) ITROX-$\mathscr{P}$ for designing (complemen-

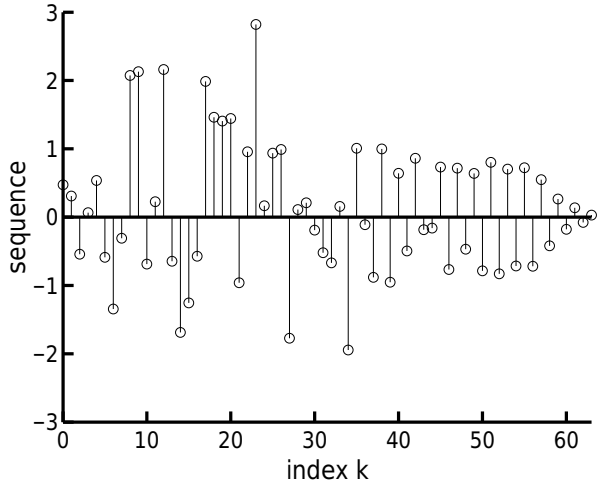

(a)

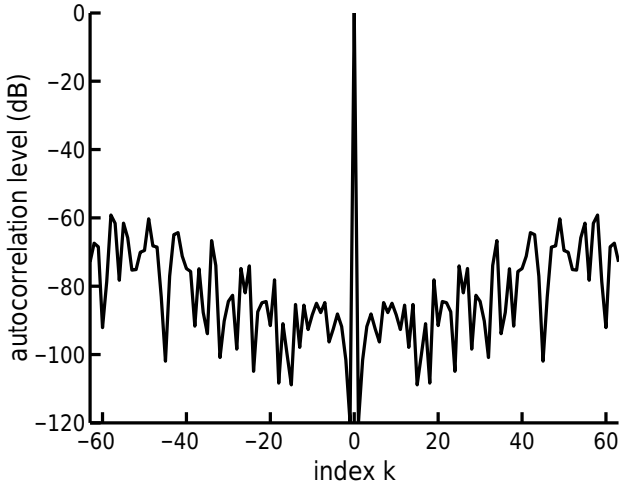

(b)

Figure 2.7. Design of a real-valued sequence (of length 64) with good aperiodic autocorrelation. (a) and (b) show the entries and the autocorrelation levels (in dB) of the sequence respectively.

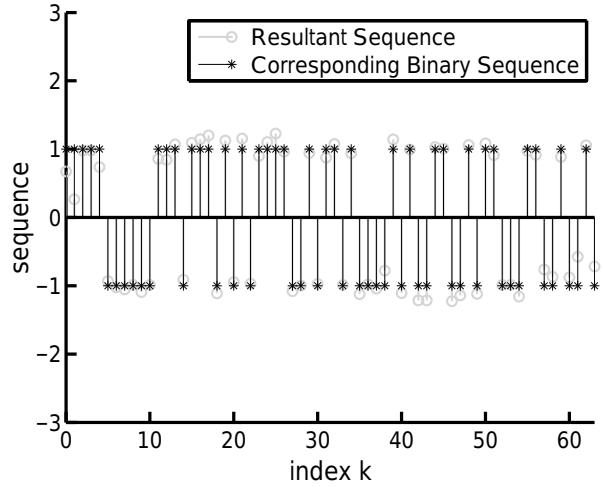

(a)

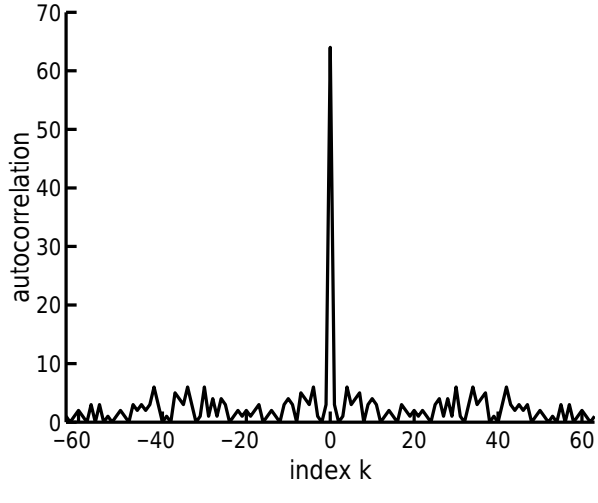

(b)

Figure 2.8. Design of a binary sequence (of length 64) with good aperiodic autocorrelation. (a) depicts the entries of the resultant sequence (i.e. the sequence provided by ITROX when stopped) along with the corresponding binary sequence (obtained by clipping the resultant sequence). The autocorrelation of the obtained binary sequence is shown in (b).

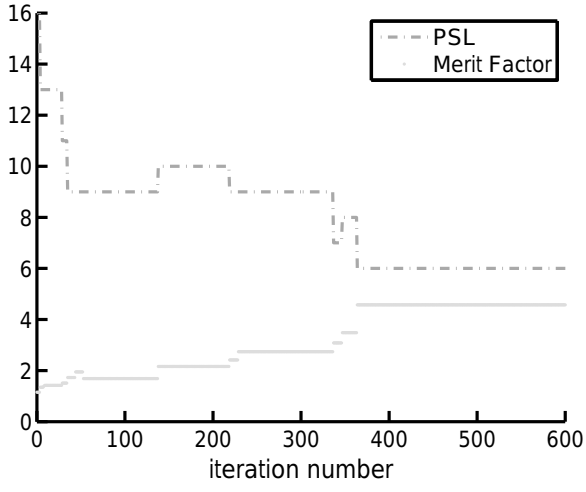

Figure 2.9. The PSL and MF vs. the iteration number for the binary sequence shown in Fig. 2.8. The binary sequence achieves a PSL value of 6 and a MF of 4.67.

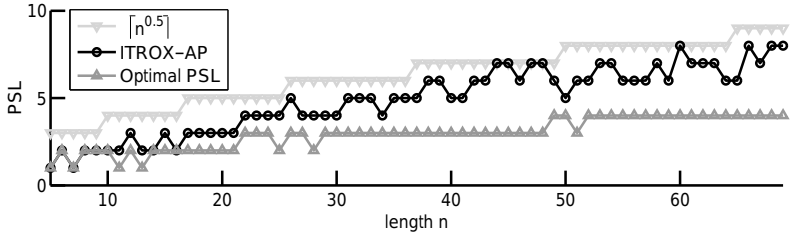

Figure 2.10. Comparison of the PSL values of binary sequences generated by ITROX-$\mathscr{AP}$ with the optimal values of PSL and the square root of lengths for $5 \leq n \leq 69$. For each length, ITROX-$\mathscr{AP}$ was used 5 times and from the 5 resultant PSL values, the best one is shown.

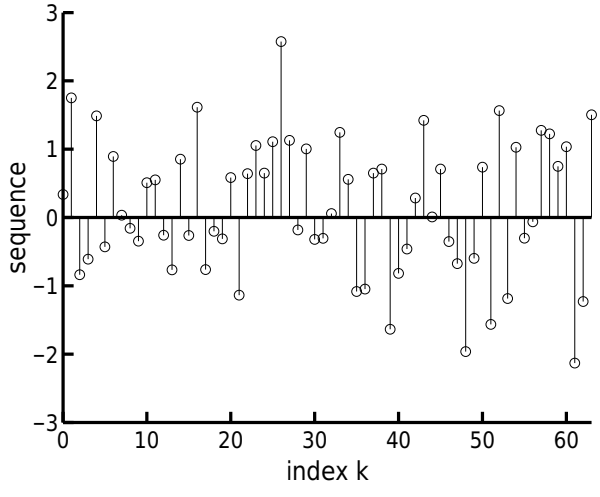

(a)

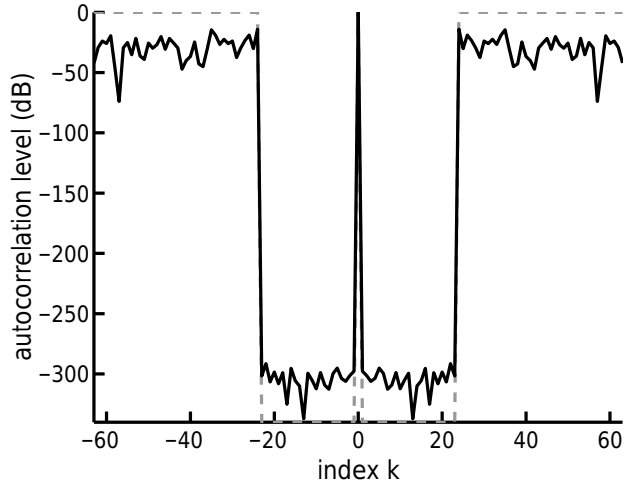

(b)

Figure 2.11. Design of a real-valued sequence (of length 64) with low aperiodic correlation zone: (a) entries of the sequence, (b) plot of the autocorrelation level of the sequence (in dB). Dashed-lines indicate the low correlation zone i.e. the lags $1 \leq |k| \leq 23$.

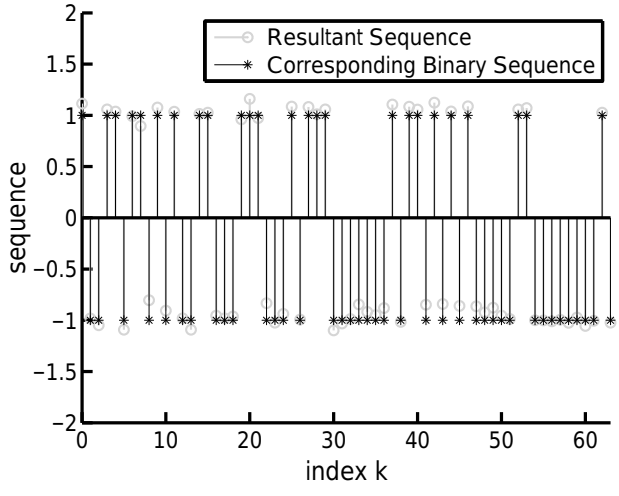

(a)

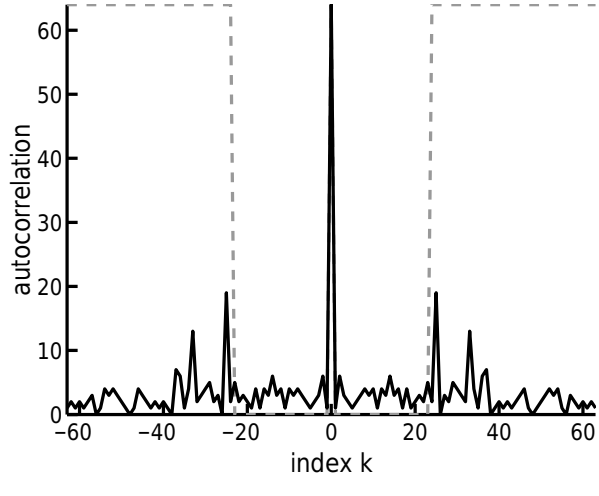

(b)

Figure 2.12. Design of a binary sequence (of length 64) with low aperiodic correlation zone: (a) the entries of the resultant sequence (i.e. the sequence provided by ITROX when stopped) along with the corresponding binary sequence (obtained by clipping), (b) plot of the autocorrelation of the obtained binary sequence. Dashed-lines indicate the low correlation zone i.e. the lags $1 \leq |k| \leq 23$.

tary sets of or single) sequences with good periodic correlation properties, (ii) ITROX-$\mathscr{AP}$ for designing (complementary sets of or single) sequences with good aperiodic correlation properties, and (iii) ITROX-$\mathscr{L}$ that extends the scope of the latter algorithms to designing (complementary sets of or single) sequences with zero or low correlation zone.

- The convergence of ITROX algorithms was studied. It was shown that ITROX is an ISL minimizer (or equivalently a merit factor maximizer) that can yield several solutions depending on initialization. The effect of ITROX iterations on the PSL metric was also investigated.
- The ability of ITROX to tackle sequence design problems with constrained alphabets was discussed. For these cases, the idea of projections on converging sets was introduced and used to modify the general form of ITROX. The convergence of this approach was also studied.
- Numerical examples were provided that confirm the potential of ITROX to tackle several sequence design problems.

Several research problems remain open. For example: (i) designing criteria that can “measure" the goodness of a function f (see Definition 2 and the discussions afterward); (ii) deriving an optimal f for given constrained and non-constrained sets; and (iii) exploring other possible applications of ITROX as well as its ability to optimize arbitrary sequence design objectives.

3. Design of Complementary Sets of Sequences

Abstract
We introduce a fast computational frequency-domain approach to designing complementary sets of sequences. Following the basic idea of CAN-based algorithms, we propose an extension of the **CAN** algorithm to complement**ary** sets of sequences (which we call CANARY). Moreover, modified versions of the proposed algorithm are derived to tackle the complementary set design problems in which low peak-to-average-power ratio (PAR), unimodular or phase-quantized sequences are of interest. Several numerical examples are provided to show the performance of CANARY.

Keywords: Autocorrelation, binary sequences, complementary sets, cyclic minimization, peak-to-average-power ratio (PAR), sidelobe level.

3.1 Introduction

An active sensing device, such as a radar system, transmits suitable waveforms into its surrounding that enable it to measure useful properties (e.g. location or speed) of peripheral objects. The transmit waveforms are generally formulated by using discrete-time sequences (see, e.g. [4]). Let $\mathbf{x} = (x(1), ..., x(N))^T$ represent such a sequence (to be designed). The aperiodic and, respectively, periodic autocorrelations of $\mathbf{x}$ are defined as

$$r(k) = \sum_{l=1}^{N-k} x(l)x^*(l+k) = r^*(-k),\ 0 \le k \le (N-1), \tag{3.1}$$

$$c(k) = \sum_{l=1}^{N} x(l)x^*(l+k)_{mod\ N} = c^*(-k),\ 0 \le k \le (N-1). \tag{3.2}$$

In general, transmit sequences $\mathbf{x}$ with small out-of-phase (i.e. $k \neq 0$) autocorrelation lags lead to a better performance of an active sensing system. As a result, there exists a rich literature on designing such sequences (see e.g. [1]-[22] and the references therein).

In order to avoid non-linear side effects and maximize the efficiency of power consumption at the transmitter, unimodular sequences (with $|x(l)| = 1$) are desirable. Moreover, for cases with more strict implementation demands, phase-quantized unimodular sequences must be considered. For unimodular sequences it is not possible to make all $\{|r(k)|\}$ much smaller than $r(0)$ (depending on the application, the needed ratio can be around 10^{-5} or even smaller). For instance, it can be easily observed that $|r(N-1)| = 1$, no matter how we design the sequence $\mathbf{x}$. In contrast with this, unimodular sequences with zero out-of-phase (i.e. perfect) periodic autocorrelation can be obtained for example via construction algorithms [8]. However, even by considering the periodic correlation, finding phase-quantized unimodular sequences with perfect periodic autocorrelation is a hard task. The difficulties in designing sequences with good autocorrelation encouraged the researchers to consider the idea of complementary sets of sequences (CSS). A set $X = \{\mathbf{x}_1, \mathbf{x}_2, \cdots, \mathbf{x}_M\}$

containing M sequences of length N is called complementary iff the autocorrelations of $\{\mathbf{x}_m\}$ sum up to zero at any out-of-phase lag, i.e.

$$\sum_{m=1}^{M} r_m(k) = 0, \quad 1 \leq |k| \leq (N-1) \tag{3.3}$$

where $r_m(k)$ represents the k^{th} autocorrelation lag of $\mathbf{x}_m$. Consequently, to measure the complementarity of a sequence set $\{\mathbf{x}_m\}$ one can consider the integrated sidelobe level (ISL) or the peak sidelobe level (PSL) metrics defined by

$$\begin{aligned} \text{ISL} &= \sum_{k=1}^{N-1} \left| \sum_{m=1}^{M} r_m(k) \right|^2, \\ \text{PSL} &= \max_k \left\{ \left| \sum_{m=1}^{M} r_m(k) \right| \right\}, \end{aligned} \tag{3.4}$$

as well as the ISL-related merit factor (MF), i.e.

$$\text{MF} = E^2 / (2\,\text{ISL}). \tag{3.5}$$

where E denotes the sum of the energy of the sequences. Complementary sets containing $M = 2$ sequences, which are known as complementary pairs, form a special case of CSS. Complementary pairs with binary (i.e. ± 1) elements were first studied in [20] and are usually referred to as Golay pairs (GP).

CSS have been applied to radar pulse compression [43], multiple-input multiple-output (MIMO) radars [44], ultrasonic ranging [45], synthetic aperture imaging [16], and ultrasonography [46]. In addition to active sensing systems, CSS have applications in code-division multiple-access (CDMA) communication schemes [14], ultra wideband (UWB) communications [18], orthogonal frequency-division multiplexing (OFDM) [22] [47], channel estimation [17], and data hiding [48]. Due to such a wide range of applications, the construction of CSS has been an active area of research during the last decades. The majority of research results on CSS have been concerned with the analytical construction of GP or CSS for restricted sequence lengths N. For example, it is shown in [49] that GPs exist for lengths of the form $N = 2^{\alpha}10^{\beta}26^{\gamma}$ where α, β and γ are nonnegative integers. Some conditions on the existence of CSS can be found in [50] and [51]. Furthermore, [51] considers the extension of GP to general CSS. A theoretical as well as computational investigation of feasible GPs of lengths $N < 100$ is accomplished in [52].

In contrast to analytical constructions, a computational design of CSS does not impose any restriction on the sequence length N or the set cardinality M. Furthermore, a computational algorithm for designing CSS can provide plenty of CSS without the need for user-tuned parameters of analytical constructions.

Such algorithms can also be used to find almost (i.e. sub-optimal) complementary sets of sequences for (N,M) values for which no CSS exists. A computational algorithm (called ITROX) for designing CSS was introduced in [45]. In this chapter, we propose an extension of the **CAN** algorithm [6] for designing complement**ary** sets of sequences (which we call CANARY). The proposed algorithm works in the frequency domain, and is generally faster than ITROX. This is due to the fact that ITROX is based on certain eigenvalue decompositions with $\mathscr{O}(MN^2)$ complexity, whereas CANARY relies on fast Fourier transform (FFT) operations with $\mathscr{O}(MN\log(N))$ complexity (the difference in computational burdens between the two algorithms can be clearly observed in practice when N grows large).

The rest of this work is organized as follows. Section II presents the CANARY algorithm for CSS design. The extension of the CANARY algorithm to phase-quantized (and other constrained) CSS is studied in Section III. Section IV is devoted to numerical examples, whereas Section V concludes the chapter.

Notation: We use bold lowercase letters for vectors and bold uppercase letters for matrices. $(.)^T$, $(.)^*$ and $(.)^H$ denote the vector/matrix transpose, the complex conjugate, and the Hermitian transpose, respectively. $\mathbf{1}$ and $\mathbf{0}$ are the all-one and all-zero vectors/matrices. $\|\mathbf{x}\|_n$ or the l_n-norm of the vector $\mathbf{x}$ is defined as $(\sum_k |\mathbf{x}(k)|^n)^{\frac{1}{n}}$ where $\{\mathbf{x}(k)\}$ are the entries of $\mathbf{x}$. The Frobenius norm of a matrix $\boldsymbol{X}$ (denoted by $\|\boldsymbol{X}\|_F$) with entries $\{\boldsymbol{X}(k,l)\}$ is equal to $\left(\sum_{k,l} |\boldsymbol{X}(k,l)|^2\right)^{\frac{1}{2}}$, whereas the l_1-norm of $\boldsymbol{X}$ (denoted as $\|\boldsymbol{X}\|_1$) is given by $\sum_{k,l} |\boldsymbol{X}(k,l)|$. The matrix $e^{j\boldsymbol{X}}$ is defined element-wisely as $\left[e^{j\boldsymbol{X}}\right]_{k,l} = e^{j[\boldsymbol{X}]_{k,l}}$. $\arg(.)$ denotes the phase angle (in radians) of the vector/matrix argument. The symbol $\odot$ stands for the Hadamard (element-wise) product of matrices. $\mathbb{C}$ represents the set of complex numbers. Finally, δ_k is the Kronecker delta function which is equal to one when $k = 0$ and to zero otherwise.

3.2 CANARY Algorithm

It is well-known that for any sequence $\mathbf{x}$ of length N with aperiodic autocorrelation lags $\{r(k)\}$ (see, e.g. [54]),

$$\Phi(\omega) \triangleq \left| \sum_{n=1}^{N} x(n) e^{-j\omega n} \right|^2 = \sum_{k=-(N-1)}^{N-1} r(k) e^{-j\omega k} \tag{3.6}$$

where $\Phi(\omega)$ is the "spectrum" of $\mathbf{x}$. Consider a complementary set $X = \{\mathbf{x}_1, \mathbf{x}_2, \cdots, \mathbf{x}_M\}$ containing M sequences of length N. It follows from the Par-

seval equality that

$$\begin{aligned} 2\,\mathrm{ISL} &= \sum_{k=-(N-1)}^{N-1} \left| \sum_{m=1}^{M} r_m(k) - MN\delta_k \right|^2 \\ &= \frac{1}{2N} \sum_{p=1}^{2N} \left[\sum_{m=1}^{M} \Phi_m(\omega_p) - MN \right]^2 \end{aligned} \tag{3.7}$$

with $\Phi_m(\omega_p)$ representing the spectrum of the m^{th} sequence at the angular frequency $\omega_p = 2p\pi/(2N)$. Therefore, the minimization of the ISL metric in (3.4) can be accomplished by minimizing the following frequency-domain metric:

$$\sum_{p=1}^{2N} \left[\sum_{m=1}^{M} \left| \sum_{n=1}^{N} x_m(n) e^{-j\omega_p n} \right|^2 - MN \right]^2. \tag{3.8}$$

Inspired by the basic idea of the CAN algorithm in [6] that considers (3.8) with $M = 1$, we propose a cyclic algorithm (which we call CANARY) for designing CSS. Let $\boldsymbol{X} \triangleq (\mathbf{x}_1\ \mathbf{x}_2\ \cdots\ \mathbf{x}_M)$ and let $\boldsymbol{A}^H$ represent the $2N \times 2N$ DFT matrix given by

$$[\boldsymbol{A}^H]_{p,n} = \frac{1}{\sqrt{2N}} e^{-jn\omega_p}, \ \ (p,n) \in \{1,2,\cdots,2N\}^2. \tag{3.9}$$

The design problem associated with the frequency-domain metric in (3.8) can be dealt with conveniently via considering the following minimization problem:

$$\min_{\boldsymbol{Z},\boldsymbol{S}} \quad \|\boldsymbol{A}^H\boldsymbol{Z} - \boldsymbol{S}\|_F \tag{3.10}$$

$$\text{s.t.} \quad (\boldsymbol{S} \odot \boldsymbol{S}^*)\mathbf{1}_M = MN\mathbf{1}_{2N}, \tag{3.11}$$

$$\boldsymbol{Z} = \begin{pmatrix} \boldsymbol{X} \\ \mathbf{0}_{N\times M} \end{pmatrix} \tag{3.12}$$

where $\boldsymbol{S}$ is an auxiliary matrix variable.

For fixed $\boldsymbol{Z}$ (equivalently fixed $\boldsymbol{X}$), the minimizer $\boldsymbol{S}$ of (3.10) can be obtained as follows. Since the constraint (3.11) is imposed row-wise, we can consider the optimization of the entries in each row of $\boldsymbol{S}$ independently. Suppose that $\overline{\boldsymbol{s}}^T$ represents a generic row of $\boldsymbol{A}^H\boldsymbol{Z}$. Then the goal is to find a vector $\boldsymbol{s}$ that solves the optimization problem:

$$\begin{aligned} \min_{\boldsymbol{s}} \quad & \|\overline{\boldsymbol{s}} - \boldsymbol{s}\|_2^2 \\ \text{s.t.} \quad & \|\boldsymbol{s}\|_2^2 = MN. \end{aligned} \tag{3.13}$$

The solution to (3.13) is simply given by

$$\boldsymbol{s} = \sqrt{MN}\,\frac{\overline{\boldsymbol{s}}}{\|\overline{\boldsymbol{s}}\|_2}. \tag{3.14}$$

In sum, let $\overline{\boldsymbol{s}}_k^T$ $(k = 1, \cdots, 2N)$ denote the k^{th} row of $\overline{\boldsymbol{S}} = \boldsymbol{A}^H \boldsymbol{Z}$. Then the minimizer $\boldsymbol{S}$ of (3.10) can be obtained as

$$\boldsymbol{S} = \sqrt{MN} \begin{pmatrix} \overline{\boldsymbol{s}}_1^T / \|\overline{\boldsymbol{s}}_1\|_2 \\ \overline{\boldsymbol{s}}_2^T / \|\overline{\boldsymbol{s}}_2\|_2 \\ \vdots \\ \overline{\boldsymbol{s}}_{2N}^T / \|\overline{\boldsymbol{s}}_{2N}\|_2 \end{pmatrix} \tag{3.15}$$

Next we study the optimization of (3.10) with respect to $\boldsymbol{Z}$. For cases in which the sequences $\{\mathbf{x}_m\}$ are not constrained, the minimizer $\boldsymbol{Z}$ of (3.10) is given by

$$[\boldsymbol{Z}]_{n,m} = \begin{cases} [\boldsymbol{A}\,\boldsymbol{S}]_{n,m} & 1 \le n \le N, \\ 0 & n > N. \end{cases} \tag{3.16}$$

However, in many practical applications, the sequences are constrained (see the discussion on this aspect in the Introduction). Particularly, we will consider unimodularity constraints as well as more general peak-to-average-power ratio (PAR) constraints. For unimodular $\boldsymbol{X}$, the minimizer $\boldsymbol{Z}$ of (3.10) can be expressed as

$$[\boldsymbol{Z}]_{n,m} = \begin{cases} e^{j \arg[\boldsymbol{A}\,\boldsymbol{S}]_{n,m}} & 1 \le n \le N, \\ 0 & n > N. \end{cases} \tag{3.17}$$

On the other hand, the minimizer $\boldsymbol{Z}$ of (3.10) for PAR constraint set, viz.

$$\mathrm{PAR}(\mathbf{x}_m) = \frac{\|\mathbf{x}_m\|_\infty^2}{\frac{1}{N}\|\mathbf{x}_m\|_2^2} \le \gamma, \;\; 1 \le m \le M, \tag{3.18}$$

can be obtained by solving the optimization problem:

$$\begin{aligned} \min_{\boldsymbol{Z}} \quad & \|\boldsymbol{Z} - \boldsymbol{A}\boldsymbol{S}\|_F \\ \text{s.t.} \quad & \|\mathbf{x}_m\|_\infty^2 \le \gamma, \; 1 \le m \le M, \\ & \|\mathbf{x}_m\|_2^2 = N, \; 1 \le m \le M, \\ & \boldsymbol{Z} = \begin{pmatrix} \boldsymbol{X} \\ \mathbf{0}_{N \times M} \end{pmatrix}. \end{aligned} \tag{3.19}$$

Interestingly, the problem (3.19) can be tackled using an efficient recursive algorithm suggested in [26]. Briefly, first we note that (3.19) can be solved via a separate optimization with respect to the sequences $\{\mathbf{x}_m\}$ (i.e. the columns

of $\boldsymbol{X}$), and that for each sequence $\mathbf{x}_m$ (3.19) boils down to a "nearest-vector" problem with PAR constraint. Let $\overline{\mathbf{x}}_m$ denote the vector containing the first N entries of the m^{th} column of $\boldsymbol{AS}$. If the magnitudes of the entries of $\overline{\mathbf{x}}_m$ are below $\sqrt{\gamma}$ then $\mathbf{x}_m = \sqrt{N}\overline{\mathbf{x}}_m/\|\overline{\mathbf{x}}_m\|_2$ is the solution. Otherwise, the entry of $\mathbf{x}_m$ corresponding to the entry of $\overline{\mathbf{x}}_m$ (say x_{max}) with maximal magnitude is given by $\sqrt{\gamma}e^{j\arg(x_{max})}$; and the other entries of $\mathbf{x}_m$ are obtained solving the same type of "nearest-vector" problem but with the remaining energy i.e. $N-\gamma$.

Based on the previous analysis, the CANARY algorithm for designing CSS is summarized in Table 3.1. Note that each iteration of CANARY is computationally efficient as it is based solely on FFT operations. As a result, the CANARY algorithm can be used for large values of N and M (e.g. $MN \sim 10^6$ or even larger).

Table 3.1. *The CANARY Algorithm*

Step 0: Initialize $\boldsymbol{Z}$ using a random $\boldsymbol{X} \in \mathbb{C}^{N\times M}$.
Step 1: Compute the minimizer $\boldsymbol{S}$ of (3.10) using (3.15).
Step 2: Depending on the constraint imposed on the sequences $\{\mathbf{x}_m\}$, compute the minimizer $\boldsymbol{Z}$ (equivalently $\boldsymbol{X}$) of (3.10) using (3.16), (3.17) or (3.19).
Step 3: Repeat steps 1 and 2 until a stop criterion is satisfied, e.g. $\|\boldsymbol{X}^{(l+1)} - \boldsymbol{X}^{(l)}\|_F \leq \varepsilon$ for some pre-defined $\varepsilon > 0$ (where $\boldsymbol{X}^{(l)}$ denotes the matrix $\boldsymbol{X}$ obtained at the l^{th} iteration).

We conclude this section with two remarks.

Remark 1: To make the chapter as concise as possible, we only derived the CANARY algorithm for aperiodic autocorrelations. However the main ideas of CANARY can also be used to design CSS with good periodic correlations. In the latter case, CANARY can be useful when single sequences with perfect periodic correlation do not exist (such as in the certain design example in the next section). Let $\widetilde{\boldsymbol{A}}^H$ denote the $N \times N$ DFT matrix. It is straightforward to verify that the design of CSS with good periodic correlations can be formulated as the following optimization problem:

$$\begin{aligned} \min_{\boldsymbol{X},\boldsymbol{S}} \quad & \|\widetilde{\boldsymbol{A}}^H\boldsymbol{X} - \boldsymbol{S}\|_F \\ \text{s.t.} \quad & (\boldsymbol{S}\odot\boldsymbol{S}^*)\mathbf{1}_{\mathbf{M}} = \mathbf{MN}\,\mathbf{1}_{\mathbf{N}} \end{aligned} \tag{3.20}$$

which can be tackled in the same manner as proposed for (3.10). ■

Remark 2: An alternative approach to designing CSS is to use the Weighted CAN (WeCAN) algorithm in [6]. To see how this can be done, let $\boldsymbol{y} \triangleq (\mathbf{x}_1^T, \mathbf{0}_{N-1}^T, \mathbf{x}_2^T, \mathbf{0}_{N-1}^T, ..., \mathbf{x}_M^T, \mathbf{0}_{N-1}^T)$ be an auxiliary sequence of length $M(2N-1)$. Note that the first N aperiodic autocorrelation lags of $\boldsymbol{y}$ (denoted by $\{R(k)\}$)

can be written as

$$R(k) = \sum_{m=1}^{M} r_m(k), \;\; 0 \leq k \leq (N-1). \tag{3.21}$$

Therefore, the sequence set $\{\mathbf{x}_m\}$ is complementary if and only if $\boldsymbol{y}$ has a zero correlation zone (ZCZ) for lags in the interval $1 \leq k \leq (N-1)$. Such a ZCZ design (with the given sequence structure) can be carried out using the WeCAN algorithm. However, this approach is computationally expensive compared to the CANARY algorithm. ■

3.3 Phase-Quantized Design

A sequence $\mathbf{x}$ of length N is phase-quantized (with phase quantization level L) iff

$$\arg(x(n)) \in \left\{0, \frac{2\pi}{L}(1), \cdots, \frac{2\pi}{L}(L-1)\right\} \tag{3.22}$$

for all $1 \leq n \leq N$. In particular, $\mathbf{x}$ is a phase-quantized unimodular sequence (with phase quantization level L) iff for any $1 \leq n \leq N$,

$$x(n) \in \left\{1, e^{j\frac{2\pi}{L}(1)}, \cdots, e^{j\frac{2\pi}{L}(L-1)}\right\}. \tag{3.23}$$

The CANARY algorithm can be used to try to find (unimodular) phase-quantized CSS (or sub-optimal CSS whenever a perfect CSS does not exist) for arbitrary N and M; however a certain modification is needed. Let $Q_L(\varphi)$ denote the closest element in the set of quantized levels in (3.22) to a given φ. Also let $v_{n,m} = |v_{n,m}|e^{j\varphi_{n,m}} = [\boldsymbol{AS}]_{n,m}$. For unimodular phase-quantized CSS (with phase quantization level L), the minimizer $\boldsymbol{Z}$ of (3.10) is given by

$$[\boldsymbol{Z}]_{n,m} = \begin{cases} e^{jQ_L(\varphi_{n,m})} & 1 \leq n \leq N, \\ 0 & n > N, \end{cases} \tag{3.24}$$

and for just phase-quantized CSS by

$$[\boldsymbol{Z}]_{n,m} = \begin{cases} |v_{n,m}|\cos(\varphi_{n,m} - Q_L(\varphi_{n,m}))\, e^{jQ_L(\varphi_{n,m})} & 1 \leq n \leq N, \\ 0 & n > N. \end{cases} \tag{3.25}$$

However, for small values of L, unimodular (or low PAR) sequences with practically optimal correlation properties are rare. In addition, we note that the objective function in (3.10) is highly multi-modal in such cases (i.e. it may have multiple local optima). Therefore, although using (3.24) (or (3.25)) monotonically decreases the objective function in (3.10), the algorithm might end up in a poor local optimum. To tackle this issue (which was noted in many

other publications such as [9], [45] and [8]), we consider a penalized version of (3.10) in the following.

We relax the unimodularity constraint to a penalization of the distance between the magnitudes of $\{x_m(n)\}_{m,n}$ and 1. Therefore, consider the optimization problem (for $\lambda > 0$):

$$\begin{aligned} \min_{\boldsymbol{X},\boldsymbol{S}} \quad & \|\boldsymbol{A}^H\boldsymbol{Z} - \boldsymbol{S}\|_F^2 + \lambda \, \|(\boldsymbol{X} \odot \boldsymbol{X}^*) - \mathbf{1}_{N\times M}\|_1 \\ \text{s.t.} \quad & (\boldsymbol{S} \odot \boldsymbol{S}^*)\mathbf{1}_M = MN\,\mathbf{1}_{2N}, \\ & \boldsymbol{Z} = \begin{pmatrix} \boldsymbol{X} \\ \mathbf{0}_{N\times M} \end{pmatrix}, \\ & \text{all } \{\mathbf{x}_m\} \text{ are phase-quantized as in (3.22).} \end{aligned} \tag{3.26}$$

The solution $\boldsymbol{S}$ of (3.26) is identical to that of (3.10). Let v be a generic element in the $N \times M$ upper sub-matrix of $\boldsymbol{AS}$. To obtain the solution $\boldsymbol{X}$ (and $\boldsymbol{Z}$) of (3.26), we note that solving (3.26) for $\boldsymbol{X}$ can be dealt with in an element-wise manner, and hence it can be reduced to the optimization problem:

$$\begin{aligned} \min_{x} \quad & |x-v|^2 + \lambda \, \big||x|^2 - 1\big| \\ \text{s.t.} \quad & x \text{ is phase-quantized as in (3.22),} \end{aligned} \tag{3.27}$$

where x denotes a generic entry of $\boldsymbol{X}$. Now let $x = |x|e^{j\varphi_x}$, $v = |v|e^{j\varphi_v}$, and note that the minimizer φ_x of (3.27) is simply given by $\varphi_x = Q_L(\varphi_v)$. Given φ_x, we can rewrite the criterion in (3.27) as

$$\begin{aligned} & |x-v|^2 + \lambda \, \big||x|^2 - 1\big| \\ = \; & \Big||x| - |v|e^{j(\varphi_v-\varphi_x)}\Big|^2 + \lambda \, \big||x|^2 - 1\big| \\ = \; & \text{Const}_1 \; + \underbrace{(|x| - |v|\cos(\varphi_v - \varphi_x))^2 + \lambda \, \big||x|^2 - 1\big|}_{f(|x|)}. \end{aligned} \tag{3.28}$$

Note that $f(|x|)$ is both continuous and lower bounded (by zero), and thus has at least one global minimum. A global minimum $|x|$ of $f(|x|)$ satisfying $|x| > 1$ should minimize

$$f(|x|) = (1+\lambda)|x|^2 - 2|x||v|\cos(\varphi_v - \varphi_x) + \text{Const}_2 \tag{3.29}$$

which implies that $|x| = |v|\cos(\varphi_v - \varphi_x)/(1+\lambda)$. Otherwise, a minimizer $|x|$ of $f(|x|)$ satisfying $|x| < 1$ should minimize

$$f(|x|) = (1-\lambda)|x|^2 - 2|x||v|\cos(\varphi_v - \varphi_x) + \text{Const}_3 \tag{3.30}$$

which implies $|x| = |v|\cos(\varphi_v - \varphi_x)/(1-\lambda)$. In sum, the minimization of (3.27) with respect to $|x|$ yields the following *soft-thresholding* type of solution

(see [55] for a similar result):

$$|x| = \begin{cases} \frac{|v|\cos(\varphi_v-\varphi_x)}{1-\lambda} & |v| < \frac{1-\lambda}{\cos(\varphi_v-\varphi_x)}, \\ 1 & \frac{1-\lambda}{\cos(\varphi_v-\varphi_x)} \le |v| \le \frac{1+\lambda}{\cos(\varphi_v-\varphi_x)}, \\ \frac{|v|\cos(\varphi_v-\varphi_x)}{1+\lambda} & |v| > \frac{1+\lambda}{\cos(\varphi_v-\varphi_x)}. \end{cases} \tag{3.31}$$

3.4 Numerical Examples

In this section, we provide numerical examples to illustrate the performance of the CANARY algorithm. The required computational times (on a PC with Intel Core i5 2.8GHz CPU, and 8.0GB memory) are reported. We use CANARY to design unimodular as well as low PAR CSS of length $N = 256$ with $M = 1$ (in which case the CSS design becomes a single sequence design), $M = 2$ (i.e. a complementary pair), and $M = 3$. We stopped the algorithm when the stop criterion was satisfied with $\varepsilon = 10^{-15}$. The computational times for designing unimodular CSS with $M = 1$, 2, and 3 were approximately 3, 175, and 254 sec, respectively. The results are shown in Fig. 3.1(a). The autocorrelation sums are normalized and expressed in dB,

$$\text{autocorrelation level (dB)} = 20\log_{10}\frac{\left|\sum_{m=1}^{M} r_m(k)\right|}{\sum_{m=1}^{M} r_m(0)}. \tag{3.32}$$

To examine CANARY when dealing with more general PAR constraints, Fig. 3.1(b) depicts the results of a similar design problem but now the constraint PAR ≤ 2 . The needed computational times were 6, 143, and 78 sec for $M = 1$, 2, and 3, respectively. As expected, the CSS designed for $M \in \{1,2\}$ and PAR ≤ 2 have better MF values compared to their corresponding CSS with PAR $= 1$ (i.e. unimodular CSS). Note that increasing M provides more degrees of freedom for CSS design. In particular, it can be observed from the figure that for $M = 3$ the autocorrelation sums of the sequences achieve values which are virtually zero (i.e. MF approaches $+\infty$).

As indicated earlier, CANARY can be used to obtain almost (i.e. sub-optimal) CSS for cases in which no CSS exists. It is known that there is no binary GP of length $N = 82$ [51]. With this in mind, we employ the CANARY algorithm to design a sub-optimal GP for $N = 82$. Using the relaxed formulation of CANARY in (3.26) five hundred times (with $\lambda = 0.5$), we have designed real-valued complementary pairs with low PAR. Next we clipped the resultant sequences to obtain sub-optimal GP and chose the best sequence pair with respect to the ISL metric. The two sequences obtained in this way are shown in Fig. 3.2(a). The average autocorrelation of the obtained binary sequences, viz.

$$\frac{1}{2}\left|\sum_{m=1}^{2} r_m(k)\right|, \quad -81 \le k \le 81 \tag{3.33}$$

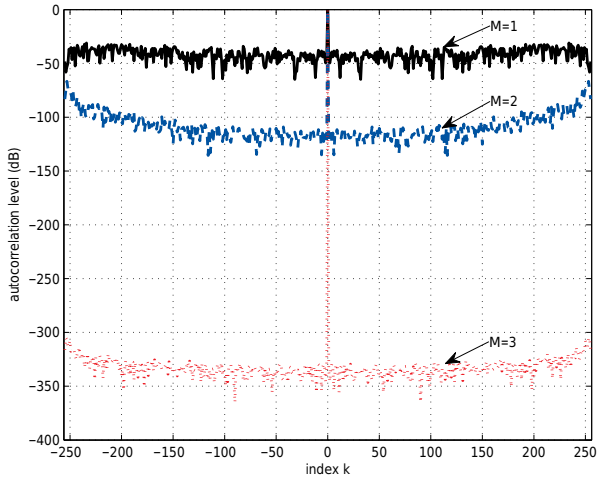

(a)

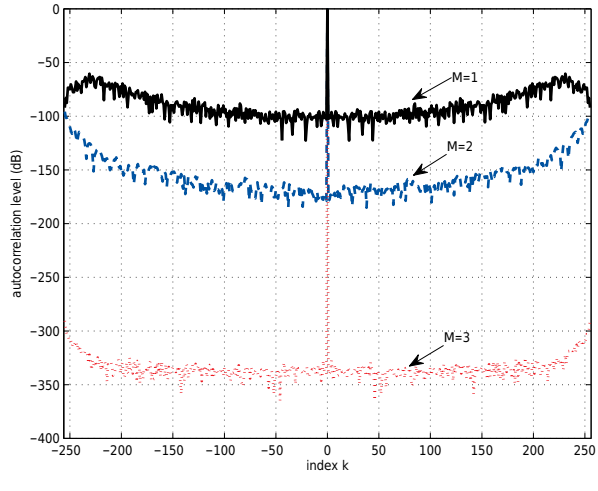

(b)

Figure 3.1. Unimodular and low PAR CSS design for $N = 256$ and $M \in \{1,2,3\}$ with the constraints: (a) PAR $= 1$ (i.e. unimodular entries), and (b) PAR ≤ 2. The autocorrelation sums achieve practically zero values as M increases to 3. The MF values corresponding to $M = 1,2,3$ in (a) and (b) are given by $(15.9, 1.0 \times 10^6, 4.0 \times 10^{29})$ and $(6.0 \times 10^4, 9.6 \times 10^8, 4.1 \times 10^{28})$, respectively.

is presented in Fig. 3.2(b). The obtained sub-optimal GP achieves a MF value of 19.88. A computational time of 41 sec was required on the PC to accomplish the task. As another example, we use the same approach to design a QAM (i.e. with $L = 4$) almost complementary pair of length $N = 82$. The results are shown in Fig. 3.2 (c)-(d). For the convenience of the reader, the resultant sequences of both binary and QAM examples are provided in Table 3.2. The obtained QAM CSS has a MF equal to 21.08. As expected the MF corresponding to the obtained QAM CSS is larger than that of the binary example; however, the binary CSS has a smaller PSL. This can be explained by the fact that CANARY is an ISL minimizer (or equivalently a MF maximizer) and not a PSL minimizer. The PAR values of the resultant sequences (before clipping) in the binary and QAM cases are (1.05,1.04) and (1.18,1.15), respectively. As the inner-product (or the distance) of the sequences in the CSS is of interest in some applications, we also report the inner-product values achieved for the above examples. The inner-product metric can be defined as $|\mathbf{x}_1^H \mathbf{x}_2|/N$, where $\mathbf{x}_1$ and $\mathbf{x}_2$ are the sequences in the obtained complementary pairs (both with energy N). The inner-product metric values corresponding to the binary and QAM examples above are 0.024 and 0.039, respectively.

Alphabet	Sequence pair
Binary	-1,1,-1,-1,1,-1,-1,-1,-1,1,-1,-1,1,-1,1,1,-1,-1,-1,-1,-1,-1,1,1,1,1,-1,1,-1,1,-1, -1,1,-1,1,1,-1,1,1,1,-1,-1,-1,-1,-1,1,-1,-1,1,-1,1,1,1,1,1,-1,1,1,-1,-1,-1,1,-1,-1,-1,1,1,-1,-1,1,-1,1,1,1,1,1,1,-1,-1,1,1,1,-1,1,-1,1,-1,1,-1,1,-1
	1,-1,-1,1,1,-1,-1,-1,1,-1,-1,1,1,-1,1,-1,-1,-1,-1,1,1,-1,-1,-1,-1,1,1,-1,-1,1,1,1,-1,-1,1,-1,1,1,-1,1,1,1,1,1,1,1,1,-1,1,1,1,1,-1,-1,-1,-1,-1,-1,1,1,1,-1,-1,-1,1,-1,1,1,-1,1,1,-1,1,1,-1,1,-1,-1,1,1,-1,1,-1,1,-1,-1,-1,1,-1,1,-1,1,-1,-1,-1,1
QAM	j,-1,j,-1,-j,1,-j,1,1,-1,-j,-1,j,1,j,j,j,1,j,-1,j,1,j,-1,j,1,-j,-1,-j,-1,j,1,j,-1,j,1,j,-1,-j,1,j,1,j,1,j,1,j,-1,j,-1,-j,1,-j,-1,j,-1,-j,-1,j,1,-j,-1,j,-1,-j,-1,j,1,-j,1,j,-1,j,1,j,1,-j,1,j,1,-j,1,j,1
	j,1,j,1,j,1,j,-1,j,-1,j,-1,-j,-1,j,1,j,-1,j,1,j,-1,-j,1,-j,1,j,-j,-j,-1,j,1,j,1,-j,-1,-j,1,j,-1,-j,1,j,-1,j,1,j,1,-j,-1,-j,1,j,-1,j,1,j,1,-j,-1,-j,1,j,-1,j,1,j,1,-j,-1,-j,1,j,-1,-j,-1,-j,1,-j,-1,j,1,j,1,j,-1,-j,-1,j,-1,j,1,-j,1,j,-j,-1,j,1,-j,1,-j,1,j,1,-j,-1,-j,1,j,-1,j,1

Table 3.2. *The obtained binary and QAM almost complementary pairs.*

Finally we provide an example to show that CANARY can find known GPs in the search space. Specifically, we consider finding a binary GP of length $N = 520$. We perturb the entries of the binary GP by zero-mean i.i.d. Gaussian random variables with a standard deviation σ that take values in the set $\{0.15, 0.25, 0.5, 0.75, 0.85\}$, and then we use the so-obtained perturbed non-binary sequences to initialize CANARY; furthermore we will do this for 1000 times to compute the average statistics. Similar to the previous example, we set $\lambda = 0.5$. For each σ, the number of the cases in which CANARY finds the original GP to the total number of tests (i.e. 1000) can be interpreted as the empirical probability p of finding the known GP. The results are reported in

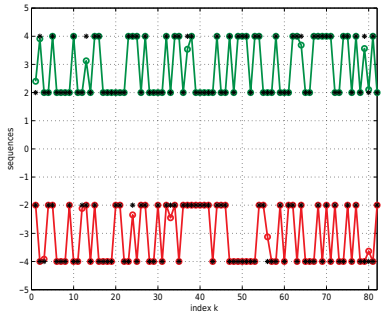

(a)

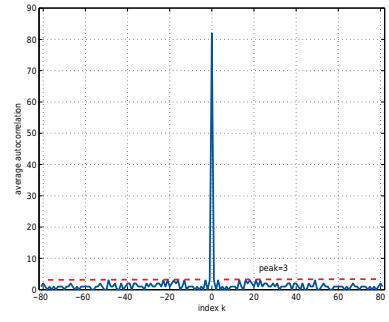

(b)

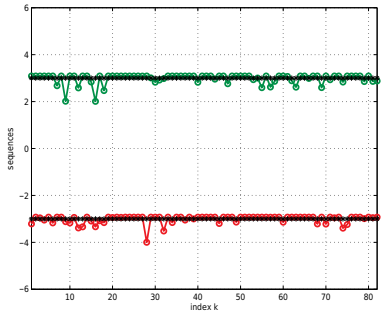

(c)

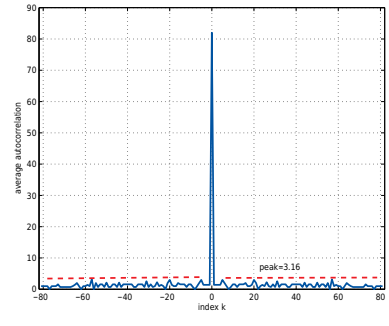

(d)

Figure 3.2. Design of a sub-optimal GP and an almost CSS (of length 82) using CANARY. (a) depicts the entries of the binary sequences (shown by $*$) and the resultant sequences of (3.26). (c) plots the absolute values of the obtained QAM sequences (shown by $*$) as well as the resultant sequences of (3.26). In both (a) and (c), a bias of $+3$ and -3 is used to distinguish the sequences. The average autocorrelations of the obtained binary/QAM sequences are shown in (b)/(d).

Table 3.3, and the empirical p decreases apparently gracefully and slowly as σ increases.

σ	0.15	0.25	0.5	0.75	0.85
p	1	1	1	0.95	0.70

Table 3.3. *The empirical probability p of finding the known GP for various perturbation levels* σ.

3.5 Concluding Remarks

The problem of CSS design has been formulated and a fast algorithm (called CANARY) for generating CSS has been proposed. The main results can be summarized as follows:

- The design of CSS was formulated as a cyclic minimization of (3.10). Several variations of this minimization problem were proposed for different sequence design constraints (depending on the application). The discussed cases were: (i) a given PAR, (ii) unimodularity of the entries of the sequences, (iii) phase-quantized sequences, and (iv) sequences with unimodular entries and quantized phase values.
- The steps of CANARY are computationally efficient, which enables usage for large (N,M). Moreover, as the sequence design problems are usually solved off-line, the computational efficiency of CANARY can be leveraged to perform an efficient search of CSS when only a single set is not enough.
- The formulation in this chapter can be exploited to deal with the CSS design for good periodic correlation properties as well. Detailed derivations were not presented for the sake of brevity.
- Numerical examples were provided to examine the performance of CANARY when dealing with different CSS design problems.

We conclude this chapter by returning to the fact that CANARY is a scheme that attempts to minimize the ISL. We note that one can generally make the PSL metric “small" by minimizing the ISL. However, a direct minimization of the PSL metric appears to be more complicated and remains a topic for future work.

4. On Meeting the Peak Correlation Bounds

Abstract
We study the problem of meeting peak periodic or aperiodic correlation bounds for complex-valued sets of sequences. To this end, the Welch, Levenstein, and Exponential bounds on the peak inner-product of sequence sets are considered and used to provide compound peak correlation bounds in both periodic and aperiodic cases. The peak aperiodic correlation bound is further improved by using the intrinsic dimension deficiencies associated with its formulation. In comparison to the compound bound, the new aperiodic bound contributes an improvement of more than 35% for some specific values of the sequence length n and set cardinality m. We study the tightness of the provided bounds by using both analytical and computational tools. In particular, novel algorithms based on alternating projections are devised to approach a given peak periodic or aperiodic correlation bound. Several numerical examples are presented to assess the tightness of the provided correlation bounds as well as to illustrate the effectiveness of the proposed methods for meeting these bounds.

Keywords: Autocorrelation, correlation bound, cross-correlation, peak sidelobe level (PSL), sequence set, Welch bound.

4.1 Introduction

Sequence sets with impulse-like autocorrelation and small cross-correlation are required in many communication and active sensing applications. For example, such sets are used in asynchronous CDMA to separate different users while performing a synchronization operation at the same time [56]. As an active sensing example, such correlation properties of the probing sequences enable the multi-input multi-output (MIMO) radars to conveniently retrieve (via matched filters) the received signals from the range bin of interest while suppressing the probing signals backscattered from other range bins [7].

Let X be a set of m sequences of length n. We assume that the sequences in X have identical energy[1], i.e. $\|\mathbf{x}\|_2^2 = \sigma$ for all $\mathbf{x} \in X$. Let $\mathbf{x}_u$ and $\mathbf{x}_v$ denote two sequences from the set X. The periodic $\{c_{u,v}(k)\}$ and aperiodic $\{r_{u,v}(k)\}$ cross-correlations of $\mathbf{x}_u$ and $\mathbf{x}_v$ are defined as

$$c_{u,v}(k) = \sum_{l=1}^{n} \mathbf{x}_u(l)\mathbf{x}_v^*(l+k)_{mod\ n}, \tag{4.1}$$

$$r_{u,v}(k) = \sum_{l=1}^{n-k} \mathbf{x}_u(l)\mathbf{x}_v^*(l+k) = r_{v,u}^*(-k), \tag{4.2}$$

for $0 \leq k \leq (n-1)$. The periodic and aperiodic autocorrelations of any $\mathbf{x}_u \in X$ are obtained from the above definitions by using $\mathbf{x}_v = \mathbf{x}_u$. Moreover, the inner product of $\mathbf{x}_u$ and $\mathbf{x}_v$ is given by $\mathbf{x}_v^H \mathbf{x}_u = c_{u,v}(0) = r_{u,v}(0)$.

The Welch bounds [57] are the most well-known theoretical limits on the collective smallness measures of both inner-products and correlations of se-

[1]For the sake of generality, an energy of σ is considered for sequences throughout the chapter. We note that the typical values of σ suggested in the literature are $\sigma = 1$ for inner-product bounds, and $\sigma = n$ for correlation bounds. However, one can easily verify that by using different values of σ leads to nothing but a scaling of the inner-product or correlation bounds.

quence sets. Several such measures along with the associated Welch lower bounds are summarized in Table 4.1. Briefly stated, the main objectives of this chapter are:

- To update the peak correlation bounds based on the current sate-of-knowledge on peak inner-product bound, as well as to propose a scheme for improvement of the aperiodic correlation bound. The proposed scheme exploits the intrinsic low dimensional properties that appear in derivation of the peak aperiodic bound. The new aperiodic peak sidelobe level (PSL) bound can be significantly larger than the previously known aperiodic bound (by more than 35% for some $(m,n) \in [2,1024] \times [2,256]$).
- To determine how close we can get to the previously known or improved PSL correlation bounds. In order to achieve this goal, a computational method is devised to approach any given (feasible) PSL level for both periodic and aperiodic correlations. To the best of our knowledge, the provided computational method is the first (non-heuristic) algorithm to tackle the problem of achieving a given low PSL.

The rest of this chapter is organized as follows. In Section 4.2, the relationship between the inner-product and correlation bounds is studied and employed to provide a derivation of peak correlation bounds. The tightness of the provided bounds along with an improvement of the aperiodic correlation bound are discussed in Section 4.3. In Section 4.4, a general framework is devised to approach a given (periodic or aperiodic) peak correlation bound. Section 4.5 is devoted to the numerical examples. Finally, Section 4.6 concludes the chapter.

Notations: We use bold lowercase letters for vectors/sequences and bold uppercase letters for matrices. $(\cdot)^T$, $(\cdot)^*$ and $(\cdot)^H$ denote the vector/matrix transpose, the complex conjugate, and the Hermitian transpose, respectively. $\mathbf{1}$ and $\mathbf{0}$ are the all-one and all-zero vectors/matrices. $\|\mathbf{x}\|_n$ is the l_n-norm of the vector $\mathbf{x}$ defined as $(\sum_k |\mathbf{x}(k)|^n)^{\frac{1}{n}}$ where $\{\mathbf{x}(k)\}$ are the entries of $\mathbf{x}$. The Frobenius norm of a matrix $\boldsymbol{X}$ (denoted by $\|\boldsymbol{X}\|_F$) with entries $\{\boldsymbol{X}(k,l)\}$ is equal to $\left(\sum_{k,l} |\boldsymbol{X}(k,l)|^2\right)^{\frac{1}{2}}$. $\mathrm{tr}\{\boldsymbol{X}\}$ denotes the trace of the matrix $\boldsymbol{X}$. $\eta_k(\boldsymbol{X})$ and $\boldsymbol{v}_k(\boldsymbol{X})$ represent the k^{th} dominant eigenvalue and the corresponding eigenvector of the Hermitian matrix $\boldsymbol{X}$, respectively. The symbol $\odot$ stands for the Hadamard (element-wise) product of matrices, whereas $\otimes$ stands for the Kronecker product of matrices. $\mathbf{x}^{\otimes n}$ is equal to $\underbrace{\mathbf{x} \otimes \mathbf{x} \otimes \cdots \otimes \mathbf{x}}_{n}$. $[n]$ denotes the set $\{1,2,\cdots,n\}$. For any $n_1, n_2 \in \mathbb{N}$, $[n_1,n_2]$ is equal to $[n_2] \backslash [n_1-1]$. $\binom{n}{k}$, often read as "n choose k", is the coefficient of the x^k-term in the polynomial expansion of the binomial power $(1+x)^n$. Finally, $\mathbb{N}$, $\mathbb{Z}$, $\mathbb{R}$ and $\mathbb{C}$ represent the set of natural, integer, real and complex numbers, respectively.

Table 4.1. *Summary of inner-product and correlation smallness measures along with the associated Welch lower bounds.*

	Metric		Metric definitions and Welch lower bounds ($\mathscr{W}$)
Inner-product	Root-mean-square (RMS) inner-product level: $I_{rms}(X)$		$I_{rms}(X) = \left(\frac{1}{m(m-1)} \sum_{u \neq v} \lvert \mathbf{x}_v^H \mathbf{x}_u \rvert^2\right)^{\frac{1}{2}} \geq$ $\overline{\mathscr{W}}_{m,n} \triangleq \sigma \sqrt{\frac{m-n}{(m-1)n}}$
	Peak inner-product level: $I_{max}(X)$		$I_{max}(X) \triangleq \max \left\{\lvert \mathbf{x}_v^H \mathbf{x}_u \rvert\right\}_{u \neq v} \geq$ $\mathscr{W}_{m,n} \triangleq \max_{s:\, \binom{n+s-1}{s} \leq m} \sigma \left(\frac{1}{m-1} \left[\frac{m}{\binom{n+s-1}{s}} - 1\right]\right)^{\frac{1}{2s}}$
Correlation	Integrated sidelobe level	Periodic case: $\mathrm{ISL}^{\mathscr{P}}(X)$	$\mathrm{ISL}^{\mathscr{P}}(X) = \sum_{u \neq v;k} \lvert c_{u,v}(k) \rvert^2 + \sum_{u;k \neq 0} \lvert c_{u,u}(k) \rvert^2 \geq$ $\overline{\mathscr{W}}^{\mathscr{P}}_{m,n} \triangleq \sigma^2 m(m-1)$
		Aperiodic case: $\mathrm{ISL}^{\mathscr{A}\mathscr{P}}(X)$	$\mathrm{ISL}^{\mathscr{A}\mathscr{P}}(X) = \sum_{u \neq v;k} \lvert r_{u,v}(k) \rvert^2 + \sum_{u;k \neq 0} \lvert r_{u,u}(k) \rvert^2 \geq$ $\overline{\mathscr{W}}^{\mathscr{A}\mathscr{P}}_{m,n} \triangleq \sigma^2 m(m-1)$
	Peak sidelobe level	Periodic case: $\mathrm{PSL}^{\mathscr{P}}(X)$	$\mathrm{PSL}^{\mathscr{P}}(X) = \max\left(\left\{\lvert c_{u,v}(k) \rvert\right\}_{u \neq v;k} \cup \left\{\lvert c_{u,u}(k) \rvert\right\}_{u;k \neq 0}\right) \geq$ $\mathscr{W}^{\mathscr{P}}_{m,n} \triangleq \max_{s:\, \binom{n+s-1}{s} \leq mn} \sigma \left(\frac{1}{mn-1} \left[\frac{mn}{\binom{n+s-1}{s}} - 1\right]\right)^{\frac{1}{2s}}$
		Aperiodic case: $\mathrm{PSL}^{\mathscr{A}\mathscr{P}}(X)$	$\mathrm{PSL}^{\mathscr{A}\mathscr{P}}(X) = \max\left(\left\{\lvert r_{u,v}(k) \rvert\right\}_{u \neq v;k} \cup \left\{\lvert r_{u,u}(k) \rvert\right\}_{u;k \neq 0}\right) \geq$ $\mathscr{W}^{\mathscr{A}\mathscr{P}}_{m,n} \triangleq \max_{s:\, \binom{2n+s-2}{s} \leq m(2n-1)} \sigma \left(\frac{1}{m(2n-1)-1} \left[\frac{m(2n-1)}{\binom{2n+s-2}{s}} - 1\right]\right)^{\frac{1}{2s}}$

4.2 A Study of the Inner-Product and Correlation Bounds

In the following, a study of the currently known inner-product and correlation bounds is accomplished. The provided background lays the ground for tightness assessments as well as the bound improvements suggested in the chapter.

4.2.1 Inner-Product Bounds

The collective smallness of the inner products of $\{\mathbf{x}_u\}$ can be measured by using the *peak inner-product level* metric:

$$I_{max}(X) = \max\left\{|\mathbf{x}_v^H \mathbf{x}_u|\right\}_{u\neq v} \tag{4.3}$$

as well as the *root-mean-square (RMS) inner-product level* metric,

$$I_{rms}(X) = \left(\frac{1}{m(m-1)}\sum_{u\neq v}|\mathbf{x}_v^H \mathbf{x}_u|^2\right)^{\frac{1}{2}} \tag{4.4}$$

where clearly $I_{max}(X) \geq I_{rms}(X)$. In [57], Welch derived lower bounds on the above collective smallness measures of the inner-product levels associated with X; the *Welch lower bounds* on $I_{max}(X)$ and $I_{rms}(X)$ are given (assuming $m > n$) by

$$I_{rms}(X) \geq \sigma\sqrt{\frac{m-n}{(m-1)n}} \triangleq \overline{\mathscr{W}}_{m,n} \tag{4.5}$$

and

$$I_{max}(X) \geq \max_{s:\ \binom{n+s-1}{s}\leq m} \sigma\left(\frac{1}{m-1}\left[\frac{m}{\binom{n+s-1}{s}}-1\right]\right)^{\frac{1}{2s}} \triangleq \mathscr{W}_{m,n}. \tag{4.6}$$

Note that both $\overline{\mathscr{W}}_{m,n}$ and $\mathscr{W}_{m,n}$ are zero for $m \leq n$.

Knowledge of inner-product bounds is essential to the derivation of both periodic and aperiodic correlation bounds. Let $\mathbf{x}_v^H \mathbf{x}_u = \sigma\cos(\phi_{u,v})$ where $\phi_{u,v}$ denotes the angle between the two vectors $\mathbf{x}_u$ and $\mathbf{x}_v$. From a geometrical point of view, the Welch peak inner-product bound provides a lower bound on the maximum of the angles $\{\phi_{u,v}\}$ among the set of m equi-norm vectors $\{\mathbf{x}_u\}$ in $\mathbb{C}^n$. A direct algebraic derivation of the inner-product bound (which appears to be simpler than that in [57]) is as follows. Let $\boldsymbol{X} \in \mathbb{C}^{n\times m}$ (with $m > n$)

represent the matrix whose columns are $\{\mathbf{x}_u\}$. Then we have that

$$\begin{aligned}\sum_{u,v}|\mathbf{x}_v^H\mathbf{x}_u|^2 &= ||\boldsymbol{X}^H\boldsymbol{X}||_F^2 = \sum_{k=1}^{n}\lambda_k^2 \\ &\geq \frac{1}{n}\left(\sum_{k=1}^{n}\lambda_k\right)^2 = \frac{1}{n}\left(\mathrm{tr}(\boldsymbol{X}^H\boldsymbol{X})\right)^2 \\ &= \frac{m^2\sigma^2}{n}\end{aligned} \tag{4.7}$$

where $\{\lambda_k\}$ are the non-zero eigenvalues of $\boldsymbol{X}^H\boldsymbol{X}$. As a result,

$$\begin{aligned}I_1(X) &\triangleq \sum_{u\neq v}|\mathbf{x}_v^H\mathbf{x}_u|^2 \\ &= \left(\sum_{u,v}|\mathbf{x}_v^H\mathbf{x}_u|^2\right) - m\sigma^2 \geq m\sigma^2\left(\frac{m}{n}-1\right)\end{aligned} \tag{4.8}$$

which implies

$$I_{\max}(X) \geq \left(\frac{I_1(X)}{m(m-1)}\right)^{\frac{1}{2}} \geq \sigma\left(\frac{1}{m-1}\left(\frac{m}{n}-1\right)\right)^{\frac{1}{2}}. \tag{4.9}$$

As an aside remark, it is straightforward to verify that for $m \leq n$, (4.7)-(4.9) yield a trivial lower bound i.e. zero.

Next observe that for any $s \in \mathbb{N}$, one can verify that $(\mathbf{x}_v^H\mathbf{x}_u)^s = (\mathbf{x}_v^{\otimes s})^H\mathbf{x}_u^{\otimes s}$. However, even though $\{\mathbf{x}_u^{\otimes s}\}$ are of length n^s, they lie in a lower dimensional subspace of $\mathbb{C}^{n^s}$. To see this, we count the number of distinct entries in any general vector $\mathbf{x}^{\otimes s}$. Note that any entry of $\mathbf{x}^{\otimes s}$ is of the form

$$(\mathbf{x}(1))^{\nu_1}(\mathbf{x}(2))^{\nu_2}\cdots(\mathbf{x}(n))^{\nu_n} \tag{4.10}$$

where $\nu_1+\nu_2+\cdots+\nu_n = s$, and $\nu_l \in \mathbb{N}\cup\{0\}$. The number of possible combinations of $(\nu_1,\nu_2,\cdots,\nu_n)$ which satisfy this same condition is given by $d = \binom{n+s-1}{s}$. Let $\boldsymbol{X}_s$ denote a matrix whose columns are $\{\mathbf{x}_u^{\otimes s}\}$. Based on the above argument, there exist a semi-unitary matrix $\boldsymbol{U} \in \mathbb{C}^{n^s\times d}$ and a rank$-d$ matrix $\boldsymbol{Y}_s \in \mathbb{C}^{d\times m}$ such that $\boldsymbol{X}_s = \boldsymbol{U}\boldsymbol{Y}_s$. By using the same approach as in (4.7) we have that

$$\sum_{u,v}|\mathbf{x}_v^H\mathbf{x}_u|^{2s} = ||\boldsymbol{X}_s^H\boldsymbol{X}_s||_F^2 = ||\boldsymbol{Y}_s^H\boldsymbol{Y}_s||_F^2 \geq \frac{m^2\sigma^{2s}}{d}. \tag{4.11}$$

It follows from (4.11) that

$$I_s(X) \triangleq \sum_{u\neq v}|\mathbf{x}_v^H\mathbf{x}_u|^{2s} \geq m\sigma^{2s}\left(\frac{m}{d}-1\right) \tag{4.12}$$

which yields

$$I_{\max}(X) \geq \sigma \left(\frac{1}{m-1} \left(\frac{m}{\binom{n+s-1}{s}} - 1 \right) \right)^{\frac{1}{2s}}. \tag{4.13}$$

The above dimension reduction scheme, which lies at the core of the higher order (i.e. with $s > 1$) Welch bounds, emphasizes the usefulness of considering hidden dimension deficiencies of the vector sets. Such dimension deficiencies play a main role in improving the peak aperiodic correlation bound in Section 4.3.2.

Due to applications in compressive sensing and synchronous CDMA, meeting the Welch bounds on the inner-products associated with sequence sets (also referred to as measurement matrices [58], codebooks [59]- [61], or Grassmannian frames [62] depending on the application) has been studied widely. It is known that the Welch bound on $I_{rms}(X)$ can be met for many (m,n) (see, e.g. [56] and the references therein). An X meeting the Welch bound on I_{rms} is called Welch-bound-equality (WBE) set [56]. On the other hand, sequence sets meeting the Welch bound on the peak inner-product level (known as maximum-Welch-bound-equality (MWBE) sets, see [56]) are hard to obtain either analytically or numerically. Examples of and some conditions for the existence of MWBE sets for given (m,n) were presented in [62]- [63]. Particularly, if MWBE sets do not exist[2] for $s = 1$ in (4.6), then they do not exist for any $s > 1$ [64]. Note that $\mathscr{W}_{m,n}$ in (4.6) associated with $s = 1$ is equal to $\overline{\mathscr{W}}_{m,n}$. These facts not only emphasize the importance of the Welch peak inner-product level bound for $s = 1$ but also imply that if the peak inner-product level of a sequence set meets the Welch bound (i.e. the Welch bound is tight) then all the inner products among the sequences in the set have the same absolute value which is equal to $\overline{\mathscr{W}}_{m,n}$. Furthermore, let the maximum of the functions in (4.6) occur for $s = s_0$. Then a necessary condition for the existence of MWBE sets for given (m,n) is [64]

$$\binom{n+s_0-1}{s_0} \leq n^2. \tag{4.14}$$

It is also known that the Welch inner-product bound can be tight only if $m \leq n^2$ [63].

Two other bounds on $I_{max}(X)$ were derived in the literature which are tighter than $\mathscr{W}_{m,n}$ for some (m,n). The latter bounds, which are not discussed in the literature as much as the Welch bound, are the *Levenstein bound* [66] [67],

$$\mathscr{L}_{m,n} \triangleq \sigma \sqrt{\frac{2m-n^2-n}{(n+1)(m-n)}} \tag{4.15}$$

[2]Note that MWBE sets exist for $s = 1$ iff (4.6) is maximized with $s = 1$ and there exist a sequence set with peak inner-product $I_{\max}(X)$ equal to the obtained value of $\mathscr{W}_{m,n}$.

for $m > n(n+1)/2$, and the *Exponential bound* [59],

$$\mathscr{E}_{m,n} \triangleq \sigma(1-2m^{\frac{-1}{n-1}}) \tag{4.16}$$

for $m > 2^{n-1}$. The above bounds can be combined with the Welch bound to yield

$$\mathscr{I}_{m,n} \triangleq \max\{\mathscr{W}_{m,n}, \mathscr{L}_{m,n}, \mathscr{E}_{m,n}\} \tag{4.17}$$

that encapsulates the current state-of-knowledge on the lower bounds for the peak inner-product level. Note that some bounds in (4.17) might not be useful (i.e. > 0) for a specific (m,n).

4.2.2 Correlation Bounds

Excluding the *in-phase* (i.e. for $k = 0$) lags of the autocorrelations of $\{\mathbf{x}_u\}$ (which equal the energy of sequences), one can measure the level of the *out-of-phase* correlations of sequences in X by using the *integrated sidelobe level* (ISL) metric:

$$\mathrm{ISL}^{\mathscr{P}}(X) = \sum_{u\neq v;\,k} |c_{u,v}(k)|^2 + \sum_{u;\,k\neq 0} |c_{u,u}(k)|^2 \tag{4.18}$$

$$\mathrm{ISL}^{\mathscr{A}\mathscr{P}}(X) = \sum_{u\neq v;\,k} |r_{u,v}(k)|^2 + \sum_{u;\,k\neq 0} |r_{u,u}(k)|^2 \tag{4.19}$$

where $\mathscr{P}$ and $\mathscr{A}\mathscr{P}$ stand for *periodic* and *aperiodic* correlations, respectively. Lower bounds on the above ISL metrics are given by [70] [71]

$$\mathrm{ISL}^{\mathscr{P}}(X) \geq \sigma^2 m(m-1) \triangleq \overline{\mathscr{W}}^{\mathscr{P}}_{m,n} \tag{4.20}$$

$$\mathrm{ISL}^{\mathscr{A}\mathscr{P}}(X) \geq \sigma^2 m(m-1) \triangleq \overline{\mathscr{W}}^{\mathscr{A}\mathscr{P}}_{m,n}. \tag{4.21}$$

Note that the ISL metric can be related to the RMS inner-product level defined in (4.4). Particularly, similar to $I_{rms}(X)$, the ISL bounds can be (nearly) met even for sequence sets with constrained alphabet [70] [71].

A different criterion for measuring the collective smallness of the out-of-phase correlations is the PSL metric:

$$\mathrm{PSL}^{\mathscr{P}}(X) = \max\left(\{|c_{u,v}(k)|\}_{u\neq v;\,k} \cup \{|c_{u,u}(k)|\}_{u;\,k\neq 0}\right) \tag{4.22}$$

$$\mathrm{PSL}^{\mathscr{A}\mathscr{P}}(X) = \max\left(\{|r_{u,v}(k)|\}_{u\neq v;\,k} \cup \{|r_{u,u}(k)|\}_{u;\,k\neq 0}\right) \tag{4.23}$$

The PSL criteria have a close relationship with the peak inner-product level metric. In particular, Welch [57] used (4.6) to derive the following lower

bounds on the periodic, and respectively, aperiodic PSL metrics:

$$\mathscr{W}^{\mathscr{P}}_{m,n} \triangleq \max_{s:\ \binom{n+s-1}{s} \leq mn} \sigma \left(\frac{1}{mn-1} \left[\frac{mn}{\binom{n+s-1}{s}} - 1 \right] \right)^{\frac{1}{2s}},$$

$$\mathscr{W}^{\mathscr{A}\mathscr{P}}_{m,n} \triangleq \max_{s:\ \binom{2n+s-2}{s} \leq m(2n-1)} \sigma \left(\frac{1}{m(2n-1)-1} \left[\frac{m(2n-1)}{\binom{2n+s-2}{s}} - 1 \right] \right)^{\frac{1}{2s}}$$

with the bounds being non-trivial for $m > 1$.

We continue this section noting that the Welch peak correlation bounds are a direct consequence of the Welch bound on inner-products. To observe this fact, let $\{\boldsymbol{Q}_k\}$ be the periodic shifting matrices defined by

$$\boldsymbol{Q}_k = \boldsymbol{Q}_{-k}^H \triangleq \begin{pmatrix} \mathbf{0}_{(n-k)\times k} & \boldsymbol{I}_{n-k} \\ \boldsymbol{I}_k & \mathbf{0}_{k\times(n-k)} \end{pmatrix}. \tag{4.24}$$

Given a sequence set $\{\mathbf{x}_u\}_{u=1}^m$ with sequences of length n and energy σ, it is straightforward to verify that the inner-products of the mn sequences $\{\boldsymbol{Q}_v \mathbf{x}_u\}_{u,v\in[m]^2}$ become the out-of-phase periodic correlations of the set $\{\mathbf{x}_u\}_{u=1}^m$. Therefore, by using the Welch inner-product bound we obtain the following lower bound on $\mathrm{PSL}^{\mathscr{P}}(X)$:

$$\mathrm{PSL}^{\mathscr{P}}(X) \geq \mathscr{W}_{mn,n} = \mathscr{W}^{\mathscr{P}}_{m,n} \tag{4.25}$$

The Welch correlation bound in the aperiodic case can be derived by additionally observing that the periodic out-of-phase correlations of $\{\widetilde{\mathbf{x}}_u\}_{u=1}^m$ where $\widetilde{\mathbf{x}}_u = (\mathbf{x}_u^T \ \mathbf{0}_{1\times(n-1)})^T$ are identical to the aperiodic out-of-phase correlations of $\{\mathbf{x}_u\}_{u=1}^m$. As a result,

$$\begin{aligned} \mathrm{PSL}^{\mathscr{A}\mathscr{P}}(X) &\geq \mathscr{W}^{\mathscr{P}}_{m,2n-1} \\ &= \mathscr{W}_{m(2n-1),2n-1} \\ &= \mathscr{W}^{\mathscr{A}\mathscr{P}}_{m,n}. \end{aligned} \tag{4.26}$$

A consequence of the above formulation is the fact that, similar to the case of inner products, the Welch peak correlation bounds can be met if and only if all out-of-phase correlation terms possess the same value. As a side consequence, the above formulation implies that the correlation lags compose the set of inner-products associated with circulant measurement matrices (or frames). Therefore, any of the obtained correlation bounds can be useful when designing measurement matrices (or frames) with circulant structure. In light of the above usage of the Welch peak inner-product bound for deriving peak correlation bounds, we can exploit the tighter peak inner-product bound $\mathscr{I}_{m,n}$ to

obtain the following *compound peak correlation bounds*:

$$\begin{aligned} \mathscr{I}^{\mathscr{P}}_{m,n} &\triangleq \mathscr{I}_{mn,n} \\ \mathscr{I}^{\mathscr{A}\mathscr{P}}_{m,n} &\triangleq \mathscr{I}^{\mathscr{P}}_{m,2n-1} = \mathscr{I}_{m(2n-1),2n-1}. \end{aligned} \tag{4.27}$$

Note that achieving the above PSL bounds is harder (both analytically and computationally) not only than meeting the ISL bounds in (4.20) but also than achieving the aforementioned peak inner-product bounds. It is worth pointing out that for designing sequence sets with constrained alphabet or with other practical limitations, the above bounds can be modified accordingly. For instance, when employing p^{th} root-of-unity (i.e. p-ary) sequences with prime p to design sequence sets with low periodic out-of-phase correlations, one can use the *Sidelnikov bound* [72] which is usually tighter (although not always) than the Welch bound. For the binary alphabet, improved lower bounds on periodic and aperiodic ISL metrics are proposed in [73] and [74], respectively.

The long-standing research problem of finding sequence sets with small out-of-phase correlations has resulted in several analytical constructions for specific values of (m,n) (see e.g. [75]- [77]). However, the analytical constructions are usually proposed for the periodic correlation case and not for the aperiodic case which is deemed to be more difficult [71]. As an example, Kasami family includes sets of binary sequences of length $n = 2^N - 1$ and cardinality $m = 2^{N/2}$ where N is an even natural number [75]. The $\mathrm{PSL}^{\mathscr{P}}$ value of a Kasami set is given by $1 + 2^{N/2}$. In addition, for odd N, Gold binary sequence sets can be constructed for $(m,n) = (2^N + 1, 2^N - 1)$ that have a $\mathrm{PSL}^{\mathscr{P}}$ value of $1 + \sqrt{2^{N+1} - 2}$ [76]. The Weil family consists of sequence sets with $n = N$ and $m = (N-1)/2$, where N is prime, that possess a $\mathrm{PSL}^{\mathscr{P}}$ value of $5 + 2\sqrt{N}$ [77]. Such sets are usually referred to as *asymptotically optimal* owing to the fact that their PSL values behave like $\mathscr{O}(\sqrt{n})$ as $n \to \infty$ similar to the behavior of Welch peak correlation bounds for $s = 1$. We refer the interested reader to [38] for further details on this aspect.

4.3 Correlation Bounds: Tightness and Improvement

By using the analytical tools provided earlier, we provide a tightness assessment of the compound correlation bounds. In order to improve the tightness condition of the bounds in the aperiodic case, a new improvement of the aperiodic bound is discussed and the obtained improvement is evaluated.

4.3.1 Tightness of $\mathscr{I}^{\mathscr{P}}_{m,n}$ and $\mathscr{I}^{\mathscr{A}\mathscr{P}}_{m,n}$

Our main results regarding the tightness of $\mathscr{I}^{\mathscr{P}}_{m,n}$ and $\mathscr{I}^{\mathscr{A}\mathscr{P}}_{m,n}$ can be briefly stated as follows. Examples of (m,n) can be provided for which the tightness

of $\mathscr{I}^{\mathscr{P}}_{m,n}$ or $\mathscr{I}^{\mathscr{A}\mathscr{P}}_{m,n}$ is straightforward to show. However, there exist (m,n) for which these bounds are not tight. Overall, the theoretical (as well as the computational) evidence suggests that *the tightness of the above bounds may be rather an exception than the rule*. The next two propositions (whose proofs are given in the Appendix) provide examples of cases in which $\mathscr{I}^{\mathscr{P}}_{m,n}$ and $\mathscr{I}^{\mathscr{A}\mathscr{P}}_{m,n}$ are tight.

Proposition 1. *The peak periodic correlation bound $\mathscr{I}^{\mathscr{P}}_{m,n}$ is tight for $(m,n) = (2,2)$.*

Proposition 2. *The peak aperiodic correlation bound $\mathscr{I}^{\mathscr{A}\mathscr{P}}_{m,n}$ is tight for $(m,n) = (2,2)$.*

Next we present a simple computational approach to find cases in which the compound peak correlation bounds are not tight. Specifically, the correlation bounds $\mathscr{I}^{\mathscr{P}}_{m,n}$ and $\mathscr{I}^{\mathscr{A}\mathscr{P}}_{m,n}$ are not tight if both conditions below hold:

1. The corresponding Welch bound is not tight, viz.

$$\begin{cases} \mathrm{PSL}^{\mathscr{P}}(X) > \mathscr{W}^{\mathscr{P}}_{m,n} & \text{periodic case,} \\ \mathrm{PSL}^{\mathscr{A}\mathscr{P}}(X) > \mathscr{W}^{\mathscr{A}\mathscr{P}}_{m,n} & \text{aperiodic case} \end{cases} \tag{4.28}$$

   for all sets X including m sequences of length n, and energy σ.
2. The Welch bound dominates both Levestein and Exponential bounds. Due to the fact that the compound bound is the maximum of Welch, Levestein and Exponential bounds, the latter condition is equivalent to

$$\begin{cases} \mathscr{I}^{\mathscr{P}}_{m,n} = \mathscr{W}^{\mathscr{P}}_{m,n} & \text{Periodic case,} \\ \mathscr{I}^{\mathscr{A}\mathscr{P}}_{m,n} = \mathscr{W}^{\mathscr{A}\mathscr{P}}_{m,n} & \text{Aperiodic case.} \end{cases} \tag{4.29}$$

Condition 1) can be verified, for example, by checking the two necessary tightness conditions of the Welch bound given in Introduction, see (4.14) and the related observations. The second condition makes sure that the compound bounds are identical to the Welch bounds. Fig. 4.1 depicts the values of $(m,n) \in [2,128] \times [2,8]$ for which the use of the above approach shows that the bounds $\mathscr{I}^{\mathscr{P}}_{m,n}$ and $\mathscr{I}^{\mathscr{A}\mathscr{P}}_{m,n}$ are not tight. The next sub-section shows that, in general, the (compound) aperiodic correlation bound is loose even more often than what is suggested by Fig. 4.1.

4.3.2 An Improvement of the Aperiodic Correlation Bound

In this sub-section, we propose an improvement of $\mathscr{I}^{\mathscr{A}\mathscr{P}}_{m,n}$. The new bound relies on the specific structure of aperiodic correlations. More concretely, one needs to observe that even though the sequence dimensions are increased by zero-padding (with the goal of deriving the aperiodic bound from the periodic

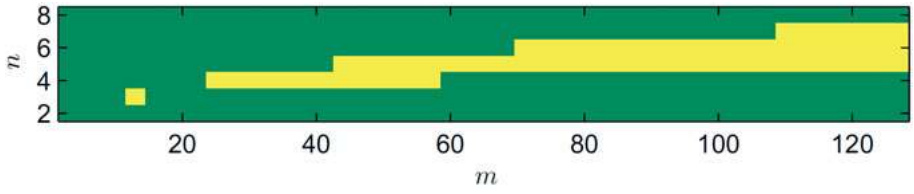

(a)

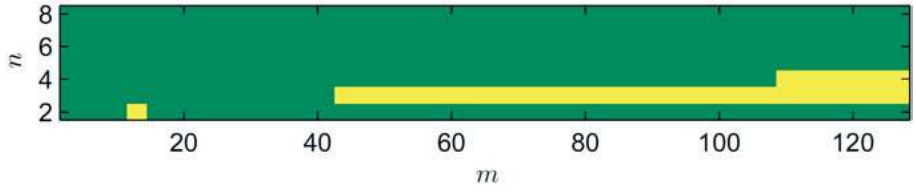

(b)

Figure 4.1. The values of $(m,n) \in [2,128] \times [2,8]$ (depicted in yellow) for which the peak correlation bounds $\mathscr{I}^{\mathscr{P}}_{m,n}$ and $\mathscr{I}^{\mathscr{A}\mathscr{P}}_{m,n}$ were found to be loose (by satisfying both conditions (4.28) and (4.29)): (a) periodic correlation, and (b) aperiodic correlation.

one), the sequences retain their intrinsic low dimensional properties. In particular, for subsets of sequences lying in lower dimensional subspaces the angles among the vectors in the set may be smaller— so the inner product may be larger. In the following, a more precise usage of this observation is proposed.

Let $n \geq 2$, and consider the sequence set

$$\{\boldsymbol{Q}_v \widetilde{\mathbf{x}}_u\}_{u\in[m],\ v\in[2n-1]}. \tag{4.30}$$

Now let k be a fixed integer such that $0 \leq k \leq n-1$. Consider the subset of sequences in (4.30) whose non-zero entries occur only in their first $n+k$ locations. It is straightforward to verify that such property holds for any $0 \leq v \leq k$. As a result, at least $m(k+1)$ sequences of (4.30) lie in the $n+k$ dimensional space associated with the first $n+k$ entries of the sequences in (4.30). This fact implies the following lower bound on the peak aperiodic correlation:

$$\mathrm{PSL}^{\mathscr{A}\mathscr{P}}(\boldsymbol{X}) \geq \mathscr{I}_{m(k+1),n+k}. \tag{4.31}$$

Note that the above observation can be made for any window of length $n+k$ over the entries of the sequences in (4.30), but does not seem to further improve the bound in (4.31). However, by using (4.31) for $0 \leq k \leq n-1$ yields

$$\mathrm{PSL}^{\mathscr{A}\mathscr{P}}(\boldsymbol{X}) \geq \max_{0\leq k\leq n-1} \mathscr{I}_{m(k+1),n+k} \triangleq \mathscr{N}^{\mathscr{A}\mathscr{P}}_{m,n}. \tag{4.32}$$

Fig. 4.2 compares the new aperiodic correlation bound $\mathscr{N}_{m,n}^{\mathscr{A}\mathscr{P}}$ with the aperiodic bound $\mathscr{I}_{m,n}^{\mathscr{A}\mathscr{P}}$. The comparison is accomplished by computing the ratio $\mathscr{N}_{m,n}^{\mathscr{A}\mathscr{P}}/\mathscr{I}_{m,n}^{\mathscr{A}\mathscr{P}}$ for $(m,n) \in [2,1024] \times [2,256]$. A considerable improvement (even by more than 35%) can be observed for some (m,n). As a specific example, we consider the case of $(m,n) = (450,250)$. In this case, the maximum of $\{\mathscr{I}_{m(k+1),n+k}\}$ occurs for $k = 11$ leading to $\mathscr{N}_{m,n}^{\mathscr{A}\mathscr{P}} = 0.0604\sigma$, whereas $\mathscr{I}_{m,n}^{\mathscr{A}\mathscr{P}} = 0.0447\sigma$. As a result, we obtain $\mathscr{N}_{m,n}^{\mathscr{A}\mathscr{P}}/\mathscr{I}_{m,n}^{\mathscr{A}\mathscr{P}} = 1.351$.

Finally, we end this section by noting that similar to $\mathscr{I}_{m,n}^{\mathscr{A}\mathscr{P}}$, the formulation of $\mathscr{N}_{m,n}^{\mathscr{A}\mathscr{P}}$ relies on the inner-product bounds $\{\mathscr{I}_{m,n}\}$ and hence, its growth rate is determined by $\{\mathscr{I}_{m,n}\}$.

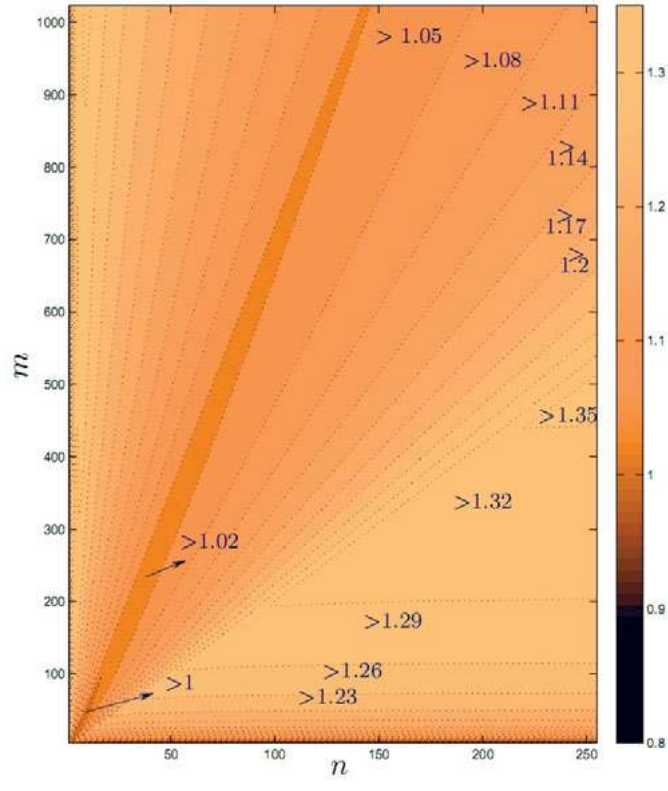

Figure 4.2. The improvement of the aperiodic correlation bound. The new bound $\mathscr{N}_{m,n}^{\mathscr{A}\mathscr{P}}$ is compared to the bound $\mathscr{I}_{m,n}^{\mathscr{A}\mathscr{P}}$ by computing the ratio $\mathscr{N}_{m,n}^{\mathscr{A}\mathscr{P}}/\mathscr{I}_{m,n}^{\mathscr{A}\mathscr{P}}$. The contours represent the areas with the indicated minimum level of improvement.

4.4 Approaching A Correlation Bound

In this section, the challenging problem of meeting a correlation bound is addressed. Particularly, it is of interest to find out how close one can get to a

given periodic or aperiodic bound. In the following, we provide a general computational framework (inspired by the formulation of the twisted product in Chapter 2) that can be used to approach any feasible correlation bound.

4.4.1 Problem Formulation

The *twisted product* of two vectors $\mathbf{x}$ and $\boldsymbol{y}$ of length n is defined as $\mathbf{x} \circlearrowright \boldsymbol{y}^H \triangleq$

$$\begin{pmatrix} \mathbf{x}(1)\boldsymbol{y}^*(1) & \mathbf{x}(2)\boldsymbol{y}^*(2) & \cdots & \mathbf{x}(n)\boldsymbol{y}^*(n) \\ \mathbf{x}(1)\boldsymbol{y}^*(2) & \mathbf{x}(2)\boldsymbol{y}^*(3) & \cdots & \mathbf{x}(n)\boldsymbol{y}^*(1) \\ \vdots & \vdots & \ddots & \vdots \\ \mathbf{x}(1)\boldsymbol{y}^*(n) & \mathbf{x}(2)\boldsymbol{y}^*(1) & \cdots & \mathbf{x}(n)\boldsymbol{y}^*(n-1) \end{pmatrix} \tag{4.33}$$

where $\mathbf{x}(k)$ and $\boldsymbol{y}(k)$ are the k^{th} entries of $\mathbf{x}$ and $\boldsymbol{y}$ respectively. In a more general context, we define the twisted product of two matrices $\boldsymbol{X} = (\mathbf{x}_1 \mathbf{x}_2 \cdots \mathbf{x}_p)$ and $\boldsymbol{Y} = (\boldsymbol{y}_1 \boldsymbol{y}_2 \cdots \boldsymbol{y}_q)$ as

$$\boldsymbol{X} \circlearrowright \boldsymbol{Y}^H \triangleq \begin{pmatrix} \mathbf{x}_1 \circlearrowright \boldsymbol{y}_1^H \\ \vdots \\ \mathbf{x}_1 \circlearrowright \boldsymbol{y}_q^H \\ \mathbf{x}_2 \circlearrowright \boldsymbol{y}_1^H \\ \vdots \\ \vdots \\ \mathbf{x}_p \circlearrowright \boldsymbol{y}_q^H \end{pmatrix} \tag{4.34}$$

where all $\{\mathbf{x}_k\}$ and $\{\boldsymbol{y}_l\}$ are of length n. Interestingly, meeting a PSL bound can be formulated by using the concept of twisted product for both periodic and aperiodic correlations. It should be observed that $\boldsymbol{X}$ meets a peak periodic correlation bound $B^{\mathscr{P}}$ if and only if the entries of

$$\boldsymbol{c} = (\boldsymbol{X} \circlearrowright \boldsymbol{X}^H)\mathbf{1}_{n\times 1} \tag{4.35}$$

satisfy

$$\begin{cases} \boldsymbol{c}(t) = \sigma & t = l(m+1)n+1,\ 0 \le l \le m-1, \\ |\boldsymbol{c}(t)| \le \mathscr{B}^{\mathscr{P}} & \text{otherwise} \end{cases} \tag{4.36}$$

where the first condition corresponds to the energy constraints on $\{\mathbf{x}_k\}$.

Next note that for any two sequences $\mathbf{x}_u, \mathbf{x}_v \in \mathbb{C}^n$ the periodic cross-correlations $\{\widetilde{c}_{u,v}(k)\}$ of $\widetilde{\mathbf{x}}_u = (\mathbf{x}_u^T\ \mathbf{0}_{1\times(n-1)})^T$ and $\widetilde{\mathbf{x}}_v = (\mathbf{x}_v^T\ \mathbf{0}_{1\times(n-1)})^T$ are given by

$$\widetilde{c}_{u,v}(k) = \begin{cases} r_{u,v}(k) & 0 \le k \le n-1, \\ r_{u,v}^*(2n-k-1) & n \le k \le 2n-2. \end{cases} \tag{4.37}$$

Consequently, a similar approach as in the case of the periodic correlation can be used to characterize the sequence sets meeting a peak aperiodic correlation bound $\mathscr{B}^{\mathscr{A}\mathscr{P}}$. Let

$$\widetilde{\boldsymbol{X}} = \begin{pmatrix} \boldsymbol{X} \\ \boldsymbol{0}_{(n-1)\times m} \end{pmatrix}. \tag{4.38}$$

Now note that $\boldsymbol{X}$ meets $\mathscr{B}^{\mathscr{A}\mathscr{P}}$ if and only if the entries of

$$\widetilde{\boldsymbol{c}} = (\widetilde{\boldsymbol{X}} \circlearrowright \widetilde{\boldsymbol{X}}^H)\boldsymbol{1}_{(2n-1)\times 1} \tag{4.39}$$

satisfy

$$\begin{cases} \widetilde{\boldsymbol{c}}(t) = \sigma & t = l(m+1)(2n-1)+1,\ 0 \le l \le m-1, \\ |\widetilde{\boldsymbol{c}}(t)| \le \mathscr{B}^{\mathscr{A}\mathscr{P}} & \text{otherwise.} \end{cases} \tag{4.40}$$

4.4.2 Computational Framework

In the sequel, we devise a computational framework based on alternating projections to approach the given bounds $\mathscr{B}^{\mathscr{P}}$ and $\mathscr{B}^{\mathscr{A}\mathscr{P}}$.

- *The Periodic Case:* Consider the convex set $\Gamma^{\mathscr{P}}_{n,m}$ of all matrices $\boldsymbol{Z}$ for which the entries of $\boldsymbol{c} = \boldsymbol{Z}\boldsymbol{1}_{n\times 1}$ satisfy the conditions in (4.36). Furthermore, consider the set

$$\Lambda^{\mathscr{P}}_{n,m} = \left\{ \boldsymbol{Z} \mid \boldsymbol{Z} = \boldsymbol{X} \circlearrowright \boldsymbol{X}^H,\ \boldsymbol{X} \in \mathbb{C}^{n\times m} \right\}. \tag{4.41}$$

Let $\Psi^{\mathscr{P}}_{m,n}(\mathscr{B}^{\mathscr{P}})$ denote the sequence sets with a peak periodic correlation equal to $\mathscr{B}^{\mathscr{P}}$. As there exists a one-to-one mapping between the two sets $\Psi^{\mathscr{P}}_{m,n}(\mathscr{B}^{\mathscr{P}})$ and $\Gamma^{\mathscr{P}}_{n,m} \cap \Lambda^{\mathscr{P}}_{n,m}$, a natural approach to find the elements of $\Psi^{\mathscr{P}}_{m,n}(\mathscr{B}^{\mathscr{P}})$ is to employ alternating projections onto the two sets $\Gamma^{\mathscr{P}}_{n,m}$ and $\Lambda^{\mathscr{P}}_{n,m}$.

Let $vec(\boldsymbol{X}) = (\mathbf{x}_1^T \mathbf{x}_2^T \cdots \mathbf{x}_m^T)^T$. It can be seen that all the entries of $\boldsymbol{X} \circlearrowright \boldsymbol{X}^H$ occur in $vec(\boldsymbol{X})\, vec^H(\boldsymbol{X})$ exactly one time. Therefore, there exists a unique re-ordering function that maps the two matrices to one another. We denote this function by $\mathscr{G} : \mathbb{C}^{m^2 n\times n} \to \mathbb{C}^{mn\times mn}$ which is such that

$$\mathscr{G}(\boldsymbol{X} \circlearrowright \boldsymbol{X}^H) = vec(\boldsymbol{X})\, vec^H(\boldsymbol{X}). \tag{4.42}$$

In words, this mapping defines the (k,l) element of the right-hand side as the corresponding let us say $(\overline{k},\overline{l})$ element of the matrix argument. As such, it can be easily generalized to any arbitrary matrix. The Frobenius norm projection $\boldsymbol{Z}^{\Lambda}_{\perp}$ of any $\boldsymbol{Z} \in \mathbb{C}^{m^2 n\times n}$ on $\Lambda^{\mathscr{P}}_{n,m}$ can be obtained as the solution to the optimization problem

$$\begin{aligned} \min_{\boldsymbol{X}_\perp, \boldsymbol{Z}^{\Lambda}_{\perp}} \quad & \|\boldsymbol{Z} - \boldsymbol{Z}^{\Lambda}_{\perp}\|_F \\ \text{s.t.} \quad & \boldsymbol{Z}^{\Lambda}_{\perp} = \boldsymbol{X}_\perp \circlearrowright \boldsymbol{X}^H_\perp \end{aligned} \tag{4.43}$$

whose objective function may be recast as:

$$\begin{aligned} \|\boldsymbol{Z}-\boldsymbol{Z}_{\perp}^{\Lambda}\|_F &= \|\boldsymbol{Z}-\boldsymbol{X}_{\perp}\circlearrowleft\boldsymbol{X}_{\perp}^{H}\|_F \\ &= \|\mathscr{G}(\boldsymbol{Z})-vec(\boldsymbol{X}_{\perp})\,vec^{H}(\boldsymbol{X}_{\perp})\|_F. \end{aligned} \tag{4.44}$$

By using (4.44), the minimizer $\boldsymbol{X}_{\perp}$ of (4.43) can be obtained as $vec(\boldsymbol{X}_{\perp}) = \sqrt{\eta_1(\mathscr{G}(\boldsymbol{Z}))}\,\boldsymbol{v}_1(\mathscr{G}(\boldsymbol{Z}))$, which yields

$$\boldsymbol{Z}_{\perp}^{\Lambda} = \boldsymbol{X}_{\perp}\circlearrowleft\boldsymbol{X}_{\perp}^{H} \tag{4.45}$$

as the optimal projection on $\Lambda_{n,m}^{\mathscr{P}}$.

Remark 1: It is worth noting that for any $\boldsymbol{X}\in\Psi_{m,n}^{\mathscr{P}}(\mathscr{B}^{\mathscr{P}})$, the value of $\eta_1(\mathscr{G}(\boldsymbol{Z}))$ for the corresponding $\boldsymbol{Z}$ represents the total energy of the sequences denoted by $\boldsymbol{X}$. Moreover, finding the close points (or the intersection) of the two sets $\Gamma_{n,m}^{\mathscr{P}}$ and $\Lambda_{n,m}^{\mathscr{P}}$ can be roughly interpreted as the maximization of $\eta_1(\mathscr{G}(\boldsymbol{Z}))$ for $\boldsymbol{Z}\in\Gamma_{n,m}^{\mathscr{P}}$. As a result, for a feasible PSL bound it can be practically assumed that $\eta_1(\mathscr{G}(\boldsymbol{Z}))>0$ throughout the projections. ■

Next, we study the Frobenius norm projection $\boldsymbol{Z}_{\perp}^{\Gamma}$ of any $\boldsymbol{Z}\in\mathbb{C}^{m^2n\times n}$ on $\Gamma_{n,m}^{\mathscr{P}}$. Such a projection can be obtained by solving the optimization problem

$$\min_{\boldsymbol{Z}_{\perp}^{\Gamma}\in\Gamma_{n,m}^{\mathscr{P}}} \quad \|\boldsymbol{Z}-\boldsymbol{Z}_{\perp}^{\Gamma}\|_F. \tag{4.46}$$

We note that the conditions (4.36) on $\boldsymbol{Z}_{\perp}^{\Gamma}\in\Gamma_{n,m}^{\mathscr{P}}$ are row-wise. Let $\boldsymbol{z}^T$ and $\boldsymbol{z}_{\perp}^T$ represent two generic rows of $\boldsymbol{Z}$ and $\boldsymbol{Z}_{\perp}^{\Gamma}$, respectively. Therefore, we consider the nearest-vector problem

$$\min_{\boldsymbol{z}_{\perp}} \quad \|\boldsymbol{z}-\boldsymbol{z}_{\perp}\|_2 \tag{4.47}$$

in which $\boldsymbol{z}_{\perp}$ is constrained either to have a given sum n, i.e. $\boldsymbol{z}_{\perp}^T\mathbf{1}=n$, or the absolute value of its sum is supposed to be upper bounded by $\mathscr{B}^{\mathscr{P}}$, viz. $|\boldsymbol{z}_{\perp}^T\mathbf{1}|\le\mathscr{B}^{\mathscr{P}}$.

To tackle the above nearest-vector problem, assume $\boldsymbol{z}^T\mathbf{1}=\alpha_1 e^{j\theta_1}$ and $\boldsymbol{z}_{\perp}^T\mathbf{1}=\alpha_2 e^{j\theta_2}$ for some $\alpha_1,\alpha_2\in\mathbb{R}_+$, $\theta_1,\theta_2\in[0,2\pi)$, and let $\boldsymbol{z}_d=\boldsymbol{z}-\boldsymbol{z}_{\perp}$. By using the Cauchy-Schwarz inequality we have that

$$\|\boldsymbol{z}_d\|_2^2 \ge \frac{|\boldsymbol{z}_d^T\mathbf{1}|^2}{\|\mathbf{1}\|_2^2} = \frac{|\alpha_1 e^{j\theta_1}-\alpha_2 e^{j\theta_2}|^2}{n} \tag{4.48}$$

where the equality is attained if and only if all the entries of $\boldsymbol{z}_d$ are identical:

$$\boldsymbol{z}_d(k) = \frac{\alpha_1 e^{j\theta_1}-\alpha_2 e^{j\theta_2}}{n}, \quad 1\le k\le n. \tag{4.49}$$

Moreover, the equality in (4.48) can be achieved for any given α_2 and θ_2 via (4.49). As a result, to minimize $\|\boldsymbol{z}-\boldsymbol{z}_{\perp}\|_2=\|\boldsymbol{z}_d\|_2$, it is sufficient to minimize

$|\alpha_1 e^{j\theta_1} - \alpha_2 e^{j\theta_2}|^2$ with respect to α_2 and θ_2. For any fixed α_2, the minimizer θ_2 of the latter criterion is given by $\theta_2 = \theta_1$. On the other hand, the optimal α_2 depends on the constraint imposed on $\boldsymbol{z}_\perp$. In particular, for the constraint $\boldsymbol{z}_\perp^T \mathbf{1} = n$ then we have the optimum $\alpha_2 = n$. In the case of the constraint $|\boldsymbol{z}_\perp^T \mathbf{1}| \leq \mathscr{B}^{\mathscr{P}}$, the minimizer α_2 is given by

$$\alpha_2 = \begin{cases} \alpha_1 & \alpha_1 \leq B^{\mathscr{P}}, \\ B^{\mathscr{P}} & \alpha_1 > B^{\mathscr{P}}. \end{cases} \tag{4.50}$$

Table 4.2 summarizes the steps of the proposed algorithm for approaching a given periodic PSL bound. Note that while the projection on the set $\Lambda_{n,m}^{\mathscr{P}}$ is performed by a rank-one approximation, the projection on the set $\Gamma_{n,m}^{\mathscr{P}}$ has a closed-form expression which leads to an even smaller computational burden.

- *The Aperiodic Case:* Similar to the derivations in the periodic case, we consider the set

$$\Lambda_{n,m}^{\mathscr{A}\mathscr{P}} = \Big\{ \boldsymbol{Z} \mid \boldsymbol{Z} = \widetilde{\boldsymbol{X}} \circlearrowleft \widetilde{\boldsymbol{X}}^H, \quad \widetilde{\boldsymbol{X}} = \begin{pmatrix} \boldsymbol{X} \\ \mathbf{0}_{(n-1)\times m} \end{pmatrix}, \boldsymbol{X} \in \mathbb{C}^{n\times m} \Big\}. \tag{4.51}$$

We define the masking matrix $\boldsymbol{M}$ as

$$\boldsymbol{M} = \begin{pmatrix} \boldsymbol{M}' & \cdots & \boldsymbol{M}' \\ \vdots & \ddots & \vdots \\ \boldsymbol{M}' & \cdots & \boldsymbol{M}' \end{pmatrix}, \quad \boldsymbol{M}'_{(2n-1)\times(2n-1)} = \begin{pmatrix} \mathbf{1}_{n\times n} & \mathbf{0} \\ \mathbf{0} & \mathbf{0} \end{pmatrix}, \tag{4.52}$$

and in addition consider the convex set $\Gamma_{n,m}^{\mathscr{A}\mathscr{P}}$ of all matrices $\boldsymbol{Z}$ such that

$$\boldsymbol{Z} \odot \mathscr{G}^{-1}(\boldsymbol{M}) = \boldsymbol{Z}, \tag{4.53}$$

where $\mathscr{G}$ is as defined in the periodic case but with dimension parameter $2n-1$ in lieu of n, and for which the entries of $\widetilde{\boldsymbol{c}} = \boldsymbol{Z}\mathbf{1}_{(2n-1)\times 1}$ satisfy the conditions in (4.40). Let $\Psi_{m,n}^{\mathscr{A}\mathscr{P}}(\mathscr{B}^{\mathscr{A}\mathscr{P}})$ denote the sequence sets with a peak aperiodic correlation equal to $\mathscr{B}^{\mathscr{A}\mathscr{P}}$. In the following, we propose an alternating projection onto the two sets $\Gamma_{n,m}^{\mathscr{A}\mathscr{P}}$ and $\Lambda_{n,m}^{\mathscr{A}\mathscr{P}}$ in order to obtain an element (if any) of $\Psi_{m,n}^{\mathscr{A}\mathscr{P}}(\mathscr{B}^{\mathscr{A}\mathscr{P}}) = \Gamma_{n,m}^{\mathscr{A}\mathscr{P}} \cap \Lambda_{n,m}^{\mathscr{A}\mathscr{P}}$ associated with the given aperiodic bound $\mathscr{B}^{\mathscr{A}\mathscr{P}}$.

Similar to the case of periodic correlation, we use the Frobenius norm as a measure of distance between the two sets. The Frobenius norm projection $\boldsymbol{Z}_\perp^\Lambda$ of any $\boldsymbol{Z} \in \mathbb{C}^{m^2(2n-1)\times(2n-1)}$ on $\Lambda_{n,m}^{\mathscr{A}\mathscr{P}}$ can be obtained as the solution to the

optimization problem

$$\begin{aligned} \min_{\boldsymbol{X}_\perp, \boldsymbol{Z}_\perp^\Lambda} \quad & \|\boldsymbol{Z} - \boldsymbol{Z}_\perp^\Lambda\|_F \\ \text{s.t.} \quad & \boldsymbol{Z}_\perp^\Lambda = \widetilde{\boldsymbol{X}}_\perp \circlearrowleft \widetilde{\boldsymbol{X}}_\perp^H \\ & \widetilde{\boldsymbol{X}}_\perp = \begin{pmatrix} \boldsymbol{X}_\perp \\ \boldsymbol{0}_{(n-1)\times m} \end{pmatrix}. \end{aligned} \tag{4.54}$$

Note that

$$\begin{aligned} \|\boldsymbol{Z} - \boldsymbol{Z}_\perp^\Lambda\|_F &= \|\boldsymbol{Z} - \widetilde{\boldsymbol{X}}_\perp \circlearrowleft \widetilde{\boldsymbol{X}}_\perp^H\|_F \\ &= \|\mathscr{G}(\boldsymbol{Z}) - vec(\widetilde{\boldsymbol{X}}_\perp)\, vec^H(\widetilde{\boldsymbol{X}}_\perp)\|_F \\ &= \|\mathscr{M}(\mathscr{G}(\boldsymbol{Z})) - vec(\boldsymbol{X}_\perp)\, vec^H(\boldsymbol{X}_\perp)\|_F \\ &\quad + \text{const.} \end{aligned} \tag{4.55}$$

where the operator $\mathscr{M}(.)$ collects the entries of the matrix argument corresponding to the non-zero entries of the masking matrix $\boldsymbol{M}$. As a result, the minimizer $\boldsymbol{X}_\perp$ of (4.54) is given by $vec(\boldsymbol{X}_\perp) = \sqrt{\eta_1(\mathscr{M}(\mathscr{G}(\boldsymbol{Z})))}\, \boldsymbol{v}_1(\mathscr{M}(\mathscr{G}(\boldsymbol{Z})))$, which consequently yields

$$\boldsymbol{Z}_\perp^\Lambda = \widetilde{\boldsymbol{X}}_\perp \circlearrowleft \widetilde{\boldsymbol{X}}_\perp^H \tag{4.56}$$

as the optimal projection on $\Lambda_{n,m}^{\mathscr{A}\mathscr{P}}$.

The Frobenius norm projection $\boldsymbol{Z}_\perp^\Gamma$ of any $\boldsymbol{Z} \in \mathbb{C}^{m^2(2n-1)\times(2n-1)}$ on $\Gamma_{n,m}^{\mathscr{A}\mathscr{P}}$ can be obtained similarly to that of $\Gamma_{n,m}^{\mathscr{P}}$ with a small modification. Note that the variables α_2 and θ_2 can be calculated by using the same arguments as for $\Gamma_{n,m}^{\mathscr{P}}$. However, the number of non-zero entries in the rows of $\boldsymbol{Z}_\perp^\Gamma$ is different. Particularly, the exact positions of non-zero entries of $\boldsymbol{Z}_\perp^\Gamma$ are given by the locations of ones in $\mathscr{G}^{-1}(\boldsymbol{M})$. Therefore, the entries of $\boldsymbol{z}_d$ are given by

$$\boldsymbol{z}_d(k) = \begin{cases} \frac{\alpha_1 e^{j\theta_1} - \alpha_2 e^{j\theta_2}}{|\boldsymbol{\mu}^T \boldsymbol{1}|} & k \in \text{supp}(\boldsymbol{\mu}), \\ 0 & \text{otherwise.} \end{cases} \tag{4.57}$$

where $\boldsymbol{\mu}$ represents the corresponding row in $\mathscr{G}^{-1}(\boldsymbol{M})$, and supp(.) denotes the set of non-zero locations in the vector argument.

Finally, the steps of the proposed alternating projections, in the periodic and aperiodic cases, are summarized in Table 4.2. Note that in both cases, each iteration of the algorithms has a $\mathscr{O}(m^2n^2)$-complexity. The obtained complexity measure is a direct consequence of the generally large cardinality (i.e. mn) of the data that the algorithms should handle as well as the hardness of the original problem (with m^2n constraints, which should be compared to the fewer constraints (i.e. m^2) for achieving a given peak inner-product level). Due to the practical interest of constrained sequence design, e.g. with finite-alphabet

or low-PAR, a modified version of the proposed algorithms that handles such cases is discussed in the Appendix. However, a more extensive discussion of the constrained sequence design is beyond the scope of this chapter.

Table 4.2. *The Proposed Algorithm for approaching a given periodic/aperiodic PSL bound*

Step 0: Initialize $\boldsymbol{X}$ with a random matrix in $\mathbb{C}^{n\times m}$;
(i) in the periodic case: set $\boldsymbol{Z}_{\perp}^{\Lambda} = \boldsymbol{X} \circlearrowleft \boldsymbol{X}^{H}$,
(ii) in the aperiodic case: set $\boldsymbol{Z}_{\perp}^{\Lambda} = \widetilde{\boldsymbol{X}} \circlearrowleft \widetilde{\boldsymbol{X}}^{H}$.
Step 1: Compute the optimal projection $\boldsymbol{Z}_{\perp}^{\Gamma}$ of $\boldsymbol{Z}_{\perp}^{\Lambda}$,
(i) in the periodic case: find $\boldsymbol{Z}_{\perp}^{\Gamma} \in \Gamma_{n,m}^{\mathscr{P}}$ by using (4.46)-(4.50).
(ii) in the aperiodic case: find $\boldsymbol{Z}_{\perp}^{\Gamma} \in \Gamma_{n,m}^{\mathscr{A}\mathscr{P}}$ by using (4.57).
Step 2: Compute the optimal projection $\boldsymbol{Z}_{\perp}^{\Lambda}$ of $\boldsymbol{Z}_{\perp}^{\Gamma}$,
(i) in the periodic case: find $\boldsymbol{Z}_{\perp}^{\Lambda} \in \Lambda_{n,m}^{\mathscr{P}}$ by using (4.45).
(ii) in the aperiodic case: find $\boldsymbol{Z}_{\perp}^{\Lambda} \in \Lambda_{n,m}^{\mathscr{A}\mathscr{P}}$ by using (4.56).
Step 3: Repeat steps 1 and 2 until a pre-defined stop criterion is satisfied, e.g. $\|\boldsymbol{Z}_{\perp}^{\Lambda} - \boldsymbol{Z}_{\perp}^{\Gamma}\|_F \leq \xi$, or $\|\boldsymbol{X}_{\perp}^{(t+1)} - \boldsymbol{X}_{\perp}^{(t)}\|_F \leq \xi$, for some $\xi > 0$, in which t denotes the iteration number.

4.5 Numerical Results

Several numerical examples will be presented to examine the performance of the proposed algorithms for approaching the peak correlation bounds. A main goal of these examples is to determine how close one can get to the peak correlation bounds via the proposed computational tools. The obtained sequence sets are provided online at `http://www.anst.uu.se/mojso279/sets`.

We employ the suggested algorithm in Table 4.2 for different values of (n,m). In the case of periodic correlation, we consider the bound $\mathscr{I}_{m,n}^{\mathscr{P}}$ in (4.27). Fig. 4.3 shows the peak periodic correlation (PSL$^{\mathscr{P}}$) values corresponding to the initializations and the obtained sequence sets along with the bound $\mathscr{I}_{m,n}^{\mathscr{P}}$, for $m \in \{2,3,4\}$ and $n \in \{2,4,5,7,8,10,12,15,16\}$. Note that due to the non-convexity of $\Lambda_{n,m}$, the problem is multi-modal (i.e. it may have many convergence points), and hence, many random initial points might be needed to achieve a certain low peak correlation level. In this example, different random initializations are considered for 40 experiments, and the resultant PSL$^{\mathscr{P}}$ of the proposed algorithm (in Table 4.2) represents the best outcome of the 40 experiments. To examine the sensitivity to choosing the initial set, well-known sequence sets including Gold, Kasami, and Weil are used as initializing sets for the (m,n) values for which they exist. Such cases are also reported in Fig. 4.3. It can be observed that $\mathscr{I}_{m,n}^{\mathscr{P}}$ can be practically met in several cases, e.g. for all n with $m = 2$. Furthermore, a considerable decrease of the peak periodic correlation obtained by using the proposed algorithm can be observed in all cases (even for the cases with well-known sets as initialization).

As discussed earlier, if the Welch bound can be met for given (m,n), then the absolute values of all out-of-phase correlations will be identical and have a value equal to the Welch bound. As an example of such behavior, we study the correlation properties of the resultant set for $(m,n) = (2,32)$. The absolute values of periodic correlations $\{c_{u,v}(k)\}$ are plotted in Fig. 4.4(a)-(c). In this case, the bound $\mathscr{I}_{m,n}^{\mathscr{P}}$ is nothing but the Welch bound $\mathscr{W}_{m,n}^{\mathscr{P}}$ corresponding to $s = 1$. As expected, all the periodic correlation levels (excluding the in-phase one) are equal to $\mathscr{W}_{m,n}^{\mathscr{P}} = \frac{32}{\sqrt{63}} \approx 4.03162$.

The mixed bound $\max\{\mathscr{N}_{m,n}^{\mathscr{A}\mathscr{P}}, \mathscr{I}_{m,n}^{\mathscr{A}\mathscr{P}}\}$ is used to conduct a similar numerical investigation in the aperiodic case. Fig. 4.5 illustrates the achieved $\text{PSL}^{\mathscr{A}\mathscr{P}}$ values by using the proposed alternating projections along with the mixed bound $\max\{\mathscr{N}_{m,n}^{\mathscr{A}\mathscr{P}}, \mathscr{I}_{m,n}^{\mathscr{A}\mathscr{P}}\}$. As expected, the bound is met for the case $(m,n) = (2,2)$ (see Proposition 2). For other cases, in which the aperiodic bound cannot be met exactly, significant reductions in the obtained $\text{PSL}^{\mathscr{A}\mathscr{P}}$ can be observed compared to the $\text{PSL}^{\mathscr{A}\mathscr{P}}$ values corresponding to the initial sets.

4.6 Concluding Remarks

Peak correlation bounds have been studied, and the problem of meeting peak periodic and aperiodic correlation bounds has been addressed. The main results can be summarized as follows:

- Welch, Levenstein, and Exponential bounds on peak inner-product level of sequence sets were discussed. Peak correlation bounds were derived based on the peak inner-product bounds.
- An improvement of the peak aperiodic correlation bound was provided.
- Analytical examples of the tightness of the peak correlation bounds were provided in both the periodic and aperiodic cases.
- Two novel algorithms were devised to tackle the problem of approaching a given periodic or aperiodic bound. Numerical examples were provided to show the potential of the proposed methods. In several cases, particularly in the case of periodic correlation, the considered peak correlation bound was met by using the proposed methods. In all examples, a significant decrease in the peak correlations of the designed sets was observed, compared to the PSL of the initial sequence sets (even for initializations by well-known sets such as Gold, Kasami and Weil families).

We believe that more studies are needed to achieve a deeper understanding and formulation of tighter peak correlation bounds. The focus of this work was on studying and on attempting to achieve peak correlation bounds when no extra constraints on the sequences were enforced. However, a modification of the algorithms to handle constrained sequence design was proposed. Extensive studies concerning constrained sequence set design, e.g. sets containing low

peak-to-average-power ratio (PAR), unimodular or root-of-unity sequences, can be interesting topics for future research.

4.7 Appendices

4.7.1 Appendix A: Proof of Proposition 1

First note that $\mathscr{I}_{2,2}^{\mathscr{P}} = \mathscr{W}_{2,2}^{\mathscr{P}}$ with $s = 1$. We provide the characterization of all sequence sets meeting the peak periodic bound $\mathscr{W}_{2,2}^{\mathscr{P}}$. Let

$$\boldsymbol{X} = \begin{pmatrix} a_1 & b_1 \\ a_2 & b_2 \end{pmatrix} \tag{4.58}$$

and observe that the out-of-phase periodic correlation levels of the two sequences $(a_1\, a_2)^T$ and $(b_1\, b_2)^T$ belong to the set $\{|2\Re(a_1a_2^*)|, |2\Re(b_1b_2^*)|, |a_1b_1^* + a_2b_2^*|, |a_1b_2^* + a_2b_1^*|\}$. The necessary and sufficient conditions for meeting the Welch peak correlation bound $\mathscr{W}_{m,n}^{\mathscr{P}}$ (for $s = 1$) imply that all the elements in the latter set should be equal to $\mathscr{W}_{2,2}^{\mathscr{P}} = \frac{2}{\sqrt{3}}$. The structure of $\boldsymbol{X}$ for meeting $\mathscr{I}_{2,2}^{\mathscr{P}}$ can be studied as follows.

By considering the energy constraint as well as the constraint $|2\Re(a_1a_2^*)| = \frac{2}{\sqrt{3}}$, we obtain that

$$\begin{cases} a_1 = \frac{1}{2}\left(e^{j\phi_1}\sqrt{2 \pm \frac{2}{\sqrt{3}}} + e^{j\phi_0}\sqrt{2 \mp \frac{2}{\sqrt{3}}}\right) \\ a_2 = \frac{1}{2}\left(e^{j\phi_1}\sqrt{2 \pm \frac{2}{\sqrt{3}}} - e^{j\phi_0}\sqrt{2 \mp \frac{2}{\sqrt{3}}}\right) \end{cases} \tag{4.59}$$

for some phase angles ϕ_0 and ϕ_1. In a similar manner, for $(b_1\, b_2)^T$ we have that

$$\begin{cases} b_1 = \frac{1}{2}\left(e^{j\theta_1}\sqrt{2 \mp \frac{2}{\sqrt{3}}} + e^{j\theta_0}\sqrt{2 \pm \frac{2}{\sqrt{3}}}\right) \\ b_2 = \frac{1}{2}\left(e^{j\theta_1}\sqrt{2 \mp \frac{2}{\sqrt{3}}} - e^{j\theta_0}\sqrt{2 \pm \frac{2}{\sqrt{3}}}\right) \end{cases} \tag{4.60}$$

with θ_0 and θ_1 being auxiliary phase angles. The result in (4.60) is also based on verifying that the assumption of the same order in "$\pm$" signs of a_1 and b_1 (as well as a_2 and b_2) in (4.59) and (4.60) violates the satisfaction of the following constraints

$$\begin{cases} |a_1b_1^* + a_2b_2^*| = \frac{2}{\sqrt{3}} \\ |a_1b_2^* + a_2b_1^*| = \frac{2}{\sqrt{3}} \end{cases} \tag{4.61}$$

On the other hand, for a_1, a_2 as given in (4.59) and b_1, b_2 as given in (4.60), the constraints in (4.61) lead to the the following equation

$$\left| e^{j(\phi_1-\theta_1)}\ \sqrt{4-4/3} \pm e^{j(\phi_0-\theta_0)}\ \sqrt{4-4/3} \right| = \frac{4}{\sqrt{3}} \tag{4.62}$$

which implies

$$\cos\left((\phi_1-\theta_1)-(\phi_0-\theta_0)\right)=0. \tag{4.63}$$

Therefore, $\Psi_{2,2}^{\mathscr{P}}(\mathscr{S}_{2,2})$ includes $\boldsymbol{X}$ characterized by (4.59) and (4.60), and with the auxiliary phase angles such that

$$(\phi_1-\theta_1)=(\phi_0-\theta_0)+(2k+1)\frac{\pi}{2}, \tag{4.64}$$

for some $k\in\mathbb{Z}$.

4.7.2 Appendix B: Proof of Proposition 2

Observe that $\mathscr{I}_{2,2}^{\mathscr{A}\mathscr{P}}=\mathscr{W}_{2,2}^{\mathscr{A}\mathscr{P}}=\frac{2}{\sqrt{5}}$ (with $s=1$) and let

$$\boldsymbol{X} \;=\; \begin{pmatrix} a_1 & b_1 \\ a_2 & b_2 \end{pmatrix}. \tag{4.65}$$

In what follows, a characterization of $\boldsymbol{X}$ that meets the aperiodic bound $\mathscr{W}_{2,2}^{\mathscr{A}\mathscr{P}}$ is derived. The set of aperiodic out-of-phase correlation levels $\{|r_{u,v}(k)|\}$ of the columns of $\boldsymbol{X}$ is given by $\{|a_1a_2^*|,|b_1b_2^*|,|a_1b_1^*+a_2b_2^*|,|a_2b_1^*|,|a_1b_2^*|\}$. By using the necessary and sufficient conditions for meeting the Welch peak correlation bound, we conclude that

$$\begin{cases} |a_1|=|b_1| \\ |a_2|=|b_2| \end{cases} \tag{4.66}$$

and that $|a_1||a_2|=\frac{2}{\sqrt{5}}$. By applying the energy constraint we obtain

$$|a_2|^4-2|a_2|^2+\frac{4}{5}=0. \tag{4.67}$$

The solutions to (4.67) are given by $|a_2|=\sqrt{1\pm\frac{\sqrt{5}}{5}}$, which also yields $|a_1|=\frac{2}{\sqrt{5\pm\sqrt{5}}}$.

To determine the phase angles of the sequences in $\boldsymbol{X}$, we employ the equation $|a_1b_1^*+a_2b_2^*|=\frac{2}{\sqrt{5}}$ which results in

$$\left||a_1|^2\,e^{j(\theta_1-\phi_1)}+|a_2|^2\,e^{j(\theta_2-\phi_2)}\right|=\frac{2}{\sqrt{5}} \tag{4.68}$$

with θ_1,θ_2,ϕ_1, and ϕ_2 being the phase angles of a_1,a_2,b_1, and b_2, respectively. Eq. (4.68) can be simplified to obtain

$$\cos\left((\theta_1-\phi_1)-(\theta_2-\phi_2)\right)=-1. \tag{4.69}$$

Consequently, $\boldsymbol{X}$ meeting $\mathscr{W}_{2,2}^{\mathscr{A}^{\mathscr{P}}}$ have the structure

$$\boldsymbol{X} = \begin{pmatrix} \frac{2}{\sqrt{5\pm\sqrt{5}}} e^{j\theta_1} & \frac{2}{\sqrt{5\pm\sqrt{5}}} e^{j\phi_1} \\ \sqrt{1\pm\frac{\sqrt{5}}{5}} e^{j\theta_2} & \sqrt{1\pm\frac{\sqrt{5}}{5}} e^{j\phi_2} \end{pmatrix} \tag{4.70}$$

such that $(\theta_1 - \phi_1) = (\theta_2 - \phi_2) + 2(k+1)\pi$ where $k \in \mathbb{Z}$.

4.7.3 Appendix C: Modified Projections for Constrained Sequence Design

With some modifications, the alternating projections proposed in Section 4.4 can be used for designing constrained sequences such as cases with finite-alphabet or low PAR. Note that in constrained cases, finding the optimal projection on the two sets $\Gamma_{n,m}$ and $\Lambda_{n,m}$ could be more complicated. However, the convergence of the projections is guaranteed if the distance between the latest projection points on the two sets is decreasing. In the following, we discuss a set of modifications that can enable the proposed approaches in Section 4.4 to tackle the constrained case.

Let $\boldsymbol{X} \in \Omega_{n,m}$ represent the required sequence structure. We revise the definition of $\Lambda_{n,m}$ by replacing the constraint $\boldsymbol{X} \in \mathbb{C}^{n\times m}$ with $\boldsymbol{X} \in \Omega_{n,m}$. Therefore, finding the projection on $\Lambda_{n,m}$ becomes equivalent to minimizing (4.44) and (4.55), in the periodic and aperiodic cases, respectively, but for $\boldsymbol{X} \in \Omega_{n,m}$. Hereafter, we study the periodic case as the extension to the aperiodic case is straightforward. Due to the fact that $\boldsymbol{X}$ has a fixed power (or Frobenius norm), minimizing (4.44) is equivalent to:

$$\begin{aligned} \min_{\boldsymbol{X}_\perp} \quad & vec^H(\boldsymbol{X}_\perp)\boldsymbol{Z}' vec(\boldsymbol{X}_\perp) \\ \text{s.t.} \quad & \boldsymbol{X}_\perp \in \Omega_{n,m} \end{aligned} \tag{4.71}$$

where $\boldsymbol{Z}' = \lambda \boldsymbol{I} + \mathscr{G}(\boldsymbol{Z})$ is positive-definite. More important, any increase in the objective function of (4.71) leads to a decrease of (4.44). Interestingly, increasing quadratic functions such as the one in (4.71), over constrained vector sets can be dealt with conveniently via the power-method like iterations proposed in [84] and [85]. Namely, considering the previously known projection on $\Lambda_{n,m}^{\mathscr{P}}$ as initialization ($\boldsymbol{X}_\perp^{(0)}$), the quadratic function in (4.71) can be increased monotonically by using the iterations:

$$\min_{\boldsymbol{X}_\perp^{(t+1)} \in \Omega_{n,m}} \left\| vec\left(\boldsymbol{X}_\perp^{(t+1)}\right) - \boldsymbol{Z}' vec\left(\boldsymbol{X}_\perp^{(t)}\right) \right\|_2 \tag{4.72}$$

The solution to (4.72) for unimodular or p-ary vector sets can be obtained analytically. In low-PAR scenarios, (4.72) can be solved using an efficient recursive algorithm developed in [26].

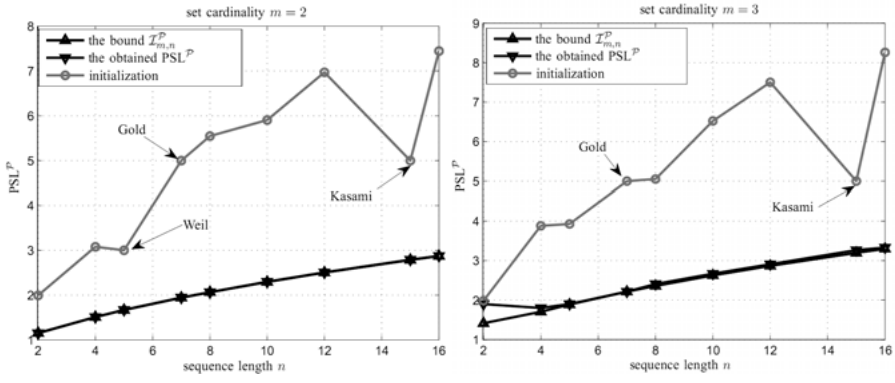

(a) (b)

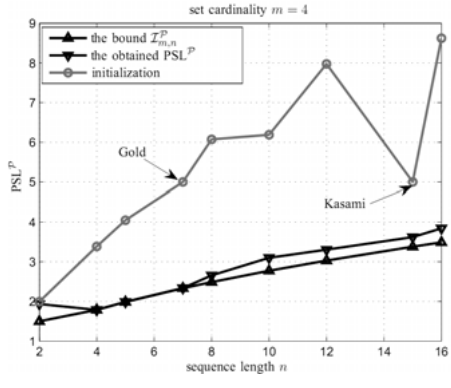

(c)

Figure 4.3. $\mathrm{PSL}^{\mathcal{P}}$ of the obtained sequence sets by using the algorithm in Table 4.2 (the periodic case), versus sequence length n, and for different set cardinalities m. Gold, Kasami, and Weil sequence sets are used to initialize the algorithm when they exist (pinpointed by arrows).

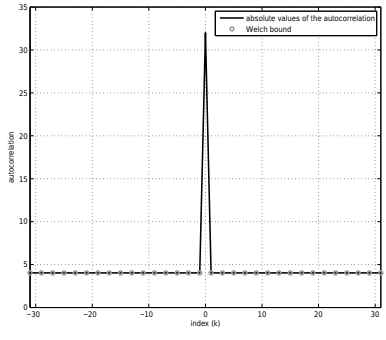

(a)

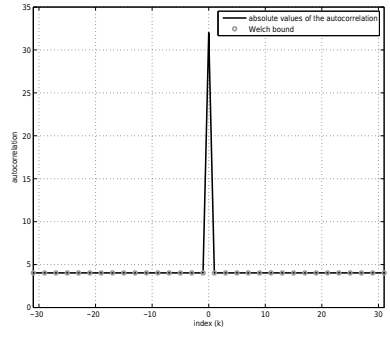

(b)

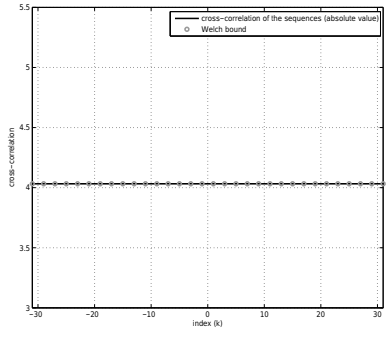

(c)

Figure 4.4. Correlation levels of the obtained sequence set for $(m,n) = (2,32)$: a) autocorrelation of the first sequence, b) autocorrelation of the second sequence, c) cross-correlation of the first and the second sequences.

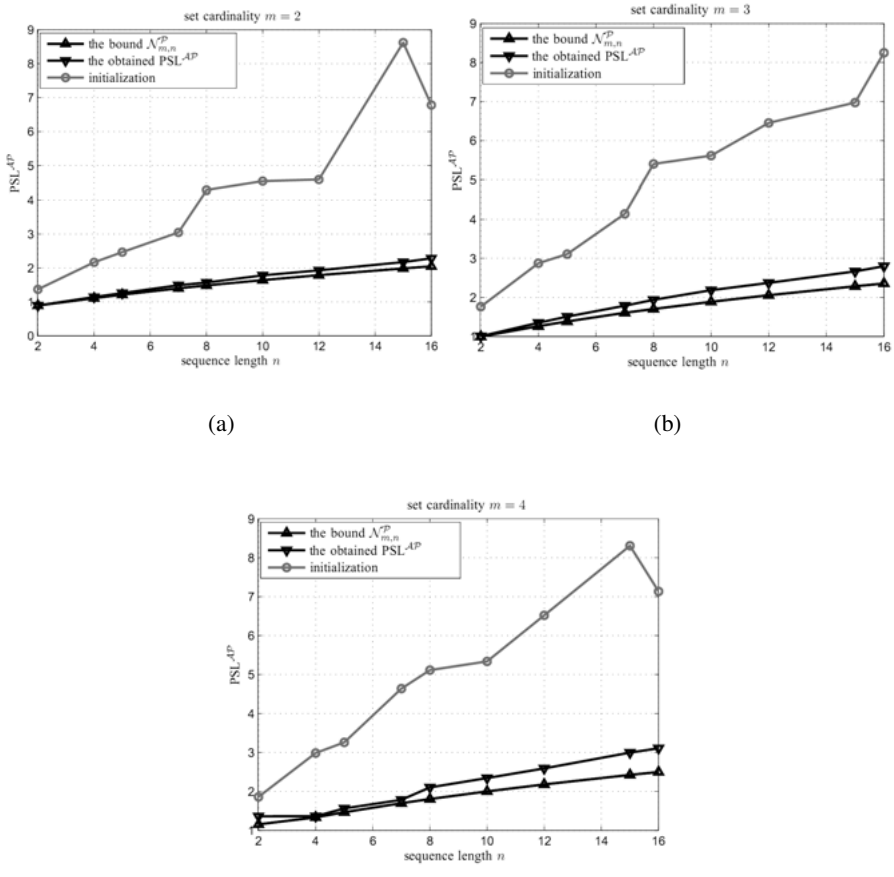

Figure 4.5. $\mathrm{PSL}^{\mathscr{A}\mathscr{P}}$ of the obtained sequence sets by using the algorithm in Table 4.2 (aperiodic case), versus sequence length *n*, for different set cardinalities *m*.

5. On Prime Root-of-Unity Sequences with Perfect Periodic Correlation

Abstract
In this chapter, Perfect Root-of-Unity Sequences (PRUS) with entries in $\alpha_p = \{x \in \mathbb{C} \mid x^p = 1\}$ (where p is a prime) are studied. A lower bound on the number of distinct phases that are used in PRUS over α_p is derived. We show that PRUS of length $L \geq p(p-1)$ must use all phases in α_p. Certain conditions on the lengths of PRUS are derived. Showing that the phase values of PRUS must follow a given difference multiset property, we derive a set of equations (which we call the principal equations) that give possible lengths of a PRUS over α_p together with their phase distributions. The usefulness of the principal equations is discussed, and guidelines for efficient construction of PRUS are provided. Through numerical results, also contributions are made to the current state-of-knowledge regarding the existence of PRUS. In particular, a combination of the developed ideas allowed us to numerically settle the problem of existence of PRUS with $(L, p) = (28, 7)$ within about two weeks— a problem whose solution (without using the ideas in this chapter) would likely take more than three million years on a standard PC.

Keywords: Perfect sequences, root-of-unity sequences, periodic autocorrelation, phase distribution, sequence construction

5.1 Introduction

Perfect Root-of-Unity Sequences (PRUS), also known as perfect N-phase [86], N-ary [87], or polyphase [88] sequences, are sequences with entries in $\alpha_N = \{x \in \mathbb{C} \mid x^N = 1\}$ and the property that all their out-of-phase periodic autocorrelations are equal to zero [39] [91]. These sequences are of interest in several applications including synchronization [92], fast startup equalization and channel estimation [86], as well as communication schemes such as Direct-Sequence Spread-Spectrum Multiple-Access (DS/SSMA) and Frequency Hopping Spread-Spectrum Multiple-Access (FH/SSMA) [93]. They can also be used as key probing sequences in active sensing, including for instance, pulse compression for continuous-wave radars [39] [93]. We note that, while sequences with good periodic correlations have many applications, there are also cases in which good aperiodic correlation properties are required. For example, in synchronization applications, sequences with good periodic correlation may be used when the sequence can be transmitted several times in succession, whereas sequences with good aperiodic correlation are required when the sequence can be used only once [92]. Interestingly, PRUS can be shown to have low autocorrelation sidelobes even in some aperiodic scenarios [93].

Note that a larger sequence length, in general, provides more degrees of freedom that can be used to improve the performance metrics in communications and sensing applications. On the other hand, sequences with short lengths can be of interest due to their lower associated costs, or in specific applications such as short-range active sensing [39] [91]. In cases where a finite-alphabet is required, the size of the alphabet plays an important role in the complexity of implementation; the smaller the alphabet size, the easier the implementation [95]. With this fact in mind, it is interesting to note that 4, 6 and 11 out of the first 8, 16 and 32 natural numbers, respectively, are

prime. The study of PRUS with prime-size alphabets is important not only because of this relatively high density of prime numbers in small alphabet sizes, but also because of the role of prime numbers as building blocks of natural numbers. A similar building block property can be seen in the PRUS case: let $n = mk$ where m and k are co-prime and assume that there exist PRUS $\boldsymbol{u} = (u_0, \cdots, u_{m-1})$ and $\boldsymbol{v} = (v_0, \cdots, v_{k-1})$ with alphabet sizes $m^\dagger$ and $k^\dagger$ respectively; then $\boldsymbol{w} = (w_0, \cdots, w_{n-1})$ where $w_l = u_{(l \bmod m)} v_{(l \bmod k)}$ is a PRUS with alphabet size $n^\dagger = m^\dagger k^\dagger$. This construction is known as Chinese Remainder Theorem (CRT) construction or simply as the direct product [96].

A general computational framework for designing sequences with optimal correlation was proposed in [83]. We note that sequences with unit-modulus entries, known as *unimodular* sequences, have been of interest due to their minimal peak-to-average power ratio (PAR). It is known that for lengths L that are *square-free* there exist an infinite number of *independent* unimodular sequences with perfect periodic correlation, see [90]. A fast computational method to find perfect unimodular sequences is proposed in [8]. Construction of *infinite* unimodular sequences with perfect correlation is studied in [98]. Algebraic constructions for perfect unimodular sequences of lengths p, $2p$, $3p$, pp' and p^s (where p and p' are prime) were introduced and studied in [99]- [103]. When it comes to root-of-unity sequences (which correspond to the finite alphabet case of the unimodular sequences), the problem appears to be more complicated. For example, it is not known whether there exists none, a few or plenty of PRUS for some lengths or alphabet sizes. Besides construction methods, some publications (e.g. [86], [104]) have introduced and used the following necessary condition on PRUS: if $\mathbf{x} = \{x_l\}_{l=0}^{L-1}$ is a PRUS of length L then

$$\left| \sum_{l=0}^{L-1} x_l \right| = \sqrt{L} \tag{5.1}$$

This necessary condition follows directly from the fact that the DFT of a PRUS has a constant magnitude (note that the DFT value at zero frequency is the sum of the sequence). In [87], several useful results are obtained which can be combined with the results in this chapter. Namely, it was shown in [87] that the existence of PRUS of length $L = mp$ (for a prime p) with entries in α_p is connected to the existence of (L, p, L, m)-relative difference sets. Using some existence results of relative difference sets, the authors in [87] prove for example that there is no PRUS of length $L = p^s$ (for $s \geq 3$), $L = 2p^s$ (for $s \geq 1$), and $L = pp'$ (for prime $p' > p$) with entries in α_p. However, the strongest claim in the literature regarding the existence (and construction) of PRUS is known as the Mow's conjecture [93]:

Mow's conjecture (for prime p): Let M(L,p) be the total number of PRUS with length L over α_p. Let $L = sq^2$, where s and q are both natural numbers

and s is square-free. Then

$$M(L,p) = \begin{cases} q!s^q\Phi^q(s)p^m, & p_{\min} = p, \\ 0, & otherwise, \end{cases} \tag{5.2}$$

where

$$p_{\min} = \begin{cases} 2sq, & for\ s\ even\ and\ m\ odd, \\ sq, & otherwise, \end{cases} \tag{5.3}$$

and the Euler totient function $\Phi(n)$ shows the number of $k \in \mathbb{Z}_n$ for which k and n are co-prime, and $\Phi(1) = 1$ by definition. Moreover, all such PRUS can be constructed using a unified approach, see [93].

Note that a proof of Mow's conjecture would imply that no PRUS of lengths other than $L = p$ and $L = p^2$ exists over α_p. In this work, PRUS with a prime-size alphabet are studied. In particular, we study the *phase distribution* of such sequences, and introduce a set of *principal equations* that can yield the possible phase distributions of PRUS for any given p and L. In general, the provided phase distributions can significantly reduce the size of search space for finding PRUS. Based on the obtained phase distributions, we also provide practical guidelines for construction of PRUS. A combination of the ideas in this chapter provides us, for example, with the possibility to numerically settle the problem of the existence of PRUS for $(L,p) = (28,7)$ within two weeks; a problem for which an exhaustive search of the associated search space is guaranteed to take more than three million years on a standard PC.

The rest of this chapter is organized as follows. In Section 5.2, the phase distribution of PRUS over α_p is discussed. We show that the phase values of PRUS over α_p must follow a specific difference multiset property. Furthermore, Section 5.2 presents the principal equations. Section 5.3 is devoted to the study of some special cases. A discussion on the usefulness of the principal equations as well as guidelines for an efficient construction of perfect sequences along with some examples are included in section 5.4. In Section 5.5, we provide our numerical results. Finally, Section 5.6 concludes the chapter.

Notation: We use bold lowercase letters for vectors/sequences and bold uppercase letters for matrices. See Table 5.1 for other notations used throughout this chapter.

5.2 Phase Study

Let $\mathbf{x} = \left\{ e^{j\frac{2\pi}{p}k_l} \right\}_{l=0}^{L-1}$ be a PRUS over α_p. In this section, we study the phase distribution of PRUS over the alphabet α_p of prime size:

Table 5.1. *Notations*

$x(k)$:	the k^{th} entry of the vector $\mathbf{x}$
$\mathbf{x}^{\updownarrow}$:	the vector containing the same entries as $\mathbf{x}$ but in reversed order
$\|\mathbf{x}\|_n$:	the l_n-norm of the vector $\mathbf{x}$, defined as $(\sum_k \|x(k)\|^n)^{\frac{1}{n}}$
$\boldsymbol{X}^*$:	the complex conjugate of a matrix $\boldsymbol{X}$
$\boldsymbol{X}^T$:	the transpose of a matrix $\boldsymbol{X}$
$\mathrm{tr}(\boldsymbol{X})$:	the trace of a matrix $\boldsymbol{X}$
$\|\boldsymbol{X}\|$:	the Frobenius norm of a matrix $\boldsymbol{X}$
$\boldsymbol{X} \odot \boldsymbol{Y}$:	the Hadamard element-wise product of two matrices $\boldsymbol{X}$ and $\boldsymbol{Y}$ of the same dimension
$\mathbf{0}_n$:	the all zero vector of length n
$\mathbf{1}_\mathbf{n}$:	the all one vector of length n
$\boldsymbol{e}_l^{(n)}$:	the l^{th} standard basis vector in $\mathbb{R}^n$
$\mathbb{N}$:	the set of natural numbers
$\mathbb{Z}$:	the set of integer numbers
$\mathbb{R}$:	the set of real numbers
$\mathbb{C}$:	the set of complex numbers
$\mathbb{Z}_n$:	the set $\{0,1,\cdots,n-1\}$
$[\cdot]$:	a multiset in which multiplicities of elements are permitted
p:	a prime number

Definition 1. *Let μ_k denote the number of times that $e^{j\frac{2\pi}{p}k}$ (for $k \in \mathbb{Z}_p$) occurs in $\mathbf{x}$. Then $\{\mu_k\}_{k=0}^{p-1}$ is called the phase distribution of $\mathbf{x}$.*

Note that all k_l are in $\mathbb{Z}_p$, and will be referred to as the *integer phases* of the sequence. The periodic autocorrelation of $\mathbf{x}$ at any lag $u \in \mathbb{Z}_L$ is defined as

$$\begin{aligned} R_u &= \sum_{l=0}^{L-1} e^{j\frac{2\pi}{p}(k_l - k_{l+u})} \\ &= \begin{cases} L & u = 0 \\ 0 & u \in \mathbb{Z}_L - \{0\} \end{cases} \end{aligned} \tag{5.4}$$

where the indices of $\{k_l\}$ are used in a periodic manner (i.e. *mod* L). It is interesting to note that R_u is a summation of terms which are also in α_p. Theorem 1 paves the way for using this observation (see Appendix 5.7.1 for a short proof):

Theorem 1. *If $\sum_{k=0}^{p-1} a_k e^{j\frac{2\pi}{p}k} = 0$ for some $a_k \in \mathbb{Z}$, then all a_k must be identical.*

Corollary 1. *If there exists a PRUS of length L over α_p then $p|L$.*

Proof: Let $u \in \mathbb{Z}_L - \{0\}$. Then it follows from (5.4) and Theorem 1 that $R_u = m\sum_{k=0}^{p-1} e^{j\frac{2\pi}{p}k} = 0$ where $m = L/p$ must be an integer. ■

The fact pointed out in Corollary 1 is already known in the literature, see e.g. [87]. However, it is worthwhile to comment on the more general case of PRUS of length L over α_N. From a number theory perspective, the authors of [106] study the *vanishing sums of roots-of-unity*, viz. $q_1+q_2+\cdots q_T=0$ with $q_l \in \alpha_N$ (for all l), and general $N \in \mathbb{N}$. In particular, they show that if $N = p_1^{a_1}\cdots p_r^{a_r}$ (with $p_1 < \cdots < p_r$) represent the prime factorization of N then a vanishing sum of T root-of-unity numbers $\{q_l\}$ (with $q_l \in \alpha_N$) can occur only if there exist non-negative integers $\{t_k\}$ such that T can be written as $T = t_1 p_1 + \cdots + t_r p_r$. Interestingly, we can use this result in the context of PRUS. Namely, the autocorrelation sums similar to that in (5.4) may become zero only if L can be written as

$$L = t_1 p_1 + \cdots + t_r p_r \tag{5.5}$$

where $\{t_k\}$ are non-negative integers. Therefore, satisfying (5.5) is a necessary condition for a PRUS of length L over α_N. Considering (5.5), also typically known as the *Frobenius coin problem* [107]- [109], can be particularly useful for showing the non-existence of PRUS when L is rather small. On the contrary, it can be shown that if $L \geq (p_1-1)(p_2-1)$ then (5.5) always has a solution.

In the sequel, we use the notation $L = mp$, $m \in \mathbb{N}$, for the length of PRUS over α_p.

Corollary 2. *Let* $\mathbf{x} = \left\{ e^{j\frac{2\pi}{p}k_l} \right\}_{l=0}^{mp-1}$ *be a PRUS of length* $L = mp$ *over* α_p. *Then for every* $s \in \mathbb{Z}_p$ *and* $u \in \mathbb{Z}_L - \{0\}$, *there exist exactly m distinct integers* $\{l\}$ *such that* $k_l \equiv k_{l+u} + s \ (mod\ p)$.

Proof: We only need to observe that, according to Theorem 1, all sums in (5.4) for $\{R_u\}_{u\in\mathbb{Z}_L-\{0\}}$ must have exactly m terms equal to $e^{j\frac{2\pi}{p}s}$ for every $s \in \mathbb{Z}_p$. ■

We note that in light of the above results, a general difference set structure is obtained [110], [111].

Definition 2. *Let* $D = [d_0, d_1, \cdots, d_{s-1}]$ *be a multiset over a group G of order v. D is a* (v,s,λ)*-difference multiset over G iff the multiset* $\Delta_D = [d_k - d_l : k,l \in \mathbb{Z}_s,\ k \neq l]$ *contains each element of G (*0 *included) exactly* λ *times.*

By this definition, the multiset of integer phases $[k_0, k_1, \cdots, k_{L-1}]$ of a PRUS of length $L = mp$ over α_p is a (p, mp, m)-difference multiset. Such an observation will enable us to study in detail the phase distribution of PRUS via Theorems 2-4. We note that there exist several construction methods for PRUS with length $L = p$; see Section 5.3 for details. Moreover, the case of $L = p$ presents some unique properties (see sub-section 5.2.1) that makes its study relevant.

We also study the PRUS of length $L = mp$, $m > 1$, and present our general results about them in sub-section 5.2.2. The next two definitions appear to be essential in order to continue our study.

Definition 3. *Let $\xi_0, \cdots, \xi_{t-1}$ be real numbers whose sum is a constant C. From the Cauchy-Schwarz inequality we have that*

$$\|\boldsymbol{\xi}\|_2^2 \geq \left(\mathbf{1_t^T}\boldsymbol{\xi}\right)^2 / t \tag{5.6}$$

where $\boldsymbol{\xi}$ is the vector with entries $\{\xi_k\}$. Therefore, $\sum_{k=0}^{t-1} \xi_k^2$ attains its minimum value when the sum is uniformly distributed over $\{\xi_k\}$. We define

$$\Gamma(C,t) \triangleq \begin{cases} C^2/t & t > 0 \\ 0 & otherwise \end{cases} \tag{5.7}$$

as the minimum value of the sum of squares of t real variables with sum C.

Definition 4. *We let $\boldsymbol{\Phi}_x$ be the circulant matrix made from the integer phases $\{k_l\}$ of the sequence $\mathbf{x}$, viz.*

$$\boldsymbol{\Phi}_x \triangleq \begin{pmatrix} k_0 & k_1 & \cdots & k_{mp-1} \\ k_{mp-1} & k_0 & \cdots & k_{mp-2} \\ \vdots & \vdots & \ddots & \vdots \\ k_1 & k_2 & \cdots & k_0 \end{pmatrix}. \tag{5.8}$$

For the l^{th} column of $\boldsymbol{\Phi}_x$, consider the location of the entries which are equal to k_l ($l = 0, \cdots, mp-1$). Considering these locations for all columns, we build an $mp \times mp$ equivalence matrix $\boldsymbol{\Phi}_e$ of $\mathbf{x}$ whose entries in the mentioned locations are 1; otherwise they are 0. We also extend the definition of $\boldsymbol{\Phi}_e$ to $\boldsymbol{\Phi}_e^{(s)}$ (with $\boldsymbol{\Phi}_e^{(0)} = \boldsymbol{\Phi}_e$), for $s \in \mathbb{Z}_p$ as follows: by finding the locations of the entries $k_{l'}$ in the l^{th} column of $\boldsymbol{\Phi}_x$ such that $k_{l'} \equiv k_l + s \pmod p$, we represent these locations in $\boldsymbol{\Phi}_e^{(s)}$ by 1, and by 0 otherwise.

The interested reader can find more details on the element-wise construction of $\{\boldsymbol{\Phi}_e^{(s)}\}$ in Section 5.4— see particularly (5.38), and the related discussions.

5.2.1 The case of $L = p$ (corresponding to $m = 1$)

Based on the above discussions, the integer phases of PRUS with length $L = p$ over α_p have a $(p, p, 1)$-difference multiset structure. Such PRUS are in close connection with prime-length binary sequences with optimal periodic correlation. A detailed discussion revealing such close relationship is provided in Appendix 5.7.2. Theorem 2 studies the phase distribution of PRUS in this case.

Theorem 2. *A PRUS of length $L = p > 2$ over α_p has exactly $\frac{1}{2}(p+1)$ distinct phases. Even more precisely, such PRUS consists of a singleton and $\frac{1}{2}(p-1)$ equi-phase pairs.*

Proof: Note that due to the $(p,p,1)$-difference multiset structure, all rows of $\mathbf{\Phi}_e$ (in this case) have exactly one 1 except the first row whose all entries are 1. Now let $\{\mu_k\}$ represent the phase distribution of the sequence, and let us assume that t of $\{\mu_k\}$ are nonzero. We have

$$\sum_{k=0}^{p-1} \mu_k = p. \tag{5.9}$$

As discussed above, by considering the rows of $\mathbf{\Phi}_e$, we conclude that there are $(2p-1)$ ones in $\mathbf{\Phi}_e$. On the other hand, since for every integer phase $k \in \mathbb{Z}_p$ we have μ_k columns with μ_k ones in each of them, the number of ones in $\mathbf{\Phi}_e$ is equal to $\sum_{k=0}^{p-1} \mu_k^2$; hence

$$\sum_{k=0}^{p-1} \mu_k^2 = 2p-1. \tag{5.10}$$

Since the sum of μ_k is constant, we have

$$2p-1 = \sum_{k=0}^{p-1} \mu_k^2 \geq \Gamma(p,t) = \frac{p^2}{t}, \tag{5.11}$$

and as a result

$$t \geq \left\lceil \frac{p^2}{2p-1} \right\rceil = \left\lceil \frac{1}{2}(p-1) + \frac{3p-1}{4p-2} \right\rceil = \frac{1}{2}(p+1) \tag{5.12}$$

where $\lceil x \rceil$ denotes the smallest integer greater than or equal to x. Now let us suppose that $t \geq \frac{1}{2}(p+1)+1 = \frac{1}{2}(p+3)$. Also let v_1 be the number of $\{\mu_k\}$ which are equal to one. Therefore

$$p = \sum_{k=0}^{p-1} \mu_k \geq v_1 + 2(t-v_1) = 2t - v_1. \tag{5.13}$$

Note that (5.13) implies $v_1 \geq 2t - p \geq 3$. This leads to a contradiction for $p = 3$ as all phases should be different; i.e. $\mu_0 = \mu_1 = \mu_2 = 1$ which yields $\sum_{k=0}^{p-1} \mu_k^2 \neq 2(3) - 1$. Next we consider the case of $p \geq 5$. Note that

$$\sum_{k=0}^{p-1} \mu_k^2 \geq v_1 + \Gamma\left(p - v_1, \frac{p+3}{2} - v_1\right). \tag{5.14}$$

By substituting (5.10) in (5.13) we get $v_1 \leq 3$ and as a result $v_1 = 3$. Now let $\mu_{k_*} \geq 2$ for some $k_* \in \mathbb{Z}_p$; then

$$\sum_{k=0}^{p-1} \mu_k^2 \geq 3 + \mu_{k_*}^2 + \Gamma\left(p - 3 - \mu_{k_*}^2, \frac{p+3}{2} - 4\right). \tag{5.15}$$

Again by substituting (5.10) in (5.15) we obtain $\mu_{k_*} \leq 3$. This shows that except for $\mu_k = 1$, the only possible values of μ_k are 2 and 3. Let us denote the number of them by v_2 and v_3, respectively. Then:

$$\begin{cases} 3 + 2v_2 + 3v_3 = p \\ 3 + 4v_2 + 9v_3 = 2p - 1 \end{cases} \tag{5.16}$$

which is not feasible for integer numbers v_2 and v_3. Thanks to the latter contradiction, we conclude that the number of distinct phases is equal to $t = \frac{1}{2}(p+1)$. In order to obtain a complete picture of the phase distribution of $\mathbf{x}$, let v_k denote the number of $\{\mu_k\}$ which are equal to k, for all $k \in \mathbb{Z}_p$. Using the inequality in (5.13) we have that $v_1 \geq 2t - p \geq 1$. On the other hand,

$$\sum_{k=0}^{p-1} \mu_k^2 \geq v_1 + \Gamma\left(p - v_1, \frac{p+1}{2} - v_1\right) \tag{5.17}$$

which implies $v_1 \leq 1$, and as a result $v_1 = 1$. If $\mu_{k_*} \geq 2$ for some $k_* \in \mathbb{Z}_p$ then

$$\sum_{k=0}^{p-1} \mu_k^2 \geq 1 + \mu_{k_*}^2 + \Gamma\left(p - 1 - \mu_{k_*}^2, \frac{p+1}{2} - 2\right). \tag{5.18}$$

As before, by substituting (5.10) in (5.18) we obtain $\mu_{k_*} \leq 2$, and hence $\mu_{k_*} = 2$. This implies that $v_2 = \frac{1}{2}(p-1)$ and $v_k = 0$ for $k > 2$ which completes the proof. ■

5.2.2 The case of $L = mp$ (general case)

As indicated earlier, the integer phases of a PRUS of length $L = mp$ over α_p build a (p, mp, m)-difference multiset, which implies that for every $u \in \mathbb{Z}_L - \{0\}$, there exist exactly m distinct integers $\{l\}$ such that $k_l = k_{l+u}$. Therefore, for an $mp \times mp$ matrix $\mathbf{\Phi}_e$ built as in Definition 4, the number of ones is equal to $mp + m(mp-1)$. Let $\{\mu_k\}$ represent the phase distribution of the sequence. Then we have that

$$\sum_{k=0}^{p-1} \mu_k = mp, \tag{5.19}$$

$$\sum_{k=0}^{p-1} \mu_k^2 = mp + m(mp-1). \tag{5.20}$$

We assume t of $\{\mu_k\}$ are nonzero, which implies

$$\begin{aligned} m^2p+m(p-1) &= \sum_{k=0}^{p-1}\mu_k^2 \\ &\geq \Gamma(mp,t)=\frac{(mp)^2}{t}, \end{aligned} \tag{5.21}$$

and as a result

$$t \geq \frac{mp^2}{(m+1)p-1}. \tag{5.22}$$

The above lower bound shows that as m increases, a larger number of phases from α_p might be needed to build a PRUS of length $L=mp$. For sufficiently large values of m we need all phases:

Theorem 3. *For $m \geq p-1$, all phase values must be used in a PRUS.*

Proof: This is a direct consequence of the lower bound in (5.22). ■

Now, for every $s \in \mathbb{Z}_p - \{0\}$ we consider the matrix $\mathbf{\Phi}_e^{(s)}$ built as in Definition 4. Based on the difference multiset property, for every $u \in \mathbb{Z}_L - \{0\}$, there exist exactly m distinct integers $\{l\}$ such that $k_{l+u} \equiv k_l + s \ (mod\ p)$. Therefore, the matrix $\mathbf{\Phi}_e^{(s)}$ has exactly m ones in each of its rows except for the first row which is all zero. This implies that $\mathbf{\Phi}_e^{(s)}$ has $m(mp-1)$ ones. On the other hand, the number of ones in $\mathbf{\Phi}_e^{(s)}$ is equal to $\sum_{k=0}^{p-1}\mu_k\mu_{k+s}$ as it equals the number of all pairs with the property $k_{l+u} \equiv k_l + s \ (mod\ p)$. Therefore, the out-of-phase correlations of the sequence $\{\mu_k\}$ are given by

$$\sum_{k=0}^{p-1}\mu_k\mu_{k+s} = m(mp-1), \quad s \in \mathbb{Z}_p - \{0\}. \tag{5.23}$$

Based on (5.19), (5.20) and (5.23), we conclude the following.

Theorem 4. *Let $\{\mu_k\}$ denote the phase distribution of a PRUS with length $L=mp$ over α_p. If we define $r_k \triangleq \mu_k - m$, then $\{r_k\}$ satisfy the following set of **principal equations**:*

$$\begin{cases} \sum_{k=0}^{p-1} r_k = 0 \\ \sum_{k=0}^{p-1} r_k^2 = m(p-1) \\ \sum_{k=0}^{p-1} r_k r_{k+s} = -m, \quad s \in \mathbb{Z}_p - \{0\}. \end{cases} \tag{5.24}$$

Solving the principal equations indicate the possible PRUS phase distributions for given L and p. It is interesting to note that if $\{r_k\}$ is a solution to

(5.24), then $\{-r_k\}$, $\{r_{-k}\}$ and $\{r_{k+l}\}$ where $l \in \mathbb{Z}_p$ are also valid solutions to (5.24). In other words, the set of principal equations induces a certain type of equivalence class on its solutions. We note that the unimodular perfect sequences enjoy a similar set of equivalence properties: let $\mathbf{x}$ be a unimodular perfect sequence, then $\mathbf{x}^*$ and $e^{j\phi}\mathbf{x}$ (where ϕ can be chosen arbitrarily) are also unimodular perfect sequences. This shows that given a solution $\{r_k\}$ to the principal equations, the solutions $\{r_{-k}\}$ and $\{r_{k+l}\}$ do not lead to new PRUS. In contrast, the solution $\{-r_k\}$ might lead to new sequences. As an aside remark, note that the second equation of (5.24) can be viewed as a *sum of squares problem*, which has been widely studied for many years. More details on this aspect are deferred to Appendix 5.7.3. The following discussion is devoted to a geometrical study of the problem.

Let $\boldsymbol{r}_0 = (r_0, \cdots, r_{p-1})^T$ and also let $\boldsymbol{r}_k$ represent the circularly shifted version of $\boldsymbol{r}_0$ by $k \in \mathbb{Z}_p$. The principal equations can be rephrased as follows over the vectors $\{\boldsymbol{r}_k\}$:

$$\begin{cases} \mathbf{1}_\mathbf{p}^\mathbf{T}\boldsymbol{r}_\mathbf{k} = \mathbf{0} \\ \|\boldsymbol{r}_k\|_2 = \sqrt{m(p-1)} \\ \boldsymbol{r}_k^T\boldsymbol{r}_l = -m, \quad k \neq l \end{cases} \tag{5.25}$$

The angle between each pair of vectors $\{(\boldsymbol{r}_k, \boldsymbol{r}_l)\}_{k\neq l}$ is given by

$$\theta = \arccos\left(\frac{\boldsymbol{r}_k^T\boldsymbol{r}_l}{\|\boldsymbol{r}_k\|_2\|\boldsymbol{r}_l\|_2}\right) = \arccos\left(\frac{-1}{p-1}\right) \tag{5.26}$$

Therefore, $\{\boldsymbol{r}_k\}_{k\in\mathbb{Z}_p}$, form a set of p vectors lying in a $(p-1)$-dimensional space which is the hyperplane orthogonal to $\mathbf{1}_\mathbf{p}$ and the angle between each pair of them is the value given in (5.26). We further note that the structure made by connecting all vertices pointed by $\{\boldsymbol{r}_k\}$ is a known multi-dimensional object called a *regular simplex* [112]. Such structures are shown in Fig. 5.1 for one, two and three dimensions. The reference [112] suggests $\{\boldsymbol{e}_k^{(p)}\}$ (i.e. the standard basis) as vertices of a regular simplex of edge $\sqrt{2}$ lying in the hyperplane $\mathbf{1}_\mathbf{p}^\mathbf{T}\mathbf{x} = \mathbf{1}$. It can be easily verified that

$$\widetilde{\boldsymbol{r}}_0 = \left((p-1)\sqrt{\frac{m}{p}}, -\sqrt{\frac{m}{p}}, \cdots, -\sqrt{\frac{m}{p}}\right)^T \in \mathbb{R}^p \tag{5.27}$$

together with its circularly shifted versions (denoted by $\{\widetilde{\boldsymbol{r}}_k\}$) satisfy the principal equations. It is also straightforward to verify that these points can be obtained from the vectors $\{\boldsymbol{e}_k^{(p)}\}$ by a scaling and a translation. As every two regular simplexes with their center at $\mathbf{0}_p$ can be obtained from each other by a set of rotations, we can find the vectors $\{\boldsymbol{r}_k\}$ by rotations of $\{\widetilde{\boldsymbol{r}}_k\}$ such that their end lie at the integral lattice. Note that as the regular simplex made by $\{\widetilde{\boldsymbol{r}}_k\}$ is in a $(p-1)$-dimensional space, its rotation could be parametrized with

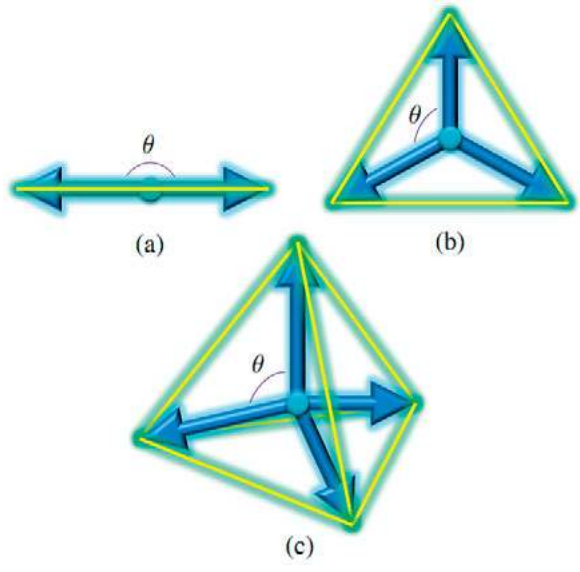

Figure 5.1. (a-c) Regular simplexes in one, two and three dimensional space. In n dimensions they can be characterized with $n+1$ vectors with the same l_2-norm and also the same angle between them as described in Eq. (5.26).

$(p-2)$ angles $\psi_0, \cdots, \psi_{p-3}$ and as a result the vectors $\{\boldsymbol{r}_k\}$ could be written as a function of $\sin\psi_k$ and $\cos\psi_k$ for $k \in \mathbb{Z}_{p-2}$. Taking into consideration the fact that $\{\boldsymbol{r}_k\}$ are integral, this gives a closed form solution for m (and as a result a closed form solution for the sequence length) as well as the phase distribution. We give an example of the usage of such a geometrical approach in Section 5.3. Nevertheless, for large values of L and p, an efficient numerical approach to tackle the principal equations is discussed in Appendix 5.7.4.

5.3 Special Cases

This section not only considers special cases associated with the principal equations but also aims to establish the connections between the results in Section 5.2 and the existing literature on PRUS. Several special cases for m and p are discussed. The cases $m = 1$ and $m = p$ are discussed because of the well-known constructions which give sequences for these values. Additionally, we study the case of $m = h^2 m'$ where a solution for the principal equations can be found for length $L' = m'p$. The special cases $p = 2$ and $p = 3$ are also discussed to give closed form solutions for the length and phase distribution of PRUS. The case $p = 3$ can be considered as an example of using the geometrical approach based on the regular simplex to solve the principal equations.

5.3.1 Special Cases of m

- $m = 1$ and $m = p$: Sequences with $m = 1$ (i.e. length $L = p$) can be constructed for example by Zadoff, Chu, Golomb polyphase, P3 and P4 methods [39]. These methods are all based on quadratic integer phases and it is easy to verify that all of them follow the distribution given in Section 5.2.1. Examples of construction methods for $m = p$ (i.e. length $L = p^2$) include Frank and P1 methods [39]. Sequences of this length contain all phase values, see Theorem 3.
- $m = h^2 m'$: Let $\{r_k^{(m')}\}$ be a solution of the principal equations for length $L' = m'p$ over α_p. Then, one can verify that $\{r_k^{(m)}\} = \{hr_k^{(m')}\}$ is a solution of the principal equations for the length $L = mp$. Interestingly, the Mow's conjecture suggests that the latter consruction of solutions for the principal equations cannot lead to new PRUS. Nevertheless, existence of such PRUS is not disproved by the principal equations.

5.3.2 Special Cases of p

- $p = 2$: Solving the principal equations, viz.

$$\mu_0^2 + \mu_1^2 = 2m^2 + m \tag{5.28}$$
$$2\mu_0\mu_1 = 2m^2 - m \tag{5.29}$$

  for this case (which is the case of perfect binary sequences) yields $\mu_0 = \frac{1}{2}\left(2m \pm \sqrt{2m}\right)$ and $\mu_1 = \frac{1}{2}\left(2m \mp \sqrt{2m}\right)$. Therefore m must be of the form $2h^2$ and as a result $\mu_0 = 2h^2 \pm h$ and $\mu_1 = 2h^2 \mp h$. This enumeration of $+1$ and -1 in perfect binary sequences can be obtained also by the necessary condition (5.1) and is mentioned in several publications including [113].
- $p = 3$: Here we use the geometrical approach discussed in Section 5.2.2 to solve the principal equations. For 3-phase perfect sequences, the vectors $\{\boldsymbol{r}_k\}$ make a two dimensional regular simplex orthogonal to $\mathbf{1_3}$, which has 3 vectors and each two of them have an angle of $\frac{2\pi}{3}$. The structure of this regular simplex is shown in Fig. 5.1(b). Let $\boldsymbol{R}_{\mathbf{1_3}}$ be the unitary rotation matrix which maps $\mathbf{1_3}$ to $\sqrt{3}\boldsymbol{e}_3^{(3)}$. Also let

$$\boldsymbol{r}'_k = \sqrt{2m}\begin{pmatrix} \cos\left(\frac{2k\pi}{3} + \psi\right) \\ \sin\left(\frac{2k\pi}{3} + \psi\right) \\ 0 \end{pmatrix} \tag{5.30}$$

for $k \in \mathbb{Z}_3$ and $\psi \in [0, 2\pi)$. Therefore, $\boldsymbol{r}_k$ is equal to $\boldsymbol{R}_{\mathbf{1_3}}^{-1} \boldsymbol{r}'_k$ for some ψ. This implies that $\boldsymbol{r}_k \in \mathbb{Z}^3$ is of the form

$$\sqrt{2m} \begin{pmatrix} \frac{\sqrt{2}}{2} \cos\left(\frac{2k\pi}{3} + \psi\right) - \frac{\sqrt{6}}{6} \sin\left(\frac{2k\pi}{3} + \psi\right) \\ \frac{\sqrt{6}}{3} \sin\left(\frac{2k\pi}{3} + \psi\right) \\ -\frac{\sqrt{2}}{2} \cos\left(\frac{2k\pi}{3} + \psi\right) - \frac{\sqrt{6}}{6} \sin\left(\frac{2k\pi}{3} + \psi\right) \end{pmatrix}$$

for $k \in \mathbb{Z}_3$. As $\{\boldsymbol{r}_k\}$ are the circularly shifted versions of each other, it is sufficient to study one of them. For $k = 0$, we infer that both $h_1 = 2\sqrt{\frac{m}{3}} \sin \psi$ (which is the second entry of $\boldsymbol{r}_0$) and $h_2 = 2\sqrt{m} \cos \psi$ (which is the difference between the first and the third entry of $\boldsymbol{r}_0$) must be integers. We conclude that $3h_1^2 + h_2^2 = 4m$ and

$$\boldsymbol{r}_0 = \frac{1}{2} \begin{pmatrix} (h_2 - h_1) \\ 2h_1 \\ -(h_2 + h_1) \end{pmatrix}. \tag{5.31}$$

Therefore, the sequence length must be of the form

$$L = \frac{1}{4} \left(9h_1^2 + 3h_2^2\right) \tag{5.32}$$

while its phase distribution is given by

$$\frac{1}{4} \left(3h_1^2 + h_2^2\right) \mathbf{1}_3 + \frac{1}{2} \begin{pmatrix} (h_2 - h_1) \\ 2h_1 \\ -(h_2 + h_1) \end{pmatrix}, \tag{5.33}$$

for integers h_1 and h_2.

5.4 PRUS: From Phase Distributions to Construction

In this section, we discuss the use of the ideas introduced earlier for an efficient search or construction of PRUS.

5.4.1 Are the Principal Equations Useful?

First we show that if $\{r_k\}$ satisfy the principal equations, then the necessary condition in (5.1) will be satisfied; i.e. the principal equations are more informative than (5.1). Let S be the sum of entries of the PRUS:

$$S \triangleq \sum_{l=0}^{mp-1} e^{j\frac{2\pi}{p}k_l} = \sum_{k=0}^{p-1} \mu_k e^{j\frac{2\pi}{p}k}. \tag{5.34}$$

For $\{r_k\}$ satisfying the principal equations:

$$\sum_{k=0}^{p-1} r_k r_{k+s} = \left(\sum_{k=0}^{p-1} r_k^2\right) - mp = -m, \quad s \in \mathbb{Z}_p - \{0\}. \tag{5.35}$$

Therefore,

$$\begin{aligned} |S|^2 &= \left|\sum_{k=0}^{p-1} \mu_k e^{j\frac{2\pi}{p}k}\right|^2 = \left|\sum_{k=0}^{p-1} r_k e^{j\frac{2\pi}{p}k}\right|^2 \\ &= \sum_{s=0}^{p-1}\left(\sum_{k=0}^{p-1} r_k r_{k+s}\right) e^{j\frac{2\pi}{p}s} = mp \end{aligned}$$

which implies the satisfaction of (5.1).

It is worth emphasizing that satisfaction of the principal equations is necessary but not sufficient for a PRUS. The necessity induced by the principal equations guarantees that if a sequence exists over α_p then it will have a specific length and phase distribution; particularly, the number of sequences which are needed to be checked for enumeration of PRUS of length L over α_p reduces from

$$p^L = \sum_{\{\mu_k \geq 0\}_{k=0}^{p-1}:\ \sum_{k=0}^{p-1}\mu_k = L} \binom{L}{\mu_0, \mu_1, \cdots, \mu_{p-1}} \tag{5.36}$$

to

$$\sum_{\{\mu_k\}_{k=0}^{p-1} \in\ \Omega} \binom{L}{\mu_0, \mu_1, \cdots, \mu_{p-1}} \tag{5.37}$$

where Ω represents the set of feasible phase distributions. Note that the expression (5.37) typically contains only a few out of $\binom{L+p-1}{p-1}$ summation terms of Eq. (5.36). Therefore, the principal equations can be used to show the impossibility of some lengths (in cases for which no feasible phase distribution exists) and to significantly reduce the size of search space of PRUS in general; see Section 5.5 for some numerical evidence on this aspect.

5.4.2 PRUS Construction: Guidelines and Examples

Once we have obtained the length and phase distribution of a PRUS, an efficient method for its construction (or further elimination of non-suitable cases) is needed. Hereafter, we aim to explain how a PRUS could be constructed using the $\{\mathbf{\Phi}_e^{(s)}\}$ matrices introduced in Section 5.2. Examples of such a construction for different scenarios are also provided.

For the $\mathbf{\Phi}_e$ matrix (built based on the equality of phases) we need an all one first row and exactly m ones in any other row. On the other hand, the

matrices $\{\mathbf{\Phi}_e^{(s)}\}_{s\neq 0}$ (built based on the inequality of phases) contain no ones in the first row and exactly m ones in the other rows. It is an important observation that *this condition is equivalent to the perfectness of the sequence* and as a result all we need is to check whether assigning different phases to indices in the sequence preserves this condition. Let us assume that the vector $\boldsymbol{\chi}_k = (\chi_k(0), \cdots, \chi_k(\mu_k - 1))^T$ contains the indices that are assigned to the k^{th} phase, i.e. $e^{j\frac{2\pi}{p}k}$. As an example, the configuration of the matrix $\mathbf{\Phi}_x$ and the corresponding vectors $\{\boldsymbol{\chi}_k\}$ are shown in Fig. 5.2 for the Frank sequence of length 9. As the $\mathbf{\Phi}_x$ matrix has a circulant structure, we can observe that rows

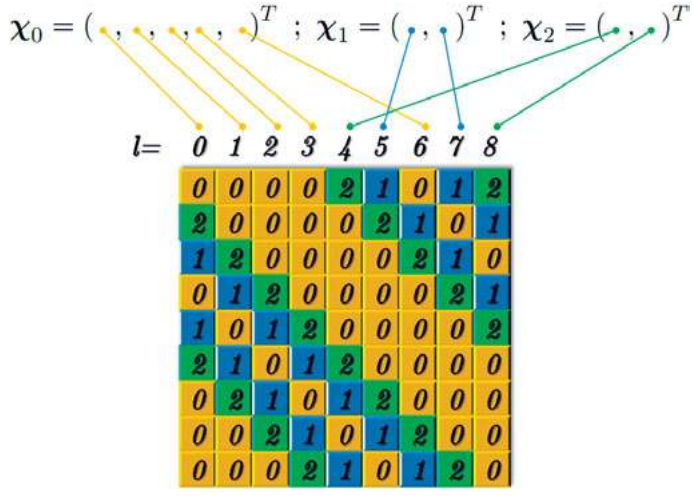

Figure 5.2. Configuration of $\mathbf{\Phi}_x$ and the vectors $\{\boldsymbol{\chi}_k\}$ for the Frank sequence of length 9.

of $\{\mathbf{\Phi}_e^{(s)}\}$ with a one in the $\chi_k(l)^{th}$ position are given by

$$(\chi_k(l) - \chi_k(1))\,\mathbf{1}_{\mu_{(\mathbf{k}+\mathbf{s})}} + \boldsymbol{\chi}^{\updownarrow}_{(\mathbf{k}+\mathbf{s})}. \tag{5.38}$$

Fig. 5.3 depicts the construction of the matrices $\{\mathbf{\Phi}_e^{(s)}\}$ for the Frank sequence of length 9 based on (5.38).

According to the above discussion, instead of the classical method based on calculation of the autocorrelation for all sequences, one can make updates of the matrices $\{\mathbf{\Phi}_e^{(s)}\}$ for each assignment of indices to phases in α_p respectively, and check whether for each assignment the number of nonzero entries in each row (except the first row) of the updated matrices $\{\mathbf{\Phi}_e^{(s)}\}$ does not exceed m. Note that since the matrices $\{\mathbf{\Phi}_e^{(s)}\}$ represent all distinct differences ($s \in \mathbb{Z}_p$ where $s = 0$ denotes the case of phase equality), they can be viewed as complementary binary matrices; i.e. (i) there exists no common positions for ones in the matrices $\{\mathbf{\Phi}_e^{(s)}\}$ (equivalently $\mathbf{\Phi}_e^{(s_1)} \odot \mathbf{\Phi}_e^{(s_2)}$ is an all zero matrix for any $s_1 \neq s_2$, where $s_1, s_2 \in \mathbb{Z}_p$), and (ii) the sum of matrices $\{\mathbf{\Phi}_e^{(s)}\}_{s\in\mathbb{Z}_p}$

is an all one matrix. Therefore, if by assigning all indices to elements of α_p, there still exists no row violating the above condition, then this shows that the number of ones in all rows of $\{\mathbf{\Phi}_e^{(s)}\}$ (except the first row) is equal to m.

It is important to note that by using the discussed idea, still we need to check all

$$\binom{L}{\mu_0, \mu_1, \cdots, \mu_{p-1}} \tag{5.39}$$

possible arrangements of entries of PRUS (with given phase distribution $\{\mu_k\}$). But the proposed method is also sensitive to unsuitable partial assignments of phases. A suitable phase arrangement is as shown in Fig. 5.2 corresponding to the Frank sequence of length 9. The method assigns $\boldsymbol{\chi}_0 = (0,1,2,3,6)^T$, $\boldsymbol{\chi}_1 = (5,7)^T$ and $\boldsymbol{\chi}_2 = (4,8)^T$ one after another and none of the matrices $\{\mathbf{\Phi}_e^{(s)}\}$ violates the above rule about the number of ones in their rows. On the other hand, there are unsuitable phase arrangements which coincide with the phase configuration of the Frank sequence. For example, suppose that the method already has assigned $\boldsymbol{\chi}_0 = (0,1,2,3,6)^T$. Now if the method assigns $\boldsymbol{\chi}_1 = (4,5)^T$ then by updating the matrices $\{\mathbf{\Phi}_e^{(s)}\}$ (as depicted in Fig. 5.4), it appears that such a partial phase arrangement violates the expected number of ones in rows of $\{\mathbf{\Phi}_e^{(s)}\}$.

Note that by recognizing any partial assignment of phases as unsuitable, the proposed construction approach avoids testing lots of sequences and thus is considerably more efficient than the classical approach. The proposed approach is summarized in Table 5.2. We refer the interested reader to a further efficiency analysis of the proposed construction method in Appendix 5.7.5.

Table 5.2. *Algorithm for efficient verification of PRUS*

Input: A sequence of length $L = mp$ with entries in α_p, whose phase distribution satisfies the principal equations in (5.24).
Step 0: Construct the vectors $\{\boldsymbol{\chi}_k\}$. Set k to zero.
Step 1: Update the matrices $\{\mathbf{\Phi}_e\}$ and $\{\mathbf{\Phi}_e^{(s)}\}_{s\neq 0}$ based on $\boldsymbol{\chi}_k$, using the positions given by (5.38).
Step 2: If the number of nonzero entries in each row (except the first row) of the updated matrices $\{\mathbf{\Phi}_e^{(s)}\}$ does not exceed m:
• **Step 1-1:** If $k < p$: increase k by one, and goto step 1.
• **Step 2-2:** If $k = p$: the sequence *is* a PRUS.
Else: stop the loop. The sequence *is not* a PRUS.

5.5 Numerical Results

We provide several numerical results that rely on the ideas discussed in the chapter. Table 5.3 presents all feasible lengths (less than or equal to 500) along

with their corresponding phase distributions for $p = 5$ and 7. Using the equivalence properties of PRUS, the $\{\mu_k\}$ sequences are circularly shifted such that μ_0 take the maximum value among all $\{\mu_k\}$. The non-existence results of [87] are used to omit some cases of (L, p) wihtout solving the principal equations. Note that by providing the phase distributions we are able to significantly reduce the size of the search space in all cases. The search space cardinality reduction induced by using the principal equations is also reported in Table 5.3.

In order to contribute to the current state-of-knowledge regarding the existence of PRUS, next we consider the unsolved cases of PRUS of length $L \leq 50$ in [87]; which are also shown in Table 5.4. As in the previous example, the size reduction of the PRUS search space is reported when the phase distributions were derived by solving the principal equations. Nevertheless, even after using the principal equations, the size of the search spaces appears to be prohibitive for an exhaustive search. To help the interpretation of the results in Table 5.4, and to see how expensive tackling such search problems can be, we consider the following analysis for the case $(L, p) = (28, 7)$:

- The initial size of the search space is $7^{28} \approx 4.60 \times 10^{23}$. Supposing that a standard PC can handle 5×10^9 simple math operations per second, we can see that a search for PRUS in this case would take more than

$$\frac{7^{28}}{(3600 \times 24 \times 365)(5 \times 10^9)} \text{ years} \tag{5.40}$$

  i.e. approximately 3 *million years*.
- Using the principal equations, we reduce the size of the search space by a factor of 5.33×10^4. On the same standard PC, an exhaustive search of PRUS for $(L, p) = (28, 7)$ in this case will take more than

$$\frac{8.63 \times 10^{18}}{(3600 \times 24 \times 365)(5 \times 10^9)} \text{ years} \tag{5.41}$$

  i.e. approximately 55 *years*.
- By employing the construction guidelines provided in Section 5.4, we developed a MATLAB code[1] to search for PRUS with $(L, p) = (28, 7)$. We used two standard PCs, which dealt with the two possible phase distribtuions of the case $(L, p) = (28, 7)$ (see Table 5.4), in parallel. Using this approach, we were able to confirm the *non-existence* of PRUS with $(L, p) = (28, 7)$ in about 2 *weeks*.

Note that due to the exponential growth in the size of search space, the questions regarding the existence of PRUS for $(L, p) = (33, 11)$ and $(L, p) = (39, 13)$ remain open.

[1] The MATLAB code associated with this experiment is provided online:
`http://www.it.uu.se/katalog/mojso279/test-p7.rar`

Table 5.3. *All possible lengths (less than or equal to* 500*) of PRUS over* α_p *for* $p = 5$ *and* 7 *together with phase distributions.*

p	Length (L)	Phase distributions $\{\mu_k\}_{k=0}^{p-1}$	Reduction in the size of search space induced by the principal equations ($\triangleq$ *initial size / final size*)
5	5	$(2,1,2,0,0)$ $(2,2,0,1,0)$	52.08
	25	$(6,6,6,6,1)$ $(9,4,4,4,4)$	1.60×10^3
	180	$(42,36,42,30,30)$ $(42,42,30,36,30)$	8.39×10^4
	220	$(52,46,34,46,42)$ $(52,46,46,42,34)$ $(54,42,46,36,42)$ $(54,46,42,42,36)$	6.31×10^4
	275	$(64,54,59,44,54)$ $(64,59,54,54,44)$ $(66,56,46,56,51)$ $(66,56,56,51,46)$	9.86×10^4
7	7	$(2,2,1,0,0,2,0)$	1.31×10^3
	28	$(6,6,4,2,2,6,2)$ $(7,5,5,2,5,2,2)$	5.33×10^4
	49	$(13,6,6,6,6,6,6)$ $(8,8,8,8,8,8,1)$	3.05×10^5
	56	$(11,10,10,5,10,5,5)$ $(11,11,6,11,6,6,5)$	4.55×10^5
	112	$(18,18,17,18,17,17,17)$ $(20,20,14,20,14,14,10)$ $(20,20,16,12,12,20,12)$ $(22,18,18,12,18,12,12)$ $(25,15,15,14,15,14,14)$	2.52×10^6
	196	$(30,30,30,30,30,30,16)$ $(33,33,26,33,26,26,19)$ $(37,30,30,23,30,23,23)$ $(40,26,26,26,26,26,26)$	1.02×10^7
	224	$(36,36,32,36,32,32,20)$ $(37,37,35,26,26,37,26)$ $(38,36,36,26,36,26,26)$ $(38,38,26,28,28,38,28)$ $(38,38,27,38,27,27,29)$ $(44,32,32,28,32,28,28)$	1.02×10^7
	372	$(62,62,55,62,55,55,41)$ $(62,62,62,48,62,48,48)$ $(64,64,50,64,50,50,50)$ $(71,57,57,50,57,50,50)$	8.23×10^7
	448	$(68,68,66,68,66,66,46)$ $(71,71,62,71,62,62,49)$ $(72,72,56,72,56,56,64)$ $(72,72,60,72,60,60,52)$ $(76,68,68,56,68,56,56)$ $(79,66,66,57,66,57,57)$ $(82,62,62,60,62,60,60)$	7.02×10^7

Table 5.4. *Remaining unsolved cases from [87], $L \leq 50$*

p	Length (L)	Phase distributions $\{\mu_k\}_{k=0}^{p-1}$	Reduction in the size of search space induced by the principal equations ($\triangleq$ *initial size / final size*)	Final size of the search space	Existence
7	28	$(6,6,4,2,2,6,2)$ $(7,5,5,2,5,2,2)$	5.33×10^4	8.63×10^{18}	**Negative**
11	33	$(8,3,2,3,3,3,2,2,2,3,2)$	2.68×10^7	8.65×10^{26}	?
13	39	$(5,1,4,5,5,3,3,1,4,3,4,0,1)$ $(5,1,1,4,4,3,5,4,5,0,3,1,3)$ $(6,3,5,3,1,5,5,2,2,3,1,2,1)$ $(6,5,1,5,2,1,1,3,3,5,2,3,2)$	1.03×10^9	2.69×10^{34}	?

Although the study of PRUS over general root-of-unity alphabet (i.e. α_N with general $N \in \mathbb{N}$) is beyond the scope of this chapter, it can be interesting to study the length/alphabet restrictions imposed by (5.5) and the remarks after Corollary 1. The eliminated cases of (L,N) via (5.5) are plotted in Fig. 5.5 for $2 \leq L,N \leq 100$. Interestingly, the prime values of N appear to support rather smaller numbers of lengths L than the nonprime values do. Via the results of Fig. 5.5 we prove the non-existence of PRUS for 3443 cases of (L,N) for $2 \leq L,N \leq 100$.

5.6 Concluding Remarks

Perfect root-of-unity sequences with prime-size alphabets have been studied. The results can be summarized as follows:

- The phase distribution of p-length PRUS over α_p was given for $p > 2$: it was shown that such sequences have $\frac{1}{2}(p+1)$ distinct phases with $\frac{1}{2}(p-1)$ of them appearing in pairs and one of them being a singleton.
- A lower bound on the number of distinct phases which must be used in a PRUS over α_p was derived. The lower bound was used to show that for PRUS of length $L \geq p(p-1)$ (i.e. $m \geq p-1$) over α_p, the sequence must use all phase values.
- Guidelines to find possible lengths (L) of PRUS over α_p were given. It was shown that integer phases of the sequence must follow a specific difference multiset property and there should exist a sequence of $\{\mu_k\}$ (introduced in Section 5.2) satisfying the principal equations. For a possible length, the phase distribution is then given by $\{\mu_k\}_{k=0}^{p-1}$.
- A geometrical analytical method to solve the principal equations was introduced for a specific p using the regular simplex. In particular, it was shown using the geometrical approach that if there exists a perfect sequence over α_3 (i.e. a 3-phase perfect sequence), its length must be of the form $L = \frac{1}{4}\left(9h_1^2 + 3h_2^2\right)$ for $(h_1,h_2) \in \mathbb{Z}^2$ and the phase distribution of the sequence was also derived.
- The usefulness of the principal equations was discussed. Given the phase distribution, guidelines for efficient construction of PRUS (in comparison to the exhaustive search) along with some examples were provided.
- Numerical evidence was provided to show the potential of using the principal equations and the construction guidelines of Section 5.4 in practice. Through numerical examples, new contributions were made to the current state of knowledge regarding the existence of PRUS.

We conclude the chapter with two remarks. First of all, while Theorem 1 shows that a uniform distribution of phases leads to perfect sequences, for *almost-perfect* sequences we may focus on *almost-uniform* distributions. A clear possibility here can be outlined as follows: in cases for which a perfect sequence does not exist, one can try to build sequences with a phase distribu-

tion which approximately satisfies the principal equations and approximately preserves the construction conditions for $\{\mathbf{\Phi}_e^{(s)}\}$ in Section 5.7.4. Finally, we would like to emphasize the possible connections between the study of PRUS and the Szemerédi theorem and related results which study the minimal size and properties of subsets of $\mathbb{Z}_n$ containing specific length arithmetic progressions (see Appendix 5.7.5). These results might be usable to further examine the existence as well as the construction for PRUS over α_p.

5.7 Appendices

5.7.1 Appendix A: Proof of Theorem 1

We prove a more general form of the theorem by using some results from the theory of algebraic numbers and minimal polynomials: a number is called algebraic iff it is a root of a polynomial with rational coefficients. The minimal polynomial $P_{min}(x)$ of an algebraic number x_0 is the polynomial with rational coefficients, minimum degree and the leading coefficient equal to 1 which satisfies $P_{min}(x_0) = 0$. It is known [117] that the minimal polynomial of the primitive n^{th} root of unity ($e^{j\frac{2\pi}{n}}$) is of degree $d = \phi(n)$ where ϕ (the Euler's totient function) shows the number of $k \in \mathbb{Z}_n$ for which k and n are co-prime. For $n = p$, p prime, the minimal polynomial is of the unique form $\sum_{k=0}^{p-1} x^k$ [118]. We conclude that if $P(e^{j\frac{2\pi}{p}}) = 0$ for a polynomial $P(x)$ with rational coefficients and degree $d = p-1$ then $P(x)$ must be equal to $w\sum_{k=0}^{p-1} x^k$ for some rational scalar w. This implies that all coefficients of $P(x)$ must be equal, which completes the proof.

5.7.2 Appendix B: Connections Between PRUS of Length $L = p$ over α_p and Binary Sequences with Optimal Periodic Correlation

Let $\mathbf{x}$ be a PRUS of length p over α_p. Let μ_k represent the number of times for which $e^{j\frac{2\pi}{p}k}$ occurs in $\mathbf{x}$. It is shown in Section 5.3.2 that the distribution of $\{\mu_k\}$ is given by

$$\begin{cases} (p-1)/2, & \mu_k = 0 \\ 1, & \mu_k = 1 \\ (p-1)/2, & \mu_k = 2 \end{cases} \tag{5.42}$$

Since $\mathbf{x}$ is perfect, it has a constant magnitude of $\sqrt{p}$ in the discrete Fourier domain. Note that the value of the discrete Fourier domain, at the frequency zero, represents the sum of the sequence $\mathbf{x}$; hence, for $\mathbf{x} = \left\{e^{j\frac{2\pi}{p}k_l}\right\}_{l=0}^{p-1}$ we

have that

$$\left|\sum_{l=0}^{p-1} e^{j\frac{2\pi}{p}k_l}\right| = \sqrt{p}, \tag{5.43}$$

or equivalently

$$\left|\sum_{k=0}^{p-1} \mu_k e^{j\frac{2\pi}{p}k}\right| = \sqrt{p}. \tag{5.44}$$

Now let $r_k = \mu_k - 1$. Therefore, (5.44) can be rewritten based on $\{r_k\}$ as

$$\left|\sum_{k=0}^{p-1} r_k e^{j\frac{2\pi}{p}k}\right| = \sqrt{p}. \tag{5.45}$$

The latter equality implies that

$$\sum_{k=0}^{p-1}\left(\sum_{l=0}^{p-1} r_l r_{l+k}\right) e^{j\frac{2\pi}{p}k} = p. \tag{5.46}$$

By applying the result of Theorem 1 to (5.46), we obtain:

$$\left(\sum_{l=0}^{p-1} r_l^2\right) - p = \sum_{l=0}^{p-1} r_l r_{l+1} = \cdots = \sum_{l=0}^{p-1} r_l r_{l+p-1}. \tag{5.47}$$

On the other hand, it is interesting to note that

$$\sum_{l=0}^{p-1} r_l^2 = \sum_{l=0}^{p-1} (\mu_l - 1)^2 = p - 1. \tag{5.48}$$

Therefore, the sequence $\{r_k\}$ has in-phase autocorrelation of $p-1$, and respectively, a constant out-of-phase autocorrelation of -1. Moreover, the distribution of $\{r_k\}$ is given by

$$\begin{cases} (p-1)/2, & r_k = -1 \\ 1, & r_k = 0 \\ (p-1)/2, & r_k = +1 \end{cases} \tag{5.49}$$

which implies that $\{r_k\}$ is a *balanced* [119] *punctured* [120] binary sequence with only one zero. Note that replacing the zero element of the sequence with $+1$ or -1 can change the out-of-phase correlation lags by 0, 2 or -2. We also note that all correlation values are congruent to the length of the sequence (i.e. p) modulo 4. Therefore, the out-of-phase correlation lags would turn to -1 for $p \equiv 3$, and to $\{1,-3\}$ for $p \equiv 1 \pmod 4$.

The discussed idea of constructing binary sequences with optimal periodic correlation from PRUS is summarized in Table 5.5. As indicated earlier, there are several methods to construct a PRUS of length p over α_p. However, we do not limit our statements to the known construction methods as it is not yet proven that the currently known construction methods cover all possible PRUS.

Table 5.5. *Construction of prime-length binary sequences with optimal periodic correlation from PRUS*

Step 0: Consider a PRUS of length $L = p$ over α_p.
Step 1: Let μ_k represent the number of times for which $e^{j\frac{2\pi}{p}k}$ occurs in the considered PRUS. Form the sequence $r_k = \mu_k - 1$.
Step 2: Replace the only zero element in $\{r_k\}$ with $+1$ or -1.

5.7.3 Appendix C: Study of the Principal Equations in (5.24) Using the Sum of Squares Problem

We note that the second equality in (5.24) may be viewed as a sum of squares problem. This approach can be applied in particular to the case of $p = 3$. For $p = 3$, Gauss showed that a natural number can be represented as the sum of three squares iff it is not of the form $4^k(8l-1)$, $(k,l) \in \mathbb{Z}^2$ [121]. For $p > 3$, one may note that according to a theorem by Lagrange every natural number can be represented as the sum of four squares [121]. The latter result implies that every natural number can be written as sum of $p > 3$ squares. We refer the interested reader to [122]- [125] for additional information on cases $p = 5$, 7, 11, and 13.

5.7.4 Appendix D: Efficient Test Method for Specific Lengths

Herein we propose an efficient method for testing if a PRUS of a specific length might exist over α_p and for determining its phase distribution. This test method is useful for cases in which the length of the needed sequence is fixed or the derivation of closed form solutions of the principal equations for the sequence length and phase distribution over a desired alphabet is deemed to be expensive. Our test method is based on two approaches to reduce the size of search space for $\{r_k\}$: (i) imposing adaptive bounds on $\{r_k\}$ and (ii) assigning $\{r_k\}$ to certain classes of residues for different integer values. A preliminary bound on $\{r_k\}$ is given by the following lemma:

Lemma 1. *Let $r_0, \cdots, r_{p-1}$ be a solution to the principal equations; then*

$$|r_k| \leq (p-1)\sqrt{\frac{m}{p}}, \qquad k \in \mathbb{Z}_p. \tag{5.50}$$

Also if r_{k_*} has the maximum absolute value among all $\{r_k\}$, then

$$|r_{k_*}| \geq \left(\sqrt{p-1}\right)\sqrt{\frac{m}{p}}. \tag{5.51}$$

Proof: From the principal equations we have $r_k = -\sum_{l\in\mathbb{Z}_p-\{k\}} r_l$, and as a result $|r_k| \le \sum_{l\in\mathbb{Z}_p-\{k\}} |r_l|$. Therefore,

$$\begin{aligned} m(p-1) &= \sum_{l=0}^{p-1} r_l^2 = r_k^2 + \sum_{l\in\mathbb{Z}_p-\{k\}} r_l^2 \\ &\ge r_k^2 + \Gamma\left(\sum_{l\in\mathbb{Z}_p-\{k\}} |r_l|, p-1\right) \\ &\ge r_k^2 + \Gamma(|r_k|, p-1) \\ &= \left(\frac{p}{p-1}\right) r_k^2 \end{aligned} \tag{5.52}$$

which yields the inequality (5.50). Next, note that

$$m(p-1) = \sum_{k=0}^{p-1} r_k^2 \le p r_{k_*}^2 \tag{5.53}$$

which implies the inequality (5.51). ■

Interestingly, similar bounds on $\{r_k\}$ could also be established in the case that some of $\{r_k\}$ are known. Let us assume that we know the values of $\{r_k\}_{k\in\mathbb{Z}_q}$ and let

$$\begin{cases} S_1 = \sum_{k=0}^{q-1} r_k \\ S_2 = \sum_{k=0}^{q-1} r_k^2 \end{cases} \tag{5.54}$$

Therefore, for every $k \in \mathbb{Z}_p - \mathbb{Z}_q$,

$$r_k = -S_1 - \sum_{l\in(\mathbb{Z}_p-\mathbb{Z}_q)-\{k\}} r_l \tag{5.55}$$

and as a result

$$\begin{aligned} m(p-1) - S_2 &= r_k^2 + \sum_{l\in(\mathbb{Z}_p-\mathbb{Z}_q)-\{k\}} r_l^2 \\ &\ge r_k^2 + \Gamma(r_k + S_1, p-q-1). \end{aligned} \tag{5.56}$$

The above quadratic inequality implies that such an arrangement of $\{r_k\}_{k\in\mathbb{Z}_q}$ might be possible only if

$$\frac{S_1^2}{p-q} + S_2 \le m(p-1), \tag{5.57}$$

and that $\{r_k\}_{k\in\mathbb{Z}_p-\mathbb{Z}_q}$ are bounded by

$$b_\pm = \frac{-S_1 \pm \sqrt{(p-q-1)\left((p-q)(m(p-1)-S_2) - S_1^2\right)}}{(p-q)}. \tag{5.58}$$

The above adaptive bounds help us make convenient successive selections of r_k.

In the following, we propose another useful idea to reduce the size of the search space, inspired by Minkowski-Hasse principle for quadratic forms [121]:

Minkowski-Hasse Principle. *A quadratic form*

$$Q(r_0,\cdots,r_{n-1}) = \sum_{(k,l)\in\mathbb{Z}_n^2} Q_{kl} r_k r_l \tag{5.59}$$

of rank n with integral coefficients represents zero over the rationals iff for any $g \in \mathbb{Z} - \{0\}$*, the congruence* $Q(r_0,\cdots,r_{n-1}) \equiv 0 \ (mod\ g)$ *has a primitive solution and in addition Q represents zero over the reals, i.e. it is indefinite.*

Let

$$\begin{cases} \sum_{k=0}^{p-1} r_k \equiv 0 \\ \sum_{k=0}^{p-1} r_k^2 \equiv m(p-1) \\ \sum_{k=0}^{p-1} r_k r_{k+s} \equiv -m, \quad s \in \mathbb{Z}_p - \{0\} \end{cases} \tag{5.60}$$

be a set of congruence *mod* $g \in \mathbb{N}$. Note that the second and third term of (5.60) are quadratic. It is also interesting to note that, as $\{r_k\}$ are bounded according to Lemma 1 and all other values are known and finite, the necessity and sufficiency of the congruence are obvious. In fact, choosing a sufficiently large g turns the congruence into an equality by adding an integral constant to r_k. The second fact we need to take into consideration is that the sum $\sum_{k=0}^{p-1} r_k,\ r_k \in \mathbb{Z}_g$, gets all the residue values in $\mathbb{Z}_g$ exactly g^{p-1} times. Therefore, by searching over all $r_k \in \mathbb{Z}_g$, the congruence set (5.60) must reduce the search space at least by a factor of g. Starting from a small g (say $g = 2$), we can omit at least $(g-1)/g$ of the search space elements by testing at most g^p elements. But, since many of these elements are redundant for different g, it turns out that for sufficiently large values of g the number of newly omitted elements is less that the number of tested elements. Therefore, a combination of this method and the adaptive bounds in (5.58) appears to be more useful. Our proposed method can be described as follows:

- **0:** Consider the integral search space Ω bounded by the inequality (5.50). Without loss of generality, we assume that r_0 has the maximum value among $\{r_k\}$ and is bounded as in (5.51). Also let $g = 2$.
- **1:** Solve the congruence set in (5.60) for g. This can be done by a brute-force search over $\mathbb{Z}_g$.
- **2:** Reduce the size of Ω by omiting elements which belong to residue classes not feasible for the congruence set in (5.60). Let Δ_g represent the number of omitted elements. If $\Delta_g > g^p$, increase g by one and goto 1.

- **3:** Consider all possible values of r_0 in Ω and update S_1 and S_2 for each of them. By considering all $k = 1, \cdots, p-1$, respectively, do the following:
  - **3.0:** Establish the bounds $b_{\pm}$ as in (5.58).
  - **3.1:** Consider all possible r_k in Ω that follow the bounds $b_{\pm}$ and their absolute value is at most equal to r_0.
  - **3.2:** Update S_1 and S_2 for each r_k considered in 3.1.
- **4:** Check whether the obtained $\{r_k\}$ satisfy the third part of the principal equations (i.e. all out-of-phase correlations of $\{r_k\}$ are $-m$).

5.7.5 Appendix E: Further Efficiency Assessment of the Proposed Construction in Section 5.4.2

To explain in more detail how the proposed approach contributes an efficient construction scheme, consider the following: let $1 + a_d(\boldsymbol{\chi}_k)$ be the length of the longest arithmetic progression with common difference d in $\boldsymbol{\chi}_k$. For a PRUS, we must have that

$$\sum_{k=0}^{p-1} a_d(\boldsymbol{\chi}_k) \leq m. \tag{5.61}$$

On the other hand, $\{a_d(\boldsymbol{\chi}_k)\}$ are not independent for different values of d as it can be checked (by construction) that

$$a_{qd}(\boldsymbol{\chi}_k) \geq \left\lfloor \frac{1}{q} a_d(\boldsymbol{\chi}_k) \right\rfloor \tag{5.62}$$

for every $q \in \mathbb{Z}_{a_d(\boldsymbol{\chi}_k)} - \{0\}$. This immediately shows that a large $a_d(\boldsymbol{\chi}_{k_*})$ (for a $k_* \in \mathbb{Z}_p$) limits not only $a_d(\boldsymbol{\chi}_k)$ where $k \in \mathbb{Z}_p - \{k_*\}$ but also $a_d(\boldsymbol{\chi}_k)$ for some other values of d. A preliminary result from (5.61) is that none of $\{\boldsymbol{\chi}_k\}$ has an arithmetic progression of length greater than $m+1$. However, the number of elements of the set $(A^{\times})$ of sequences for which the assigned vectors $\boldsymbol{\chi}_0, \cdots, \boldsymbol{\chi}_l$ ($l \in \mathbb{Z}_p$) are not feasible according to (5.61) and (5.62) is significantly larger than the number of sequences for which at least one of the elements of the set $\{\boldsymbol{\chi}_0, \cdots, \boldsymbol{\chi}_l\}$ has an arithmetic progression of length greater than $m+1$. We further note that $A^{\times}$ is a subset of all sequences that the proposed construction approach identifies as unsuitable for PRUS before assigning all $\{\boldsymbol{\chi}_k\}_{k \in \mathbb{Z}_p}$.

Acknowledgement

The authors are grateful to Prof. Matthew Geoffrey Parker for his detailed comments on an early version of this chapter.

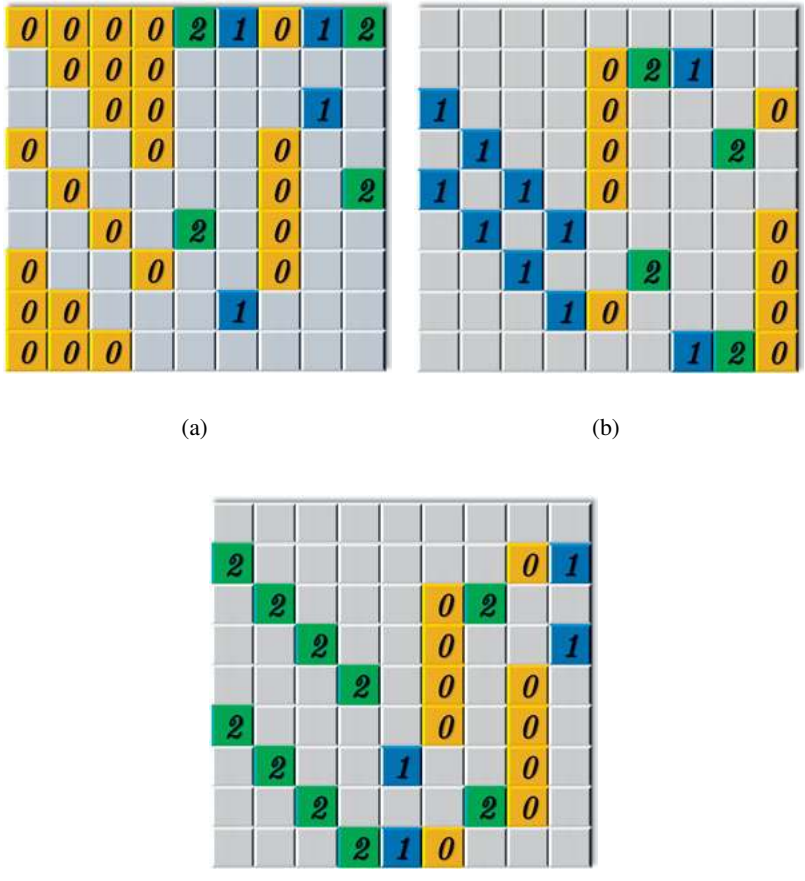

Figure 5.3. (a-c) Construction of the matrices $\{\mathbf{\Phi}_e^{(s)}\}$ for the Frank sequence of length 9 and integer phase differences equal to $s = 0$ (i.e. equality of phases), 1 and 2 respectively. The positions of 1s are shown by the corresponding phases that satisfy the difference s.

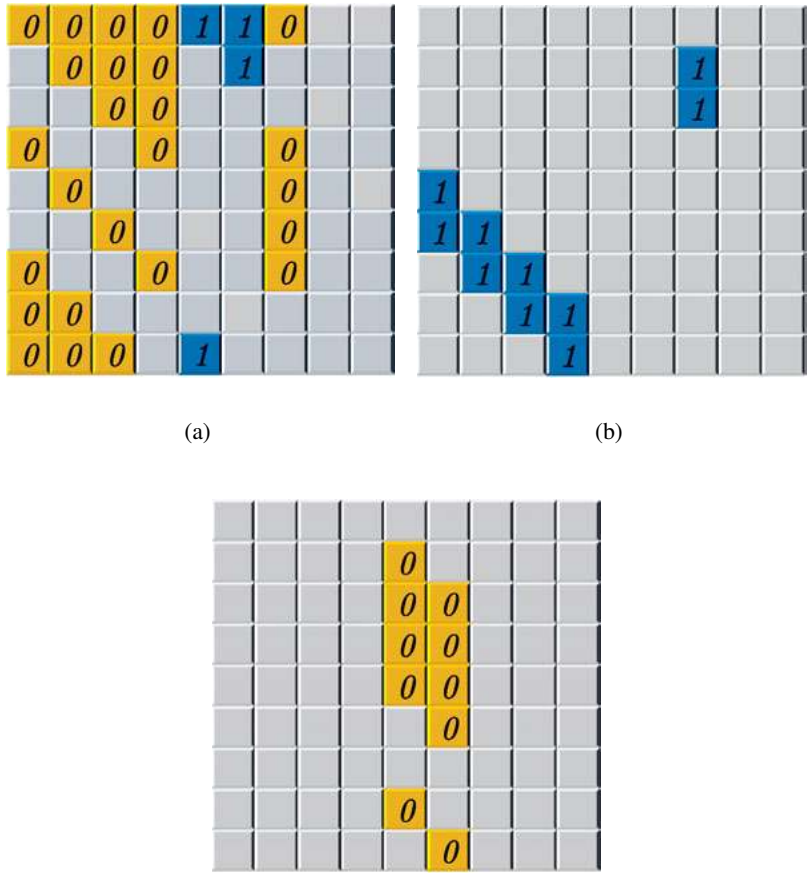

(a) (b)

(c)

Figure 5.4. (a-c) Updated matrices $\{\mathbf{\Phi}_e^{(s)}\}$ for an unsuitable phase arrangement which coincides with the phase configuration of the Frank sequence (integer phase differences are equal to $s = 0$, 1 and 2 for (a), (b) and (c) respectively). The positions of 1s are shown by the corresponding phases that satisfy the difference s. $\boldsymbol{\chi}_1 = (4,5)^T$ is assigned after considering $\boldsymbol{\chi}_0 = (0,1,2,3,6)^T$ and as a result the number of 1s in the second and ninth row of (a) are more than $m = 3$.

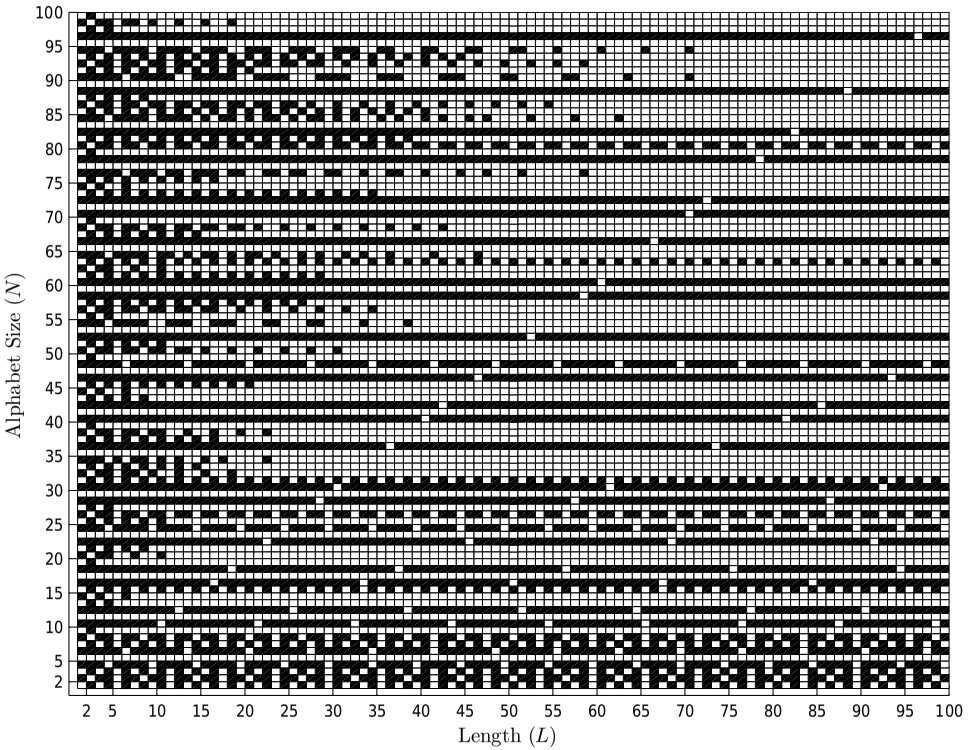

Figure 5.5. The eliminated PRUS cases (represented by black squares) of (L,N) by solving (5.5) for $2 \leq L,N \leq 100$. The results in this figure prove the non-existence of PRUS for 3443 cases of (L,N) for $2 \leq L,N \leq 100$.

6. Design of Piecewise Linear Polyphase Sequences with Good Correlation Properties

Abstract
We devise a computational approach for designing polyphase sequences with two key properties; (i) a phase argument which is piecewise linear, and (ii) an impulse-like autocorrelation. The proposed approach relies on fast Fourier transform (FFT) operations and thus can be used efficiently to design sequences with a large length or alphabet size. Moreover, using the suggested method, one can construct many new such polyphase sequences which were not known and/or could not be constructed by the previous formulations in the literature. Several numerical examples are provided to show the performance of the proposed design framework in different scenarios.

Keywords: Autocorrelation, peak-to-average-power ratio (PAR), polyphase sequences, radar codes, waveform design

6.1 Introduction

A judicious approach to sequence design for active sensing and communication systems is to seek for sequences with small *out-of-phase* autocorrelations, also referred to as good correlation properties [89], [91]. The periodic (c_k) and aperiodic (r_k) autocorrelations of a sequence $\mathbf{x} \in \mathbb{C}^N$ are defined as

$$c_k \triangleq \sum_{l=1}^{N} \mathbf{x}(l)\mathbf{x}^*(l+k)_{mod\ N}, \quad 0 \le k \le (N-1) \tag{6.1}$$

$$r_k \triangleq \sum_{l=1}^{N-k} \mathbf{x}(l)\mathbf{x}^*(l+k) = r_{-k}^*, \; 0 \le k \le (N-1) \tag{6.2}$$

where in both cases, the lag $k = 0$ represents the energy of $\mathbf{x}$, and the out-of-phase lags are those with $k \neq 0$.

We note that, in many applications, the sequences $\mathbf{x}$ with good correlation properties are not only constrained to have low *peak-to-average power ratio* (PAR),

$$\text{PAR} \triangleq \frac{\|\mathbf{x}\|_\infty^2}{\frac{1}{N}\|\mathbf{x}\|_2^2}, \tag{6.3}$$

but are also assumed to be *finite-alphabet*. In terms of PAR, the best squences are those with unimodular entries (i.e. $|\mathbf{x}(l)| = 1, \forall l$). As a result, the construction of finite-alphabet unimodular sequences has been studied widely in the literature. In particular, several (analytical) constructions are available in this case: such sequences for any given length can be constructed for example by Zadoff, Chu, Golomb polyphase, P3 and P4 methods [39]. Other constructions include Frank, P1, P2, Px, and PAT methods that work only when the length is a perfect square ($N = M^2$) [39], [129]. Note that the latter constructions present a unique property in their phase values, namely that their phase argument is *piecewise linear*. A generic piecewise linear polyphase sequence

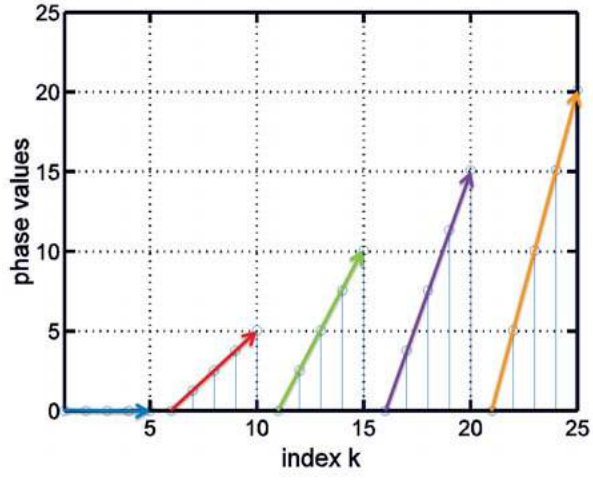

Figure 6.1. The phase values of the Frank sequence $\{\mathbf{x}(k)\}_{k=1}^{N}$ of length $N = 25$ [39], illustrated based on the formulation in (6.4)-(6.6) with $\phi_{m,1} = 0$ and $\eta_m = 2\pi(m-1)/5$, $1 \leq m \leq 5$.

of length $N = MK$ can be formulated as follows [129]. Let the matrix

$$\mathbf{\Phi} = \begin{pmatrix} \varphi_{1,1} & \varphi_{1,2} & \cdots & \varphi_{1,K} \\ \varphi_{2,1} & \varphi_{2,2} & \cdots & \varphi_{2,K} \\ \vdots & \vdots & \ddots & \vdots \\ \varphi_{M,1} & \varphi_{M,2} & \cdots & \varphi_{M,K} \end{pmatrix} \tag{6.4}$$

include the phase values of a unimodular sequence $\mathbf{x}$ via the identity

$$\mathbf{x} = e^{j(vec(\mathbf{\Phi}^T))}. \tag{6.5}$$

Then $\mathbf{x}$ is a piecewise linear polyphase sequence (with parameters M and K) iff

$$\eta_m \triangleq \eta_{m,k} = \varphi_{m,k+1} - \varphi_{m,k} \tag{6.6}$$

is a fixed constant for $1 \leq k \leq K-1$. Note that piecewise linear polyphase sequences are beneficial to practical implementations owing to the smaller number of variables involved in their construction, as well as their simple structure. As an example, Fig. 6.1 illustrates the phase values of the Frank sequence of length $N = 25$, with $M = K = 5$.

In this chapter, a fast computational method for designing piecewise linear polyphase sequences with good correlation is proposed. Particularly, we discuss in detail the sequence design for desirable aperiodic correlation. The reasons for choosing aperiodic correlation (and not its periodic counterpart) are the following; (i) piecewise linear polyphase sequences with optimal periodic correlation are already known in the literature (for instance the Frank

sequence), and (ii) the aperiodic autocorrelations are of specific interest due to the higher difficulty of the associated design problem, see e.g. [83]. We also note that a modification of the proposed formulations to tackle the periodic case is straightforward. The contributions of this work can be summarized as follows:

- The analytical construction methods yield polyphase sequences with limited alphabet sizes. As a result, the proposed method can lead to considerable improvements upon the currently known piecewise linear polyphase sequences by alphabet size enlargement.
- The suggested formulation provides the possibility of designing piecewise linear polyphase sequences for lengths $N = MK$ which are not *perfect square*, i.e. for scenarios in which $(M,K) \neq (\sqrt{N},\sqrt{N})$.

Consequently, using the proposed method, one can construct a new set of piecewise linear polyphase sequences with good correlation properties; a set with large cardinality whose majority of elements are not known and/or cannot be constructed with currently known formulations. See Section 3 for some numerical examples.

Notation: We use bold lowercase letters for vectors and bold uppercase letters for matrices. $(.)^T$, $(.)^*$ and $(.)^H$ denote the vector/matrix transpose, the complex conjugate, and the Hermitian transpose, respectively. $\mathbf{1}$ and $\mathbf{0}$ are the all-one and all-zero vectors/matrices. $\|\mathbf{x}\|_n$ or the l_n-norm of the vector $\mathbf{x}$ is defined as $(\sum_k |\mathbf{x}(k)|^n)^{\frac{1}{n}}$ where $\{\mathbf{x}(k)\}$ are the entries of $\mathbf{x}$. The symbol $\odot$ stands for the Hadamard element-wise product of matrices. $vec(\boldsymbol{X})$ is a vector obtained by stacking the columns of $\boldsymbol{X}$ successively. Finally, $\mathbb{Z}_Q$ denotes the set $\{0,1,\cdots,Q-1\}$.

6.2 The Proposed Method

Let $N = MK$ represent a twin factorization of N. Based on the formulation in Section 6.1, a piecewise-linear polyphase sequence $\mathbf{x}$ can be written as

$$\mathbf{x} = \begin{pmatrix} e^{j\varphi_1}\mathbf{x}_1 \\ e^{j\varphi_2}\mathbf{x}_2 \\ \vdots \\ e^{j\varphi_M}\mathbf{x}_M \end{pmatrix}; \quad \mathbf{x}_m = \begin{pmatrix} 1 \\ e^{j\eta_m} \\ \vdots \\ e^{j(K-1)\eta_m} \end{pmatrix}, \forall m, \tag{6.7}$$

where $\varphi_m = \varphi_{m,1}$. Note that, depending on the factorization of N, the parameter M (which denotes the number of linear segments in the phase argument) can attain different values ranging from 1 to N; particularly, the case of $M = 1$ leads to a structure that resembles the steering vectors associated with uniform linear arrays, while $M = N$ corresponds to a sequence design with no piecewise-linearity constraint at all. We assume that the elements of $\mathbf{x}$ belong

to the Q-ary alphabet $\Omega_Q = \left\{ e^{j2k\pi/Q} : \ k \in \mathbb{Z}_Q \right\}$. Accordingly, we assume that $\{\varphi_m\}$ and $\{\eta_m\}$ are of the form $2\pi k/Q$, with $k \in \mathbb{Z}_Q$.

In the following, we employ the CAN computational framework introduced in [6]. From an intuitive point of view, a sequence with zero out-of-phase periodic correlation has a flat spectrum in the frequency domain— in particular, the more flat the spectrum, the smaller the out-of-phase periodic correlations. The CAN algorithm in [6] (see also [89]) provides the mathematical formalism that confirms such observations. Namely, the periodic out-of-phase correlations of a sequence $\mathbf{x}$ can be minimized conveniently via the optimization problem:

$$\begin{aligned} \min_{\mathbf{x},\boldsymbol{\nu}} \quad & \left\| \boldsymbol{A}^H \mathbf{x} - \boldsymbol{\nu} \right\|_2^2 \\ \text{s.t.} \quad & \boldsymbol{\nu} \text{ is unimodular,} \end{aligned} \tag{6.8}$$

where $\mathbf{x}$ is constrained, e.g. as in (6.7), and $\boldsymbol{A}$ denotes the $N \times N$ (inverse) DFT matrix, whose (l,p)-element is given by

$$[A]_{l,p} = \frac{1}{\sqrt{N}} e^{j2\pi lp/N}, \quad l,p = 1,\ldots,N. \tag{6.9}$$

Note that the aperiodic correlations of $\mathbf{x}$ are given by the periodic correlations of the sequence

$$\widetilde{\mathbf{x}} = \begin{pmatrix} \mathbf{x} \\ \mathbf{0}_{N-1} \end{pmatrix}. \tag{6.10}$$

Therefore, CAN considers the following frequency-domain design problem to *minimize* the aperiodic out-of-phase correlations of $\mathbf{x}$:

$$\begin{aligned} \min_{\widetilde{\mathbf{x}},\widetilde{\boldsymbol{\nu}}} \quad & \left\| \widetilde{\boldsymbol{A}}^H \widetilde{\mathbf{x}} - \widetilde{\boldsymbol{\nu}} \right\|_2^2 \\ \text{s.t.} \quad & \widetilde{\boldsymbol{\nu}} \text{ is unimodular,} \end{aligned} \tag{6.11}$$

in which $\mathbf{x}$ is constrained as described earlier, and $\widetilde{\boldsymbol{A}}$ denotes the $(2N-1) \times (2N-1)$ (inverse) DFT matrix. For given $\widetilde{\mathbf{x}}$, the minimization of (6.11) with respect to $\widetilde{\boldsymbol{\nu}}$ is straightforward, viz.

$$\widetilde{\boldsymbol{\nu}} = e^{j \arg(\widetilde{\boldsymbol{A}}^H \widetilde{\mathbf{x}})}. \tag{6.12}$$

Due to the various constraints on $\mathbf{x}$ including the piecewise linearity and a given phase alphabet, the optimization of (6.11) with respect to $\widetilde{\mathbf{x}}$ (or equivalently $\mathbf{x}$) appears to be more complicated. However, to achieve a monotonically decreasing objective function, one can simply employ a separate optimization of (6.11) with respect to the variables $\{\varphi_m\}$ and $\{\eta_m\}$. In order to

obtain the minimizer $\{\varphi_m\}$ of (6.11) for fixed $\widetilde{\boldsymbol{\nu}}$ and $\{\eta_m\}$, we note that the objective function can be rewritten as

$$\begin{aligned}\left\|\widetilde{\boldsymbol{A}}^H\widetilde{\mathbf{x}}-\widetilde{\boldsymbol{\nu}}\right\|_2^2 &= \left\|\widetilde{\mathbf{x}}-\widetilde{\boldsymbol{A}}\widetilde{\boldsymbol{\nu}}\right\|_2^2 \\ &= \left\|\begin{pmatrix} e^{j\varphi_1}\mathbf{x}_1 \\ e^{j\varphi_2}\mathbf{x}_2 \\ \vdots \\ e^{j\varphi_M}\mathbf{x}_M \end{pmatrix} - \begin{pmatrix} \widehat{\boldsymbol{\nu}}_1 \\ \widehat{\boldsymbol{\nu}}_2 \\ \vdots \\ \widehat{\boldsymbol{\nu}}_M \end{pmatrix}\right\|_2^2 \\ &\qquad +\text{const}_1 \\ &= \left\|\begin{pmatrix} e^{j\varphi_1}\mathbf{1}_{\mathbf{K}} \\ e^{j\varphi_2}\mathbf{1}_{\mathbf{K}} \\ \vdots \\ e^{j\varphi_M}\mathbf{1}_{\mathbf{K}} \end{pmatrix} - \begin{pmatrix} \widehat{\boldsymbol{\nu}}_1 \odot \mathbf{x}_1^* \\ \widehat{\boldsymbol{\nu}}_2 \odot \mathbf{x}_2^* \\ \vdots \\ \widehat{\boldsymbol{\nu}}_M \odot \mathbf{x}_M^* \end{pmatrix}\right\|_2^2 \\ &\qquad +\text{const}_1\end{aligned} \tag{6.13}$$

where $\widehat{\boldsymbol{\nu}}_m$ denotes the column vector consisting of the m^{th} K-tuple in the vector $\widetilde{\boldsymbol{A}}\widetilde{\boldsymbol{\nu}}$. Let $\boldsymbol{u}_m = \widehat{\boldsymbol{\nu}}_m \odot \mathbf{x}_m^*$ for $1 \le m \le M$. Then it is easy to verify that the minimization of (6.13) may be decoupled for different $\{\varphi_m\}$; namely, the minimizer $\varphi_m \triangleq 2\pi g_m/Q$ of (6.13) is given by the solution to the following optimization problem:

$$\min_{g_m \in \mathbb{Z}_Q} \quad \sum_{k=1}^{K} \left| e^{j\varphi_m} - \boldsymbol{u}_m(k) \right|^2. \tag{6.14}$$

Consequently, the minimizer φ_m of (6.13) becomes

$$\varphi_m = \Psi_Q\left(\arg\left(\sum_{k=1}^{K} \boldsymbol{u}_m(k)\right)\right), \quad 1 \le m \le M, \tag{6.15}$$

where $\Psi_Q(.)$ yields the closest phase value to the argument in the Q-ary alphabet. Now suppose $\{\varphi_m\}$ and $\widetilde{\boldsymbol{\nu}}$ (equivalently $\{\widehat{\boldsymbol{\nu}}_m\}$) are given. According to (6.13), the minimization of (6.11) with respect to $\{\eta_m\}$ may be accomplished using the optimization problems

$$\begin{aligned} \min_{\mathbf{x}_m} \quad & \left\|\mathbf{x}_m - e^{-j\varphi_m}\widehat{\boldsymbol{\nu}}_m\right\|_2^2 \\ \text{s.t.} \quad & \mathbf{x}_m \text{ has the structure in (6.7),} \end{aligned} \tag{6.16}$$

Table 6.1. *The Proposed Algorithm for Designing Piecewise-Linear Polyphase Sequences with Good Correlation*

Input parameters: sequence length$=N$, alphabet size$=Q$, twin factorization of N into (M,K).
Step 0: Initialize the variables $\{\varphi_m\}$ and $\{\eta_m\}$ of the form $2\pi k/Q$ ($k \in \mathbb{Z}_Q$) randomly (or set the values by a previously known sequence). **Step 1**: Form the sequence $\mathbf{x}$ using (6.7), based on the current values of $\{\varphi_m\}$ and $\{\eta_m\}$. **Step 2**: Compute $\widetilde{\boldsymbol{\nu}}$ using (6.12). **Step 3**: Compute $\{\varphi_m\}$ using (6.15). **Step 4**: Compute $\{\eta_m\}$ using (6.17). **Step 5**: Let $\varepsilon = \left\|\widetilde{\boldsymbol{A}}^H\widetilde{\mathbf{x}} - \widetilde{\boldsymbol{\nu}}\right\|_2$. Repeat the steps 1-4 until $$\varepsilon^{(s)} = \varepsilon^{(s-1)},$$ where s denotes the iteration number.

for $1 \le m \le M$. Let $\eta_m \triangleq 2\pi h_m/Q$, and note that one can restate the objective function of (6.16) as

$$\begin{aligned}
&\left\|\mathbf{x}_m - e^{-j\varphi_m}\widehat{\boldsymbol{\nu}}_m\right\|_2^2 \\
&\quad = \sum_{k=1}^{K}\left|e^{j2\pi h_m(k-1)/Q} - e^{-j\varphi_m}\widehat{\boldsymbol{\nu}}_m(k)\right|^2 \\
&\quad = \text{const}_2 - 2\,\Re\left\{\sum_{k=1}^{K}(e^{-j\varphi_m}\widehat{\boldsymbol{\nu}}_m(k))e^{-j2\pi h_m(k-1)/Q}\right\}.
\end{aligned}$$

Hence, the optimization problem in (6.16) is equivalent to

$$\max_{h_m\in\mathbb{Z}_Q} \quad \Re\left\{\sum_{k=1}^{K}(e^{-j\varphi_m}\widehat{\boldsymbol{\nu}}_m(k))\,e^{-j2\pi h_m(k-1)/Q}\right\}. \tag{6.17}$$

Interestingly, the solution to (6.17) can be obtained efficiently using an FFT operation due to the fact that the objective function represents the real-part of the Q-point DFT sequence associated with $\{e^{-j\varphi_m}\widehat{\boldsymbol{\nu}}_m(k)\}_{k=1}^{K}$.

Finally, the steps of the proposed method are summarized in Table 6.1. We note that the approach proposed in this work relies on FFT operations and hence can be used efficiently for large lengths N, or phase alphabet sizes Q.

6.3 Numerical Results and Discussions

We provide several numerical examples to show the performance of the proposed method. As discussed earlier, the method can be employed to design piecewise linear polyphase sequences of non-square length. We use the proposed approach to design a piecewise linear polyphase sequence of length $N = 128$ with $(M,K) = (16,8)$ and $Q = 128$. The obtained sequence along with its normalized autocorrelation level,

$$\text{autocorrelation level (dB)} \triangleq 20\log_{10}\left|\frac{r_k}{r_0}\right| \tag{6.18}$$

are presented in Fig. 6.2. The correlation peak sidelobe level (PSL), viz.

$$\text{PSL} \triangleq \max\{|r_k|\}_{k=1}^{N-1}, \tag{6.19}$$

of the sequences obtained during the iterations of the proposed algorithm is shown in Fig. 6.3. A significant reduction in the PSL of the sequences vs. iteration number can be observed. We note that CAN minimizes an upper bound on the PSL metric, and hence, the resultant PSL values in Fig. 3 are not monotonically decreasing; see [6] and [83] for more details related to this observation.

Next, we consider improving upon a certain piecewise linear polyphase sequence with good correlation. As an example, we use the PAT sequence [129] of length $N = 256$ in order to initialize the algorithm in Table 1. PAT sequences were proposed recently, and have a PSL value which is the minimum of those of Frank, P1, P2, and Px. While improving the correlation properties of a PAT sequence by using numerical methods is not simple, the said properties can be enhanced by considering an alphabet size Q larger than that used by the PAT sequences which is $2\sqrt{N}$. In order to show the potential of such an approach in enhancing the correlation properties, we choose a large alphabet size by setting Q to 2^{16}. Fig. 6.4 depicts the normalized autocorrelation level of the PAT sequence, as well as the level corresponding to the proposed method. The PSL value corresponding to the initial PAT sequence is equal to 11.3086, while the obtained sequence has a PSL value of 5.6359.

Finally, it can be interesting to examine how the factorization of N into (M,K) affects the correlation properties of the obtained sequences. To study this aspect, we consider $N = 2^2 \times 3^2 \times 5 = 180$, and $Q = N$. For all 18 divisors of $N = 180$, we use the proposed algorithm 15 times with different random initializations. Fig. 6.5 plots the best PSL values for each case, obtained in the 15 trials . A considerable reduction in the obtained PSL values can be seen as M grows large. To explain this behavior, we note that the number of free variables, i.e. degrees of freedom (DOFs) of the problem, is determined by the number of variables $\{\varphi_m\}$ and $\{\eta_m\}$:

$$\#\text{DOFs} = \begin{cases} 2M & M \leq N/2, \\ M & M = N. \end{cases} \tag{6.20}$$

As a result, the number of DOFs is increasing with M, which lays the ground for a better performance of the method in terms of the correlation PSL. However, increasing M might increase the complexity of implementing the sequences in practice— a trade off which should be dealt with wisely.

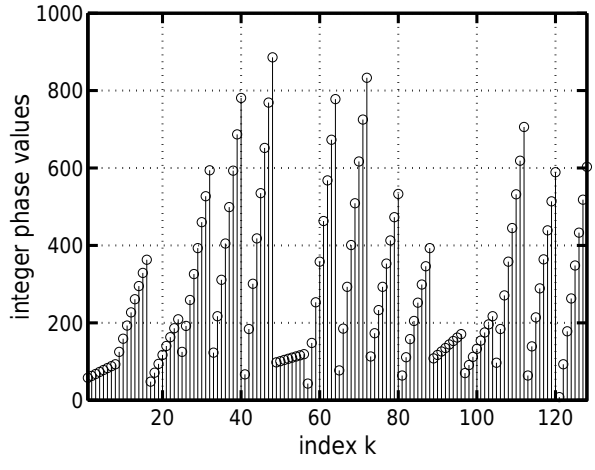

(a)

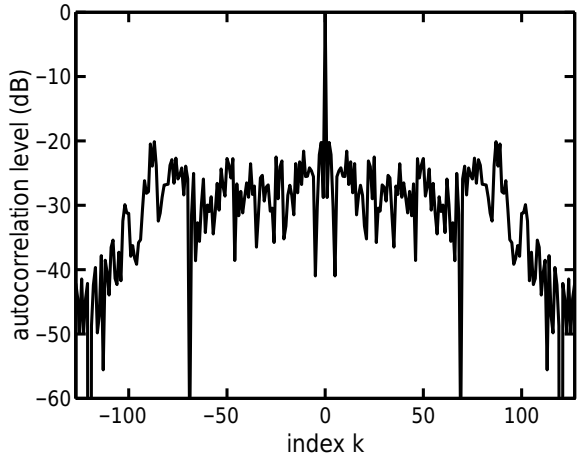

(b)

Figure 6.2. Design of a piecewise linear polyphase sequence (of length $N = 128$) with good aperiodic autocorrelation, and parameters $(M,k) = (16,8)$, $Q = 128$: (a) the integer phases ($\triangleq$ phase values $\times Q/(2\pi)$) of the sequence; (b) the autocorrelation levels of the sequence.

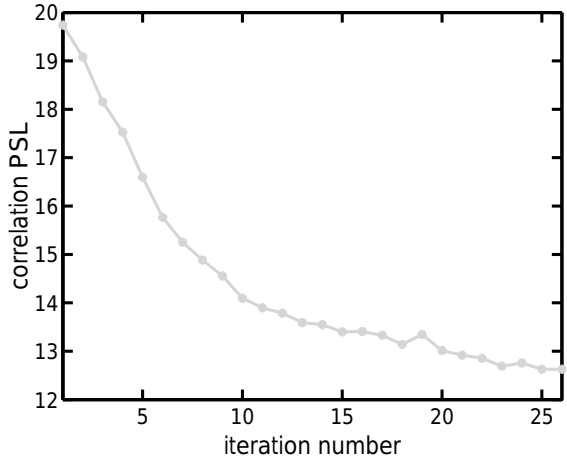

Figure 6.3. The PSL values versus iteration number associated with the obtained sequences through the iterations of the proposed algorithm.

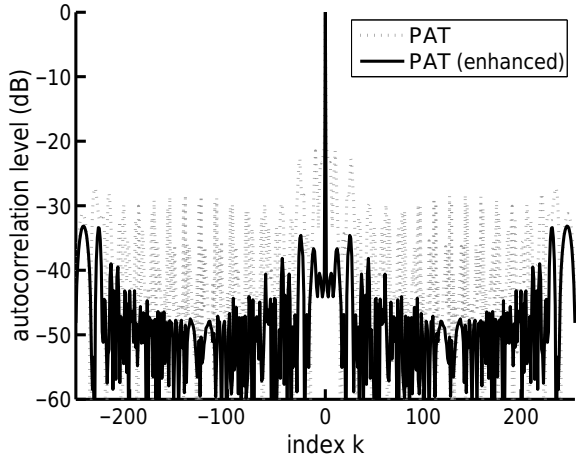

Figure 6.4. Enhancement of the aperiodic correlation properties of the PAT sequence of length $N = 256$ via alphabet size enlargement. The figure shows the normalized autocorrelation level of the initial PAT sequence, along with that of the enhanced sequence obtained by the proposed method.

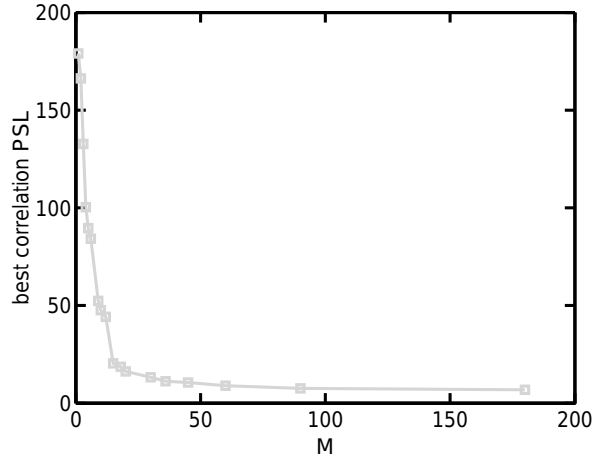

Figure 6.5. The best PSL values obtained in 15 trials of the proposed method with different random initializations for $N = 180$, and M set to various divisors of N.

Part II:
SNR and MSE Performance Metrics

7. Design of Unimodular Codes via Quadratic Optimization

Abstract
The NP-hard problem of optimizing a quadratic form over the unimodular vector set arises in radar code design scenarios as well as other active sensing and communication applications. To tackle this problem (which we call unimodular quadratic program (UQP)), several computational approaches are devised and studied. Power method-like iterations are introduced for local optimization of UQP. Furthermore, a **m**onotonically **er**ror-bound **i**mproving **t**echnique (MERIT) is proposed to obtain the global optimum or a local optimum of UQP with good sub-optimality guarantees. The provided sub-optimality guarantees are case-dependent and may outperform the $\pi/4$ approximation guarantee of semi-definite relaxation. Several numerical examples are presented to illustrate the performance of the proposed method. The examples show that for several cases, including rank-deficient matrices, the proposed methods can solve UQPs efficiently in the sense of sub-optimality guarantee and computational time.

Keywords: Code design, radar codes, unimodular codes, quadratic programming, peak-to-average-power ratio (PAR)

7.1 Introduction

Unimodular codes are used in many active sensing and communication systems mainly as a result of the their optimal (i.e. unity) peak-to-average-power ratio (PAR). The design of such codes can be often formulated as the optimization of a quadratic form (see sub-section 7.1.1 for examples). Therefore, we will study the problem

$$\text{UQP:} \quad \max_{\boldsymbol{s}\in\Omega^n} \boldsymbol{s}^H \boldsymbol{R}\boldsymbol{s} \tag{7.1}$$

where $\boldsymbol{R} \in \mathbb{C}^{n\times n}$ is a given Hermitian matrix, Ω represents the unit circle, i.e. $\Omega = \{s \in \mathbb{C} : \ |s| = 1\}$ and UQP stands for Unimodular Quadratic Program(ming).

Notation: We use bold lowercase letters for vectors/sequences and bold uppercase letters for matrices. $(\cdot)^T$, $(\cdot)^*$ and $(\cdot)^H$ denote the vector/matrix transpose, the complex conjugate, and the Hermitian transpose, respectively. $\mathbf{1}$ and $\mathbf{0}$ are the all-one and all-zero vectors/matrices. $\boldsymbol{e}_k$ is the k^{th} standard basis vector in $\mathbb{C}^n$. $\|\mathbf{x}\|_n$ or the l_n-norm of the vector $\mathbf{x}$ is defined as $(\sum_k |\mathbf{x}(k)|^n)^{\frac{1}{n}}$ where $\{\mathbf{x}(k)\}$ are the entries of $\mathbf{x}$. The Frobenius norm of a matrix $\boldsymbol{X}$ (denoted by $\|\boldsymbol{X}\|_F$) with entries $\{\boldsymbol{X}(k,l)\}$ is equal to $\left(\sum_{k,l} |\boldsymbol{X}(k,l)|^2\right)^{\frac{1}{2}}$. We use $\Re(\boldsymbol{X})$ and $\Im(\boldsymbol{X})$ to denote the matrices obtained by collecting the real parts, and respectively, the imaginary parts of the entries of $\boldsymbol{X}$. The matrix $e^{j\boldsymbol{X}}$ is defined element-wisely as $\left[e^{j\boldsymbol{X}}\right]_{k,l} = e^{j[\boldsymbol{X}]_{k,l}}$. $\arg(.)$ denotes the phase angle (in radians) of the vector/matrix argument. $\mathbb{E}[.]$ stands for the expectation operator. $\mathbf{Diag}(.)$ denotes the diagonal matrix formed by the entries of the vector argument, whereas $\mathbf{diag}(.)$ denotes the vector formed by collecting the diagonal entries of the matrix argument. $\sigma_k(\boldsymbol{X})$ represents the k^{th} maximal eigenvalue of $\boldsymbol{X}$. The symbol $\odot$ stands for the Hadamard (element-wise) product of matrices. The operator notation $\oplus$ stands for the Minkowski sum of the two sets. Finally, $\mathbb{R}$ and $\mathbb{C}$ represent the set of real and complex numbers, respectively.

7.1.1 Motivating Applications

To motivate the UQP formulation considered above, we present four scenarios in which a design problem in active sensing or communication boils down to an UQP.

• *Designing codes that optimize the SNR or the CRLB:* We consider a monostatic radar which transmits a linearly encoded burst of pulses. The observed backscattered signal $\boldsymbol{v}$ can be written as (see, e.g. [131]):

$$\boldsymbol{v} = a(\boldsymbol{c} \odot \boldsymbol{p}) + \boldsymbol{w}, \tag{7.2}$$

where a represents channel propagation and backscattering effects, $\boldsymbol{w}$ is the disturbance/noise component, $\boldsymbol{c}$ is the unimodular vector containing the code elements, $\boldsymbol{p} = (1, e^{j2\pi f_d T_r}, \cdots, e^{j2\pi(n-1)f_d T_r})^T$ is the temporal steering vector with f_d and T_r being the target Doppler frequency and pulse repetition time, respectively.

Under the assumption that $\boldsymbol{w}$ is a zero-mean complex-valued circular Gaussian vector with known positive definite covariance matrix $\mathbb{E}[\boldsymbol{w}\boldsymbol{w}^H] = \boldsymbol{M}$, the signal-to-noise ratio (SNR) is given by [132]

$$\text{SNR} = |a|^2 \boldsymbol{c}^H \boldsymbol{R} \boldsymbol{c} \tag{7.3}$$

where $\boldsymbol{R} = \boldsymbol{M}^{-1} \odot (\boldsymbol{p}\boldsymbol{p}^H)^*$. Therefore, the problem of designing codes optimizing the SNR of the radar system can be formulated directly as an UQP. Additionally, the Cramer-Rao lower bound (CRLB) for the target Doppler frequency estimation (which yields a lower bound on the variance of any unbiased target Doppler frequency estimator) is given by [132]

$$\begin{aligned} \text{CRLB} &= \left(2|a|^2 (\boldsymbol{c} \odot \boldsymbol{p} \odot \boldsymbol{u})^H \boldsymbol{M}^{-1} (\boldsymbol{c} \odot \boldsymbol{p} \odot \boldsymbol{u})\right)^{-1} \\ &= \left(2|a|^2 \boldsymbol{c}^H \boldsymbol{R}' \boldsymbol{c}\right)^{-1} \end{aligned} \tag{7.4}$$

where $\boldsymbol{u} = (0, j2\pi T_r, \cdots, j2\pi(n-1)T_r)^T$ and $\boldsymbol{R}' = \boldsymbol{M}^{-1} \odot (\boldsymbol{p}\boldsymbol{p}^H)^* \odot (\boldsymbol{u}\boldsymbol{u}^H)^*$. Therefore the minimization of CRLB can also be formulated as an UQP. For the simultaneous optimization of SNR and CRLB see [132].

• *Synthesizing cross ambiguity functions (CAFs):* The ambiguity function (which is widely used in active sensing applications [4] [39]) represents the two-dimensional response of the matched filter to a signal with time delay τ and Doppler frequency shift f. The more general concept of cross ambiguity function occurs when the matched filter is replaced by a mismatched filter. The cross ambiguity function (CAF) is defined as

$$\chi(\tau, f) = \int_{-\infty}^{\infty} u(t) v^*(t+\tau) e^{j2\pi f t} dt \tag{7.5}$$

where $u(t)$ and $v(t)$ are the transmit signal and the receiver filter, respectively (the ambiguity function is obtained from (7.5) with $v(t) = u(t)$). In several

applications $u(t)$ and $v(t)$ are given by:

$$u(t) = \sum_{k=1}^{n} x_k p_k(t), \quad v(t) = \sum_{k=1}^{n} y_k p_k(t) \tag{7.6}$$

where $\{p_k(t)\}$ are pulse-shaping functions (with the rectangular pulse as a common example), and

$$\mathbf{x} = (x_1 \cdots x_n)^T, \ \ \boldsymbol{y} = (y_1 \cdots y_n)^T \tag{7.7}$$

are the code and, respectively, the filter vectors. The design problem of synthesizing a desired CAF has a small number of free variables (i.e. the entries of the vectors $\mathbf{x}$ and $\boldsymbol{y}$) compared to the large number of constraints arising from two-dimensional matching criteria (to a given $|\chi(\tau, f)|$). Therefore, the problem is generally considered to be difficult and there are not many methods to synthesize a desired (cross) ambiguity function. Below, we describe briefly the cyclic approach of [133] for CAF design.

The problem of matching a desired $|\chi(\tau, f)| = d(\tau, f)$ can be formulated as the minimization of the criterion [133]

$$g(\mathbf{x}, \boldsymbol{y}, \phi) = \tag{7.8}$$
$$\int_{-\infty}^{\infty}\int_{-\infty}^{\infty} w(\tau, f) \left| d(\tau, f) e^{j\phi(\tau, f)} - \boldsymbol{y}^H \boldsymbol{J}(\tau, f)\mathbf{x} \right|^2 d\tau df$$

where $\boldsymbol{J}(\tau, f) \in \mathbb{C}^{n\times n}$ is given, $w(\tau, f)$ is a weighting function that specifies the CAF area which needs to be emphasized and $\phi(\tau, f)$ represent auxiliary phase variables. It is not difficult to see that for fixed $\mathbf{x}$ and $\boldsymbol{y}$, the minimizer $\phi(\tau, f)$ is given by $\phi(\tau, f) = \arg\{\boldsymbol{y}^H \boldsymbol{J}(\tau, f)\mathbf{x}\}$. For fixed $\phi(\tau, f)$ and $\mathbf{x}$, the criterion g can be written as

$$\begin{aligned} g(\boldsymbol{y}) &= \boldsymbol{y}^H \boldsymbol{D}_1 \boldsymbol{y} - \boldsymbol{y}^H \boldsymbol{B}^H \mathbf{x} - \mathbf{x}^H \boldsymbol{B}\boldsymbol{y} + \text{const}_1 \\ &= (\boldsymbol{y} - \boldsymbol{D}_1^{-1}\boldsymbol{B}^H\mathbf{x})^H \boldsymbol{D}_1 (\boldsymbol{y} - \boldsymbol{D}_1^{-1}\boldsymbol{B}^H\mathbf{x}) + \text{const}_2 \end{aligned} \tag{7.9}$$

where $\boldsymbol{B}$ and $\boldsymbol{D}_1$ are given matrices in $\mathbb{C}^{n\times n}$ [133]. Due to practical considerations, the transmit coefficients $\{x_k\}$ must have low PAR values. However, the receiver coefficients $\{y_k\}$ need not be constrained in such a way. Therefore, the minimizer $\boldsymbol{y}$ of $g(\boldsymbol{y})$ is given by $\boldsymbol{y} = \boldsymbol{D}_1^{-1}\boldsymbol{B}^H\mathbf{x}$. Similarly, for fixed $\phi(\tau, f)$ and $\boldsymbol{y}$, the criterion g can be written as

$$g(\mathbf{x}) = \mathbf{x}^H \boldsymbol{D}_2 \mathbf{x} - \mathbf{x}^H \boldsymbol{B}\boldsymbol{y} - \boldsymbol{y}^H \boldsymbol{B}^H \mathbf{x} + \text{const}_3 \tag{7.10}$$

where $\boldsymbol{D}_2 \in \mathbb{C}^{n\times n}$ is given [133]. If a unimodular code vector $\mathbf{x}$ is desired then the optimization of $g(\mathbf{x})$ is an UQP as $g(\mathbf{x})$ can be written as

$$g(\mathbf{x}) = \begin{pmatrix} e^{j\varphi}\mathbf{x} \\ e^{j\varphi} \end{pmatrix}^H \begin{pmatrix} \boldsymbol{D}_2 & -\boldsymbol{B}\boldsymbol{y} \\ -(\boldsymbol{B}\boldsymbol{y})^H & 0 \end{pmatrix} \begin{pmatrix} e^{j\varphi}\mathbf{x} \\ e^{j\varphi} \end{pmatrix} + \text{const}_3 \tag{7.11}$$

where $\varphi \in [0, 2\pi)$ is a free phase variable.

- *Steering vector estimation in adaptive beamforming:* Consider a linear array with n antennas. The output of the array at time instant k can be expressed as [134]

$$\mathbf{x}_k = s_k \boldsymbol{a} + \boldsymbol{n}_k \tag{7.12}$$

with $\{s_k\}$ being the signal waveform, $\boldsymbol{a}$ the associated steering vector (with $|[\boldsymbol{a}]_l| = 1$, $1 \leq l \leq n$), and $\boldsymbol{n}_k$ the vector accounting for all independent interferences.

The true steering vector is usually unknown in practice, and it can therefore be considered as an unimodular vector to be determined [135]. Define the sample covariance matrix of $\{\mathbf{x}_k\}$ as $\widehat{\boldsymbol{R}} = \frac{1}{T}\sum_{k=1}^{T} \mathbf{x}_k \mathbf{x}_k^H$ where T is the number of training data samples. Assuming some prior knowledge on $\boldsymbol{a}$ (which can be represented by $\arg(\boldsymbol{a})$ being in a given sector Θ), the problem of estimating the steering vector can be formulated as [136]

$$\begin{aligned} \min_{\boldsymbol{a}} \ & \boldsymbol{a}^H \widehat{\boldsymbol{R}}^{-1} \boldsymbol{a} \\ \text{s.t. } & \arg(\boldsymbol{a}) \in \Theta, \end{aligned} \tag{7.13}$$

hence an UQP-type problem. Such problems can be tackled using general local optimization techniques or the optimization scheme introduced in Section 7.3.

- *Maximum likelihood (ML) detection of unimodular codes:* Assume the linear model

$$\boldsymbol{y} = \boldsymbol{Q}\boldsymbol{s} + \boldsymbol{n} \tag{7.14}$$

where $\boldsymbol{Q}$ represents a multiple-input multiple-output (MIMO) channel, $\boldsymbol{y}$ is the received signal, $\boldsymbol{n}$ is the additive white Gaussian noise and $\boldsymbol{s}$ contains the unimodular symbols which are to be estimated. The ML detection of $\boldsymbol{s}$ may be stated as

$$\widehat{\boldsymbol{s}}_{ML} = \arg \min_{\boldsymbol{s} \in \Omega^n} \|\boldsymbol{y} - \boldsymbol{Q}\boldsymbol{s}\|_2 \tag{7.15}$$

It is straightforward to verify that the above optimization problem is equivalent to the UQP [138]:

$$\min_{\overline{\boldsymbol{s}} \in \Omega^{n+1}} \ \overline{\boldsymbol{s}}^H \boldsymbol{R} \overline{\boldsymbol{s}} \tag{7.16}$$

where

$$\boldsymbol{R} = \begin{pmatrix} \boldsymbol{Q}^H\boldsymbol{Q} & -\boldsymbol{Q}^H\boldsymbol{y} \\ -\boldsymbol{y}^H\boldsymbol{Q} & 0 \end{pmatrix}, \overline{\boldsymbol{s}} = \begin{pmatrix} e^{j\varphi}\boldsymbol{s} \\ e^{j\varphi} \end{pmatrix} \tag{7.17}$$

and where $\varphi \in [0, 2\pi)$ is a free phase variable.

7.1.2 Related Work

In [139], the NP-hardness of UQP is proven by employing a reduction from an NP-complete matrix partitioning problem. The UQP in (7.1) is often studied along with the following (also NP-hard) related problem in which the decision variables are discrete:

$$m\text{-UQP: } \max_{\boldsymbol{s}\in\Omega_m^n} \boldsymbol{s}^H\boldsymbol{R}\boldsymbol{s} \tag{7.18}$$

where $\Omega_m = \{1, e^{j\frac{2\pi}{m}}, \cdots, e^{j\frac{2\pi}{m}(m-1)}\}$. Note that the latter problem coincides with the UQP in (7.1) as $m \to \infty$. The authors of [140] show that when the matrix $\boldsymbol{R}$ is rank-deficient (more precisely, when $d = \text{rank}(\boldsymbol{R})$ behaves like $\mathscr{O}(1)$ with respect to the problem dimension) the m-UQP problem can be solved in polynomial-time and they propose a $\mathscr{O}((mn/2)^{2d})$-complexity algorithm to solve (7.18). However, such algorithms are not applicable to the UQP which corresponds to $m \to \infty$.

Studies on polynomial-time (or efficient) algorithms for UQP (and m-UQP) have been extensive (e.g. see [137]-[152] and the references therein). In particular, the semi-definite relaxation (SDR) technique has been one of the most appealing approaches to the researchers. To derive an SDR, we note that $\boldsymbol{s}^H\boldsymbol{R}\boldsymbol{s} = \text{tr}(\boldsymbol{s}^H\boldsymbol{R}\boldsymbol{s}) = \text{tr}(\boldsymbol{R}\boldsymbol{s}\boldsymbol{s}^H)$. Hence, the UQP can be rewritten as

$$\begin{aligned} &\max_{\boldsymbol{S}} \text{tr}(\boldsymbol{R}\boldsymbol{S}) \\ &\text{s.t. } \boldsymbol{S} = \boldsymbol{s}\boldsymbol{s}^H,\ \boldsymbol{s} \in \Omega^n. \end{aligned} \tag{7.19}$$

If we relax (7.19) by removing the rank constraint on $\boldsymbol{S}$ then the result is a semi-definite program:

$$\begin{aligned} \text{SDP: } &\max_{\boldsymbol{S}} \text{tr}(\boldsymbol{R}\boldsymbol{S}) \\ &\text{s.t. } [\boldsymbol{S}]_{k,k} = 1,\ \ 1 \le k \le n, \\ &\boldsymbol{S} \text{ is positive semi-definite.} \end{aligned} \tag{7.20}$$

The above SDP can be solved in polynomial time using interior-point methods [145]. The approximation of the UQP solution based on the SDP solution can be accomplished in several ways. For example, we can approximate the phase values of the solution $\boldsymbol{s}$ using a rank-one approximation of $\boldsymbol{S}$. A more effective approach for guessing $\boldsymbol{s}$ is based on randomized approximations (see [139], [146] and [147]). A detailed guideline for randomized approximation of the UQP solution can be found in [147]. In addition, we refer the interested reader to the survey of the rich literature on SDR in [2].

In order to formalize the quality assessment of the UQP solutions, let $\boldsymbol{s}$ be the approximate solution to a given UQP. We assume that $\boldsymbol{R}$ is positive semidefinite (such an assumption can be made without loss of generality, see

Section 7.2.1). Then the *approximation ratio (δ)* associated with $\boldsymbol{s}$ is given by

$$\delta \triangleq \frac{\boldsymbol{s}^H \boldsymbol{R}\boldsymbol{s}}{\max_{\boldsymbol{s}' \in \Omega^n} \boldsymbol{s}'^H \boldsymbol{R}\boldsymbol{s}'}. \tag{7.21}$$

The approximation ratio is usually unknown, because the global optimum of the problem is not known. However, an optimization method may offer a *sub-optimality guarantee (γ)*, i.e. a lower bound on the quality of the approximate solution:

$$\delta \geq \gamma. \tag{7.22}$$

Herein, we present the existing (analytically derived) sub-optimality guarantee for SDR. Let v_{SDR} be the expected value of the UQP objective at the obtained randomized solution. Let v_{opt} represent the optimal value of the UQP objective. We have

$$\gamma v_{opt} \leq v_{SDR} \leq v_{opt} \tag{7.23}$$

with the sub-optimality guarantee coefficient $\gamma = \pi/4$ [139] [148]. Note that the sub-optimality coefficient of the solution obtained by SDR can be arbitrarily close to $\pi/4$ (e.g., see [148]). For the sake of brevity, in the sequel the abbreviation SDR will be used for semidefinite relaxations followed by the randomization procedure.

7.1.3 Contributions of this Work

Besides SDR, the literature does not offer many other numerical approaches to tackle UQP. In this chapter, a specialized local optimization scheme for UQP is proposed. The proposed computationally efficient local optimization approach can be used to tackle UQP as well as improve upon the solutions obtained by other methods such as SDR. Furthermore, a **m**onotonically **er**ror-bound **i**mproving **t**echnique (called MERIT) is introduced to obtain the global optimum or a local optimum of UQP with good sub-optimality guarantees. Note that:

- MERIT provides real-time case-dependent sub-optimality guarantees (γ) during its iterations. To the best of our knowledge, such guarantees for UQP were not known prior to this work. Using MERIT one may obtain better performance guarantees compared to the analytical worst-case guarantees (such as $\gamma = \pi/4$ for SDR).
- The provided case-dependent sub-optimality guarantees are of practical importance in decision making scenarios. For instance in some cases the UQP solution obtained by SDR (or other optimization methods) might achieve good objective values, and equivalently good approximation ratios δ (this is indeed the case for some practical examples, see Section

7.6). However, unless the goodness of the obtained solution is known (which can be determined using the proposed bounds), the solution cannot be trusted.
- Using MERIT, numerical evidence is provided to show that several UQPs (particularly those with low rank) can be solved efficiently without sacrificing the solution accuracy.

Finally, we believe that the general ideas of this work can be adopted to tackle m-UQP as the finite alphabet case of UQP. However, a detailed study of m-UQP is beyond the scope of this chapter.

The rest of this work is organized as follows. Section 7.2 discusses several properties of UQP. Section 7.3 introduces a specialized local optimization method that resembles the well-known power method. Section 7.4 presents a cone approximation that is used in Section 7.5 to derive the algorithmic form of MERIT for UQP. Several numerical examples are provided in section 7.6. Finally, Section 7.7 concludes the chapter.

7.2 Some Properties of UQP

In this section, we study several properties of UQP. The discussed properties lay the grounds for a better understanding of UQP as well as the tools proposed to tackle it in the following sections.

7.2.1 Basic Properties

The UQP formulation in (7.1) covers both maximization and minimization of quadratic forms (one can obtain the minimization of the quadratic form in (7.1) by considering $-\boldsymbol{R}$ in lieu of $\boldsymbol{R}$). In addition, without loss of generality, the Hermitian matrix $\boldsymbol{R}$ can be assumed to be positive (semi)definite. If $\boldsymbol{R}$ is not positive (semi)definite, we can make it so using the diagonal loading technique (i.e. $\boldsymbol{R} \leftarrow \boldsymbol{R} + \lambda \boldsymbol{I}$ where $\lambda \geq -\sigma_n(\boldsymbol{R})$). Note that such a diagonal loading does not change the solution of UQP as $\boldsymbol{s}^H(\boldsymbol{R}+\lambda \boldsymbol{I})\boldsymbol{s} = \boldsymbol{s}^H\boldsymbol{R}\boldsymbol{s} + \lambda n$. Next, we note that if $\widetilde{\boldsymbol{s}}$ is a solution to UQP then $e^{j\phi}\widetilde{\boldsymbol{s}}$ (for any $\phi \in [0, 2\pi)$) is also a valid solution. To establish connections among different UQPs, Theorem 1 presents a bijection among the set of matrices leading to the same solution.

Theorem 1. *Let $\mathscr{K}(\boldsymbol{s})$ represent the set of matrices $\boldsymbol{R}$ for which a given $\boldsymbol{s} \in \Omega^n$ is the global optimizer of UQP. Then*

1. *$\mathscr{K}(\boldsymbol{s})$ is a convex cone.*
2. *For any two vectors $\boldsymbol{s}_1, \boldsymbol{s}_2 \in \Omega^n$, the one-to-one mapping (where $\boldsymbol{s}_0 = \boldsymbol{s}_1^* \odot \boldsymbol{s}_2$)*

$$\boldsymbol{R} \in \mathscr{K}(\boldsymbol{s}_1) \Longleftrightarrow \boldsymbol{R} \odot (\boldsymbol{s}_0 \boldsymbol{s}_0^H) \in \mathscr{K}(\boldsymbol{s}_2) \tag{7.24}$$

holds among the matrices in $\mathscr{K}(\boldsymbol{s}_1)$ and $\mathscr{K}(\boldsymbol{s}_2)$.

Proof: See the Appendix. ■

It is interesting to note that in light of the above result, the characterization of the cone $\mathscr{K}(\boldsymbol{s})$ for any given $\boldsymbol{s} = \widetilde{\boldsymbol{s}}$ leads to a complete characterization of all $\mathscr{K}(\boldsymbol{s})$, $\boldsymbol{s} \in \Omega^n$, and thus solving any UQP. However, the NP-hardness of UQP suggests that such a tractable characterization cannot be expected. Further discussions regarding the characterization of $\mathscr{K}(\boldsymbol{s})$ are deferred to Section 7.4.

7.2.2 Analytical Solutions to UQP

There exist cases for which the analytical global optima of UQP are easy to obtain. In this sub-section, we consider two such cases which will be used in Section 7.4 to provide an approximate characterization of $\mathscr{K}(\boldsymbol{s})$. A special example is the case in which $e^{j\arg(\boldsymbol{R})}$ (see the notation definition in the Introduction) is a rank-one matrix. More precisely, let $\boldsymbol{R} = \boldsymbol{R}_1 \odot (\widetilde{\boldsymbol{s}}\widetilde{\boldsymbol{s}}^H)$ where $\boldsymbol{R}_1$ is a real-valued Hermitian matrix with non-negative entries and $\widetilde{\boldsymbol{s}} \in \Omega^n$. A simple special case of this example is when $\boldsymbol{R}$ is a rank-one matrix itself. In this case, it can be easily verified that $\boldsymbol{R}_1 \in \mathscr{K}(\mathbf{1}_{n\times 1})$. Therefore, using Theorem 1 one concludes that $\boldsymbol{R} \in \mathscr{K}(\widetilde{\boldsymbol{s}})$ i.e. $\boldsymbol{s} = \widetilde{\boldsymbol{s}}$ yields the global optimum of UQP. As another example, Theorem 2 considers the case for which the matrix $\boldsymbol{R}$ has a repeated largest eigenvalue.

Theorem 2. *Let $\boldsymbol{R}$ be a Hermitian matrix with eigenvalue decomposition $\boldsymbol{R} = \boldsymbol{U}\boldsymbol{\Sigma}\boldsymbol{U}^H$. Suppose $\boldsymbol{\Sigma}$ is of the form*

$$\boldsymbol{\Sigma} = \mathbf{Diag}([\underbrace{\sigma_1 \ \cdots \ \sigma_1}_{m \text{ times}} \ \sigma_2 \ \cdots \ \sigma_{n-m+1}]^T) \tag{7.25}$$

$$\sigma_1 > \sigma_2 \geq \cdots \geq \sigma_{n-m+1}$$

and let $\boldsymbol{U}_m$ be the matrix made from the first m columns of $\boldsymbol{U}$. Now suppose $\widetilde{\boldsymbol{s}} \in \Omega^n$ lies in the linear space spanned by the columns of $\boldsymbol{U}_m$, i.e. there exists a vector $\boldsymbol{\alpha} \in \mathbb{C}^m$ such that

$$\widetilde{\boldsymbol{s}} = \boldsymbol{U}_m \boldsymbol{\alpha}. \tag{7.26}$$

Then $\widetilde{\boldsymbol{s}}$ is a global optimizer of UQP.

Proof: If $\widetilde{\boldsymbol{s}}$ satisfies (24), then it belongs to the span of the m dominant eigenvectors of $\boldsymbol{R}$, and hence it is also a dominant eigenvector of $\boldsymbol{R}$. This fact implies that $\widetilde{\boldsymbol{s}}$ is the global optimizer of the quadratic optimization (even without the unimodularity constraint) which completes the proof. ■

We end this section by noting that the solution to an UQP is not necessarily unique. For any set of unimodular vectors $\{\boldsymbol{s}_1, \boldsymbol{s}_2, \cdots, \boldsymbol{s}_k\}$, $k \leq n$, we can use

the Gram-Schmidt process to obtain a unitary matrix $\boldsymbol{U}$ the first k columns of which span the same linear space as $\boldsymbol{s}_1, \boldsymbol{s}_2, \cdots, \boldsymbol{s}_k$. In this case, Theorem 2 suggests a method to construct a matrix $\boldsymbol{R}$ (by choosing a $\boldsymbol{\Sigma}$ with k identical largest eigenvalues) for which all $\boldsymbol{s}_1, \boldsymbol{s}_2, \cdots, \boldsymbol{s}_k$ are global optimizers of the corresponding UQP.

7.3 Power Method for UQP

Due to its NP-hard nature, UQP has in general a highly multi-modal optimization objective. Finding the local optima of UQP is not only useful to tackle the problem itself (particularly for UQP-related problems such as (7.13)), but also to improve the UQP approximate solutions obtained by SDR or other optimization techniques. In this section, we introduce a computationally efficient procedure (to obtain a local optimum of UQP) which resembles the well-known power method for computing the dominant eigenvalue/vector pairs of matrices.

Assume that $\boldsymbol{R}$ is positive definite and let $\{\boldsymbol{s}^{(t+1)}\}_{t=0}^{\infty}$ be a sequence of unimodular codes where $\boldsymbol{s}^{(t+1)}$ is the minimizer of the following criterion:

$$\min_{\boldsymbol{s}^{(t+1)} \in \Omega^n} \|\boldsymbol{s}^{(t+1)} - \boldsymbol{R}\boldsymbol{s}^{(t)}\|_2 \tag{7.27}$$

The minimizing vector $\boldsymbol{s}^{(t+1)}$ of (7.27) is simply given by the following *power method-like* iteration:

$$\boldsymbol{s}^{(t+1)} = e^{j \arg(\boldsymbol{R}\boldsymbol{s}^{(t)})} \tag{7.28}$$

Note that

$$\|\boldsymbol{s}^{(t+1)} - \boldsymbol{R}\boldsymbol{s}^{(t)}\|_2^2 = \text{const} - 2\Re\{\boldsymbol{s}^{(t+1)H}\boldsymbol{R}\boldsymbol{s}^{(t)}\} \tag{7.29}$$

As a result, $\boldsymbol{s}^{(t+1)}$ is equivalently the maximizer of the criterion $\Re\{\boldsymbol{s}^{(t+1)H}\boldsymbol{R}\boldsymbol{s}^{(t)}\}$. Moreover, if $\boldsymbol{s}^{(t+1)} \neq \boldsymbol{s}^{(t)}$ we have that

$$(\boldsymbol{s}^{(t+1)} - \boldsymbol{s}^{(t)})^H \boldsymbol{R} (\boldsymbol{s}^{(t+1)} - \boldsymbol{s}^{(t)}) > 0 \tag{7.30}$$

which implies

$$\begin{aligned} \boldsymbol{s}^{(t+1)H}\boldsymbol{R}\boldsymbol{s}^{(t+1)} &> 2\Re\{\boldsymbol{s}^{(t+1)H}\boldsymbol{R}\boldsymbol{s}^{(t)}\} - \boldsymbol{s}^{(t)H}\boldsymbol{R}\boldsymbol{s}^{(t)} \\ &> \boldsymbol{s}^{(t)H}\boldsymbol{R}\boldsymbol{s}^{(t)} \end{aligned} \tag{7.31}$$

as $\Re\{\boldsymbol{s}^{(t+1)H}\boldsymbol{R}\boldsymbol{s}^{(t)}\} > \boldsymbol{s}^{(t)H}\boldsymbol{R}\boldsymbol{s}^{(t)}$. Therefore, the UQP objective is increasing through the power method-like iterations in (7.28). On the other hand, the UQP objective is upper bounded by $\sum_{k,l} |\boldsymbol{R}(k,l)|$, and thus the said iterations are convergent in the sense of the UQP objective value. We further note that

the increase in the UQP objective is lower bounded (within a multiplicative constant) by the l_2-norm of the difference of the unimodular codes in successive iterations, viz.

$$\begin{aligned} & \boldsymbol{s}^{(t+1)H}\boldsymbol{R}\boldsymbol{s}^{(t+1)} - \boldsymbol{s}^{(t)H}\boldsymbol{R}\boldsymbol{s}^{(t)} \\ = \; & (\boldsymbol{s}^{(t+1)} - \boldsymbol{s}^{(t)})^H \boldsymbol{R} (\boldsymbol{s}^{(t+1)} - \boldsymbol{s}^{(t)}) \\ & + 2\Re\{\boldsymbol{s}^{(t+1)H}\boldsymbol{R}\boldsymbol{s}^{(t)}\} - 2\boldsymbol{s}^{(t)H}\boldsymbol{R}\boldsymbol{s}^{(t)} \\ > \; & (\boldsymbol{s}^{(t+1)} - \boldsymbol{s}^{(t)})^H \boldsymbol{R} (\boldsymbol{s}^{(t+1)} - \boldsymbol{s}^{(t)}) \\ \geq \; & \sigma_n(\boldsymbol{R}) \, \|\boldsymbol{s}^{(t+1)} - \boldsymbol{s}^{(t)}\|_2^2 \end{aligned} \tag{7.32}$$

Due to the fact that the sequence $\{\boldsymbol{s}^{(t)H}\boldsymbol{R}\boldsymbol{s}^{(t)}\}$ is convergent, (7.32) implies that $\|\boldsymbol{s}^{(t+1)} - \boldsymbol{s}^{(t)}\|_2$ is also converging to zero through the iterations in (7.28).

It is also important to observe that the power method-like iterations do not stop before reaching a local optimum or saddle point of UQP. A limit point $\widetilde{\boldsymbol{s}}$ of (7.28) can be characterized by the equation

$$\boldsymbol{R}\widetilde{\boldsymbol{s}} = \boldsymbol{v} \odot \widetilde{\boldsymbol{s}} \tag{7.33}$$

where $\boldsymbol{v}$ is real-valued and non-negative. On the other hand, the stationary points $\widetilde{\boldsymbol{s}}$ of UQP (associated with $\boldsymbol{R}$) may be characterized as $\boldsymbol{R}\widetilde{\boldsymbol{s}} = \boldsymbol{v} \odot \widetilde{\boldsymbol{s}}$, where $\boldsymbol{v}$ is real-valued (see Appendix 7.8.2 for a detailed derivation). Therefore, the limit points of (7.28) form a subset of the stationary points of UQP. We refer to the subset of UQP stationary points satisfying (7.33) as the *stable points* of UQP. A characterization of the UQP optima can also be found in Appendix 7.8.2. Namely, $\boldsymbol{s}$ is a local maximum of UQP if and only if $\boldsymbol{V} \geq \boldsymbol{R}$, where $\boldsymbol{V} = \mathbf{Diag}(\boldsymbol{v})$. Due to the positive definiteness of $\boldsymbol{R}$, the latter condition implies that for any local maximum of UQP $\boldsymbol{v}$ is non-negative. As a result, the set of the local maxima of UQP (including its global optima) is simply a subset of the stable points of UQP.

Remark 1: The application of the power method-like iterations introduced above is not limited to the optimization of quadratic forms over the unimodular vector set. If one can minimize the criterion in (7.27) for a particular constraint on $\boldsymbol{s}^{(t+1)}$, say $\boldsymbol{s}^{(t+1)} \in \Psi$, then all the arguments accompanying (7.27)-(7.32) are valid and they yield an optimization of quadratic forms over Ψ. An interesting practical example is the more general problem of quadratic optimization over PAR constrained codes (see e.g. [147] and [150]) that can be cast as

$$\begin{aligned} & \max_{\boldsymbol{s}} \; \boldsymbol{s}^H \boldsymbol{R} \boldsymbol{s} \\ & \text{s.t.} \;\; |\boldsymbol{s}(k)| \leq \sqrt{\gamma}, \; \forall k, \\ & \qquad \|\boldsymbol{s}\|_2^2 = n. \end{aligned} \tag{7.34}$$

where γ denotes the maximal tolerable PAR value. The related power method-like iterations, namely

$$\begin{aligned} \min_{\boldsymbol{s}^{(t+1)}} \ & \|\boldsymbol{s}^{(t+1)} - \boldsymbol{R}\boldsymbol{s}^{(t)}\|_2 \\ \text{s.t.} \ & |\boldsymbol{s}^{(t+1)}(k)| \leq \sqrt{\gamma}, \ \forall k, \\ & \|\boldsymbol{s}^{(t+1)}\|_2^2 = n. \end{aligned} \tag{7.35}$$

are *nearest-vector* problems that can be solved efficiently via an algorithm devised in [26]. ■

7.4 Results on the cone $\mathscr{K}(\mathbf{s})$

While a complete tractable characterization of $\mathscr{K}(\boldsymbol{s})$ cannot be expected (due to the NP-hardness of UQP), approximate characterizations of $\mathscr{K}(\boldsymbol{s})$ are possible. The goal of this section is to provide an approximate characterization of the cone $\mathscr{K}(\boldsymbol{s})$ which can be used to tackle the UQP problem.

Theorem 3. *For any given $\boldsymbol{s} = (e^{j\phi_1}, \cdots, e^{j\phi_n})^T \in \Omega^n$, let $\mathscr{C}(\boldsymbol{V}_{\boldsymbol{s}})$ represent the convex cone of matrices $\boldsymbol{V}_{\boldsymbol{s}} = \boldsymbol{D} \odot (\boldsymbol{s}\boldsymbol{s}^H)$ where $\boldsymbol{D}$ is any real-valued symmetric matrix with non-negative off-diagonal entries. Also let $\mathscr{C}_{\boldsymbol{s}}$ represent the convex cone of matrices with $\boldsymbol{s}$ being their dominant eigenvector (i.e the eigenvector corresponding to the maximal eigenvalue). Then for any $\boldsymbol{R} \in \mathscr{K}(\boldsymbol{s})$, there exists $\alpha_0 \geq 0$ such that for all $\alpha \geq \alpha_0$,*

$$\boldsymbol{R} + \alpha \boldsymbol{s}\boldsymbol{s}^H \in \mathscr{C}(\boldsymbol{V}_{\boldsymbol{s}}) \oplus \mathscr{C}_{\boldsymbol{s}}. \tag{7.36}$$

The proof of Theorem 3 will be presented in several steps (Theorems 4-7 and thereafter). As indicated earlier, a global optimum of UQP is also a stable point of UQP. In what follows, we prove Theorem 3 by proving a more general result, namely that (7.36) is also satisfied if $\boldsymbol{s}$ is a stable point of UQP (characterized by (7.33)). However, since $\boldsymbol{s}$ is the global optimum of UQP for all matrices in $\mathscr{C}_{\boldsymbol{s}}$ and $\mathscr{C}(\boldsymbol{V}_{\boldsymbol{s}})$, the case of $\alpha_0 = 0$ can occur only when $\boldsymbol{s}$ is a global optimum of UQP associated with $\boldsymbol{R}$. An intuitive illustration of the result in Theorem 3 is shown in Fig. 7.1.

Suppose $\boldsymbol{s}$ is a stable point of UQP associated with a given positive definite matrix $\boldsymbol{R}$, and let $\theta_{k,l} = [\arg(\boldsymbol{R})]_{k,l}$. We define the matrix $\boldsymbol{R}_+^{\boldsymbol{s}}$ as

$$\boldsymbol{R}_+^{\boldsymbol{s}}(k,l) = \begin{cases} |\boldsymbol{R}(k,l)|\cos(\theta_{k,l} - (\phi_k - \phi_l)) & (k,l) \in \Theta, \\ 0 & otherwise \end{cases} \tag{7.37}$$

where Θ represents the set of all (k,l) such that $|\theta_{k,l} - (\phi_k - \phi_l)| < \pi/2$. Now, let ρ be a positive real number such that

$$\rho > \max_{(k,l) \notin \Theta} \left\{ |\boldsymbol{R}(k,l)\cos(\theta_{k,l} - (\phi_k - \phi_l))| \right\} \tag{7.38}$$

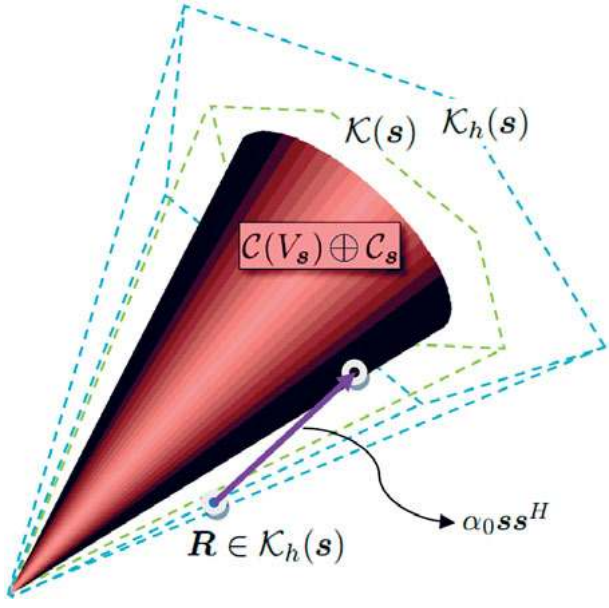

Figure 7.1. An illustration of the result in Theorem 3. $\mathscr{K}_h(\boldsymbol{s})$ denotes the convex cone of matrices with $\boldsymbol{s}$ as a stable point of the associated UQPs.

and consider the sequence of matrices $\{\boldsymbol{R}^{(t)}\}$ defined (in an iterative manner) by $\boldsymbol{R}^{(0)} = \boldsymbol{R}$, and

$$\boldsymbol{R}^{(t+1)} = \boldsymbol{R}^{(t)} - (\boldsymbol{R}_+^{\boldsymbol{s}\,(t)} - \rho \mathbf{1}_{n\times n}) \odot (\boldsymbol{s}\boldsymbol{s}^H) \tag{7.39}$$

for $t \geq 0$. The next two theorems (whose proofs are given in the Appendix) study some useful properties of the sequence $\{\boldsymbol{R}^{(t)}\}$.

Theorem 4. *$\{\boldsymbol{R}^{(t)}\}$ is convergent in at most two iterations:*

$$\boldsymbol{R}^{(t)} = \boldsymbol{R}^{(2)}, \ \ \forall\, t \geq 2. \tag{7.40}$$

Theorem 5. *$\boldsymbol{R}^{(t)}$ is a function of ρ. Let ρ and ρ' both satisfy the criterion (7.38). At the convergence of $\{\boldsymbol{R}^{(t)}\}$ (which is attained for $t = 2$) we have:*

$$\boldsymbol{R}^{(2)}(\rho') = \boldsymbol{R}^{(2)}(\rho) + (\rho' - \rho)(\boldsymbol{s}\boldsymbol{s}^H). \tag{7.41}$$

Using the above results, Theorems 6 (whose proof is given in the Appendix) and 7 pave the way for a constructive proof of Theorem 3.

Theorem 6. *If $\boldsymbol{s}$ is a stable point of the UQP associated with $\boldsymbol{R}^{(0)} = \boldsymbol{R}$ then it is also a stable point of the UQPs associated with $\boldsymbol{R}^{(1)}$ and $\boldsymbol{R}^{(2)}$. Furthermore, $\boldsymbol{s}$ is an eigenvector of $\boldsymbol{R}^{(2)}$ corresponding to the eigenvalue $n\rho$.*

Theorem 7. *If $\boldsymbol{s}$ is a stable point of UQP for $\boldsymbol{R}^{(0)} = \boldsymbol{R}$ then it will be the dominant eigenvector of $\boldsymbol{R}^{(2)}$ if ρ is sufficiently large. In particular, let μ be the largest eigenvalue of $\boldsymbol{R}^{(2)}$ which belongs to an eigenvector other than $\boldsymbol{s}$. Then for any $\rho \geq \mu/n$, $\boldsymbol{s}$ is a dominant eigenvector of $\boldsymbol{R}^{(2)}$.*

Proof: We know from Theorem 6 that $\boldsymbol{s}$ is an eigenvector of $\boldsymbol{R}^{(2)}$ corresponding to the eigenvalue $n\rho$. However, if $\boldsymbol{s}$ is not the dominant eigenvector of $\boldsymbol{R}^{(2)}$, Theorem 5 implies that increasing ρ would not change any of the eigenvalues/vectors of $\boldsymbol{R}^{(2)}$ except that it increases the eigenvalue corresponding to $\boldsymbol{s}$. As a result, for $\boldsymbol{s}$ to be the dominant eigenvector of $\boldsymbol{R}^{(2)}$ we only need ρ to satisfy $n\rho \geq \mu$ or equivalently $\rho \geq \mu/n$, which concludes the proof. ■

Returning to Theorem 3, note that $\boldsymbol{R}$ can be written as

$$\begin{aligned} \boldsymbol{R} &= \boldsymbol{R}^{(0)} \\ &= \boldsymbol{R}^{(2)} + (\boldsymbol{R}_{+}^{\boldsymbol{s}\,(0)} + \boldsymbol{R}_{+}^{\boldsymbol{s}\,(1)}) \odot (\boldsymbol{s}\boldsymbol{s}^H) - 2\rho\boldsymbol{s}\boldsymbol{s}^H. \end{aligned} \tag{7.42}$$

For sufficiently large ρ (satisfying both (7.38) and the condition of Theorem 7) we have that

$$\boldsymbol{R} + 2\rho\boldsymbol{s}\boldsymbol{s}^H = \boldsymbol{R}^{(2)} + (\boldsymbol{R}_{+}^{\boldsymbol{s}\,(0)} + \boldsymbol{R}_{+}^{\boldsymbol{s}\,(1)}) \odot (\boldsymbol{s}\boldsymbol{s}^H) \tag{7.43}$$

where $\boldsymbol{R}^{(2)} \in \mathscr{C}_{\boldsymbol{s}}$ and $(\boldsymbol{R}_{+}^{\boldsymbol{s}\,(0)} + \boldsymbol{R}_{+}^{\boldsymbol{s}\,(1)}) \odot (\boldsymbol{s}\boldsymbol{s}^H) \in \mathscr{C}(\boldsymbol{V}_{\boldsymbol{s}})$. Theorem 3 can thus be directly satisfied using Eq. (7.43) with $\alpha_0 = 2\rho$.

We conclude this section with two remarks. First of all, the above proof of Theorem 3 does not attempt to derive the minimal α_0. In the following section we study a computational method to obtain an α_0 which is as small as possible. Secondly, we can use $\mathscr{C}(\boldsymbol{V}_{\boldsymbol{s}}) \oplus \mathscr{C}_{\boldsymbol{s}}$ as an approximate characterization of $\mathscr{K}(\boldsymbol{s})$ noting that the accuracy of such a characterization can be measured by the minimal value of α_0. An explicit formulation of a sub-optimality guarantee for a solution of UQP based on the above $\mathscr{K}(\boldsymbol{s})$ approximation is derived in the following section.

7.5 MERIT for UQP

Using the previous results, namely the one-to-one mapping introduced in Theorem 1 and the approximation of $\mathscr{K}(\boldsymbol{s})$ derived in Section 7.4, we build a sequence of matrices (for which the UQP global optima are known) whose distance from a given matrix is decreasing. The proposed iterative approach can be used to solve for the global optimum of UQP or at least to obtain a local optimum (with an upper bound on the sub-optimality of the solution). The sub-optimality guarantees are derived noting that the proposed method decreases an upper bound on the sub-optimality of the obtained UQP solution in each iteration.

We know from Theorem 3 that if $\boldsymbol{s}$ is a stable point of the UQP associated with $\boldsymbol{R}$ then there exist matrices $\boldsymbol{Q_s} \in \mathscr{C}_{\boldsymbol{s}}$, $\boldsymbol{P_s} \in \mathscr{C}(\boldsymbol{V_s})$ and a scalar $\alpha_0 \geq 0$ such that

$$\boldsymbol{R} + \alpha_0 \boldsymbol{s}\boldsymbol{s}^H = \boldsymbol{Q_s} + \boldsymbol{P_s}. \tag{7.44}$$

Eq. (7.44) can be rewritten as

$$\boldsymbol{R} + \alpha_0 \boldsymbol{s}\boldsymbol{s}^H = (\boldsymbol{Q_1} + \boldsymbol{P_1}) \odot (\boldsymbol{s}\boldsymbol{s}^H) \tag{7.45}$$

where $\boldsymbol{Q_1} \in \mathscr{C}_{\boldsymbol{1}}$, $\boldsymbol{P_1} \in \mathscr{C}(\boldsymbol{V_1})$. We first consider the case of $\alpha_0 = 0$ which corresponds to the global optimality of $\boldsymbol{s}$.

7.5.1 Global Optimization of UQP (the Case of $\alpha_0 = 0$)

Consider the optimization problem:

$$\min_{\boldsymbol{s} \in \Omega^n, \boldsymbol{Q_1} \in \mathscr{C}_{\boldsymbol{1}}, \boldsymbol{P_1} \in \mathscr{C}(\boldsymbol{V_1})} \|\boldsymbol{R} - (\boldsymbol{Q_1} + \boldsymbol{P_1}) \odot (\boldsymbol{s}\boldsymbol{s}^H)\|_F \tag{7.46}$$

Note that, as $\mathscr{C}_{\boldsymbol{1}} \oplus \mathscr{C}(\boldsymbol{V_1})$ is a convex cone, the global optimizers $\boldsymbol{Q_1}$ and $\boldsymbol{P_1}$ of (7.46) for any given $\boldsymbol{s}$ can be easily found. On the other hand, the problem of finding an optimal $\boldsymbol{s}$ for fixed $\boldsymbol{R_1} = \boldsymbol{Q_1} + \boldsymbol{P_1}$ is non-convex and hence more difficult to solve globally (see below for details).

We will assume that $\boldsymbol{R_1}$ is a positive definite matrix. To justify this assumption let $\overline{\boldsymbol{R}} = \boldsymbol{R} \odot (\boldsymbol{s}\boldsymbol{s}^H)^*$ and note that the eigenvalues of $\overline{\boldsymbol{R}}$ are exactly the same as those of $\boldsymbol{R}$, hence $\overline{\boldsymbol{R}}$ is positive definite. Suppose that we have

$$\begin{cases} \mathbf{x}^H \overline{\boldsymbol{R}} \mathbf{x} > \varepsilon, \ \ \forall \text{ unit-norm } \mathbf{x} \in \mathbb{C}^{n \times 1} \\ \|\overline{\boldsymbol{R}} - \boldsymbol{R_1}\|_F \leq \varepsilon \end{cases} \tag{7.47}$$

for some $\varepsilon \geq 0$. It follows from (7.47) that

$$\begin{aligned} \mathbf{x}^H \boldsymbol{R_1} \mathbf{x} &\geq \mathbf{x}^H \overline{\boldsymbol{R}} \mathbf{x} - |\mathbf{x}^H \overline{\boldsymbol{R}} \mathbf{x} - \mathbf{x}^H \boldsymbol{R_1} \mathbf{x}| \\ &> \varepsilon - |\mathbf{x}^H (\overline{\boldsymbol{R}} - \boldsymbol{R_1}) \mathbf{x}| \\ &\geq \varepsilon - |\sigma_1 (\overline{\boldsymbol{R}} - \boldsymbol{R_1})| \\ &\geq \varepsilon - \|\overline{\boldsymbol{R}} - \boldsymbol{R_1}\|_F \geq 0 \end{aligned} \tag{7.48}$$

which implies that $\boldsymbol{R_1}$ is also a positive definite matrix. The conditions in (7.47) can be met as follows. By considering the partial minimization of (7.46) only with respect to the component of $\boldsymbol{R_1}$ in $\mathscr{C}(\boldsymbol{V_1})$ (namely $\boldsymbol{P_1}$) we observe that any positive (i.e. with $\lambda > 0$) diagonal loading of $\boldsymbol{R}$, which leads to the same diagonal loading of $\overline{\boldsymbol{R}}$ (as $\overline{\boldsymbol{R}} + \lambda \boldsymbol{I} = \boldsymbol{R} \odot (\boldsymbol{s}\boldsymbol{s}^H)^* + \lambda \boldsymbol{I} = (\boldsymbol{R} + \lambda \boldsymbol{I}) \odot (\boldsymbol{s}\boldsymbol{s}^H)^*$), will be absorbed[1] in $\boldsymbol{P_1}$. Therefore, a positive diagonal

[1] i.e. the optimal $\boldsymbol{P_1}$ will be the same as before but with the same diagonal loading.

loading of $\boldsymbol{R}$ does not change $\|\overline{\boldsymbol{R}}-\boldsymbol{R_1}\|_F$ but increases $\mathbf{x}^H\overline{\boldsymbol{R}}\mathbf{x}$ by λ. We also note that due to $\|\overline{\boldsymbol{R}}-\boldsymbol{R_1}\|_F$ being monotonically decreasing through the iterations of the method, if the conditions in (7.47) hold for the solution obtained in any iteration, it will hold for all the iterations afterward.

In the following, we study a suitable diagonal loading of $\boldsymbol{R}$ that ensures meeting the conditions in (7.47). Next the optimization of the function in (7.46) is discussed through a separate optimization over the three variables of the problem.

• *Diagonal loading of* $\boldsymbol{R}$*:* As will be explained later, we can compute $\boldsymbol{Q_1}$ and $\boldsymbol{P_1}$, (hence $\boldsymbol{R_1}=\boldsymbol{Q_1}+\boldsymbol{P_1}$) for any initialization of $\boldsymbol{s}$. In order to guarantee the positive definiteness of $\boldsymbol{R_1}$, define

$$\varepsilon_0 \triangleq \|\overline{\boldsymbol{R}}-\boldsymbol{R_1}\|_F. \tag{7.49}$$

Then we suggest to diagonally load $\boldsymbol{R}$ with $\lambda>\lambda_0=-\sigma_n(\boldsymbol{R})+\varepsilon_0$:

$$\boldsymbol{R}\leftarrow\boldsymbol{R}+\lambda\boldsymbol{I}. \tag{7.50}$$

• *Optimization with respect to* $\boldsymbol{Q_1}$*:* We restate the objective function of (7.46) as

$$\begin{aligned} & \|\boldsymbol{R}-(\boldsymbol{Q_1}+\boldsymbol{P_1})\odot(\boldsymbol{s}\boldsymbol{s}^H)\|_F \\ = \;& \|\underbrace{\left(\boldsymbol{R}\odot(\boldsymbol{s}\boldsymbol{s}^H)^*-\boldsymbol{P_1}\right)}_{\boldsymbol{R}_Q}-\boldsymbol{Q_1}\|_F. \end{aligned} \tag{7.51}$$

Given $\boldsymbol{R}_Q$, the partial minimization of (7.46) with respect to $\boldsymbol{Q_1}$ can be written as

$$\min_{\boldsymbol{Q_1}\in\mathscr{C}_{\boldsymbol{1}}} \|\boldsymbol{R}_Q-\boldsymbol{Q_1}\|_F. \tag{7.52}$$

which is equivalent to

$$\begin{aligned} &\min_{\boldsymbol{Q_1},\rho} \|\boldsymbol{R}_Q-\boldsymbol{Q_1}\|_F \\ &\text{s.t. } \boldsymbol{Q_1}\mathbf{1}=\rho\mathbf{1}, \\ &\quad \sigma_1(\boldsymbol{Q_1})=\rho. \end{aligned} \tag{7.53}$$

In [**?**], the authors have derived an explicit solution for the optimization problem

$$\begin{aligned} &\min_{\boldsymbol{Q_1}} \|\boldsymbol{R}_Q-\boldsymbol{Q_1}\|_F \\ &\text{s.t. } \boldsymbol{Q_1}\mathbf{1}=\rho\mathbf{1}.\ (\rho=\text{given}) \end{aligned} \tag{7.54}$$

The explicit solution of (7.54) is given by

$$\begin{aligned} & \boldsymbol{Q_1}(\rho) \\ = \;& \rho\boldsymbol{I}_n+(\boldsymbol{I}_n-\frac{\mathbf{1}_{n\times n}}{n})(\boldsymbol{R}_Q-\rho\boldsymbol{I}_n)(\boldsymbol{I}_n-\frac{\mathbf{1}_{n\times n}}{n}) \\ = \;& \boldsymbol{R}_Q+\frac{\rho}{n}\mathbf{1}_{n\times n}-\frac{2}{n}(\boldsymbol{R}_Q\mathbf{1}_{n\times n})+\frac{1}{n^2}(\mathbf{1}_{n\times n}\boldsymbol{R}_Q\mathbf{1}_{n\times n}) \end{aligned} \tag{7.55}$$

Note that

$$\boldsymbol{Q_1}(\rho') - \boldsymbol{Q_1}(\rho) = (\rho' - \rho)(\mathbf{1}_{n\times 1}/\sqrt{n})(\mathbf{1}_{n\times 1}/\sqrt{n})^T \tag{7.56}$$

which implies that except for the eigenpair $(\mathbf{1}_{n\times 1}/\sqrt{n}, \rho)$, all other eigenvalue/vectors are independent of ρ. Let ρ_0 represent the maximal eigenvalue of $\boldsymbol{Q_1}(0)$ corresponding to an eigenvector other than $\mathbf{1}_{n\times 1}/\sqrt{n}$. More interesting, the set of the optimal solutions of (7.54) for different ρ form a line in $\mathbb{C}^{n^2}$ described as in (7.56). Therefore, (7.52) is equivalent to

$$\begin{aligned} \min_{\rho} \|\boldsymbol{R}_Q - \boldsymbol{Q_1}(\rho)\|_F \\ \text{s.t. } \rho \geq \rho_0. \end{aligned} \tag{7.57}$$

It follows from (7.55) that

$$\|\boldsymbol{R}_Q - \boldsymbol{Q_1}(\rho)\|_F^2 = \sum_{k=1}^{n} n \left| \frac{\rho}{n} - \frac{2G_k}{n} + \frac{H}{n^2} \right|^2 \tag{7.58}$$

where G_k and H are the sum of the k^{th} row and, respectively, the sum of all entries of $\boldsymbol{R}_Q$. The ρ that minimizes (7.58) is given by

$$\rho = \frac{1}{n} \sum_{k=1}^{n} \Re \left(2G_k - \frac{H}{n} \right) = \frac{H}{n} \tag{7.59}$$

which implies that the minimizer $\rho = \rho_\star$ of (7.57) is equal to

$$\rho_\star = \begin{cases} \frac{H}{n} & \frac{H}{n} \geq \rho_0, \\ \rho_0 & \text{otherwise.} \end{cases} \tag{7.60}$$

Finally, the optimal solution $\boldsymbol{Q_1}$ to (7.52) is given by

$$\boldsymbol{Q_1} = \boldsymbol{Q_1}(\rho_\star). \tag{7.61}$$

• *Optimization with respect to* $\boldsymbol{P_1}$*:* Similar to the previous case, (7.46) can be rephrased as

$$\min_{\boldsymbol{Q_1} \in \mathscr{C}(\boldsymbol{V_1})} \|\boldsymbol{R}_P - \boldsymbol{P_1}\|_F \tag{7.62}$$

where $\boldsymbol{R}_P = \boldsymbol{R} \odot (\boldsymbol{s}\boldsymbol{s}^H)^* - \boldsymbol{Q_1}$. The solution of (7.62) is simply given by

$$\boldsymbol{P_1}(k,l) = \begin{cases} \boldsymbol{R}'_P(k,l) & \boldsymbol{R}'_P(k,l) \geq 0 \text{ or } k = l, \\ 0 & \text{otherwise} \end{cases} \tag{7.63}$$

where $\boldsymbol{R}'_P = \Re\{\boldsymbol{R}_P\}$.

• *Optimization with respect to* $\boldsymbol{s}$*:* Suppose that $\boldsymbol{Q_1}$ and $\boldsymbol{P_1}$ are given and that

$\boldsymbol{R_1} = \boldsymbol{Q_1} + \boldsymbol{P_1}$ is a positive definite matrix (see the discussion on this aspect following Eq. (7.46)). Then we have

$$\begin{aligned} & \|\boldsymbol{R} - \boldsymbol{R_1} \odot (\boldsymbol{s}\boldsymbol{s}^H)\|_F^2 \\ = \; & \|\boldsymbol{R} - \mathbf{Diag}(\boldsymbol{s})\, \boldsymbol{R_1}\, \mathbf{Diag}(\boldsymbol{s}^*)\|_F^2 \\ = \; & \mathrm{tr}(\boldsymbol{R}^2) + \mathrm{tr}(\boldsymbol{R_1}^2) - 2\Re\{\mathrm{tr}(\boldsymbol{R}\, \mathbf{Diag}(\boldsymbol{s})\, \boldsymbol{R_1}\, \mathbf{Diag}(\boldsymbol{s}^*))\}. \end{aligned} \tag{7.64}$$

Note that only the third term of (7.64) is a function of $\boldsymbol{s}$. Moreover, it can be verified that [151]

$$\mathrm{tr}(\boldsymbol{R}\, \mathbf{Diag}(\boldsymbol{s})\, \boldsymbol{R_1}\, \mathbf{Diag}(\boldsymbol{s}^*)) = \boldsymbol{s}^H (\boldsymbol{R} \odot \boldsymbol{R_1}^T)\boldsymbol{s}. \tag{7.65}$$

As $\boldsymbol{R} \odot \boldsymbol{R_1}^T$ is positive definite, we can employ the power method-like iterations introduced in (7.28) to decrease the criterion in (7.46), i.e. starting from the current $\boldsymbol{s} = \boldsymbol{s}^{(0)}$, a local optimum of the problem can be obtained by the iterations

$$\boldsymbol{s}^{(t+1)} = e^{j \arg((\boldsymbol{R} \odot \boldsymbol{R_1}^T)\boldsymbol{s}^{(t)})}. \tag{7.66}$$

Remark 2: Note that the ability of using more general constraints (e.g. the PAR constraint) in the power method-like iterations means that MERIT can deal with such generalized constraints. This is basically due to the fact that the optimization of the MERIT criterion with respect to $\boldsymbol{s}$ is accomplished via the power method-like iterations. ■

Finally, the proposed algorithmic optimization of (7.46) based on the above results is summarized in Table 7.1-A.

7.5.2 Achieving a Local Optimum of UQP (the Case of $\alpha_0 > 0$)

There exist examples for which the objective function in (7.46) does not converge to zero. As a result, the proposed method cannot obtain a global optimum of UQP in such cases. However, it is still possible to obtain a local optimum of UQP for some $\alpha_0 > 0$. To do so, we solve the optimization problem,

$$\min_{\boldsymbol{s} \in \Omega, \boldsymbol{Q_1} \in \mathscr{C}_1, \boldsymbol{P_1} \in \mathscr{C}(\boldsymbol{V_1})} \|\boldsymbol{R}' - (\boldsymbol{Q_1} + \boldsymbol{P_1}) \odot (\boldsymbol{s}\boldsymbol{s}^H)\|_F \tag{7.67}$$

with $\boldsymbol{R}' = \boldsymbol{R} + \alpha_0 \boldsymbol{s}\boldsymbol{s}^H$, for increasing α_0. It is worth pointing out that achieving a zero value for the criterion in (7.67) implies $\boldsymbol{R} + \alpha_0 \boldsymbol{s}\boldsymbol{s}^H \in \mathscr{K}(\boldsymbol{s})$. As a result, there exists a non-negative $\boldsymbol{v} \in \mathbb{R}^n$ such that

$$(\boldsymbol{R} + \alpha_0 \boldsymbol{s}\boldsymbol{s}^H)\boldsymbol{s} = \boldsymbol{v} \odot \boldsymbol{s}. \tag{7.68}$$

Consequently,

$$\boldsymbol{R}\boldsymbol{s} = (\boldsymbol{v} - n\alpha_0 \mathbf{1}) \odot \boldsymbol{s} \tag{7.69}$$

Table 7.1. *The MERIT Algorithm*

(A) The case of $\alpha_0 = 0$

Step 0: Initialize the variables $\boldsymbol{Q_1}$ and $\boldsymbol{P_1}$ with $\boldsymbol{I}$. Let $\boldsymbol{s}$ be a random vector in Ω^n.
Step 1: Perform the diagonal loading of $\boldsymbol{R}$ as in (7.49)-(7.50) (note that this diagonal loading is sufficient to keep $\boldsymbol{R_1} = \boldsymbol{Q_1} + \boldsymbol{P_1}$ always positive definite).
Step 2: Obtain the minimum of (7.46) with respect to $\boldsymbol{Q_1}$ as in (7.61).
Step 3: Obtain the minimum of (7.46) with respect to $\boldsymbol{P_1}$ using (7.63).
Step 4: Minimize (7.46) with respect to $\boldsymbol{s}$ using (7.66).
Step 5: Goto step 2 until a stop criterion is satisfied, e.g. $\|\boldsymbol{R} - (\boldsymbol{Q_1} + \boldsymbol{P_1}) \odot (\boldsymbol{s}\boldsymbol{s}^H)\|_F \leq \varepsilon_0$ (or if the number of iterations exceeded a predefined maximum number).

(B) The case of $\alpha_0 > 0$

Step 0: Initialize the variables $(\boldsymbol{s}, \boldsymbol{Q_1}, \boldsymbol{P_1})$ using the results obtained by the optimization of (7.46) as in Table 7.1-A.
Step 1: Set δ (the step size for increasing α_0 in each iteration). Let δ_0 be the minimal δ to be considered and $\alpha_0 = 0$.
Step 2: Let $\alpha_0^{pre} = \alpha_0$, $\alpha_0^{new} = \alpha_0 + \delta$ and $\boldsymbol{R}' = \boldsymbol{R} + \alpha_0^{new}\boldsymbol{s}\boldsymbol{s}^H$.
Step 3: Solve (7.67) using the steps 2-5 in Table 7.1-A (particularly step 4 must be applied to (7.71)).
Step 4: If $\|\boldsymbol{R}' - (\boldsymbol{Q_1} + \boldsymbol{P_1}) \odot (\boldsymbol{s}\boldsymbol{s}^H)\|_F \leq \varepsilon_0$ do:

- **Step 4-1**: If $\delta \geq \delta_0$, let $\delta \leftarrow \delta/2$ and initialize (7.67) with the previously obtained variables $(\boldsymbol{s}, \boldsymbol{Q_1}, \boldsymbol{P_1})$ for $\alpha_0 = \alpha_0^{pre}$. Goto step 2.
- **Step 4-2**: If $\delta < \delta_0$, stop.

Else, let $\alpha_0 = \alpha_0^{new}$ and goto step 2.

which implies $\boldsymbol{s}$ is a stationary point of the UQP associated with $\boldsymbol{R}$.

The optimization problem in (7.67) can be tackled using the same tools as proposed for (7.46). In particular, note that increasing α_0 decreases (7.67). To observe this, suppose that the solution $(\boldsymbol{s}, \boldsymbol{Q_1}, \boldsymbol{P_1})$ of (7.67) is given for an $\alpha_0 \geq 0$. The minimization of (7.67) with respect to $\boldsymbol{Q_1}$ for $\alpha_0^{new} = \alpha_0 + \delta$ ($\delta > 0$) yields $\widetilde{\boldsymbol{Q}}_{\boldsymbol{1}} \in \mathscr{C}_{\boldsymbol{1}}$ such that

$$\begin{aligned} & \|\boldsymbol{R} + \alpha_0^{new}\boldsymbol{s}\boldsymbol{s}^H - (\widetilde{\boldsymbol{Q}}_{\boldsymbol{1}} + \boldsymbol{P_1}) \odot (\boldsymbol{s}\boldsymbol{s}^H)\|_F \\ \leq \; & \|\boldsymbol{R} + \alpha_0^{new}\boldsymbol{s}\boldsymbol{s}^H - ((\boldsymbol{Q_1} + \delta \boldsymbol{1}\boldsymbol{1}^T) + \boldsymbol{P_1}) \odot (\boldsymbol{s}\boldsymbol{s}^H)\|_F \\ = \; & \|\boldsymbol{R} + \alpha_0 \boldsymbol{s}\boldsymbol{s}^H - (\boldsymbol{Q_1} + \boldsymbol{P_1}) \odot (\boldsymbol{s}\boldsymbol{s}^H)\|_F \end{aligned} \tag{7.70}$$

where $\boldsymbol{Q_1} + \delta \boldsymbol{1}\boldsymbol{1}^T \in \mathscr{C}_{\boldsymbol{1}}$. The optimization of (7.67) with respect to $\boldsymbol{P_1}$ can be dealt with as before (see (7.46)) and it leads to a further decrease of the objective function. Furthermore,

$$\begin{aligned} & \|\boldsymbol{R} + \alpha_0 \boldsymbol{s}\boldsymbol{s}^H - (\boldsymbol{Q_1} + \boldsymbol{P_1}) \odot (\boldsymbol{s}\boldsymbol{s}^H)\|_F \\ = \; & \|\boldsymbol{R} + \lambda' \boldsymbol{I} - (\boldsymbol{Q_1} + \boldsymbol{P_1} - \alpha_0 \boldsymbol{1}\boldsymbol{1}^T + \lambda' \boldsymbol{I}) \odot (\boldsymbol{s}\boldsymbol{s}^H)\|_F \end{aligned} \tag{7.71}$$

which implies that a solution $\boldsymbol{s}$ of (7.67) can be obtained via optimizing (7.71) with respect to $\boldsymbol{s}$ in a similar way as we described for (7.46) provided that $\lambda' \geq 0$ is such that $\boldsymbol{Q_1} + \boldsymbol{P_1} - \alpha_0 \boldsymbol{1}\boldsymbol{1}^T + \lambda' \boldsymbol{I}$ is positive definite. Finally, note that the obtained solution $(\boldsymbol{s}, \boldsymbol{Q_1}, \boldsymbol{P_1})$ of (7.46) can be used to initialize the corresponding variables in (7.67). In effect, the solution of (7.67) for any α_0 can be used for the initialization of (7.67) with an increased α_0.

Based on the above discussion and the fact that small values of α_0 are of interest, a bisection approach can be used to obtain α_0. The proposed method for obtaining a local optimum of UQP along with the corresponding α_0 is described in Table 7.1-B. Using the proposed algorithm, the task of finding the minimal α_0 can be accomplished within *finite number of steps*, see Appendix 7.8.6.

7.5.3 Sub-Optimality Analysis

In this sub-section, we show how the proposed method can provide real-time sub-optimality guarantees and bounds during its iterations. Let $\alpha_0 = 0$ (as a result $\boldsymbol{R}' = \boldsymbol{R}$) and define

$$\boldsymbol{E} \triangleq \boldsymbol{R}' - \underbrace{(\boldsymbol{Q_1} + \boldsymbol{P_1}) \odot (\boldsymbol{s}\boldsymbol{s}^H)}_{\boldsymbol{R_s}} \tag{7.72}$$

where $\boldsymbol{Q_1} \in \mathscr{C}_1$ and $\boldsymbol{P_1} \in \mathscr{C}(\boldsymbol{V_1})$. By construction, the global optimum of the UQP associated with $\boldsymbol{R_s}$ is $\boldsymbol{s}$. We have that

$$\begin{aligned} \max_{\boldsymbol{s}' \in \Omega^n} \boldsymbol{s}'^H \boldsymbol{R} \boldsymbol{s}' &\leq \max_{\boldsymbol{s}' \in \Omega^n} \boldsymbol{s}'^H \boldsymbol{R_s} \boldsymbol{s}' + \max_{\boldsymbol{s}' \in \Omega^n} \boldsymbol{s}'^H \boldsymbol{E} \boldsymbol{s}' \\ &\leq \max_{\boldsymbol{s}' \in \Omega^n} \boldsymbol{s}'^H \boldsymbol{R_s} \boldsymbol{s}' + n\sigma_1(\boldsymbol{E}) \\ &= \boldsymbol{s}^H \boldsymbol{R_s} \boldsymbol{s} + n\sigma_1(\boldsymbol{E}) \end{aligned} \tag{7.73}$$

Furthermore,

$$\begin{aligned} \max_{\boldsymbol{s}' \in \Omega^n} \boldsymbol{s}'^H \boldsymbol{R} \boldsymbol{s}' &\geq \max_{\boldsymbol{s}' \in \Omega^n} \boldsymbol{s}'^H \boldsymbol{R_s} \boldsymbol{s}' + \min_{\boldsymbol{s}' \in \Omega^n} \boldsymbol{s}'^H \boldsymbol{E} \boldsymbol{s}' \\ &\geq \max_{\boldsymbol{s}' \in \Omega^n} \boldsymbol{s}'^H \boldsymbol{R_s} \boldsymbol{s}' + n\sigma_n(\boldsymbol{E}) \\ &= \boldsymbol{s}^H \boldsymbol{R_s} \boldsymbol{s} + n\sigma_n(\boldsymbol{E}) \end{aligned} \tag{7.74}$$

As a result, an upper bound and a lower bound on the objective function for the global optimum of (7.46) can be obtained *at each iteration*. In accordance to what discussed earlier, as

$$|\sigma_1(\boldsymbol{E})| \leq \|\boldsymbol{E}\|_F, \; |\sigma_n(\boldsymbol{E})| \leq \|\boldsymbol{E}\|_F \tag{7.75}$$

if $\|\boldsymbol{E}\|_F$ converges to zero we conclude from (7.73) and (7.74) that

$$\max_{\boldsymbol{s}' \in \Omega^n} \boldsymbol{s}'^H \boldsymbol{R} \boldsymbol{s}' = \boldsymbol{s}^H \boldsymbol{R_s} \boldsymbol{s} = \boldsymbol{s}^H \boldsymbol{R} \boldsymbol{s} \tag{7.76}$$

and hence $\boldsymbol{s}$ is the global optimum of the UQP associated with $\boldsymbol{R}$ (i.e. a sub-optimality guarantee of $\gamma = 1$ is achieved).

Next, suppose that we have to increase α_0 in order to obtain the convergence of $\|\boldsymbol{E}\|_F$ to zero. In such a case, we have that $\boldsymbol{R} = \boldsymbol{R_s} - \alpha_0 \boldsymbol{s}\boldsymbol{s}^H$ and as a result, $\max_{\boldsymbol{s}' \in \Omega^n} \boldsymbol{s}'^H \boldsymbol{R_s} \boldsymbol{s}' - \alpha_0 n^2 \leq \max_{\boldsymbol{s}' \in \Omega^n} \boldsymbol{s}'^H \boldsymbol{R} \boldsymbol{s}' \leq \max_{\boldsymbol{s}' \in \Omega^n} \boldsymbol{s}'^H \boldsymbol{R_s} \boldsymbol{s}'$ or equivalently,

$$\boldsymbol{s}^H \boldsymbol{R_s} \boldsymbol{s} - \alpha_0 n^2 \leq \max_{\boldsymbol{s}' \in \Omega^n} \boldsymbol{s}'^H \boldsymbol{R} \boldsymbol{s}' \leq \boldsymbol{s}^H \boldsymbol{R_s} \boldsymbol{s}. \tag{7.77}$$

The provided case-dependent sub-optimality guarantee is thus given by

$$\gamma = \frac{\boldsymbol{s}^H \boldsymbol{R} \boldsymbol{s}}{\boldsymbol{s}^H \boldsymbol{R_s} \boldsymbol{s}} = 1 - \frac{\alpha_0 n^2}{\boldsymbol{s}^H \boldsymbol{R_s} \boldsymbol{s}} = \frac{\boldsymbol{s}^H \boldsymbol{R} \boldsymbol{s}}{\boldsymbol{s}^H \boldsymbol{R} \boldsymbol{s} + \alpha_0 n^2}. \tag{7.78}$$

The following section provides empirical evidence to the fact that (7.78) can yield tighter sub-optimality guarantees than the currently known approximation guarantee of $\pi/4$ for SDR.

7.6 Numerical Examples

In order to examine the performance of the proposed method, several numerical examples will be presented. Random Hermitian matrices $\boldsymbol{R}$ are generated

using the formula

$$\boldsymbol{R} = \sum_{k=1}^{n} \mathbf{x}_k \mathbf{x}_k^H \tag{7.79}$$

where $\{\mathbf{x}_k\}$ are random vectors in $\mathbb{C}^n$ whose real-part and imaginary-part elements are i.i.d. with a standard Gaussian distribution $\mathcal{N}(0,1)$. In all cases, we stopped the iterations when $\|\boldsymbol{E}\|_F \leq 10^{-9}$.

We use the MERIT algorithm to solve the UQP for a random positive definite matrix of size $n = 16$. The obtained values of the UQP objective for the true matrix $\boldsymbol{R}$ and the approximated matrix $\boldsymbol{R_s}$ as well as the sub-optimality bounds (derived in (7.73) and (7.74)) are depicted in Fig. 7.2 versus the iteration number. In this example, a sub-optimality guarantee of $\gamma = 1$ is achieved which implies that the method has successfully obtained the global optimum of the considered UQP. A computational time of 3.653 sec was required to accomplish the task on a standard PC. For the sake of comparison, we also use the power method-like iterations discussed in Section 7.3, and MERIT, as well as the curvilinear search of [137] with Barzilai-Borwein (BB) step size, to solve an UQP ($n = 10$) based on the same initialization. The resultant UQP objectives along with required times (in sec) versus iteration number are plotted in Fig. 7.3. It can be observed that the power method-like iterations approximate the UQP solution much faster than the curvilinear search of [137]. On the other hand, both methods are much faster than MERIT. This type of behavior, which is not unexpected, is due to the fact that MERIT is not designed solely for local optimization; indeed, MERIT relies on a considerable over-parametrization in its formulation which is the cost paid for easily derivable sub-optimality guarantees. In general, one may employ the power method-like iterations to obtain a fast approximation of the UQP solution (e.g. by using several initializations), whereas for obtaining sub-optimality guarantees one can resort to MERIT.

Next, we approximate the UQP solutions for 20 full-rank random positive definite matrices of sizes $n \in \{8, 16, 32, 64\}$. Inspired by [140] and [152], we also consider rank-deficient matrices $\boldsymbol{R} = \sum_{k=1}^{d} \mathbf{x}_k \mathbf{x}_k^H$ where $\{\mathbf{x}_k\}$ are as in (7.79), but $d \ll n$. The performance of MERIT for different values of d is shown in Table 7.2. Interestingly, the solution of UQP for rank-deficient matrices appears to be more efficiently obtained than for full-rank matrices. We also employ SDR [147] to solve the same UQPs. Note also that given the solutions obtained by MERIT and SDR as well as the sub-optimality guarantee of MERIT, a case-dependent sub-optimality guarantee for SDR can be computed as

$$\gamma_{\text{SDR}} \triangleq \gamma_{\text{MERIT}} \left(\frac{v_{SDR}}{v_{MERIT}} \right). \tag{7.80}$$

This can be used to examine the goodness of the solutions obtained by SDR. In this example, we continue the randomization procedure of SDR until reaching

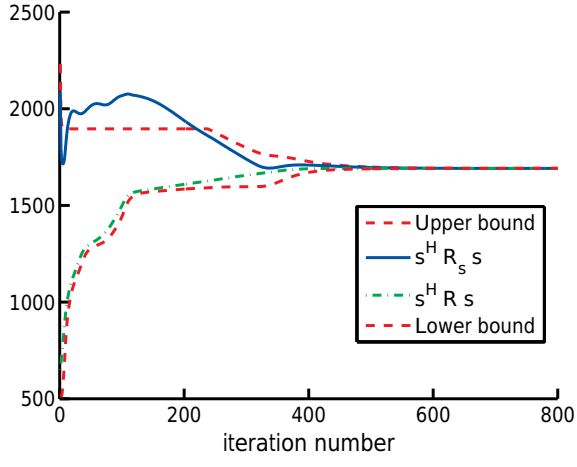

(a)

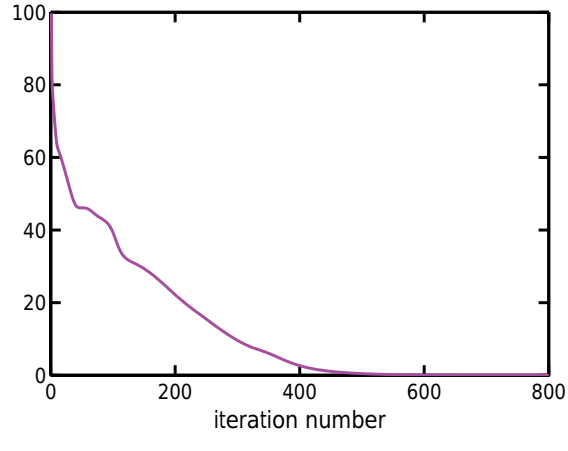

(b)

Figure 7.2. Different metrics versus the iteration number for an UQP solved by MERIT. (a) the UQP objective corresponding to the true matrix $\boldsymbol{R}$, the approximated matrix $\boldsymbol{R_s}$ and also the upper/lower bounds at each iteration. The sub-optimality bounds are updated using (7.73)-(7.74). (b) the criterion $\|\boldsymbol{E}\|_F = \|\boldsymbol{R} - \boldsymbol{R}_s\|_F$ (it reaches values which are practically zero).

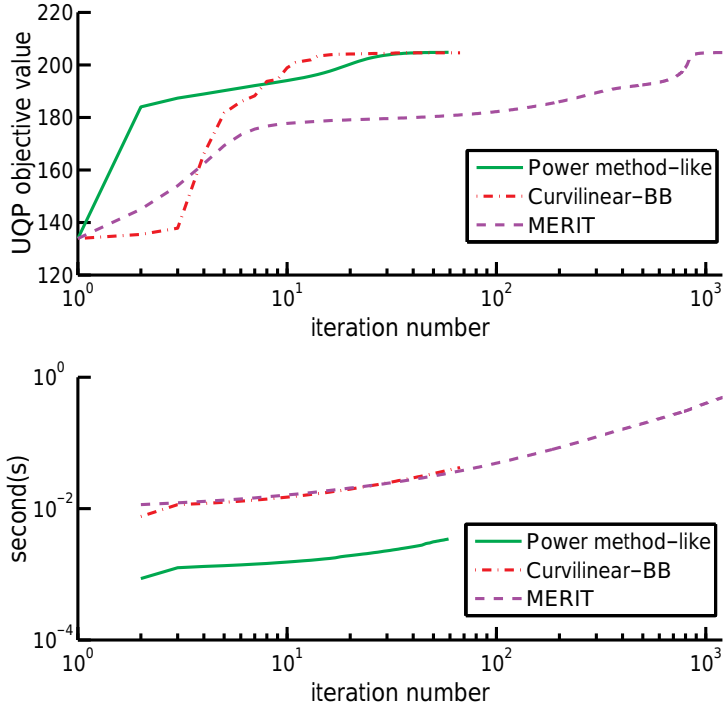

Figure 7.3. A comparison of power method-like iterations, the curvilinear search of [137] with Barzilai-Borwein (BB) step size, and MERIT: (top) the UQP objective; (bottom) the required time for solving an UQP ($n = 10$) with same initialization. The computation times for the three methods were 3.44×10^{-3}, 4.22×10^{-2}, and 4.89×10^{-1} (all in sec), respectively.

the same UQP objective as for MERIT. The results can be found in Table 7.2. The results imply that, although the average SDR time is less than MERIT in some cases, the average MERIT time appears to outperform that of SDR for larger dimensions n or lower matrix ranks d.

As discussed earlier, the UQP formulation occurs in different code design scenarios. An interesting code design problem arises when synthesizing waveforms that have good resolution properties in range and Doppler [3]-[5],[28]-[90]. In the following, we consider the design of a thumbtack CAF (see the definitions in Section 7.1.1):

$$d(\tau,f)=\begin{cases} n & (\tau,f)=(0,0), \\ 0 & \text{otherwise.} \end{cases} \tag{7.81}$$

Suppose $n=53$, let T be the time duration of the total waveform, and let $t_p=T/n$ represent the time duration of each sub-pulse. Define the weighting function as

$$w(\tau,f)=\begin{cases} 1 & (\tau,f)\in\Psi\backslash\Psi_{ml}, \\ 0 & \text{otherwise,} \end{cases} \tag{7.82}$$

where $\Psi=[-10t_p,10t_p]\times[-2/T,2/T]$ is the region of interest and $\Psi_{ml}=([-t_p,t_p]\backslash\{0\})\times([-1/T,1/T]$
$\backslash\{0\})$ is the mainlobe area which is excluded due to the sharp changes near the origin of $d(\tau,f)$. Note that the time delay τ and the Doppler frequency f are typically normalized by T and $1/T$, respectively, and as a result the value of t_p can be chosen freely without changing the performance of CAF design. The synthesis of the desired CAF is accomplished via the cyclic minimization of (7.8) with respect to $\mathbf{x}$ and $\boldsymbol{y}$ (see Section 7.1.1). In particular, we use MERIT to obtain a unimodular $\mathbf{x}$ in each iteration. A Björck code is used to initialize both vectors $\mathbf{x}$ and $\boldsymbol{y}$. The Björck code of length $n=p$ (where p is a prime number for which $p\equiv 1\ (\mod 4)$) is given by $\boldsymbol{b}(k)=e^{j(\frac{k}{p})\arccos\left(1/(1+\sqrt{p})\right)}$, $0\leq k<p$, with $(\frac{k}{p})$ denoting the Legendre symbol. Fig. 7.4 depicts the normalized CAF modulus of the Björck code (i.e. the initial CAF) and the obtained CAF using the UQP formulation in (7.11) and the proposed method. Despite the fact that designing CAF with a unimodular transmit vector $\mathbf{x}$ is a rather difficult problem, MERIT is able to efficiently suppress the CAF sidelobes in the region of interest.

7.7 Concluding Remarks

A computational approach to the NP-hard problem of optimizing a quadratic form over the unimodular vector set (called UQP) has been introduced. The main results can be summarized as follows:

n	Rank (d)	#problems for which $\gamma = 1$	Average γ	Minimum γ	Average MERIT CPU time (sec)	$\frac{\text{Average SDR time}}{\text{Average MERIT time}}$
8	*2*	17	0.9841	0.8184	0.13	1.08
	8	16	0.9912	0.9117	0.69	0.81
16	*2*	15	0.9789	0.8301	1.06	2.08
	4	13	0.9773	0.8692	1.58	0.95
	16	4	0.9610	0.8693	3.54	0.92
32	*2*	9	0.9536	0.8190	47.04	4.79
	6	4	0.9077	0.8106	55.59	2.44
	32	2	0.9031	0.8021	94.90	1.12
64	*2*	3	0.8893	0.8177	406.56	4.34
	8	1	0.8567	0.7727	560.35	2.07
	64	0	0.8369	0.7811	1017.69	1.85

Table 7.2. *Comparison of the performance of MERIT (see Table 7.1) and SDR [147] when solving the UQP for* 20 *random positive definite matrices of different sizes n and ranks d.*

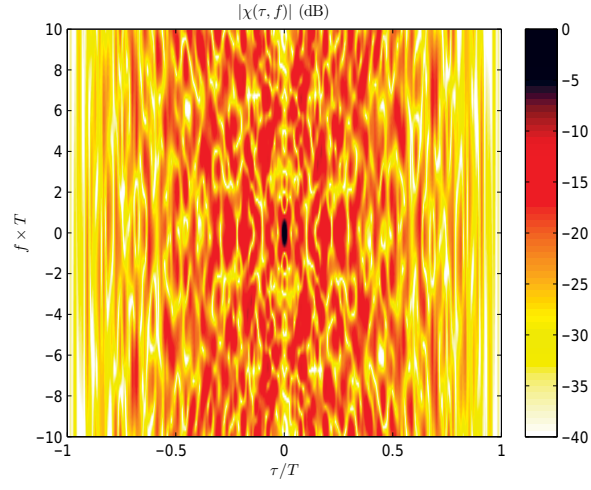

(a)

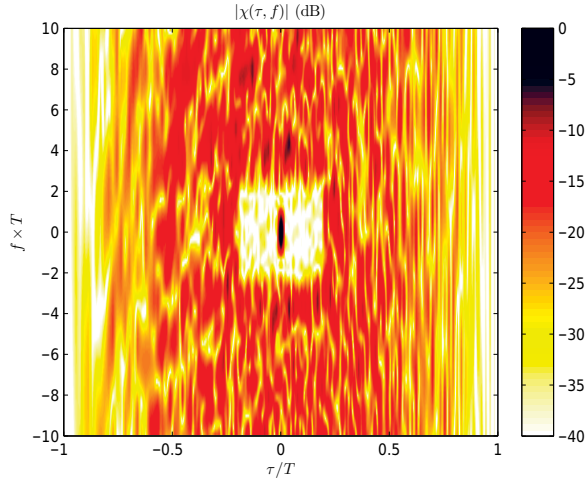

(b)

Figure 7.4. The normalized CAF modulus for (a) the Björck code of length $n = 53$ (i.e. the initial CAF), and (b) the UQP formulation in (7.11) and MERIT.

- Power method-like iterations were devised for local optimization. The proposed method was shown to be useful not only for the quadratic optimization over unimodular codes but also for some other types of code constraints. The particular example of PAR constrained code design was discussed in some detail.
- It was shown that the set of matrices $\mathscr{K}(\boldsymbol{s})$ leading to the same solution $\boldsymbol{s}$ as the global optimum of UQP is a convex cone. An one-to-one mapping between any two such convex cones was introduced and an approximate characterization of $\mathscr{K}(\boldsymbol{s})$ was proposed.
- Using the approximate characterization of $\mathscr{K}(\boldsymbol{s})$, an iterative approach (called MERIT) to the UQP was proposed. It was shown that MERIT provides real-time case-dependent sub-optimality guarantees during its iterations. The available numerical evidence shows that the sub-optimality guarantees obtained by MERIT may be better than the currently known approximation guarantee of $\pi/4$ for SDR.

We note that more rigorous efficiency assessments of the method would be useful. It is clear that $\mathscr{C}(\boldsymbol{V}_{\boldsymbol{s}}) \oplus \mathscr{C}_{\boldsymbol{s}} \subset \mathscr{K}(\boldsymbol{s})$. A possible approach would be to determine how large is the part of $\mathscr{K}(\boldsymbol{s})$ that is "covered" by $\mathscr{C}(\boldsymbol{V}_{\boldsymbol{s}}) \oplus \mathscr{C}_{\boldsymbol{s}}$; a research problem which is left for future work. Furthermore, a study of m-UQP using the ideas in this chapter will be the subject of a future research.

7.8 Appendices

7.8.1 Appendix A: Proof of Theorem 1

In order to verify the first part of the theorem, consider any two matrices $\boldsymbol{R}_1, \boldsymbol{R}_2 \in \mathscr{K}(\widetilde{\boldsymbol{s}})$. For any two non-negative scalars γ_1, γ_2 we have that

$$\boldsymbol{s}^H(\gamma_1\boldsymbol{R}_1 + \gamma_2\boldsymbol{R}_2)\boldsymbol{s} = \gamma_1\boldsymbol{s}^H\boldsymbol{R}_1\boldsymbol{s} + \gamma_2\boldsymbol{s}^H\boldsymbol{R}_2\boldsymbol{s}. \tag{7.83}$$

Clearly, if some $\boldsymbol{s} = \widetilde{\boldsymbol{s}}$ is the global maximizer of both $\boldsymbol{s}^H\boldsymbol{R}_1\boldsymbol{s}$ and $\boldsymbol{s}^H\boldsymbol{R}_2\boldsymbol{s}$ then it is the global maximizer of $\boldsymbol{s}^H(\gamma_1\boldsymbol{R}_1 + \gamma_2\boldsymbol{R}_2)\boldsymbol{s}$ which implies $\gamma_1\boldsymbol{R}_1 + \gamma_2\boldsymbol{R}_2 \in \mathscr{K}(\widetilde{\boldsymbol{s}})$.

The second part of the theorem can be shown noting that

$$\begin{aligned} \boldsymbol{s}_2^H(\boldsymbol{R} \odot (\boldsymbol{s}_0\boldsymbol{s}_0^H))\boldsymbol{s}_2 &= (\boldsymbol{s}_0^* \odot \boldsymbol{s}_2)^H\boldsymbol{R}(\boldsymbol{s}_0^* \odot \boldsymbol{s}_2) \\ &= \boldsymbol{s}_1^H\boldsymbol{R}\boldsymbol{s}_1 \end{aligned} \tag{7.84}$$

for all $\boldsymbol{s}_1, \boldsymbol{s}_2 \in \Omega^n$ and $\boldsymbol{s}_0 = \boldsymbol{s}_1^* \odot \boldsymbol{s}_2$. Therefore, if $\boldsymbol{R} \in \mathscr{K}(\widetilde{\boldsymbol{s}}_1)$ then $\boldsymbol{R} \odot (\widetilde{\boldsymbol{s}}_0\widetilde{\boldsymbol{s}}_0^H) \in \mathscr{K}(\widetilde{\boldsymbol{s}}_2)$ (for $\widetilde{\boldsymbol{s}}_0 = \widetilde{\boldsymbol{s}}_1^* \odot \widetilde{\boldsymbol{s}}_2$) and vice versa.

7.8.2 Appendix B: Characterization of the Stationary Points and Optima of UQP

Let $\boldsymbol{s} = (e^{j\phi_1}, \cdots, e^{j\phi_n})^T$ and note that

$$\begin{aligned} L &= \boldsymbol{s}^H \boldsymbol{R} \boldsymbol{s} = \sum_{k,l} \boldsymbol{R}(k,l) e^{j(\phi_l - \phi_k)} \\ &= \frac{1}{2} \left(\sum_{k,l} \boldsymbol{R}(k,l) e^{j(\phi_l - \phi_k)} + \sum_{k,l} \boldsymbol{R}(l,k) e^{j(\phi_k - \phi_l)} \right). \end{aligned} \tag{7.85}$$

To obtain the stationary points of UQP (associated with $\boldsymbol{R}$) one can write the following partial derivative equations for all $1 \leq k_0 \leq n$:

$$\begin{aligned} \frac{\partial L}{\partial \phi_{k_0}} &= \frac{1}{2} \Bigg(-j \sum_l \boldsymbol{R}(k_0,l) e^{j(\phi_l - \phi_{k_0})} \\ &\qquad + j \sum_l \boldsymbol{R}(l,k_0) e^{j(\phi_{k_0} - \phi_l)} \Bigg) \\ &= \Im \left\{ e^{-j\phi_{k_0}} \left(\sum_l \boldsymbol{R}(k_0,l) e^{j\phi_l} \right) \right\} = 0 \end{aligned} \tag{7.86}$$

which implies that there exist $v_{k_0} \in \mathbb{R}$ such that

$$\sum_l \boldsymbol{R}(k_0,l) e^{j\phi_l} = v_{k_0} e^{j\phi_{k_0}}. \tag{7.87}$$

Considering the above set of equations for all $1 \leq k_0 \leq n$ yields the characterization of the stationary points of L as

$$\boldsymbol{R}\widetilde{\boldsymbol{s}} = \boldsymbol{v} \odot \widetilde{\boldsymbol{s}} \tag{7.88}$$

where $\boldsymbol{v} \in \mathbb{R}^n$. Based on the latter characterization of the stationary points, we study the optima of UQP by employing the second derivatives of L. For any $l_0 \neq k_0$ we have that

$$\begin{aligned} \frac{\partial^2 L}{\partial \phi_{k_0} \partial \phi_{l_0}} &= \frac{1}{2} \Big(-j(j) \boldsymbol{R}(k_0,l_0) e^{j(\phi_{l_0} - \phi_{k_0})} \\ &\qquad + j(-j) \boldsymbol{R}(l_0,k_0) e^{j(\phi_{k_0} - \phi_{l_0})} \Big) \\ &= \Re\{ \boldsymbol{R}(k_0,l_0) e^{j(\phi_{l_0} - \phi_{k_0})} \}. \end{aligned} \tag{7.89}$$

For $l_0 = k_0$ we can write

$$\begin{aligned}\frac{\partial^2 L}{\partial \phi_{k_0}^2} &= \frac{1}{2}\Bigg(-j(-j)\sum_{l\neq k_0}\boldsymbol{R}(k_0,l)e^{j(\phi_l-\phi_{k_0})} \\ &\qquad +j(j)\sum_{l\neq k_0}\boldsymbol{R}(l,k_0)e^{j(\phi_{k_0}-\phi_l)}\Bigg) \\ &= \Re\{\boldsymbol{R}(k_0,k_0)-v_{k_0}\}.\end{aligned} \tag{7.90}$$

Therefore, the Hessian matrix associated with L is given by $\boldsymbol{H} = \Re\{\boldsymbol{R}\odot(\boldsymbol{s}\boldsymbol{s}^H)^* - \boldsymbol{V}\}$ where $\boldsymbol{V} = \mathbf{Diag}(\boldsymbol{v})$. As a direct consequence, $\boldsymbol{s}$ is a local maximum of UQP iff $\boldsymbol{H} \leq 0$, or equivalently $\boldsymbol{V} \geq \boldsymbol{R}$.

7.8.3 Appendix C: Proof of Theorem 4

It is worthwhile to observe that the convergence rate of $\{\boldsymbol{R}^{(t)}\}$ is not dependent on the problem dimension (n), as each entry of $\{\boldsymbol{R}^{(t)}\}$ is treated independently from the other entries (i.e. all the operations are element-wise). Therefore, without loss of generality we study the convergence of one entry (say $\{\boldsymbol{R}^{(t)}(k,l)\} = \{r_t e^{j\theta_t}\}$) in the following.

Note that in cases for which $|\theta_t - (\phi_k - \phi_l)| > \pi/2$, the next element of the sequence $\{r_t e^{j\theta_t}\}$ can be written as

$$r_{t+1}e^{j\theta_{t+1}} = r_t e^{j\theta_t} + \rho e^{j(\phi_k-\phi_l)} \tag{7.91}$$

which implies that the proposed operation tends to make θ_t closer to $(\phi_k - \phi_l)$ in each iteration, and finally puts θ_t within the $\pi/2$ distance from $(\phi_k - \phi_l)$.

Let us suppose that $|\theta_0 - (\phi_k - \phi_l)| > \pi/2$, and that the latter phase criterion remains satisfied for all θ_t, $t < T$. We have that

$$r_T e^{j\theta_T} = r_0 e^{j\theta_0} + T\rho e^{j(\phi_k-\phi_l)} \tag{7.92}$$

which yields

$$r_T\cos(\theta_T - (\phi_k-\phi_l)) = r_0\cos(\theta_0-(\phi_k-\phi_l)) + T\rho. \tag{7.93}$$

Therefore it takes only $T = \lceil -r_0\cos(\theta_0-(\phi_k-\phi_l))/\rho\rceil = 1$ iteration for θ_t to stand within the $\pi/2$ distance from $(\phi_k - \phi_l)$.

Now, suppose that $|\theta_0 - (\phi_k - \phi_l)| \leq \pi/2$. For every $t \geq 1$ we can write that

$$\begin{aligned}r_{t+1}e^{j\theta_{t+1}} &= r_t e^{j\theta_t} + \rho e^{j(\phi_k-\phi_l)} \\ &\quad -r_t\cos(\theta_t-(\phi_k-\phi_l))e^{j(\phi_k-\phi_l)} \\ &= e^{j(\phi_k-\phi_l)}\left(\rho + jr_t\sin(\theta_t-(\phi_k-\phi_l))\right).\end{aligned} \tag{7.94}$$

Let $\delta_{t+1} = r_{t+1}e^{j\theta_{t+1}} - r_t e^{j\theta_t}$. The first equality in (7.94) implies that

$$\delta_{t+1} = e^{j(\phi_k-\phi_l)}(\rho - r_t\cos(\theta_t - (\phi_k-\phi_l))). \tag{7.95}$$

On the other hand, the second equality in (7.94) implies that

$$\begin{aligned}\delta_{t+1} &= e^{j(\phi_k-\phi_l)}(\rho + jr_t\sin(\theta_t-(\phi_k-\phi_l))) \\ &\quad -e^{j(\phi_k-\phi_l)}(\rho + jr_{t-1}\sin(\theta_{t-1}-(\phi_k-\phi_l))) \\ &= je^{j(\phi_k-\phi_l)}(r_t\sin(\theta_t-(\phi_k-\phi_l)) \\ &\qquad -r_{t-1}\sin(\theta_{t-1}-(\phi_k-\phi_l)))\end{aligned} \tag{7.96}$$

for all $t \geq 1$. Note that in (7.95) and (7.96), δ_{t+1} is a complex number having different phases. We conclude

$$\delta_{t+1} = 0, \ \ \forall\, t \geq 1 \tag{7.97}$$

which shows that the sequence $\{r_t e^{j\theta_t}\}$ is convergent in one iteration. In sum, every entry of the matrix R will converge in at most two iterations (i.e. at most one to achieve a phase value within the $\pi/2$ distance from $(\phi_k - \phi_l)$, and one iteration thereafter).

7.8.4 Appendix D: Proof of Theorem 5

We use the same notations as in the proof of Theorem 4. If $|\theta_0 - (\phi_k - \phi_l)| \leq \pi/2$ then

$$\begin{aligned}r_2e^{j\theta_2} &= r_1e^{j\theta_1} \\ &= r_0e^{j\theta_0} + \rho e^{j(\phi_k-\phi_l)} \\ &- r_0\cos(\theta_0-(\phi_k-\phi_l))e^{j(\phi_k-\phi_l)}.\end{aligned} \tag{7.98}$$

On the other hand, if $|\theta_0 - (\phi_k - \phi_l)| > \pi/2$ we have that $r_1e^{j\theta_1} = r_0e^{j\theta_0} + \rho e^{j(\phi_k-\phi_l)}$. As a result, $r_1\cos(\theta_1 - (\phi_k-\phi_l)) = \rho + r_0\cos(\theta_0-(\phi_k-\phi_l))$ which implies

$$\begin{aligned}r_2e^{j\theta_2} &= r_1e^{j\theta_1} + \rho e^{j(\phi_k-\phi_l)} \\ &\quad -r_1\cos(\theta_1-(\phi_k-\phi_l))e^{j(\phi_k-\phi_l)} \\ &= \underbrace{r_0e^{j\theta_0} + \rho e^{j(\phi_k-\phi_l)}}_{r_1e^{j\theta_1}} + \rho e^{j(\phi_k-\phi_l)} \\ &\quad -\underbrace{(\rho + r_0\cos(\theta_0-(\phi_k-\phi_l)))}_{r_1\cos(\theta_1-(\phi_k-\phi_l))}e^{j(\phi_k-\phi_l)} \\ &= r_0e^{j\theta_0} + \rho e^{j(\phi_k-\phi_l)} \\ &\quad -r_0\cos(\theta_0-(\phi_k-\phi_l))e^{j(\phi_k-\phi_l)}.\end{aligned} \tag{7.99}$$

Now, it is easy to verify that (7.41) follows directly from (7.98) and (7.99).

7.8.5 Appendix E: Proof of Theorem 6

If $\boldsymbol{s}$ is a stable point of UQP associated with $\boldsymbol{R}^{(0)} = \boldsymbol{R}$ then we have that $\arg(\boldsymbol{s}) = \arg(\boldsymbol{R}\boldsymbol{s})$. Let $\boldsymbol{R}\boldsymbol{s} = \boldsymbol{v} \odot \boldsymbol{s}$ where $\boldsymbol{v}$ is a non-negative real-valued vector in $\mathbb{R}^n$. It follows that

$$\boldsymbol{v}(k)e^{j\phi_k} = \sum_{l=1}^{n} |\boldsymbol{R}(k,l)|e^{j\theta_{k,l}}e^{j\phi_l} \tag{7.100}$$

or equivalently

$$\boldsymbol{v}(k) = \sum_{l=1}^{n} |\boldsymbol{R}(k,l)|e^{j(\theta_{k,l}-(\phi_k-\phi_l))} \tag{7.101}$$

which implies that

$$\begin{cases} \sum_{l=1}^{n} |\boldsymbol{R}(k,l)|\cos(\theta_{k,l}-(\phi_k-\phi_l)) \geq 0 \\ \sum_{l=1}^{n} |\boldsymbol{R}(k,l)|\sin(\theta_{k,l}-(\phi_k-\phi_l)) = 0 \end{cases} \tag{7.102}$$

for all $1 \leq k \leq n$. Now, note that the recursive formula of the sequence $\{\boldsymbol{R}^{(t)}\}$ can be rewritten as

$$\boldsymbol{R}^{(t+1)} = \boldsymbol{R}^{(t)} - \mathbf{Diag}(\boldsymbol{s})\ (\boldsymbol{R}_{+}^{\boldsymbol{s}\,(t)} - \rho \mathbf{1}_{n\times n})\ \mathbf{Diag}(\boldsymbol{s}^*) \tag{7.103}$$

and as a result,

$$\boldsymbol{R}^{(t+1)}\boldsymbol{s} = \boldsymbol{R}^{(t)}\boldsymbol{s} - \mathbf{Diag}(\boldsymbol{s})\ (\boldsymbol{R}_{+}^{\boldsymbol{s}\,(t)} - \rho \mathbf{1}_{n\times n})\ \mathbf{1}_{n\times 1}. \tag{7.104}$$

It follows from (7.104) that if $\boldsymbol{s}$ is a stable point of the UQP associated with $\boldsymbol{R}^{(t)}$ (which implies the existence of non-negative real-valued vector $\boldsymbol{v}^{(t)}$ such that $\boldsymbol{R}^{(t)}\boldsymbol{s} = \boldsymbol{v}^{(t)} \odot \boldsymbol{s}$), then there exists $\boldsymbol{v}^{(t+1)} \in \mathbb{R}^n$ for which $\boldsymbol{R}^{(t+1)}\boldsymbol{s} = \boldsymbol{v}^{(t+1)} \odot \boldsymbol{s}$ and therefore,

$$\begin{aligned} \boldsymbol{v}^{(t+1)}(k)\, e^{j\phi_k} &= \sum_{l=1}^{n} |\boldsymbol{R}^{(t)}(k,l)|e^{j\theta_{k,l}}e^{j\phi_l} \\ &- \left(\left(\sum_{l=1}^{n} \boldsymbol{R}_{+}^{\boldsymbol{s}\,(t)}(k,l)\right) - n\rho\right) e^{j\phi_k}. \end{aligned} \tag{7.105}$$

Eq. (7.105) can be rewritten as

$$\begin{aligned} \boldsymbol{v}^{(t+1)}(k) &= \sum_{l=1}^{n} |\boldsymbol{R}^{(t)}(k,l)|e^{j(\theta_{k,l}-(\phi_k-\phi_l))} \\ &- \left(\sum_{l=1}^{n} \boldsymbol{R}_{+}^{\boldsymbol{s}\,(t)}(k,l)\right) + n\rho \end{aligned} \tag{7.106}$$

As indicated earlier, $\boldsymbol{s}$ being a stable point for $\boldsymbol{R}^{(0)}$ assures that the imaginary part of (7.106) is zero. To show that $\boldsymbol{s}$ is a stable point of the UQP associated with $\boldsymbol{R}^{(t+1)}$, we only need to verify that $\boldsymbol{v}^{(t+1)}(k) \geq 0$:

$$\begin{aligned} \boldsymbol{v}^{(t+1)}(k) &= \sum_{l=1}^{n} |\boldsymbol{R}^{(t)}(k,l)| \cos(\theta_{k,l} - (\phi_k - \phi_l)) \\ &- \left(\sum_{l=1}^{n} \boldsymbol{R}_{+}^{\boldsymbol{s}\,(t)}(k,l) \right) + n\rho \\ &= n\rho \\ &+ \sum_{l:\ (k,l) \notin \Theta} |\boldsymbol{R}^{(t)}(k,l)| \cos(\theta_{k,l} - (\phi_k - \phi_l)) \end{aligned} \tag{7.107}$$

Now note that the positivity of $\boldsymbol{v}^{(t+1)}(k)$ is concluded from (7.38). In particular, based on the discussions in the proof of Theorem 4, for $t = 1$, there is no $\theta_{k,l}$ such that $|\theta_{k,l} - (\phi_k - \phi_l)| \geq \pi/2$ and therefore $\boldsymbol{v}^{(2)}(k) = n\rho$ for all $1 \leq k \leq n$. As a result,

$$\boldsymbol{R}^{(2)}\boldsymbol{s} = n\rho\boldsymbol{s} \tag{7.108}$$

which implies that $\boldsymbol{s}$ is an eigenvector of $\boldsymbol{R}^{(2)}$ corresponding to the eigenvalue $n\rho$.

7.8.6 Appendix F: Finding the Minimal α_0 in Table 7.1-B (Case of $\alpha_0 > 0$) Requires a Finite Number of Steps

The results of Section 7.4 provide a theoretical upper bound on the minimal α_0 for which $\boldsymbol{R} + \alpha_0 \boldsymbol{s}\boldsymbol{s}^H \in \mathscr{C}(\boldsymbol{V}_{\boldsymbol{s}}) \oplus \mathscr{C}_{\boldsymbol{s}}$. Note that $\mathscr{C}(\boldsymbol{V}_{\boldsymbol{s}}) \oplus \mathscr{C}_{\boldsymbol{s}}$ is a convex cone, implying that any such α_0 (for which $\boldsymbol{R} + \alpha_0 \boldsymbol{s}\boldsymbol{s}^H \in \mathscr{C}(\boldsymbol{V}_{\boldsymbol{s}}) \oplus \mathscr{C}_{\boldsymbol{s}}$) would easily set the objective function of (7.67) to zero. Eq. (7.43) suggests that any $\alpha_0 \geq 2\rho$ can serve as the upper bound for the minimal α_0. Theorem 7 suggests that any $\rho \geq \mu/n$, where μ is the largest eigenvalue of $\boldsymbol{R}^{(2)}$ belonging to an eigenvector other than $\boldsymbol{s}$, can be used to construct such an upper bound on the minimal α_0. Using the results of Theorems 5 and 6 along with (7.43) implies that it is sufficient to consider

$$\begin{aligned} \rho &= \sigma_1 \left(\boldsymbol{R}^{(2)}(0) \right) / n \\ &= \sigma_1 \left(\boldsymbol{R} - (\boldsymbol{R}_{+}^{\boldsymbol{s}\,(0)} + \boldsymbol{R}_{+}^{\boldsymbol{s}\,(1)}) \odot (\boldsymbol{s}\boldsymbol{s}^H) \right) / n \\ &\leq \frac{3}{n} \|\boldsymbol{R}\|_F \end{aligned} \tag{7.109}$$

due to the definition of $\boldsymbol{R}_{+}^{\boldsymbol{s}}$ in (7.37). As a result, it is sufficient to consider

$$\alpha_0 = 2\rho \leq \frac{6}{n} \|\boldsymbol{R}\|_F \tag{7.110}$$

as an upper bound on the values of α_0 for which the objective function of (7.67) attains zero. It was shown in (7.70) that the objective function of (7.67) is monotonically decreasing with respect to α_0. Considering a step size δ for increasing α_0, it takes at most

$$\eta_1 = \left\lceil \left(\frac{6}{n} \|\boldsymbol{R}\|_F \right) / \delta \right\rceil \tag{7.111}$$

steps to achieve $f(\alpha_0^{new}) \triangleq \|\boldsymbol{R}' - (\boldsymbol{Q_1} + \boldsymbol{P_1}) \odot (\boldsymbol{s}\boldsymbol{s}^H)\|_F \leq \varepsilon_0$ in Step 4 of Table 7.1-B, where the bisection procedure starts. In each bisection, the step size δ will be divided by 2, until reaching a priori given precision (δ_0) of the obtained α_0. More precisely, let us suppose $(\alpha_0^{pre}, \alpha_0^{new}) = (\alpha_0, \alpha_0 + \delta)$ where $f(\alpha_0^{new}) = f(\alpha_0 + \delta) \leq \varepsilon_0$. At the next step, the bisection approach uses the new pair $(\alpha_0^{pre}, \alpha_0^{new}) = (\alpha_0, \alpha_0 + \delta/2)$ to check whether $f(\alpha_0 + \delta/2) \leq \varepsilon_0$. If $f(\alpha_0 + \delta/2) \leq \varepsilon_0$ then the bisection approach will be recursively applied for $(\alpha_0^{pre}, \alpha_0^{new}) = (\alpha_0, \alpha_0 + \delta/2)$. Otherwise, the algorithm considers $(\alpha_0^{pre}, \alpha_0^{new}) = (\alpha_0 + \delta/2, \alpha_0 + \delta)$ as the new candidate for applying the bisection procedure. Therefore, the number of steps required to obtain α_0 with a fixed precision δ_0 is given by

$$\eta_2 = \lceil \log_2(\delta/\delta_0) \rceil . \tag{7.112}$$

The latter result proves the finiteness of required number of steps for finding the minimal α_0— thanks to the upper bound $\eta_1 + \eta_2$ on the required steps.

Acknowledgement

We would like to thank Prof. Antonio De Maio for providing us with the MATLAB code for SDR. Moreover, we would like to thank Prof. Joakim Jaldén and the four anonymous reviewers for their constructive and to-the-point comments that helped us significantly in clarifying the ideas of this work.

8. Radar Code Design for Detection of Moving Targets

Abstract
In this chapter, we study the problem of pulsed-radar transmit code design for detection of moving targets in the presence of signal-dependent clutter. For unknown target Doppler shift, the optimal detector does not lead to a closed-form expression. Therefore, we resort to average and worst-case performance metrics of the optimal detector for code design. We propose several algorithms under two novel frameworks to solve highly non-convex design problems. We also consider low-peak-to-average-power ratio code design.

Keywords: Clutter, code design, moving target detection, optimal detector, peak-to-average-power ratio.

8.1 Introduction

Radars as well as many other active sensing systems face the simultaneous effects of signal-dependent and independent interferences. The signal-dependent interference, usually known as clutter, is the echo of the transmitted signals produced by uninteresting obstacles. On the other hand, the signal-independent interferences include various types of noise, jamming, and other unwanted emissions. Due to the difference between the target velocity and motions of the clutter scatteres, Doppler shifts of the moving targets play an important role in distinguishing the targets from clutter background. However, the target Doppler shift is usually unknown at the transmitter. Considering such an ambiguity along with the presence of clutter, and the practical implementation demands for low peak-to-average-power ratio (PAR) make the transmit code design a challenging task.

The signal design for radar performance improvement has been an active area of research in the last decades; however, the majority of previous works have considered either stationary target or clutter-free scenarios. The effect of clutter has been considered in early studies for stationary targets, or targets with known Doppler shifts (see e.g. [155–159]). In [160] a solution for the case of a stationary target with no clutter motion was derived; more concretely, [160] proposed a method for obtaining the spectrum of the optimal transmit signal, which is later used for the code's approximate synthesis. A related problem to that of [160] has been considered in [161] with a discrete-time model and PAR constraint (see also [162, 163]). In [164], two signal design approaches based on mutual information (MI) and signal-to-interference-plus noise ratio (SINR) metrics have been considered for stationary extended target recognition. Signal design for detection performance improvement of multiple-input multiple-output (MIMO) radars has been studied in [165] and [166] for stationary targets in the absence of clutter motion (see also [167]). Moreover, [168] considers stationary target classification for MIMO radars in white noise background. Some clutter-free scenarios are discussed in [169–171]. The unknown Doppler shift of the target has been taken into account in [172] and [173]. The reference [172] considers the worst-case

code design problem for clutter-free cases under a similarity constraint to a given code. The ideas of [172] are generalized in [173] where the PAR constraint is included.

In this chapter, we study the problem of radar signal design for detection of a moving target in the presence of clutter. Two different design methodologies including *average* and *worst-case* approaches are considered to handle the fact that the Doppler shift of the target is often unknown at the transmit side. The corresponding optimization problems are highly non-convex. To tackle these problems, we propose several novel algorithms under two frameworks for unconstrained and constrained design. Particularly, we introduce the **Co**nvexification via **Re**parametrization (CoRe) framework which considers a relaxation of the original design problem to a core semi-definite program (SDP), that we call CSDP. The CSDP is then followed by a code synthesis stage. Moreover, another framework based on a **C**yclic **A**lgorithm for **D**irect **CO**de **DE**sign (which we call CADCODE) is proposed to carry out a direct code design via cyclic minimization. The key contributions of this chapter are:

- The simultaneous presence of clutter (i.e. the signal-dependent interference) and the unknown Doppler shift of the moving targets is considered. To the best of our knowledge, designing codes for improving detection performance in such cases has not been addressed in the literature prior to this work.
- To deal with the unknown Doppler shift of the target, both average and worst-case performance metrics of the optimal detector (with known Doppler shift) are considered for code design. The connections between the considered metrics and the detection performance are also addressed. As a result, the proposed code design schemes enable the user with the possibility to choose the desired performance guarantees (at any occurred scenario) freely.
- The PAR constraint is taken into account in the code design. Several extensions of the proposed methods are derived to handle such constrained code design problems.
- Using the CSDP solution in the CoRe framework, computational upper bounds on the achievable values of the average and worst-case performance metrics are provided. The obtained upper bounds can be used as benchmarks to examine the goodness of codes obtained by different code design methods. In addition, they provide the system designers with a better insight into the optimal system performance in various scenarios.

The rest of this chapter is organized as follows. In Section II, we present the data modeling and derive the optimal detectors for both known and unknown target Doppler shift. The average design is studied in Section III. This section also includes a presentation of the CoRe and CADCODE frameworks. Section IV is dedicated to the worst-case code design. The PAR constrained code design is considered in Section V. Several numerical examples are provided in Section VI. Finally, Section VII concludes the chapter.

Notation: We use bold lowercase letters for vectors and bold uppercase letters for matrices. $(\cdot)^T$, $(\cdot)^*$ and $(\cdot)^H$ denote the vector/matrix transpose, the complex conjugate, and the Hermitian transpose, respectively. $\boldsymbol{I}_N$ represents the identity matrix in $\mathbb{C}^{N\times N}$. $\mathbf{1}$ and $\mathbf{0}$ are the all-one and the all-zero vectors/matrices. $\boldsymbol{e}_k$ is the k^{th} standard basis vector in $\mathbb{C}^N$. The Frobenius norm of a matrix $\boldsymbol{X}$ (denoted by $\|\boldsymbol{X}\|_F$) with entries $\{X_{k,l}\}$ is equal to $\left(\sum_{k,l}|X_{k,l}|^2\right)^{\frac{1}{2}}$. The l_2-norm of a vector $\mathbf{x}$ is denoted by $\|\mathbf{x}\|$. The symbol $\odot$ stands for the Hadamard (element-wise) product of matrices. $\mathrm{tr}(\cdot)$ is the trace of a square matrix argument. The notations $\lambda_{max}(\cdot)$ and $\lambda_{min}(\cdot)$ indicate the principal and the minor eigenvalues of a Hermitian matrix, respectively. $\mathbf{Diag}(\cdot)$ denotes the diagonal matrix formed by the entries of the vector argument, whereas $\mathbf{diag}(\cdot)$ denotes the vector formed by collecting the diagonal entries of the matrix argument. $\mathrm{E}\{\cdot\}$ stands for the statistical expectation operator. We write $\boldsymbol{A}\succeq\boldsymbol{B}$ iff $\boldsymbol{A}-\boldsymbol{B}$ is positive semi-definite, and $\boldsymbol{A}\succ\boldsymbol{B}$ iff $\boldsymbol{A}-\boldsymbol{B}$ is positive-definite. Finally, $\Re(\cdot)$ and $\arg(\cdot)$ denote the real-part and the phase angle (in radians) of the complex-valued argument.

8.2 Data Modeling and Optimal Detector

8.2.1 Data Modeling

We consider a narrow-band pulsed-radar system using a train of pulses. The baseband transmit signal can be formulated as

$$s(t)=\sum_{n=0}^{N-1}a_n\,\phi(t-nT_{PRI}) \tag{8.1}$$

where $\phi(.)$ is the basic unit-energy transmit pulse (with time duration τ_p), T_{PRI} is the pulse repetition interval ($T_{PRI}\gg\tau_p$), and $\{a_n\}_{n=0}^{N-1}$ are the weights that are to be optimally designed.

At the transmitter, the baseband signal is modulated by a carrier frequency ω_c. The backscattered signal from a point-like moving target can be expressed as

$$r(t)=\alpha_t s(t-\tau)e^{j(\omega_c+\nu)(t-\tau)}+c(t)+w(t) \tag{8.2}$$

where α_t is the amplitude of the target echo (accounting for target reflectivity and channel effects), τ and ν denote the target delay and Doppler shift, respectively, $c(t)$ is the clutter component, and $w(t)$ represents the signal-independent interferences.

We assume that both $c(t)$ and $w(t)$ are Gaussian random processes. In particular, we assume that the clutter component is the signal echo produced by many individual point scatterers (distributed across the delay and Doppler domains) which are statistically independent. Under such an assumption, $c(t)$

can be formulated as [156]

$$c(t) = \sum_{k=1}^{N_{\rm ct}} \sum_{l=1}^{N_{\rm cd}} \rho_{kl} s(t-\tau_k) e^{j(\omega_c+\omega_l)(t-\tau_k)} \tag{8.3}$$

where $N_{\rm ct}$ and $N_{\rm cd}$ are the number of clutter scatterers in the delay and Doppler domains[1], respectively, and ρ_{kl} is the amplitude of a specific clutter scatterer at time delay τ_k and Doppler shift ω_l (due to the clutter motion).

Note that in radar applications, the pulse $\phi(t)$ and its time-shifted versions can be used as an orthonormal basis for signal recovery at the receiver. More precisely, the matched filter $\phi^*(-t)$ is usually applied to the downconverted received signal (i.e. $r(t)e^{-j\omega_c t}$) and the output of the matched filter is then sampled at the time delays corresponding to the range-cell under test, i.e. $t = nT_{PRI} + \tau$ for $0 \le n \le N-1$. The discrete-time received signal $\boldsymbol{r}$ for the range-cell corresponding to the time delay τ can be written as (see Appendix A for a derivation)

$$\boldsymbol{r} = \alpha\, \boldsymbol{a} \odot \boldsymbol{p} + \boldsymbol{a} \odot \boldsymbol{c} + \boldsymbol{w} \tag{8.4}$$

where $\alpha = \alpha_t e^{-j\omega_c \tau}$, $\boldsymbol{a} \triangleq [a_0 \;\; a_1 \;\; \ldots \;\; a_{N-1}]^T$ is the code vector (to be designed), $\boldsymbol{p} \triangleq [1 \;\; e^{j\omega} \;\; \ldots \;\; e^{j(N-1)\omega}]^T$ with ω being the normalized Doppler shift of the target, $\boldsymbol{c}$ is the vector corresponding to the clutter component, and the vector $\boldsymbol{w}$ represents the signal-independent interferences[2]. A detailed construction of $\boldsymbol{c}$ and $\boldsymbol{w}$ from the continuous variables $c(t)$ and $w(t)$ can also be found in Appendix 8.8.1. Herein we remark on the fact that (8.4) refers to the cases with unambiguous clutter scatterers.

Using (8.4), the target detection problem can be cast as the following binary hypothesis test:

$$\begin{cases} \mathrm{H}_0: & \boldsymbol{r} = \boldsymbol{a} \odot \boldsymbol{c} + \boldsymbol{w} \\ \mathrm{H}_1: & \boldsymbol{r} = \alpha \boldsymbol{a} \odot \boldsymbol{p} + \boldsymbol{a} \odot \boldsymbol{c} + \boldsymbol{w} \end{cases} \tag{8.5}$$

Note that the covariance matrices of $\boldsymbol{c}$ and $\boldsymbol{w}$ (denoted by $\boldsymbol{C}$ and $\boldsymbol{M}$) can be assumed to be priori known (e.g. they can be obtained by using geographical, meteorological, or pre-scan information) [177] [176]. As to the target, we assume α is a zero-mean complex Gaussian random variable with variance σ_T^2 (i.e. Swerling-I model).

8.2.2 Optimal Detector for A Priori Known Doppler Shift

Let $\mathbf{x} = \boldsymbol{D}^{-1/2}\boldsymbol{r}$ with $\boldsymbol{D} = \boldsymbol{M} + \boldsymbol{A}\boldsymbol{C}\boldsymbol{A}^H$, and $\boldsymbol{A} = \mathrm{Diag}(\boldsymbol{a})$ (that is referred to as *code matrix* in the sequel). The detection problem in (8.5) can equivalently be

[1] It is assumed that the number of the independent scatterers is sufficiently large such that the central limit theorem holds and the Gaussian distribution for $c(t)$ can be justified (see e.g., [156] [174] [175]).

[2] Note that in the data model (8.4) we neglect the effects of the antenna pattern; however, the results can be straightforwardly extended to include these effects (see e.g. [176]).

expressed in terms of $\mathbf{x}$. More precisely, for a known target Doppler shift, the problem in (8.5) is equivalent to:

$$\begin{cases} \mathrm{H}_0: & \mathbf{x} \sim \mathscr{CN}(\mathbf{0}, \boldsymbol{I}) \\ \mathrm{H}_1: & \mathbf{x} \sim \mathscr{CN}(\mathbf{0}, \boldsymbol{S}+\boldsymbol{I}) \end{cases} \tag{8.6}$$

where $\boldsymbol{S} = \sigma_T^2 \boldsymbol{D}^{-1/2}(\boldsymbol{a} \odot \boldsymbol{p})(\boldsymbol{a} \odot \boldsymbol{p})^H \boldsymbol{D}^{-1/2}$. The optimal detector compares the likelihood-ratio associated with the above problem, i.e. the ratio of the pdf of $\mathbf{x}$ under H_1 over that of H_0, with a detection threshold. According to (8.6), the likelihood-ratio for the problem is given by

$$\mathscr{L}(\mathbf{x}) = \frac{1}{\det(\boldsymbol{S}+\boldsymbol{I})} \left(\frac{\exp\left(-\mathbf{x}^H (\boldsymbol{S}+\boldsymbol{I})^{-1} \mathbf{x}\right)}{\exp\left(-\mathbf{x}^H \mathbf{x}\right)} \right). \tag{8.7}$$

By taking logarithm and removing the constants, the following expression is obtained for the optimal detector:

$$|\boldsymbol{r}^H \left(\boldsymbol{M} + \boldsymbol{A}\boldsymbol{C}\boldsymbol{A}^H\right)^{-1} (\boldsymbol{a} \odot \boldsymbol{p})|^2 \underset{\mathrm{H}_1}{\overset{\mathrm{H}_0}{\lessgtr}} \eta \tag{8.8}$$

where η is the detection threshold. Note that the above detector is nothing but a whitening process, a matched filtering, and a square-law detection. The performance of the above detector depends on the following SNR [178, Chapter 8]

$$\lambda = \sigma_T^2 (\boldsymbol{a} \odot \boldsymbol{p})^H \left(\boldsymbol{M} + \boldsymbol{A}\boldsymbol{C}\boldsymbol{A}^H\right)^{-1} (\boldsymbol{a} \odot \boldsymbol{p}). \tag{8.9}$$

It is interesting to observe that the above performance metric is invariant to a phase-shift of the code vector $\boldsymbol{a}$, i.e. the code vectors $\boldsymbol{a}$ and $e^{j\varphi}\boldsymbol{a}$ (for any $\varphi \in [0, 2\pi]$) result in the same value of the SNR.

8.2.3 Optimal Detector for an Unknown Doppler Shift

The target Doppler shift ω is usually unknown at the transmitter. In such cases, the detector of (8.8) does not hold true anymore. The optimal detector for the detection problem in (8.5) in cases where ω is unknown is obtained by considering the pdf of ω. The distribution of the vector $\boldsymbol{r}$ (and $\mathbf{x}$) are no longer Gaussian under H_1 and the optimal detector does not lead to a closed-form expression. More precisely, let $f(\omega)$ denote the pdf of ω. The optimal detector is obtained by considering the average likelihood-ratio [178]:

$$\mathscr{L}(\mathbf{x}) = \int_\Omega \mathscr{L}(\mathbf{x}|\omega) f(\omega)\, d\omega \tag{8.10}$$

which results in the following detector [179]

$$\int_\Omega \frac{1}{1+\lambda} \exp\left(\frac{\sigma_T^2 \boldsymbol{r}^H \boldsymbol{D}^{-1} (\boldsymbol{a} \odot \boldsymbol{p})(\boldsymbol{a} \odot \boldsymbol{p})^H \boldsymbol{D}^{-1} \boldsymbol{r}}{1+\lambda} \right) f(\omega)\, d\omega \underset{\mathrm{H}_1}{\overset{\mathrm{H}_0}{\lessgtr}} \eta' \tag{8.11}$$

where $\Omega = [\omega_l, \omega_u]$ denotes the considered interval for the target Doppler shift[3] ω and λ is given by (8.9). It is worth mentioning that the values of ω_l and ω_u and the pdf of ω can be obtained in practice using prior knowledge about the type of target (e.g. knowing if the target is an airplane, a ship, or a missile), rough estimates of the target Doppler shift obtained by pre-scan procedures, and employing cognitive methods [177] [180]. Usually, a uniform distribution for ω is considered over Ω to model the uncertainty of the target Doppler shift [176].

8.3 Code Design in Average Sense

Code design to improve the detection performance of the system for a known target Doppler shift ω can be accomplished by the maximization of the following performance metric[4] for a given ω:

$$\begin{aligned}
&(\boldsymbol{a}\odot\boldsymbol{p})^H\left(\boldsymbol{M}+\boldsymbol{A}\boldsymbol{C}\boldsymbol{A}^H\right)^{-1}(\boldsymbol{a}\odot\boldsymbol{p}) \\
&=\mathrm{tr}\left\{\boldsymbol{A}^H(\boldsymbol{M}+\boldsymbol{A}\boldsymbol{C}\boldsymbol{A}^H)^{-1}\boldsymbol{A}\boldsymbol{p}\boldsymbol{p}^H\right\} \\
&=\mathrm{tr}\left\{\left((\boldsymbol{A}^H\boldsymbol{M}^{-1}\boldsymbol{A})^{-1}+\boldsymbol{C}\right)^{-1}\boldsymbol{p}\boldsymbol{p}^H\right\}.
\end{aligned} \tag{8.12}$$

In cases where target Doppler shift is unknown, the expressions for the corresponding optimal detector and its performance metrics are too complicated to be used for code design (see also [181] [182]). In such a circumstance, we consider the following design metric (referred to as average metric):

$$\mathrm{tr}\left\{\left(\boldsymbol{A}^{-1}\boldsymbol{M}\boldsymbol{A}^{-H}+\boldsymbol{C}\right)^{-1}\boldsymbol{W}\right\} \tag{8.13}$$

where $\boldsymbol{W}=\mathrm{E}\{\boldsymbol{p}\boldsymbol{p}^H\}$. The mathematical background for selection of such metric is as follows: It can be shown (see below) that maximizing the above metric results in maximization of a lower bound on the J-divergence [183] associated with the detection problem in (8.5) for unknown ω. Furthermore, for large SNR regimes, maximization of the above metric approximates well the maximization of the J-divergence. More precisely, the J-divergence associated with the binary hypothesis test is given by [181]

$$\mathscr{J} \;=\; \mathrm{E}\{\log(\mathscr{L}(\mathbf{x}))|\mathrm{H}_1\}-\mathrm{E}\{\log(\mathscr{L}(\mathbf{x}))|\mathrm{H}_0\}. \tag{8.14}$$

Therefore, for the detection problem in (8.5) in cases where ω is unknown we can write

$$\mathscr{J}=E\{\mathscr{J}|\omega\}. \tag{8.15}$$

[3]Note that Ω can also be the union of several intervals.

[4]In what follows, we assume that all the code elements are non-zero.

For a given ω, the detection problems in (8.5) and (8.6) are equivalent, and hence $\mathscr{J}|\omega$ can be derived considering (8.6) as:

$$\mathscr{J}|\omega = \left(-\log(1+\lambda)+\frac{\lambda^2+\lambda}{1+\lambda}\right)-\left(-\log(1+\lambda)+\frac{\lambda}{1+\lambda}\right)=\frac{\lambda^2}{1+\lambda} \tag{8.16}$$

where λ is defined in (8.9). Now observe that $g(x)=x^2/(1+x)$ is a convex function. Consequently, using Jensen inequality we conclude

$$\mathscr{J} = \mathrm{E}\left\{\frac{\lambda^2}{1+\lambda}\right\} \geq \underbrace{\frac{(\mathrm{E}\{\lambda\})^2}{1+\mathrm{E}\{\lambda\}}}_{\mathscr{J}_{LB}}. \tag{8.17}$$

Furthermore, $g(x)=x^2/(1+x)$ is a monotonically increasing function. As a result, maximization of the $\mathrm{E}\{\lambda\}$ leads to maximization of the $\mathscr{J}_{LB}$ in the above inequality. Owing to the fact that the considered metric in (8.13) is equal to $\mathrm{E}\{\lambda\}$, the maximization of the average metric leads to maximization of the lower bound $\mathscr{J}_{LB}$ on the J-divergence $\mathscr{J}$. An analysis of the tightness of the bound $\mathscr{J}_{LB}$ is presented in Appendix 8.8.2. The J-divergence has an asymptotic relationship with the detection performance of a hypothesis test and can also be considered as a bound on the detection performance [184] [183].

Remark 1: Note that $\mathscr{J} = \mathrm{E}\left\{\lambda - 1 + \frac{1}{\lambda+1}\right\}$ and hence for large SNR, i.e. large λ, we have $\mathscr{J} \approx \mathrm{E}\{\lambda\}-1$. As a result, in such cases, maximization of the considered average metric approximates well the maximization of the J-divergence. A similar approximation has also been used in [184] for radar signal design. With similar calculations, for small λ, it can be shown that maximization of the average metric is approximately equivalent to maximization of the Mutual Information associated with the problem (8.5) (that is given by $\mathrm{E}\{\log(1+\lambda)\}$). For known ω, the average metric is identical to the performance metric in (8.12) and directly determines the performance of the optimal detector. ■

To optimize the detection performance, the average metric (8.13) can be maximized under an energy constraint:

$$\begin{aligned} \max_{\boldsymbol{A}} \quad & \mathrm{tr}\left\{\left(\boldsymbol{A}^{-1}\boldsymbol{M}\boldsymbol{A}^{-H}+\boldsymbol{C}\right)^{-1}\boldsymbol{W}\right\} \\ \text{subject to} \quad & \mathrm{tr}\left\{\boldsymbol{A}\boldsymbol{A}^H\right\} \leq e \end{aligned} \tag{8.18}$$

where e denotes the maximum energy that can be used for transmission. Note that if $\boldsymbol{A}$ is claimed to be a solution to (8.18) with $\mathrm{tr}\{\boldsymbol{A}\boldsymbol{A}^H\} < e$, then $\gamma\boldsymbol{A}$ (for some $\gamma > 1$ such that $\gamma\mathrm{tr}\{\boldsymbol{A}\boldsymbol{A}^H\} = e$) is feasible but leads to a larger value of the objective function. Therefore, the energy constraint in (8.18) is active. In the following, we propose two different frameworks to tackle the code optimization problem in (8.18).

8.3.1 Convexification via Reparametrization (CoRe)

First, we introduce the CoRe framework which is based on a relaxation of the optimization problem in (8.18). In particular, we show that a relaxed version of the code design problem in (8.18) can be formulated as an SDP. Let

$$\boldsymbol{X} \triangleq \boldsymbol{A}^H \boldsymbol{M}^{-1} \boldsymbol{A} \tag{8.19}$$

and observe that $\boldsymbol{X} \succ \boldsymbol{0}$. The energy constraint of (8.18) can be rewritten noting that

$$\mathrm{tr}\{\boldsymbol{X}\} = \mathrm{tr}\{\boldsymbol{A}^H \boldsymbol{M}^{-1} \boldsymbol{A}\} = \sum_{k=1}^{N} m_{kk} |a_k|^2 \tag{8.20}$$

where $\{m_{kk}\}_{k=1}^N$ are the diagonal entries of the positive-definite matrix $\boldsymbol{M}^{-1}$. Using (8.20), the energy of the code can be alternatively written as

$$\mathrm{tr}\{\boldsymbol{A}^H \boldsymbol{A}\} = \mathrm{tr}\{\boldsymbol{X}\boldsymbol{G}\} \tag{8.21}$$

where $\boldsymbol{G} \triangleq (\boldsymbol{M}^{-1} \odot \boldsymbol{I})^{-1}$ is a diagonal matrix with diagonal entries $\{1/m_{kk}\}_{k=1}^N$.

Next, we reformulate (8.18) as a convex optimization problem w.r.t. $\boldsymbol{X}$. Note that there exists $\boldsymbol{B} \in \mathbb{C}^{N \times N}$ such that $\boldsymbol{C} = \boldsymbol{B}\boldsymbol{B}^H$. Using the matrix inversion lemma we have that

$$(\boldsymbol{X}^{-1} + \boldsymbol{C})^{-1} = \boldsymbol{X} - \boldsymbol{X}\boldsymbol{B}(\boldsymbol{I} + \boldsymbol{B}^H \boldsymbol{X}\boldsymbol{B})^{-1} \boldsymbol{B}^H \boldsymbol{X}. \tag{8.22}$$

Let $\delta = \mathrm{rank}(\boldsymbol{W})$, and let $\boldsymbol{W} = \sum_{k=1}^{\delta} \boldsymbol{w}_k \boldsymbol{w}_k^H$. As a result,

$$\begin{aligned} &\mathrm{tr}\left\{ \left(\boldsymbol{A}^{-1} \boldsymbol{M} \boldsymbol{A}^{-H} + \boldsymbol{C}\right)^{-1} \boldsymbol{W} \right\} = \mathrm{tr}\left\{ (\boldsymbol{X}^{-1} + \boldsymbol{C})^{-1} \boldsymbol{W} \right\} \\ &= \textstyle\sum_{k=1}^{\delta} \left\{ \boldsymbol{w}_k^H \boldsymbol{X} \boldsymbol{w}_k - \boldsymbol{w}_k^H \boldsymbol{X}\boldsymbol{B}(\boldsymbol{I} + \boldsymbol{B}^H \boldsymbol{X}\boldsymbol{B})^{-1} \boldsymbol{B}^H \boldsymbol{X} \boldsymbol{w}_k \right\}. \end{aligned} \tag{8.23}$$

To maximize (8.23), each term in the latter summation can be dealt with by means of a linear matrix inequality (LMI) using auxiliary variables $\{\beta_k\}$:

$$\begin{aligned} &\beta_k \geq -\boldsymbol{w}_k^H \boldsymbol{X} \boldsymbol{w}_k + \boldsymbol{w}_k^H \boldsymbol{X}\boldsymbol{B}(\boldsymbol{I} + \boldsymbol{B}^H \boldsymbol{X}\boldsymbol{B})^{-1} \boldsymbol{B}^H \boldsymbol{X} \boldsymbol{w}_k \\ &\Leftrightarrow \begin{bmatrix} \beta_k + \boldsymbol{w}_k^H \boldsymbol{X} \boldsymbol{w}_k & \boldsymbol{w}_k^H \boldsymbol{X}\boldsymbol{B} \\ \boldsymbol{B}^H \boldsymbol{X} \boldsymbol{w}_k & \boldsymbol{I} + \boldsymbol{B}^H \boldsymbol{X}\boldsymbol{B} \end{bmatrix} \succeq \boldsymbol{0}. \end{aligned} \tag{8.24}$$

In light of Eqs. (8.21) and (8.23), and the LMIs introduced in (8.24), the optimization problem (8.18) boils down (in a relaxed form) to the following core SDP (CSDP):

$$\begin{aligned} \text{CSDP:} \quad \min_{\boldsymbol{X}, \{\beta_k\}_{k=1}^{\delta}} \quad & \sum_{k=1}^{\delta} \beta_k \\ \text{subject to} \quad & \begin{bmatrix} \beta_k + \boldsymbol{w}_k^H \boldsymbol{X} \boldsymbol{w}_k & \boldsymbol{w}_k^H \boldsymbol{X}\boldsymbol{B} \\ \boldsymbol{B}^H \boldsymbol{X} \boldsymbol{w}_k & \boldsymbol{I} + \boldsymbol{B}^H \boldsymbol{X}\boldsymbol{B} \end{bmatrix} \succeq \boldsymbol{0}, \quad \forall\, k, \\ & \mathrm{tr}\{\boldsymbol{X}\boldsymbol{G}\} \leq e, \\ & \boldsymbol{X} \succ \boldsymbol{0}. \end{aligned} \tag{8.25}$$

Note that the above CSDP can be solved in polynomial-time (e.g. see [185] in which an $O(N^{3.5})$-complexity algorithm is introduced to solve such SDPs). The global optimum $\boldsymbol{X}$ of the above CSDP can be used to synthesize the code matrix $\boldsymbol{A}$. To obtain $\boldsymbol{A}$ such that $\boldsymbol{A}^H\boldsymbol{M}^{-1}\boldsymbol{A} \cong \boldsymbol{X}$, we consider the optimization problem

$$\begin{aligned} \min_{\boldsymbol{A},\boldsymbol{Q}} \quad & \|\boldsymbol{X}^{1/2}\boldsymbol{Q} - \boldsymbol{A}^H\boldsymbol{M}^{-1/2}\|_F^2 \\ \text{subject to} \quad & \boldsymbol{Q}\boldsymbol{Q}^H = \boldsymbol{I} \end{aligned} \tag{8.26}$$

where $\boldsymbol{Q}$ is an auxiliary matrix. In the following, we propose an efficient cyclic algorithm for solving (8.26). For any fixed code matrix $\boldsymbol{A}$, (8.26) leads to the maximization problem:

$$\begin{aligned} \max_{\boldsymbol{Q}} \quad & \Re\left(\text{tr}\left\{\boldsymbol{X}^{1/2}\boldsymbol{Q}\boldsymbol{M}^{-1/2}\boldsymbol{A}\right\}\right) \\ \text{subject to} \quad & \boldsymbol{Q}\boldsymbol{Q}^H = \boldsymbol{I}. \end{aligned} \tag{8.27}$$

Interestingly, a similar problem to (8.27) has been studied in [186] where an explicit solution was derived. Let $\boldsymbol{V}_1\boldsymbol{S}\boldsymbol{V}_2^H$ represent the singular value decomposition (SVD) of $\boldsymbol{M}^{-1/2}\boldsymbol{A}\boldsymbol{X}^{1/2}$. Then the explicit solution of (8.27) is given by $\boldsymbol{V}_2\boldsymbol{V}_1^H$ (see [186] for details). Furthermore, for fixed $\boldsymbol{Q}$, the solution of (8.26) w.r.t. the code matrix $\boldsymbol{A}$ can be obtained solving the problem:

$$\min_{\boldsymbol{A}} \ \text{tr}\left\{\boldsymbol{A}^H\boldsymbol{M}^{-1}\boldsymbol{A}\right\} - 2\Re\left(\text{tr}\left\{\boldsymbol{X}^{1/2}\boldsymbol{Q}\boldsymbol{M}^{-1/2}\boldsymbol{A}\right\}\right) \tag{8.28}$$

which can be rewritten (in vectorized form) as

$$\min_{\boldsymbol{a}} \ \boldsymbol{a}^H(\boldsymbol{M}^{-1} \odot \boldsymbol{I})\boldsymbol{a} - 2\Re(\boldsymbol{b}^H\boldsymbol{a}) \tag{8.29}$$

with $\boldsymbol{b} \triangleq \text{diag}(\boldsymbol{X}^{1/2}\boldsymbol{Q}^*\boldsymbol{M}^{-1/2})$. The solution $\boldsymbol{a}$ of (8.29) is given by

$$\boldsymbol{a} = (\boldsymbol{M}^{-1} \odot \boldsymbol{I})^{-1}\boldsymbol{b} = \boldsymbol{G}\boldsymbol{b}. \tag{8.30}$$

Remark 2: Note that the aim of the synthesis problem (8.26) is to provide $\boldsymbol{A}$ such that $\boldsymbol{A}^H\boldsymbol{M}^{-1}\boldsymbol{A} \cong \boldsymbol{X}$, and also that an energy constraint has already been imposed when obtaining the $\boldsymbol{X}$ (see (8.25)). Therefore, in (8.26), we do not consider the energy constraint, as it has been implicitly imposed. However, one might be interested to explicitly consider the energy constraint in (8.26). In this case, the optimization problem for fixed $\boldsymbol{Q}$ is convex w.r.t. $\boldsymbol{A}$ and hence can be solved efficiently (but (8.30) does not hold). Note that it was numerically observed that the difference between explicitly imposing the energy constraint in (8.26) and the considered synthesis problem in the chapter is very minor. ■

The steps of the CoRe framework are summarized in Table 8.1. It is worth mentioning that as the solution $\boldsymbol{X}$ to the CSDP does not necessarily possess

the desired structure in (8.19), some degradation of the metric in (8.13) can be expected at the synthesis stage. In other words, the CSDP solution in (8.25) provides an upper bound on the average metric. This upper bound can be used to assess the quality of code design methods as well as the system performance in various scenarios.

Table 8.1. *CoRe for Optimal Code Design Using the Average Metric*

Step 1: Solve the CSDP of (8.25) to obtain its global optimum $\boldsymbol{X}$.
Step 2 *(The synthesis stage)*: Initialize $\boldsymbol{a}$ with a random vector in $\mathbb{C}^N$.
Step 2-1: Compute $\boldsymbol{Q} = \boldsymbol{V}_2\boldsymbol{V}_1^H$ where $\boldsymbol{V}_1\boldsymbol{S}\boldsymbol{V}_2^H$ represents the SVD of $\boldsymbol{M}^{-1/2}\boldsymbol{A}\boldsymbol{X}^{1/2}$.
Step 2-2: Compute $\boldsymbol{a} = \boldsymbol{G}\,\mathrm{diag}(\boldsymbol{X}^{1/2}(\boldsymbol{Q}^*)\boldsymbol{M}^{-1/2})$.
Step 2-3: Repeat steps 2-1 and 2-2 until a pre-defined stop criterion is satisfied, e.g. $\|\boldsymbol{a}^{(k+1)} - \boldsymbol{a}^{(k)}\| \leq \varepsilon$ for some $\varepsilon > 0$, where the superscript k denotes the iteration number.

8.3.2 Cyclic Algorithm for Direct COde DEsign (CADCODE)

In this sub-section, we propose the CADCODE framework for solving (8.18) directly w.r.t. the code matrix $\boldsymbol{A}$.

We begin by noting that as $\boldsymbol{W} \succeq \boldsymbol{0}$ there must exist a full column-rank matrix $\boldsymbol{V} \in \mathbb{C}^{N\times\delta}$ such that $\boldsymbol{W} = \boldsymbol{V}\boldsymbol{V}^H$ (particularly observe that $\boldsymbol{V} = [\boldsymbol{w}_1\ \boldsymbol{w}_2\ ...\ \boldsymbol{w}_\delta]$ yields such decomposition of $\boldsymbol{W}$). As a result,

$$\begin{aligned} \mathrm{tr}\left\{\left((\boldsymbol{A}^H\boldsymbol{M}^{-1}\boldsymbol{A})^{-1} + \boldsymbol{C}\right)\boldsymbol{W}\right\} &= \mathrm{tr}\left\{\boldsymbol{A}^H(\boldsymbol{M}+\boldsymbol{A}\boldsymbol{C}\boldsymbol{A}^H)^{-1}\boldsymbol{A}\boldsymbol{W}\right\} \\ &= \mathrm{tr}\left\{\boldsymbol{V}^H\boldsymbol{A}^H(\boldsymbol{M}+\boldsymbol{A}\boldsymbol{C}\boldsymbol{A}^H)^{-1}\boldsymbol{A}\boldsymbol{V}\right\}. \end{aligned} \tag{8.31}$$

Let $\boldsymbol{\Theta} \triangleq \theta\boldsymbol{I} - \boldsymbol{V}^H\boldsymbol{A}^H(\boldsymbol{M}+\boldsymbol{A}\boldsymbol{C}\boldsymbol{A}^H)^{-1}\boldsymbol{A}\boldsymbol{V}$ with a sufficiently large θ such that $\boldsymbol{\Theta} \succ \boldsymbol{0}$ (a detailed calculation of the diagonal loading parameter θ can be found in Appendix 8.8.3). Note that the optimization problem (8.18) is equivalent to the minimization problem

$$\begin{aligned} \min_{\boldsymbol{A}} \quad & \mathrm{tr}\{\boldsymbol{\Theta}\} \\ \text{subject to} \quad & \mathrm{tr}\{\boldsymbol{A}^H\boldsymbol{A}\} \leq e. \end{aligned} \tag{8.32}$$

Now define

$$\boldsymbol{R} \triangleq \begin{bmatrix} \theta\boldsymbol{I} & \boldsymbol{V}^H\boldsymbol{A}^H \\ \boldsymbol{A}\boldsymbol{V} & \boldsymbol{M}+\boldsymbol{A}\boldsymbol{C}\boldsymbol{A}^H \end{bmatrix} \tag{8.33}$$

and observe that for $\boldsymbol{U} \triangleq [\boldsymbol{I}_\delta\ \ \boldsymbol{0}_{N\times\delta}]^T$ we have

$$\boldsymbol{U}^H\boldsymbol{R}^{-1}\boldsymbol{U} = \boldsymbol{\Theta}^{-1}. \tag{8.34}$$

To tackle (8.32) let $g(\boldsymbol{A},\boldsymbol{Y}) \triangleq \mathrm{tr}\{\boldsymbol{Y}^H\boldsymbol{R}\boldsymbol{Y}\}$ (with $\boldsymbol{Y}$ being an auxiliary variable), and consider the following minimization problem:

$$\begin{aligned} \min_{\boldsymbol{A},\boldsymbol{Y}} \quad & g(\boldsymbol{A},\boldsymbol{Y}) \\ \text{subject to} \quad & \boldsymbol{Y}^H\boldsymbol{U} = \boldsymbol{I} \\ & \mathrm{tr}\{\boldsymbol{A}^H\boldsymbol{A}\} \leq e. \end{aligned} \tag{8.35}$$

For fixed $\boldsymbol{A}$, the minimizer $\boldsymbol{Y}$ of (8.35) can be obtained using Result 35 in [187, p. 354] as

$$\boldsymbol{Y} = \boldsymbol{R}^{-1}\boldsymbol{U}(\boldsymbol{U}^H\boldsymbol{R}^{-1}\boldsymbol{U})^{-1}. \tag{8.36}$$

On the other hand, for fixed $\boldsymbol{Y}$, the minimization of $g(\boldsymbol{Y},\boldsymbol{A})$ w.r.t. $\boldsymbol{A}$ yields the following convex quadratically-constrained quadratic program (QCQP):

$$\begin{aligned} \min_{\boldsymbol{a}} \quad & \boldsymbol{a}^H\left((\boldsymbol{Y}_2\boldsymbol{Y}_2^H)\odot\boldsymbol{C}^T\right)\boldsymbol{a} + 2\Re(\boldsymbol{d}^H\boldsymbol{a}) \\ \text{subject to} \quad & \boldsymbol{a}^H\boldsymbol{a} \leq e \end{aligned} \tag{8.37}$$

where $\boldsymbol{Y} \triangleq [\boldsymbol{Y}_{1\ \delta\times\delta}\ \ \boldsymbol{Y}_{2\ N\times\delta}]^T$ and $\boldsymbol{d} \triangleq \mathrm{diag}(\boldsymbol{V}^*\boldsymbol{Y}_1^*\boldsymbol{Y}_2^T)$. Note that the positive semi-definiteness of $(\boldsymbol{Y}_2\boldsymbol{Y}_2^H)\odot\boldsymbol{C}^T$ guarantees the convexity of (8.37). The QCQP in (8.37) can be solved efficiently using the Lagrange multiplier method (see Appendix 8.8.4).

It is straightforward to verify that at the minimizer $\boldsymbol{Y}$ of (8.35),

$$g(\boldsymbol{Y},\boldsymbol{A}) = \mathrm{tr}\{\boldsymbol{\Theta}\}. \tag{8.38}$$

From this property, we conclude that each step of the cyclic minimization of (8.35) leads to a decrease of $\mathrm{tr}\{\boldsymbol{\Theta}\}$. Indeed, let $f(\boldsymbol{A}) = \mathrm{tr}\{\boldsymbol{\Theta}\}$ and note that

$$\begin{aligned} f\left(\boldsymbol{A}^{(k+1)}\right) &= g\left(\boldsymbol{Y}^{(k+2)},\boldsymbol{A}^{(k+1)}\right) \\ &\leq g\left(\boldsymbol{Y}^{(k+1)},\boldsymbol{A}^{(k+1)}\right) \\ &\leq g\left(\boldsymbol{Y}^{(k+1)},\boldsymbol{A}^{(k)}\right) = f\left(\boldsymbol{A}^{(k)}\right) \end{aligned} \tag{8.39}$$

where the superscript k denotes the iteration number. The first and the second inequality in (8.39) hold true due to the minimization of $g(\boldsymbol{A},\boldsymbol{Y})$ w.r.t. $\boldsymbol{Y}$ and $\boldsymbol{A}$, respectively. As a result, *CADCODE converges to a stationary point of (8.18).* It is worth noting that the minimization steps of CADCODE (which are summarized in Table 8.2) are solved either analytically or using standard interior-point methods [188].

8.4 Code Design in Worst-Case Sense

Following the optimization schemes proposed for code design in the average-sense, we extend our derivations in order to handle the unknown Doppler shift

Table 8.2. *CADCODE for Optimal Code Design Using the Average Metric*

Step 0: Initialize the code vector $\boldsymbol{a}$ using a random vector in $\mathbb{C}^N$, and form $\boldsymbol{R}$ as defined in (8.33).
Step 1: Compute $\boldsymbol{Y} = \boldsymbol{R}^{-1}\boldsymbol{U}(\boldsymbol{U}^H\boldsymbol{R}^{-1}\boldsymbol{U})^{-1}$.
Step 2: Solve the optimization problem (8.37) to obtain the code vector $\boldsymbol{a}$.
Step 3: Repeat steps 1 and 2 until a pre-defined stop criterion is satisfied, e.g. $\|\boldsymbol{a}^{(k+1)} - \boldsymbol{a}^{(k)}\| \leq \varepsilon$ for some $\varepsilon > 0$, where k denotes the iteration number.

of the target in a *worst-case* scenario. The worst-case approach has been considered in [172] and [173] for clutter-free scenarios. These works also address the connection between the worst-case metric and the detection performance (see also [128] for a related problem). Considering the performance metric of the detector (8.8), the *worst-case metric* (for an unknown Doppler shift in the interval $[\omega_l, \omega_u]$) is defined as

$$\min_{\omega_l \leq \omega \leq \omega_u} \quad \mathrm{tr}\left\{ \left((\boldsymbol{A}^H \boldsymbol{M}^{-1} \boldsymbol{A})^{-1} + \boldsymbol{C} \right)^{-1} \boldsymbol{p}\boldsymbol{p}^H \right\}. \tag{8.40}$$

The maximization of the worst-case metric boils down to the max-min problem:

$$\begin{aligned} \max_{\boldsymbol{A}} \min_{\omega_l \leq \omega \leq \omega_u} \quad & \mathrm{tr}\left\{ \left((\boldsymbol{A}^H \boldsymbol{M}^{-1} \boldsymbol{A})^{-1} + \boldsymbol{C} \right)^{-1} \boldsymbol{p}\boldsymbol{p}^H \right\} \\ \text{subject to} \quad & \mathrm{tr}\left\{ \boldsymbol{A}^H \boldsymbol{A} \right\} \leq e \end{aligned} \tag{8.41}$$

which can be rewritten (using a slack variable t) as

$$\begin{aligned} \max_{\boldsymbol{A}, t} \quad & \{t\} \\ \text{subject to} \quad & \\ & \mathrm{tr}\left\{ \left((\boldsymbol{A}^H \boldsymbol{M}^{-1} \boldsymbol{A})^{-1} + \boldsymbol{C} \right)^{-1} \boldsymbol{p}\boldsymbol{p}^H \right\} - t \geq 0, \quad \forall\ \omega \in [\omega_l, \omega_u], \\ & \mathrm{tr}\left\{ \boldsymbol{A}^H \boldsymbol{A} \right\} \leq e. \end{aligned} \tag{8.42}$$

Note that (8.42) is a non-convex optimization problem with infinitely many nonlinear constraints. In the following, we make use of an extension of the CoRe framework to tackle (8.42).

Using a new variable $\boldsymbol{Z} = \left((\boldsymbol{A}^H \boldsymbol{M}^{-1} \boldsymbol{A})^{-1} + \boldsymbol{C} \right)^{-1}$, one can recast (8.42) (in a relaxed form) as

$$\begin{aligned} \max_{\boldsymbol{Z}, t} \quad & \{t\} \\ \text{subject to} \quad & \\ & \boldsymbol{p}^H \boldsymbol{Z} \boldsymbol{p} - t \geq 0, \quad \forall\ \omega \in [\omega_l, \omega_u], \qquad (8.44) \\ & \mathrm{tr}\left\{ (\boldsymbol{Z}^{-1} - \boldsymbol{C})^{-1} \boldsymbol{G} \right\} \leq e. \qquad (8.45) \end{aligned} \tag{8.43}$$

Observe that for any $\omega \in [\omega_l, \omega_u]$, the constraint (8.44) is equivalent to

$$h(\omega) \triangleq z_0 - t + 2\Re\left(\sum_{k=1}^{N-1} z_k e^{-jk\omega}\right) \geq 0 \tag{8.46}$$

where

$$z_k \triangleq \sum_{i=1}^{N-k} Z_{i+k,i}, \quad 0 \leq k \leq N-1. \tag{8.47}$$

We use Theorem 3.2 of [189] (which is stated as Theorem 1 below) to obtain an SDP representation of (8.46).

Theorem 1. *The trigonometric polynomial* $\tilde{h}(\omega) = z_0 + 2\Re\left(\sum_{k=1}^{N-1} z_k e^{-jk\omega}\right)$ *is non-negative for any* $\omega \in [\omega_0 - \omega_1, \omega_0 + \omega_1]$ *(with* $0 < \omega_1 < \pi$*) iff there exist an* $N \times N$ *Hermitian matrix* $\boldsymbol{Z}_1 \succeq \boldsymbol{0}$ *and an* $(N-1) \times (N-1)$ *Hermitian matrix* $\boldsymbol{Z}_2 \succeq \boldsymbol{0}$ *such that*

$$\boldsymbol{z} = \boldsymbol{F}_1^H \left(\mathrm{diag}(\boldsymbol{F}_1 \boldsymbol{Z}_1 \boldsymbol{F}_1^H) + \boldsymbol{q} \odot \mathrm{diag}(\boldsymbol{F}_2 \boldsymbol{Z}_2 \boldsymbol{F}_2^H)\right) \tag{8.48}$$

where $\boldsymbol{z} = [z_0\ z_1\ ...\ z_{N-1}]^T$, $\boldsymbol{q} = [q_0\ q_1\ ...\ q_{n-1}]^T$ *with* $q_k = \cos(2\pi k/n - \omega_0) - \cos(\omega_1)$, $\boldsymbol{F}_1 = [\mathbf{f}_0\ ...\ \mathbf{f}_{N-1}]$ *and* $\boldsymbol{F}_2 = [\mathbf{f}_0\ ...\ \mathbf{f}_{N-2}]$ *in which* $\mathbf{f}_k = [1\ e^{-jk\theta}\ \ ...\ e^{-j(n-1)k\theta}]^T$ *with* $\theta = 2\pi/n$, *and* $n \geq 2N-1$.

Note that the SDP representation of (8.46) can be derived by employing the above results with $n = 2N-1$, $\omega_0 = (\omega_l + \omega_u)/2$, and $\omega_1 = \omega_0 - \omega_l$.

Next we obtain an LMI representation for the constraint (8.45). Let $\boldsymbol{G} = \mathrm{Diag}([G_1\ G_2\ ...\ G_N]) = \sum_{m=1}^{N} \boldsymbol{g}_m \boldsymbol{g}_m^H$ (where $\boldsymbol{g}_m = \sqrt{G_m}\boldsymbol{e}_m$), and note that

$$\mathrm{tr}\left\{(\boldsymbol{Z}^{-1} - \boldsymbol{C})^{-1}\boldsymbol{G}\right\} = \sum_{m=1}^{N} \left\{\boldsymbol{g}_m^H \boldsymbol{Z} \boldsymbol{g}_m + \boldsymbol{g}_m^H \boldsymbol{Z}\boldsymbol{B}(\boldsymbol{I} - \boldsymbol{B}^H \boldsymbol{Z}\boldsymbol{B})^{-1}\boldsymbol{B}^H \boldsymbol{Z}\boldsymbol{g}_m\right\}. \tag{8.49}$$

Similar to the derivation of CoRe in the average-sense code design, we consider the following LMI characterization:

$$\begin{aligned} \boldsymbol{g}_m^H \boldsymbol{Z} \boldsymbol{g}_m + \boldsymbol{g}_m^H \boldsymbol{Z}\boldsymbol{B}(\boldsymbol{I} - \boldsymbol{B}^H \boldsymbol{Z}\boldsymbol{B})^{-1}\boldsymbol{B}^H \boldsymbol{Z}\boldsymbol{g}_m &\leq \gamma_m \\ \Leftrightarrow \quad \begin{bmatrix} \gamma_m - \boldsymbol{g}_m^H \boldsymbol{Z}\boldsymbol{g}_m & \boldsymbol{g}_m^H \boldsymbol{Z}\boldsymbol{B} \\ \boldsymbol{B}^H \boldsymbol{Z}\boldsymbol{g}_m & \boldsymbol{I} - \boldsymbol{B}^H \boldsymbol{Z}\boldsymbol{B} \end{bmatrix} &\succeq 0 \end{aligned} \tag{8.50}$$

where $\{\gamma_m\}$ are auxiliary variables. Therefore, the SDP related to the worst-case code design can be expressed as[5]:

$$\begin{aligned}
\text{CSDP:} \quad & \max_{t,\boldsymbol{Z},\boldsymbol{Z}_1,\boldsymbol{Z}_2,\{\gamma_m\}_{m=1}^N} \{t\} \qquad (8.51)\\
& \text{subject to}\\
& \boldsymbol{z} = t\boldsymbol{e}_1 + \boldsymbol{F}_1^H \left(\text{diag}(\boldsymbol{F}_1\boldsymbol{Z}_1\boldsymbol{F}_1^H) + \boldsymbol{q} \odot \text{diag}(\boldsymbol{F}_2\boldsymbol{Z}_2\boldsymbol{F}_2^H)\right),\\
& \begin{bmatrix} \gamma_m - \boldsymbol{g}_m^H\boldsymbol{Z}\boldsymbol{g}_m & \boldsymbol{g}_m^H\boldsymbol{Z}\boldsymbol{B} \\ \boldsymbol{B}^H\boldsymbol{Z}\boldsymbol{g}_m & \boldsymbol{I} - \boldsymbol{B}^H\boldsymbol{Z}\boldsymbol{B} \end{bmatrix} \succeq \boldsymbol{0}, \ \forall\, m,\\
& \sum_{m=1}^N \gamma_m \le e,\\
& \boldsymbol{I} - \boldsymbol{B}^H\boldsymbol{Z}\boldsymbol{B} \succ \boldsymbol{0},\\
& \boldsymbol{Z} \succ \boldsymbol{0},\ \boldsymbol{Z}_1 \succeq \boldsymbol{0},\ \boldsymbol{Z}_2 \succeq \boldsymbol{0}.
\end{aligned}$$

To synthesize the code matrix $\boldsymbol{A}$ from the CSDP solution $\boldsymbol{Z}$ of (8.51), we will consider a synthesis stage similar to that of the average-sense code design in sub-section 8.3.1 (observe that $(\boldsymbol{Z}^{-1} - \boldsymbol{C})^{-1} = \boldsymbol{X}$). The CoRe framework for obtaining optimized codes using the worst-case metric is summarized in Table 8.3. Although solving (8.51) yields a global optimum of the CSDP, the further synthesis step leads to an approximate solution $\boldsymbol{A}$ of the original problem in (8.42). Therefore, the CSDP solution of (8.51) provides an upper bound on the possible values of the worst-case metric. Note that the results can be straightforwardly extended to the case in which Ω is a union of several intervals.

Table 8.3. *CoRe for Optimal Code Design Using the Worst-Case Metric*

Step 1: Solve CSDP in (8.51) to obtain its global optimum $\boldsymbol{Z}$.
Step 2 *(The synthesis stage)*: Initialize the code vector $\boldsymbol{a}$ with a random vector in $\mathbb{C}^N$.
Step 2-1: Compute $\boldsymbol{Q} = \boldsymbol{V}_2\boldsymbol{V}_1^H$ where $\boldsymbol{V}_1\boldsymbol{S}\boldsymbol{V}_2^H$ represents the SVD of $\boldsymbol{M}^{-1/2}\boldsymbol{A}(\boldsymbol{Z}^{-1} - \boldsymbol{C})^{-1/2}$.
Step 2-2: Compute the code vector as

$$\boldsymbol{a} = \boldsymbol{G}\ \text{diag}\left((\boldsymbol{Z}^{-1} - \boldsymbol{C})^{-1/2}\boldsymbol{Q}^*\boldsymbol{M}^{-1/2}\right).$$

Step 2-3: Repeat steps 2-1 and 2-2 until a pre-defined stop criterion is satisfied, e.g. $\|\boldsymbol{a}^{(k+1)} - \boldsymbol{a}^{(k)}\| \le \varepsilon$ for some $\varepsilon > 0$, where k denotes the iteration number.

Remark 3: The reader might observe the fact that the code synthesis stage is meaningful only if $\boldsymbol{Z} \prec \boldsymbol{C}^{-1}$, and hence might be willing to add such constraint

[5]We have also included the constraint $\boldsymbol{I} - \boldsymbol{B}^H\boldsymbol{Z}\boldsymbol{B} \succ \boldsymbol{0}$ in the CSDP (8.51) to ensure a meaningful synthesis stage (see Remark 3 below).

to the constraint set of (8.51). To clarify this issue, note that using the matrix inversion lemma we have

$$(\boldsymbol{Z}^{-1}-\boldsymbol{C})^{-1}=\boldsymbol{Z}+\boldsymbol{Z}\boldsymbol{B}(\boldsymbol{I}-\boldsymbol{B}^H\boldsymbol{Z}\boldsymbol{B})^{-1}\boldsymbol{B}^H\boldsymbol{Z}. \tag{8.52}$$

As $\boldsymbol{Z}$ of (8.51) is a positive-definite matrix, and the constraint set in (8.51) implies $\boldsymbol{I}-\boldsymbol{B}^H\boldsymbol{Z}\boldsymbol{B}\succ\boldsymbol{0}$, we conclude from (8.52) that $\boldsymbol{Z}^{-1}-\boldsymbol{C}\succ\boldsymbol{0}$. Therefore, the constraint $\boldsymbol{Z}\prec\boldsymbol{C}^{-1}$ is already taken into account via the constraints in (8.51). Moreover, adding the constraint $\boldsymbol{Z}\prec\boldsymbol{C}^{-1}$ separately would limit our design to the case of a non-singular $\boldsymbol{C}$. ■

8.5 Constrained Code Design

In order to use the power resources efficiently and to avoid non-linear effects at the transmitter, sequences with low PAR values are of practical interest in many applications [126] [173]. In this section, we consider code design via CoRe and CADCODE frameworks under an arbitrary PAR constraint, viz.

$$\mathrm{PAR}(\boldsymbol{a})=\frac{\max\limits_{m}\{|a_m|^2\}}{\frac{1}{N}\|\boldsymbol{a}\|^2}\leq\zeta. \tag{8.53}$$

It is possible to synthesize low-PAR codes from the CSDP solution of the CoRe framework. To keep the chapter concise, we only use the CoRe formulation in an average sense (note that for a worst-case scenario we have $(\boldsymbol{Z}^{-1}-\boldsymbol{C})^{-1}=\boldsymbol{X}$). In this case, the optimization problem (8.26) can be reformulated as

$$\begin{aligned}\min_{\boldsymbol{A},\boldsymbol{Q}}\quad & \|\boldsymbol{X}^{1/2}\boldsymbol{Q}-\boldsymbol{A}^H\boldsymbol{M}^{-1/2}\|_F^2\\ \text{subject to}\quad & \boldsymbol{Q}\boldsymbol{Q}^H=\boldsymbol{I}\\ & \mathrm{PAR}(\boldsymbol{a})\leq\zeta.\end{aligned} \tag{8.54}$$

Therefore, for fixed $\boldsymbol{Q}$ we have the code synthesis problem:

$$\begin{aligned}\max_{\boldsymbol{a}}\quad & \boldsymbol{a}^H(\boldsymbol{M}^{-1}\odot\boldsymbol{I})\boldsymbol{a}-2\Re\left(\boldsymbol{b}^H\boldsymbol{a}\right)\\ \text{subject to}\quad & \max_{m=0,\cdots,N-1}\{|a_m|^2\}\leq\zeta,\\ & \|\boldsymbol{a}\|^2=N.\end{aligned} \tag{8.55}$$

On the other hand, the low-PAR code design using the CADCODE framework can be handled in a similar manner. The minimization of $g(\boldsymbol{Y},\boldsymbol{A})$ in (8.35) w.r.t. a low-PAR code vector $\boldsymbol{a}$ can be accomplished using the optimization

problem

$$\begin{aligned} \min_{\boldsymbol{a}} \quad & \boldsymbol{a}^H \left((\boldsymbol{Y}_2 \boldsymbol{Y}_2^H) \odot \boldsymbol{C}^T \right) \boldsymbol{a} + 2\Re(\boldsymbol{d}^H \boldsymbol{a}) \\ \text{subject to} \quad & \max_{m=0,\cdots,N-1} \{|a_m|^2\} \leq \zeta, \\ & \|\boldsymbol{a}\|^2 = N. \end{aligned} \tag{8.56}$$

We note that both (8.55) and (8.56) are non-convex QCQPs with PAR constraint and known to be NP-hard in general [173]. In the following, we consider the formulation of (8.55) (without loss of generality). The optimization problem in (8.55) is equivalent to

$$\begin{aligned} \min_{\boldsymbol{a}} \quad & \widetilde{\boldsymbol{a}}^H \boldsymbol{J}\, \widetilde{\boldsymbol{a}} \\ \text{subject to} \quad & \max_{m=0,\cdots,N-1} \{|a_m|^2\} \leq \zeta, \\ & \|\boldsymbol{a}\|^2 = N \end{aligned} \tag{8.57}$$

where $\widetilde{\boldsymbol{a}} = [\boldsymbol{a} \;\; 1]^T$, and

$$\boldsymbol{J} = \begin{bmatrix} \boldsymbol{M}^{-1} \odot \boldsymbol{I} & -\boldsymbol{b} \\ -\boldsymbol{b}^H & 0 \end{bmatrix}.$$

For any $\mu > \lambda_{max}(\boldsymbol{J})$ we can reformulate the latter problem as

$$\begin{aligned} \max_{\boldsymbol{a}} \quad & \widetilde{\boldsymbol{a}}^H \boldsymbol{K}\, \widetilde{\boldsymbol{a}} \\ \text{subject to} \quad & \max_{m=0,\cdots,N-1} \{|a_m|^2\} \leq \zeta, \\ & \|\boldsymbol{a}\|^2 = N \end{aligned} \tag{8.58}$$

with $\boldsymbol{K} = \mu \boldsymbol{I}_{N+1} - \boldsymbol{J}$. Interestingly, derivation of the power-method like iterations in [84] [190] can be extended to the case of PAR-constrained $\boldsymbol{a}$. As a result, the discussed iterations can be applied (after a small modification) to obtain a local optimum of (8.58). More precisely, the code vector $\boldsymbol{a}$ of the $(l+1)^{th}$ iteration (denoted by $\boldsymbol{a}^{(l+1)}$) can be obtained from the last estimate of $\boldsymbol{a}$, i.e. $\boldsymbol{a}^{(l)}$, via solving the optimization problem

$$\begin{aligned} \max_{\boldsymbol{a}^{(l+1)}} \quad & \|\boldsymbol{a}^{(l+1)} - \widehat{\boldsymbol{a}}^{(l)}\| \\ \text{subject to} \quad & \max_{m=0,\cdots,N-1} \{|a_m^{(l+1)}|^2\} \leq \zeta, \\ & \|\boldsymbol{a}^{(l+1)}\|^2 = N \end{aligned} \tag{8.59}$$

where $\widehat{\boldsymbol{a}}^{(l)}$ represents the vector containing the first N entries of $\boldsymbol{K}\, \widetilde{\boldsymbol{a}}^{(l)}$. The optimization problem (8.59) is a "nearest-vector" problem with PAR constraint.

Such PAR constrained problems can be tackled using a recursive algorithm proposed in [191] that can be described briefly as follows: for cases in which the magnitudes of the entries of $\widehat{\boldsymbol{a}}^{(l)}$ are below $\sqrt{\zeta}$, one can easily observe that $\boldsymbol{a}^{(l+1)} = \sqrt{N}\widehat{\boldsymbol{a}}^{(l)}/\|\widehat{\boldsymbol{a}}^{(l)}\|$ is the solution. Otherwise, let $\widehat{a}_0$ denote the entry of $\widehat{\boldsymbol{a}}^{(l)}$ with maximum absolute value. Then the entry of $\boldsymbol{a}^{(l+1)}$ corresponding to $\widehat{a}_0$ is given by $\sqrt{\zeta}e^{j\arg(\widehat{a}_0)}$. Recursively, the other entries of $\boldsymbol{a}^{(l+1)}$ can be obtained solving the same type of "nearest-vector" problem but with the remaining energy i.e. $N-\zeta$.

Finally, we note that as a scaling does not affect the PAR metric (see (8.53)), the low-PAR codes obtained by CoRe or the CADCODE framework can be scaled to fit any desired level of energy. The steps of CoRe and CADCODE presented in Table I and Table II should be modified for designing low-PAR codes. More precisely, the optimization problems in (8.55) in step 2-2 of CoRe (average design) and (8.56) in step 2 of CADCODE are solved via the power method-like iterations provided above.

Remark 4 (unimodular code design): In case of unimodular code design, i.e. $\zeta = 1$, we have

$$\begin{aligned} &\mathrm{tr}\left\{\boldsymbol{A}^H\boldsymbol{M}^{-1}\boldsymbol{A}\right\} = \boldsymbol{a}^H(\boldsymbol{M}^{-1}\odot\boldsymbol{I})\boldsymbol{a} \\ &= N\,\mathrm{tr}\left\{\boldsymbol{M}^{-1}\odot\boldsymbol{I}\right\} = N\,\mathrm{tr}\left\{\boldsymbol{G}^{-1}\right\} \end{aligned} \tag{8.60}$$

and hence the optimization problem in (8.55) is equivalent to:

$$\begin{aligned} \max_{\boldsymbol{a}} \quad & \Re(\boldsymbol{b}^H\boldsymbol{a}) \\ \text{subject to} \quad & |a_m| = 1,\ 0 \le m \le N-1 \end{aligned} \tag{8.61}$$

where $\boldsymbol{b} = \mathrm{diag}(\boldsymbol{X}^{1/2}\boldsymbol{Q}^*\boldsymbol{M}^{-1/2})$. The maximizer $\boldsymbol{a}$ of (8.61) is simply given by $\boldsymbol{a} = \exp(j\arg(\boldsymbol{b}))$. As to the CADCODE framework, unimodular codes can alternatively be obtained by defining

$$\boldsymbol{R} \triangleq \begin{bmatrix} \theta\boldsymbol{I} & \boldsymbol{V}^H \\ \boldsymbol{V} & (\boldsymbol{A}^H\boldsymbol{M}^{-1}\boldsymbol{A})^{-1} + \boldsymbol{C} \end{bmatrix} \tag{8.62}$$

with sufficiently large θ (see Appendix C). Note that for $g(\boldsymbol{Y},\boldsymbol{A}) = \mathrm{tr}\{\boldsymbol{Y}^H\boldsymbol{R}\boldsymbol{Y}\}$ with above $\boldsymbol{R}$, eqs. (8.34) and (8.38) hold true. Therefore, for fixed $\boldsymbol{Y}$ the minimization of $g(\boldsymbol{Y},\boldsymbol{A})$ w.r.t. $\boldsymbol{A}$ can be simplified as the following homogeneous QCQP:

$$\begin{aligned} \min_{\boldsymbol{A}} \quad & \mathrm{tr}\left\{\boldsymbol{Y}_2\boldsymbol{Y}_2^H\boldsymbol{A}^H\boldsymbol{M}\boldsymbol{A}\right\} \\ \text{subject to} \quad & |a_m| = 1,\ 0 \le m \le N-1 \end{aligned} \tag{8.63}$$

where $\boldsymbol{Y} = [\boldsymbol{Y}_{1\ \delta\times\delta}\ \ \boldsymbol{Y}_{2\ N\times\delta}]$. The unimodular quadratic programm in (8.63) is NP-hard in general and can be tackled via a technique similar to that of (8.58). ■

8.6 Numerical Examples

Numerical results will be provided to examine the performance of the proposed methods. Several code design examples for the average metric and the worst-case metric in both constrained and unconstrained cases are included. In particular, we provide a comparison between the code designs in the average and worst-case scenarios using SNR defined in (8.9).

Throughout the numerical examples, we assume that the signal-independent interference can be modeled as a first-order auto-regressive process with parameters $\rho_{\text{int}} = 0.5$ and p_{int}, as well as a white noise at the receiver with the variance σ_n^2:

$$M_{m,n} = \sigma_n^2 \delta[m-n] + p_{\text{int}} \rho_{\text{int}}^{|m-n|},\ 1 \le m,n \le N \tag{8.64}$$

with $\delta[m-n]$ being the discrete-time Kronecker delta function. Furthermore, for clutter we let

$$C_{m,n} = \sigma_c^2 \rho^{(m-n)^2},\ 1 \le m,n \le N \tag{8.65}$$

with $\rho = 0.8$. Note that the model in (8.65) can be used for many natural clutter sources [192]. In this section, we consider $\sigma_c^2 = 1, \sigma_n^2 = 0.01$, and $p_{\text{int}} = 1$ unless otherwise explicitly stated. As to the unknown target Doppler shift, we assume ω is uniformly distributed over Ω. The CVX package has been used to solve the convex problems in the various approaches of this chapter [193]. The extensions of the CoRe and CADCODE frameworks to the case of unimodular code design ($\zeta = 1$) are referred to as CoRe-U and CADCODE-U, respectively (for CoRe and CADCODE without suffix "U" we do not consider the PAR constraint).

8.6.1 Average Sense Design

Herein we consider an example of code design for a Doppler shift interval of $[\omega_l, \omega_u] = [-1, 1]$. We use the proposed algorithms (both CoRe and CADCODE frameworks) to design optimal codes of length $N = 16$. The results are shown in Fig. 8.1(a). The goodness of the resultant codes is investigated using two benchmarks: (i) the upper bound on the average metric obtained by solving the CSDP in (8.25), and (ii) the average metric corresponding to the uncoded system (using the transmit code $\boldsymbol{a} = \sqrt{\frac{e}{N}}\mathbf{1}$).

It can be observed from Fig. 8.1(a) that, as expected, a coded system employing CoRe, CoRe-U, CADCODE, or CADCODE-U outperforms the uncoded system. It is also practically observed that the performance obtained by the randomly generated codes is similar to that of the all-one code used in the uncoded system. We also note that, compared to CoRe, the CADCODE framework leads to slightly larger values of the average metric. This behaviour can be explained noting that CADCODE presumably circumvents the optimality losses arising in the synthesis stage of CoRe. In other words, CADCODE

directly converges to a stationary point of the design problem and there is no synthesis loss associated with the provided code; whereas, the obtained code via CoRe is associated with some synthesis loss. Moreover, Fig. 8.1(a) reveals that the quality of the codes obtained via constrained designs is very similar to that of unconstrained designs. However, there are minor degradations due to imposing the constraints. We also observe the saturation phenomenon in Fig. 8.1(a). More precisely, for sufficiently large values of the transmit energy (i.e. e), the increase in the average metric is negligible. Note that, the value of the average metric (for non-singular $\boldsymbol{C}$) asymptotically converges to:

$$\lim_{e\to\infty} \mathrm{tr}\left\{\left((\boldsymbol{A}^H\boldsymbol{M}^{-1}\boldsymbol{A})^{-1}+\boldsymbol{C}\right)^{-1}\boldsymbol{W}\right\} = \mathrm{tr}\{\boldsymbol{C}^{-1}\boldsymbol{W}\}. \tag{8.66}$$

Next we study the performance of the proposed algorithms w.r.t. the detection performance of the optimal detector (for unknown Doppler shift) stated in (8.11). To this end, we consider the target with $\sigma_T^2 = 10$, transmit energy $e = 10$, and use 100000 sets of random generated data to simulate receiver operating characteristic (ROC). The optimal detector in (8.11) is implemented by numerically evaluating the associated integral. ROCs corresponding to CoRe and CADCODE algorithms (constrained and unconstrained case) as well as to the uncoded system are depicted in Fig. 8.1(b). As expected, the detection performance obtained by devised methods outperforms that of the uncoded system. Minor differences can be observed between ROCs associated with various algorithms. The practical implementation of the optimal detector in (8.11) might be hard. Therefore, we also consider a conventional GLR detector that well approximates the behavior of the optimal detector ([194] [180]):

$$\max_{\omega\in\Omega} \frac{|\boldsymbol{r}^H\left(\boldsymbol{M}+\boldsymbol{A}\boldsymbol{C}\boldsymbol{A}^H\right)^{-1}(\boldsymbol{a}\odot\boldsymbol{p})|^2}{(\boldsymbol{a}\odot\boldsymbol{p})^H\left(\boldsymbol{M}+\boldsymbol{A}\boldsymbol{C}\boldsymbol{A}^H\right)^{-1}(\boldsymbol{a}\odot\boldsymbol{p})} \underset{\mathrm{H_1}}{\overset{\mathrm{H_0}}{\lessgtr}} \eta'' \tag{8.67}$$

In practical situations, a discrete set of target Doppler shifts in Ω is considered in lieu of Ω for the maximization. Fig. 8.1(c), plots the detection performance of the above detector for the coded and uncoded systems (employing 50 points in the Ω for the maximization). As expected, there exist minor degradations in the detection performance of the systems as compared with the performance of the optimal detector shown in Fig. 8.1(b). This figure corresponds to CADCODE but similar performances were observed for the other proposed methods.

The effect of the code length N on the value of the average metric is illustrated in Fig. 8.2 for a fixed transmit energy $e = 10$. It can be seen that as N grows large, the quality of the proposed coding schemes improves substantially (compared to the uncoded system). This is due to the fact that for a large N the code design problem has more degrees of freedom. It can also be observed in Fig. 8.2 that for any fixed length, CoRe and CADCODE provide similar results.

The detection performance of the system depends on the energy of the clutter and interference. To investigate the effects of the aforementioned parameters on the system performance, we define the clutter-to-noise ratio (CNR) and the interference-to-noise ratio (INR):

$$CNR = \frac{\sigma_c^2\, e}{\sigma_n^2}$$
$$INR = \frac{p_{\text{int}}}{\sigma_n^2}$$

To measure the performance improvement in different scenarios, we consider the improvement of the average metric (8.13) (i.e., $\text{metric}^{\text{imp}}$) and the relative increment of the detection probability associated with the optimal detector (8.11) (i.e., P_d^{inc}) w.r.t. the uncoded system:

$$\text{metric}^{\text{imp}} = \frac{\text{average metric}^{coded}}{\text{average metric}^{uncoded}}$$
$$P_d^{\text{inc}} = P_d^{coded} - P_d^{uncoded}$$

The values of $\text{metric}^{\text{imp}}$ and P_d^{inc} for different CNRs have been shown in Table 8.4. The reported values are associated with $e = 5$, INR $= 20$ dB, $\sigma_T^2 = 5$ and are obtained via changing σ_c^2. Note that these values correspond to CAD-CODE but similar behaviors were observed for the other methods. As to the P_d^{inc}, the ROC of the optimal detector (8.11) is considered for $P_{fa} = 10^{-3}$. It is observed that P_d^{inc} is an increasing function of $\text{metric}^{\text{imp}}$. This can be explained via considering the mathematical reasoning for using the average metric (see section III). Furthermore, as expected, increasing the energy of clutter leads to the decreasing of $\text{metric}^{\text{imp}}$ (and so P_d^{inc}). Indeed, for sufficiently large values of CNR, the term $\boldsymbol{A}^{-1}\boldsymbol{M}\boldsymbol{A}^{-H}$ can be neglected as compared with $\boldsymbol{C}$ in (8.13); therefore, the effect of the code matrix $\boldsymbol{A}$ on the detection performance is minor (see the similar discussion on the saturation phenomenon).

Table 8.4. *The values of* $\text{metric}^{\text{imp}}$ *and* P_d^{inc} *for different CNRs (CADCODE).*

CNR	10 dB	15 dB	20 dB	25 dB	30 dB
$\text{metric}^{\text{imp}}$	6.65 dB	6.1 dB	5.3 dB	3.9 dB	2.2 dB
P_d^{inc}	0.32	0.31	0.28	0.23	0.15

Next we perform a similar analysis to probe the detection performance of the system for different values of INR. Herein we consider $e = 5$, CNR $= 20$ dB, $\sigma_T^2 = 5$ and report the values of $\text{metric}^{\text{imp}}$ and P_d^{inc} associated with CAD-CODE in Table 8.5 (by changing p_{int}). It is observed that in low INRs, the performance improvement is minor; this can be explained by noting the fact that such situations refer to clutter-limited cases. By increasing the energy of

interference (i.e., going from clutter-limited conditions to interference-limited conditions), the performance improvement increases. This observation is related to the fact that the the proposed methods have better ability for reducing the effects of the signal-independent interference (as compared with the signal-dependent clutter). Also, it is expected that for large enough values of INR, the detection probabilities of both coded and uncoded systems significantly reduce; hence P_d^{inc} becomes small.

Table 8.5. *The values of* $\text{metric}^{\text{imp}}$ *and* P_d^{inc} *for different INRs (CADCODE).*

INR	10 dB	15 dB	20 dB	25 dB	30 dB
$\text{metric}^{\text{imp}}$	2.2 dB	3.9 dB	5.3 dB	6.2 dB	6.6 dB
P_d^{inc}	0.08	0.13	0.28	0.42	0.42

8.6.2 Worst-Case Sense Design

We consider a worst-case design example with code length $N = 16$, transmit energy $e = 10$, and the Doppler shift interval $\Omega = [-1.5, -0.5] \cup [0.5, 1.5]$. The assessment of the codes in the worst-case design is performed using: (i) the CSDP solution of (8.51) which leads to an upper bound on the worst-case metric, and (ii) the worst-case metric values associated with the uncoded system.

The SNR corresponding to i) and ii) above and to the coded system using CoRe as well as CoRe-U are shown in Fig. 8.3(a) versus the target Doppler shift ω for $\sigma_T^2 = 1$. The optimized CoRe and CoRe-U codes outperform the uncoded system significantly. Moreover, a minor difference between the lowest SNR of the optimized codes can be observed. Note that near $\omega = 0$, all the curves show worse values as compared to other values of ω. This is due to the overlapping of the target and clutter in the frequency domain.

The detection probability can be used to obtain further insights into the behaviour of the worst-case metric for code optimization. We consider the worst-case detection probabilities w.r.t. the Doppler shift of the target. Let $\tilde{\omega}$ denote the Doppler shift corresponding to the smallest achievable performance metric w.r.t ω, viz.

$$\tilde{\omega} = \underset{\omega_l \le \omega \le \omega_u}{\operatorname{argmin}} \operatorname{tr}\left\{ \left((\boldsymbol{A}^H \boldsymbol{M}^{-1} \boldsymbol{A})^{-1} + \boldsymbol{C} \right)^{-1} \boldsymbol{p}\boldsymbol{p}^H \right\}. \tag{8.68}$$

The values of $\tilde{\omega}$ were computed via the Newton method. The worst-case detection probability is calculated via results of [173] as

$$P_{d,worst} = \exp\left(\frac{\log(P_{fa})}{1 + \tilde{\lambda}} \right) \tag{8.69}$$

where P_{fa} denotes probability of false alarm and $\tilde{\lambda}$ is the value of λ for $\tilde{\omega}$. Using the obtained $\tilde{\omega}$ and (8.69), Fig. 8.3(b) shows the worst-case detection probabilities for the CSDP solution and the CoRe code versus target strength σ_T^2 for $P_{fa} = 10^{-6}$. Using CoRe and CoRe-U, a substantial improvement of $P_{d,worst}$ is evident compared to the uncoded system. Due to the unimodularity constraint, CoRe-U yields a slightly lower worst-case detection probability compared to CoRe.

8.6.3 Comparison of the Average and Worst-Case Designs

The average and worst-case metrics are independent of the target Doppler shift; however, one can use the SNR (for various ω) to compare the average and the worst-case designs. To compare the two designs, we consider a code length of $N = 16$, transmit energy $e = 10$, $\sigma_T^2 = 1$, and two different Doppler shift intervals $[-2,-1] \cup [1,2]$ and $[-2,-0.5] \cup [0.5,2]$. Fig. 8.4(a)-(b) plot the SNRs corresponding to the CSDP solution in (8.25), the code obtained by CoRe for the average design, the CSDP solution in (8.51) and the code obtained by CoRe for the worst-case design. These sub-figures also show the SNR corresponding to the case in which the target Doppler shift is known. Note that for the aforementioned case, the optimized code is obtained via the maximization of (8.12) for each Doppler and hence various target Doppler shifts lead to various optimal codes. The SNR associated with the known Doppler case always has the largest values compared with other feasible codes. However, the CSDP solution (8.51) possesses larger minimum SNR values when compared to other curves; but the optimized code corresponding to the CSDP solution (8.51) is associated with a certain synthesis loss that leads to slightly lower minimum value as compared to the known Doppler case. The codes obtained via the worst-case design provide better minimum SNR values whereas the codes obtained via the average design possess larger average SNR values. Furthermore, there exist nulls near $\omega = 0$ due to the overlapping of the target and clutter spectra. In addition, the CSDP solution of the worst-case design can be considered to be rather "conservative" when compared to that of the average design. Herein we remark on the fact that the worst-case design does not require the p.d.f of the target Doppler shift on the desired interval Ω; whereas, the average design depends on the aforementioned p.d.f. Fig. 8.4(c)-(d) depict the detection probabilities corresponding to sub-figures Fig. 8.4(a)-(b). The values of detection probability are obtained via considering (8.69) with $P_{fa} = 10^{-6}$ and $\sigma_T^2 = 10$. Observations similar to those about sub-figures Fig. 8.4(a)-(b) can be made from these sub-figures as well.

8.7 Concluding Remarks

The problem of radar code design for moving target detection in the presence of clutter was considered. Several algorithms were proposed using two novel frameworks for unconstrained or constrained code design in such scenarios. The main results can be summarized as follows:

- A new discrete-time formulation was introduced in (8.4) for moving target detection using pulsed-radars in the presence of clutter (considering motions of the clutter scatterers). The optimal detectors for both known Doppler shift and unknown Doppler shifts are presented. To handle the unknown Doppler shift of the target, the code design problem was considered using both average and worst-case performance metrics of the optimal detector for known Doppler shifts. The connection between the considered metrics and the detection performance are addressed.
- The Convexification via Reparametrization (CoRe) framework was proposed to deal with the highly non-convex design problems. CoRe is based on a relaxation (reparametrization) of the metric optimization problems followed by a synthesis stage. The CoRe framework was used to develop two separate algorithms for obtaining optimal codes in both average and worst-case designs.
- The CoRe framework is based on a core SDP (called CSDP) which can be solved efficiently (in polynomial-time). The CSDP solution of CoRe was used to synthesize the optimal codes w.r.t. the original design problem. The code synthesis was accomplished using a cyclic optimization of a similarity criterion. The CSDP solution provides an upper bound on the average metric in different design scenarios.
- A Cyclic Algorithm for Direct COde DEsign, namely the CADCODE framework, was suggested to tackle the average code design problem directly. In CADCODE, the code design objective function is iteratively minimized via a cyclic minimization of an auxiliary function of the code matrix. The convergence of CADCODE was studied. It was shown that each step of CADCODE can be performed either using the available analytical solutions or solving a convex QCQP.
- The design problems when PAR constrained codes are of interest were also considered. The derivations of CoRe and CADCODE were extended to tackle such constrained problems.
- Several numerical examples were provided to show the potential of the proposed algorithms. It was observed that the codes obtained by CADCODE generally have slightly larger metrics in comparison to those obtained using the synthesis stage of CoRe. The CSDP solution of the worst-case design appears to be rather “conservative" when compared to that of the average design.

Finally we note that, in this chapter, the covariance matrices of the clutter and interference assumed to be a priori known. However, in practice, the ma-

trices are not exactly known and need to be estimated. The code design problem considering uncertainty of the prior knowledge about statistics of clutter and interference can be an interesting topic for future research.

8.8 Appendices

8.8.1 Appendix A: Derivation of the Discrete-Time Model

It follows from (8.1) and (8.2) that the n^{th} lag of the receiver filter output sampled at $t = nT_{PRI} + \tau$ can be written as

$$\begin{aligned} r_n &= (r(t)e^{-j\omega_c t}) \star \phi^*(-t)\Big|_{t=nT_{PRI}+\tau} \qquad (8.70)\\ &= \int_{-\infty}^{+\infty} r(x)e^{-j\omega_c x}\phi^*(x-nT_{PRI}-\tau)dx \\ &= \int_{-\infty}^{+\infty} \alpha_t e^{-j(\omega_c+\nu)\tau}\sum_{m=0}^{N-1} a_m \phi(x-mT_{PRI}-\tau)e^{j\nu x}\phi^*(x-nT_{PRI}-\tau)dx \\ &+ \int_{-\infty}^{+\infty}\sum_{k=1}^{N_{\rm ct}}\sum_{l=1}^{N_{\rm cd}}\sum_{m=0}^{N-1} e^{-j(\omega_c+\omega_l)\tau_k}\rho_{kl}a_m\phi(x-mT_{PRI}-\tau_k)e^{j\omega_l x} \\ &\qquad\qquad \phi^*(x-nT_{PRI}-\tau)dx \\ &+ \int_{-\infty}^{+\infty} w(x)e^{-j\omega_c x}\phi^*(x-nT_{PRI}-\tau)dx \end{aligned}$$

where $\star$ denotes the convolution operator. For the first term at the right-hand side (RHS) of (8.70) we have that

$$\begin{aligned} &\alpha_t \sum_{m=0}^{N-1} a_m e^{-j\omega_c\tau}e^{j\nu mT_{PRI}} \qquad (8.71)\\ &\times \int_{-\infty}^{+\infty}\phi(x-mT_{PRI}-\tau)\phi^*(x-nT_{PRI}-\tau)e^{j\nu(x-mT_{PRI}-\tau)}dx \\ &= \alpha e^{jn\omega}\sum_{m=0}^{N-1} a_m \Psi_{\rm m,n}(0,\nu) \end{aligned}$$

where $\alpha \triangleq \alpha_t e^{-j\omega_c\tau}$, $\omega \triangleq \nu T_{PRI}$, and $\Psi_{\rm m,n}(t_d,\omega_d)$ is the cross-ambiguity function of $\phi(t-mT_{PRI})$ and $\phi(t-nT_{PRI})$ at $t_d = 0$ and Doppler shift ω_d, which is generally defined as

$$\Psi_{\rm m,n}(t_d,\omega_d) = \int_{-\infty}^{+\infty}\phi(x-mT_{PRI})\phi^*(x-nT_{PRI}-t_d)e^{j\omega_d(x-mT_{PRI})}dx. \quad (8.72)$$

Note that $\phi(t-mT_{PRI})$ and $\phi(t-nT_{PRI})$ are non-overlapping for any $n \neq m$. As $\Psi_{n,n}(.,.)$ is not dependent on n, we exploit the notation brevity $\Psi(.,.) =$

$\Psi_{n,n}(.,.)$ and further assume $\Psi(0,\nu) \approx 1$ (this assumption implies the Doppler tolerable property [192] for the basic pulse $\phi(.)$ and has also been considered in several other publications, e.g., [173] [176] and references therein). Therefore, (8.71) becomes

$$\alpha a_n e^{jn\omega} \Psi(0,\nu) \tag{8.73}$$

The second term at the RHS of (8.70) can be rewritten as

$$\begin{aligned} &\sum_{k=1}^{N_{\rm ct}} \sum_{l=1}^{N_{\rm cd}} \rho_{kl} e^{-j(\omega_c+\omega_l)\tau_k} \sum_{m=0}^{N-1} a_m \\ &\times \int_{-\infty}^{+\infty} \phi(x - mT_{PRI} - \tau_k) e^{j\omega_l x} \phi^*(x - nT_{PRI} - \tau) dx \\ &= \sum_{k=1}^{N_{\rm ct}} \sum_{l=1}^{N_{\rm cd}} \rho_{kl} e^{-j\omega_c \tau_k} \sum_{m=0}^{N-1} a_m e^{j\omega_l m T_{PRI}} \Psi_{\rm m,n}(\tau - \tau_k, \omega_l) \end{aligned} \tag{8.74}$$

For unambiguous-range clutter scatterers we have $|\tau - \tau_k| < T_{PRI} - \tau_p$ and hence it is observed that $\phi(x - mT_{PRI} - \tau_k)$ and $\phi^*(x - nT_{PRI} - \tau)$ are non-overlapping for $n \neq m$. Hence for any $n \neq m$ we have that $\Psi_{\rm m,n}(\tau - \tau_k, \omega_l) = 0$ and as a result, (8.74) can be simplified as

$$\begin{aligned} &a_n \underbrace{\left(\sum_{k=1}^{N_{\rm ct}} \sum_{l=1}^{N_{\rm cd}} \rho_{kl} e^{-j\omega_c \tau_k} e^{jn\omega_l T_{PRI}} \Psi(\tau - \tau_k, \omega_l) \right)}_{c_n} \\ &= a_n c_n \end{aligned} \tag{8.75}$$

Finally, we denote the last term at the RHS of (8.70) by w_n to obtain the discrete-time signal model as

$$\boldsymbol{r} = \alpha \boldsymbol{a} \odot \boldsymbol{p} + \boldsymbol{a} \odot \boldsymbol{c} + \boldsymbol{w} \tag{8.76}$$

where $\boldsymbol{r} \triangleq [r_0\ r_1\ \ \ldots\ \ r_{N-1}]^T$, $\boldsymbol{p} \triangleq [1\ e^{j\omega}\ \ \ldots\ \ e^{j(N-1)\omega}]^T$, and $\boldsymbol{w} \triangleq [w_0\ w_1\ \ \ldots\ \ w_{N-1}]^T$.

The covariance matrices of Gaussian random vectors $\boldsymbol{w}$ and $\boldsymbol{c}$ are required for the proposed code design algorithms. Let

$$\mathrm{E}\left\{\boldsymbol{w}\boldsymbol{w}^H\right\} \triangleq \boldsymbol{M},\ \ \mathrm{E}\left\{\boldsymbol{c}\boldsymbol{c}^H\right\} \triangleq \boldsymbol{C}. \tag{8.77}$$

To compute the entries of $\boldsymbol{M}$ one can write

$$\begin{aligned} M_{m,n} &= \mathrm{E}\{w_m w_n^*\} \\ &= \int_{-\infty}^{+\infty} \int_{-\infty}^{+\infty} \mathrm{E}\{w(x) w^*(y)\} e^{-j\omega_{\rm c}(x-y)} \\ &\quad \times \phi^*(x - mT_{PRI} - \tau) \phi(y - nT_{PRI} - \tau)\, dxdy \\ &= \int_{-\infty}^{+\infty} \int_{-\infty}^{+\infty} R_w(x,y) e^{-j\omega_{\rm c}(x-y)} \\ &\quad \times \phi^*(x - mT_{PRI} - \tau) \phi(y - nT_{PRI} - \tau)\, dxdy \end{aligned} \tag{8.78}$$

where $R_w(x,y)$ is the statistical auto-correlation function of the random process[6] $w(t)$. In particular, it is interesting to derive the entries of $\boldsymbol{C}$ as it provides useful insights into the importance of the ambiguity function of $\phi(.)$ as well as the other parameters that form $\boldsymbol{C}$. The entries of $\boldsymbol{C}$ can be computed as

$$\begin{aligned} C_{m,n} &= \mathrm{E}\{c_m c_n^*\} \qquad (8.79)\\ &= \sum_k \sum_l \sum_p \sum_q \mathrm{E}\{\rho_{kl}\rho_{pq}^*\}\,\mathrm{E}\{\left(e^{-j\omega_c\tau_k} e^{jm\omega_l T_{PRI}} \Psi(|\tau-\tau_k|,\omega_l)\right)\\ &\quad \times \left(e^{j\omega_c\tau_p} e^{-jn\omega_q T_{PRI}} \Psi^*(|\tau-\tau_p|,\omega_q)\right)\}\\ &= \sum_k \sum_l \mathrm{E}\{|\rho_{kl}|^2\}\,\mathrm{E}\{|\Psi(|\tau-\tau_k|,\omega_l)|^2 e^{j(m-n)\omega_l T_{PRI}}\} \end{aligned}$$

where $\mathrm{E}\{\rho_{kl}\}$ is assumed to be zero (without loss of generality). It is worth noting that $C_{m,n}$ is dependent on the variances of $\{\rho_{kl}\}$, the ambiguity function of $\phi(.)$ (i.e. $\Psi(.,.)$), as well as the statistical distributions of τ_k and ω_l .

8.8.2 Appendix B: Tightness Assessment of the Lower Bound $\mathscr{J}_{LB}$ on the J-Divergence

We define the following relative error to measure the tightness of the lower bound $\mathscr{J}_{LB}$ on the J-divergence:

$$\mathscr{E} \triangleq \frac{\mathscr{J} - \mathscr{J}_{LB}}{\mathscr{J}_{LB}}. \qquad (8.80)$$

Let $\lambda_0 = \mathrm{E}\{\lambda\}$. Note that using (8.17), we have

$$\mathscr{J} = \mathrm{E}\left\{\lambda - 1 + \frac{1}{\lambda+1}\right\} \qquad (8.81)$$

and hence, the numerator of the relative error $\mathscr{E}$ can be simplified as:

$$\begin{aligned} \mathscr{J} - \mathscr{J}_{LB} &= \mathrm{E}\left\{\lambda - 1 + \frac{1}{\lambda+1}\right\} - \left\{\lambda_0 - 1 + \frac{1}{\lambda_0+1}\right\} \qquad (8.82)\\ &= \mathrm{E}\left\{\frac{1}{1+\lambda}\right\} - \frac{1}{1+\lambda_0}. \end{aligned}$$

Note that there exists $\lambda_1 \geq 0$ for which $\lambda \geq \lambda_1$, for all ω. Therefore, we have $\mathrm{E}\left\{\frac{1}{1+\lambda}\right\} \leq \frac{1}{1+\lambda_1}$. Consequently, $\mathscr{E}$ can be upper bounded as:

$$\mathscr{E} \leq \frac{\lambda_0 - \lambda_1}{{\lambda_0}^2(1+\lambda_1)} \leq \frac{1}{\lambda_0}. \qquad (8.83)$$

[6]Note that in the case of white noise, $M_{m,n}$ is zero for $m \neq n$ and $M_{n,n}$ is equal to the variance of the noise.

The above analysis shows that for *sufficiently large* values of λ_0 the value of relative error $\mathscr{E}$ approaches zero. Hereafter, a numerical study of the tightness of the $\mathscr{J}_{LB}$ is provided. We first evaluate the relative error $\mathscr{E}$ for various intervals of ω. We consider $e = 16$, $\sigma_T^2 = 1$, and other parameters as those of Section VI. The value of the J-divergence is calculated by numerically evaluating the integral. Fig. 8.5(a) depicts two dimensional curve of the average of the $\mathscr{E}$ for 1000 random code vectors $\boldsymbol{a}$ versus ω' and ω''. Each point of the curve is associated with the Doppler shift interval $[\min(\omega', \omega''), \max(\omega', \omega'')]$. It is observed that the average $\mathscr{E}$ is significantly small. Moreover, as expected, average $\mathscr{E}$ is zero when $\omega' = \omega''$ (which corresponds to known Doppler shift equal to ω'). Next we investigate the behavior of the relative error with respect to the transmit energy e and target strength σ_T^2. The results are illustrated in Fig. 8.5(b) by considering 1000 random code vectors $\boldsymbol{a}$ and $\Omega = [-.75, 1.95]$ (corresponds to a peak of $\mathscr{E}$ in Fig. 8.5(a)). Small values of the average relative error can be seen in the figure. Furthermore, by increasing e or σ^2, the average $\mathscr{E}$ decreases. This observation is also compatible with the behavior of the $\mathscr{E}$ upper bound in (8.83).

8.8.3 Appendix C: Derivation of the Variable θ

We note that θ should be sufficiently large such that Θ in (8.32) becomes positive definite. Particularly, θ should satisfy the matrix inequality

$$\theta \boldsymbol{I} - \boldsymbol{V}^H (\boldsymbol{A}^{-1} \boldsymbol{M} \boldsymbol{A}^{-H} + \boldsymbol{C})^{-1} \boldsymbol{V} \succ \boldsymbol{0} \tag{8.84}$$

or equivalently $\theta > \lambda_{max}\left(\boldsymbol{V}^H (\boldsymbol{A}^{-1} \boldsymbol{M} \boldsymbol{A}^{-H} + \boldsymbol{C})^{-1} \boldsymbol{V}\right)$. Note that

$$\lambda_{max}\left(\boldsymbol{V}^H (\boldsymbol{A}^{-1} \boldsymbol{M} \boldsymbol{A}^{-H} + \boldsymbol{C})^{-1} \boldsymbol{V}\right) \leq \lambda_{max}\left((\boldsymbol{A}^{-1} \boldsymbol{M} \boldsymbol{A}^{-H} + \boldsymbol{C})^{-1}\right) \lambda_{max}(\boldsymbol{W}). \tag{8.85}$$

Furthermore, one can verify that

$$\begin{aligned} \lambda_{min}(\boldsymbol{A}^{-1} \boldsymbol{M} \boldsymbol{A}^{-H}) &= \min_{\|\mathbf{x}\|=1} \left((\boldsymbol{A}^{-H} \mathbf{x})^H \boldsymbol{M} (\boldsymbol{A}^{-H} \mathbf{x})\right) \\ &\geq \left(\min_m \left\{|a_m|^{-1}\right\}\right)^2 \left(\min_{\|\mathbf{x}\|=1} \mathbf{x}^H \boldsymbol{M} \mathbf{x}\right) \\ &\geq \frac{1}{e} \lambda_{min}(\boldsymbol{M}) \end{aligned} \tag{8.86}$$

which implies

$$\begin{aligned} \lambda_{min}(\boldsymbol{A}^{-1} \boldsymbol{M} \boldsymbol{A}^{-H} + \boldsymbol{C}) &\geq \lambda_{min}(\boldsymbol{A}^{-1} \boldsymbol{M} \boldsymbol{A}^{-H}) + \lambda_{min}(\boldsymbol{C}) \\ &\geq \frac{1}{e} \lambda_{min}(\boldsymbol{M}) + \lambda_{min}(\boldsymbol{C}). \end{aligned} \tag{8.87}$$

As a result, setting

$$\theta = \frac{\lambda_{max}(\boldsymbol{W})}{\frac{1}{e} \lambda_{min}(\boldsymbol{M}) + \lambda_{min}(\boldsymbol{C})} \tag{8.88}$$

ensures $\Theta \succ \mathbf{0}$.

In the case of unimodular code design, we have that $|a_m| = 1$ (for all m). Therefore, in order to guarantee the positive definiteness of $\boldsymbol{R}$ in (8.62), it is sufficient to set

$$\theta = \frac{\lambda_{max}(\boldsymbol{W})}{\lambda_{min}(\boldsymbol{M}) + \lambda_{min}(\boldsymbol{C})}. \tag{8.89}$$

8.8.4 Appendix D: Solution to the QCQP in (8.37)

The convex QCQP in (8.37) can be solved using the Lagrange multiplier method . Let

$$h(\boldsymbol{a}, \mu) = \boldsymbol{a}^H \left(\boldsymbol{Y}_2 \boldsymbol{Y}_2^H \odot \boldsymbol{C}^T \right) \boldsymbol{a} + 2\Re \left(\boldsymbol{d}^H \boldsymbol{a} \right) + \mu (\boldsymbol{a}^H \boldsymbol{a} - e) \tag{8.90}$$

represent the Lagrangian function with μ being the non-negative Lagrange multiplier associated with the energy constraint (such that $(\boldsymbol{Y}_2 \boldsymbol{Y}_2^H) \odot \boldsymbol{C}^T + \mu \boldsymbol{I} \succ \mathbf{0}$). For fixed μ, the unconstrained minimizer $\boldsymbol{a}$ of $h(\boldsymbol{a}, \mu)$ is given by

$$\boldsymbol{a}_\mu = -(\boldsymbol{Y}_2 \boldsymbol{Y}_2^H \odot \boldsymbol{C}^T + \mu \boldsymbol{I})^{-1} \boldsymbol{d}. \tag{8.91}$$

It is straightforward to derive that

$$h(\boldsymbol{a}_\mu, \mu) = -\boldsymbol{d}^H (\boldsymbol{Y}_2 \boldsymbol{Y}_2^H \odot \boldsymbol{C}^T + \mu \boldsymbol{I})^{-1} \boldsymbol{d} - \mu e \tag{8.92}$$

The $h(\boldsymbol{a}_\mu, \mu)$ is a concave function w.r.t. $\mu \geq 0$ and hence the maximizer μ of (8.92) is immediate by imposing the criterion $\frac{\partial}{\partial \mu} h(\boldsymbol{a}_\mu, \mu) = 0$ which implies

$$\boldsymbol{d}^H (\boldsymbol{Y}_2 \boldsymbol{Y}_2^H \odot \boldsymbol{C}^T + \mu \boldsymbol{I})^{-2} \boldsymbol{d} = e. \tag{8.93}$$

Moreover, note that

$$\frac{\partial}{\partial \mu} \left(\boldsymbol{d}^H (\boldsymbol{Y}_2 \boldsymbol{Y}_2^H \odot \boldsymbol{C}^T + \mu \boldsymbol{I})^{-2} \boldsymbol{d} \right) = -2 \boldsymbol{d}^H (\boldsymbol{Y}_2 \boldsymbol{Y}_2^H \odot \boldsymbol{C}^T + \mu \boldsymbol{I})^{-3} \boldsymbol{d} < 0. \tag{8.94}$$

Therefore, the left hand side of (8.93) is a monotonically decreasing function of μ and hence the solution μ of (8.93) can be obtained efficiently via, for example, the Newton method. Once (8.93) is solved, the optimum $\boldsymbol{a}$ is calculated using (8.91).

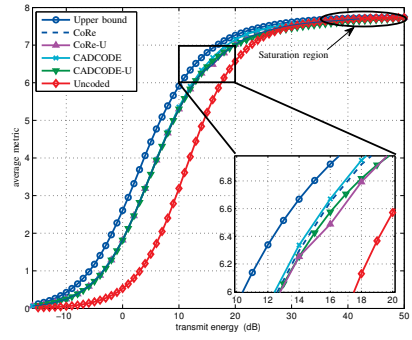

(a)

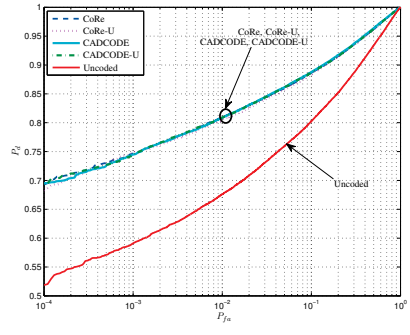

(b)

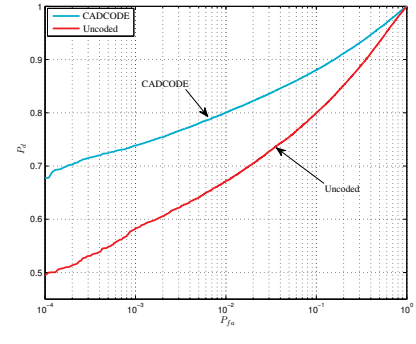

(c)

Figure 8.1. The design of optimized codes of length $N = 16$ using the average metric. (a) depicts the average metric for different methods as well as the uncoded system vs. the transmit energy. (b) plots the ROC of the optimal detector associated with the same codes (as in sub-figure (a)) with $\sigma_T^2 = 10$ and $e = 10$. (c) depicts the ROC of the GLR detector (8.67) for the coded system (CADCODE) and uncoded one.

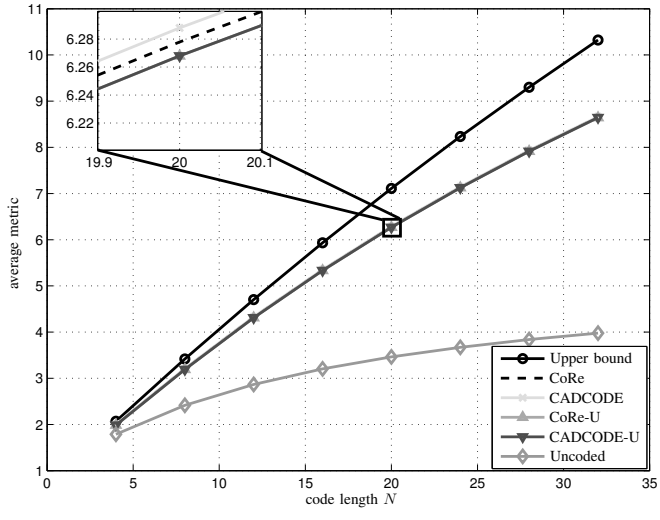

Figure 8.2. The average metric associated with the upper bound (i.e. the CSDP solution in (8.25)), CoRe, CADCODE, CoRe-U, CADCODE-U, and the uncoded system vs. the code length N. A transmit energy of $e = 10$ was considered.

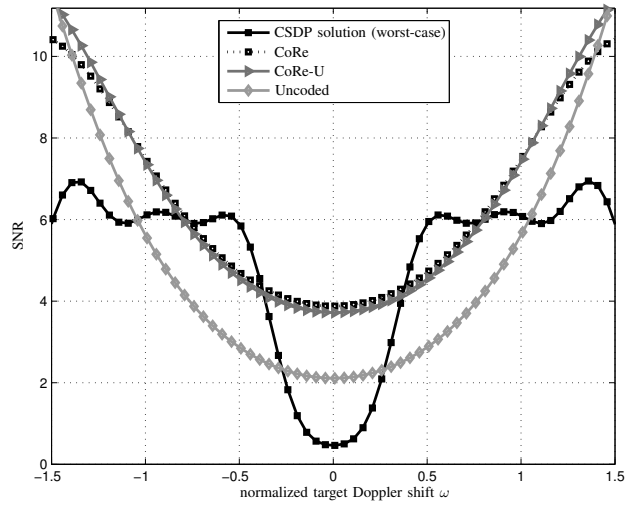

(a)

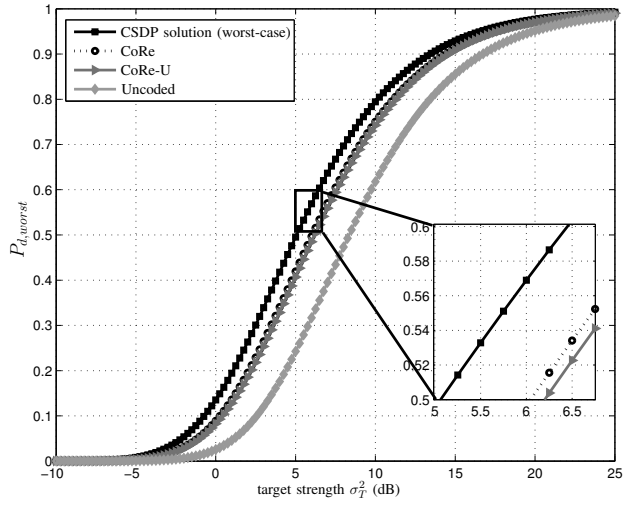

(b)

Figure 8.3. (a) The SNR for the CSDP solution, CoRe, CoRe-U, and the uncoded system vs. the normalized target Doppler shift for $N = 16$ and $e = 10$. (b) The worst-case detection probability of the CSDP solution, CoRe, CoRe-U, and the uncoded system vs. the target strength σ_T^2 for the same designs as in sub-figure (a).

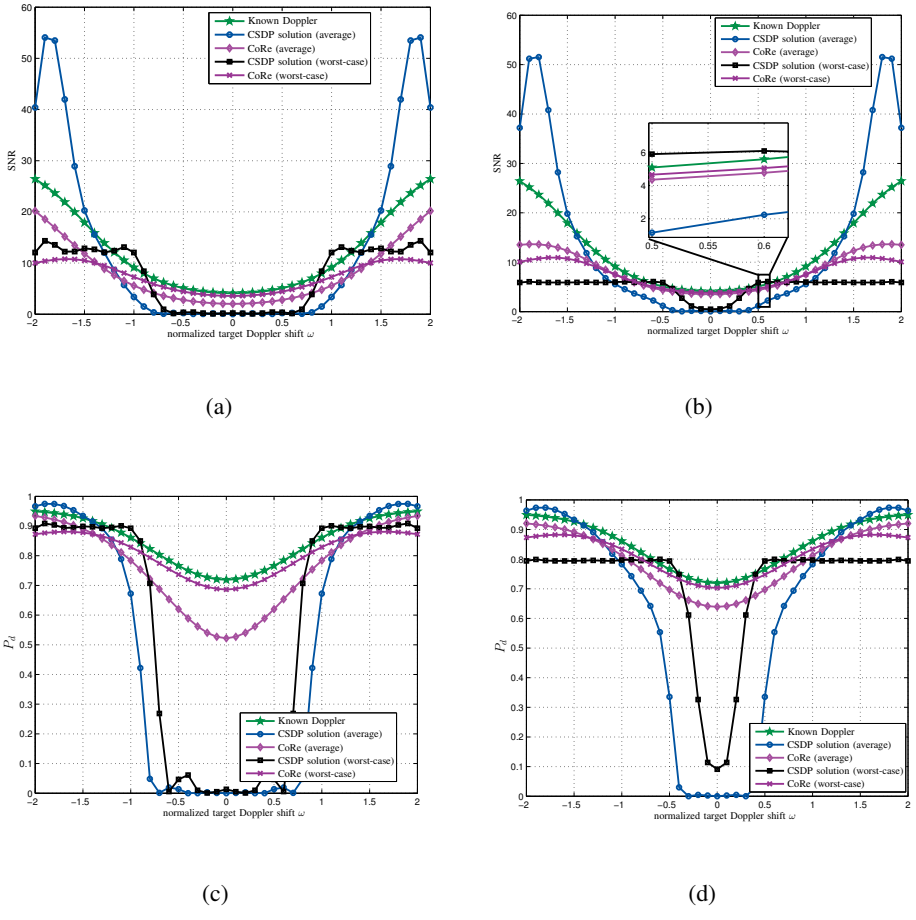

Figure 8.4. Comparison of the average and worst-case code design approaches for $N = 16$, $e = 10$, and two different normalized target Doppler shift intervals Ω: (a) the SNR for $[-2,-1] \cup [1,2]$ ($\sigma_T^2 = 1$), (b) the SNR for $[-2,-0.5] \cup [0.5,2]$ ($\sigma_T^2 = 1$), (c) the detection probability for $[-2,-1] \cup [1,2]$ ($\sigma_T^2 = 10$), and (d) the detection probability for $[-2,-0.5] \cup [0.5,2]$ ($\sigma_T^2 = 10$).

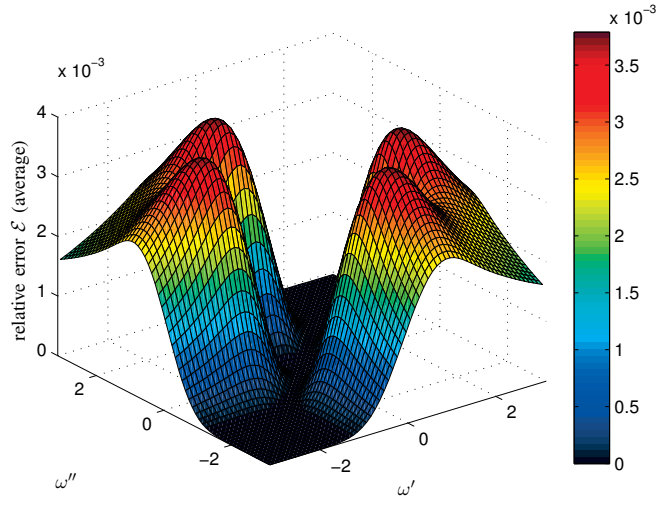

(a)

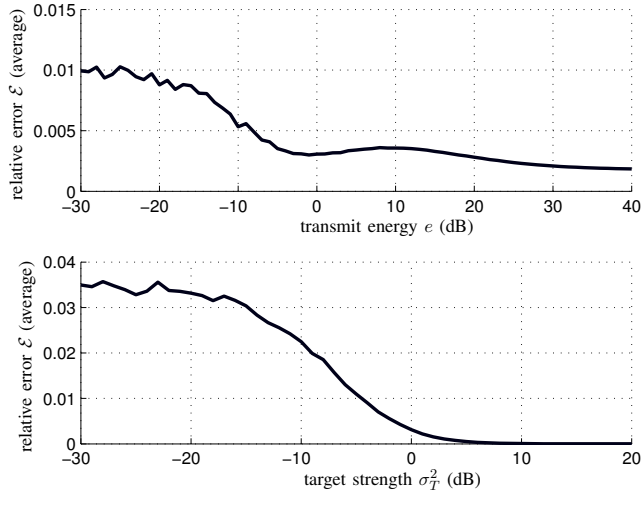

(b)

Figure 8.5. A numerical analysis of the tightness of the lower bound $\mathscr{J}_{LB}$ on the J-divergence. (a) plots the average relative error $\mathscr{E}$ for various intervals of $\omega = [\min(\omega', \omega''), \max(\omega', \omega'')]$. (b) depicts the behavior of the average relative error $\mathscr{E}$ versus transmit energy e and target strength σ_T^2.

9. Joint Design of the Receive Filter and Transmit Sequence for Active Sensing

Abstract
Due to its long-standing importance, the problem of designing the receive filter and transmit sequence for clutter/interference rejection in active sensing has been studied widely in the last decades. In this letter, we propose a cyclic optimization of the transmit sequence and the receive filter. The proposed approach can handle arbitrary peak-to-average-power ratio (PAR) constraints on the transmit sequence, and can be used for large dimension designs (with $\sim 10^3$ variables) even on an ordinary PC.

Keywords: Clutter rejection, peak-to-average-power ratio (PAR), probing signal, receive filter.

9.1 Introduction and Problem Formulation

A key design problem in cognitive active sensing is to jointly optimize the probing sequence and the receive filter (using *apriori* knowledge on clutter/interference) in order to minimize the estimation error of the target parameters. Let $\boldsymbol{s} = (s_1\, s_2 \cdots s_N)^T$ denote the transmit sequence which is used to modulate the train of pulses [39]. In the following, we adopt the discrete model in [196] to formulate the problem. Particularly, we assume that the received baseband signal satisfies the following equation:

$$\boldsymbol{y} = \boldsymbol{A}^H \boldsymbol{\alpha} + \boldsymbol{\varepsilon} \tag{9.1}$$

with

$$\mathbf{A}^H = \begin{pmatrix} s_1 & 0 & \cdots & 0 & s_N & s_{N-1} & \cdots & s_2 \\ s_2 & s_1 & & \vdots & 0 & s_N & & \vdots \\ \vdots & \vdots & \ddots & 0 & \vdots & \vdots & \ddots & s_N \\ s_N & s_{N-1} & \cdots & s_1 & 0 & 0 & \cdots & 0 \end{pmatrix}, \tag{9.2}$$

$$\boldsymbol{\alpha} = (\alpha_0\ \alpha_1\ \cdots\ \alpha_{N-1}\ \alpha_{-(N-1)}\ \cdots\ \alpha_{-1})^T \tag{9.3}$$

where $\{\alpha_k\}$ are the scattering coefficients of different range cells, and $\boldsymbol{\varepsilon}$ denotes the signal independent interference. We also assume that

$$\begin{aligned} \mathbb{E}\{\boldsymbol{\varepsilon}\boldsymbol{\varepsilon}^H\} &= \boldsymbol{\Gamma}, \\ \mathbb{E}\{|\alpha_k|^2\} &= \beta,\ \ k \neq 0 \end{aligned} \tag{9.4}$$

where the interference covariance matrix $\boldsymbol{\Gamma}$, and the average clutter power β are given (e.g. they are obtained by some pre-scan procedures [197]), and that $\boldsymbol{\varepsilon}$ and $\{\alpha_k\}$ have zero mean and are independent of each other. The estimation of the scattering coefficient of current interest α_0 can be accomplished using a matched filter. However, an estimate of α_0 with generally smaller mean square error (MSE) can be obtained via a suitable mismatched filtering (MMF) of the received data. The MMF estimate of α_0 is given by $\widehat{\alpha}_0 = (\boldsymbol{w}^H \boldsymbol{y})/(\boldsymbol{w}^H \boldsymbol{s})$ where

$\boldsymbol{w} \in \mathbb{C}^N$ is the MMF vector. The MSE of the above estimate of α_0 can be expressed as

$$\mathrm{MSE}(\widehat{\alpha}_0) = \mathbb{E}\left\{ \left| \frac{\boldsymbol{w}^H \boldsymbol{y}}{\boldsymbol{w}^H \boldsymbol{s}} - \alpha_0 \right|^2 \right\} = \frac{\boldsymbol{w}^H \boldsymbol{R} \boldsymbol{w}}{|\boldsymbol{w}^H \boldsymbol{s}|^2} \tag{9.5}$$

where

$$\boldsymbol{R} = \beta \sum_{0<|k|\leq(N-1)} \boldsymbol{J}_k \boldsymbol{s}\boldsymbol{s}^H \boldsymbol{J}_k^H + \boldsymbol{\Gamma} \tag{9.6}$$

and $\{\boldsymbol{J}_k\}$ are the shifting matrices defined by

$$[\boldsymbol{J}_k]_{l,m} = [\boldsymbol{J}_{-k}^H]_{l,m} \triangleq \delta_{m-l-k}. \tag{9.7}$$

where $\delta_{(.)}$ denotes the Kronecker delta function. The principal objective of the **c**ognitive **re**ceiver and **w**aveform (CREW) design of $\boldsymbol{w}$ and $\boldsymbol{s}$ is to minimize the MSE of $\widehat{\alpha}_0$ (see e.g. [196] for a review of the relevant literature of this design). In the following section, a new approach to CREW is presented.

9.2 CREW(cyclic)

In this section, we propose a cyclic minimization of the MSE criterion in (9.5). For fixed $\boldsymbol{s}$, the minimization of (9.5) with respect to (w.r.t.) $\boldsymbol{w}$ results in the closed-form expression:

$$\boldsymbol{w} = \boldsymbol{R}^{-1} \boldsymbol{s} \tag{9.8}$$

to within a multiplicative constant. For fixed $\boldsymbol{w}$, the minimizing transmit code $\boldsymbol{s}$ of (9.5) can be obtained as follows. Note that

$$\begin{aligned} \boldsymbol{w}^H \boldsymbol{R} \boldsymbol{w} &= \boldsymbol{w}^H \left(\beta \sum_{0<|k|\leq(N-1)} \boldsymbol{J}_k \boldsymbol{s}\boldsymbol{s}^H \boldsymbol{J}_k^H + \boldsymbol{\Gamma} \right) \boldsymbol{w} \\ &= \boldsymbol{s}^H \underbrace{\left(\beta \sum_{0<|k|\leq(N-1)} \boldsymbol{J}_k^H \boldsymbol{w}\boldsymbol{w}^H \boldsymbol{J}_k \right)}_{\boldsymbol{Q}} \boldsymbol{s} + \underbrace{\boldsymbol{w}^H \boldsymbol{\Gamma} \boldsymbol{w}}_{\mu}. \end{aligned} \tag{9.9}$$

As a result, the design metric in (9.5) can be rewritten as

$$\mathrm{MSE}(\widehat{\alpha}_0) = \frac{\boldsymbol{w}^H \boldsymbol{R} \boldsymbol{w}}{|\boldsymbol{w}^H \boldsymbol{s}|^2} = \frac{\boldsymbol{s}^H \boldsymbol{Q} \boldsymbol{s} + \mu}{\boldsymbol{s}^H \boldsymbol{W} \boldsymbol{s}} \tag{9.10}$$

where $\boldsymbol{W} = \boldsymbol{w}\boldsymbol{w}^H$. We observe that both the numerator and denominator of (9.10) are quadratic in $\boldsymbol{s}$. To deal with the minimization of (9.10), we exploit

the idea of fractional programming [198]. Let $a(\boldsymbol{s}) = \boldsymbol{s}^H \boldsymbol{Q}\boldsymbol{s} + \mu$, $b(\boldsymbol{s}) = \boldsymbol{s}^H \boldsymbol{W}\boldsymbol{s}$, and note that for MSE to be finite we must have $b(\boldsymbol{s}) > 0$. Moreover, let $f(\boldsymbol{s}) = \mathrm{MSE}(\widehat{\alpha}_0) = a(\boldsymbol{s})/b(\boldsymbol{s})$ and suppose that $\boldsymbol{s}_\star$ denotes the current value of $\boldsymbol{s}$. We define $g(\boldsymbol{s}) \triangleq a(\boldsymbol{s}) - f(\boldsymbol{s}_\star)b(\boldsymbol{s})$, and $\boldsymbol{s}_\dagger \triangleq \arg\min_{\boldsymbol{s}} g(\boldsymbol{s})$. It is straightforward to verify that $g(\boldsymbol{s}_\dagger) \leq g(\boldsymbol{s}_\star) = 0$. Consequently, we have that $g(\boldsymbol{s}_\dagger) = a(\boldsymbol{s}_\dagger) - f(\boldsymbol{s}_\star)b(\boldsymbol{s}_\dagger) \leq 0$ which implies

$$f(\boldsymbol{s}_\dagger) \leq f(\boldsymbol{s}_\star) \tag{9.11}$$

as $b(\boldsymbol{s}_\dagger) > 0$. Therefore, $\boldsymbol{s}_\dagger$ can be considered as a new vector $\boldsymbol{s}$ which decreases $f(\boldsymbol{s})$. Note that for (9.11) to hold, $\boldsymbol{s}_\dagger$ does not necessarily have to be a minimizer of $g(s)$; indeed, it is enough if $\boldsymbol{s}_\dagger$ is such that $g(\boldsymbol{s}_\dagger) \leq g(\boldsymbol{s}_\star)$.

For a given MMF vector $\boldsymbol{w}$, and any $\boldsymbol{s}_\star$ of the minimizer $\boldsymbol{s}$ of (9.10) we have (assuming $\|\boldsymbol{s}\|_2^2 = N$):

$$g(\boldsymbol{s}) = \boldsymbol{s}^H(\boldsymbol{Q} + (\mu/N)\boldsymbol{I} - f(\boldsymbol{s}_\star)\boldsymbol{W})\boldsymbol{s} = \boldsymbol{s}^H \boldsymbol{T}\boldsymbol{s} \tag{9.12}$$

where $\boldsymbol{T} \triangleq \boldsymbol{Q} + (\mu/N)\boldsymbol{I} - f(\boldsymbol{s}_\star)\boldsymbol{W}$. Now, let λ be a real number larger than the maximum eigenvalue of $\boldsymbol{T}$. Then the minimization of (9.10) w.r.t. unimodular $\boldsymbol{s}$ can be cast as the following unimodular quadratic program (UQP) [84]:

$$\begin{aligned} \max_{\boldsymbol{s}} \quad & \boldsymbol{s}^H \widetilde{\boldsymbol{T}}\boldsymbol{s} \\ \text{s.t.} \quad & |s_k| = 1, \;\; 1 \leq k \leq N, \end{aligned} \tag{9.13}$$

in which $\widetilde{\boldsymbol{T}} \triangleq \lambda \boldsymbol{I} - \boldsymbol{T}$ is positive definite. Note that (9.13) is NP-hard in general (see, e.g. [139]). A possible approach to deal with (9.13) is to employ the semi-definite relaxation (SDR) method which is widely used in the literature. However, SDR is based on a core semi-definite program (SDP) which makes it computationally expensive as N grows large. To tackle (9.13) efficiently, in [84] a set of *power method-like* iterations was introduced that can be used to monotonically increase the criterion in (9.13) (or equivalently decrease $f(\boldsymbol{s})$); namely, the vector $\boldsymbol{s}$ is updated using the nearest-vector problem

$$\begin{aligned} \min_{\boldsymbol{s}^{(t+1)}} \quad & \left\| \boldsymbol{s}^{(t+1)} - \widetilde{\boldsymbol{T}}\boldsymbol{s}^{(t)} \right\|_2 \\ \text{s.t.} \quad & \left| s_k^{(t+1)} \right| = 1, \;\; 1 \leq k \leq N. \end{aligned} \tag{9.14}$$

The solution of (9.14) is simply given by $\boldsymbol{s}^{(t+1)} = e^{j \arg(\widetilde{\boldsymbol{T}}\boldsymbol{s}^{(t)})}$. A proof of monotonically increasing behavior of the associated UQP objective function through the above power method-like iterations is presented in Appendix A.

In many applications, unimodularity (i.e. unit PAR) is not required for the transmit sequence $\boldsymbol{s}$. As a result, one can consider a more general PAR constraint, viz. $\mathrm{PAR} = \|\boldsymbol{s}\|_\infty^2/(\frac{1}{N}\|\boldsymbol{s}\|_2^2) \leq \gamma$ for designing $\boldsymbol{s}$. In such a situation, a similar formulation as in the case of unimodular $\boldsymbol{s}$ can be used. More concretely, a decrease of the MSE criterion in (9.10) for a PAR constrained $\boldsymbol{s}$ can

be achieved via increasing the objective function of the following optimization problem:

$$\begin{aligned} \max_{\boldsymbol{s}} \quad & \boldsymbol{s}^H \widetilde{\boldsymbol{T}} \boldsymbol{s} \\ \text{s.t.} \quad & |s_k| \le \sqrt{\gamma}, \;\; 1 \le k \le N, \\ & \|\boldsymbol{s}\|_2^2 = N \end{aligned} \tag{9.15}$$

where $\widetilde{\boldsymbol{T}}$ is defined as in (9.13). To this end, we note that the derivation of the power method-like iterations in [84] can be conveniently generalized to the case with a PAR constraint. In particular, one can increase the objective function of (9.15) by updating $\boldsymbol{s}$ using the nearest-vector problem

$$\begin{aligned} \min_{\boldsymbol{s}^{(t+1)}} \quad & \left\| \boldsymbol{s}^{(t+1)} - \widetilde{\boldsymbol{T}} \boldsymbol{s}^{(t)} \right\|_2 \\ \text{s.t.} \quad & \left| s_k^{(t+1)} \right| \le \sqrt{\gamma}, \;\; 1 \le k \le N, \\ & \left\| \boldsymbol{s}^{(t+1)} \right\|_2^2 = N \end{aligned} \tag{9.16}$$

which can be solved efficiently via a recursive algorithm suggested in [26].

The CREW(cyclic) algorithm derived above is summarized in Table 9.1. Note that the matrices $\boldsymbol{R}$ and $\boldsymbol{Q}$ can be computed efficiently by employing fast Fourier transform (FFT) operations. We refer the interested reader to Appendix B for the derivation of such an efficient computational scheme.

Table 9.1. *CREW(cyclic)*

Step 0: Initialize the transmit sequence $\boldsymbol{s}$ with a unimodular (or low PAR) vector in $\mathbb{C}^N$.
Step 1: Compute the matrix $\boldsymbol{R}$, and find the optimal MMF vector $\boldsymbol{w}$ using (9.8).
Step 2 Compute the scalar μ, and the matrices $\boldsymbol{Q}$ and $\boldsymbol{W}$. Use t as the internal iteration counter of step 2, and while $f(\boldsymbol{s}^{(t)}) - f(\boldsymbol{s}^{(t+1)}) > \delta$ (for some fixed $\delta > 0$) do:
Step 2-1: Form the matrix $\widetilde{\boldsymbol{T}}$ (as defined in (9.13)) using the
current vector $\boldsymbol{s}$.
Step 2-2: Employ the power method-like iterations following
(9.14) or (9.16) (depending on the code constraint) to update $\boldsymbol{s}$;
until convergence.
Step 3: Repeat steps 1 and 2 until a stop criterion is satisfied, e.g. $\left\|\text{MSE}^{(v+1)} - \text{MSE}^{(v)}\right\| < \varepsilon$ for some given $\varepsilon > 0$, where v denotes the outer loop iteration number.

9.3 Discussion and Numerical Examples

In this section, we examine the performance of CREW(cyclic) by comparing it with three methods previously devised in [196]; namely CAN-MMF, CREW(gra) and CREW(fre). The CAN-MMF method employs the CAN algorithm in [6] to design a transmit sequence with good correlation properties. As a result, the design of the transmit waveform is independent of the receive filter. The receive filter of CAN-MMF is obtained by (9.8). Note that no prior knowledge of interference is used in the waveform design of CAN-MMF. CREW(gra) is a gradient based algorithm for minimizing (9.5) which can only deal with the unimodularity constraint. Moreover, a large number of iterations is needed by CREW(gra) until convergence and, in each iteration, the update of the gradient vector is time consuming. CREW(fre) is a frequency-based approach that yields globally optimal values of the spectrum of the transmit waveform as well as the receive filter for a relaxed version of the original waveform design problem, and hence in general does not provide an optimal solution to the latter problem. Like CAN-MMF, CREW(fre) can handle both unimodularity and PAR constraints. Moreover, it can be used to design relatively long sequences due to the leveraged FFT operations.

We adopt the same simulation examples as in [196]. Particularly, we consider the following interference covariance matrix:

$$\boldsymbol{\Gamma} = \sigma_J^2 \boldsymbol{\Gamma}_J + \sigma^2 \boldsymbol{I} \tag{9.17}$$

where $\sigma_J^2 = 100$ and $\sigma^2 = 0.1$ are the jamming and noise powers, respectively, and the jamming covariance matrix $\boldsymbol{\Gamma}_J$ is given by $[\boldsymbol{\Gamma}_J]_{k,l} = q_{k-l}$ where $\left(q_0 q_1 \cdots q_{N-1} q_{-(N-1)} \cdots q_{-1}\right)$ can be obtained by an inverse FFT (IFFT) of the jamming power spectrum $\{\eta_p\}$ at frequencies $(p-1)/(2N-1)$, $p = 1, \cdots, 2N-1$. We set the average clutter power to $\beta = 1$. Furthermore, the Golomb sequence is used to initialize the transmit code $\boldsymbol{s}$ for all the algorithms.

As the first example, we consider a spot jamming located at a normalized frequency $f_0 = 0.2$, with a power spectrum given by

$$\eta_p = \begin{cases} 1, & p = \lfloor (2N-1) f_0 \rfloor \\ 0, & \text{elsewhere,} \end{cases} \quad p = 1, \cdots, 2N-1. \tag{9.18}$$

Fig. 9.1(a) shows the MSE values corresponding to CAN-MMF, CREW(fre), CREW(gra), and CREW(cyclic), under the unimodularity constraint, for various sequence lengths. In order to include the CREW(gra) algorithm in the comparison, we show its MSE only for $N \leq 300$ since CREW(gra) is computationally prohibitive for $N > 300$ on an ordinary PC. Fig. 9.1(b) depicts the MSE values obtained by the different algorithms under the constraint PAR ≤ 2 on the transmit sequence. One can observe that CREW(cyclic) provides the smallest MSE values for all sequence lengths. In particular, CREW(cyclic) outperforms CAN-MMF and CREW(fre) under both constraints. Due to the fact that both CREW(gra) and CREW(cyclic) are MSE optimizers, the performances of the two methods are almost identical under the unimodularity

constraint for $N \leq 300$. On the other hand, compared to CREW(gra), the CREW(cyclic) algorithm can be used to design longer sequences (even more than $N \sim 1000$) owing to its relatively small computational burden. Furthermore, CREW(cyclic) can handle not only the unimodularity constraint but also more general PAR constraints.

Next we consider a barrage jamming located in the normalized frequency band $[f_1, f_2] = [0.2, 0.3]$, and with a power spectrum given by

$$\eta_p = \begin{cases} 1, & \lfloor (2N-1)f_1 \rfloor \leq p \leq \lfloor (2N-1)f_2 \rfloor \\ 0, & \text{elsewhere,} \end{cases} \quad p = 1, \cdots, 2N-1. \quad (9.19)$$

Fig. 9.2(a) plots the MSE values obtained by CAN-MMF, CREW(fre), CREW (gra) and CREW(cyclic) under the unimodularity constraint. Similar to the previous example, the performances of CREW(gra) and CREW(cyclic) are almost identical for $N \leq 300$, and the CREW(cyclic) algorithm outperforms the other algorithms for all the sequence lengths. Fig. 9.2(b) presents the MSE values provided by CAN-MMF, CREW(fre) and CREW(cyclic) for the constraint PAR ≤ 2 on the transmit sequence. It can be observed that CREW(cyclic) yields a lower MSE than the other algorithms for all lengths.

According to Fig. 9.3, although an iteration of CREW(fre) is more computationally efficient than an iteration of CREW(cyclic), the overall CPU time of CREW(fre) until convergence is comparable to that of CREW(cyclic) due to the fact that CREW(fre) generally needs more iterations than cyclic CREW until convergence. The results leading to Fig. 9.3 were obtained using a PC with Intel Core 2 Duo T5250 1.5GHz CPU, and 1.5GB memory.

9.4 Appendices

9.4.1 Appendix A: Effectiveness of the Power Method-like Iterations in (9.14) and (9.16)

We show that the power method-like iterations in (9.14) and (9.16) yield a monotonic increase of the objective functions of the associated UQPs. Let $\boldsymbol{s}^{(t+1)}$ be an update of the vector s obtained by the aforementioned power method-like iterations. Note that for fixed $\boldsymbol{s}^{(t)}$, the update vector $\boldsymbol{s}^{(t+1)}$ is the minimizer of the criterion

$$\left\| \boldsymbol{s}^{(t+1)} - \widetilde{\boldsymbol{T}} \boldsymbol{s}^{(t)} \right\|_2^2 = \text{const} - 2\Re\{\boldsymbol{s}^{(t+1)H} \widetilde{\boldsymbol{T}} \boldsymbol{s}^{(t)}\} \quad (9.20)$$

or, equivalently, the maximizer of the criterion $\Re\{\boldsymbol{s}^{(t+1)H} \widetilde{\boldsymbol{T}} \boldsymbol{s}^{(t)}\}$ in the search space satisfying the constraints. We have that

$$(\boldsymbol{s}^{(t+1)} - \boldsymbol{s}^{(t)})^H \widetilde{\boldsymbol{T}} (\boldsymbol{s}^{(t+1)} - \boldsymbol{s}^{(t)}) \geq 0 \quad (9.21)$$

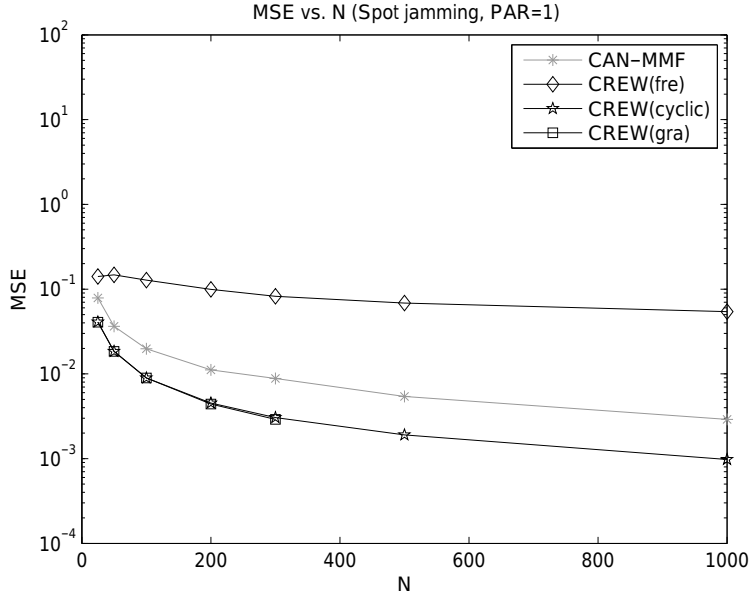

(a)

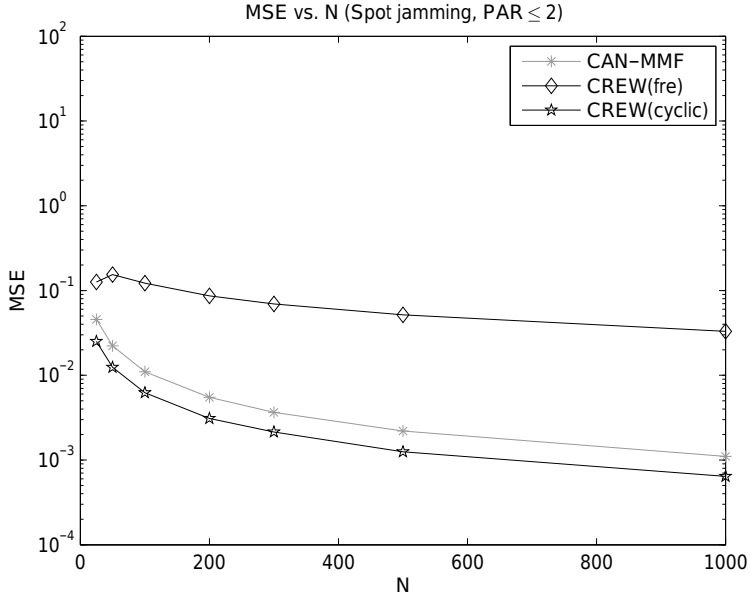

(b)

Figure 9.1. MSE values obtained by the different design algorithms for a spot jamming with normalized frequency $f_0 = 0.2$, and the following PAR constraints on the transmit sequence: (a) PAR$=1$ (unimodularity constraint), (b) PAR ≤ 2.

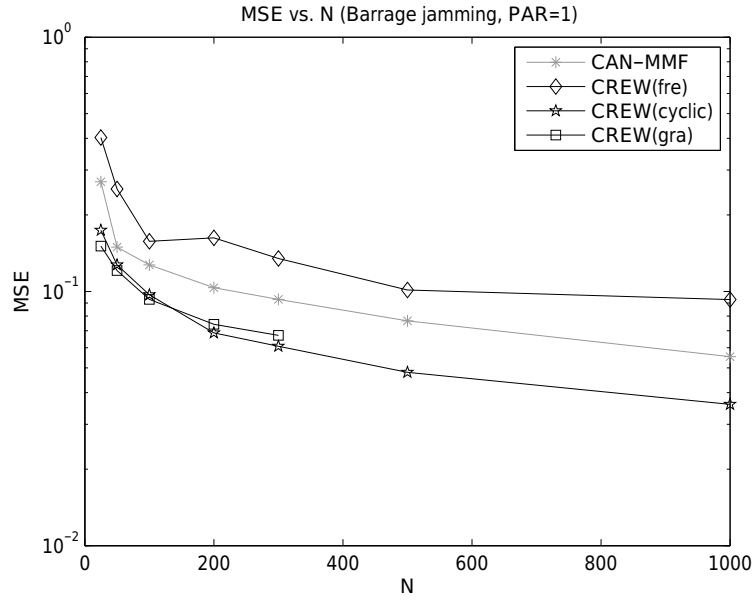

(a)

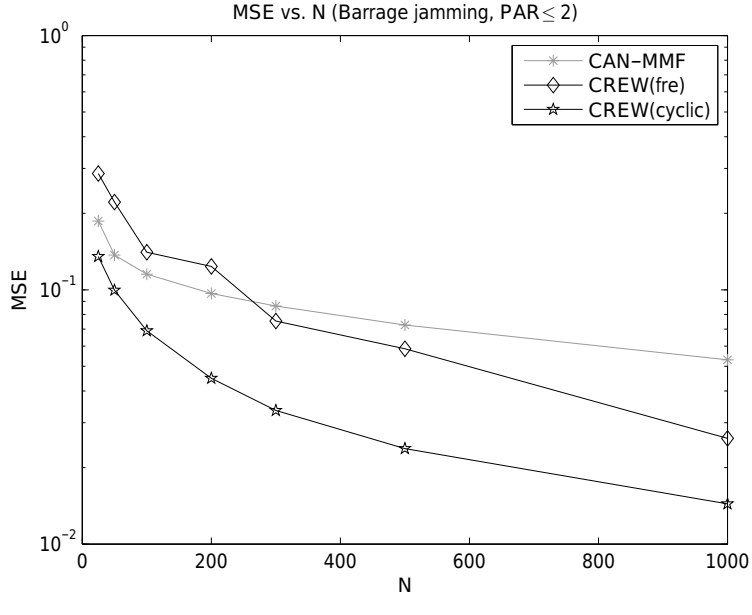

(b)

Figure 9.2. MSE values obtained by the different design algorithms for a barrage jamming in the normalized frequency interval $[f_1, f_2] = [0.2, 0.3]$ and the following constraints on the transmit sequence: (a) PAR$= 1$ (unimodularity constraint), (b) PAR ≤ 2.

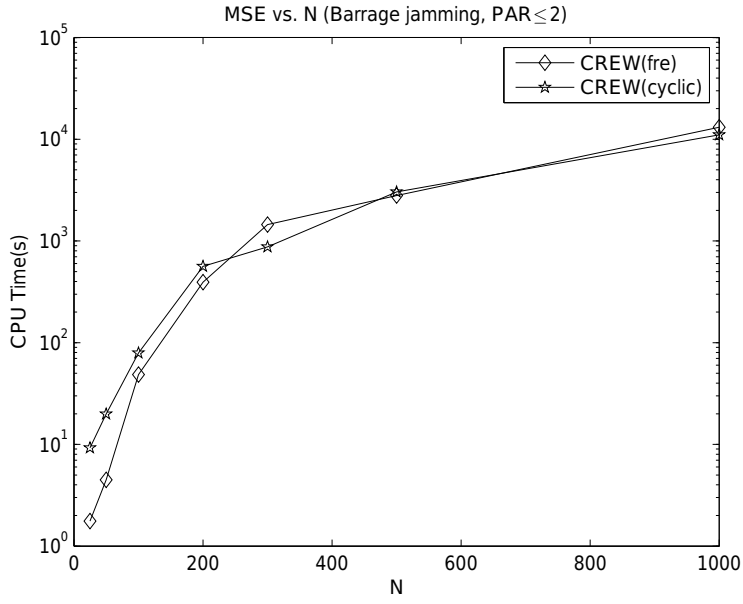

Figure 9.3. CPU time of CREW(fre) and CREW(cyclic) for the barrage jamming, and various sequence lengths N, under the constraint of PAR ≤ 2.

which implies

$$\begin{aligned} \boldsymbol{s}^{(t+1)H}\widetilde{\boldsymbol{T}}\boldsymbol{s}^{(t+1)} &\geq 2\Re\{\boldsymbol{s}^{(t+1)H}\widetilde{\boldsymbol{T}}\boldsymbol{s}^{(t)}\} - \boldsymbol{s}^{(t)H}\widetilde{\boldsymbol{T}}\boldsymbol{s}^{(t)} \\ &\geq \boldsymbol{s}^{(t)H}\widetilde{\boldsymbol{T}}\boldsymbol{s}^{(t)} \end{aligned} \tag{9.22}$$

as $\Re\{\boldsymbol{s}^{(t+1)H}\widetilde{\boldsymbol{T}}\boldsymbol{s}\} \geq \boldsymbol{s}^{(t)H}\widetilde{\boldsymbol{T}}\boldsymbol{s}^{(t)}$.

9.4.2 Appendix B: Efficient Computation of $\mathbf{R}$ and $\mathbf{Q}$

We have that

$$\boldsymbol{R} + \beta\boldsymbol{s}\boldsymbol{s}^H = \beta \sum_{0\leq|k|\leq(N-1)} \boldsymbol{J}_k\boldsymbol{s}\boldsymbol{s}^H\boldsymbol{J}_k^H = \beta\boldsymbol{A}^H\boldsymbol{A}. \tag{9.23}$$

The entries of $\boldsymbol{A}^H\boldsymbol{A}$ are nothing but the aperiodic autocorrelations of $\boldsymbol{s}$:

$$[\mathbf{A}^H\mathbf{A}]_{l,m} = r_{l-m} \tag{9.24}$$

where

$$r_k = \sum_{l=k+1}^{N} s_l s_{l-k}^* = r_{-k}^* \tag{9.25}$$

for $0 \leq k \leq N-1$. Note that the aperiodic autocorrelations $\{r_k\}$ of $\boldsymbol{s}$ are identical to the periodic autocorrelations of the sequence $\widetilde{\boldsymbol{s}} = (\boldsymbol{s}^T \ \mathbf{0}_{N-1}^T)^T$ where $\mathbf{0}$ denotes the all-zero vector. As a result, one can obtain $\{r_k\}$ by calculating the Inverse FFT (IFFT) of $\{|v_k|^2\}$, where the sequence $\{v_k\}$ is the FFT of $\widetilde{\boldsymbol{s}}$. Once $\{r_k\}$ are calculated, the matrix $\boldsymbol{R}$ can be obtained using (9.23)-(9.24).

In order to compute the matrix $\boldsymbol{Q}$, we note that

$$\begin{aligned} \boldsymbol{Q} &= \beta \sum_{0<|k|\leq(N-1)} \boldsymbol{J}_k^H \boldsymbol{w}\boldsymbol{w}^H \boldsymbol{J}_k \\ &= \beta \sum_{0<|k|\leq(N-1)} \boldsymbol{J}_k \boldsymbol{w}\boldsymbol{w}^H \boldsymbol{J}_k^H \end{aligned} \tag{9.26}$$

which implies that by using the variable $\boldsymbol{w}$ in lieu of $\boldsymbol{s}$, the matrix $\boldsymbol{Q}$ can be obtained via the same technique as devised above for the computation of $\boldsymbol{R}$.

10. Joint Doppler-Robust Design of the Receive Filter and Transmit Sequence in the Presence of Signal-Dependent Interference

Abstract
In this chapter, we study the joint design of Doppler robust transmit sequence and receive filter to improve the performance of an active sensing system dealing with signal-dependent interference. The signal-to-noise-plus-interference (SINR) of the filter output is considered as the performance measure of the system. The design problem is cast as a max-min optimization problem to robustify the system SINR with respect to the unknown Doppler shifts of the targets. To tackle the design problem, which belongs to a class of NP-hard problems, we devise a novel method (which we call DESIDE) to obtain optimized pairs of transmit sequence and receive filter sharing the desired robustness property. The proposed method is based on a cyclic maximization of SINR expressions with relaxed rank-one constraints, and is followed by a novel synthesis stage. We devise synthesis algorithms to obtain high quality pairs of transmit sequence and receive filter that well approximate the behavior of the optimal SINR (of the relaxed problem) with respect to target Doppler shift. Several numerical examples are provided to analyze the performance obtained by DESIDE.

Keywords: Code design, Doppler shift, interference, receive filter, robust design, synthesis, transmit sequence

10.1 Introduction

The performance of an active sensing system can be significantly improved by judiciously designing its transmit sequence and receive filter. Such a design usually deals with several challenges including the fact that Doppler shifts of moving targets are often unknown at the transmit side, the existence of signal-dependent interference as well as signal-independent interference at the receive side, and practical constraints such as similarity to a given code.

Joint design of the transmit sequence and the receive filter has been considered in a large number of studies during the last decades. Most of the works have been concerned with either stationary targets or targets with known Doppler shifts (see e.g. [155–159, 165, 199, 200]). In [160], considering a stationary target, a frequency domain approach has been employed to obtain an optimal receive filter and corresponding optimal energy spectral density of the transmit signal; then a synthesis procedure has been used to approximately provide the time domain signal. The works of [161] and [190] consider a related problem to that of [160] under a peak-to-average power ratio (PAR) constraint. The reference [176] deals with joint design of transmit sequence and receive filter under a similarity constraint in cases where the Doppler shift of the target is known. In [162], constant-modulus transmit sequences are considered in a framework similar to that of [176]. Several researches consider signal-independent clutter scenarios (see e.g. [170, 172, 173, 201, 202]). The unknown Doppler shift of the target has been taken into account in [172] and [173]. The reference [172] considers Doppler robust code design problem for signal-independent clutter cases under a similarity constraint. The ideas of [172] are generalized in [173] where the PAR constraint is also imposed.

In this chapter, we devise a novel method for **D**oppl**e**r robu**s**t jo**i**nt **de**sign of transmit sequence and receive filter (which we call DESIDE) in the presence

of clutter. We focus on radar systems but the design methodology can be useful for other active sensing systems such as sonar, seismic exploration, etc. We consider the SINR at the output of the receive filter as the performance measure. Besides an energy constraint, a similarity constraint is imposed on the transmit sequence to control certain characteristics of the transmit waveform. The design problem is cast as a max-min optimization and shown to belong to a class of NP-hard problems. We devise a cyclic maximization to tackle a relaxed version of the design problem. Furthermore, we propose a synthesis stage to obtain optimized pairs of transmit sequences and receive filters which possess the desired Doppler robustness.

The rest of this chapter is organized as follows. The data modeling and problem formulation are presented in Section 10.2. Section 10.3 contains the steps for the derivation of the cyclic approach to tackle the relaxed problem. The required synthesis stage is discussed in Section 10.4. Numerical results are provided in Section 10.5. Finally, conclusions are drawn in Section 10.6.

Notation: We use bold lowercase letters for vectors and bold uppercase letters for matrices. $(\cdot)^T$, $(\cdot)^*$ and $(\cdot)^H$ denote the vector/matrix transpose, the complex conjugate, and the Hermitian transpose, respectively. $\boldsymbol{I}$ represents the identity matrix in $\mathbb{C}^{N\times N}$. $\mathbf{1}$ and $\mathbf{0}$ are the all-one and the all-zero vectors/matrices. $\boldsymbol{e}_k$ is the k^{th} standard basis vector in $\mathbb{C}^N$. The l_2-norm of a vector $\mathbf{x}$ is denoted by $\|\mathbf{x}\|$. The symbol $\odot$ stands for the Hadamard (element-wise) product of matrices. $\mathrm{tr}(\cdot)$ is the trace of a square matrix argument. The notations $\lambda_{max}(\cdot)$ and $\lambda_{min}(\cdot)$ indicate the principal and the minor eigenvalues of a Hermitian matrix, respectively. $\mathbf{Diag}(\cdot)$ denotes the diagonal matrix formed by the entries of the vector argument, whereas $\mathbf{diag}(\cdot)$ denotes the vector formed by collecting the diagonal entries of the matrix argument. We write $\boldsymbol{A} \succeq \boldsymbol{B}$ iff $\boldsymbol{A}-\boldsymbol{B}$ is positive semi-definite, and $\boldsymbol{A} \succ \boldsymbol{B}$ iff $\boldsymbol{A}-\boldsymbol{B}$ is positive-definite. $\Re(\cdot)$ and $\arg(\cdot)$ denote the real-part and the phase angle (in radians) of the complex-valued argument. Finally, $\mathbb{N}$, $\mathbb{R}$ and $\mathbb{C}$ represent the set of natural, real and complex numbers, respectively.

10.2 Problem Formulation

We consider a radar system with (slow-time) transmit sequence $\mathbf{x} \in \mathbb{C}^N$ and receive filter $\boldsymbol{w} \in \mathbb{C}^N$. The discrete-time received signal backscattered from a moving target corresponding to the range-azimuth cell under the test can be modeled as (see, e.g. [162, 176], and [201]):

$$\boldsymbol{r} = \alpha_T \mathbf{x} \odot \boldsymbol{p}(\nu) + \boldsymbol{c} + \boldsymbol{n}, \tag{10.1}$$

where α_T is a complex parameter associated with backscattering effects of the target as well as propagation effects, $\boldsymbol{p}(\nu) = [1, e^{j\nu}, \ldots, e^{j(N-1)\nu}]^T$ with ν being the normalized target Doppler shift (expressed in radians), $\boldsymbol{c}$ is the N-dimensional column vector containing clutter (signal-dependent interference)

samples, and $\boldsymbol{n}$ is the N-dimensional column vector of (signal-independent) interference samples. The vector $\boldsymbol{c}$ is the superposition of the returns from different uncorrelated scatterers located at various range-azimuth bins and can be expressed as [176]

$$\boldsymbol{c} = \sum_{k=0}^{N_c-1} \sum_{i=0}^{L-1} \alpha_{(k,i)} \boldsymbol{J}_k \left(\boldsymbol{s} \odot \boldsymbol{p}(\nu_{d_{(k,i)}}) \right)$$

where $N_c \leq N$ is the number of range rings[1] that interfere with the range-azimuth bin of interest $(0,0)$, L is the number of discrete azimuth sectors, $\alpha_{(k,i)}$ and $\nu_{d_{(k,i)}}$ denote the echo and the normalized Doppler shift, respectively, of the scatterer in the range-azimuth bin (k,i), and $\boldsymbol{J}_k$ denotes the aperiodic shifting matrix for $0 \leq k \leq N_c - 1$, viz.

$$\boldsymbol{J}_k(l,m) = \begin{cases} 1 & \text{if} \quad l-m=k \\ 0 & \text{if} \quad l-m \neq k \end{cases} \qquad (l,m) \in \{1,\ldots,N\}^2$$

with $\boldsymbol{J}_{-k} = \boldsymbol{J}_k^T$.

The SINR at the output of the receive filter can be formulated as

$$\text{SINR}(\nu) = \frac{|\alpha_T|^2 \left| \boldsymbol{w}^H \left(\mathbf{x} \odot \boldsymbol{p}(\nu) \right) \right|^2}{\boldsymbol{w}^H \boldsymbol{\Sigma}_{\boldsymbol{c}}(\mathbf{x}) \boldsymbol{w} + \boldsymbol{w}^H \boldsymbol{M} \boldsymbol{w}} \tag{10.2}$$

where $\boldsymbol{M} \triangleq \mathrm{E}\{\boldsymbol{n}\boldsymbol{n}^H\}$ and $\boldsymbol{\Sigma}_{\boldsymbol{c}}(\mathbf{x})$ is the covariance matrix of $\boldsymbol{c}$ given by [176]

$$\boldsymbol{\Sigma}_{\boldsymbol{c}}(\mathbf{x}) = \sum_{k=0}^{N_c-1} \sum_{i=0}^{L-1} \sigma_{(k,i)}^2 \boldsymbol{J}_k \boldsymbol{\Gamma}(\mathbf{x},(k,i)) \boldsymbol{J}_k^T \tag{10.3}$$

with $\sigma_{(k,i)}^2 = \mathrm{E}\left[|\alpha_{(k,i)}|^2 \right]$ being the mean interfering power associated with the clutter patch located at the $(k,i)^{th}$ range-azimuth bin whose Doppler shift is supposed to be uniformly distributed in the interval $\Omega_c = \left(\bar{\nu}_{d_{(k,i)}} - \frac{\varepsilon_{(k,i)}}{2}, \bar{\nu}_{d_{(k,i)}} + \frac{\varepsilon_{(k,i)}}{2} \right)$ [201]. Herein $\boldsymbol{\Gamma}(\mathbf{x},(k,i)) = \text{Diag}(\mathbf{x}) \boldsymbol{\Phi}_{\varepsilon_{(k,i)}}^{\bar{\nu}_{d_{(k,i)}}} \text{Diag}(\mathbf{x})^H$ where $\boldsymbol{\Phi}_{\varepsilon_{(k,i)}}^{\bar{\nu}_{d_{(k,i)}}}(l,m)$ is the covariance matrix of $\boldsymbol{p}(\nu_{d_{(k,i)}})$ [176], viz.

$$\boldsymbol{\Phi}_{\varepsilon_{(k,i)}}^{\bar{\nu}_{d_{(k,i)}}}(l,m) = \begin{cases} 1 & \text{if} \quad l=m \\ e^{\left(j(l-m)\bar{\nu}_{d_{(k,i)}} \right)} \frac{\sin[0.5(l-m)\varepsilon_{(k,i)}]}{[0.5(l-m)\varepsilon_{(k,i)}]} & \text{if} \quad l \neq m \end{cases}, \qquad (l,m) \in \{1,\ldots,N\}^2. \tag{10.4}$$

[1] Note that the model considers the general case of range ambiguous clutter and reduces to unambiguous range scenario for $N_c = 1$. See [176] and [201] for justifications of the employed model and several examples of scenes that can be modeled in this way.

Note that the expression for $\mathbf{\Phi}_{\varepsilon_{(k,i)}}^{\bar{v}_{d_{(k,i)}}}(l,m)$ can be modified to consider cases with an arbitrary statistical distribution of the Doppler shifts of the clutter scatterers.

In this study we assume that the parameters of clutter and signal-independent interference are known at the transmit side by using cognitive (knowledge-aided) methods [176] [177]. We consider the SINR in (10.2) as the performance measure of the system [176] [201] and aim to find a robust design of the transmit sequence and the receive filter with respect to the unknown Doppler shift of the target[2]. In addition to an energy constraint, a similarity constraint is imposed on the transmit sequence [203] [176] [204]:

$$\|\mathbf{x}-\mathbf{x}_0\|^2 \leq \delta\,, \tag{10.5}$$

where the parameter $\delta \geq 0$ rules the size of the similarity region and $\mathbf{x}_0$ is a given sequence. There are several reasons that justify the use of a similarity constraint in the design of a radar sequence. The unconstrained optimization of SINR can lead to signals with significant modulus variations, poor range resolution, high peak sidelobe levels, and more generally with an undesired ambiguity function behavior. These drawbacks can be partially circumvented imposing the similarity constraint (10.5) on the sought radar code [176] [203] [204]. Comprehensive simulations have been performed in [176] [172] [203] and [205] to illustrate how the properties of the ambiguity function (e.g. range resolution, sidelobe levels, etc.) and modulus variations associated with the optimized code can be controlled via the value of δ in the similarity constraint. By doing so, it is required that the solution be similar to a known sequence $\mathbf{x}_0$ which has some good properties such as constant modulus, reasonable range resolution, and peak sidelobe level.

The problem of Doppler robust joint design of transmit sequence $\mathbf{x}$ and receive filter $\boldsymbol{w}$ under the similarity constraint can be cast as the following max-min optimization problem

$$\mathscr{P}\left\{\begin{array}{ll} \max\limits_{\mathbf{x},\boldsymbol{w}} \min\limits_{\nu} & \dfrac{\left|\boldsymbol{w}^H\left(\mathbf{x}\odot\boldsymbol{p}(\nu)\right)\right|^2}{\boldsymbol{w}^H\mathbf{\Sigma}_{\boldsymbol{c}}(\mathbf{x})\,\boldsymbol{w}+\boldsymbol{w}^H\boldsymbol{M}\boldsymbol{w}} \\ \text{subject to} & \|\mathbf{x}\|^2 = e \\ & \|\mathbf{x}-\mathbf{x}_0\|^2 \leq \delta \\ & \nu \in \Omega \end{array}\right. \tag{10.6}$$

where $\Omega = [\nu_l, \nu_u] \subseteq [-\pi, \pi]$ denotes a given interval of the target Doppler shift ν and e denotes the maximum available transmit energy. Note that for

[2]The target Doppler shift can be estimated at the receiver, e.g. via a bank of filters matched to different Doppler frequencies [180]; however, the Doppler shifts of the targets are usually unknown at the transmit side and hence we consider a robust design with respect to the target Doppler shift. The design approach can also be useful for a robust confirmation process, so as to account for target Doppler estimation errors.

a priori known target Doppler shift $\tilde{\nu}$ (i.e. $\Omega = [\tilde{\nu}, \tilde{\nu}]$), the problem $\mathscr{P}$ boils down to the considered problem in [176].

Remark 1: Note that a similar discrete-time data modeling and problem formulation applies to fast-time coding systems. In that case, the entries of $\mathbf{x}$ denote (complex) weights of the sub-pulses within a transmit pulse. Moreover, the normalized target Doppler shift ν is proportional to the system bandwidth (as opposed to the slow-time scheme for which ν is proportional to the pulse repetition frequency of the system); hence in such a case, the Doppler robust design would be concerned with high speed moving targets. As to the expressions, the formulation of the covariance matrix $\boldsymbol{\Sigma}_{\boldsymbol{c}}(\mathbf{x})$ in (10.3) should be modified. More precisely, for fast-time coding scenarios, the summation over k in (10.3) should be performed for $0 < |k| \leq N-1$. We refer interested readers to the references [161] and [180] for more details on this aspect. ■

To realize the hardness of the above problem, let z' and $\bar{\mathbf{x}}_\star$ denote a slack variable and an optimal solution $\mathbf{x}$ to the problem $\mathscr{P}$, respectively. The optimal $\boldsymbol{w}$ is obtained via solving the following optimization problem:

$$\begin{cases} \max\limits_{\boldsymbol{w},z'} & \dfrac{z'}{\boldsymbol{w}^H \boldsymbol{\Sigma}_{\boldsymbol{c}}(\bar{\mathbf{x}}_\star)\,\boldsymbol{w} + \boldsymbol{w}^H \boldsymbol{M} \boldsymbol{w}} \\ \text{subject to} & \boldsymbol{w}^H \left(\bar{\mathbf{x}}_\star \bar{\mathbf{x}}_\star^H \odot \boldsymbol{p}(\nu)\boldsymbol{p}(\nu)^H\right) \boldsymbol{w} \geq z' \\ & \forall \nu \in \Omega. \end{cases} \tag{10.7}$$

The above quadratic fractional program can be recast equivalently as (see Lemma 2 below and [206]):

$$\mathscr{P}_{NP} \begin{cases} \max\limits_{\boldsymbol{w},z'} & z' \\ \text{subject to} & \boldsymbol{w}^H \left(\boldsymbol{\Sigma}_{\boldsymbol{c}}(\bar{\mathbf{x}}_\star) + \boldsymbol{M}\right) \boldsymbol{w} \leq 1 \\ & \boldsymbol{w}^H \left(\bar{\mathbf{x}}_\star \bar{\mathbf{x}}_\star^H \odot \boldsymbol{p}(\nu)\boldsymbol{p}(\nu)^H\right) \boldsymbol{w} \geq z' \\ & \forall \nu \in \Omega. \end{cases} \tag{10.8}$$

The optimization problem $\mathscr{P}_{NP}$ is a quadratically constrained quadratic program (QCQP) with infinitely many non-convex constraints. This class of QCQPs is known to be NP-hard in general [172] [207, Chapter 4] [208]. Note that solving the optimization problem $\mathscr{P}$ with respect to $(\boldsymbol{w}, \mathbf{x}, \nu)$ is at least as hard as solving the problem $\mathscr{P}_{NP}$.

The following lemma helps tackling the optimization problem $\mathscr{P}$ via providing two alternative expressions for the objective function in problem $\mathscr{P}$.

Lemma 1. *Let $\boldsymbol{X} = \mathbf{x}\mathbf{x}^H$ and $\boldsymbol{W} = \boldsymbol{w}\boldsymbol{w}^H$. The $SINR(\nu)$ can be alternatively expressed with respect to $\boldsymbol{X}$ and $\boldsymbol{W}$ as follows:*

$$SINR(\nu) = \frac{|\alpha_T|^2 \boldsymbol{p}(\nu)^H (\boldsymbol{W} \odot \boldsymbol{X}^*)\, \boldsymbol{p}(\nu)}{\mathrm{tr}\{(\boldsymbol{\Sigma}_{\boldsymbol{c}}(\boldsymbol{X}) + \boldsymbol{M})\, \boldsymbol{W}\}} \tag{10.9}$$

$$= \frac{|\alpha_T|^2 \boldsymbol{p}(\nu)^H (\boldsymbol{W} \odot \boldsymbol{X}^*)\, \boldsymbol{p}(\nu)}{\mathrm{tr}\left\{\left(\boldsymbol{\Theta}_{\boldsymbol{c}}(\boldsymbol{W}) + (\frac{\beta}{e})\boldsymbol{I}\right) \boldsymbol{X}\right\}} \tag{10.10}$$

where $\beta = \mathrm{tr}\{\boldsymbol{M}\boldsymbol{W}\}$, *and*

$$\boldsymbol{\Sigma}_{\boldsymbol{c}}(\boldsymbol{X}) = \sum_{k=0}^{N_c-1}\sum_{i=0}^{L-1}\sigma_{(k,i)}^2\boldsymbol{J}_k\left(\boldsymbol{X}\odot\boldsymbol{\Phi}_{\varepsilon_{(k,i)}}^{\bar{\nu}_{d_{(k,i)}}}\right)\boldsymbol{J}_k^T, \tag{10.11}$$

$$\boldsymbol{\Theta}_{\boldsymbol{c}}(\boldsymbol{W}) = \sum_{k=0}^{N_c-1}\sum_{i=0}^{L-1}\sigma_{(k,i)}^2\left(\left(\boldsymbol{J}_k^T\boldsymbol{W}\boldsymbol{J}_k\right)\odot\left(\boldsymbol{\Phi}_{\varepsilon_{(k,i)}}^{\bar{\nu}_{d_{(k,i)}}}\right)^*\right). \tag{10.12}$$

Proof: See Appendix 10.7.1. ■

To deal with the design problem $\mathscr{P}$, consider the following optimization problem:

$$\mathscr{P}'\left\{\begin{array}{ll}\max\limits_{\boldsymbol{X},\boldsymbol{W}}\min\limits_{\nu} & \dfrac{\boldsymbol{p}(\nu)^H(\boldsymbol{W}\odot\boldsymbol{X}^*)\boldsymbol{p}(\nu)}{\mathrm{tr}\{(\boldsymbol{\Sigma}_{\boldsymbol{c}}(\boldsymbol{X})+\boldsymbol{M})\boldsymbol{W}\}}\\ \text{subject to} & \mathrm{tr}\{\boldsymbol{X}\}=e\\ & \mathrm{tr}\{\boldsymbol{X}\boldsymbol{X}_0\}\geq\varepsilon_\delta\\ & \mathrm{rank}(\boldsymbol{X})=1\\ & \mathrm{rank}(\boldsymbol{W})=1\\ & \boldsymbol{X}\succeq\boldsymbol{0}\\ & \boldsymbol{W}\succeq\boldsymbol{0}\\ & \nu\in\Omega\end{array}\right. \tag{10.13}$$

where $\boldsymbol{X}_0=\mathbf{x}_0\mathbf{x}_0^H$ and $\varepsilon_\delta=((2e-\delta)/2)^2$. Let $(\boldsymbol{W},\boldsymbol{X})$ denote an optimal solution to the above problem. Using Lemma 1 and the results of [203], it can be easily verified that an optimal solution to $\mathscr{P}$ is given by $(\boldsymbol{w},\mathbf{x}e^{j\arg(\mathbf{x}^H\mathbf{x}_0)})$ with $\boldsymbol{W}=\boldsymbol{w}\boldsymbol{w}^H$ and $\boldsymbol{X}=\mathbf{x}\mathbf{x}^H$.

Now observe that both the objective function and the rank constraints in $\mathscr{P}'$ are non-convex. In addition, $\boldsymbol{p}(\nu)$ belongs to a non-convex set for $\nu\in\Omega$. In the sequel, we relax the rank-one constraints on $\boldsymbol{X}$ and $\boldsymbol{W}$ in $\mathscr{P}'$ to obtain the relaxed problem $\mathscr{P}_1$:

$$\mathscr{P}_1\left\{\begin{array}{ll}\max\limits_{\boldsymbol{X},\boldsymbol{W}}\min\limits_{\nu} & \dfrac{\boldsymbol{p}(\nu)^H(\boldsymbol{W}\odot\boldsymbol{X}^*)\boldsymbol{p}(\nu)}{\mathrm{tr}\{(\boldsymbol{\Sigma}_{\boldsymbol{c}}(\boldsymbol{X})+\boldsymbol{M})\boldsymbol{W}\}}\\ \text{subject to} & \mathrm{tr}\{\boldsymbol{X}\}=e\\ & \mathrm{tr}\{\boldsymbol{X}\boldsymbol{X}_0\}\geq\varepsilon_\delta\\ & \boldsymbol{X}\succeq\boldsymbol{0}\\ & \boldsymbol{W}\succeq\boldsymbol{0}\\ & \nu\in\Omega.\end{array}\right. \tag{10.14}$$

The expression $\frac{|\alpha_T|^2\boldsymbol{p}(\nu)^H(\boldsymbol{W}\odot\boldsymbol{X}^*)\boldsymbol{p}(\nu)}{\mathrm{tr}\{(\boldsymbol{\Sigma}_{\boldsymbol{c}}(\boldsymbol{X})+\boldsymbol{M})\boldsymbol{W}\}}$ for rank-one $\boldsymbol{X}$ and $\boldsymbol{W}$ (i.e., $\boldsymbol{X}=\mathbf{x}\mathbf{x}^H$ and $\boldsymbol{W}=\boldsymbol{w}\boldsymbol{w}^H$) is equal to $SINR(\nu)$ (see Lemma 1). When the rank constraints are omitted (i.e., for arbitrary $\boldsymbol{X}\succeq\boldsymbol{0}$ and $\boldsymbol{W}\succeq\boldsymbol{0}$), the expression $\frac{|\alpha_T|^2\boldsymbol{p}(\nu)^H(\boldsymbol{W}\odot\boldsymbol{X}^*)\boldsymbol{p}(\nu)}{\mathrm{tr}\{(\boldsymbol{\Sigma}_{\boldsymbol{c}}(\boldsymbol{X})+\boldsymbol{M})\boldsymbol{W}\}}$ may be used in lieu of $SINR(\nu)$ and it will be denoted by $\widetilde{SINR}_{relax}(\nu)$ in the following. $SINR(\nu)$ is the restriction of $\widetilde{SINR}_{relax}(\nu)$ over the space of the rank-one positive semi-definite matrices $\boldsymbol{X}$ and $\boldsymbol{W}$ (due

to the relaxation of the rank-one constraints on $\boldsymbol{X}$ and $\boldsymbol{W}$). The optimization problem $\mathscr{P}_1$ is still non-convex and will be discussed in the next section.

10.3 The Proposed Method to Tackle the Relaxed Problem $\mathscr{P}_1$

In this section, we devise a novel cyclic algorithm (which we call DESIDE-R as it deals with the relaxed version of the original problem) to tackle the non-convex optimization problem $\mathscr{P}_1$. In a cyclic algorithm, the optimization variables are partitioned into two parts; then, by starting from an initial point, optimization is cyclically performed with respect to each part (while the another part is fixed) [209]. In the following, we consider the maximization problem $\mathscr{P}_1$ with respect to $(\boldsymbol{X},\boldsymbol{W})$ where $\boldsymbol{X}$ and $\boldsymbol{W}$ are the two partitions. The obtained pair $(\boldsymbol{W}_\star,\boldsymbol{X}_\star)$ which maximizes $\widetilde{SINR}_{relax}(\nu)$ will be used later to synthesize the optimized transmit sequence/receive filter pair $(\mathbf{x}_\star,\boldsymbol{w}_\star)$. The synthesis stage is addressed in Section 10.4.

- *Optimal $\boldsymbol{X}$ for fixed $\boldsymbol{W}$*:

Let $\widetilde{t}\in\mathbb{R}$ denote a slack variable. For fixed $\boldsymbol{W}$, the optimization in (10.14) is equivalent to the following maximization problem:

$$\mathscr{P}_X\left\{\begin{array}{ll}\underset{\boldsymbol{X},\widetilde{t}}{\max} & \dfrac{\widetilde{t}}{\mathrm{tr}\left\{\left(\boldsymbol{\Theta}_{\boldsymbol{c}}(\boldsymbol{W})+(\frac{\beta}{e})\boldsymbol{I}\right)\boldsymbol{X}\right\}}\\ \text{subject to} & \boldsymbol{p}(\nu)^H(\boldsymbol{W}\odot\boldsymbol{X}^*)\,\boldsymbol{p}(\nu)\geq\widetilde{t},\ \ \forall\,\nu\in\Omega\\ & \mathrm{tr}\{\boldsymbol{X}\}=e\\ & \mathrm{tr}\{\boldsymbol{X}\boldsymbol{X}_0\}\geq\varepsilon_\delta\\ & \boldsymbol{X}\succeq\boldsymbol{0}.\end{array}\right. \tag{10.15}$$

Note that the above problem is feasible and has a finite-valued objective function over the constraint set (see eq. (10.29)). Moreover, problem $\mathscr{P}_X$ is a linear-fractional maximization problem with infinitely many constraints (see the first constraint in (10.15)). Inspired by Charnes-Cooper transform for tackling linear fractional programs [210], we let $\boldsymbol{Y}=s\boldsymbol{X}, t=s\widetilde{t}$ for an auxiliary variable $s\geq 0$, and consider the following optimization problem:

$$\mathscr{P}'_X\left\{\begin{array}{ll}\underset{\boldsymbol{Y},t,s}{\max} & t\\ \text{subject to} & \mathrm{tr}\left\{\left(\boldsymbol{\Theta}_{\boldsymbol{c}}(\boldsymbol{W})+(\frac{\beta}{e})\boldsymbol{I}\right)\boldsymbol{Y}\right\}=1\\ & \boldsymbol{p}(\nu)^H(\boldsymbol{W}\odot\boldsymbol{Y}^*)\,\boldsymbol{p}(\nu)\geq t,\ \ \forall\,\nu\in\Omega\\ & \mathrm{tr}\{\boldsymbol{Y}\}=e\,s\\ & \mathrm{tr}\{\boldsymbol{Y}\boldsymbol{X}_0\}\geq\varepsilon_\delta\,s\\ & \boldsymbol{Y}\succeq\boldsymbol{0}\\ & s\geq 0.\end{array}\right. \tag{10.16}$$

Lemma 2. *The optimization problems $\mathscr{P}_X$ and $\mathscr{P}'_X$ are equivalent. More precisely, they share the same optimal values and their corresponding solutions can be uniquely obtained from each other.*

Proof: Let $(\boldsymbol{X}_\star, \widetilde{t}_\star)$ and $v(\mathscr{P}_X)$ denote an optimal solution and the optimal value of the problem $\mathscr{P}_X$, respectively. Note that $\mathrm{tr}\left\{\left(\boldsymbol{\Theta}_{\boldsymbol{c}}(\boldsymbol{W}) + (\frac{\beta}{e})\boldsymbol{I}\right)\boldsymbol{Y}\right\} > 0$ because $\beta > 0$. It is straightforward to verify that

$$(\boldsymbol{Y}, t, s) = \left(\frac{\boldsymbol{X}_\star}{\mathrm{tr}\left\{\left(\boldsymbol{\Theta}_{\boldsymbol{c}}(\boldsymbol{W}) + (\frac{\beta}{e})\boldsymbol{I}\right)\boldsymbol{X}_\star\right\}}, \frac{\widetilde{t}_\star}{\mathrm{tr}\left\{\left(\boldsymbol{\Theta}_{\boldsymbol{c}}(\boldsymbol{W}) + (\frac{\beta}{e})\boldsymbol{I}\right)\boldsymbol{X}_\star\right\}}, \frac{1}{\mathrm{tr}\left\{\left(\boldsymbol{\Theta}_{\boldsymbol{c}}(\boldsymbol{W}) + (\frac{\beta}{e})\boldsymbol{I}\right)\boldsymbol{X}_\star\right\}}\right) \tag{10.17}$$

is feasible for the problem $\mathscr{P}'_X$. Also observe that the value of the objective function of $\mathscr{P}'_X$ for $(\boldsymbol{Y}, t, s)$ in (10.17) is given by

$$\frac{t_\star}{\mathrm{tr}\left\{\left(\boldsymbol{\Theta}_{\boldsymbol{c}}(\boldsymbol{W}) + (\frac{\beta}{e})\boldsymbol{I}\right)\boldsymbol{X}_\star\right\}} \tag{10.18}$$

and note that (10.18) is equal to $v(\mathscr{P}_X)$. Therefore, for the optimal value of the problem $\mathscr{P}'_X$, i.e. $v(\mathscr{P}'_X)$, we have

$$v(\mathscr{P}'_X) \geq v(\mathscr{P}_X). \tag{10.19}$$

Next let $(\boldsymbol{Y}_\star, t_\star, s_\star)$ denote an optimal solution to the problem $\mathscr{P}'_X$. Note that $s_\star \neq 0$ because $s_\star = 0$ leads to $\boldsymbol{Y}_\star = \boldsymbol{0}$ (a contradiction, see the first constraint in $\mathscr{P}'_X$). One can check that $(\boldsymbol{Y}_\star/s_\star, t_\star/s_\star)$ is feasible for the problem $\mathscr{P}_X$ with corresponding objective value equal to $t_\star$. Owing to the fact that $v(\mathscr{P}'_X) = t_\star$, the following inequality holds between $v(\mathscr{P}'_X)$ and $v(\mathscr{P}_X)$:

$$v(\mathscr{P}'_X) \leq v(\mathscr{P}_X). \tag{10.20}$$

Finally, eqs. (10.19) and (10.20) yield $v(\mathscr{P}'_X) = v(\mathscr{P}_X)$ and the proof is concluded. ■

Now observe that $\mathscr{P}'_X$ is a convex problem with infinitely many constraints. To deal with the constraint set, we note that the constraint $\boldsymbol{p}(\nu)^H(\boldsymbol{W} \odot \boldsymbol{Y}^*)\boldsymbol{p}(\nu) \geq t$, $\forall\, \nu \in \Omega$ implies the non-negativity of a trigonometric polynomial of ν over the interval Ω. More specifically, let

$$z_k \triangleq \sum_{i=1}^{N-k} Z_{i+k,i}, \quad 0 \leq k \leq N-1, \tag{10.21}$$

and $\boldsymbol{z} = [z_0, z_1, \ldots, z_{N-1}]^T$ with $\boldsymbol{Z} = \boldsymbol{W} \odot \boldsymbol{Y}^*$. It is straightforward to verify that for any $\nu \in \Omega$, the aforementioned constraint is equivalent to

$$h(\nu) \triangleq z_0 - t + 2\Re\left(\sum_{k=1}^{N-1} z_k e^{-jk\nu}\right) \geq 0. \tag{10.22}$$

Interestingly, a semidefinite representation of the constraint (10.22) can be obtained via Theorem 3.4 in [189] which we quote below.

Theorem 2. *The trigonometric polynomial* $\tilde{h}(\nu) = \widetilde{z}_0 + 2\Re\left(\sum_{k=1}^{N-1} \widetilde{z}_k e^{-jk\nu}\right)$ *is non-negative for any* $\nu \in [\nu_0 - \nu_1, \nu_0 + \nu_1]$ *(with* $0 < \nu_1 < \pi$*) iff there exist an* $N \times N$ *Hermitian matrix* $\boldsymbol{Z}_1 \succeq \boldsymbol{0}$ *and an* $(N-1) \times (N-1)$ *Hermitian matrix* $\boldsymbol{Z}_2 \succeq \boldsymbol{0}$ *such that*

$$\widetilde{\boldsymbol{z}} = \boldsymbol{F}_1^H \left(\mathrm{diag}(\boldsymbol{F}_1 \boldsymbol{Z}_1 \boldsymbol{F}_1^H) + \boldsymbol{q} \odot \mathrm{diag}(\boldsymbol{F}_2 \boldsymbol{Z}_2 \boldsymbol{F}_2^H)\right) \tag{10.23}$$

where $\widetilde{\boldsymbol{z}} = [\widetilde{z}_0, \widetilde{z}_1, \ldots, \widetilde{z}_{N-1}]^T$, $\boldsymbol{q} = [q_0, q_1, \ldots, q_{n-1}]^T$ *with* $q_k = \cos(2\pi k/n - \nu_0) - \cos(\nu_1)$, $\boldsymbol{F}_1 = [\mathbf{f}_0, \ldots, \mathbf{f}_{N-1}]$ *and* $\boldsymbol{F}_2 = [\mathbf{f}_0, \ldots, \mathbf{f}_{N-2}]$ *in which* $\mathbf{f}_k = [1, e^{-jk\theta}, \ldots, e^{-j(n-1)k\theta}]^T$ *with* $\theta = 2\pi/n$*, and* $n \geq 2N-1$.

Note that an SDP representation of (10.22) is immediate by employing the above results with $\widetilde{\boldsymbol{z}} = \boldsymbol{z}$, $n = 2N-1$, $\nu_0 = (\nu_l + \nu_u)/2$, and $\nu_1 = \nu_0 - \nu_l$. Consequently, $\mathscr{P}'_X$ is equivalent to the following SDP:

$$\mathscr{SDP}_X \left\{ \begin{array}{ll} \max\limits_{\boldsymbol{Y}, \boldsymbol{Z}_1, \boldsymbol{Z}_2, t, s} & t \\ \text{subject to} & \mathrm{tr}\left\{\left(\boldsymbol{\Theta}_{\boldsymbol{c}}(\boldsymbol{W}) + (\frac{\beta}{e})\boldsymbol{I}\right)\boldsymbol{Y}\right\} = 1 \\ & \boldsymbol{z} = t\boldsymbol{e}_1 + \boldsymbol{F}_1^H \left(\mathrm{diag}(\boldsymbol{F}_1 \boldsymbol{Z}_1 \boldsymbol{F}_1^H) + \boldsymbol{q} \odot \mathrm{diag}(\boldsymbol{F}_2 \boldsymbol{Z}_2 \boldsymbol{F}_2^H)\right) \\ & \mathrm{tr}\{\boldsymbol{Y}\} = e\,s \\ & \mathrm{tr}\{\boldsymbol{Y}\boldsymbol{X}_0\} \geq \varepsilon_\delta\, s \\ & \boldsymbol{Y} \succeq \boldsymbol{0} \\ & \boldsymbol{Z}_1 \succeq \boldsymbol{0} \\ & \boldsymbol{Z}_2 \succeq \boldsymbol{0} \\ & s \geq 0. \end{array} \right. \tag{10.24}$$

Remark 2: The derivation of $\mathscr{SDP}_X$ can be extended to deal with cases where Ω is a union of several (non-overlapping) sub-intervals of $[-\pi, \pi]$. More precisely, for each of such sub-intervals, the SDP representation associated with the corresponding constraint (obtained via Theorem 1) can be added to the constraint set of $\mathscr{SDP}_X$. ■

Let $(\boldsymbol{Y}, \boldsymbol{Z}_1, \boldsymbol{Z}_2, t, s)$ denote an optimal solution to $\mathscr{SDP}_X$. The corresponding optimal $\boldsymbol{X}$ (i.e., an optimal solution to $\mathscr{P}_X$) for fixed $\boldsymbol{W}$ is given by $\boldsymbol{Y}/s$ (see Lemma 2).

- *Optimal* $\boldsymbol{W}$ *for fixed* $\boldsymbol{X}$:

Using Lemma 1, $\mathscr{P}_1$ can be recast into the following equivalent form for fixed $\boldsymbol{X}$:

$$\mathscr{P}_W \begin{cases} \max\limits_{\boldsymbol{W},\check{t}} & \dfrac{\check{t}}{\mathrm{tr}\{(\boldsymbol{\Sigma_c}(\boldsymbol{X})+\boldsymbol{M})\boldsymbol{W}\}} \\ \text{subject to} & \boldsymbol{p}(\nu)^H(\boldsymbol{W}\odot\boldsymbol{X}^*)\boldsymbol{p}(\nu)\geq\check{t},\ \forall\,\nu\in\Omega \\ & \boldsymbol{W}\succeq\boldsymbol{0} \end{cases} \tag{10.25}$$

where $\check{t}$ denotes a slack variable. The above problem can be tackled in a way similar to the case of obtaining $\boldsymbol{X}$ for fixed $\boldsymbol{W}$. In particular, using Lemma 2 as well as Theorem 1, we obtain the following SDP:

$$\mathscr{SDP}_W \begin{cases} \max\limits_{\boldsymbol{W},\boldsymbol{Z}_1',\boldsymbol{Z}_2',\check{t}} & \check{t} \\ \text{subject to} & \mathrm{tr}\{(\boldsymbol{\Sigma_c}(\boldsymbol{X})+\boldsymbol{M})\boldsymbol{W}\}=1 \\ & \boldsymbol{z}'=\check{t}\boldsymbol{e}_1+\boldsymbol{F}_1^H\left(\mathrm{diag}(\boldsymbol{F}_1\boldsymbol{Z}_1'\boldsymbol{F}_1^H)+\boldsymbol{q}\odot\mathrm{diag}(\boldsymbol{F}_2\boldsymbol{Z}_2'\boldsymbol{F}_2^H)\right) \\ & \boldsymbol{W}\succeq\boldsymbol{0} \\ & \boldsymbol{Z}_1'\succeq\boldsymbol{0} \\ & \boldsymbol{Z}_2'\succeq\boldsymbol{0} \end{cases} \tag{10.26}$$

where $\boldsymbol{z}'$ is given by

$$z_k'=\sum_{i=1}^{N-k}Z_{i+k,i}',\quad 0\leq k\leq N-1, \tag{10.27}$$

with $\boldsymbol{Z}'=\boldsymbol{W}\odot\boldsymbol{X}^*$.

Remark 3: It might be interesting in practice to control the shape of the cross-ambiguity function of the transmit sequence $\mathbf{x}$ and the receive filter $\boldsymbol{w}$. An approach would then be to require that the variables $\boldsymbol{w}$ and $\mathbf{x}$ are sufficiently similar to given $\boldsymbol{w}_0$ and $\mathbf{x}_0$, respectively, which possess desirable cross-ambiguity properties. The Doppler robust design for controlling the shape of the cross-ambiguity function could therefore be cast as the following optimization problem:

$$\mathscr{P}_{cross} \begin{cases} \max\limits_{\mathbf{x},\boldsymbol{w}}\ \min\limits_{\nu} & \dfrac{\left|\boldsymbol{w}^H(\mathbf{x}\odot\boldsymbol{p}(\nu))\right|^2}{\boldsymbol{w}^H\boldsymbol{\Sigma}_{\boldsymbol{c}}(\mathbf{x})\boldsymbol{w}+\boldsymbol{w}^H\boldsymbol{M}\boldsymbol{w}} \\ \text{subject to} & \|\mathbf{x}-\mathbf{x}_0\|^2\leq\delta \\ & \|\boldsymbol{w}-\boldsymbol{w}_0\|^2\leq\delta_w \\ & \|\mathbf{x}\|^2=e \\ & \nu\in\Omega \end{cases} \tag{10.28}$$

where δ_w rules the size of the similarity region for the receive filter. The problem $\mathscr{P}_{cross}$ can be tackled in a way similar to (10.6). ■

The steps of DESIDE-R are summarized in Table 10.1. Each iteration of the proposed method is handled via solving two SDPs, i.e., $\mathscr{SDP}_W$ and $\mathscr{SDP}_X$. The complexity of solving the SDPs with accuracy of ε_a is given by

$\mathcal{O}(N^{3.5}\log(\varepsilon_a^{-1}))$ [185]. A synthesis stage is proposed in the next section to compute high quality transmit sequence/receive filter pairs $(\boldsymbol{w}_\star, \mathbf{x}_\star)$ from the solutions $(\boldsymbol{W}_\star, \boldsymbol{X}_\star)$ obtained herein.

Table 10.1. *DESIDE-R method for solving the relaxed problem* $\mathscr{P}_1$

Step 0: Initialize $\boldsymbol{X}$ with $\mathbf{x}\mathbf{x}^H$ where $\mathbf{x}$ is a random vector in $\mathbb{C}^N$.
Step 1: Solve the problem $\mathscr{SDP}_W$ in (10.26) to obtain $\boldsymbol{W}$.
Step 2: Solve the problem $\mathscr{SDP}_X$ in (10.24) to obtain $\boldsymbol{X}$.
Step 3: Repeat steps 1 and 2 until a pre-defined stop criterion is satisfied, e.g. $\lvert \min_{\nu\in\Omega} \widetilde{SINR}_{relax}(\nu)^{(\kappa+1)} - \min_{\nu\in\Omega} \widetilde{SINR}_{relax}(\nu)^{(\kappa)} \rvert \leq \mu$ for a given $\mu > 0$.

• *Convergence and the* $\widetilde{SINR}_{relax}$ *metric*:

By cyclically solving $\mathscr{SDP}_X$ and $\mathscr{SDP}_W$ in DESIDE-R, it can be easily verified that the resulting $\{\min_{\nu\in\Omega} \widetilde{SINR}^{(\kappa)}_{relax}(\nu)\}_{\kappa\in\mathbb{N}}$ is a monotonically increasing sequence [209]. Furthermore, $\min_{\nu\in\Omega} \widetilde{SINR}_{relax}(\nu)$ is bounded from above; indeed we have that

$$\begin{aligned}
\min_{\nu\in\Omega} \widetilde{SINR}_{relax}(\nu) &\leq \frac{\boldsymbol{p}(\nu)^H (\boldsymbol{W}\odot\boldsymbol{X}^*)\,\boldsymbol{p}(\nu)}{\mathrm{tr}\{\boldsymbol{W}\,(\boldsymbol{\Sigma}_{\boldsymbol{c}}(\mathbf{x})+\boldsymbol{M})\}} \\
&\leq \frac{\|\boldsymbol{p}(\nu)\|^2 \lambda_{max}(\boldsymbol{W}\odot\boldsymbol{X}^*)}{\mathrm{tr}\{\boldsymbol{M}\boldsymbol{W}\}} \\
&\leq \frac{N\,\mathrm{tr}\{\boldsymbol{W}\}\,\mathrm{tr}\{\boldsymbol{X}\}}{\mathrm{tr}\{\boldsymbol{M}\boldsymbol{W}\}} \\
&\leq \frac{N e}{\lambda_{min}(\boldsymbol{M})}. \qquad (10.29)
\end{aligned}$$

The third inequality above holds true because $\mathrm{tr}\{\boldsymbol{W}\odot\boldsymbol{X}^*\} \leq \mathrm{tr}\{\boldsymbol{W}\}\,\mathrm{tr}\{\boldsymbol{X}\}$; and for the last inequality we have used the fact that $\mathrm{tr}\{\boldsymbol{M}\boldsymbol{W}\} \geq \lambda_{min}(\boldsymbol{M})\,\mathrm{tr}\{\boldsymbol{W}\}$ [211]. Eq. (10.29) along with the increasing property of $\{\min_{\nu\in\Omega} \widetilde{SINR}^{(\kappa)}_{relax}(\nu)\}_{\kappa\in\mathbb{N}}$ ensure the convergence of the sequence of the objective function values.

10.4 The Synthesis Stage

As discussed earlier, a judicious synthesis of the optimized transmit sequence $\mathbf{x}_\star$ and receive filter $\boldsymbol{w}_\star$ from the obtained $(\boldsymbol{W}_\star, \boldsymbol{X}_\star)$ is required to maintain the Doppler robustness. If $\boldsymbol{W}_\star$ is rank-one, $\boldsymbol{w}_\star$ is available via considering $\boldsymbol{W}_\star = \boldsymbol{w}_\star\boldsymbol{w}_\star^H$; whereas if $\boldsymbol{X}_\star = \mathbf{x}\mathbf{x}^H$, for $\mathbf{x}_\star$ we have $\mathbf{x}_\star = \mathbf{x}e^{j\arg(\mathbf{x}^H\mathbf{x}_0)}$. The rank behavior of SDP solutions, tightness of the semidefinite relaxation, and synthesis methods have been investigated in the literature (see e.g. [212–214],

and references therein). For example, it is known that for a solvable[3] SDP with M constraints, there exists an optimal solution of rank at most equal to $\sqrt{M}$ [212]. However, the result does not ensure the existence of rank-one solutions for the case considered in this chapter due to the fact that $\mathscr{SDP}_X$ and $\mathscr{SDP}_W$ have $N+3$ and $N+1$ constraints, respectively. Herein we remark on the fact that the ranks of $\boldsymbol{W}_\star$ and $\boldsymbol{X}_\star$ depend on the employed starting point in addition to the parameters of the design problem. In cases where the rank of either $\boldsymbol{W}_\star$ or $\boldsymbol{X}_\star$ is larger than one, the synthesis of $\boldsymbol{w}_\star$ or $\mathbf{x}_\star$ is more complicated. To tackle this problem, this section initially considers the rank-one decomposition method [215]. Then we devise novel synthesis algorithms to design pairs of $(\boldsymbol{w}_\star, \mathbf{x}_\star)$ possessing the desired robustness.

10.4.1 The Rank-One Decomposition Method

The main result of the rank-one decomposition method can be summarized as follows [215]:

Theorem 3. *Let $\boldsymbol{X}$ be a non-zero $N \times N$ complex Hermitian positive semidefinite matrix (with $N \geq 3$) and $\{\boldsymbol{A}_1, \boldsymbol{A}_2, \boldsymbol{A}_3, \boldsymbol{A}_4\}$ be Hermitian matrices. Suppose that $(\mathrm{tr}\{\boldsymbol{Y}\boldsymbol{A}_1\}, \mathrm{tr}\{\boldsymbol{Y}\boldsymbol{A}_2\}, \mathrm{tr}\{\boldsymbol{Y}\boldsymbol{A}_3\}, \mathrm{tr}\{\boldsymbol{Y}\boldsymbol{A}_4\}) \neq (0,0,0,0)$ for any non-zero complex Hermitian positive semidefinite matrix $\boldsymbol{Y}$ of size $N \times N$. Then,*

- *if $\mathrm{rank}(\boldsymbol{X}) \geq 3$, one can find, in polynomial time, a rank-one matrix $\mathbf{x}\mathbf{x}^H$ such that $\mathbf{x}$ (synthetically denoted as $\mathbf{x} = \mathscr{D}_1(\boldsymbol{X}, \boldsymbol{A}_1, \boldsymbol{A}_2, \boldsymbol{A}_3, \boldsymbol{A}_4)$) is in the $\mathrm{range}(\boldsymbol{X})$, and*

$$\mathbf{x}^H \boldsymbol{A}_i \mathbf{x} = \mathrm{tr}\{\boldsymbol{X}\boldsymbol{A}_i\}, \quad i = 1,2,3,4;$$

- *if $\mathrm{rank}(\boldsymbol{X}) = 2$, for any $\boldsymbol{z}$ not in the range space of $\boldsymbol{X}$, one can find a rank-one matrix $\mathbf{x}\mathbf{x}^H$ such that $\mathbf{x}$ (synthetically denoted as $\mathbf{x} = \mathscr{D}_2(\boldsymbol{X}, \boldsymbol{A}_1, \boldsymbol{A}_2, \boldsymbol{A}_3, \boldsymbol{A}_4)$) is in the linear subspace spanned by $\{\boldsymbol{z}\} \cup \mathrm{range}(\boldsymbol{X})$, and*

$$\mathbf{x}^H \boldsymbol{A}_i \mathbf{x} = \mathrm{tr}\{\boldsymbol{X}\boldsymbol{A}_i\}, \quad i = 1,2,3,4.$$

Proof: see [215, Theorem 2.3]. ■

Let $(\boldsymbol{W}_\star, \boldsymbol{X}_\star)$ denote an optimal solution to $\mathscr{P}_1$, and let

$$\nu_\star \quad = \quad \mathrm{argmin}_{\nu \in \Omega} \ \boldsymbol{p}(\nu)^H (\boldsymbol{W}_\star \odot \boldsymbol{X}_\star^*) \boldsymbol{p}(\nu). \tag{10.30}$$

Considering Theorem 3 and the problem $\mathscr{P}_W$, a suitable rank-one matrix $\boldsymbol{w}_\star \boldsymbol{w}_\star^H$ can be found such that

$$\mathrm{tr}\{\underbrace{(\boldsymbol{\Sigma}_c(\boldsymbol{X}_\star) + \boldsymbol{M})}_{\boldsymbol{Q}_1} \boldsymbol{W}_\star\} = \boldsymbol{w}_\star^H \boldsymbol{Q}_1 \boldsymbol{w}_\star \tag{10.31}$$

[3] Meaning that the SDP is feasible, bounded, and its optimal value is attained (see [185] for more details).

and that

$$\begin{cases} \mathrm{tr}\{\underbrace{\left(\boldsymbol{X}_\star \odot (\boldsymbol{p}(\nu_\star)\boldsymbol{p}(\nu_\star)^H)\right)}_{\boldsymbol{Q}_2}\boldsymbol{W}_\star\} = \boldsymbol{w}_\star^H \boldsymbol{Q}_2 \boldsymbol{w}_\star \\ \mathrm{tr}\{\underbrace{\left(\boldsymbol{X}_\star \odot (\boldsymbol{p}(\nu')\boldsymbol{p}(\nu')^H)\right)}_{\boldsymbol{Q}_3}\boldsymbol{W}_\star\} = \boldsymbol{w}_\star^H \boldsymbol{Q}_3 \boldsymbol{w}_\star \\ \mathrm{tr}\{\underbrace{\left(\boldsymbol{X}_\star \odot (\boldsymbol{p}(\nu'')\boldsymbol{p}(\nu'')^H)\right)}_{\boldsymbol{Q}_4}\boldsymbol{W}_\star\} = \boldsymbol{w}_\star^H \boldsymbol{Q}_4 \boldsymbol{w}_\star \end{cases} \tag{10.32}$$

where ν' and ν'' are two arbitrary Doppler shifts in Ω. The equations in (10.32) have been written using the identity

$$\boldsymbol{p}(\nu)^H (\boldsymbol{W}_\star \odot \boldsymbol{X}_\star^*)\, \boldsymbol{p}(\nu) = \mathrm{tr}\{\left(\boldsymbol{X}_\star \odot (\boldsymbol{p}(\nu)\boldsymbol{p}(\nu)^H)\right)\boldsymbol{W}_\star\}. \tag{10.33}$$

Note that Theorem 2 lays the ground for considering two more Doppler frequencies (i.e. ν' and ν'') other than $\nu_\star$. This leads to a receive filter $\boldsymbol{w}_\star$ with a behavior more similar to that of $\boldsymbol{W}_\star$ with respect to target Doppler shift ν. Consequently, $\boldsymbol{w}_\star$ is obtained via $\boldsymbol{w}_\star = \mathscr{D}_1(\boldsymbol{W}_\star, \boldsymbol{Q}_1, \boldsymbol{Q}_2, \boldsymbol{Q}_3, \boldsymbol{Q}_4)$ or $\boldsymbol{w}_\star = \mathscr{D}_2(\boldsymbol{W}_\star, \boldsymbol{Q}_1, \boldsymbol{Q}_2, \boldsymbol{Q}_3, \boldsymbol{Q}_4)$ for cases where $\mathrm{rank}(\boldsymbol{W}_\star) \geq 3$ or $\mathrm{rank}(\boldsymbol{W}_\star) = 2$, respectively. Note that the condition $(\mathrm{tr}\,(\boldsymbol{Y}\boldsymbol{Q}_1)\,, \mathrm{tr}\,(\boldsymbol{Y}\boldsymbol{Q}_2)\,, \mathrm{tr}\,(\boldsymbol{Y}\boldsymbol{Q}_3),\ \mathrm{tr}\,(\boldsymbol{Y}\boldsymbol{Q}_4)) \neq (0,0,0,0)$ on the matrices $\boldsymbol{Q}_1, \boldsymbol{Q}_2, \boldsymbol{Q}_3$, and $\boldsymbol{Q}_4$ in Theorem 3 is satisfied; more precisely, there exists $(a_1, a_2, a_3, a_4) \in \mathbb{R}_+^4$ such that $a_1\boldsymbol{Q}_1 + a_2\boldsymbol{Q}_2 + a_3\boldsymbol{Q}_3 + a_4\boldsymbol{Q}_4 \succ \boldsymbol{0}$ (see [216]).

The $\mathbf{x}_\star$ can be obtained in a similar way; particularly,

$$\mathbf{x}_\star = \mathscr{D}_\zeta(\boldsymbol{X}_\star, \boldsymbol{R}_1, \boldsymbol{R}_2, \boldsymbol{X}_0, \boldsymbol{I}) \tag{10.34}$$

($\zeta = 1$ or 2 depending on the rank of $\boldsymbol{X}_\star$) where

$$\boldsymbol{R}_1 = \boldsymbol{\Theta}_c(\boldsymbol{W}_\star) + (\beta/e)\boldsymbol{I} \tag{10.35}$$

$$\boldsymbol{R}_2 = \boldsymbol{W}_\star \odot \left((\boldsymbol{p}(\nu_\star)\boldsymbol{p}(\nu_\star)^H\right)^*. \tag{10.36}$$

10.4.2 New Algorithms for Synthesis Stage

As explained earlier, the rank-one decomposition method can deal with at most four trace equalities for the synthesis of the receive filter and the transmit sequence. This ability allows for considering the values of the $\widetilde{SINR}_{relax}(\nu)$ at three Doppler shifts ν for the receive filter synthesis (and one Doppler shift for synthesis of the transmit sequence). However, the pair $(\boldsymbol{w}_\star, \mathbf{x}_\star)$ obtained by applying Theorem 2 can lead to $SINR(\nu)$ whose behavior with respect to target Doppler shift is not "sufficiently" close to the behavior of the $\widetilde{SINR}_{relax}(\nu)$. It means that the $SINR(\nu)$ can have significantly lower minimum value with respect to ν. In this subsection, we devise novel algorithms to synthesize high

quality $\boldsymbol{w}_\star$ and $\mathbf{x}_\star$ from the solutions to the problem $\mathscr{P}_1$, i.e. $\boldsymbol{W}_\star$ and $\boldsymbol{X}_\star$. The idea is to consider the values of $\boldsymbol{p}(\nu)^H\left(\boldsymbol{W}_\star \odot \boldsymbol{X}_\star^*\right)\boldsymbol{p}(\nu)$ as the optimal energy spectral density (ESD) associated with the transmit sequence and the receive filter. The sought receive filter $\boldsymbol{w}_\star$ and transmit sequence $\mathbf{x}_\star$ are obtained to approximate well the behavior of the optimal ESD with respect to ν. Due to the fact that $\widetilde{SINR}_{relax}(\nu)$ (of $(\boldsymbol{W}_\star, \boldsymbol{X}_\star)$) is a scaled version of the optimal ESD (see (10.9)), we deal with the denominator of the $\widetilde{SINR}_{relax}(\nu)$ by imposing constraints in the synthesis problems.

Let $\{\nu_1, \nu_2, \cdots, \nu_K\}$ denote a discrete set of target Doppler shifts "uniformly distributed" over Ω, and consider the following quantities:

$$g_k \triangleq \boldsymbol{p}_k^H\left(\boldsymbol{W}_\star \odot \boldsymbol{X}_\star^*\right)\boldsymbol{p}_k \in \mathbb{R}_+,\ 1 \le k \le K \tag{10.37}$$

where $\boldsymbol{p}_k = \boldsymbol{p}(\nu_k)$. We define the vector $\mathbf{g} = [g_1, g_2, \cdots, g_K]^T$ as the optimal ESD.

• *Receive filter synthesis:* Herein the aim is to synthesize the optimized receive filter for given $(\boldsymbol{W}_\star, \boldsymbol{X}_\star)$. Observe that

$$\boldsymbol{p}_k^H\left(\boldsymbol{w}\boldsymbol{w}^H \odot \boldsymbol{X}_\star^*\right)\boldsymbol{p}_k = \boldsymbol{w}^H \underbrace{\left(\boldsymbol{p}_k\boldsymbol{p}_k^H \odot \boldsymbol{X}_\star\right)}_{\boldsymbol{T}_k}\boldsymbol{w}. \tag{10.38}$$

Note also that $\boldsymbol{T}_k \succeq \mathbf{0}$ for all k and so that there must exist $\boldsymbol{V}_k$ (of rank d_k) such that $\boldsymbol{T}_k = \boldsymbol{V}_k\boldsymbol{V}_k^H$. Moreover, considering $\boldsymbol{w}^H\boldsymbol{V}_k\boldsymbol{V}_k^H\boldsymbol{w} \approx g_k$, we can write

$$\boldsymbol{V}_k^H\boldsymbol{w} \approx \sqrt{g_k}\boldsymbol{u}_k,\ 1 \le k \le K, \tag{10.39}$$

where all $\boldsymbol{u}_k \in \mathbf{C}^{d_k}$ are unit-norm. Therefore, the receive filter $\boldsymbol{w}_\star$ can be found as the minimizer of the following metric:

$$\|\boldsymbol{A}\boldsymbol{w} - \boldsymbol{u} \odot \boldsymbol{b}\|^2 \tag{10.40}$$

where $\boldsymbol{A}^H = [\boldsymbol{V}_1, \boldsymbol{V}_2, \cdots, \boldsymbol{V}_K]$, $\boldsymbol{u} = [\boldsymbol{u}_1^T, \boldsymbol{u}_2^T, \cdots, \boldsymbol{u}_K^T]^T$, and $\boldsymbol{b} = [\sqrt{g_1}\mathbf{1}^\mathbf{T}, \sqrt{\mathbf{g_2}}\mathbf{1}^\mathbf{T}, \cdots, \sqrt{\mathbf{g_K}}\mathbf{1}^\mathbf{T}]^\mathbf{T}$. Note that the optimal $\widetilde{SINR}_{relax}(\nu)$ (corresponding to $(\boldsymbol{W}_\star, \boldsymbol{X}_\star)$) is a scaled version of the optimal ESD for given $(\boldsymbol{W}_\star, \boldsymbol{X}_\star)$ (see (10.9)). As a result, to obtain the receive filter that yields $SINR(\nu)$ values close to $\widetilde{SINR}_{relax}(\nu)$, we should also take into account the denominator of the $\widetilde{SINR}_{relax}(\nu)$, viz.

$$\gamma = \mathrm{tr}\{\left(\boldsymbol{\Sigma_c}\left(\boldsymbol{X}_\star\right) + \boldsymbol{M}\right)\boldsymbol{W}_\star\}. \tag{10.41}$$

Consequently, we consider the following optimization problem to obtain $\boldsymbol{w}_\star$:

$$\mathscr{P}_w^{synt}\ \begin{cases} \min\limits_{\boldsymbol{w},\boldsymbol{u}} & \|\boldsymbol{A}\boldsymbol{w} - \boldsymbol{u} \odot \boldsymbol{b}\|^2 \\ \text{subject to} & \boldsymbol{w}^H\boldsymbol{G}\boldsymbol{w} \le \gamma \\ & \|\boldsymbol{u}_k\|^2 = 1,\ 1 \le k \le K \end{cases} \tag{10.42}$$

with $\boldsymbol{G} = \boldsymbol{\Sigma_c}\left(\boldsymbol{X}_\star\right) + \boldsymbol{M}$. In the sequel, we propose a cyclic minimization to tackle the non-convex problem $\mathscr{P}_w^{synt}$.

For fixed $\boldsymbol{w}$, the problem $\mathscr{P}_w^{synt}$ boils down to the non-convex problem:

$$\begin{cases} \min\limits_{\boldsymbol{u}} & \left\| \begin{pmatrix} \boldsymbol{a}_1 \\ \boldsymbol{a}_2 \\ \cdot \\ \cdot \\ \boldsymbol{a}_K \end{pmatrix} - \begin{pmatrix} \sqrt{g_1}\boldsymbol{u}_1 \\ \sqrt{g_2}\boldsymbol{u}_2 \\ \cdot \\ \cdot \\ \sqrt{g_K}\boldsymbol{u}_K \end{pmatrix} \right\|^2 \\ \text{subject to} & \|\boldsymbol{u}_k\|^2 = 1,\ 1 \le k \le K \end{cases} \tag{10.43}$$

where $\boldsymbol{a}_k$ contains the entries of $\boldsymbol{A}\boldsymbol{w}$ corresponding to $\boldsymbol{u}_k$ for $1 \le k \le K$. The above minimization can be decoupled into K minimization problems of the following form:

$$\begin{cases} \min\limits_{\boldsymbol{u}_k} & \|\boldsymbol{a}_k - \sqrt{g_k}\boldsymbol{u}_k\|^2 \\ \text{subject to} & \|\boldsymbol{u}_k\|^2 = 1. \end{cases} \tag{10.44}$$

The solution to the above nearest-vector problem is simply given by

$$\boldsymbol{u}_k = \frac{\boldsymbol{a}_k}{\|\boldsymbol{a}_k\|}. \tag{10.45}$$

For fixed $\boldsymbol{u}$, the problem $\mathscr{P}_w^{synt}$ is equivalent to the following QCQP:

$$\begin{cases} \min\limits_{\boldsymbol{w}} & \boldsymbol{w}^H\boldsymbol{A}^H\boldsymbol{A}\boldsymbol{w} - 2\Re\{(\boldsymbol{u}\odot\boldsymbol{b})^H\boldsymbol{A}\boldsymbol{w}\} \\ \text{subject to} & \boldsymbol{w}^H\boldsymbol{G}\boldsymbol{w} \le \gamma. \end{cases} \tag{10.46}$$

Note that the positive definiteness of the matrices $\boldsymbol{A}^H\boldsymbol{A}$ and $\boldsymbol{G}$ ensures the convexity of the above QCQP. As a result, this QCQP can be solved efficiently via interior point methods or Lagrange multipliers [195].

• *Transmit sequence synthesis:* A technique similar to the above one can be used for transmit sequence synthesis. More precisely, we have

$$\boldsymbol{p}_k^H\left((\mathbf{x}\mathbf{x}^H)^*\odot\boldsymbol{W}_\star\right)\boldsymbol{p}_k = \mathbf{x}^H\underbrace{\left((\boldsymbol{p}_k\boldsymbol{p}_k^H)^*\odot\boldsymbol{W}_\star\right)}_{\widetilde{\boldsymbol{T}}_k}\mathbf{x}. \tag{10.47}$$

Therefore, minimization of the following metric can be employed for transmit sequence synthesis:

$$\|\widetilde{\boldsymbol{A}}\mathbf{x} - \widetilde{\boldsymbol{u}}\odot\boldsymbol{b}\|^2 \tag{10.48}$$

where $\widetilde{\boldsymbol{T}}_k = \widetilde{\boldsymbol{V}}_k\widetilde{\boldsymbol{V}}_k^H$, $\widetilde{\boldsymbol{A}}^H = [\widetilde{\boldsymbol{V}}_1, \widetilde{\boldsymbol{V}}_2, \cdots, \widetilde{\boldsymbol{V}}_K]$ and $\widetilde{\boldsymbol{u}}, \boldsymbol{b}$ are defined similarly to the case of receive filter design ($\widetilde{\boldsymbol{u}}_k \in \mathbb{C}^{\widetilde{d}_k}$ with $\widetilde{d}_k$ being the rank of $\widetilde{\boldsymbol{V}}_k$). Note that for transmit sequence synthesis, the similarity and energy constraints should be taken into account in addition to the denominator of the $\widetilde{SINR}_{relax}(v)$. Consequently, we consider the following optimization problem to synthesize the

sought transmit sequence:

$$\mathscr{P}_x^{synt} \left\{ \begin{array}{ll} \min\limits_{\mathbf{x},\widetilde{\boldsymbol{u}}} & \|\widetilde{\boldsymbol{A}}\mathbf{x} - \widetilde{\boldsymbol{u}} \odot \boldsymbol{b}\|^2 \\ \text{subject to} & \mathbf{x}^H \boldsymbol{\Theta}_{\boldsymbol{c}}(\boldsymbol{W}_\star)\mathbf{x} \leq \zeta \\ & \|\mathbf{x}\|^2 \leq e \\ & \Re\{\mathbf{x}^H \mathbf{x}_0\} \geq \varepsilon \\ & \|\widetilde{\boldsymbol{u}}_k\|^2 = 1, 1 \leq k \leq K \end{array} \right. \tag{10.49}$$

where $\zeta = \text{tr}\{\boldsymbol{X}_\star \boldsymbol{\Theta}_{\boldsymbol{c}}(\boldsymbol{W}_\star)\}$ and $\varepsilon = e - \delta/2$. Let $\bar{\mathbf{x}}$ denote the optimal solution $\mathbf{x}$ to the above problem. Note that $\mathbf{x}_\star = \sqrt{e}\frac{\bar{\mathbf{x}}}{\|\bar{\mathbf{x}}\|}$ is such that $\|\mathbf{x}_\star\|^2 = e$, and $\Re\{\mathbf{x}_\star^H \mathbf{x}_0\} \geq \varepsilon$. Therefore, one can consider $\mathbf{x}_\star$ as the optimized transmit sequence $\mathbf{x}_\star$ which lies in the desired similarity region and is feasible for the problem $\mathscr{P}$.

The non-convex optimization problem $\mathscr{P}_x^{synt}$ can be dealt with via a cyclic minimization similar to that used for $\mathscr{P}_w^{synt}$. For fixed $\mathbf{x}$, the solution to the k^{th} resulting nearest-vector problem is given by

$$\widetilde{\boldsymbol{u}}_k = \frac{\widetilde{\boldsymbol{a}}_k}{\|\widetilde{\boldsymbol{a}}_k\|} \tag{10.50}$$

where $\widetilde{\boldsymbol{a}}_k$ includes the entries of $\widetilde{\boldsymbol{A}}\mathbf{x}$ corresponding to $\widetilde{\boldsymbol{u}}_k$ for $1 \leq k \leq K$. On the other hand, the case of fixed $\boldsymbol{u}$ is handled by solving the following convex QCQP:

$$\left\{ \begin{array}{ll} \min\limits_{\mathbf{x}} & \mathbf{x}^H \left(\widetilde{\boldsymbol{A}}^H \widetilde{\boldsymbol{A}}\right)\mathbf{x} - 2\Re\{(\widetilde{\boldsymbol{u}} \odot \boldsymbol{b})^H \widetilde{\boldsymbol{A}}\mathbf{x}\} \\ \text{subject to} & \mathbf{x}^H \boldsymbol{\Theta}_{\boldsymbol{c}}(\boldsymbol{W}_\star)\mathbf{x} \leq \zeta \\ & \|\mathbf{x}\|^2 \leq e \\ & \Re\{\mathbf{x}^H \mathbf{x}_0\} \geq \varepsilon. \end{array} \right. \tag{10.51}$$

Remark 4: Note that the $\mathbf{x}_\star$ synthesized via the rank-one decomposition is a feasible point for the above convex QCQP. Indeed, the output of the rank-one decomposition procedure in Section IV-A can be used as a feasible starting point for the proposed cyclic minimization to obtain the transmit sequence. This can also be done for the receive filter synthesis. ■

The steps of DESIDE can be summarized as in Table 10.2. The first step consists of applying DESIDE-R to the relaxed problem $\mathscr{P}_1$ (see Table 10.1). Steps 2 and 3 aim to synthesize high quality receive filters and transmit sequences, respectively. The cyclic minimizations in step 2 is terminated when a pre-defined stop criterion is satisfied; e.g. $\|\boldsymbol{w}^{(i+1)} - \boldsymbol{w}^{(i)}\| \leq \xi$ for a given $\xi > 0$ where i denotes the iteration number. A similar criterion can be used to terminate the algorithm in the step 3. Note that the obtained $\mathbf{x}$ after satisfying the stop criterion in the step 3 is scaled to obtain $\mathbf{x}_\star$ with energy e. The complexity of DESIDE can be addressed considering DESIDE-R and the synthesis stage. The complexity of each iteration of DESIDE-R is $\mathscr{O}(N^{3.5})$

(see the discussion above Table I). The complexity of each iteration of the proposed synthesis stage is determined by the complexity of solving the QCQPs in eqs. (10.46) and (10.51). These QCQPs can be solved via described methods in [185] with $\mathscr{O}(N^3)$ complexity.

Table 10.2. *The DESIDE Method for obtaining Doppler robust pair of transmit sequence and receive filter*

Step 1 (Solving the relaxed problem): Apply DESIDE-R method to the optimization problem $\mathscr{P}_1$ to obtain the pair of $(\boldsymbol{W}_\star, \boldsymbol{X}_\star)$.
Step 2 (Receive filter synthesis): If $\boldsymbol{W}_\star$ is rank-one, perform an eigendecomposition $\boldsymbol{W}_\star = \boldsymbol{w}_\star \boldsymbol{w}_\star^H$ to obtain $\boldsymbol{w}_\star$. Otherwise, initialize $\boldsymbol{w}$ with a random vector in $\mathbb{C}^N$ and do the following operations until a pre-defined stop criterion is satisfied:

- Obtain $\boldsymbol{u}$ by solving the optimization problem in (10.43) using (10.45).
- Solve the convex QCQP in (10.46) to obtain $\boldsymbol{w}$.

Step 3 (Transmit sequence synthesis): If $\boldsymbol{X}_\star$ is rank-one, perform an eigendecomposition $\boldsymbol{X}_\star = \mathbf{x}\mathbf{x}^H$ to obtain $\mathbf{x}_\star = \mathbf{x} e^{j \arg(\mathbf{x}^H \mathbf{x}_0)}$. Otherwise, initialize $\mathbf{x}$ with a random vector in $\mathbb{C}^N$ and do the following operations until a predefined stop criterion is satisfied:

- Obtain $\widetilde{\boldsymbol{u}}$ by solving the optimization problem in (10.49) for fixed $\mathbf{x}$ using (10.50).
- Solve the convex QCQP in (10.51) to obtain $\mathbf{x}$.

10.5 Numerical Examples

In this section we provide several numerical examples to examine the effectiveness of DESIDE method. Throughout the simulations, unless otherwise explicitly stated, we consider a code length[4] $N = 20$, number of interfering range rings $N_c = 2$, and number azimuth sectors $L = 100$. The interfering signals backscattered from various azimuth sectors are weighted according to the azimuth beam-pattern characteristic of a typical linear array (see [176] for details). A uniformly distributed clutter is assumed with $\sigma^2_{(k,i)} = \sigma^2 = 100$ for all (k,i). In addition, we let the Doppler shifts of the clutter scatterers be uniformly distributed over the interval $\Omega_c = [\bar{\nu}_d - \frac{\varepsilon}{2}, \bar{\nu}_d + \frac{\varepsilon}{2}] = [-0.1, 0.1]$ [192]. As to the target, we set $\alpha_T = 1$. Concerning the covariance matrix $\boldsymbol{M}$ of the signal-independent interference, it is assumed that $\boldsymbol{M}_{m,n} = \rho^{|m-n|}$ with parameter ρ. Regarding the similarity constraint, the generalized Barker code is used

[4] It is expected that the output SINR of the receive filter increases by increasing N due to the increase in the number of degrees of freedom for the design problem (see e.g. [217]) and the longer coherent processing interval [192].

for sequence $\mathbf{x}_0$ [218]. This is a constant modulus sequence which has good correlation properties [176]. The size of the similarity region is controlled by $\delta_0 = \delta/e$. The total transmit energy e is supposed to be equal to the sequence length N. The convex optimization problems are solved via the CVX toolbox [193].

10.5.1 The Effect of the Design Parameters

• *The width of* Ω *and the correlations between the interference samples*

The performance of the system generally depends on the width of target Doppler shift interval Ω and the correlations between the interference samples (controlled by the parameter ρ). Herein the non-robust design (i.e., with a priori known target Doppler shift $\tilde{\nu}$) of the transmit sequence and receive filter (with a similarity constraint) [176], i.e. the solution to the following problem:

$$\begin{cases} \max\limits_{\mathbf{x},\boldsymbol{w}} SINR(\tilde{\nu}) & \\ \text{subject to} & \|\mathbf{x}\|^2 = e \\ & \|\mathbf{x}-\mathbf{x}_0\|^2 \leq \delta \end{cases} \tag{10.52}$$

is considered as a benchmark for comparisons. The effects of the width of interval Ω and the value of ρ are investigated in Fig. 10.1, where the values of $SINR(\nu)$ obtained by DESIDE (with $\mu = 10^{-3}$ and $\delta_0 = 0.5$) are compared with those of the non-robust design for two intervals $\Omega = [1,3]$, $\Omega = [1.5,2.5]$ and for $\rho \in \{0, 0.2, 0.5\}$. For the non-robust design, we reasonably set $\tilde{\nu}$ equal to $\frac{\nu_l+\nu_u}{2}$ with $\Omega = [\nu_l, \nu_u]$. In all examples, it is observed that DESIDE provides a robust $SINR(\nu)$ over the considered interval Ω of target Doppler shifts. The minimum value of $SINR(\nu)$ obtained by DESIDE outperforms that of the non-robust design significantly. The superiority of DESIDE is highlighted by observing that for a considerable range of the target Doppler shift ν, the $SINR(\nu)$ obtained by DESIDE is around 10 dB larger than that of the non-robust design. Furthermore, for any fixed ρ, the minimum value of $SINR(\nu)$ in the interval $\Omega = [1,3]$ is less than that for $\Omega = [1.5,2.5]$. As expected, the wider range of target Doppler shift leads to a more restricted design. Another observation is that for a fixed interval Ω, the minimum values of $SINR(\nu)$ increase as ρ increases. The observation is compatible with the behavior of the upper bound on the $\min_{\nu\in\Omega} \widetilde{SINR}_{relax}(\nu)$ in (10.29)- by increasing the value of ρ, the value of $\lambda_{min}(\boldsymbol{M})$ decreases and the upper bound on the $\widetilde{SINR}_{relax}(\nu)$ becomes larger. Note that in these examples, the ranks of the optimal $\boldsymbol{W}_\star$ and $\boldsymbol{X}_\star$ were equal to one (see section 10.5.4) and hence the obtained pairs of the transmit sequence and the receive filter are *optimal* for the problem $\mathscr{P}$.

• *Size of the similarity region*

Examples for the robust design of transmit sequences and receive filters with various sizes of similarity region are now provided. The values of $SINR(\nu)$

obtained by DESIDE for different δ_0 in $\{0.01, 0.2, 0.4, 0.8\}$ are depicted in Fig. 10.2. The robustness property with respect to the target Doppler shift ν is observed in all examples. As expected, the larger the δ_0, the larger the worst value of the $SINR(\nu)$. This is due to a larger feasibility set for the optimization problem $\mathscr{SDP}_X$ and the fact that the optimal $\boldsymbol{W}_\star$ and $\boldsymbol{X}_\star$ are rank-one.

10.5.2 Convergence of DESIDE-R

Examples of the convergence of DESIDE-R are depicted in Fig. 10.3. This figure shows the values of the objective function (in the maximization problem $\mathscr{P}_1$) obtained through the iterations $\kappa \in \mathbb{N}$ (with κ denoting the iteration number) for $\rho = 0.2$, $\delta_0 = 0.5$, as well as two intervals $\Omega = [1,3]$ and $\Omega = [1.5, 2.5]$. As expected, the cyclic maximization approach which is devised to tackle $\mathscr{P}_1$ leads to a monotonically increasing objective function $\min_{\nu\in\Omega} \widetilde{SINR}_{relax}(\nu)$. The values of the objective function for $\Omega = [1.5, 2.5]$ are larger than those for $\Omega = [1,3]$ (see the discussions associated with Fig. 10.1). Note that both $\boldsymbol{W}_\star$ and $\boldsymbol{X}_\star$ are rank-one here, and as a result, the obtained pairs of the transmit sequence and receive filter are *optimal* for the original design problem $\mathscr{P}$.

10.5.3 A Fast-Time Coding Example

As mentioned earlier (see Remark 1), the problem formulation and the design method can also be applied to fast-time coding systems. We present an example of such an application by considering $N = 32$ and $N_c = N$. The target Doppler shift ν is assumed to be in the interval $\Omega = [-0.1, 0.1]$. The considered maximum target Doppler shift corresponds to a target with an approximate velocity of Mach 4 illuminating by an L-band radar of sampling frequency 1 MHz. Owing to the fact that normalized Doppler shift in this case is proportional to the system bandwidth, we neglect the effect of the Doppler shifts of clutter scatterers. Fig. 10.4 shows the obtained $SINR(\nu)$ by DESIDE as well as the results for the non-robust design, for $\sigma^2 = 10$, $\delta_0 = 1$, and $\rho = 0$. It is observed that employing DESIDE leads to performance robustness of the system. In this example, the result obtained by DESIDE outperforms that of the non-robust design for $|\nu| \geq 0.035$. Moreover, the obtained $\boldsymbol{W}_\star$ and $\boldsymbol{X}_\star$ were rank-one too, similar to the examples presented earlier.

10.5.4 The Synthesis Algorithms

The performance analysis of the synthesis algorithms is performed by considering cases where the ranks of the solutions to the relaxed problem $\mathscr{P}_1$ are larger than one. We consider 20 random starting points for the synthesis algorithms (with $\xi = 10^{-3}$) and report the best result. In the first example, we assume $\Omega = [1,2]$, $\Omega_c = [-0.25, 0.25]$, $\sigma^2 = 100$, $\delta_0 = 0.1$. For a random initial-

ization, DESIDE-R provides $(\boldsymbol{W}_\star, \boldsymbol{X}_\star)$ with $\text{rank}(\boldsymbol{W}_\star) = 2$ and $\text{rank}(\boldsymbol{X}_\star) = 1$ (it was numerically observed that as long as $\Omega \cap \Omega_c = \varnothing$, the rank of W_* is equal to one for most of the employed random initial points). The optimal ESD corresponding to the pair $(\boldsymbol{W}_\star, \boldsymbol{X}_\star)$ is shown in Fig. 10.5(a). The values of $SINR(\nu)$ for the synthesized $\boldsymbol{w}_\star$ and $\mathbf{x}_\star$ are shown in Fig. 10.5(b). This figure also includes the optimal $\widetilde{SINR}_{relax}(\nu)$ (corresponding to $(\boldsymbol{W}_\star, \boldsymbol{X}_\star)$) and the result of applying the rank-one decomposition method. For the latter method, the best result is obtained with $\nu_\star = 1.71$, $\nu' = 1.3$, and $\nu'' = 1.5$. It is observed that using the proposed synthesis algorithm leads to values of $SINR(\nu)$ that are close to the optimal ones. Fig. 10.5(c) shows the optimal $\widetilde{SINR}_{relax}(\nu)$, $SINR(\nu)$ for $(\boldsymbol{w}_\star, \mathbf{x}_\star)$ synthesized via the proposed algorithm and the result of rank-one decomposition method for another case in which $\Omega = [1,3]$. The performance of the rank-one decomposition method is degraded considerably whereas the difference between the results of the proposed algorithm and $\widetilde{SINR}_{relax}(\nu)$ is minor. This can be explained by noting that the rank-one decomposition method can consider the values of the optimal $\widetilde{SINR}_{relax}(\nu)$ at up to three points, i.e., $\nu_\star, \nu'$, and ν''. On the other hand, the proposed method considers a constrained synthesis problem to approximate the values of optimal $\widetilde{SINR}_{relax}(\nu)$ for an arbitrary set of discrete ν. To measure the goodness of the synthesis algorithms, we define the following loss metric:

$$\mathscr{L} \triangleq 10 \log \left(\frac{\min_{\nu \in \Omega} SINR(\nu)}{\min_{\nu \in \Omega} \widetilde{SINR}_{relax}(\nu)} \right). \tag{10.53}$$

In this example, the loss metric $\mathscr{L}$ for the proposed method and the rank-one decomposition method are equal to -0.25 dB and -4.1 dB, respectively. Next we study the effect of the number of optimal ESD samples, i.e. K, on the performance of the proposed synthesis stage. The results for a transmit sequence synthesis example are illustrated in Fig. 10.5(d). For this example, we have $\Omega = [0,2], \Omega_c = [-0.125, 0.125]$, and $\delta_0 = 0.3$. Note that it was numerically observed that the rank of $\boldsymbol{X}_\star$ is equal to one as long as $\Omega \cap \Omega_c = \varnothing$. The figure shows the absolute values of loss metric $\mathscr{L}$ versus K. It is seen that the performance improvement for $K \geq 50$ is negligible. Another observation is that there is about -2 dB loss even for sufficiently large values of K. This might be due to imposing more constraints in the sequence synthesis as compared to the case of filter synthesis. In the example of Fig. 10.5(d), the loss of the rank-decomposition method is around -13 dB; here the latter method can take into account just one point of the optimal $\widetilde{SINR}_{relax}(\nu)$, i.e., $\nu_\star$.

10.6 Concluding Remarks

A joint robust design of the transmit sequence and receive filter was considered for cases where the Doppler shift of the target is unknown. A novel

method (called DESIDE) was proposed to tackle the design problem under the similarity constraint. The main results can be summarized as follows:

- The robust design problem was cast as a max-min problem by using the model which considers the effects of the interfering clutter scatterers at various range-azimuth bins and internal Doppler shifts of these scatterers. It was shown that for a given optimal transmit sequence, the problem can equivalently be written as a QCQP with infinitely many non-convex constraints and hence the design problem in general belongs to a class of NP-hard problems.
- DESIDE was devised to tackle the design problem. The method consists of solving a relaxed version of the design problem (via DESIDE-R) as well as a synthesis stage:
  - DESIDE-R was based on a reformulation of $SINR(v)$ by considering $\boldsymbol{W} = \boldsymbol{w}\boldsymbol{w}^H$ and $\boldsymbol{X} = \mathbf{x}\mathbf{x}^H$, relaxation of the rank-one constraints on the aforementioned matrices, and cyclic maximization of the relaxed problem. For fixed receive filter, the relaxed optimization problem was equivalently expressed as an SDP by using a transformation (inspired by Charnes-Cooper transform) and an SDP representation of the infinitely many affine constraints. Using a similar technique, an SDP was obtained in the fixed transmit sequence case.
  - New algorithms were devised to synthesize the receive filters and transmit sequences from the solutions to the relaxed problem. The synthesis algorithms aim to fit the $\widetilde{SINR}_{relax}(v)$ values associated with the solutions provided by DESIDE-R. The synthesis stage is cast as constrained non-convex problems which were dealt with via cyclic minimization.
- The effectiveness of the devised methods was illustrated by providing several numerical examples. It was shown that the DESIDE system performance possesses a considerable robustness with respect to the target Doppler shift. The numerical analysis of the proposed synthesis algorithms confirms that high quality pairs of receive filter and transmit sequence can be synthesized from the solutions to the relaxed problem.

The design problem considered in this chapter is based on known parameters of clutter and signal-independent interference. Robust design of transmit sequences and receive filters with respect to uncertainties in clutter and interference parameters in addition to the target Doppler shift is a possible topic for future research.

10.7 Appendix

10.7.1 Appendix A: Proof of Lemma 1

Note that the numerator of $SINR(\nu)$ in (10.2) can be rewritten as

$$\begin{aligned} |\alpha_T|^2 \left|\boldsymbol{w}^H (\mathbf{x} \odot \boldsymbol{p}(\nu))\right|^2 &= |\alpha_T|^2 \boldsymbol{w}^H (\mathbf{x} \odot \boldsymbol{p}(\nu))(\mathbf{x} \odot \boldsymbol{p}(\nu))^H \boldsymbol{w} \\ &= |\alpha_T|^2 (\mathbf{x} \odot \boldsymbol{p}(\nu))^H \boldsymbol{w}\boldsymbol{w}^H (\mathbf{x} \odot \boldsymbol{p}(\nu)) \\ &= |\alpha_T|^2 \boldsymbol{p}(\nu)^H \left(\boldsymbol{w}\boldsymbol{w}^H \odot \left(\mathbf{x}\mathbf{x}^H\right)^*\right) \boldsymbol{p}(\nu) \end{aligned} \tag{10.54}$$

where in the last equality we have used standard properties of the Hadamard product [211]. As to the denominator of $SINR(\nu)$ in (10.2), it is straightforward to verify that, for all (k,i),

$$\begin{aligned} \boldsymbol{\Gamma}(\mathbf{x},(k,i)) &= \mathrm{Diag}(\mathbf{x}) \boldsymbol{\Phi}_{\varepsilon_{(k,i)}}^{\bar{\nu}_{d_{(k,i)}}} \mathrm{Diag}(\mathbf{x})^H \\ &= \mathbf{x}\mathbf{x}^H \odot \boldsymbol{\Phi}_{\varepsilon_{(k,i)}}^{\bar{\nu}_{d_{(k,i)}}}. \end{aligned} \tag{10.55}$$

Using the matrix variable $\boldsymbol{X} = \mathbf{x}\mathbf{x}^H$ and substituting the above identity in (10.3) we obtain that

$$\boldsymbol{\Sigma_c}(\boldsymbol{X}) \triangleq \boldsymbol{\Sigma_c}(\mathbf{x}) = \sum_{k=0}^{N_c-1} \sum_{i=0}^{L-1} \sigma_{(k,i)}^2 \boldsymbol{J}_k \left(\boldsymbol{X} \odot \boldsymbol{\Phi}_{\varepsilon_{(k,i)}}^{\bar{\nu}_{d_{(k,i)}}}\right) \boldsymbol{J}_k^T. \tag{10.56}$$

As a result, eq. (10.54) and (10.56) yield the expression of $SINR(\nu)$ in (10.9).

To derive the alternative expression of $SINR(\nu)$ in (10.10), we begin by considering the result of the Lemma 3.1 in [176] which implies

$$\boldsymbol{w}^H \boldsymbol{\Sigma_c}(\mathbf{x}) \boldsymbol{w} = \sum_{k=0}^{N_c} \sum_{k=0}^{L-1} \sigma_{(k,i)}^2 \mathbf{x}^T \mathrm{Diag}(\boldsymbol{J}_{-k}\boldsymbol{w}^*) \boldsymbol{\Phi}_{\varepsilon_{(k,i)}}^{\bar{\nu}_{d_{(k,i)}}} \mathrm{Diag}(\boldsymbol{J}_{-k}\boldsymbol{w}) \mathbf{x}^*. \tag{10.57}$$

Note also that

$$\mathrm{Diag}(\boldsymbol{J}_{-k}\boldsymbol{w}^*) \boldsymbol{\Phi}_{\varepsilon_{(k,i)}}^{\bar{\nu}_{d_{(k,i)}}} \mathrm{Diag}(\boldsymbol{J}_{-k}\boldsymbol{w}) = (\boldsymbol{J}_{-k}\boldsymbol{w}^*\boldsymbol{w}^T\boldsymbol{J}_{-k}^T) \odot \boldsymbol{\Phi}_{\varepsilon_{(k,i)}}^{\bar{\nu}_{d_{(k,i)}}}, \forall k. \tag{10.58}$$

Therefore, using (10.58) as well as the fact that the covariance matrix $\boldsymbol{\Sigma_c}(\mathbf{x}) \succeq \mathbf{0}$, we can write

$$\boldsymbol{w}^H \boldsymbol{\Sigma_c}(\mathbf{x}) \boldsymbol{w} = \mathbf{x}^H \boldsymbol{\Theta_c}(\boldsymbol{W}) \mathbf{x} \tag{10.59}$$

where $\boldsymbol{W} = \boldsymbol{w}\boldsymbol{w}^H$ and

$$\boldsymbol{\Theta_c}(\boldsymbol{W}) = \sum_{k=0}^{N_c-1} \sum_{i=0}^{L-1} \sigma_{(k,i)}^2 \left((\boldsymbol{J}_k^T \boldsymbol{W} \boldsymbol{J}_k) \odot \left(\boldsymbol{\Phi}_{\varepsilon_{(k,i)}}^{\bar{\nu}_{d_{(k,i)}}}\right)^*\right). \tag{10.60}$$

Now let $\beta = \boldsymbol{w}^H \boldsymbol{M} \boldsymbol{w}$, and observe that

$$\boldsymbol{w}^H \boldsymbol{\Sigma_c}(\mathbf{x}) \boldsymbol{w} + \boldsymbol{w}^H \boldsymbol{M} \boldsymbol{w} = \mathrm{tr}\left\{\left(\boldsymbol{\Theta_c}(\boldsymbol{W}) + \left(\frac{\beta}{e}\right) \boldsymbol{I}\right) \boldsymbol{X}\right\}. \tag{10.61}$$

The above identity and eq. (10.54) prove the validity of the alternative expression of $SINR(\boldsymbol{v})$ in (10.10). ■

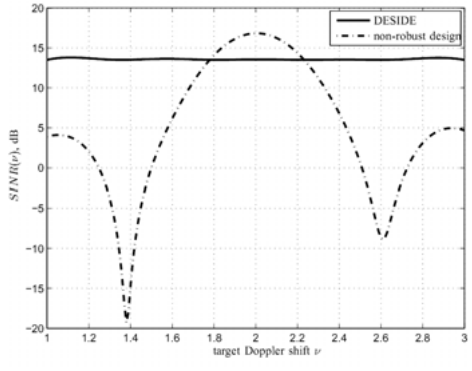

(a)

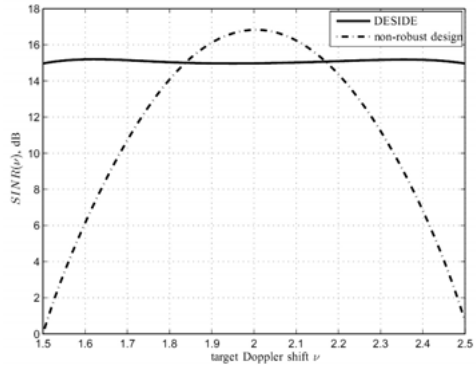

(b)

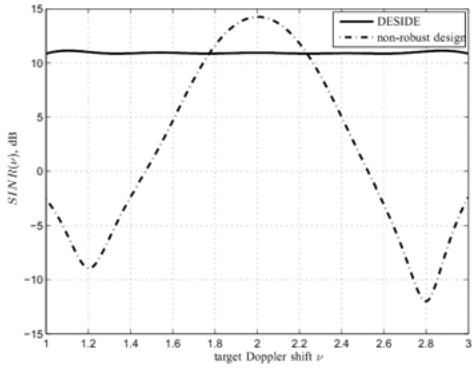

(c)

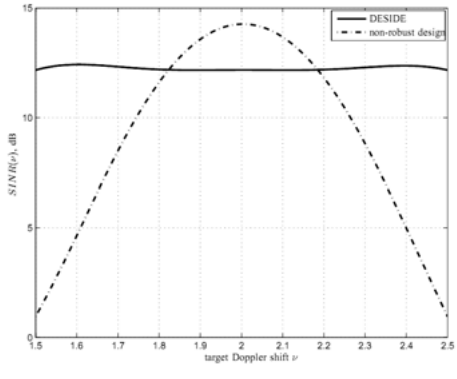

(d)

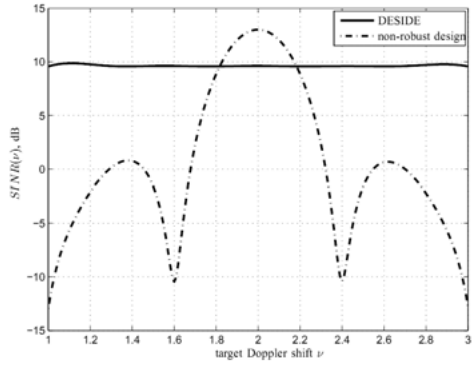

(e)

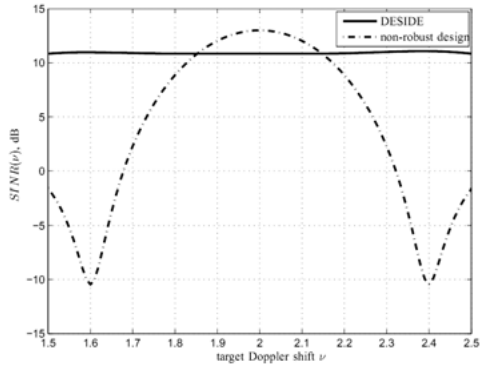

(f)

Figure 10.1. Design examples for various target Doppler shift intervals Ω and various ρ: (a) $\Omega = [1,3]$ and $\rho = 0.5$, (b) $\Omega = [1.5,2.5]$ and $\rho = 0.5$, (c) $\Omega = [1,3]$ and $\rho = 0.2$, (d) $\Omega = [1.5,2.5]$ and $\rho = 0.2$, (e) $\Omega = [1,3]$ and $\rho = 0$, (f) $\Omega = [1.5,2.5]$ and $\rho = 0$.

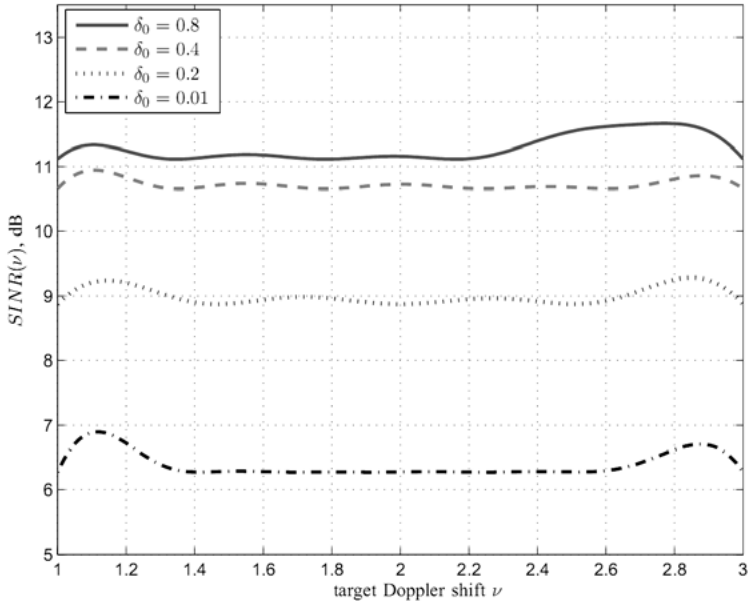

Figure 10.2. Design examples for various sizes of the similarity region: $SINR(\nu)$ obtained by DESIDE versus target Doppler shift ν for $\delta_0 = 0.01, 0.2, 0.4$, and 0.8.

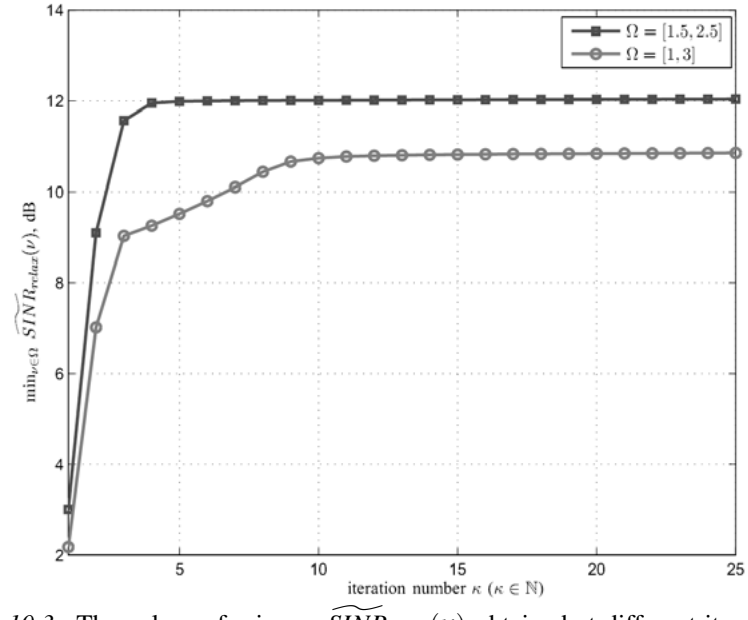

Figure 10.3. The values of $\min_{\nu\in\Omega} \widetilde{SINR}_{relax}(\nu)$ obtained at different iterations of DESIDE-R for $\rho = 0.2$, $\delta = 0.5$ as well as two intervals $\Omega = [1,3]$ and $\Omega = [1.5, 2.5]$.

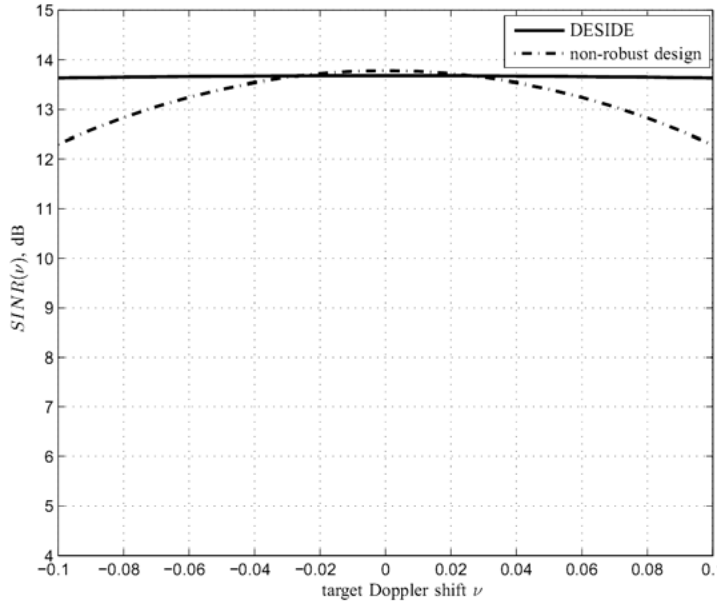

Figure 10.4. Design example for a fast-time coding system.

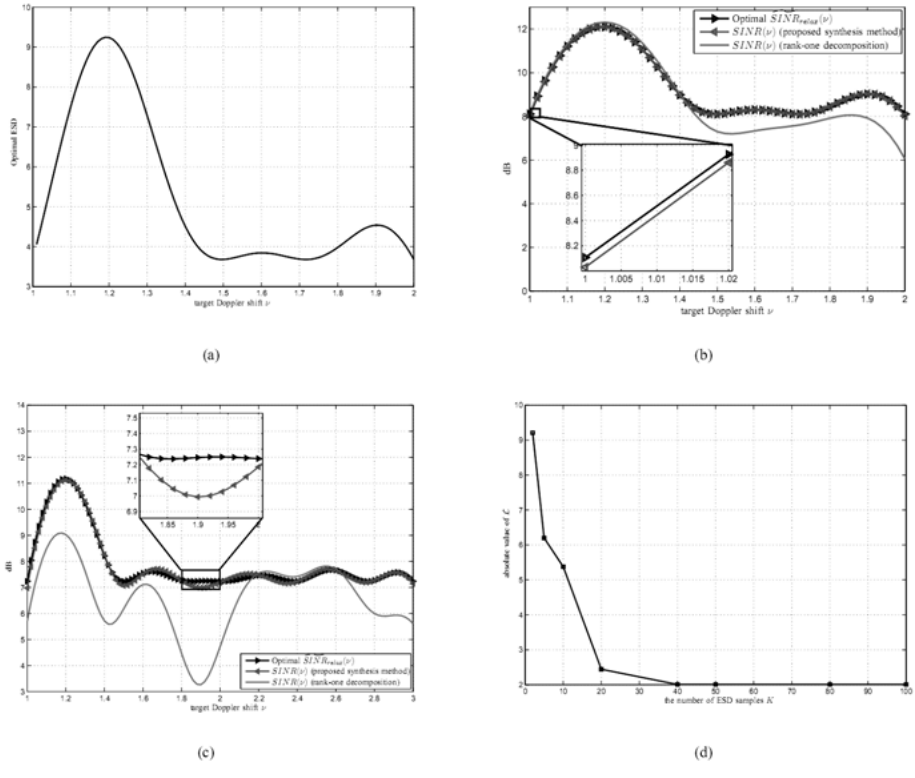

Figure 10.5. Results obtained with the proposed synthesis algorithms: (a) an optimal ESD, (b) results of the filter synthesis corresponding to part (a), (c) another filter synthesis example, (d) absolute value of the loss metric $\mathscr{L}$ of the transmit sequence synthesis versus the number of ESD samples K for the considered transmit sequence synthesis example. The zoomed areas in (b) and (c) show the values of the optimal $\widetilde{SINR}_{relax}(\nu)$ and $SINR(\nu)$ of the proposed synthesis method in the neighborhoods of their minimum values.

Part III:
Information-Theoretic Criteria

11. Unified Optimization Framework for Multi-Static Radar Code Design using Information-Theoretic Criteria

Abstract
In this chapter, we study the problem of code design to improve the detection performance of multi-static radar in the presence of clutter (i.e., a signal-dependent interference). To this end, we briefly present a discrete-time formulation of the problem as well as the optimal detector in the presence of Gaussian clutter. Due to the lack of analytical expression for receiver operation characteristic (ROC), code design based on ROC is not feasible. Therefore, we consider several popular information-theoretic criteria including Bhattacharyya distance, Kullback-Leibler (KL) divergence, J-divergence, and mutual information (MI) as design metrics. The code optimization problems associated with different information-theoretic criteria are obtained and cast under a unified framework. We propose two general methods based on Majorization-Minimization to tackle the optimization problems in the framework. The first method provides optimal solutions via successive majorizations whereas the second one consists of a majorization step, a relaxation, and a synthesis stage. Moreover, derivations of the proposed methods are extended to tackle the code design problems with a peak-to-average ratio power (PAR) constraint. Using numerical investigations, a general analysis of the coded system performance, computational efficiency of the proposed methods, and the behavior of the information-theoretic criteria is provided.

Keywords: Code design, information-theoretic criteria, multi-static radar, majorization-minimization, peak-to-average power ratio (PAR)

11.1 Introduction

Signal design for detection performance improvement has been a long-term research topic in the radar literature.

Active radars deal with both signal-dependent as well as signal-independent interferences. Indeed, the signals backscattered from undesired obstacles (known as clutter) depend on the transmit signal, whereas noise, unwanted emissions, and jammer emissions do not depend on the transmit signal.

The effect of the clutter has been considered in early studies for single-input single-output (SISO) systems [155–159]. The aim of these studies is to maximize the signal-to-interference-plus-noise-ratio (SINR) by means of joint optimization of the transmit signal and the receive filter. The results of [219] and [220] are recent extensions of [159] which use different methods to tackle some related problems. In [160], a solution for the optimal energy spectral density (ESD) of the transmit signal as well as a method for approximate synthesis of the signal have been presented for SISO systems. Problems related to that of [160] have been considered in [161] and [176] for cases where practical constraints such as low peak-to-average-power ratio (PAR) and similarity to a given code are imposed in the design stage. The work of [221] employs mutual information (MI) as design metric for target detection and estimation. In [164], two signal design approaches based on MI and SINR have been studied for extended target recognition in SISO systems. KL-divergence has been considered in [222] for target classification.

In multi-static scenarios, the interpretation of the detection performance is not easy in general and in several cases expressions for detection perfor-

mance are too complicated to be amenable to utilization as design metrics (see e.g. [182] [184]). In such circumstances, information-theoretic criteria can be considered as design metrics to guarantee some types of optimality for the obtained signals. For example, in [184] an approach similar to that of [160] has been applied to the case of multi-static radars with one transmit antenna, and a concave approximation of the J-divergence has been used as the design metric. MI has been considered as a design metric for non-orthogonal multiple-input multiple-output (MIMO) radar signal design in [171] for clutter-free scenarios. A problem related to that of [171] has been studied in [223] where Kullback-Leibler (KL) divergence and J-divergence are used as design metrics. In [169], KL-divergence and MI have been taken into account for MIMO radar signal design in the absence of clutter. Information-theoretic criteria have also been used in research subjects related to the detection problem. The authors in [168] study the target classification for MIMO radars using minimum mean-square error (MMSE) and the MI criterion assuming no clutter. The reference [183] employs Bhatacharyya distance, KL-divergence, and J-divergence for signal design of a communication system with multiple transmit antennas. MI has also been used to investigate the effect of the jammer on MIMO radar performance in clutter-free situations in [170].

In this chapter, we provide a unified framework for multi-static radar code design in the presence of clutter. Although closed-form expressions for the probability of detection and the probability of false alarm of the optimal detector are available, the analytical receiver operating characteristic (ROC) does not exist. As such, we employ several information-theoretic criteria that are widely used in the literature (see e.g. [169, 171, 183]), namely Bhattacharyya distance, KL-divergence, J-divergence, and MI as metrics for code design. In particular, we express these metrics in terms of the code vector and then present corresponding optimization problems. We show that the arising optimization problems can be conveniently dealt with using a unified framework. To tackle the code design problem, two novel methods based on Majorization-Minimization (MaMi) technique are devised. In the first method (which we call Sv-MaMi) successive majorizations are employed, whereas the second one (which we call Re-MaMi) is based on majorizations, a relaxation, and a synthesis stage. We also extend the proposed methods to the code design problem with PAR constraints and to the case of multiple transmitters (with orthogonal transmission). To the best of our knowledge, no study of code design with PAR constraints using information-theoretic criteria was conducted prior to this work.

The rest of this chapter is organized as follows. In Section 11.2, we present a discrete-time formulation of the detection problem as well as the optimal detector. We briefly review different information-theoretic criteria in Section 11.3 and cast the associated optimization problems under a unified framework. Section 11.4 contains the derivations of the steps of Sv-MaMi to deal with the optimization problems formulated in the unified framework presented in Sec-

tion 11.3. Re-MaMi is introduced in Section 11.5 as an alternative approach to obtain optimized codes of the arising optimization problems. Extensions of the design problem to the cases of PAR-constrained design and multiple transmitters (with orthogonal transmission) are discussed in Section 11.6. Numerical examples are provided in Section 11.7. Finally, conclusions are drawn in Section 11.8.

Notation: We use bold lowercase letters for vectors and bold uppercase letters for matrices. $(.)^T$, $(.)^*$ and $(.)^H$ denote the vector/matrix transpose, the complex conjugate, and the Hermitian transpose, respectively. $\boldsymbol{I}_N$ represents the identity matrix in $\mathbb{C}^{N\times N}$. $\|\boldsymbol{X}\|_F$ denotes the Frobenius norm of a matrix $\boldsymbol{X}$. The notations $\mu_{max}(\cdot)$ and $\mu_{min}(\cdot)$ indicate the principal and the minor eigenvalues of a Hermitian matrix, respectively. The l_2-norm of a vector $\mathbf{x}$ is denoted by $\|\mathbf{x}\|_2$. tr$(.)$ is the trace of a square matrix argument. blkDiag$(.)$ denotes the block diagonal matrix formed by its arguments. We write $\boldsymbol{A} \succeq \boldsymbol{B}$ iff $\boldsymbol{A}-\boldsymbol{B}$ is positive semi-definite, and $\boldsymbol{A} \succ \boldsymbol{B}$ iff $\boldsymbol{A}-\boldsymbol{B}$ is positive-definite. E$\{.\}$ stands for the statistical expectation operator. $\mathscr{CN}(\boldsymbol{\omega},\boldsymbol{\Sigma})$ denotes the circularly symmetric complex Gaussian distribution with mean $\boldsymbol{\omega}$ and covariance $\boldsymbol{\Sigma}$. The symbol $\sim$ is used to show the distribution of a random variable/vector. Finally, $\Re(.)$ denotes the real-part of the complex-valued argument.

11.2 Data Modeling and the Optimal Detector

11.2.1 Data Modeling

We consider a multi-static pulsed-radar with one transmitter and N_r widely separated receive antennas. The baseband transmit signal can be formulated as

$$s(t) = \sum_{n=1}^{N} a_n \phi(t-[n-1]T_P) \tag{11.1}$$

where $\phi(t)$ is the basic unit-energy transmit pulse (with time duration τ_p), T_P is the pulse repetition period ($T_P \gg \tau_p$), and $\{a_n\}_{n=1}^N$ are the deterministic coefficients that are to be "optimally" determined. The vector $\boldsymbol{a} \triangleq [a_1 \;\; a_2 \;\; \ldots \;\; a_N]^T$ is referred to as the code vector of the radar system.

The baseband signal received at the k^{th} antenna backscattered from a stationary target can be written as

$$r_k(t) = \alpha_k s(t-\tau_k) + c_k(t) + w_k(t) \tag{11.2}$$

where α_k is the amplitude of the target return (including the channel effects), $c_k(t)$ is the clutter component, $w_k(t)$ is a Gaussian random process representing the signal-independent interference component (including various types of noise, interference, and jamming), and τ_k is the time corresponding to propagation delay for the path from the transmitter to the target and thereafter to the k^{th} receiver.

In what follows, we consider a few typical assumptions in the radar literature which are key to the derivations that will appear in this chapter.

Assumption 1. *We assume that the clutter component at the k^{th} receiver is composed of signal echoes produced by many stationary point scatterers (located within unambiguous-range with respect to the k^{th} receiver [192]). The amplitudes and arrival times of the echoes are assumed to be statistically independent [175, 225].*

According to Assumption 1, the clutter component can be expressed as

$$c_k(t) = \sum_{v=1}^{N_c} \rho_{k,v} s(t - \tau_{k,v}) \tag{11.3}$$

where N_c is the number of point scatterers, $\rho_{k,v}$ is the "amplitude" of the v^{th} scatterer observed by the k^{th} receive antenna, and $\tau_{k,v}$ is the propagation delay at the k^{th} receiver corresponding to the v^{th} scatterer for which we have $\tau_{k,v} \leq T_p$.

At the k^{th} receiver, the received signal is matched filtered by $\phi^*(-t)$. Then range-gating is performed by sampling the output of the matched filter at time slots corresponding to a specific radar cell. Note that the detection for a specific radar cell can be accomplished using a successive chain of operations including directional transmission and reception as well as range-gating at each receiver [226].

The discrete-time signal corresponding to a certain radar cell for the k^{th} receiver can be described as (see Appendix A):

$$r_{k,n} = \alpha_k a_n + \widetilde{\rho}_k a_n + w_{k,n} \tag{11.4}$$

where $r_{k,n}$ is the output of the matched filter at the k^{th} receiver sampled at $t = (n-1)T_p + \tau_k$, $\widetilde{\rho}_k$ is a zero-mean complex Gaussian random variable (RV) with variance $\sigma^2_{c,k}$ associated with the clutter scatterers, and $w_{k,n}$ denotes the n^{th} sample of $w_k(t)$ when filtered by $\phi^*(-t)$ at the k^{th} receiver. Using a vector notation, we can write

$$\mathbf{r}_k \triangleq \mathbf{s}_k + \mathbf{c}_k + \mathbf{w}_k = \alpha_k \mathbf{a} + \widetilde{\rho}_k \mathbf{a} + \mathbf{w}_k \tag{11.5}$$

where $\mathbf{r}_k \triangleq [r_{k,1} \;\; r_{k,2} \;\; \cdots \;\; r_{k,N}]^T$, $\mathbf{w}_k \triangleq [w_{k,1} \;\; w_{k,2} \;\; \cdots \;\; w_{k,N}]^T$, $\boldsymbol{s}_k \triangleq \alpha_k \boldsymbol{a}$, and $\boldsymbol{c}_k \triangleq \widetilde{\rho}_k \boldsymbol{a}$.

We further make the following assumptions:

Assumption 2. *The Swerling-I model is used for the amplitude of the target echo, i.e. $\alpha_k \sim \mathscr{CN}(0, \sigma_k^2)$ for any stationary target [160, 184].*

Assumption 3. *The second-order statistics of the target, clutter, and interference components at the k^{th} receiver (i.e. $\sigma_k^2, \sigma_{c,k}^2$, and $\mathrm{E}\{\boldsymbol{w}_k \boldsymbol{w}_k^H\}$) are assumed to be known.*

The above assumption is common for radar systems using cognitive (knowledge-aided) methods that employ geographical, meteorological, National Land Cover Data (NLCD), and the information of the previous scan to interactively learn and extract the characteristics of the environment (see e.g. [162, 176, 177, 227, 228]).

Assumption 4. *The random variables in the set $\{\alpha_k\}_{k=1}^{N_r}$ are statistically independent. Such a statistical independence is also considered for random variables/vectors in the sets $\{\widetilde{\rho}_k\}_{k=1}^{N_r}$ and $\{\boldsymbol{w}_k\}_{k=1}^{N_r}$.*

Assumption 4 is well-justified, due to the fact that the receivers are widely separated [171, 184].

11.2.2 Optimal Detector

Using all the received signals, the target detection leads to the following binary hypothesis problem

$$\begin{cases} \mathrm{H}_0: & \mathbf{r} = \mathbf{c} + \mathbf{w} \\ \mathrm{H}_1: & \mathbf{r} = \mathbf{s} + \mathbf{c} + \boldsymbol{w} \end{cases} \tag{11.6}$$

where $\mathbf{r}$, $\mathbf{s}$, $\mathbf{c}$, and $\boldsymbol{w}$ are defined by column-wise stacking of $\mathbf{r}_k, \mathbf{s}_k, \mathbf{c}_k$, and $\mathbf{w}_k$ for $k = 1, 2, ..., N_r$; more precisely, $\mathbf{r} \triangleq [\mathbf{r}_1^T \ \cdots \ \mathbf{r}_{N_r}^T]^T$, $\mathbf{s} \triangleq [\mathbf{s}_1^T \ \cdots \ \mathbf{s}_{N_r}^T]^T$, $\mathbf{c} \triangleq [\mathbf{c}_1^T \ \cdots \ \mathbf{c}_{N_r}^T]^T$, and $\mathbf{w} \triangleq [\mathbf{w}_1^T \ \cdots \ \mathbf{w}_{N_r}^T]^T$.

Let $\{\boldsymbol{M}_k\}$ denote the covariance matrices of Gaussian random vectors $\{\boldsymbol{w}_k\}$. Further let $\boldsymbol{S}, \boldsymbol{C}$, and $\boldsymbol{M}$ represent the the covariance matrices of $\boldsymbol{s}, \boldsymbol{c}$, and $\boldsymbol{w}$, respectively. Using the aforementioned assumptions we have that

$$\begin{aligned} \mathbf{S} &= \mathrm{blkDiag}(\sigma_1^2 \mathbf{a}\mathbf{a}^H, \sigma_2^2 \mathbf{a}\mathbf{a}^H, \ldots, \sigma_{N_r}^2 \mathbf{a}\mathbf{a}^H) \\ \mathbf{C} &= \mathrm{blkDiag}(\sigma_{c,1}^2 \mathbf{a}\mathbf{a}^H, \sigma_{c,2}^2 \mathbf{a}\mathbf{a}^H, \ldots, \sigma_{c,N_r}^2 \mathbf{a}\mathbf{a}^H) \\ \boldsymbol{M} &= \mathrm{blkDiag}(\mathbf{M}_1, \mathbf{M}_2, \ldots, \mathbf{M}_{N_r}). \end{aligned} \tag{11.7}$$

Consequently, the underlying detection problem can be equivalently expressed as

$$\begin{cases} \mathrm{H}_0 : \mathbf{x} \sim \mathscr{CN}(\mathbf{0}, \mathbf{I}) \\ \mathrm{H}_1 : \mathbf{x} \sim \mathscr{CN}(\mathbf{0}, \mathbf{DSD} + \mathbf{I}) \end{cases} \tag{11.8}$$

where $\mathbf{x} \triangleq \mathbf{Dr}$, $\mathbf{D} \triangleq (\mathbf{C} + \boldsymbol{M})^{-\frac{1}{2}} = \mathrm{blkDiag}(\boldsymbol{D}_1, \boldsymbol{D}_2, \ldots, \boldsymbol{D}_{N_r})$ with $\mathbf{D}_k \triangleq (\sigma_{c,k}^2 \mathbf{a}\mathbf{a}^H + \mathbf{M}_k)^{-\frac{1}{2}}$. Note that both $\boldsymbol{D}$ and $\boldsymbol{S}$ in (11.8) depend on the transmit code $\boldsymbol{a}$.

The optimal detector for (11.8) can be obtained by applying the estimator-correlator theorem [178, chapter 13] as:

$$\sum_{k=1}^{N_r} \sigma_k^2 \mathbf{x}_k^H \mathbf{D}_k \mathbf{a}\mathbf{a}^H \mathbf{D}_k (\sigma_k^2 \mathbf{D}_k \mathbf{a}\mathbf{a}^H \mathbf{D}_k + \mathbf{I})^{-1} \mathbf{x}_k \underset{\mathrm{H}_1}{\overset{\mathrm{H}_0}{\lessgtr}} \eta \tag{11.9}$$

where η is the detection threshold, and

$$\mathbf{x}_k = \mathbf{D}_k \mathbf{r}_k \,. \tag{11.10}$$

In particular, by defining

$$\begin{aligned} \lambda_k &\triangleq \sigma_k^2 \boldsymbol{a}^H \boldsymbol{D}_k^2 \boldsymbol{a}, \\ \theta_k &\triangleq \frac{\mathbf{a}^H \mathbf{D}_k \mathbf{x}_k}{\|\boldsymbol{a}^H \boldsymbol{D}_k\|_2}, \end{aligned} \tag{11.11}$$

the canonical form of the detector in (11.9) can be obtained as

$$T(\boldsymbol{\theta}) \triangleq \sum_{k=1}^{N_r} \frac{\lambda_k |\theta_k|^2}{1+\lambda_k} \underset{\mathrm{H}_1}{\overset{\mathrm{H}_0}{\lessgtr}} \eta \tag{11.12}$$

where $\boldsymbol{\theta} \triangleq [\theta_1 \;\; \theta_2 \;\; \cdots \;\; \theta_{N_r}]^T$.

11.3 Optimal Code Design

In this section, we aim to obtain the optimal transmit signals by judiciously designing the code vector $\boldsymbol{a}$. A reasonable approach to code design is to exploit the knowledge of the analytical receiver operating characteristic (ROC) which enables the designer to obtain the largest possible value of the probability of detection P_d for a given value of the probability of false alarm P_{fa} via optimal selection of the design parameters. However, this method cannot be used if the analytical ROC is not amenable to a closed-form expression which is the case for the problem considered in this chapter. Particularly, even though closed-form expressions for P_d and P_{fa} can be obtained by applying the results of [182], derivation of the analytical ROC is not possible. In such cases, one can resort to information-theoretic criteria including Bhattacharyya distance, KL-divergence, J-divergence, and MI (see the Introduction). In what follows, the goal is to improve the detection performance by maximizing the aforementioned information-theoretic criteria over the code vector $\boldsymbol{a}$. Interestingly, the corresponding optimization problems can be dealt with conveniently using a unified optimization framework.

11.3.1 Information-Theoretic Design Metrics

• **Bhattacharyya distance**: Bhattacharyya distance $\mathscr{B}$ measures the distance between two probability density functions (pdf). In a binary hypothesis testing

problem $T(H_0, H_1)$, the design parameters can be chosen such that the Bhattacharyya distance $\mathscr{B}$ between the pdfs of the observation under H_0 and H_1 is maximized. Note that the Bhattacharyya distance provides an upper bound on P_{fa}, and at the same time yields a lower bound on P_d [183]. Therefore, maximization of the Bhattacharyya distance minimizes the upper bound on P_{fa} while it maximizes the lower bound on P_d[1].

The Bhattacharyya distance $\mathscr{B}$ for two multivariate Gaussian distributions, $\mathscr{CN}(\mathbf{0}, \boldsymbol{\Sigma}_1)$ and $\mathscr{CN}(\mathbf{0}, \boldsymbol{\Sigma}_2)$, can be expressed as [183]:

$$\mathscr{B} = \log\left(\frac{\det(0.5(\boldsymbol{\Sigma}_1 + \boldsymbol{\Sigma}_2))}{\sqrt{\det(\boldsymbol{\Sigma}_1)\det(\boldsymbol{\Sigma}_2)}}\right). \tag{11.13}$$

By applying (11.13) to the problem in (11.8) we obtain

$$\begin{aligned}
\mathscr{B} &= \log\left(\frac{\det(\boldsymbol{I} + 0.5\boldsymbol{DSD})}{\sqrt{\det(\boldsymbol{I} + \boldsymbol{DSD})}}\right) \\
&= \sum_{k=1}^{N_r} \log\left(\frac{\det(\mathbf{I} + 0.5\sigma_k^2 \mathbf{D}_k \mathbf{a}\mathbf{a}^H \mathbf{D}_k)}{\sqrt{\det(\mathbf{I} + \sigma_k^2 \mathbf{D}_k \mathbf{a}\mathbf{a}^H \mathbf{D}_k)}}\right) \\
&= \sum_{k=1}^{N_r} \log\left(\frac{1 + 0.5\lambda_k}{\sqrt{1 + \lambda_k}}\right).
\end{aligned} \tag{11.14}$$

The second equality in (11.14) holds due to the block-diagonal structure of the matrices $\boldsymbol{S}$ and $\boldsymbol{D}$. The last equality follows from the fact that the eigenvalues of the matrix $\mathbf{I} + \sigma_k^2 \mathbf{D}_k \mathbf{a}\mathbf{a}^H \mathbf{D}_k$ include $(N-1)$ ones and the maximum eigenvalue which is given by $1 + \sigma_k^2 \boldsymbol{a}^H \mathbf{D}_k^2 \mathbf{a} = 1 + \lambda_k$. Eventually the underlying code design problem can be formulated as

$$\begin{aligned}
\max_{\mathbf{a}, \lambda_k} \quad & \sum_{k=1}^{N_r} \log\left(\frac{1 + 0.5\lambda_k}{\sqrt{1 + \lambda_k}}\right) \\
\text{subject to} \quad & \lambda_k = \sigma_k^2 \boldsymbol{a}^H (\sigma_{\mathrm{c},k}^2 \mathbf{a}\mathbf{a}^H + \mathbf{M}_k)^{-1} \boldsymbol{a} \\
& \|\boldsymbol{a}\|_2^2 \leqslant e,
\end{aligned} \tag{11.15}$$

where e denotes the total transmit energy.

• **KL-divergence**: The KL-divergence $\mathscr{D}(f_0 \| f_1)$ is another metric to measure the "distance" between two pdfs f_0 and f_1. Consider a binary hypothesis testing problem with $f_0 = f(\boldsymbol{r}|\mathrm{H}_0)$ and $f_1 = f(\boldsymbol{r}|\mathrm{H}_1)$. The Stein Lemma states that for any fixed P_{fa} [183]

$$\mathscr{D}(f(\boldsymbol{r}|\mathrm{H}_0) \| f(\boldsymbol{r}|\mathrm{H}_1)) = \lim_{N \to \infty} \left(-\frac{1}{N} \log(1 - P_d)\right) \tag{11.16}$$

[1]This is due to the fact that $P_d \geq 1 - \delta^{-1/2} e^{-\mathscr{B}}$ and $P_{fa} \leq \delta^{1/2} e^{-\mathscr{B}}$ where δ is the likelihood threshold [229].

which implies that (for any fixed P_{fa}) the maximization of the KL-divergence metric leads to an asymptotic maximization of P_d (we refer the interested reader to [230, Chapter 4], [183], [231, Theorem 1], [232], and references therein for some bounds on the detection performance associated with the KL-divergence). In addition, we have that [183]

$$\mathscr{D}(f(\boldsymbol{r}|\mathrm{H}_0)\|f(\boldsymbol{r}|\mathrm{H}_1)) = -\mathrm{E}\{\log(\mathscr{L})|\mathrm{H}_0\} \tag{11.17}$$

where $\mathscr{L}$ is the likelihood ratio defined as

$$\mathscr{L} \triangleq \frac{f(\boldsymbol{r}|\mathrm{H}_1)}{f(\boldsymbol{r}|\mathrm{H}_0)}.$$

Using (11.12), (11.17) and the identity $\log(\mathscr{L}) = T(\boldsymbol{\theta}) - \log\det(\mathbf{I}+\mathbf{DSD})$ [178], the KL-divergence associated with (11.8) can be obtained as

$$\mathscr{D}(f(\boldsymbol{r}|\mathrm{H}_0)\|f(\boldsymbol{r}|\mathrm{H}_1)) = \sum_{k=1}^{N_r}\left\{\log(1+\lambda_k) - \frac{\lambda_k}{1+\lambda_k}\right\}.$$

As a result, the problem of code design by maximizing the KL-divergence metric can be stated as:

$$\begin{aligned} \max_{\mathbf{a},\lambda_k} \quad & \sum_{k=1}^{N_r}\left\{\log(1+\lambda_k) - \frac{\lambda_k}{1+\lambda_k}\right\} \\ \text{subject to} \quad & \lambda_k = \sigma_k^2 \boldsymbol{a}^H(\sigma_{\mathrm{c},k}^2 \mathbf{a}\mathbf{a}^H + \mathbf{M}_k)^{-1}\boldsymbol{a} \\ & \|\boldsymbol{a}\|_2^2 \leqslant e. \end{aligned} \tag{11.18}$$

• **J-divergence**: The J-divergence metric, denoted herein as $\mathscr{J}$, is another measure of the distance between two pdfs and it is defined as

$$\mathscr{J} \triangleq \mathscr{D}(f_0\|f_1) + \mathscr{D}(f_1\|f_0). \tag{11.19}$$

According to Stein Lemma [230, Chapter 4], in a binary hypothesis testing problem (with $f_0 = f(\boldsymbol{r}|\mathrm{H}_0)$ and $f_1 = f(\boldsymbol{r}|\mathrm{H}_1)$), and for any fixed P_d, we can write

$$\mathscr{D}(f(\boldsymbol{r}|\mathrm{H}_1)\|f(\boldsymbol{r}|\mathrm{H}_0)) = \lim_{N\to\infty}\left(-\frac{1}{N}\log(P_{fa})\right). \tag{11.20}$$

Eq. (11.16) and (11.20) along with other properties and bounds associated with the J-divergence (see e.g [230, Chapter 4], [231, Theorem 1], [233], [183], and references therein) have motivated several authors to consider $\mathscr{J}$ as the design metric for radar signal design (see [184], [183], [234], and references therein). For the binary hypothesis testing problem in (11.8) with $f_0 = f(\boldsymbol{r}|\mathrm{H}_0)$ and $f_1 = f(\boldsymbol{r}|\mathrm{H}_1)$, we have that [183]

$$\begin{aligned} \mathscr{J} &= \mathrm{E}\{(\mathscr{L}-1)\log(\mathscr{L})|\mathrm{H}_0\} \\ &= \left(\int \frac{f(\boldsymbol{r}|\mathrm{H}_1)}{f(\boldsymbol{r}|\mathrm{H}_0)}\log(\mathscr{L})f(\boldsymbol{r}|\mathrm{H}_0)d\boldsymbol{r}\right) - \mathrm{E}\{\log(\mathscr{L})|H_0\} \\ &= \mathrm{E}\{\log(\mathscr{L})|H_1\} - \mathrm{E}\{\log(\mathscr{L})|H_0\}. \end{aligned}$$

Using (11.21) along with similar calculations as in the case of KL-divergence, the J-divergence metric associated with (11.8) can be obtained as

$$\mathscr{J} = \sum_{k=1}^{N_r} \frac{\lambda_k^2}{1+\lambda_k}. \tag{11.21}$$

Consequently, the corresponding code design problem can be expressed as

$$\begin{aligned} \max_{\mathbf{a},\lambda_k} \quad & \sum_{k=1}^{N_r} \frac{\lambda_k^2}{1+\lambda_k} \\ \text{subject to} \quad & \lambda_k = \sigma_k^2 \boldsymbol{a}^H (\sigma_{c,k}^2 \mathbf{a}\mathbf{a}^H + \mathbf{M}_k)^{-1} \boldsymbol{a} \\ & \|\boldsymbol{a}\|_2^2 \leqslant e. \end{aligned} \tag{11.22}$$

• **Mutual information**: MI is another metric that has been used for radar transmit signal design (see the Introduction). The MI between the amplitude of the target return and the received signal is often considered as a design criterion. For the relationship between MI and minimum mean-square error (MMSE) estimation see e.g. [235]. Note that the larger the MI the better the MMSE estimation [201, Chapter 2]. Note also that, the optimal detector for Gaussian pdfs has a close relationship to the MMSE estimation (see e.g. the estimator-correlator theorem in [178, Chapter 5 and 13]) in the sense that better estimation leads to detection performance improvements [171]. Furthermore, a comprehensive mathematical motivation for using MI as a metric in radar signal design is provided in [201, Chapter 2] and [221] using rate-distortion function, Fano's inequality, and Shannon's noisy channel coding theorem. Additionally, the results of [236] relate the MI and Bayes risk in statistical decision problems. An analysis of the connection between Bayesian classification performance and MI has also been performed in [237]. The MI metric associated with (11.8) is given by [238]

$$\begin{aligned} \mathscr{M} &= \log\left((\pi e)^N \det(\mathbf{I}+\mathbf{DSD})\right) - \log\left((\pi e)^N \det(\mathbf{I})\right) \\ &= \sum_{k=1}^{N_r} \log\left(\det(\mathbf{I}+\sigma_k^2 \mathbf{D}_k \mathbf{a}\mathbf{a}^H \mathbf{D}_k)\right) - \sum_{k=1}^{N_r} \log\left(\det(\mathbf{I})\right) \\ &= \sum_{k=1}^{N_r} \log(1+\lambda_k) \end{aligned} \tag{11.23}$$

where the second equality follows from the block-diagonal structures of $\mathbf{D}$ and $\mathbf{S}$, and the third equality holds due to the fact that $\left\{\sigma_k^2 \mathbf{D}_k \mathbf{a}\mathbf{a}^H \mathbf{D}_k\right\}$ are rank-one. Therefore, the $\mathscr{M}$-optimal code $\boldsymbol{a}$ is the solution to the following

maximization problem:

$$\begin{array}{ll} \max\limits_{\mathbf{a},\lambda_k} & \sum\limits_{k=1}^{N_r} \log(1+\lambda_k) \\ \text{subject to} & \lambda_k = \sigma_k^2 \boldsymbol{a}^H (\sigma_{\mathrm{c},k}^2 \mathbf{a}\mathbf{a}^H + \mathbf{M}_k)^{-1} \boldsymbol{a} \\ & \|\boldsymbol{a}\|_2^2 \leqslant e. \end{array} \tag{11.24}$$

11.3.2 Unified Framework

Herein we cast the optimization problems corresponding to various information-theoretic criteria discussed earlier under a unified optimization framework. Indeed, we consider the following general form of the optimization problems in (11.15), (11.18), (11.22), and (11.24):

$$\begin{array}{ll} \max\limits_{\mathbf{a},\lambda_k} & \sum\limits_{k=1}^{N_r} f_{\mathscr{I}}(\lambda_k) + g_{\mathscr{I}}(\lambda_k) \\ \text{subject to} & \lambda_k = \sigma_k^2 \boldsymbol{a}^H (\sigma_{\mathrm{c},k}^2 \mathbf{a}\mathbf{a}^H + \mathbf{M}_k)^{-1} \boldsymbol{a} \\ & \|\boldsymbol{a}\|_2^2 \leqslant e, \end{array} \tag{11.25}$$

where $\mathscr{I} \in \{\mathscr{B}, \mathscr{D}, \mathscr{J}, \mathscr{M}\}$, and $f_{\mathscr{I}}(.)$ and $g_{\mathscr{I}}(.)$ are concave and convex functions for any $\mathscr{I}$, respectively. More precisely, we have that

$$\begin{cases} f_{\mathscr{B}}(\lambda_k) = \log(1+0.5\lambda_k), & g_{\mathscr{B}}(\lambda_k) = -\frac{1}{2}\log(1+\lambda_k), \\ f_{\mathscr{D}}(\lambda_k) = \log(1+\lambda_k), & g_{\mathscr{D}}(\lambda_k) = \frac{1}{1+\lambda_k} - 1, \\ f_{\mathscr{J}}(\lambda_k) = 0, & g_{\mathscr{J}}(\lambda_k) = \frac{\lambda_k^2}{1+\lambda_k}, \\ f_{\mathscr{M}}(\lambda_k) = \log(1+\lambda_k), & g_{\mathscr{M}}(\lambda_k) = 0. \end{cases}$$

Remark 1: In the case of spatially wide-sense stationary (up to a power scale) signal-independent interferences, we have that $\mathbf{M}_k = \sigma_{w,k}^2 \widetilde{\boldsymbol{M}}$, $k = 1, 2, .., N_r$ (see e.g. [171]). In such a situation, a closed-form solution to the optimization problem (11.25) can be obtained. In particular, note that for any $\boldsymbol{M}_k$, a simplified expression of λ_k can be obtained using the matrix inversion lemma as:

$$\begin{aligned} \lambda_k &= \sigma_k^2 \boldsymbol{a}^H \left(\boldsymbol{M}_k^{-1} - \sigma_{\mathrm{c,k}}^2 \frac{\boldsymbol{M}_k^{-1} \mathbf{a}\mathbf{a}^H \boldsymbol{M}_k^{-1}}{1 + \sigma_{\mathrm{c,k}}^2 \mathbf{a}^H \boldsymbol{M}_k^{-1} \mathbf{a}} \right) \boldsymbol{a} \\ &= \frac{\sigma_k^2 \boldsymbol{a}^H \boldsymbol{M}_k^{-1} \boldsymbol{a}}{1 + \sigma_{\mathrm{c,k}}^2 \boldsymbol{a}^H \boldsymbol{M}_k^{-1} \boldsymbol{a}}. \end{aligned} \tag{11.26}$$

Therefore, one can recast (11.25) as the following optimization problem:

$$\begin{aligned} \max_{\mathbf{a}} \quad & \sum_{k=1}^{N_r} q_{\mathscr{I}}\left(\frac{\sigma_k^2 \boldsymbol{a}^H \boldsymbol{M}_k^{-1} \boldsymbol{a}}{1+\sigma_{\mathrm{c,k}}^2 \boldsymbol{a}^H \boldsymbol{M}_k^{-1} \boldsymbol{a}}\right) \\ \text{subject to} \quad & \|\boldsymbol{a}\|_2^2 \leq e, \end{aligned} \tag{11.27}$$

where $q_{\mathscr{I}}(.) = f_{\mathscr{I}}(.) + g_{\mathscr{I}}(.)$. Let $v_\star$ denote the optimal value of (11.27). We have that

$$v_\star \leq \sum_{k=1}^{N_r} q_{\mathscr{I}}(\widetilde{\boldsymbol{a}}_{k,\mathscr{I}}) \tag{11.28}$$

with $\widetilde{\boldsymbol{a}}_{k,\mathscr{I}}$ being the maximizer of $q_{\mathscr{I}}(.)$ subject to $\|\boldsymbol{a}\|^2 \leq e$ for fixed k. Now we claim that $\boldsymbol{a}_\star = \sqrt{e}\boldsymbol{u}$ with $\boldsymbol{u}$ being the minor eigenvector of $\widetilde{\boldsymbol{M}}$ is an optimal solution to the optimization problem in (11.27). To observe this fact, note that the $\boldsymbol{a}_\star$ maximizes λ_k, for any k, subject to the energy constraint because λ_k is an increasing function of $\boldsymbol{a}^H \boldsymbol{M}_k^{-1} \boldsymbol{a}$. Moreover, $q_{\mathscr{I}}(\lambda_k)$ is an increasing function of λ_k for all $\mathscr{I} \in \{\mathscr{B}, \mathscr{D}, \mathscr{J}, \mathscr{M}\}$ (see Appendix B) and hence $\widetilde{\boldsymbol{a}}_{k,\mathscr{I}} = \boldsymbol{a}_\star$ for all $k, \mathscr{I}$. Consequently, $\boldsymbol{a} = \boldsymbol{a}_\star$ yields the upper bound on $v_\star$ for all $\mathscr{I} \in \{\mathscr{B}, \mathscr{D}, \mathscr{J}, \mathscr{M}\}$. ■

We use the Majorization-Minimization (or Minorization-Maximization) techniques to tackle the non-convex problems in (11.25). Majorization-Minimization (MaMi) is an iterative technique that can be used for obtaining a solution to the general minimization problem [209] [239]:

$$\begin{aligned} \min_{\boldsymbol{z}} \quad & \widetilde{f}(\boldsymbol{z}) \\ \text{subject to} \quad & c(\boldsymbol{z}) \leq 0 \end{aligned} \tag{11.29}$$

where $\widetilde{f}(.)$ and $c(.)$ are non-convex functions. Each iteration (say the l^{th} iteration) of MaMi consists of two steps:

- Majorization Step: Finding $p^{(l)}(\boldsymbol{z})$ such that its minimization is simpler than that of $\widetilde{f}(\boldsymbol{z})$ and $p^{(l)}(\boldsymbol{z})$ majorizes $\widetilde{f}(\boldsymbol{z})$, i.e.,

$$\begin{aligned} p^{(l)}(\boldsymbol{z}) &\geq \widetilde{f}(\boldsymbol{z}), \ \forall \boldsymbol{z} \\ p^{(l)}\left(\boldsymbol{z}^{(l-1)}\right) &= \widetilde{f}\left(\boldsymbol{z}^{(l-1)}\right) \end{aligned} \tag{11.30}$$

  with $\boldsymbol{z}^{(l-1)}$ being the value of $\boldsymbol{z}$ at the $(l-1)^{th}$ iteration.
- Minimization Step: Solving the optimization problem,

$$\begin{aligned} \min_{\boldsymbol{z}} \quad & p^{(l)}(\boldsymbol{z}) \\ \text{subject to} \quad & c(\boldsymbol{z}) \leq 0. \end{aligned} \tag{11.31}$$

  to obtain $\boldsymbol{z}^{(l)}$.

Note that applying the Majorization-Minimization technique to the optimization problem in (11.29) decreases the value of the objective function $\widetilde{f}(\boldsymbol{z})$ at each iteration. Indeed, we have

$$\begin{aligned}\widetilde{f}\left(\boldsymbol{z}^{(l-1)}\right) = p^{(l)}\left(\boldsymbol{z}^{(l-1)}\right) &\geq p^{(l)}\left(\boldsymbol{z}^{(l)}\right) \\ &\geq \widetilde{f}\left(\boldsymbol{z}^{(l)}\right).\end{aligned} \tag{11.32}$$

The first inequality above follows from the minimization step in (11.31) and the second inequality holds true due to the majorization step in (11.30). The descent property in (11.32) guarantees the convergence of the sequence $\{\widetilde{f}(\boldsymbol{z}^{(l)})\}$ (assuming $\widetilde{f}(\boldsymbol{z})$ is bounded from below). Generally, the goodness of the obtained solution (i.e. $\boldsymbol{z}$ after the convergence) depends on the employed starting point. The optimality of the obtained solution $\boldsymbol{z}$ has been addressed in [209,239,240], where the solution $\boldsymbol{z}$ was shown to be a stationary point of $\widetilde{f}(\boldsymbol{z})$ (under some mild conditions). It is worth mentioning that a similar monotonically increasing behavior is guaranteed for Minorization-Maximization technique. Such a behavior of the values of the objective function is important when considering the objective as a measure of the code performance.

Remark 2: Note that the objective function $\sum_{k=1}^{N_r} q_{\mathscr{I}}(\lambda_k)$ in the problem (11.25) is bounded from above. To observe this fact, note that λ_k for all k can be upper bounded (considering (11.26)) as

$$\begin{aligned}\lambda_k = \frac{\sigma_k^2 \boldsymbol{a}^H \boldsymbol{M}_k^{-1} \boldsymbol{a}}{1+\sigma_{\mathrm{c},\mathrm{k}}^2 \boldsymbol{a}^H \boldsymbol{M}_k^{-1} \boldsymbol{a}} &\leq \frac{\sigma_k^2 \|\boldsymbol{a}\|_2^2 \mu_{max}(\boldsymbol{M}_k^{-1})}{1+\sigma_{\mathrm{c},\mathrm{k}}^2 \|\boldsymbol{a}\|_2^2 \mu_{min}(\boldsymbol{M}_k^{-1})} \\ &\leq \frac{\sigma_k^2 e\, \mu_{min}^{-1}(\boldsymbol{M}_k)}{1+\sigma_{\mathrm{c},\mathrm{k}}^2 e\, \mu_{max}^{-1}(\boldsymbol{M}_k)}.\end{aligned} \tag{11.33}$$

Due to the fact that $q_{\mathscr{I}}(\lambda_k)$ is a monotonically increasing function of λ_k for all k and $\mathscr{I}$ (see Appendix B), the above equation leads to an upper bound on the objective function in (11.25) for all k and $\mathscr{I}$. ■

In the following sections, we propose two novel algorithms based on MaMi to yield optimized solutions to (11.25).

11.4 Code Design using Successive Majorizations

In this section, we propose a novel algorithm based on successive majorizations (which we call Sv-MaMi) to obtain an optimal code $\boldsymbol{a}$. In particular, we apply successive majorizations to the optimization problem in (11.25) and show the following:

Theorem 1. *(Sv-MaMi algorithm) The solution $\boldsymbol{a} = \boldsymbol{a}_\star$ of (11.25) can be obtained iteratively by solving the following convex quadratically constrained*

quadratic program (QCQP) (at the $(l+1)^{th}$ iteration):

$$\begin{aligned} \min_{\mathbf{a}} \quad & \boldsymbol{a}^H \left(\sum_{k=1}^{N_r} \phi_{k,\mathscr{I}}^{(l)} \boldsymbol{M}_k^{-1} \right) \boldsymbol{a} - \Re \left(\left(\sum_{k=1}^{N_r} \boldsymbol{d}_{k,\mathscr{I}}^{(l)} \right)^H \boldsymbol{a} \right) \\ \textit{subject to} \quad & \|\boldsymbol{a}\|_2^2 \leqslant e, \end{aligned} \tag{11.34}$$

where the positive constant $\{\phi_{k,\mathscr{I}}^{(l)}\}$ and the vectors $\{\boldsymbol{d}_{k,\mathscr{I}}^{(l)}\}$ depend on $\mathscr{I} \in \{\mathscr{B}, \mathscr{D}, \mathscr{J}, \mathscr{M}\}$ and will be given below.

In the sequel, we provide a proof of Theorem 1. We begin by noting that the convex function $g_{\mathscr{I}}(.)$ can be minorized using its supporting hyperplane at any given $\lambda_k = \lambda_k^{(l)}$, viz.

$$g_{\mathscr{I}}(\lambda_k) \geq g_{\mathscr{I}}\left(\lambda_k^{(l)}\right) + g'_{\mathscr{I}}\left(\lambda_k^{(l)}\right)\left(\lambda_k - \lambda_k^{(l)}\right) \tag{11.35}$$

which implies that

$$\sum_{k=1}^{N_r} g_{\mathscr{I}}(\lambda_k) \geq \sum_{k=1}^{N_r} g_{\mathscr{I}}\left(\lambda_k^{(l)}\right) + \sum_{k=1}^{N_r} g'_{\mathscr{I}}\left(\lambda_k^{(l)}\right)\left(\lambda_k - \lambda_k^{(l)}\right). \tag{11.36}$$

Herein $\lambda_k^{(l)}$ denote the λ_k obtained at the l^{th} iteration and $g'_{\mathscr{I}}(.)$ denote the first-order derivative of $g_{\mathscr{I}}(.)$ for $\mathscr{I} \in \{\mathscr{B}, \mathscr{D}, \mathscr{J}, \mathscr{M}\}$.

Now observe that using (11.26), the optimal code $\boldsymbol{a} = \boldsymbol{a}_\star$ can be obtained in an iterative manner solving the following maximization at the $(l+1)^{th}$ iteration:

$$\max_{\mathbf{a},\lambda_k} \quad \sum_{k=1}^{N_r} f_{\mathscr{I}}(\lambda_k) + g'_{\mathscr{I}}\left(\lambda_k^{(l)}\right)\lambda_k \tag{11.37}$$

$$\text{subject to} \quad \lambda_k = \gamma_k - \frac{\gamma_k}{1 + \beta_k \boldsymbol{a}^H \boldsymbol{M}_k^{-1} \boldsymbol{a}} \tag{11.38}$$

$$\|\boldsymbol{a}\|_2^2 \leq e, \tag{11.39}$$

where $\gamma_k = \frac{\sigma_k^2}{\sigma_{\mathrm{c,k}}^2}$ and $\beta_k = \sigma_{\mathrm{c,k}}^2$. Note that the above problem is non-convex due to the non-affine equality constraint (11.38).

The following Lemmas pave the way toward the derivation of the convex QCQPs of Theorem 1 corresponding to $\mathscr{I} \in \{\mathscr{B}, \mathscr{D}, \mathscr{J}, \mathscr{M}\}$.

Lemma 1. *If $f(x)$ is twice differentiable and if there exists $U > 0$ such that $f''(x) \leq U$ for all x, then for any given $\tilde{x}$, the convex quadratic function*

$$f(\tilde{x}) + f'(\tilde{x})(x - \tilde{x}) + \frac{1}{2}U(x - \tilde{x})^2 \tag{11.40}$$

majorizes f at $\tilde{x}$.

Proof: See [239, Section 3.4]. ■

Lemma 2. *Let $f(x)$ be an even function (i.e. $f(x) = f(-x)$ for all $x \in \mathbb{R}$), and assume that $\frac{f'(x)}{x}$ is decreasing over the interval $[0,\infty)$. Then the function*

$$f(\tilde{x}) + \frac{f'(\tilde{x})}{2\tilde{x}}(x^2 - \tilde{x}^2) \tag{11.41}$$

majorizes f at $\tilde{x}$.

Proof: See [241, Theorem 4.5]. ■

Lemma 3. *Let $f(x) = -\log(1+\mu - \frac{\mu}{1+\eta x^2})$ for some $\mu, \eta > 0$. Then for all $x, \tilde{x} \in \mathbb{R}$ we have that*

$$f(x) \leq f(\tilde{x}) + \frac{\eta}{1+\eta\tilde{x}^2}(x^2 - \tilde{x}^2) - \frac{2\eta\tilde{x}(1+\mu)}{1+\eta(1+\mu)\tilde{x}^2}(x-\tilde{x}) + \eta(1+\mu)(x-\tilde{x})^2.$$

Proof: We can rewrite $f(x)$ as

$$f(x) = \log(1+\eta x^2) - \log(1+\eta x^2 + \mu\eta x^2). \tag{11.42}$$

The first term satisfies the conditions in Lemma 11.4 and hence its majorizer is given by

$$\log(1+\eta x^2) \leq \log(1+\eta\tilde{x}^2) + \frac{\eta}{1+\eta\tilde{x}^2}(x^2 - \tilde{x}^2).$$

Moreover, let $f_2(x) = -\log(1+\eta x^2 + \mu\eta x^2)$. It is straightforward to verify that

$$\begin{aligned} f_2''(x) &= \frac{4\eta^2(1+\mu)^2x^2 - 2\eta(1+\mu)(1+\eta x^2(1+\mu))}{1+\eta^2(1+\mu)^2x^4 + 2\eta(1+\mu)x^2} \\ &\leq 2\eta(1+\mu)\frac{2\eta(1+\mu)x^2}{1+2\eta(1+\mu)x^2} \leq 2\eta(1+\mu). \end{aligned}$$

Consequently, $f_2(x)$ can be majorized using Lemma 11.4, and hence the proof is concluded. ■

- **Bhattacharyya distance:** For $\mathscr{I} = \mathscr{B}$, substituting $\{\lambda_k\}$ of (11.38) into the objective function of (11.37) leads to the following expression for the objective function:

$$\sum_{k=1}^{N_r}\left[\log\left(1 + 0.5\gamma_k - 0.5\frac{\gamma_k}{1+\beta_k \boldsymbol{a}^H \boldsymbol{M}_k^{-1}\boldsymbol{a}}\right) + \frac{0.5}{1+\lambda_k^{(l)}}\left(\frac{\gamma_k}{1+\beta_k \boldsymbol{a}^H \boldsymbol{M}_k^{-1}\boldsymbol{a}}\right)\right] \tag{11.43}$$

where

$$\lambda_k^{(l)} \quad = \quad \gamma_k - \frac{\gamma_k}{1+\beta_k y_k^{(l)}}. \tag{11.44}$$

A minorizer of the logarithmic term can be obtained immediately by employing Lemma 11.4 with $x_k = \sqrt{\boldsymbol{a}^H \boldsymbol{M}_k^{-1} \boldsymbol{a}}$, $\mu = 0.5\gamma_k$, and $\eta = \beta_k$. To deal with the expression $\frac{\gamma_k}{1+\beta_k \boldsymbol{a}^H \boldsymbol{M}_k^{-1} \boldsymbol{a}}$ in (11.43) conveniently, we use the convexity of the function $\frac{1}{1+\beta x}$ for $\beta > 0$ which implies

$$\frac{1}{1+\beta x} \geq \frac{1}{1+\beta \tilde{x}} - \frac{\beta}{(1+\beta \tilde{x})^2}(x - \tilde{x}), \quad \forall\, x, \tilde{x}. \tag{11.45}$$

As a result, a minorizer of $\frac{\gamma_k}{1+\beta_k \boldsymbol{a}^H \boldsymbol{M}_k^{-1} \boldsymbol{a}}$ can be obtained by considering the above inequality for $x_k = \boldsymbol{a}^H \boldsymbol{M}_k^{-1} \boldsymbol{a}$ and $\beta = \beta_k$. Furthermore, by replacing the summation terms in (11.43) for each k with the obtained minorizers (using Lemma 11.4 and eq. (11.45)) and removing the constants, the criterion in (11.43) turns to:

$$\sum_{k=1}^{N_r} \Bigg[- \left(\frac{\beta_k}{1+\beta_k y_k^{(l)}} + \beta_k(1+0.5\gamma_k) + \frac{0.5\gamma_k}{1+\lambda_k^{(l)}} \, \frac{\beta_k}{(1+\beta_k y_k^{(l)})^2} \right) \boldsymbol{a}^H \boldsymbol{M}_k^{-1} \boldsymbol{a}$$
$$+ \left(\frac{2\beta_k(1+0.5\gamma_k)\sqrt{y_k^{(l)}}}{1+\beta_k y_k^{(l)}(1+0.5\gamma_k)} + 2\beta_k(1+0.5\gamma_k)\sqrt{y_k^{(l)}} \right) \sqrt{\boldsymbol{a}^H \boldsymbol{M}_k^{-1} \boldsymbol{a}} \Bigg] \tag{11.46}$$

where

$$y_k^{(l)} = (\boldsymbol{a}^{(l)})^H \boldsymbol{M}_k^{-1} \boldsymbol{a}^{(l)}. \tag{11.47}$$

Yet, due to the non-concavity of the terms $\left\{ \sqrt{\boldsymbol{a}^H \boldsymbol{M}_k^{-1} \boldsymbol{a}} \right\}$, dealing with the maximization of the criterion in (11.46) appears to be complicated. However, $\sqrt{\boldsymbol{a}^H \boldsymbol{M}_k^{-1} \boldsymbol{a}}$ can be minorized using its supporting hyperplane at any given $\tilde{\boldsymbol{a}}$; more precisely,

$$\sqrt{\boldsymbol{a}^H \boldsymbol{M}_k^{-1} \boldsymbol{a}} \geq \sqrt{\tilde{\boldsymbol{a}}^H \boldsymbol{M}_k^{-1} \tilde{\boldsymbol{a}}} + \Re \left(\frac{\tilde{\boldsymbol{a}}^H \boldsymbol{M}_k^{-1}}{\sqrt{\tilde{\boldsymbol{a}}^H \boldsymbol{M}_k^{-1} \tilde{\boldsymbol{a}}}} (\boldsymbol{a} - \tilde{\boldsymbol{a}}) \right). \tag{11.48}$$

The above inequality holds true due to the convexity of the function $h(\mathbf{x}) = \|\mathbf{x}\|_2$ and the fact that the gradient of $h(\mathbf{x})$ is given by $\nabla h(\mathbf{x}) = \frac{\mathbf{x}}{\|\mathbf{x}\|_2}$. Ultimately, by using eq. (11.46) and (11.48) as well as removing the constants, the optimization problem associated with the $(l+1)^{th}$ iteration of Sv-MaMi

for $\mathscr{I} = \mathscr{B}$ is as follows:

$$\begin{aligned} \min_{\mathbf{a}} \quad & \boldsymbol{a}^H \left(\sum_{k=1}^{N_r} \phi_{k,\mathscr{B}}^{(l)} \boldsymbol{M}_k^{-1} \right) \boldsymbol{a} - \Re \left(\left(\sum_{k=1}^{N_r} \boldsymbol{d}_{k,\mathscr{B}}^{(l)} \right)^H \boldsymbol{a} \right) \\ \text{subject to} \quad & \|\boldsymbol{a}\|_2^2 \leqslant e, \end{aligned} \tag{11.49}$$

where

$$\begin{aligned} \phi_{k,\mathscr{B}}^{(l)} &\triangleq \left(\frac{\beta_k}{1+\beta_k y_k^{(l)}} + \beta_k(1+0.5\gamma_k) + \frac{0.5\gamma_k}{1+\lambda_k^{(l)}} \, \frac{\beta_k}{(1+\beta_k y_k^{(l)})^2} \right) \\ \boldsymbol{d}_{k,\mathscr{B}}^{(l)} &\triangleq \left(\frac{2\beta_k(1+0.5\gamma_k)}{1+\beta_k y_k^{(l)}(1+0.5\gamma_k)} + 2\beta_k(1+0.5\gamma_k) \right) \boldsymbol{M}_k^{-1} \boldsymbol{a}^{(l)}. \end{aligned} \tag{11.50}$$

Note that as $\phi_{k,\mathscr{B}}^{(l)} > 0$ and $\boldsymbol{M}_k \succ \mathbf{0}$, the above problem is a convex QCQP.

- **KL-Divergence:** In the case of $\mathscr{I} = \mathscr{D}$, using (11.37) and (11.38) (and dropping the constants) leads to the following expression for the corresponding objective function:

$$\sum_{k=1}^{N_r} \left[\log \left(1 + \gamma_k - \frac{\gamma_k}{1+\beta_k \boldsymbol{a}^H \boldsymbol{M}_k^{-1} \boldsymbol{a}} \right) + \left(\frac{1}{1+\lambda_k^{(l)}} \right)^2 \left(\frac{\gamma_k}{1+\beta_k \boldsymbol{a}^H \boldsymbol{M}_k^{-1} \boldsymbol{a}} \right) \right]. \tag{11.51}$$

The logarithmic term in (11.51) can be handled via Lemma 11.4 by setting $x_k = \sqrt{\boldsymbol{a}^H \boldsymbol{M}_k^{-1} \boldsymbol{a}}, \mu = \gamma_k$, and $\eta = \beta_k$. Moreover, the expression $\frac{\gamma_k}{1+\beta_k \boldsymbol{a}^H \boldsymbol{M}_k^{-1} \boldsymbol{a}}$ can be minorized using (11.48). Consequently, using a similar approach as in the case of the Bhattacharrya distance, the optimization problem associated with the $(l+1)^{th}$ iteration of Sv-MaMi for $\mathscr{I} = \mathscr{D}$ is given by:

$$\begin{aligned} \min_{\mathbf{a}} \quad & \boldsymbol{a}^H \left(\sum_{k=1}^{N_r} \phi_{k,\mathscr{D}}^{(l)} \boldsymbol{M}_k^{-1} \right) \boldsymbol{a} - \Re \left(\left(\sum_{k=1}^{N_r} \boldsymbol{d}_{k,\mathscr{D}}^{(l)} \right)^H \boldsymbol{a} \right) \\ \text{subject to} \quad & \|\boldsymbol{a}\|_2^2 \leqslant e, \end{aligned} \tag{11.52}$$

where

$$\begin{aligned} \phi_{k,\mathscr{D}}^{(l)} &\triangleq \left(\frac{\beta_k}{1+\beta_k y_k^{(l)}} + \beta_k(1+\gamma_k) + \left(\frac{\gamma_k}{1+\lambda_k^{(l)}} \right)^2 \left(\frac{\beta_k}{(1+\beta_k y_k^{(l)})^2} \right) \right) \\ \boldsymbol{d}_{k,\mathscr{D}}^{(l)} &\triangleq \left(\frac{2\beta_k(1+\gamma_k)}{1+\beta_k y_k^{(l)}(1+\gamma_k)} + 2\beta_k(1+\gamma_k) \right) \boldsymbol{M}_k^{-1} \boldsymbol{a}^{(l)}. \end{aligned}$$

• **J-Divergence:** In this case, (11.37) boils down to the following non-convex optimization problem:

$$\begin{aligned} \min_{\mathbf{a}} \quad & \sum_{k=1}^{N_r} \gamma_k w_k^{(l)} \left(\frac{1}{1+\beta_k \boldsymbol{a}^H \boldsymbol{M}_k^{-1} \boldsymbol{a}} \right) \\ \text{subject to} \quad & \|\boldsymbol{a}\|_2^2 \leq e, \end{aligned} \tag{11.53}$$

with $w_k^{(l)} = 1 - \frac{1}{(1+\lambda_k^{(l)})^2} > 0$. Note that in contrast to the case of Bhattacharyya distance and KL-divergence (see eqs. (11.43) and (11.51)), the expression $\frac{1}{1+\beta_k \boldsymbol{a}^H \boldsymbol{M}_k^{-1} \boldsymbol{a}}$ appears in a *minimization* problem. We consider a majorization of the function $\frac{1}{1+\eta x^2}$ (note that $\frac{1}{1+\eta x^2} = \frac{1}{1+\beta_k \boldsymbol{a}^H \boldsymbol{M}_k^{-1} \boldsymbol{a}}$ when $x_k = \sqrt{\boldsymbol{a}^H \boldsymbol{M}_k^{-1} \boldsymbol{a}}$, $\eta = \beta_k$). One can derive a majorizer for the aforementioned function via Lemma 11.4, viz.

$$\frac{1}{1+\eta x^2} \leq \frac{1}{1+\eta \tilde{x}^2} - \frac{2\eta \tilde{x}}{(1+\eta \tilde{x}^2)^2}(x-\tilde{x}) + \frac{1}{2} U (x-\tilde{x})^2. \tag{11.54}$$

Note that we have

$$\frac{d^2}{dx^2}\left(\frac{1}{1+\eta x^2} \right) = \frac{6\eta^2 x^2 - 2\eta}{(1+\eta x^2)^3} \leq 6\eta$$

which implies that (11.54) holds true for $U = 6\eta$. Therefore, by minorizing $\sqrt{\boldsymbol{a}^H \boldsymbol{M}_k^{-1} \boldsymbol{a}}$ using (11.48), the following QCQP is obtained for the $(l+1)^{th}$ iteration of Sv-MaMi for $\mathscr{I} = \mathscr{J}$:

$$\begin{aligned} \min_{\mathbf{a}} \quad & \boldsymbol{a}^H \left(\sum_{k=1}^{N_r} \phi_{k,\mathscr{J}}^{(l)} \boldsymbol{M}_k^{-1} \right) \boldsymbol{a} - \Re \left(\left(\sum_{k=1}^{N_r} \boldsymbol{d}_{k,\mathscr{J}}^{(l)} \right)^H \boldsymbol{a} \right) \\ \text{subject to} \quad & \|\boldsymbol{a}\|_2^2 \leqslant e, \end{aligned} \tag{11.55}$$

where

$$\begin{aligned} \phi_{k,\mathscr{J}}^{(l)} &\triangleq 3\beta_k \gamma_k w_k^{(l)} \\ \boldsymbol{d}_{k,\mathscr{J}}^{(l)} &\triangleq \left(\frac{2\beta_k \gamma_k w_k^{(l)}}{(1+\beta_k y_k^{(l)})^2} + 6\beta_k \right) \boldsymbol{M}_k^{-1} \boldsymbol{a}^{(l)}. \end{aligned} \tag{11.56}$$

• **Mutual Information:** The derivation of the QCQP corresponding to $\mathscr{I} = \mathscr{M}$ is straightforward. In particular, using Lemma 11.4 as well as (11.48) we obtain the following QCQP:

$$\begin{aligned} \min_{\mathbf{a}} \quad & \boldsymbol{a}^H \left(\sum_{k=1}^{N_r} \phi_{k,\mathscr{M}}^{(l)} \boldsymbol{M}_k^{-1} \right) \boldsymbol{a} - \Re \left(\left(\sum_{k=1}^{N_r} \boldsymbol{d}_{k,\mathscr{M}}^{(l)} \right)^H \boldsymbol{a} \right) \\ \text{subject to} \quad & \|\boldsymbol{a}\|_2^2 \leqslant e, \end{aligned} \tag{11.57}$$

Table 11.1. *The Sv-MaMi Algorithm for* $\mathscr{I} \in \{\mathscr{B}, \mathscr{D}, \mathscr{J}, \mathscr{M}\}$

Step 0: Initialize $\boldsymbol{a}$ with a random vector in $\mathbb{C}^N$ and set the iteration number l to 0.
Step 1: Solve the QCQP problem in (11.34) to obtain $\boldsymbol{a}^{(l+1)}$; set $l \leftarrow l+1$.
Step 2: Compute $\phi_{k,\mathscr{I}}^{(l)}$ and $\boldsymbol{d}_{k,\mathscr{I}}^{(l)}$ corresponding to the metric $\mathscr{I}$.
Step 3: Repeat steps 1 and 2 until a pre-defined stop criterion is satisfied, e.g. $\|\boldsymbol{a}^{(l+1)} - \boldsymbol{a}^{(l)}\|_2 \leq \xi$ for some $\xi > 0$.

where

$$\begin{aligned} \phi_{k,\mathscr{M}}^{(l)} &\triangleq \left(\frac{\beta_k}{1+\beta_k y_k^{(l)}} + \beta_k(1+\gamma_k) \right) \\ \boldsymbol{d}_{k,\mathscr{M}}^{(l)} &\triangleq \left(\frac{2\beta_k(1+\gamma_k)}{1+\beta_k y_k^{(l)}(1+\gamma_k)} + 2\beta_k(1+\gamma_k) \right) \boldsymbol{M}_k^{-1} \boldsymbol{a}^{(l)}. \end{aligned} \tag{11.58}$$

Table 11.1 summarizes the steps of Sv-MaMi. Note that the convex QCQP of the first step can be solved very efficiently (see e.g. [195]). Moreover, the derivations of Sv-MaMi algorithm can be extended to tackle code design problems in which a PAR-constrained code is required. Such an extension is discussed in Section VI.

Remark 3 (Saturation Phenomenon): It might be of interest to investigate the behavior of the considered information-theoretic criteria when the transmit energy e grows large. Let $\bar{\boldsymbol{a}}$ represent the unit-norm version of $\boldsymbol{a}$ (i.e. $\boldsymbol{a} = \sqrt{e}\,\bar{\boldsymbol{a}}$) and note that:

$$\lim_{e\to\infty} q_{\mathscr{I}} \left(\gamma_k - \frac{\gamma_k}{1 + e\beta_k \bar{\boldsymbol{a}}^H \boldsymbol{M}_k^{-1} \bar{\boldsymbol{a}}} \right) = q_{\mathscr{I}}(\gamma_k). \tag{11.59}$$

In light of the above equality, one can observe that all information-theoretic criteria $q_{\mathscr{I}}$ for $\mathscr{I} \in \{\mathscr{B}, \mathscr{D}, \mathscr{J}, \mathscr{M}\}$ tend to constant values in $\mathbb{R}_+$ as $e \to \infty$. We refer to this behavior of the considered metrics as the saturation phenomenon, meaning that for sufficiently large values of the transmit energy e, the performance improvement obtained by choosing $\boldsymbol{a}$ or by increasing e is negligible. Interestingly, it might still be reasonable to increase the transmit energy of the system. Indeed our previous arguments rely on the fact that a fixed radar cell is considered; however, increasing e extends the detection range (or coverage) of the system. ■

11.5 Code Design using MaMi and Relaxation

In this section, we propose another algorithm based on MaMi to tackle the optimization problems formulated in (11.25). The suggested algorithm (which

we call Re-MaMi) employs a relaxation of the rank constraint on the code matrix $\boldsymbol{A} = \boldsymbol{a}\boldsymbol{a}^H$ such that each iteration of MaMi can be handled as a convex optimization problem. In particular, we have the following result:

Theorem 2. *(Re-MaMi algorithm) The solution code matrix $\boldsymbol{A} = \boldsymbol{A}_\star$ (with relaxed rank constraint) can be obtained iteratively by solving the following convex problem (at the $(l+1)^{th}$ iteration):*

$$\begin{aligned} \max_{\mathbf{A}} \quad & \sum_{k=1}^{N_r} \left[f_{\mathscr{I}}\left(N\gamma_k - \gamma_k \operatorname{tr}\{(\boldsymbol{M}_k + \beta_k \boldsymbol{A})^{-1}\boldsymbol{M}_k\}\right) + h_{k,\mathscr{I}}^{(l)}(\boldsymbol{A}) \right] \\ \textit{subject to} \quad & \operatorname{tr}\{\boldsymbol{A}\} \leqslant e \\ & \boldsymbol{A} \succeq \boldsymbol{0}, \end{aligned} \tag{11.60}$$

where $h_{k,\mathscr{I}}^{(l)}(\boldsymbol{A})$ denotes a concave function of $\boldsymbol{A}$, for $\mathscr{I} \in \{\mathscr{B}, \mathscr{D}, \mathscr{J}, \mathscr{M}\}$, that will be given in explicit form below.

In what follows, we present a proof of Theorem 2 and then discuss the synthesis of optimized $\boldsymbol{a}_\star$ from the obtained $\boldsymbol{A}_\star$. First note that using matrix inversion lemma, λ_k can be rewritten as

$$\begin{aligned} \lambda_k &= \sigma_k^2 \boldsymbol{a}^H (\sigma_{c,k}^2 \boldsymbol{a}\boldsymbol{a}^H + \boldsymbol{M}_k)^{-1}\boldsymbol{a} = \sigma_k^2 \operatorname{tr}\{(\sigma_{c,k}^2 \boldsymbol{a}\boldsymbol{a}^H + \boldsymbol{M}_k)^{-1}\boldsymbol{a}\boldsymbol{a}^H\} \qquad (11.61) \\ &= \sigma_k^2 \operatorname{tr}\{(\sigma_{c,k}^2 \boldsymbol{A} + \boldsymbol{M}_k)^{-1}\boldsymbol{A}\} = \frac{\sigma_k^2}{\sigma_{c,k}^2} \operatorname{tr}\{\boldsymbol{I} - (\boldsymbol{I} + \sigma_{c,k}^2 \boldsymbol{M}_k^{-1}\boldsymbol{A})^{-1}\} \\ &= N\frac{\sigma_k^2}{\sigma_{c,k}^2} - \frac{\sigma_k^2}{\sigma_{c,k}^2} \operatorname{tr}\{(\boldsymbol{M}_k + \sigma_{c,k}^2 \boldsymbol{A})^{-1}\boldsymbol{M}_k\} \triangleq N\gamma_k - \gamma_k \operatorname{tr}\{(\boldsymbol{M}_k + \beta_k \boldsymbol{A})^{-1}\boldsymbol{M}_k\} \end{aligned}$$

where $\boldsymbol{A} = \boldsymbol{a}\boldsymbol{a}^H$. As a result, using (11.61) and (11.36), the optimal code matrix $\boldsymbol{A} = \boldsymbol{A}_\star$ can be obtained iteratively via solving the following optimization problem at the $(l+1)^{th}$ iteration:

$$\max_{\mathbf{A}, \lambda_k} \quad \sum_{k=1}^{N_r} f_{\mathscr{I}}(\lambda_k) + g'_{\mathscr{I}}\left(\lambda_k^{(l)}\right) \lambda_k \tag{11.62}$$

$$\text{subject to} \quad \lambda_k = N\gamma_k - \gamma_k \operatorname{tr}\left\{(\boldsymbol{M}_k + \beta_k \boldsymbol{A})^{-1}\boldsymbol{M}_k\right\} \tag{11.63}$$

$$\operatorname{tr}\{\boldsymbol{A}\} \leqslant e \tag{11.64}$$

$$\boldsymbol{A} \succeq \boldsymbol{0} \tag{11.65}$$

$$\operatorname{rank}(\boldsymbol{A}) = 1. \tag{11.66}$$

Note that the above problem is non-convex due to the non-affine equality constraints in (11.63) and (11.66). Hereafter, we relax the rank-one constraint (11.66). Moreover, when the term $\left\{g'_{\mathscr{I}}\left(\lambda_k^{(l)}\right)\lambda_k\right\}$ is not concave (with respect to $\boldsymbol{A}$), a further minorization will be needed in order to make the problem convex. Let $h_{k,\mathscr{I}}^{(l)}(\boldsymbol{A})$ (to be discussed shortly) denote a concave function

that minorizes $g'_{\mathscr{I}}\left(\lambda_k^{(l)}\right)\lambda_k$ (we let $h_{k,\mathscr{I}}^{(l)} = g'_{\mathscr{I}}\left(\lambda_k^{(l)}\right)\lambda_k$ when $g'_{\mathscr{I}}\left(\lambda_k^{(l)}\right)\lambda_k$ is concave itself).

Remark 4: Note that for $\boldsymbol{A} \succeq \boldsymbol{0}$ of rank δ, there exists a $\boldsymbol{V} \in \mathbb{C}^{N\times\delta}$ such that $\boldsymbol{A} = \boldsymbol{V}\boldsymbol{V}^H$. As a result, considering (11.61) we have

$$\begin{aligned} N\gamma_k - \gamma_k \operatorname{tr}\{(\boldsymbol{M}_k + \beta_k\boldsymbol{A})^{-1}\boldsymbol{M}_k\} &= \sigma_k^2 \operatorname{tr}\{(\sigma_{c,k}^2\boldsymbol{A} + \boldsymbol{M}_k)^{-1}\boldsymbol{A}\} \\ &= \sigma_k^2 \operatorname{tr}\{\boldsymbol{V}^H(\sigma_{c,k}^2\boldsymbol{A} + \boldsymbol{M}_k)^{-1}\boldsymbol{V}\} > 0 \end{aligned}$$

which implies that the argument of the function $f_{\mathscr{I}}(.)$ in (11.62) remains positive even in the case in which no rank constraint on $\boldsymbol{A}$ is imposed. Moreover, note that $\operatorname{tr}\{(\boldsymbol{M}_k + \beta_k\boldsymbol{A})^{-1}\boldsymbol{M}_k\}$ is a convex function of $\boldsymbol{A}$. Consequently, $f_{\mathscr{I}}\left(N\gamma_k - \gamma_k \operatorname{tr}\{(\boldsymbol{M}_k + \beta_k\boldsymbol{A})^{-1}\boldsymbol{M}_k\}\right)$ is a concave function of $\boldsymbol{A}$ as $f_{\mathscr{I}}(.)$ is an increasing function (for all $\mathscr{I}$). ■

Selecting a suitable function $h_{k,\mathscr{I}}^{(l)}(\boldsymbol{A})$ depends on the code design metric:

• **Bhattacharyya distance:** By substituting λ_k of (11.63) as well as $g'_{\mathscr{B}}\left(\lambda_k^{(l)}\right)$, the objective function in (11.62) for $\mathscr{I} = \mathscr{B}$ can be rewritten (by omitting constants) as

$$\begin{aligned} &\sum_{k=1}^{N_r}\Big[\log\left(1 + 0.5N\gamma_k - 0.5\gamma_k \operatorname{tr}\{(\boldsymbol{M}_k + \beta_k\boldsymbol{A})^{-1}\boldsymbol{M}_k\}\right) \\ &+ \frac{0.5\gamma_k}{1+\lambda_k^{(l)}} \operatorname{tr}\{(\boldsymbol{M}_k + \beta_k\boldsymbol{A})^{-1}\boldsymbol{M}_k\}\Big] \end{aligned}$$

where $\lambda_k^{(l)} = N\gamma_k - \gamma_k \operatorname{tr}\{(\boldsymbol{M}_k + \beta_k\boldsymbol{A}^{(l)})^{-1}\boldsymbol{M}_k\}$ with $\boldsymbol{A}^{(l)}$ being the $\boldsymbol{A}$ obtained at the l^{th} iteration. As mentioned in Remark 4 the logarithmic term is concave; however, the second term is convex with respect to (w.r.t.) $\boldsymbol{A}$, and hence a minorization is needed to tackle the problem.

Lemma 4. *Let $h(\boldsymbol{A}) = \operatorname{tr}\{(\boldsymbol{M}_k + \beta_k\boldsymbol{A})^{-1}\boldsymbol{M}_k\}$. A minorizer of $h(\boldsymbol{A})$ at $\boldsymbol{A} = \tilde{\boldsymbol{A}}$ is given by*

$$\tilde{h}(\boldsymbol{A}) = \operatorname{tr}\{(\boldsymbol{M}_k + \beta_k\tilde{\boldsymbol{A}})^{-1}\boldsymbol{M}_k\} - \beta_k \operatorname{tr}\{(\boldsymbol{M}_k + \beta_k\tilde{\boldsymbol{A}})^{-1}\boldsymbol{M}_k(\boldsymbol{M}_k + \beta_k\tilde{\boldsymbol{A}})^{-1}(\boldsymbol{A} - \tilde{\boldsymbol{A}})\}.$$

Proof: See Appendix C. ■

By applying Lemma 11.5 to (11.67), we can recast the maximization step at the $(l+1)^{th}$ iteration of Re-MaMi for $\mathscr{I} = \mathscr{B}$ as follows:

$$\begin{aligned} \max_{\mathbf{A}} \quad & \sum_{k=1}^{N_r}\left[\log\left(1 + 0.5N\gamma_k - 0.5\gamma_k \operatorname{tr}\{(\boldsymbol{M}_k + \beta_k\boldsymbol{A})^{-1}\boldsymbol{M}_k\}\right) + h_{k,\mathscr{B}}^{(l)}(\boldsymbol{A})\right] \\ \text{subject to} \quad & \operatorname{tr}\{\boldsymbol{A}\} \leqslant e \qquad (11.67) \\ & \boldsymbol{A} \succeq \boldsymbol{0}, \end{aligned}$$

where

$$h^{(l)}_{k,\mathscr{B}}(\boldsymbol{A}) \triangleq -\operatorname{tr}\left\{\boldsymbol{F}^{(l)}_{k,\mathscr{B}}\boldsymbol{A}\right\}, \tag{11.68}$$
$$\boldsymbol{F}^{(l)}_{k,\mathscr{B}} \triangleq \frac{0.5\,\gamma_k\beta_k}{1+\lambda^{(l)}_k}\left(\boldsymbol{M}_k+\beta_k\boldsymbol{A}^{(l)}\right)^{-1}\boldsymbol{M}_k\left(\boldsymbol{M}_k+\beta_k\boldsymbol{A}^{(l)}\right)^{-1}.$$

• **KL-divergence:** By substituting λ_k and $g'_{\mathscr{D}}(\lambda^{(l)}_k)$ in (11.62), it can be easily verified that (11.62) includes the expression $\operatorname{tr}\{(\boldsymbol{M}_k+\beta_k\boldsymbol{A})^{-1}\boldsymbol{M}_k\}$ with positive sign. Therefore, similar to the case of Bhattacharyya distance, the following convex problem can be derived (using Lemma 11.5) at the $(l+1)^{th}$ iteration of Re-MaMi for $\mathscr{I}=\mathscr{D}$:

$$\begin{aligned}\max_{\mathbf{A}} \quad & \sum_{k=1}^{N_r}\left[\log\left(1+N\gamma_k-\gamma_k\operatorname{tr}\{(\boldsymbol{M}_k+\beta_k\boldsymbol{A})^{-1}\boldsymbol{M}_k\}\right)+h^{(l)}_{k,\mathscr{D}}(\boldsymbol{A})\right]\\ \text{subject to} \quad & \operatorname{tr}\{\boldsymbol{A}\}\leqslant e\\ & \boldsymbol{A}\succeq\mathbf{0},\end{aligned} \tag{11.69}$$

where

$$\begin{aligned}h^{(l)}_{k,\mathscr{D}}(\boldsymbol{A}) &\triangleq -\operatorname{tr}\left\{\boldsymbol{F}^{(l)}_{k,\mathscr{D}}\boldsymbol{A}\right\},\\ \boldsymbol{F}^{(l)}_{k,\mathscr{D}} &\triangleq \frac{\gamma_k\beta_k}{\left(1+\lambda^{(l)}_k\right)^2}\left(\boldsymbol{M}_k+\beta_k\boldsymbol{A}^{(l)}\right)^{-1}\boldsymbol{M}_k\left(\boldsymbol{M}_k+\beta_k\boldsymbol{A}^{(l)}\right)^{-1}\end{aligned} \tag{11.70}$$

• **J-divergence:** For the case of $\mathscr{I}=\mathscr{J}$, the relaxed version of the maximization in (11.62)-(11.66) is equivalent to the optimization problem:

$$\begin{aligned}\min_{\mathbf{A}} \quad & \sum_{k=1}^{N_r}\gamma_k w^{(l)}_k\operatorname{tr}\left\{(\boldsymbol{M}_k+\beta_k\boldsymbol{A})^{-1}\boldsymbol{M}_k\right\}\\ \text{subject to} \quad & \operatorname{tr}\{\boldsymbol{A}\}\leqslant e\\ & \boldsymbol{A}\succeq\mathbf{0},\end{aligned} \tag{11.71}$$

where $w^{(l)}_k = 1-(\frac{1}{1+\lambda^{(l)}_k})^2$ and $h^{(l)}_{k,\mathscr{J}} = -\gamma_k w^{(l)}_k\operatorname{tr}\left\{(\boldsymbol{M}_k+\beta_k\boldsymbol{A})^{-1}\boldsymbol{M}_k\right\}$.

Note that Remark 4 ensures that $w^{(l)}_k>0$ for all (k,l), and hence (11.71) is a convex optimization problem due to the convexity of $\operatorname{tr}\{\boldsymbol{X}^{-1}\}$ w.r.t. $\boldsymbol{X}\succ\mathbf{0}$. Note also that the optimization problem in (11.71) can be recast as a semi-definite program (SDP) by considering an SDP representation of the $\operatorname{tr}\{\boldsymbol{X}^{-1}\}$ minimization (see e.g. [167]).

• **Mutual information:** Using the relaxation of the rank-one constraint for the case of $\mathscr{I}=\mathscr{M}$, one obtains the following form of the optimization

problem in (11.62)-(11.66):

$$\begin{aligned} \max_{\mathbf{A}} \quad & \sum_{k=1}^{N_r} \log\left(1+N\gamma_k-\gamma_k \operatorname{tr}\{(\boldsymbol{M}_k+\beta_k\boldsymbol{A})^{-1}\boldsymbol{M}_k\}\right) \\ \text{subject to} \quad & \operatorname{tr}\{\boldsymbol{A}\} \leqslant e \\ & \boldsymbol{A} \succeq \boldsymbol{0}. \end{aligned} \tag{11.72}$$

Note that the above relaxed version of the optimization in (11.62)-(11.66) is a convex problem that can be solved in one iteration of Re-MaMi (as no majorization is required, i.e. $h^{(l)}_{k,\mathscr{M}}(\boldsymbol{A})=0$).

We end this section by discussing the synthesis stage required for Re-MaMi. Once the proposed Re-MaMi algorithm converges to $\boldsymbol{A}_\star$, the corresponding code $\boldsymbol{a}_\star$ can be obtained as follows. If $\operatorname{rank}(\boldsymbol{A}_\star)=1$, the local optimum obtained for the relaxed problem in (11.60) yields a local optimum of (11.25) via $\boldsymbol{A}_\star=\boldsymbol{a}_\star\boldsymbol{a}_\star^H$. Otherwise, a synthesis loss is unavoidable due to the rank of $\boldsymbol{A}_\star$ being larger than 1. The rank behavior of the matrix obtained from the relaxed problem and the associated rank-one approximations have been discussed in the literature particularly for semi-definite relaxations (see e.g. [212, 213] and references therein). Least-squares (LS) synthesis is a common approach to synthesize the optimized codes [212]. The LS criterion can be formulated as:

$$\min_{\boldsymbol{a}} \ \|\boldsymbol{A}_\star-\boldsymbol{a}\boldsymbol{a}^H\|_F^2 \ \text{ subject to } \ \|\boldsymbol{a}\|_2^2=e. \tag{11.73}$$

The solution to the above problem is simply given by $\sqrt{e}\widetilde{\boldsymbol{b}}$ where $\widetilde{\boldsymbol{b}}$ is the principal eigenvector of $\boldsymbol{A}_\star$. Inspired by the randomization technique in the literature (see e.g. [212] and the references therein), here we employ randomization as an alternative approach of code synthesis. In the randomization technique, several feasible random vectors $\{\boldsymbol{a}_m\}_{m=1}^L$ are generated (e.g. according to the distribution $\mathscr{CN}(\boldsymbol{0},\boldsymbol{A}_\star)$) and $\boldsymbol{a}_\star$ is obtained as

$$\boldsymbol{a}_\star=\arg\max_m\{\widetilde{q}_{\mathscr{I}}(\boldsymbol{a}_m)\} \tag{11.74}$$

where $\widetilde{q}_{\mathscr{I}}(\cdot)$ denotes the objective function in (11.60).

The steps of Re-MaMi algorithm are summarized in Table 11.2. Note that the first step of Re-MaMi (for all $\mathscr{I}\in\{\mathscr{B},\mathscr{D},\mathscr{J},\mathscr{M}\}$) contains a convex problem which can be solved efficiently via interior point methods [188]. Modification of Re-MaMi to obtain optimized codes under a PAR constraint is discussed in the next section.

11.6 Extensions of the Design Methods

In this section we provide two extensions of the previous design methods to PAR-constrained codes and the case of multiple transmitters. In order to use

Table 11.2. *The Re-MaMi Algorithm for* $\mathscr{I} \in \{\mathscr{B}, \mathscr{D}, \mathscr{J}, \mathscr{M}\}$

Step 0: Initialize $\boldsymbol{A}$ with a random matrix in $\mathbb{C}^{N\times N}$ and set the iteration number l to 0.
Step 1: Solve the convex problem in (11.60) to obtain $\boldsymbol{A}^{(l+1)}$; set $l \leftarrow l+1$.
Step 2: Compute $h^{(l)}_{k,\mathscr{I}}(\boldsymbol{A})$ corresponding to the metric $\mathscr{I}$.
Step 3: Repeat steps 1 and 2 until a pre-defined stop criterion is satisfied, e.g. $\|\boldsymbol{A}^{(l+1)} - \boldsymbol{A}^{(l)}\|_F \leq \xi$ for some $\xi > 0$.
Step 4 (*Synthesis stage*): Synthesize the optimized code $\boldsymbol{a}_\star$ using the approaches in (11.73) or (11.74).

the power resources efficiently and to avoid non-linear effects at the transmitter, codes with low PAR values are of practical interest in many applications [173] [126]. To the best of our knowledge, no study of code design with PAR constraints using information-theoretic criteria was conducted prior to this work. This section also includes the extension of the design methods to deal with the case of multiple transmitters with orthogonal transmission.

11.6.1 PAR-Constrained Code Design

In this subsection, we extend the derivations of Sv-MaMi and Re-MaMi for code design with an arbitrary PAR constraint, viz.

$$\mathrm{PAR}(\boldsymbol{a}) = \frac{\max\limits_{n} \{|a_n|^2\}}{\frac{1}{N}\|\boldsymbol{a}\|_2^2} \leq \zeta. \tag{11.75}$$

For Sv-MaMi the PAR constrained problem that must be solved is:

$$\begin{aligned} \min_{\mathbf{a}} \quad & \boldsymbol{a}^H \left(\sum_{k=1}^{N_r} \phi^{(l)}_{k,\mathscr{I}} \boldsymbol{M}_k^{-1} \right) \boldsymbol{a} - \Re\left(\left(\sum_{k=1}^{N_r} \boldsymbol{d}^{(l)}_{k,\mathscr{I}} \right)^H \boldsymbol{a} \right) \\ \text{subject to} \quad & \max_{n=1,\ldots,N} \{|a_n|^2\} \leq \zeta \\ & \|\boldsymbol{a}\|_2^2 = N. \end{aligned} \tag{11.76}$$

For Re-MaMi, one can consider the PAR constraint in the synthesis stage, which for LS synthesis leads to the following optimization problem:

$$\begin{aligned} \max_{\boldsymbol{a}} \quad & \boldsymbol{a}^H \boldsymbol{A} \boldsymbol{a} \\ \text{subject to} \quad & \max_{n=1,\ldots,N} \{|a_n|^2\} \leq \zeta \\ & \|\boldsymbol{a}\|_2^2 = N. \end{aligned} \tag{11.77}$$

Note that the QCQPs in (11.76) and (11.77) are non-convex optimization problems and known to be NP-hard [173]. Also note that the problem in (11.76)

can be recast in a form similar to (11.77), viz.

$$\begin{aligned} \min_{\boldsymbol{a}} \quad & \widehat{\boldsymbol{a}}^H \boldsymbol{J}\, \widehat{\boldsymbol{a}} \\ \text{subject to} \quad & \max_{n=1,\cdots,N} \{|a_n|^2\} \leq \zeta \\ & \|\boldsymbol{a}\|_2^2 = N \end{aligned} \tag{11.78}$$

where $\widehat{\boldsymbol{a}} = [\boldsymbol{a} \;\; 1]^T$, and

$$\boldsymbol{J} = \begin{bmatrix} \left(\sum_{k=1}^{N_r} \phi_{k,\mathscr{I}}^{(l)} \boldsymbol{M}_k^{-1}\right) & -0.5\left(\sum_{k=1}^{N_r} \boldsymbol{d}_{k,\mathscr{I}}^{(l)}\right) \\ -0.5\left(\sum_{k=1}^{N_r} \boldsymbol{d}_{k,\mathscr{I}}^{(l)}\right)^H & 0 \end{bmatrix}.$$

In what follows, we will explain how to solve (11.76) but, of course, (11.77) can be tackled in the same way. Let $\boldsymbol{K} = \mu \boldsymbol{I}_{N+1} - \boldsymbol{J}$ for any $\mu > \mu_{max}(\boldsymbol{J})$. Next observe that the problem in (11.78) is equivalent to:

$$\begin{aligned} \max_{\boldsymbol{a}} \quad & \widehat{\boldsymbol{a}}^H \boldsymbol{K}\, \widehat{\boldsymbol{a}} \\ \text{subject to} \quad & \max_{n=1,\cdots,N} \{|a_n|^2\} \leq \zeta \\ & \|\boldsymbol{a}\|_2^2 = N. \end{aligned} \tag{11.79}$$

The above problem can be tackled using the power-method in [190]. More precisely, the code vector $\boldsymbol{a}$ at the $(p+1)^{th}$ iteration can be obtained from $\boldsymbol{a}^{(p)}$, via solving the optimization problem

$$\begin{aligned} \max_{\boldsymbol{a}^{(p+1)}} \quad & \|\boldsymbol{a}^{(p+1)} - \breve{\boldsymbol{a}}^{(p)}\| \\ \text{subject to} \quad & \max_{n=1,\cdots,N} \{|a_n^{(p+1)}|^2\} \leq \zeta \\ & \|\boldsymbol{a}^{(p+1)}\|_2^2 = N \end{aligned} \tag{11.80}$$

where $\breve{\boldsymbol{a}}^{(p)}$ represents the vector containing the first N entries of $\boldsymbol{K}\, \widehat{\boldsymbol{a}}^{(p)}$. The optimization problem (11.80) is a "nearest-vector" problem with PAR constraint. Such PAR constrained problems can be tackled using an algorithm proposed in [191]. Note that the codes obtained as above can be scaled to fit any desired level of transmit energy as a scaling does not affect the PAR metric (see (11.75)). We refer the interested reader to [173] for using the randomization technique when a PAR constraint is imposed.

11.6.2 The Case of Multiple Transmitters

Here we discuss the extension of the design problem to the case of multiple transmit antennas that emit orthogonal signals. Let $\widetilde{s}_m(t)$ and $\boldsymbol{a}_m$ denote the

passband version and associated code vector of the m^{th} transmit signal, respectively. Assume that $\{\widetilde{s}_m(t)\}_{m=1}^{N_t}$ are well-separated in the frequency domain such that the signal echoes corresponding to each transmitter can be extracted at the k^{th} receiver. Then, the discrete-time signal at the k^{th} receiver due to the m^{th} transmitter can be expressed as

$$\mathbf{r}_{k,m} = \alpha_{k,m}\mathbf{a}_m + \widetilde{\rho}_{k,m}\mathbf{a}_m + \mathbf{w}_{k,m},\ m = 1,2,...,N_t; k = 1,2,...,N_r \tag{11.81}$$

where $\alpha_{k,m}$ denotes the "amplitude" of the target return and $\widetilde{\rho}_{k,m}$ is associated with the clutter, both corresponding to the k^{th} receiver and the m^{th} transmitter, and $\boldsymbol{w}_{k,m}$ denotes the interference at the k^{th} receive antenna corresponding to the m^{th} frequency band. Making assumptions similar to those stated in Section I leads to the following optimal detector:

$$\sum_{m=1}^{N_t}\sum_{k=1}^{N_r}\frac{\lambda_{k,m}|\theta_{k,m}|^2}{1+\lambda_{k,m}} \underset{\mathrm{H}_1}{\overset{\mathrm{H}_0}{\lessgtr}} \eta' \tag{11.82}$$

with $\lambda_{k,m} \triangleq \sigma_{k,m}^2 \boldsymbol{a}_m^H \boldsymbol{D}_{k,m}^2 \boldsymbol{a}_m$, and

$$\theta_{k,m} \triangleq \frac{\mathbf{a}_m^H \mathbf{D}_{k,m}^2 \mathbf{r}_{k,m}}{\|\boldsymbol{a}_m^H \boldsymbol{D}_{k,m}\|_2}, \tag{11.83}$$

$$\boldsymbol{D}_{k,m} \triangleq \left(\sigma_{\mathrm{c},(k,m)}^2 \boldsymbol{a}_m \boldsymbol{a}_m^H + \boldsymbol{M}_{k,m}\right)^{-1/2}. \tag{11.84}$$

Herein $\sigma_{\mathrm{c},(k,m)}^2$ and $\boldsymbol{M}_{k,m}$ denote the variance of $\widetilde{\rho}_{k,m}$ and covariance matrix of $\boldsymbol{w}_{k,m}$, respectively.

It is now straightforward to verify that the code design problem for the case of multiple transmitters can be dealt with using a modified version of (11.25):

$$\begin{aligned} \max_{\{\mathbf{a}_m\},\{\lambda_{k,m}\}} \quad & \sum_{m=1}^{N_t}\sum_{k=1}^{N_r} f_{\mathscr{I}}(\lambda_{k,m}) + g_{\mathscr{I}}(\lambda_{k,m}) \\ \text{subject to} \quad & \lambda_{k,m} = \sigma_{k,m}^2 \boldsymbol{a}_m^H (\sigma_{\mathrm{c},(k,m)}^2 \mathbf{a}_m \mathbf{a}_m^H + \mathbf{M}_{k,m})^{-1} \boldsymbol{a}_m, \\ & \|\boldsymbol{a}_m\|_2^2 \leqslant e_m \ \ \forall m, \end{aligned} \tag{11.85}$$

where e_m denotes the maximum available transmit energy for the m^{th} transmit antenna. Next observe that the above optimization problem is separable w.r.t m. Therefore, the code design procedure associated with each transmitter can be independently handled using the proposed methods in this chapter.

11.7 Simulation Results

In this section, we present several numerical examples to examine the performance of the proposed algorithms. In particular, we compare the system

performance for coded and uncoded (employing the code vector $\boldsymbol{a} = \sqrt{\frac{e}{N}}\mathbf{1}$) scenarios. Comparisons between the computational costs of Sv-MaMi and Re-MaMi are also included. Moreover, the behavior of the information-theoretic criteria is assessed when e varies.

Throughout this section, we assume the code length $N = 10$, the number of receivers $N_r = 4$, variances of the target components given by $\sigma_k^2 = 1$ (for $1 \leq k \leq 4$), and variances of the clutter components given by $(\sigma_{c,1}^2, \sigma_{c,2}^2, \sigma_{c,3}^2, \sigma_{c,4}^2) = (0.125, 0.25, .5, 1)$. Furthermore, we assume that the k^{th} interference covariance matrix $\boldsymbol{M}_k$ is given by $[\boldsymbol{M}_k]_{m,n} = (1 - 0.15k)^{|m-n|}$. The ROC is used to evaluate the detection performance of the system. Particularly, P_d and P_{fa} are calculated using their analytical expressions (see eqs. (32)-(34) in [182]). Then the ROC is plotted by numerically eliminating the detection threshold. The CVX toolbox [193] is used for solving the MaMi convex optimization problems.

Fig. 11.1(a)-(d) show the ROCs associated with the coded system (employing the optimized codes) as well as the uncoded system for $e = 10$ and $\mathscr{I} \in \{\mathscr{B}, \mathscr{D}, \mathscr{J}, \mathscr{M}\}$. The plotted ROCs correspond to the obtained codes using Sv-MaMi, Re-MaMi with either randomization (with $L = 50$) or LS, and the uncoded system. Theses figures also show the results of PAR-constrained code design with PAR$= 1$ (i.e. constant modulus) for Sv-MaMi and Re-MaMi (LS). It can be observed that the performance of the coded system (for all $\mathscr{I}$) outperforms that of the uncoded system significantly. Furthermore, the codes obtained by Sv-MaMi lead to slightly better performance compared to the codes provided by Re-MaMi as Sv-MaMi circumvents the synthesis loss. Note also the superiority of synthesis via randomization when compared to the LS synthesis. As to the constrained design, it can be seen that imposing the PAR constraint leads to a minor performance degradation (for all criteria) when compared to the unconstrained design. The fact that Sv-MaMi (PAR$= 1$) outperforms Re-MaMi (PAR$= 1$) complies with the related observation for the unconstrained case. In this example, the detection performances corresponding to various criteria are similar. However, this behavior does not generally hold true (see e.g. [183, 230, 231] and [223] for details on this aspect).

In Fig. 11.2 (a)-(d), the error norm has been depicted versus the iteration number for both Sv-MaMi and Re-MaMi. The error norm for Sv-MaMi and Re-MaMi is defined as $\|\boldsymbol{a}^{(l+1)} - \boldsymbol{a}^{(l)}\|_2$ and $\|\boldsymbol{A}^{(l+1)} - \boldsymbol{A}^{(l)}\|_F$, respectively. It can be observed that Re-MaMi converges much faster than Sv-MaMi. This observation can be explained by noting that in Sv-MaMi several majorizations have been applied successively. However, the complexity per iteration of Sv-MaMi is less than that of Re-MaMi because each iteration of Sv-MaMi can be handled efficiently by solving a convex QCQP. Another observation is that for the metrics $\mathscr{B}$ and $\mathscr{D}$, both algorithms require more iterations for convergence when compared to $\mathscr{J}$ and $\mathscr{M}$. This might be due to the more complicated form of the objective functions associated with $\mathscr{B}$ and $\mathscr{D}$. Note that for $\mathscr{I} =$

$\mathscr{M}$, Re-MaMi not only needs just one iteration to converge but also it provides the globally optimal solution to the relaxed optimization problem owing to its convexity (see (11.72)).

The required computation time of Sv-MaMi and Re-MaMi (employing randomization with $L = 50$) for various criteria is shown in Table 11.3. Due to the fact that the convergence time is dependent on the starting point as well as the stop criterion, the reported times are averaged for 100 random starting points on a standard PC (with Intel Core i5 2.8GHz CPU and 8GB memory) assuming $\xi = 10^{-4}$. It can be observed from this table that for $\mathscr{I} \in \{\mathscr{J}, \mathscr{M}\}$, Re-MaMi converges much faster than it does in the case of $\mathscr{I} \in \{\mathscr{B}, \mathscr{D}\}$. This can be explained by considering the required iteration numbers for different $\mathscr{I}$. Furthermore, the computational times of Sv-MaMi are almost the same for all criteria. In sum, from a computational point of view, it can be concluded that Re-MaMi is preferable for $\mathscr{I} \in \{\mathscr{J}, \mathscr{M}\}$ whereas Sv-MaMi is more suitable for $\mathscr{I} \in \{\mathscr{B}, \mathscr{D}\}$. It is also practically observed that there is no considerable difference between computational time of Re-MaMi with either LS or randomization with $L = 50$.

The behavior of various information-theoretic criteria versus the transmit energy e is investigated in Fig. 11.3 (a)-(d) for the coded system (using Sv-MaMi with PAR$=1$, and without PAR constraint) as well as the uncoded system. This figure also illustrates the saturation phenomenon. We observe from Fig. 11.3 that a saturation of the coded system always occurs before that in the uncoded system, which was expected: employing an optimized code enables the system to perform closer to the best possible performance at lower values of e. For all criteria, an approximate decrease of 14.5 dB in the required transmit energy of the coded system (with PAR$=1$) is observed for $e = 10$ as for Fig. 11.1 (see above).

Table 11.3. *Comparison of the average computational times (in sec.) of Sv-MaMi and Re-MaMi on a standard PC*

Algorithm \ Criterion	$\mathscr{B}$	$\mathscr{D}$	$\mathscr{J}$	$\mathscr{M}$
Sv-MaMi	20.31	20.86	16.88	18.91
Re-MaMi	49.01	27.71	2.51	3.16

11.8 Conclusions

Multi-static radar code design schemes based on information-theoretic criteria were considered in the presence of clutter. Two general methods were proposed to tackle the highly non-linear and non-convex design optimization problems using the Majorization-Minimization (MaMi) technique. The main results can be summarized as follows:

- A discrete-time formulation of the problem as well as the associated optimal detector were presented. Due to the lack of analytical ROC, information-theoretic criteria were used as design metrics, viz. the Bhattacharyya distance, KL-divergence, J-divergence, and the Mutual information. Using these metrics, optimization problems corresponding to the original code design problem were derived.
- A unified framework was proposed to describe all the arising optimization problems. Two methods called Sv-MaMi and Re-MaMi (based on the MaMi technique) were devised to solve these optimization problems:
  i) Sv-MaMi uses successive (linear as well as quadratic) majorizations such that each iteration of the algorithm can be handled using a convex QCQP.
  ii) Re-MaMi consists of majorization steps, rank-one constraint relaxation, and a synthesis stage. A least-squares approach and a randomization technique were used for code synthesis.
- The proposed methods were extended to PAR-constrained code design problems and to the case of multiple transmitters (with orthogonal transmission).
- Numerical examples were provided to examine the proposed methods. It was observed that Re-MaMi is computationally more efficient for $\mathscr{I} \in \{\mathscr{J}, \mathscr{M}\}$. On the other hand, for $\mathscr{I} \in \{\mathscr{B}, \mathscr{D}\}$ Sv-MaMi is preferable. The metric's saturation phenomenon, as the transmit energy increases, was also investigated.

Note that stationary targets were considered in this work. Optimal code design using information-theoretic criteria in the case of moving targets can be an interesting topic for future research.

11.9 Appendices

11.9.1 Appendix A: Derivation of the Discrete-Time Model

It follows from (11.1) and (11.2) that the n^{th} sample of the output of the matched filter at the k^{th} receiver can be written as

$$\begin{aligned} r_{k,n} &= r_k(t) \star \phi^*(-t)\Big|_{t=(n-1)T_p+\tau_k} = \int_{-\infty}^{+\infty} r_k(\tau)\phi^*(\tau-[n-1]T_p-\tau_k)d\tau \\ &= \int_{-\infty}^{+\infty} \alpha_k \sum_{i=1}^{N} a_i \phi(\tau-[i-1]T_p-\tau_k)\phi^*(\tau-[n-1]T_p-\tau_k)d\tau \\ &+ \int_{-\infty}^{+\infty} \sum_{v=1}^{N_c} \rho_{k,v} \sum_{i=1}^{N} a_i \phi(\tau-[i-1]T_p-\tau_{k,v})\phi^*(\tau-[n-1]T_p-\tau_k)d\tau \\ &+ \int_{-\infty}^{+\infty} w_k(\tau)\phi^*(\tau-[n-1]T_p-\tau_k)d\tau. \end{aligned} \tag{11.86}$$

Let Q_u denote the u^{th} integral in the right-hand side of the above equation. Since $\{\phi(t-[n-1]T_p)\}_{n=1}^{N}$ are non-overlapping and have unit energy, Q_1 can be simplified as

$$Q_1 = \alpha_k \sum_{i=1}^{N} a_i \delta[i-n] = a_n \alpha_k. \tag{11.87}$$

Furthermore, we have that

$$Q_2 = \sum_{v=1}^{N_c} \rho_{k,v} \left(\sum_{i=1}^{N} a_i \Psi_{n,i}(\tau_k - \tau_{k,v}) \right) \tag{11.88}$$

where $\Psi_{n,i}(t)$ is the cross-correlation function of $\phi(\tau-[i-1]T_p)$ and $\phi(\tau-[n-1]T_p)$ defined by

$$\Psi_{n,i}(t) \triangleq \int_{-\infty}^{+\infty} \phi(\tau-[i-1]T_p-t)\phi^*(\tau-[n-1]T_p)d\tau. \tag{11.89}$$

For unambiguous-range clutter scatterers (i.e. scatterers with $\tau_{k,v} \leq T_p$) [192], $\Psi_{n,i}(\tau_k-\tau_{k,v})$ is zero for $i \neq n$ because $\phi(t-[i-1]T_p-\tau_{k,v})$ and $\phi(t-[n-1]T_p-\tau_k)$ are non-overlapping[2]. Therefore, Q_2 can be rewritten as

$$Q_2 = a_n \left(\sum_{v=1}^{N_c} \rho_{k,v} \Psi_{n,n}(\tau_k-\tau_{k,v}) \right) \triangleq a_n \widetilde{\rho}_k. \tag{11.90}$$

Note that $w_{k,n} \triangleq Q_3$ represents the filtered version of the interference. Finally, we can simplify (11.86) as

$$r_{k,n} = a_n \alpha_k + a_n \widetilde{\rho}_k + w_{k,n}, \quad \text{for} \quad k = 1,2,..,N_r \quad \text{and} \quad n = 1,2,..,N$$

According to Assumption 3, $\beta_{k,v} \triangleq \rho_{k,v}\Psi_{n,n}(\tau_k-\tau_{k,v})$ are independent RVs, for $v = 1,2,...,N_c$. Consequently, $\widetilde{\rho}_k = \sum_{v=1}^{N_c} \beta_{k,v}$ can be modeled, using the central limit theorem [225], as a zero-mean complex Gaussian RV with variance $\sigma_{c,k}^2$. Note that $\sigma_{c,k}^2$ can be calculated using $\Psi_{n,n}(\cdot)$ and the distribution of the $(\tau_k-\tau_{k,v})$ [156].

11.9.2 Appendix B: Monotonically Increasing Behavior of the Function $q_{\mathscr{I}}(\lambda_k)$

For $\mathscr{I} = \mathscr{B}$, we have $q_{\mathscr{I}}(\lambda_k) = \log \frac{1+.5\lambda_k}{\sqrt{1+\lambda_k}}$. Therefore, the first-order derivative of $q_{\mathscr{B}}(\lambda_k)$ is given by

$$\frac{d}{d\lambda_k} q_{\mathscr{B}}(\lambda_k) = \frac{0.25\lambda_k}{(1+\lambda_k)(1+0.5\lambda_k)}. \tag{11.91}$$

[2]Note that $\tau_k \geq \tau_p$, otherwise τ_k corresponds to a blind range of the system [192].

Similarly, for the first-order derivative of $q_{\mathscr{D}}(\lambda_k)$ we have

$$\frac{d}{d\lambda_k} q_{\mathscr{D}}(\lambda_k) = \frac{\lambda_k}{(\lambda_k+1)^2}. \tag{11.92}$$

As to the J-divergence, one can easily verify that

$$\frac{d}{d\lambda_k} q_{\mathscr{J}}(\lambda_k) = \frac{\lambda_k^2+2\lambda_k}{(1+\lambda_k)^2}. \tag{11.93}$$

Due to the fact that the right-hand side in eqs. (11.91), (11.92), and (11.93) are non-negative for $\lambda_k \geq 0$, the function $q_{\mathscr{I}}(\lambda_k)$ is monotonically increasing for $\mathscr{I}$ in $\{\mathscr{B}, \mathscr{D}, \mathscr{J}\}$. Moreover, the case of $\mathscr{I} = \mathscr{M}$ simply leads to the monotonically increasing function $q_{\mathscr{M}}(\lambda_k) = \log(1+\lambda_k)$.

11.9.3 Appendix C: Proof of Lemma 4

First note that $\widetilde{h}(\widetilde{\boldsymbol{A}}) = h(\widetilde{\boldsymbol{A}})$. In addition, $\widetilde{h}(\boldsymbol{A}) \leq \mathrm{tr}\{(\boldsymbol{M}_k + \beta_k \boldsymbol{A})^{-1} \boldsymbol{M}_k\}$ for every pair of positive semidefinite matrices $\boldsymbol{A}, \widetilde{\boldsymbol{A}} \in \mathbb{C}^{N\times N}$ if

$$(\boldsymbol{M}_k + \beta_k \boldsymbol{A})^{-1} - (\boldsymbol{M}_k + \beta_k \widetilde{\boldsymbol{A}})^{-1} + (\boldsymbol{M}_k + \beta_k \widetilde{\boldsymbol{A}})^{-1} (\beta_k \boldsymbol{A} - \beta_k \widetilde{\boldsymbol{A}})(\boldsymbol{M}_k + \beta_k \widetilde{\boldsymbol{A}})^{-1} \succeq \boldsymbol{0}. \tag{11.94}$$

Observe that $(\beta_k \boldsymbol{A} - \beta_k \widetilde{\boldsymbol{A}}) = (\boldsymbol{M}_k + \beta_k \boldsymbol{A}) - (\boldsymbol{M}_k + \beta_k \widetilde{\boldsymbol{A}})$. Therefore, using the variables $\boldsymbol{X} = (\boldsymbol{M}_k + \beta_k \boldsymbol{A})$ and $\boldsymbol{Y} = (\boldsymbol{M}_k + \beta_k \widetilde{\boldsymbol{A}})$, one can rewrite the left-hand side of (11.94) as

$$\boldsymbol{X}^{-1} - \boldsymbol{Y}^{-1} + \boldsymbol{Y}^{-1}(\boldsymbol{X} - \boldsymbol{Y})\boldsymbol{Y}^{-1} = (\boldsymbol{I} - \boldsymbol{Y}^{-1}\boldsymbol{X})\boldsymbol{X}^{-1}(\boldsymbol{I} - \boldsymbol{X}\boldsymbol{Y}^{-1}).$$

Now it is straightforward to verify that the right-hand side of the above equation is always positive semi-definite as $\boldsymbol{X}^{-1} \succ \boldsymbol{0}$ and $(\boldsymbol{I} - \boldsymbol{X}\boldsymbol{Y}^{-1}) = (\boldsymbol{I} - \boldsymbol{Y}^{-1}\boldsymbol{X})^H$.

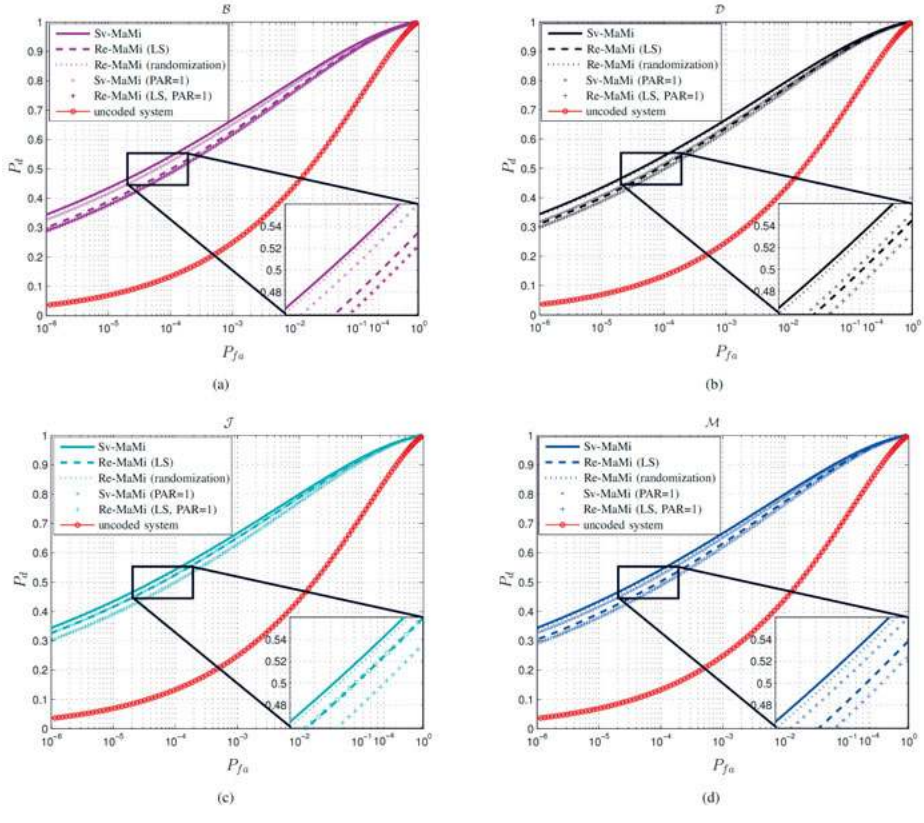

Figure 11.1. ROCs corresponding to the obtained codes using Sv-MaMi and Re-MaMi (both PAR-constrained and unconstrained) as well as the uncoded system for different design metrics: a) $\mathscr{B}$, b) $\mathscr{D}$, c) $\mathscr{J}$, and d) $\mathscr{M}$. For unconstrained design using Re-MaMi algorithm, results of both LS synthesis and randomization are shown.

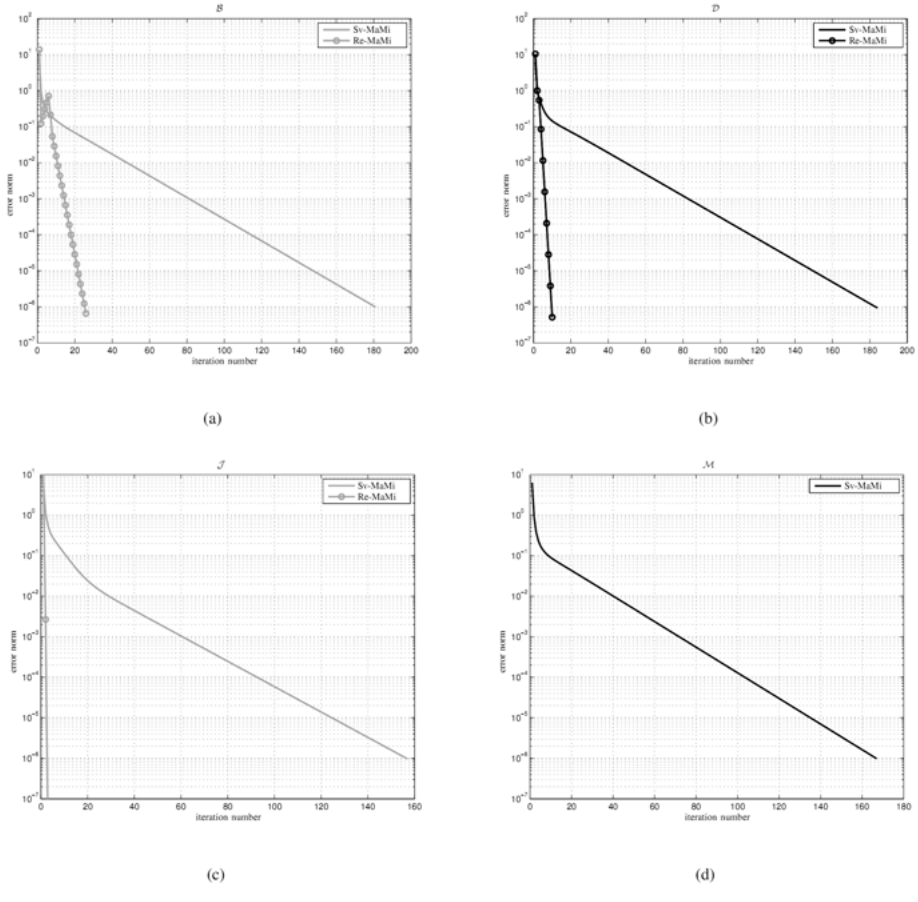

Figure 11.2. Error norm versus iteration number for Sv-MaMi/Re-MaMi and different design metrics: a) $\mathscr{B}$, b) $\mathscr{D}$, c) $\mathscr{J}$, and d) $\mathscr{M}$. For the case of $\mathscr{M}$, Re-MaMi converges in one iteration.

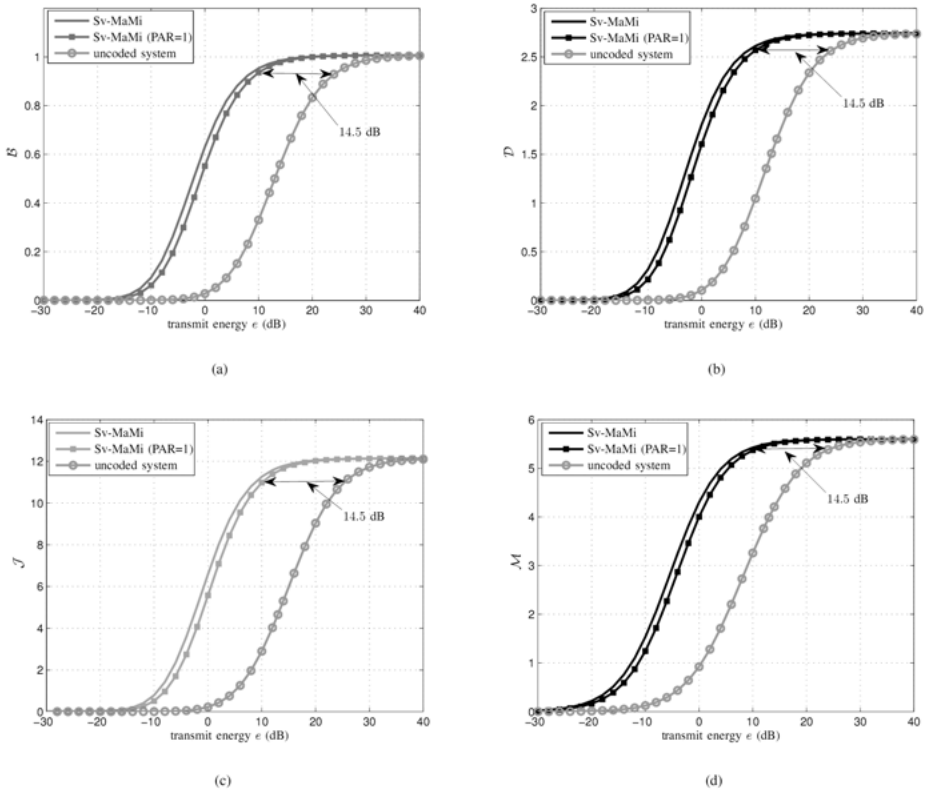

Figure 11.3. Behavior of various information-theoretic criteria versus transmit energy e for the coded and the uncoded systems: a) $\mathscr{B}$, b) $\mathscr{D}$, c) $\mathscr{J}$, and d) $\mathscr{M}$. Results for Sv-MaMi with PAR$=1$ and with no PAR constraint are shown.

Part IV:
Sparsity-Related Metrics

12. Search for Costas Arrays via Sparse Representation

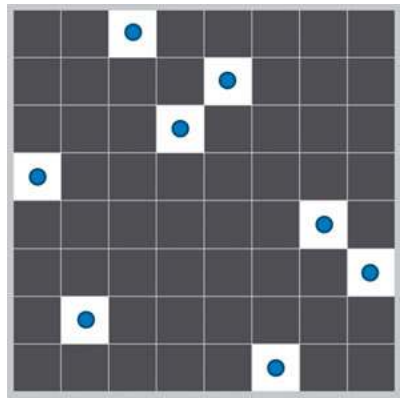

Figure 12.1. A Costas array of size 8×8.

Abstract
Costas arrays are mainly known as a certain type of optimized time-frequency coding pattern for sonar and radar. In order to fulfill the need for effective computational approaches to find Costas arrays, in this chapter, we propose a sparse formulation of the Costas array search problem. The new sparse representation can pave the way for using an extensive number of methods offered by the sparse signal recovery literature. It is further shown that Costas arrays can be obtained using an equivalent quadratic program with linear constraints. A numerical approach is devised and used to illustrate the performance of the proposed formulations.

Keywords: Code design, Costas arrays, frequency hopping, radar codes, sparsity

12.1 Introduction

Costas arrays have been studied in engineering and mathematics for around half a century— however, many related fundamental questions are not yet answered [242] [243]. The definition of a Costas array is fairly straightforward:

Definition 1. *A Costas array is a set of n points lying on the squares of an $n \times n$ checkerboard, such that each row and column contains only one point, and all of the $\binom{n}{2}$ displacement vectors*[1] *between each pair of points are distinct.*

Fig. 12.1 shows an example of a Costas array of size 8×8. Costas arrays are mainly known as time-frequency coding patterns that optimize the performance of sonars and radars. They have also shown promising applications in data hiding and mobile radio [244] [245]. The usefulness of Costas arrays in sonar and radar applications can be seen more clearly by the following alternative definition of Costas arrays:

[1]Note that the points in the checkerboard can be associated with position vectors (initiated from an arbitrary origin). Then the displacement vectors are the differences of such position vectors.

Definition 2. *A permutation matrix $\boldsymbol{P}$ of size $n \times n$ represents a Costas array if and only if for any pair of integers $(r,s) \neq (0,0)$, $|r| \leq n$, $|s| \leq n$, the two-dimensional (2D) correlation function $c(r,s)$ associated with $\boldsymbol{P}$ satisfies*

$$c(r,s) = \sum_{k=1}^{n} \sum_{l=1}^{n} \boldsymbol{P}(k,l)\boldsymbol{P}(k+r,l+s) \leq 1 \tag{12.1}$$

where $\boldsymbol{P}$ is extended with zeros when required.

Note that the low 2D correlation character described in (12.1) leads to a low *ambiguity* in detection of moving targets. Due to their importance, several analytical construction methods have been proposed for Costas arrays [246]. Thanks to such constructions, Costas arrays are known for an infinite number of orders n. On the other hand, it is not yet known whether Costas arrays exist for all n.

Using computer clusters, the enumeration of Costas arrays has been accomplished via brute-force computational methods for all $n \leq 29$ [247]. However, the size of the search space is reported to grow exponentially with n, which makes the problem of finding Costas arrays impossible to tackle via exhaustive search when n grows large [248]. With such issues in mind, in this chapter (Sections 12.2 and 12.3), we propose a sparse formulation of the Costas array search problem:

- We believe that the sparse formulation introduced in this chapter lays the ground for using the many methods offered by the extensive literature on sparse signal recovery— which can lead to more effective numerical approaches than the exhaustive search.
- To the best of our knowledge, this work is the first to cast the Costas array search problem as an optimization problem, in a form which is well-known in the signal processing community.

Based on the proposed formulation, and in order to show its performance, a numerical approach is devised and used to find a Costas array in Section 12.4.

Notation: We use bold lowercase letters for vectors and bold uppercase letters for matrices. $(\cdot)^T$ denotes the vector/matrix transpose. $\mathbf{1}$ and $\mathbf{0}$ are the all-one and all-zero vectors/matrices. $\boldsymbol{e}_k$ and $\widetilde{\boldsymbol{e}}_k$ are the k^{th} standard basis vectors in $\mathbb{R}^n$, and $\mathbb{R}^{n^2}$, respectively. $vec(\boldsymbol{X})$ is a vector obtained by stacking the columns of $\boldsymbol{X}$ successively. $\|\mathbf{x}\|_n$ or the l_n-norm of the vector $\mathbf{x}$ is defined as $(\sum_k |\mathbf{x}(k)|^n)^{\frac{1}{n}}$ where $\{\mathbf{x}(k)\}$ are the entries of $\mathbf{x}$; for $n = 0$, $\|\mathbf{x}\|_0$ is given by the number of nonzero entries of $\mathbf{x}$. Finally, the symbol $\otimes$ stands for the Kronecker product of matrices.

12.2 Costas Arrays: A Linear Formulation

In this section, we introduce a linear interpretation of the Costas array constraints. Particularly, we show that such constraints can be expressed as an

under-determined linear system of equations along with some linear inequalities. To this end, we propose the following geometrically equivalent definition of Costas arrays:

Definition 3. *A Costas array is a set of n points lying on the squares of an $n \times n$ checkerboard, such that (i) each row and column contains only one point (**permutation property**), and that (ii) no four points form a parallelogram; moreover no three equidistant points occur on the same line (**distinctness property**).*

Let the binary matrix $\boldsymbol{X}_{n\times n}$ (with entries in $\{0,1\}$) denote a Costas array, and let $\mathbf{x} = vec(\boldsymbol{X})$. Assuming binary variables, the permutation property in Definition 3 can be expressed by the linear equality constraint:

$$\boldsymbol{A}\mathbf{x} = \mathbf{1}_{\mathbf{2n}\times\mathbf{1}} \triangleq \boldsymbol{b} \tag{12.2}$$

where

$$\boldsymbol{A}_{2n\times n^2} = \begin{pmatrix} \boldsymbol{O}_1 & \boldsymbol{O}_2 & \cdots & \boldsymbol{O}_n \\ \boldsymbol{I} & \boldsymbol{I} & \cdots & \boldsymbol{I} \end{pmatrix} \tag{12.3}$$

and $\boldsymbol{O}_k = \boldsymbol{e}_k \otimes \mathbf{1}_{\mathbf{n}}^{\mathbf{T}}$. We further note that the distinctness property in Definition 3 can be formulated using a number of linear inequalities. Suppose that the location indices $\{i_1, i_2, i_3, i_4\}$ in $\mathbf{x}$ represent the vertices of a parallelogram in $\boldsymbol{X}$. To avoid forming such a parallelogram, it is sufficient to add the inequality

$$\begin{aligned} \mathbf{x}(i_1) + \mathbf{x}(i_2) + \mathbf{x}(i_3) + \mathbf{x}(i_4) \leq 3, \\ \text{i.e. } (\widetilde{\boldsymbol{e}}_{i_1} + \widetilde{\boldsymbol{e}}_{i_2} + \widetilde{\boldsymbol{e}}_{i_3} + \widetilde{\boldsymbol{e}}_{i_4})^T \mathbf{x} \leq 3 \end{aligned} \tag{12.4}$$

to the constraint set. Furthermore, any pattern of equidistant points on the same line, represented by the location indices $\{i_1, i_2, i_3\}$ in $\mathbf{x}$, can be avoided by the linear inequality constraint

$$\begin{aligned} \mathbf{x}(i_1) + \mathbf{x}(i_2) + \mathbf{x}(i_3) \leq 2, \\ \text{i.e. } (\widetilde{\boldsymbol{e}}_{i_1} + \widetilde{\boldsymbol{e}}_{i_2} + \widetilde{\boldsymbol{e}}_{i_3})^T \mathbf{x} \leq 2. \end{aligned} \tag{12.5}$$

By including the linear constraints associated with all possible parallelograms and three equidistant points on a same line in the checkerboard, one can formulate the distinctness property in the following unified form:

$$\boldsymbol{A}'\mathbf{x} \leq \boldsymbol{b}'. \tag{12.6}$$

Note that although $\boldsymbol{A}'$ and $\boldsymbol{b}'$ can be hardly formulated in an explicit form, they are easy to generate algorithmically. An example of such an algorithmic construction of $(\boldsymbol{A}', \boldsymbol{b}')$ is given in Table 12.1. Finally, a binary vector $\mathbf{x}_{n^2\times 1}$ represents a Costas array if and only if it is a solution to the linear system

$$\begin{cases} \boldsymbol{A}\mathbf{x} = \boldsymbol{b}, \\ \boldsymbol{A}'\mathbf{x} \leq \boldsymbol{b}'. \end{cases} \tag{12.7}$$

Table 12.1. *An algorithmic construction of* $(\boldsymbol{A}', \boldsymbol{b}')$

Step 1: For all triples (i_1, i_2, i_3) (not on the same row/column) sorted by their row number in the checkerboard do:
Step 1-1: If i_2 is in the middle of i_1 and i_3,
Step 1-1-1: Add the row vector $(\widetilde{\boldsymbol{e}}_{i_1} + \widetilde{\boldsymbol{e}}_{i_2} + \widetilde{\boldsymbol{e}}_{i_3})^T$ at the bottom of $\boldsymbol{A}'$, and 2 at the bottom of $\boldsymbol{b}'$.
Step 1-2: Else,
Step 1-2-1: Find the 4^{th} vertices $\{i_4\}$ corresponding to the two parallelograms that can be formed using the available vertices (i_1, i_2, i_3) with i_1 as the vertex with the minimum row number.
Step 1-2-2: For any of the two possible locations $\{i_4\}$ which occur inside the checkerboard, include the row vector $(\widetilde{\boldsymbol{e}}_{i_1} + \widetilde{\boldsymbol{e}}_{i_2} + \widetilde{\boldsymbol{e}}_{i_3} + \widetilde{\boldsymbol{e}}_{i_4})^T$ at the bottom of $\boldsymbol{A}'$, and 3 at the bottom of $\boldsymbol{b}'$.

As indicated earlier, the linear system in (12.7) contains $2n$ equality constraints. We refer the interested reader to the Appendix for enumeration results regarding the inequality constraints in (12.7).

12.3 Sparse Representation of Costas Arrays

It is interesting to observe that the binary constraint on $\mathbf{x}$ can be omitted if one seeks for the *sparsest* solution of the linear system in (12.7). Consider the following optimization problem:

$$P_0: \min_{\mathbf{x} \in \mathbb{R}^{n^2}} \quad \|\mathbf{x}\|_0 \tag{12.8}$$

$$\text{s.t.} \quad \begin{cases} \boldsymbol{A}\mathbf{x} = \boldsymbol{b}, \\ \boldsymbol{A}'\mathbf{x} \leq \boldsymbol{b}', \\ \mathbf{0} \leq \mathbf{x} \leq \mathbf{1} \end{cases} \tag{12.9}$$

Theorem 1. *Every solution of* P_0 *represents a Costas array, and vice versa.*

Proof: According to the equality constraint in (12.9), every solution of P_0 has at least one nonzero element in the location indices corresponding to each row/column of the checkerboard. This implies that every solution $\mathbf{x}$ to P_0 has an l_0-norm of at least n. On the other hand, if $\|\mathbf{x}\|_0 = n$, the satisfaction of the equality constraint in (12.9) implies that $\mathbf{x}$ denotes a permutation matrix, and as a result, the satisfaction of the inequality constraint in (12.9) shows that $\mathbf{x}$ represents a Costas array. Moreover, any $\mathbf{x}$ representing a Costas array is a feasible solution to the linear system in (12.9) with the minimum l_0-norm, i.e. n. ■

Note that the sparse formulation above paves the way for employing many existing, as well as emerging sparse signal recovery techniques in the literature. The recovery of sparse signals subject to linear constraints has been

studied widely in the past decade, see [249]- [255] and the references therein. We note that as the l_1-norm of any feasible $\mathbf{x} \geq \mathbf{0}$ of P_0 is constant, it is not possible to employ the convex l_1 *minimization* alternative of P_0, although it is a common practice in sparse signal recovery [252]. From a geometrical point of view, the solutions to P_0, i.e. the sparsest solutions to (12.7), have the maximum Euclidean distance from the origin. In other words, P_0 is equivalent to

$$P_2 : \max_{\mathbf{x} \in \mathbb{R}^{n^2}} \quad \|\mathbf{x}\|_2 \tag{12.10}$$

$$\text{s.t.} \quad \begin{cases} \boldsymbol{A}\mathbf{x} = \boldsymbol{b}, \\ \boldsymbol{A}'\mathbf{x} \leq \boldsymbol{b}', \\ \mathbf{0} \leq \mathbf{x} \leq \mathbf{1} \end{cases} \tag{12.11}$$

To observe this fact, we recall that the equality constraint $\boldsymbol{A}\mathbf{x} = \boldsymbol{b}$ implies a constant sum of entries corresponding to each row/column of $\boldsymbol{X}$. Using such a constant-sum property, the connection between the solutions of P_0 and P_2 can be studied in a constructive way. Let $\mathbf{x}(k) \geq \mathbf{x}(l)$, and $\alpha > 0$. Then it is easy to verify that

$$(\mathbf{x}(k) + \alpha)^2 + (\mathbf{x}(l) - \alpha)^2 > (\mathbf{x}(k))^2 + (\mathbf{x}(l))^2. \tag{12.12}$$

The latter inequality implies that the l_2-norm of $\mathbf{x}$ can be increased monotonically by decreasing the small elements of $\mathbf{x}$ and increasing the large elements of $\mathbf{x}$ at the same rate— i.e. enhancing sparsity while increasing the l_2-norm. The latter result can be applied to a feasible $\mathbf{x}$ of P_0, meaning that a solution $\mathbf{x}$ of P_0 has the minimal l_0-norm (i.e. n) and at the same time the maximal l_2-norm (i.e. $\sqrt{n}$) among all feasible candidates in the search space of P_0.

We end this section with two remarks. First of all, the linear system in (12.9) and (12.11) describes a convex polytope, which we call the *Costas ball* in the sequel. Based on the above discussion, Costas arrays can be viewed as the farthest subset (in Euclidean sense) of vertices of the Costas ball from the origin, that intersect with the n^2-sphere

$$\boldsymbol{B}_{n^2} = \{\mathbf{x} \in \mathbb{R}^{n^2} : \ \|\mathbf{x}\|_2^2 = n\}. \tag{12.13}$$

This observation is illustrated in Fig. 12.2. Second, both optimization problems P_0 and P_2 are NP-hard in general; see [255], and [256], [257]. Nevertheless, such new formulations might be employed to devise numerical methods that can handle the Costas array search problems more effectively than the brute-force methods.

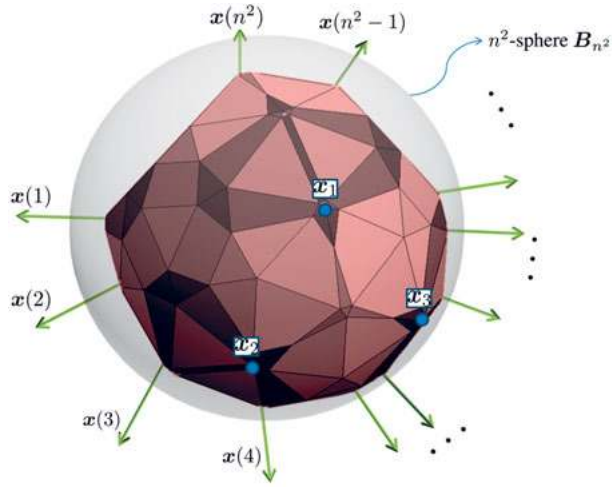

Figure 12.2. An intuitive illustration of the Costas ball and the Costas arrays ($\{\mathbf{x}_k\}$, shown by the blue dots) possessing maximal l_2-norm. Costas arrays intersect with the n^2-sphere $\boldsymbol{B}_{n^2}$.

12.4 A Numerical Approach— Along with an Illustrative Example

In order to show the potential of the proposed sparse formulation, we consider a reweighted iterative approach to tackle P_2. More precisely, starting from a random positive weight vector $\boldsymbol{w}^{(1)} \in \mathbb{R}^{n^2}$, we obtain the variable $\mathbf{x}^{(k)}$ (at the k^{th} iteration) using the linear program:

$$P_2 - reweighted: \max_{\mathbf{x}^{(k)} \in \mathbb{R}^{n^2}} \quad \boldsymbol{w}^{T\ (k)} \mathbf{x}^{(k)} \tag{12.14}$$

$$\text{s.t.} \quad \begin{cases} \boldsymbol{A}\mathbf{x}^{(k)} = \boldsymbol{b}, \\ \boldsymbol{A}'\mathbf{x}^{(k)} \leq \boldsymbol{b}', \\ \mathbf{0} \leq \mathbf{x}^{(k)} \leq \mathbf{1} \end{cases} \tag{12.15}$$

where the weight vector is updated as

$$\boldsymbol{w}^{(k+1)} = \mathbf{x}^{(k)} + \boldsymbol{\varepsilon}, \ \ k \geq 1 \tag{12.16}$$

and $\boldsymbol{\varepsilon}$ is a random vector in $\mathbb{R}^{n^2}$ consisting of elements with i.i.d. standard Gaussian distribution $\mathcal{N}(0, \sigma)$. Note that $P_2 - reweighted$ aims to (approximately) maximize the l_2-norm, while it also provides a randomized leverage to skip the local optima of P_2 (corresponding to some vertices of the Costas ball with an l_2-norm less than $\sqrt{n}$). We stop the iterations when $\mathbf{x}$ becomes binary, and hence will represent a Costas array.

We note that, the reweighted method in (12.14)-(12.16) typically requires more iterations until convergence as n grows large. As an example, we consider using the proposed iterative approach to find a Costas array of size 8×8;

a size which enables us to present the results through iterations. Due to the binary (i.e. $0/1$) nature of the ultimate results, we use a standard deviation σ of 0.5. The resultant 2D patterns $\boldsymbol{X}^{(k)} = vec^{-1}\left(\mathbf{x}^{(k)}\right)$ are shown in Fig. 12.3. In this example, the algorithm finds a Costas array after 6 iterations. It is worth observing that the 2D patterns obtained from successive iterations appear to be rather correlated (i.e. similar); at the same time, the obtained Costas array looks rather different from the pattern obtained at the end of the first iteration.

Finally, it is worthwhile to mention that, for large n, efficient implementation of the proposed approaches is crucial, and may be considered as an interesting topic for future works.

12.5 Appendix

12.5.1 Appendix A: The Number of Inequality Constraints in (12.7)

We begin by observing that the number of distinct (k,l)-vectors[2] in an $n \times n$ checkerboard is given by $(n-|k|+1)(n-|l|+1)$. Note that (i) the pattern described by three equidistant points on the same line is also a parallelogram whose two vertices share the same location. Moreover, (ii) each parallelogram including a (k,l)-edge is uniquely determined by placing two (k,l) vectors in the checkerboard. The number of all parallelograms including a (k,l)-edge in the $n \times n$ checkerboard is thus given by

$$\binom{(n-|k|+1)(n-|l|+1)}{2}. \tag{12.17}$$

Now we should exclude the parallelograms which have two vertices on the same row/column, except those for which the two mentioned vertices are exactly at the same location. The number of such parallelograms with two vertices on the same row is given by the number of $(t,2l)$-vectors with $-(n-2|l|+2) \leq t \leq n$. Similarly, the number of such parallelograms with two vertices on the same column is given by the number of $(2k,t)$-vectors with $-(n-2|k|+2) \leq t \leq n$. On the other hand, the number of parallelograms with a (k,l)-edge and two vertices sharing the same location is given by the number of $(2k,2l)$-vectors in the checkerboard. In sum, the number of parallelograms including a (k,l)-edge for which no two vertices occur on the same

[2] i.e. the displacement vectors that map a point location (i,j) to the location $(i+k, j+l)$ in the checkerboard.

row/column unless they share a same location is equal to

$$\begin{aligned} f_{k,l} &= \binom{(n-|k|+1)(n-|l|+1)}{2} \\ &\quad - \sum_{t=-(n-2|l|+2)}^{n} (n-2|l|+1)(n-|t|+1) \\ &\quad - \sum_{t=-(n-2|k|+2)}^{n} (n-2|k|+1)(n-|t|+1) \\ &\quad +2\,(n-2|k|+1)(n-2|l|+1) \end{aligned} \tag{12.18}$$

We note that by considering all $1 \leq k \leq n-1$ and $1 \leq |l| \leq n-1$, each parallelogram (except those with two vertices in the same location) will be counted two times in $\{f_{k,l}\}$. Therefore, the number of all parallelograms (corresponding to the linear inequality constraints) becomes

$$\begin{aligned} T_n &= \frac{1}{2}\sum_{k=1}^{n-1} \sum_{1\leq|l|\leq n-1} f_{k,l} \\ &+ \frac{1}{2}\sum_{k=1}^{n-1} \sum_{1\leq|l|\leq n-1} (n-2|k|+1)(n-2|l|+1). \end{aligned} \tag{12.19}$$

Finally, it is worthwhile to observe that $f_{k,l} = \mathscr{O}(n^4)$ which implies that $T_n = \mathscr{O}(n^6)$ according to (12.19).

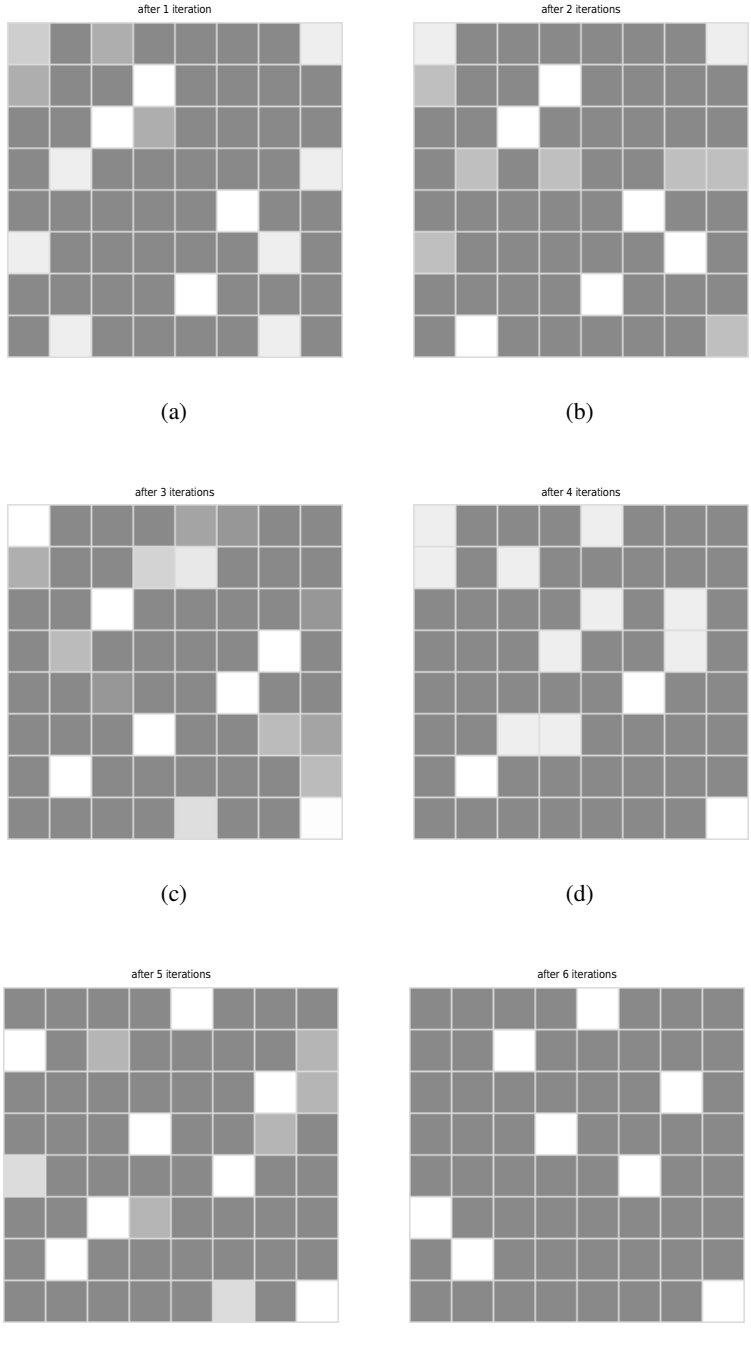

Figure 12.3. The 2D patterns $\boldsymbol{X}^{(k)} = vec^{-1}\left(\mathbf{x}^{(k)}\right)$ obtained using the iterative reweighted approach proposed in (12.14)-(12.16). The values are shown using grayscale intensity. In this example, the method finds a Costas array after 6 iterations.

13. Sparsity-Aware Radar Waveform Synthesis

Abstract
Owing to the inherent sparsity of the target scene, compressed sensing (CS) has been successfully employed in radar applications. It is known that the performance of target scene recovery in CS scenarios depends highly on the coherence of the sensing matrix (CSM), which is determined by the radar transmit waveform. In this chapter, we present a cyclic optimization algorithm to effectively reduce the CSM via a judicious design of the radar waveform. The proposed method provides a reduction in the size of the Gram matrix associated with the sensing matrix, and moreover, relies on the fast Fourier transform (FFT) operations to improve the computation speed. As a result, the suggested algorithm can be used for large dimension designs (with $\gtrsim 100$ variables) even on an ordinary PC. The effectiveness of the proposed algorithm is illustrated through numerical examples.

Keywords: Compressed sensing, mutual coherence, radar, sensing matrix, sparsity, waveform synthesis

13.1 Introduction and System Modeling

A primary interest in radar is the inverse problem of recovering the target scene from the noisy measurements. For a radar working under the conventional Nyquist-Shannon sampling framework, the sampling rate is constrained to be at least twice the highest frequency component in the received signal, in order to reconstruct the target scene accurately. In many cases, particularly for ultra wide band (UWB) radar, such a requirement is hardly achieved using the currently employed analog to digital converters (ADCs); not to mention the large computational burden caused by the processing of the data with high sampling rates.

The new framework of compressed sensing (CS) may promise a solution to such difficulties [258, 259]. To observe how, note that in practical radar applications, the target scene is typically sparse— i.e. there is usually a small number of targets that we are concerned with. In order to recover the data with lower sampling rates, CS relies on two criteria: (i) *sparsity*, which is related to the signal of interest (i.e. the target scene), and (ii) *incoherence*, which is related to the sensing modality to be designed. Note that CS-based formulations have been successfully developed for MIMO radar [261, 262], synthetic aperture radar (SAR) [263], as well as the inverse synthetic aperture radar (ISAR) [264].

In radar applications, the sensing modality is determined by the transmit sequence $\boldsymbol{s}$. The design problem can be formulated as follows. Suppose the target scene (in the range-Doppler plane) is discretized via a $N_r \times N_d$ grid, and

define the time delay and Doppler shift matrices as

$$\boldsymbol{T}^r = \begin{pmatrix} \mathbf{0}_{r\times N} \\ \boldsymbol{I}_{N\times N} \\ \mathbf{0}_{(N_r-r-1)\times N} \end{pmatrix}, \qquad r = 0,1,\cdots,N_r-1, \tag{13.1}$$

$$\boldsymbol{F}^d = \begin{pmatrix} \omega_M^0 & 0 & \cdots & 0 \\ 0 & \omega_M^1 & \cdots & 0 \\ \vdots & \vdots & \ddots & \vdots \\ 0 & 0 & \cdots & \omega_M^{N-1} \end{pmatrix}^d, d = 0,1,\cdots,N_d-1,$$

where N is the length of transmit sequence $\boldsymbol{s}$, $\omega_M = e^{j\frac{2\pi}{M}}$ is the M^{th} root-of-unity. Thus, the discrete received signal can be formulated as (see [265–267] for details)

$$\boldsymbol{x} = \sum_{d=0}^{N_d-1}\sum_{r=0}^{N_r-1} \alpha_{r,d} \underbrace{\boldsymbol{T}^r\boldsymbol{F}^d\boldsymbol{s}}_{\triangleq\boldsymbol{\varphi}_{r,d}} + \boldsymbol{e} \tag{13.2}$$

where $\alpha_{r,d}$ denotes the complex scattering coefficient corresponding to the $(r,d)^{\text{th}}$ element of the grid, and $\boldsymbol{e}$ accounts for noise and all other unwanted interferences. Note that (13.2) can be recast in matrix form as

$$\boldsymbol{x} = \boldsymbol{\Phi}\boldsymbol{\alpha} + \boldsymbol{e} \tag{13.3}$$

where $\boldsymbol{\Phi} = (\boldsymbol{\varphi}_{0,0}, \boldsymbol{\varphi}_{0,1}, \ldots, \boldsymbol{\varphi}_{N_r-1,N_d-1})$ and $\boldsymbol{\alpha} = (\alpha_{0,0}, \alpha_{0,1}, \ldots, \alpha_{N_r-1,N_d-1})^T$. The goal of a radar system is to estimate the location, speed, and the radar cross-section (RCS) of the targets; in other words, to find the vector $\boldsymbol{\alpha}$ in the above equation. As discussed earlier, $\boldsymbol{\alpha}$ in (13.3) is usually sparse. Therefore, different methods from the CS literature can be used for designing $\boldsymbol{s}$ (equivalently an optimized sening matrix $\boldsymbol{\Phi}$), as well as to seek for the sparse $\boldsymbol{\alpha}$ in (13.3).

Notation: We use bold lowercase letters for vectors and bold uppercase letters for matrices. $(.)^T$ and $(.)^H$ denote the vector/matrix transpose and the Hermitian transpose, respectively. $\mathbf{0}$ is the all-zero vector/matrix. $vec(\boldsymbol{X})$ is a vector obtained by stacking the columns of $\boldsymbol{X}$ successively. $\|\mathbf{x}\|_n$ or the l_n-norm of the vector $\mathbf{x}$ is defined as $(\sum_k |\mathbf{x}(k)|^n)^{\frac{1}{n}}$ where $\{\mathbf{x}(k)\}$ are the entries of $\mathbf{x}$. The Frobenius norm of a matrix $\boldsymbol{X}$ (denoted by $\|\boldsymbol{X}\|_F$) is equal to $\|vec(\boldsymbol{X})\|_2$. Finally, $\mathbb{C}$ represents the set of complex numbers.

13.2 Mutual Coherence

The mutual coherence, also known as the coherence of the sensing matrix (CSM) [269], is a useful metric to measure the incoherence required by CS,

which can be defined as

$$\mu(\boldsymbol{\Phi}) \triangleq \max_{(r,d)\neq(r',d')} \frac{|\boldsymbol{\varphi}_{r,d}^H \boldsymbol{\varphi}_{r',d'}|}{\|\boldsymbol{\varphi}_{r,d}\|_2 \|\boldsymbol{\varphi}_{r',d'}\|_2}. \tag{13.4}$$

Suppose that the number of non-zero entries associated with the target scene $\tilde{\boldsymbol{\alpha}}$ satisfies the following inequality

$$\|\tilde{\boldsymbol{\alpha}}\|_0 < \frac{1}{2}\left(1 + \frac{1}{\mu(\boldsymbol{\Phi})}\right). \tag{13.5}$$

Then $\tilde{\boldsymbol{\alpha}}$ is necessarily the sparsest solution of the linear equation $\boldsymbol{x} = \boldsymbol{\Phi}\boldsymbol{\alpha}$. Moreover, fast greedy algorithms such as the basis pursuit (BP) or the orthogonal matching pursuit (OMP) are guaranteed to find the correct solution $\boldsymbol{\alpha}$ [259, 267]. A suitable approach to describe $\mu(\boldsymbol{\Phi})$ is via the Gram matrix $\boldsymbol{G} \triangleq \tilde{\boldsymbol{\Phi}}^H \tilde{\boldsymbol{\Phi}}$, where $\tilde{\boldsymbol{\Phi}}$ is the column-normalized version of $\boldsymbol{\Phi}$. Consequently, $\mu(\boldsymbol{\Phi})$ can be stated as

$$\mu(\boldsymbol{\Phi}) = \max_{k\neq l} |\boldsymbol{G}(k,l)| \tag{13.6}$$

where $\{|\boldsymbol{G}(k,l)|\}_{k\neq l}$ are the *coherence coefficients* associated with the sensing matrix $\boldsymbol{\Phi}$.[1]

Note that a matrix $\boldsymbol{\Phi}$ with low coherence corresponds to a Gram matrix $\boldsymbol{G}$ which is close to identity $\boldsymbol{I}_{N_r N_d}$. As a result, one can reduce the incoherence conveniently via the optimization problem:

$$\min_{\boldsymbol{\Phi}} \|\boldsymbol{G} - \boldsymbol{I}\|_F^2. \tag{13.7}$$

Due to its quartic objective, (13.7) is deemed to be easier to tackle compared to (13.6); however, a large number of variables can make the problem prohibitive. In the next section, we will discuss a more effective approach that formulates a quadratic alternative of (13.7), and particularly facilitates using the fast Fourier transform (FFT) operations to tackle the problem.

13.3 Waveform Synthesis

Due to practical constraints, unimodular sequences (with $|\boldsymbol{s}(k)| = 1, \forall\, k$) are very desirable for transmission purposes [89]. As a result, we consider the design of unimodular transmit sequences $\boldsymbol{s}$ in the following.

We begin the design formulation noting that the coherence between any two arbitrary columns of the matrix $\tilde{\boldsymbol{\Phi}}$ (and equivalently the corresponding

[1] We note that, according to the formulation in (13.2), the coherence coefficients can also be associated with the transmit sequence $\boldsymbol{s}$.

element in the Gram matrix $\boldsymbol{G}$) can be written as

$$\begin{aligned}\tilde{\boldsymbol{\varphi}}_{r,d}^{H}\tilde{\boldsymbol{\varphi}}_{r',d'} &= \left(\frac{1}{\sqrt{N}}\boldsymbol{T}^{r}\boldsymbol{F}^{d}\boldsymbol{s}\right)^{H}\left(\frac{1}{\sqrt{N}}\boldsymbol{T}^{r'}\boldsymbol{F}^{d'}\boldsymbol{s}\right)\\ &= \frac{1}{N}\left(\boldsymbol{s}^{H}\boldsymbol{F}^{dH}\boldsymbol{T}^{rH}\right)\left(\boldsymbol{T}^{r'}\boldsymbol{F}^{d'}\boldsymbol{s}\right)\\ &= \frac{1}{N}\boldsymbol{s}^{H}\boldsymbol{F}^{dH}\widetilde{\boldsymbol{T}}_{\Delta r}\boldsymbol{F}^{d'}\boldsymbol{s} \end{aligned} \tag{13.8}$$

where $\widetilde{\boldsymbol{T}}_{\Delta r} = \boldsymbol{T}^{rH}\boldsymbol{T}^{r'}$, and $\Delta r = r' - r$. Based on the above equation, it is easy to verify that the terms formulated in (13.8) are identical for all (r, r') with the same Δr. Therefore, the Gram matrix $\boldsymbol{G}$ has a specific structure that can be exploited. Namely, using (13.8) the objective function in (13.7) can be rewritten as

$$\begin{aligned}\|\boldsymbol{G}-\boldsymbol{I}\|_F^2 &= \left\|\begin{pmatrix} \widetilde{\boldsymbol{G}}_0 & \widetilde{\boldsymbol{G}}_1 & \cdots & \widetilde{\boldsymbol{G}}_{N_r-1} \\ \widetilde{\boldsymbol{G}}_{-1} & \widetilde{\boldsymbol{G}}_0 & \cdots & \widetilde{\boldsymbol{G}}_{N_r-2} \\ \vdots & \vdots & \ddots & \vdots \\ \widetilde{\boldsymbol{G}}_{1-N_r} & \widetilde{\boldsymbol{G}}_{2-N_r} & \cdots & \widetilde{\boldsymbol{G}}_0 \end{pmatrix} - \boldsymbol{I}\right\|_F^2\\ &= \sum_{r=-(N-1)}^{N-1}\gamma_r^2\,\|\widetilde{\boldsymbol{G}}_r - \boldsymbol{I}\delta_r\|_F^2 \end{aligned} \tag{13.9}$$

where

$$\widetilde{\boldsymbol{G}}_r = \boldsymbol{X}^{H}\widetilde{\boldsymbol{T}}_r\boldsymbol{X}, \tag{13.10}$$

$$\boldsymbol{X} = (\boldsymbol{x}_0, \boldsymbol{x}_1, \ldots, \boldsymbol{x}_{N_d-1}), \tag{13.11}$$

$$\boldsymbol{x}_d = \frac{1}{\sqrt{N}}\boldsymbol{F}^{d}\boldsymbol{s} \quad , \quad d = 0, 1, \ldots, N_d - 1, \tag{13.12}$$

$$\gamma_r^2 = \begin{cases} N_r - |r|, & |r| < N_r, \\ 0, & \text{otherwise}, \end{cases} \tag{13.13}$$

and δ_r denotes the Kronecker delta function which is one if $r = 0$, and is zero otherwise. It is worth observing that (13.9) contributes a significant reduction in the size of the matrix variables.

Next note that $\widetilde{\boldsymbol{T}}_r$ is a shifting matrix, and hence $\widetilde{\boldsymbol{G}}_r$ can be viewed as the covariance matrix of the vectors $\{\mathbf{x}_d\}$ corresponding to the time lag r. Based

on this observation, the following Parseval-type equality holds [270]:

$$\begin{aligned}\|\boldsymbol{G}-\boldsymbol{I}\|_F^2 &= \sum_{r=-(N-1)}^{N-1} \gamma_r^2 \|\widetilde{\boldsymbol{G}}_r - \boldsymbol{I}\delta_r\|_F^2 \\ &= \frac{1}{2N}\sum_{p=1}^{2N} \left\| \boldsymbol{\Psi}\left(\frac{2\pi p}{2N}\right) - \gamma_0 \boldsymbol{I} \right\|_F^2 \end{aligned} \tag{13.14}$$

in which

$$\boldsymbol{\Psi}(\omega) = \sum_{r=-(N-1)}^{N-1} \gamma_r \boldsymbol{X}^H \widetilde{\boldsymbol{T}}_r \boldsymbol{X}\, e^{-j\omega r}. \tag{13.15}$$

Interestingly, the frequency domain criterion in (13.14) has the same form as (28) in [270]. Therefore, we employ a similar approach to tackle the problem herein. In particular, the $\boldsymbol{\Psi}(\omega)$ defined in (13.15) can also be written in the form

$$\boldsymbol{\Psi}(\omega) = \boldsymbol{Z}^H(\omega)\boldsymbol{\Gamma}\boldsymbol{Z}(\omega) \tag{13.16}$$

with

$$\boldsymbol{Z}(\omega) = (\boldsymbol{z}(1)e^{-j\omega}, \ldots, \boldsymbol{z}(N)e^{-j\omega N})^T, \tag{13.17}$$

$$\boldsymbol{z}(n) = (\boldsymbol{x}_0(n), \ldots, \boldsymbol{x}_{N_d-1}(n))^T \tag{13.18}$$

for $1 \le n \le N$, and

$$\boldsymbol{\Gamma} = \begin{pmatrix} \gamma_0 & \gamma_1 & \cdots & \gamma_{N-1} \\ \gamma_{-1} & \gamma_0 & \cdots & \vdots \\ \vdots & \vdots & \ddots & \gamma_1 \\ \gamma_{-N+1} & \cdots & \gamma_{-1} & \gamma_0 \end{pmatrix}. \tag{13.19}$$

As a result, we have that

$$\|\boldsymbol{G}-\boldsymbol{I}\|_F^2 = \frac{1}{2N}\sum_{p=1}^{2N} \|\boldsymbol{Z}_p^H \boldsymbol{\Gamma} \boldsymbol{Z}_p - \gamma_0 \boldsymbol{I}\|_F^2 \tag{13.20}$$

where $\boldsymbol{Z}_p \triangleq \boldsymbol{Z}(2\pi p/(2N))$. Now note that $\|\widetilde{\boldsymbol{G}}_0 - \boldsymbol{I}\|_F^2$ is a constant, and thus, a diagonal loading of $\boldsymbol{\Gamma}$ does not change the solution to (13.7). Let $\tilde{\boldsymbol{\Gamma}} = \boldsymbol{\Gamma} + \lambda \boldsymbol{I}$, with λ being a non-negative scalar that can ensure $\tilde{\boldsymbol{\Gamma}} \ge 0$. Consequently, one can reduce the incoherence of $\boldsymbol{\Phi}$ conveniently using the following quadratic almost-equivalent form of (13.20), see [89, 270]:

$$\begin{aligned} \min_{\boldsymbol{s},\boldsymbol{U}_p} \quad & \sum_{p=1}^{2N} \|\boldsymbol{C}\boldsymbol{Z}_p - \sqrt{\gamma_0}\boldsymbol{U}_p\|_F^2 \\ \text{s.t.} \quad & |\boldsymbol{s}_n| = 1, \qquad n = 1, \ldots, N, \\ & \boldsymbol{U}_p^H \boldsymbol{U}_p = \boldsymbol{I},\ p = 1, \ldots, 2N, \end{aligned} \tag{13.21}$$

where $\boldsymbol{C}$ is the Hermitian square root of $\tilde{\boldsymbol{\Gamma}}$, i.e. $\boldsymbol{C}^H\boldsymbol{C} = \tilde{\boldsymbol{\Gamma}}$.

To tackle the minimization problem in (13.21), we adopt a cyclic method as follows. For given $\{\boldsymbol{Z}_p\}_{p=1}^{2N}$ (equivalently a given transmit sequence $\boldsymbol{s}$), let $\boldsymbol{Z}_p^H\boldsymbol{C}^H = \boldsymbol{U}_1\boldsymbol{\Sigma}\boldsymbol{U}_2^H$ represent the *economy-size* singular value decomposition (SVD) of $\boldsymbol{Z}_p^H\boldsymbol{C}^H$, with $\boldsymbol{U}_1$ being an $N_d \times N_d$ unitary matrix, $\boldsymbol{\Sigma}$ being an $N_d \times N_d$ diagonal matrix and $\boldsymbol{U}_2$ being an $N \times N_d$ semi-unitary matrix. Then the minimizer $\boldsymbol{U}_p$ of (13.21) is given by [270]

$$\boldsymbol{U}_p = \boldsymbol{U}_2\boldsymbol{U}_1^H. \tag{13.22}$$

Similar to the WeCAN algorithm in [270], the computation of $\boldsymbol{C}\boldsymbol{Z}_p$ can be performed using the FFT operation. To observe how, let

$$\tilde{\boldsymbol{X}}_m = \boldsymbol{C}^T \odot (\boldsymbol{x}_m, \boldsymbol{x}_m, \ldots, \boldsymbol{x}_m)_{N\times N} \tag{13.23}$$

for $0 \le m \le N_d - 1$, and

$$\boldsymbol{F} = \sqrt{2N}\boldsymbol{A}^H\tilde{\boldsymbol{F}}, \quad \tilde{\boldsymbol{F}} = \begin{pmatrix} \tilde{\boldsymbol{X}}_0 & \cdots & \tilde{\boldsymbol{X}}_{N_d-1} \\ \boldsymbol{0}_{N\times N} & \cdots & \boldsymbol{0}_{N\times N} \end{pmatrix} \tag{13.24}$$

where $\boldsymbol{A}$ denotes the $2N \times 2N$ (inverse) DFT matrix, whose (l,p)-element is given by

$$[A]_{l,p} = \frac{1}{\sqrt{2N}} e^{j2\pi lp/(2N)}, \quad l,p = 1,\ldots,2N. \tag{13.25}$$

Using the above formulations, one can observe that the $N \times N_d$ matrix $\boldsymbol{C}\boldsymbol{Z}_p$ may be obtained by reshaping the $NN_d \times 1$ vector $\boldsymbol{f}_p$ into each column of $\boldsymbol{C}\boldsymbol{Z}_p$, where $\boldsymbol{f}_p^T$ represents the p^{th} row of $\boldsymbol{F}$.

Next we discuss the minimization of (13.21) with respect to $\boldsymbol{s}$ for given $\{\boldsymbol{U}_p\}_{p=1}^{2N}$. Let

$$\boldsymbol{V}_{2N\times NN_d} = (\boldsymbol{v}_1, \boldsymbol{v}_2, \ldots, \boldsymbol{v}_{2N})^T \tag{13.26}$$

where $\boldsymbol{v}_p = \sqrt{\gamma_0}\, vec(\boldsymbol{U}_p)$, $1 \le p \le 2N$. Then the criterion in (13.21) can be written as

$$\begin{aligned} \sum_{p=1}^{2N} \|\boldsymbol{C}\boldsymbol{Z}_p - \sqrt{\gamma_0}\boldsymbol{U}_p\|_F^2 &= \left\| \sqrt{2N}\boldsymbol{A}^H\tilde{\boldsymbol{F}} - \boldsymbol{V} \right\|_F^2 \\ &= 2N \left\| \tilde{\boldsymbol{F}} - \frac{1}{\sqrt{2N}}\boldsymbol{A}\boldsymbol{V} \right\|_F^2. \end{aligned} \tag{13.27}$$

Note that (13.27) can be minimized with respect to each element of $\boldsymbol{s}$ in a separate manner. Particularly, we can consider minimizing the following criterion with respect to s (a generic element of $\boldsymbol{s}$):

$$\sum_{k=1}^{NN_d} |\mu_k s - \nu_k|^2 = \text{const} - 2\Re\left[\left(\sum_{k=1}^{NN_d} \mu_k^* \nu_k \right) s^* \right] \tag{13.28}$$

Table 13.1. *The Proposed Algorithm for Sparsity-Aided Transmit Sequence Design*

Step 0: Initialize the transmit sequence $\boldsymbol{s}$ with a random unimodular sequence (or by a good existing sequence). Calculate the Hermitian square root $\boldsymbol{C}$ of $\tilde{\boldsymbol{\Gamma}}$.
Step 1: Fix $\boldsymbol{s}$ (equivalently $\{\boldsymbol{Z}_p\}_{p=1}^{2N}$) and compute $\{\boldsymbol{U}_p\}_{p=1}^{2N}$ using (13.22).
Step 2: Fix $\{\boldsymbol{U}_p\}_{p=1}^{2N}$ and compute $\boldsymbol{s}$ using (13.29).
Step 3: Repeat steps 1 and 2 until a stop criterion is satisfied, e.g. $\|\boldsymbol{s}^{(t+1)}-\boldsymbol{s}^{(t)}\|_F < \varepsilon$ for some given $\varepsilon > 0$, where t denotes the total iteration number.

where $\{\mu_k\}$ are given by the elements of $\tilde{\boldsymbol{F}}$ that contain s, and ν_k is given by the element of $\frac{1}{\sqrt{2N}}\boldsymbol{AV}$ whose position is the same as that of μ_k in $\tilde{\boldsymbol{F}}$. Hence, the unimodular s minimizing (13.28) is

$$s = e^{j\varphi},\ \varphi = \arg\left(\sum_{k=1}^{NN_d} \mu_k^* \nu_k\right). \tag{13.29}$$

Finally, the steps of the proposed algorithm for designing the transmit sequence $\boldsymbol{s}$ are summarized in Table 13.1.

13.4 Numerical Examples

13.4.1 Incoherence

We consider employing the proposed method to design a transmit sequence $\boldsymbol{s}$ of length $N = 127$, using the Alltop sequence as initialization, for a target scene with $N_r = 20$ range and $N_d = 15$ Doppler bins. The Alltop sequence is known to yield a desirable incoherence property of the sensing matrix $\boldsymbol{\Phi}$ [266], and is defined for prime lengths $N > 5$ as

$$\boldsymbol{s}(n) = e^{j\frac{2\pi}{N}n^3}, \quad n = 1,2,\ldots,N. \tag{13.30}$$

In a type of example inspired by [267], we compare the coherence coefficients associated with the Alltop sequence, and those of the optimized sequence obtained by the proposed method. Furthermore, we include the results obtained by using the coherence reduction approach in [267] initialized by the Alltop sequence. The results are shown in Fig. 13.1. It can be observed from Fig. 13.1 that the proposed method in this work and the approach in [267] can lead to a similar coherence distribution. On the other hand, both methods outperform the Alltop sequence in terms of incoherence.

13.4.2 Target Scene Recovery

In order to verify the effectiveness of the optimized sequences, we examine the root mean-square errors (RMSEs) of the target scene recovery for different sparsity orders $K = \|\boldsymbol{\alpha}\|_0$. We construct the sparse vectors $\boldsymbol{\alpha}$ by choosing K non-zero locations in the vector, with identical chance for all $\binom{N_d N_r}{K}$ assignments of the non-zero locations, and consider random positive RCS values for the non-zero locations. We let $N = 127$, $N_r = 20$, $N_d = 15$, and set the signal-to-noise ratio to 0dB. Based on these settings, we use the OMP algorithm for the recovery of $\boldsymbol{\alpha}$. The results leading to Fig. 13.2 are obtained by averaging the RMSE values for 500 Monte Carlo experiments (with different random initializations). Once again, the proposed method and the approach in [267] present a very similar performance. However, according to Fig. 13.2, the optimized sequences obtained by both methods can yield a smaller RMSE compared to that of Alltop sequence; particularly when the sparsity order K grows large. We note that for larger values of K, a low incoherence of the sensing matrix $\boldsymbol{\Phi}$ becomes more crucial to an accurate reconstruction of the target scene; see (13.5).

13.4.3 Computation Time

Finally, we compare the computation times required by the proposed method and the coherence reduction approach devised in [267], when performing the sequence design for various lengths N of the transmit sequence. Herein, we set $M = 10$, $N_d = 8$, and $N_r = N$. It can be observed from Fig. 13.3 that the computation time of the design algorithm in [267] is growing rapidly as N grows large. In contrary, the proposed algorithm can be used for comparably large lengths of the transmit sequence, e.g. $N \gtrsim 100$. The results leading to Fig. 13.3 were obtained by averaging the computation times over 100 experiments (with different random initializations) using a PC with Intel Core i5 CPU 750 @2.67GHz, and 8GB memory.

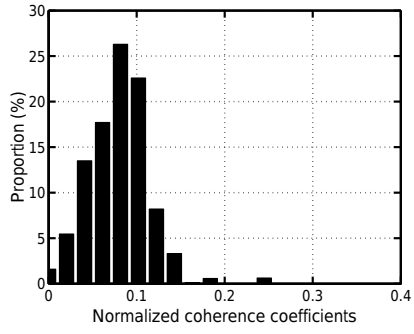

(a)

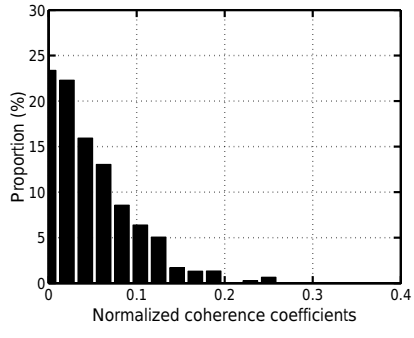

(b)

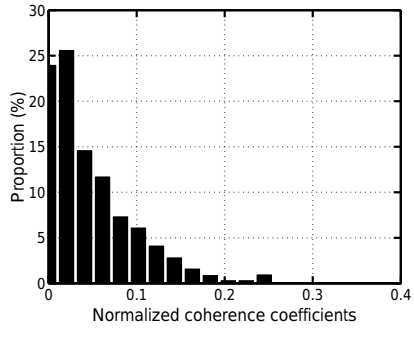

(c)

Figure 13.1. Distribution of the coherence coefficients associated with (a) Alltop sequence, and (b-c) the optimized sequences obtained by the proposed method and the coherence reduction approach in [267], respectively, using the Alltop sequence as initialization.

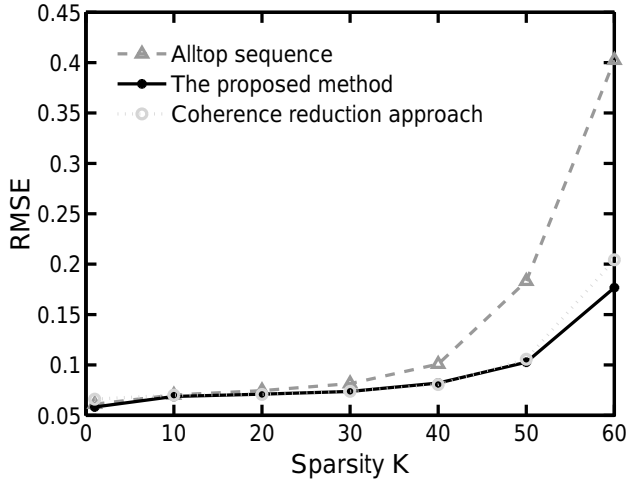

Figure 13.2. Comparison of the recovery error for sensing matrices built based on the Alltop sequence and the optimized sequences obtained by the proposed method and the approach in [267], for different sparsity orders K of the target scene $\boldsymbol{\alpha}$.

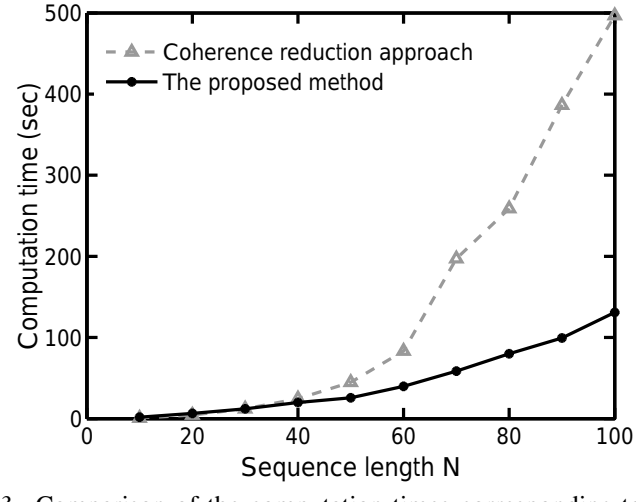

Figure 13.3. Comparison of the computation times corresponding to the proposed method and the design algorithm devised in [267], for different lengths N of the transmit sequence.

Part V:
Beam-Pattern Matching Metrics

14. Single-Stage Transmit Beamforming Design for MIMO Radar

Abstract
MIMO radar beamforming algorithms usually consist of a signal covariance matrix synthesis stage, followed by signal synthesis to fit the obtained covariance matrix. In this chapter, we propose a radar beamforming algorithm (called Beam-Shape) that performs a single-stage radar transmit signal design; i.e. no prior covariance matrix synthesis is required. Beam-Shape's theoretical as well as computational characteristics, include: (i) the possibility of considering signal structures such as low-rank, discrete-phase or low-PAR, and (ii) the significantly reduced computational burden for beampattern matching scenarios with large grid size. The effectiveness of the proposed algorithm is illustrated through numerical examples.

Keywords: Beamforming, multi-input multi-output (MIMO) radar, peak-to-average-power ratio (PAR), signal design

14.1 Introduction

A key problem in the radar literature is the transmit signal design for matching a desired beampattern. In contrast to conventional phased-array radar, multiple-input multiple-output (MIMO) radar uses its antennas to transmit independent waveforms, and thus provides extra degrees of freedom (DOF) [273] [274]. As a result, MIMO radars can achieve beampatterns which might be impossible for phased-arrays [275] [276]. The MIMO radar transmit beampattern design approaches in the literature require two stages in general (see, e.g. [275]- [284]). The first stage consists of the design of the transmit covariance matrix $\boldsymbol{R}$. The design of $\boldsymbol{R}$ can be typically performed using convex optimization tools. Next, the transmit signals (under practical constraints) are designed in order to fit the obtained covariance matrix.

In this chapter, we present a novel approach (which we call *Beam-Shape*) for "shaping" the transmit beam of MIMO radar via a single-stage transmit signal design. We consider the transmit beamspace processing (TBP) scheme [281] [286] for system modeling (see Section 14.2 for details). Due to different practical (or computational) demands, two optimization problems are considered for both TBP weight matrix design as well as a direct design of the transmit signal. In comparison to the two-stage framework of beamforming approaches in the literature:

- Beam-Shape is able to directly consider in its formulation the matrix rank or signal constraints (such as low peak-to-average-power ratio (PAR), or discrete-phase); an advantage which generally is not shared with the covariance matrix design. As a result, the matching optimization problem will produce optimized solutions considering all the constraints of the original problem at once, and may thus avoid the optimality losses imposed by a further signal synthesis stage. See Section 14.4 for some numerical illustrations.
- In beamforming scenarios with large grid size, Beam-Shape appears to have a significantly smaller computational burden compared to the two-stage framework. See the related discussions in Sections 14.3 and 14.4.

Notation: We use bold lowercase letters for vectors and bold uppercase letters for matrices. $(\cdot)^T$, $(\cdot)^*$ and $(\cdot)^H$ denote the vector/matrix transpose, the complex conjugate, and the Hermitian transpose, respectively. $\mathbf{1}$ and $\mathbf{0}$ are the all-one and all-zero vectors/matrices. The symbol $\odot$ stands for the Hadamard (element-wise) product of matrices. $\|\mathbf{x}\|_n$ or the l_n-norm of the vector $\mathbf{x}$ is defined as $(\sum_k |\mathbf{x}(k)|^n)^{\frac{1}{n}}$ where $\{\mathbf{x}(k)\}$ are the entries of $\mathbf{x}$. The Frobenius norm of a matrix $\boldsymbol{X}$ (denoted by $\|\boldsymbol{X}\|_F$) with entries $\{\boldsymbol{X}(k,l)\}$ is equal to $\left(\sum_{k,l} |\boldsymbol{X}(k,l)|^2\right)^{\frac{1}{2}}$. We use $\Re(\boldsymbol{X})$ and $\Im(\boldsymbol{X})$ to denote the matrices obtained by collecting the real parts, and respectively, the imaginary parts of the entries of $\boldsymbol{X}$. Finally, $\mathscr{Q}_p(\boldsymbol{X})$ yields the closest *p-ary phase matrix* with entries from the set $\{2k\pi/p : k = 0, 1, \cdots, p-1\}$, in an element-wise sense, to an argument *phase matrix* $\boldsymbol{X}$.

14.2 Problem Formulation

Consider a MIMO radar system with M antennas and let $\{\theta_l\}_{l=1}^L$ denote a fine grid of the angular sector of interest. Under the assumption that the transmitted probing signals are narrow-band and the propagation is non-dispersive, the steering vector of the transmit array (at location θ_l) can be written as

$$\boldsymbol{a}(\theta_l) = \left(e^{j2\pi f_0 \tau_1(\theta_l)}, e^{j2\pi f_0 \tau_2(\theta_l)}, \ldots, e^{j2\pi f_0 \tau_M(\theta_l)}\right)^T, \tag{14.1}$$

where f_0 denotes the carrier frequency of the radar, and $\tau_m(\theta_l)$ is the time needed by the transmitted signal of the m^{th} antenna to arrive at the target location θ_l.

In lieu of transmitting M partially correlated waveforms, the TBP technique employs K orthogonal waveforms that are linearly mixed at the transmit array via a weighting matrix $\boldsymbol{W} \in \mathbb{C}^{M\times K}$. The number of orthogonal waveforms K can be determined by counting the number of *significant* eigenvalues of the matrix [286]:

$$\boldsymbol{A} = \sum_{l=1}^{L} \boldsymbol{a}(\theta_l)\boldsymbol{a}^H(\theta_l). \tag{14.2}$$

The parameter K can be chosen such that the sum of the K dominant eigenvalues of $\boldsymbol{A}$ exceeds a given percentage of the total sum of eigenvalues [286]. Note that *usually $K \ll M$ (especially when M is large)* [286] [288]. Let $\boldsymbol{\Phi}$ be the matrix containing K orthonormal TBP waveforms, viz.

$$\boldsymbol{\Phi} = (\boldsymbol{\varphi}_1, \boldsymbol{\varphi}_2, \ldots, \boldsymbol{\varphi}_K)^T \in \mathbb{C}^{K\times N}, \quad K \leq M \tag{14.3}$$

where $\boldsymbol{\varphi}_k \in \mathbb{C}^{N\times 1}$ denotes the k^{th} waveform (or sequence). The transmit signal matrix can then be written as $\boldsymbol{S} = \boldsymbol{W}\boldsymbol{\Phi} \in \mathbb{C}^{M\times N}$, and the transmit beampattern

becomes

$$\begin{aligned} P(\theta_l) &= \|\boldsymbol{S}^H \boldsymbol{a}(\theta_l)\|_2^2 \\ &= \boldsymbol{a}^H(\theta_l)\boldsymbol{W}\boldsymbol{\Phi}\boldsymbol{\Phi}^H\boldsymbol{W}^H\boldsymbol{a}(\theta_l) \\ &= \boldsymbol{a}^H(\theta_l)\boldsymbol{W}\boldsymbol{W}^H\boldsymbol{a}(\theta_l) \\ &= \|\boldsymbol{W}^H\boldsymbol{a}(\theta_l)\|_2^2. \end{aligned} \tag{14.4}$$

Eq. (14.4) sheds light on two different perspectives for radar beampattern design. Observe that matching a desired beampattern may be accomplished by considering $\boldsymbol{W}$ as the design variable. Doing so, one can control the rank (K) of the covariance matrix $\boldsymbol{R} = \boldsymbol{S}\boldsymbol{S}^{\boldsymbol{H}} = \boldsymbol{W}\boldsymbol{W}^{\boldsymbol{H}}$ by fixing the dimensions of $\boldsymbol{W} \in \mathbb{C}^{M\times K}$. This idea becomes of particular interest for the phased-array radar formulation with $K = 1$. Note that considering the optimization problem with respect to $\boldsymbol{W}$ for small K may significantly reduce the computational costs. On the other hand, imposing practical signal constraints (such as discrete-phase or low PAR) while considering $\boldsymbol{W}$ as the design variable appears to be difficult. In such cases, one can resort to a direct beampattern matching by choosing $\boldsymbol{S}$ as the design variable.

In light of the above discussion, we consider beampattern matching problem formulations for designing either $\boldsymbol{W}$ or $\boldsymbol{S}$ as follows. Let $P_d(\theta_l)$ denote the desired beampattern. According to the last equality in (14.4), $P_d(\theta_l)$ can be synthesized exactly if and only if there exist a unit-norm vector $\boldsymbol{p}(\theta_l)$ such that

$$\boldsymbol{W}^H\boldsymbol{a}(\theta_l) = \sqrt{P_d(\theta_l)}\boldsymbol{p}(\theta_l). \tag{14.5}$$

Therefore, by considering $\{\boldsymbol{p}(\theta_l)\}_l$ as auxiliary design variables, the beampattern matching via weight matrix design can be dealt with conveniently via the optimization problem:

$$\min_{\boldsymbol{W},\alpha,\{\boldsymbol{p}(\theta_l)\}} \quad \sum_{l=1}^{L} \left\| \boldsymbol{W}^H\boldsymbol{a}(\theta_l) - \alpha\sqrt{P_d(\theta_l)}\boldsymbol{p}(\theta_l) \right\|_2^2 \tag{14.6}$$

$$\text{s.t.} \qquad (\boldsymbol{W}\odot\boldsymbol{W}^*)\mathbf{1} = \tfrac{E}{M}\mathbf{1}, \tag{14.7}$$

$$\|\boldsymbol{p}(\theta_l)\|_2 = 1,\ \forall l, \tag{14.8}$$

where (14.7) is the transmission energy constraint at each transmitter with E being the total energy, and α is a scalar accounting for the energy difference between the desired beampattern and the transmitted beam. Similarly, the beampattern matching problem with $\boldsymbol{S}$ as the design variable can be formulated as

$$\min_{\boldsymbol{S},\alpha,\{\boldsymbol{p}(\theta_l)\}} \quad \sum_{l=1}^{L} \left\| \boldsymbol{S}^H\boldsymbol{a}(\theta_l) - \alpha\sqrt{P_d(\theta_l)}\boldsymbol{p}(\theta_l) \right\|_2^2 \tag{14.9}$$

$$\text{s.t.} \qquad (\boldsymbol{S}\odot\boldsymbol{S}^*)\mathbf{1} = \tfrac{E}{M}\mathbf{1}, \tag{14.10}$$

$$\|\boldsymbol{p}(\theta_l)\|_2 = 1,\ \forall l, \tag{14.11}$$

$$\boldsymbol{S} \in \Psi, \tag{14.12}$$

where Ψ is the desired set of transmit signals. The above beampattern matching formulations pave the way for an algorithm (which we call Beam-Shape) that can perform a direct matching of the beampattern with respect to the weight matrix $\boldsymbol{W}$ or the signal $\boldsymbol{S}$, without requiring an intermediate synthesis of the covariance matrix.

14.3 Beam-Shape

We begin by considering the beampattern matching formulation in (14.6). For fixed $\boldsymbol{W}$ and α, the minimizer $\boldsymbol{p}(\theta_l)$ of (14.6) is given by

$$\boldsymbol{p}(\theta_l) = \frac{\boldsymbol{W}^H \boldsymbol{a}(\theta_l)}{\|\boldsymbol{W}^H \boldsymbol{a}(\theta_l)\|_2}. \tag{14.13}$$

Let $P \triangleq \sum_{l=1}^{L} P_d(\theta_l)$. For fixed $\boldsymbol{W}$ and $\{\boldsymbol{p}(\theta_l)\}$ the minimizer α of (14.6) can be obtained as

$$\alpha = \Re\left\{ \left(\sum_{l=1}^{L} \sqrt{P_d(\theta_l)} \boldsymbol{p}^H(\theta_l) \boldsymbol{W}^H \boldsymbol{a}(\theta_l) \right) / P \right\}. \tag{14.14}$$

Using (14.13), the expression for α can be further simplified as

$$\alpha = \left(\sum_{l=1}^{L} \sqrt{P_d(\theta_l)} \left\| \boldsymbol{W}^H \boldsymbol{a}(\theta_l) \right\|_2 \right) / P. \tag{14.15}$$

Now assume that $\{\boldsymbol{p}(\theta_l)\}$ and α are fixed. Note that

$$\begin{aligned} Q(\boldsymbol{W}) &= \sum_{l=1}^{L} \|\boldsymbol{W}^H \boldsymbol{a}(\theta_l) - \alpha \sqrt{P_d(\theta_l)} \boldsymbol{p}(\theta_l)\|_2^2 \\ &= \mathrm{tr}(\boldsymbol{W}\boldsymbol{W}^H \boldsymbol{A}) - 2\Re\{\mathrm{tr}(\boldsymbol{W}\boldsymbol{B})\} + P\alpha^2 \end{aligned} \tag{14.16}$$

where $\boldsymbol{A}$ is as defined in (14.2), and

$$\boldsymbol{B} = \sum_{l=1}^{L} \alpha \sqrt{P_d(\theta_l)} \boldsymbol{p}(\theta_l) \boldsymbol{a}^H(\theta_l). \tag{14.17}$$

By dropping the constant part in $Q(\boldsymbol{W})$, we have

$$\begin{aligned} \widetilde{Q}(\boldsymbol{W}) &= \mathrm{tr}(\boldsymbol{W}\boldsymbol{W}^H \boldsymbol{A}) - 2\Re\{\mathrm{tr}(\boldsymbol{W}\boldsymbol{B})\} \\ &= \mathrm{tr}\left(\begin{pmatrix} \boldsymbol{W} \\ \boldsymbol{I} \end{pmatrix}^H \underbrace{\begin{pmatrix} \boldsymbol{A} & -\boldsymbol{B}^H \\ -\boldsymbol{B} & \boldsymbol{0} \end{pmatrix}}_{\triangleq \boldsymbol{C}} \underbrace{\begin{pmatrix} \boldsymbol{W} \\ \boldsymbol{I} \end{pmatrix}}_{\triangleq \widetilde{\boldsymbol{W}}} \right). \end{aligned} \tag{14.18}$$

Therefore, the minimization of (14.6) with respect to $\boldsymbol{W}$ is equivalent to

$$\min_{\boldsymbol{W}} \quad \operatorname{tr}\left(\widetilde{\boldsymbol{W}}^H \boldsymbol{C} \widetilde{\boldsymbol{W}}\right) \tag{14.19}$$

$$\text{s.t.} \quad (\boldsymbol{W} \odot \boldsymbol{W}^*)\mathbf{1} = \tfrac{E}{M}\mathbf{1}, \tag{14.20}$$

$$\widetilde{\boldsymbol{W}} = \left(\boldsymbol{W}^T \; \boldsymbol{I}\right)^T. \tag{14.21}$$

As a result of the energy constraint in (14.20), $\widetilde{\boldsymbol{W}}$ has a fixed Frobenius norm, and hence a diagonal loading of $\boldsymbol{C}$ does not change the solution to (14.19). Therefore, (14.19) can be written in the following equivalent form:

$$\max_{\boldsymbol{W}} \quad \operatorname{tr}\left(\widetilde{\boldsymbol{W}}^H \widetilde{\boldsymbol{C}} \widetilde{\boldsymbol{W}}\right) \tag{14.22}$$

$$\text{s.t.} \quad (\boldsymbol{W} \odot \boldsymbol{W}^*)\mathbf{1} = \tfrac{E}{M}\mathbf{1}, \tag{14.23}$$

$$\widetilde{\boldsymbol{W}} = \left(\boldsymbol{W}^T \; \boldsymbol{I}\right)^T \tag{14.24}$$

where $\widetilde{\boldsymbol{C}} = \lambda \boldsymbol{I} - \boldsymbol{C}$, with λ being larger than the maximum eigenvalue of $\boldsymbol{C}$. In particular, *an increase in the objective function of (14.22) leads to a decrease of the objective function in (14.6).* Although (14.22) is non-convex, a monotonically increasing sequence of the objective function in (14.22) may be obtained (see Appendix A for a proof) via a generalization of the *power method-like iterations* proposed in [84] and [85], namely:

$$\boldsymbol{W}^{(t+1)} = \sqrt{\frac{E}{M}}\, \eta\left(\begin{pmatrix} \boldsymbol{I}_{M\times M} \\ \mathbf{0} \end{pmatrix}^T \widetilde{\boldsymbol{C}} \widetilde{\boldsymbol{W}}^{(t)}\right) \tag{14.25}$$

where the iterations may be initialized with the latest approximation of $\boldsymbol{W}$ (used as $\boldsymbol{W}^{(0)}$), t denotes the internal iteration number, and $\eta(\cdot)$ is a row-scaling operator that makes the rows of the matrix argument have unit-norm.

Next we study the optimization problem in (14.9). Thanks to the similarity of the problem formulation to (14.6), the derivations of the minimizers $\{\boldsymbol{p}(\theta_l)\}$ and α of (14.9) remain the same as for (14.6). Moreover, the minimization of (14.9) with respect to the constrained $\boldsymbol{S}$ can be formulated as the following optimization problem:

$$\max_{\boldsymbol{S}} \quad \operatorname{tr}\left(\widetilde{\boldsymbol{S}}^H \widetilde{\boldsymbol{C}} \widetilde{\boldsymbol{S}}\right) \tag{14.26}$$

$$\text{s.t.} \quad (\boldsymbol{S} \odot \boldsymbol{S}^*)\mathbf{1} = \tfrac{E}{M}\mathbf{1}, \tag{14.27}$$

$$\widetilde{\boldsymbol{S}} = \left(\boldsymbol{S}^T \boldsymbol{I}\right)^T, \; \boldsymbol{S} \in \Psi \tag{14.28}$$

with $\widetilde{\boldsymbol{C}}$ being the same as in (14.22). An increasing sequence of the objective function in (14.26) can be obtained via power method-like iterations that exploit the following nearest-matrix problem (see Appendix A for a sketched

proof):

$$\min_{\boldsymbol{S}^{(t+1)}} \quad \left\| \boldsymbol{S}^{(t+1)} - \begin{pmatrix} \boldsymbol{I}_{M\times M} \\ \boldsymbol{0} \end{pmatrix}^T \widetilde{\boldsymbol{C}}\widetilde{\boldsymbol{S}}^{(t)} \right\|_F \tag{14.29}$$

$$\text{s.t.} \quad (\boldsymbol{S}^{(t+1)} \odot \boldsymbol{S}^{*(t+1)})\mathbf{1} = \tfrac{E}{M}\mathbf{1}, \;\; \boldsymbol{S}^{(t+1)} \in \Psi. \tag{14.30}$$

Obtaining the solution to (14.29) for some constraint sets Ψ such as real-valued, unimodular, or p-ary matrices is straightforward (see Appendix B), viz.

$$\boldsymbol{S}^{(t+1)} = \begin{cases} \sqrt{\frac{E}{M}}\,\eta\left(\Re\left\{\widehat{\boldsymbol{S}}^{(t)}\right\}\right), & \Psi = \text{real-values matrices}, \\ e^{j\arg\left(\widehat{\boldsymbol{S}}^{(t)}\right)}, & \Psi = \text{unimodular matrices}, \\ e^{j\mathscr{Q}_p\left(\arg\left(\widehat{\boldsymbol{S}}^{(t)}\right)\right)}, & \Psi = p\text{-ary matrices}, \end{cases} \tag{14.31}$$

where

$$\widehat{\boldsymbol{S}}^{(t)} = \begin{pmatrix} \boldsymbol{I}_{M\times M} \\ \boldsymbol{0} \end{pmatrix}^T \widetilde{\boldsymbol{C}}\widetilde{\boldsymbol{S}}^{(t)}. \tag{14.32}$$

Furthermore, the case of PAR-constrained $\boldsymbol{S}$ can be handled efficiently via a recursive algorithm devised in [289].

Finally, the Beam-Shape algorithm for beampattern matching via designing the weight matrix $\boldsymbol{W}$ or the transmit signal $\boldsymbol{S}$ is summarized in Table 14.1. Note that the focus of signal design formulation in (9) is on the beampattern matching in MIMO scenarios. In particular, (9) does not take into account the signal and beampattern auto/cross-correlation properties which are of interest in some radar applications using match filtering. Nevertheless, the numerical results in Section IV show that the signals obtained from (9) can also have desirable correlation/ambiguity properties presumably due to their pseudorandom appearance in the N-dimensional space. We refer the interested reader to Part I of this thesis for several computational methods related to (MIMO) signal design with good correlation properties.

Remark: A brief comparison of the computational complexity of the Beam-Shape algorithm and the two-stage beamforming approaches in the literature is as follows. The design of the covariance matrix $\boldsymbol{R} \in \mathbb{C}^{M\times M}$ for the two-stage framework can be done using a semi-definite program (SDP) representation with $\mathscr{O}(L)$ constraints. The corresponding SDP may be solved with $\mathscr{O}(\max\{M,L\}^4 M^{1/2}\log(1/\varepsilon))$ complexity, where $\varepsilon > 0$ denotes the solution accuracy [2]. Using the formulation in [276], the design of $\boldsymbol{W}$ or $\boldsymbol{S}$ (for fitting the given covariance matrix) leads to an iterative approach with an iteration complexity of $\mathscr{O}(M^2K + KM^2 + K^3)$, or $\mathscr{O}(M^2N + NM^2 + N^3)$, respectively. On the other hand, Beam-Shape is an iterative method with an iteration complexity of $\mathscr{O}(M(L+KH)(M+K))$ for designing $\boldsymbol{W}$, and $\mathscr{O}(M(L+NH)(M+$

Table 14.1. *The Beam-Shape algorithm for MIMO radar beamforming*

Step 0: Calculate the matrix $\boldsymbol{A}$ using (14.2). Choose random α and $\{\boldsymbol{p}(\theta_l)\}$ and initialize the matrix $\boldsymbol{B}$ using (14.17).
Step 1: Use the power method-like iterations in (14.25) (until convergence) to obtain $\boldsymbol{W}$, or (14.29) to obtain $\boldsymbol{S}$.
Step 2: Update $\{\boldsymbol{p}(\theta_l)\}$, α, and $\boldsymbol{B}$ using (14.13), (14.15), and (14.17), respectively.
Step 3: Repeat steps 1 and 2 until a stop criterion is satisfied, e.g. $\|\boldsymbol{W}^{(v+1)} - \boldsymbol{W}^{(v)}\|_F < \varepsilon$ for some given $\varepsilon > 0$, where v denotes the total iteration number.

$N)$) for designing $\boldsymbol{S}$; where H denotes the number of required internal iterations of the power method-like methods discussed in (14.25) or (14.29). The above results suggest that *Beam-Shape may be more computationally efficient when the grid size (L) grows large*. The next section provides numerical examples for further computational efficiency comparison between the two approaches. ■

14.4 Numerical Examples with Discussions

In this section, we provide several numerical examples to show the potential of Beam-Shape in applications. Consider a MIMO radar with a uniform linear array (ULA) comprising $M = 32$ antennas with half-wavelength spacing between adjacent antennas. The total transmit power is set to $E = MN$. The angular pattern covers $[-90^\circ, 90^\circ]$ with a mesh grid size of 1° and the desired beampattern is given by

$$P_d(\theta) = \begin{cases} 1, \ \theta \in [\widehat{\theta}_k - \Delta, \widehat{\theta}_k + \Delta] \\ 0, \ \text{otherwise} \end{cases} \tag{14.33}$$

where $\widehat{\theta}_k$ denotes the direction of a target of interest and 2Δ is the chosen beamwidth for each target. In the following examples, we assume 3 targets located at $\widehat{\theta}_1 = -45^\circ$, $\widehat{\theta}_2 = 0^\circ$ and $\widehat{\theta}_3 = 45^\circ$ with a beamwidth of 24° ($\Delta = 12^\circ$). The results are compared with those obtained via the covariance matrix synthesis-based (CMS) approach proposed in [275] and [276]. For the sake of a fair comparison, we define the mean square error (MSE) of a beampattern matching as

$$\text{MSE} \triangleq \sum_{l=1}^{L} \left| \boldsymbol{a}^H(\theta_l) \boldsymbol{R} \boldsymbol{a}(\theta_l) - P_d(\theta_l) \right|^2 \tag{14.34}$$

which is the typical optimality criterion for the covariance matrix synthesis in the literature (including the CMS in [275] and [276]).

We begin with the design of the weight matrix $\boldsymbol{W}$ using the formulation in (14.6). In particular, we consider $K = M$ corresponding to a general MIMO radar, and $K = 1$ which corresponds to a phased-array. The results are shown in Fig. 14.1. For $K = M$, The MSE values obtained by Beam-Shape and CMS are 1.79 and 1.24, respectively. Note that a smaller MSE value was expected for CMS in this case, as CMS obtains $\boldsymbol{R}$ (or equivalently $\boldsymbol{W}$) by globally minimizing the MSE in (14.34). On the other hand, in the phased-array example (Fig. 14.1(b)), Beam-Shape yields an MSE value of 3.72, whereas the MSE value obtained by CMS is 7.21. Such a behavior was also expected due to the embedded rank constraint when designing $\boldsymbol{W}$ by Beam-Shape, while CMS appears to face a considerable loss during the synthesis of the rank-constrained $\boldsymbol{W}$.

Next we design the transmit signal $\boldsymbol{S}$ using the formulation in (14.9). In this example, $\boldsymbol{S}$ is constrained to be unimodular (i.e. $|\boldsymbol{S}(k,l)| = 1$), which corresponds to a unit PAR. Fig. 14.2 compares the performances of Beam-Shape and CMS for two different lengths of the transmit sequences, namely $N = 8$ (Fig. 14.2(a)) and $N = 128$ (Fig. 14.2(b)). In the case of $N = 8$, Beam-Shape obtains an MSE value of 1.80 while the MSE value obtained by CMS is 2.73. For $N = 128$, the MSE values obtained by Beam-Shape and CMS are 1.74 and 1.28, respectively. Given the fact that $M = 32$, the case of $N = 128$ provides a large number of DOFs for CMS when fitting $\boldsymbol{S}\boldsymbol{S}^H$ to the obtained $\boldsymbol{R}$ in the covariance matrix synthesis stage, whereas for $N = 8$ the number of DOFs is rather limited.

As discussed earlier, the range/Doppler resolution properties of the obtained signals are of interest in some radar applications. Therefore, we also show the (normalized) average absolute value of $M = 32$ discrete ambiguity functions (AFs) associated with the transmit signals in $\boldsymbol{S}$ (Fig. 14.3(a)), as well as the (normalized) average absolute value of $\binom{M}{2} = 496$ discrete cross ambiguity functions (CAFs) associated with $\boldsymbol{S}$ (Fig. 14.3(b)), both for $N = 128$. The discrete-CAF of two signal vectors $\boldsymbol{s}_1$ and $\boldsymbol{s}_2$ of length N is defined as [89]

$$\overline{r}(k,p) \triangleq \sum_{n=1}^{N} \boldsymbol{s}_1(n)\boldsymbol{s}_2^*(n-k)\, e^{-j2\pi\frac{(n-k)p}{N}}, \qquad (14.35)$$
$$-N+1 \le k \le N-1,\ -N/2 \le p \le N/2-1.$$

It is interesting to observe that the signals in this example have satisfactory ambiguity properties, which is likely due to their pseudorandom character in the N-dimensional space.

Finally, it can be interesting to examine the performance of Beam-Shape in scenarios with large grid size L. To this end, we compare the computation times of Beam-Shape and CMS for different L, using the same problem setup for designing $\boldsymbol{S}$ (as the above example) but for $N = M = 32$. According to Fig. 14.4, the overall CPU time of CMS is growing rapidly as L increases, which implies that CMS can hardly be used for beamforming design with large grid

sizes (e.g. $L \gtrsim 10^3$). In contrast, Beam-Shape runs well for large L, even for $L \sim 10^6$ on a standard PC. The results leading to Fig. 14.4 were obtained by averaging the computation times for 100 experiments (with different random initializations) using a PC with Intel Core i5 CPU 750 @2.67GHz, and 8GB memory.

14.5 Appendices

14.5.1 Appendix A: Power Method-Like Iterations Monotonically Increase the Objective Functions in (14.22) and (14.26)

In the following, we study the power method-like iterations for designing $\boldsymbol{W}$ in (14.22). The extension of the results to the design of $\boldsymbol{S}$ in (14.26) is straightforward. For fixed $\boldsymbol{W}^{(t)}$, observe that the update matrix $\boldsymbol{W}^{(t+1)}$ is the minimizer of the criterion

$$\left\| \widetilde{\boldsymbol{W}}^{(t+1)} - \widetilde{\boldsymbol{C}} \widetilde{\boldsymbol{W}}^{(t)} \right\|_2^2 = \text{const} - 2\Re \left\{ \text{tr} \left(\widetilde{\boldsymbol{W}}^{(t+1)H} \widetilde{\boldsymbol{C}} \widetilde{\boldsymbol{W}}^{(t)} \right) \right\} \tag{14.36}$$

or, equivalently, the maximizer of the criterion

$$\Re \left\{ \text{tr} \left(\widetilde{\boldsymbol{W}}^{(t+1)H} \widetilde{\boldsymbol{C}} \widetilde{\boldsymbol{W}}^{(t)} \right) \right\} \tag{14.37}$$

in the search space satisfying the given fixed-norm constraint on the rows of $\boldsymbol{W}$ (for $\boldsymbol{S}$, one should also consider the constraint set Ψ). Therefore, for the optimizer $\widetilde{\boldsymbol{W}}^{(t+1)}$ of (14.22) we must have

$$\Re \left\{ \text{tr} \left(\widetilde{\boldsymbol{W}}^{(t+1)H} \widetilde{\boldsymbol{C}} \widetilde{\boldsymbol{W}}^{(t)} \right) \right\} \geq \text{tr} \left(\widetilde{\boldsymbol{W}}^{(t)H} \widetilde{\boldsymbol{C}} \widetilde{\boldsymbol{W}}^{(t)} \right). \tag{14.38}$$

Moreover, as $\widetilde{\boldsymbol{C}}$ is positive-definite:

$$\text{tr} \left(\left(\widetilde{\boldsymbol{W}}^{(t+1)} - \widetilde{\boldsymbol{W}}^{(t)} \right)^H \widetilde{\boldsymbol{C}} \left(\widetilde{\boldsymbol{W}}^{(t+1)} - \widetilde{\boldsymbol{W}}^{(t)} \right) \right) \geq 0 \tag{14.39}$$

which along with (14.38) implies

$$\text{tr} \left(\widetilde{\boldsymbol{W}}^{(t+1)H} \widetilde{\boldsymbol{C}} \widetilde{\boldsymbol{W}}^{(t+1)} \right) \geq \text{tr} \left(\widetilde{\boldsymbol{W}}^{(t)H} \widetilde{\boldsymbol{C}} \widetilde{\boldsymbol{W}}^{(t)} \right), \tag{14.40}$$

and hence, a monotonic increase of the objective function in (14.22).

14.5.2 Appendix B: Derivation of the Constrained Solutions in (14.31)

- $\Psi =$ real-values matrices: In this case, the objective function of (14.29) can be reformulated as

$$\left\| \boldsymbol{S}^{(t+1)} - \widehat{\boldsymbol{S}}^{(t)} \right\|_F^2 = \left\| \boldsymbol{S}^{(t+1)} - \Re\left\{ \widehat{\boldsymbol{S}}^{(t)} \right\} \right\|_F^2 + \underbrace{\left\| \Im\left\{ \widehat{\boldsymbol{S}}^{(t)} \right\} \right\|_F^2}_{const.}. \quad (14.41)$$

  As a result, similar to (14.25) the minimizer $\boldsymbol{S}^{(t+1)}$ of (14.29) can be obtained via a scaling as

$$\boldsymbol{S}^{(t+1)} = \sqrt{\frac{E}{M}}\, \eta\left(\Re\left\{ \widehat{\boldsymbol{S}}^{(t)} \right\} \right). \quad (14.42)$$

- $\Psi =$ unimodular matrices: The closest element on the unit-circle to a given complex number may be obtained by scaling (i.e. projecting) the number on the unit-circle (and keeping its phase argument). The minimizing unimodular signal $\boldsymbol{S}^{(t+1)}$ of (14.29) can be computed in an element-wise manner, due to the fact that all elements of $\boldsymbol{S}^{(t+1)}$ are then optimal, namely

$$\boldsymbol{S}^{(t+1)} = e^{j \arg\left(\widehat{\boldsymbol{S}}^{(t)} \right)}. \quad (14.43)$$

- $\Psi = p$-ary matrices: Similar to the previous case, the minimizing p-ary signal $\boldsymbol{S}^{(t+1)}$ of (14.29) can be computed in an element-wise manner, which yields

$$\boldsymbol{S}^{(t+1)} = e^{j \mathscr{Q}_p\left(\arg\left(\widehat{\boldsymbol{S}}^{(t)} \right) \right)}. \quad (14.44)$$

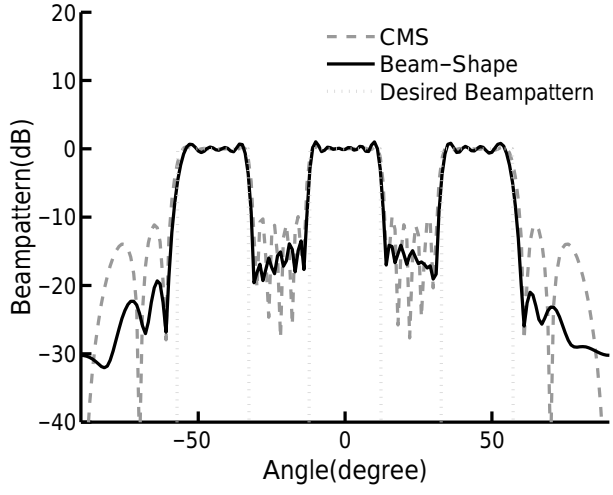

(a)

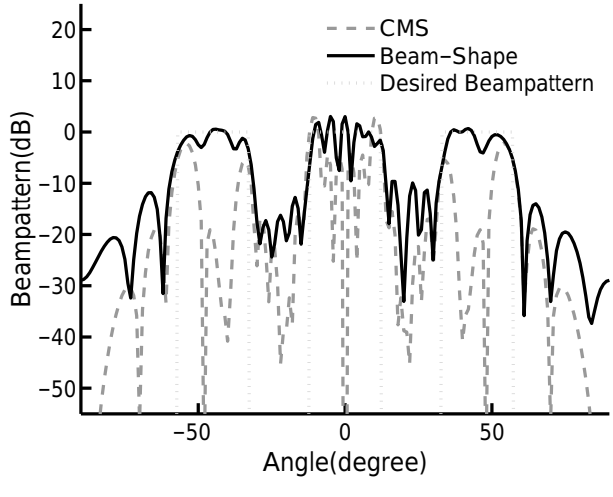

(b)

Figure 14.1. Comparison of radar beampattern matchings obtained by CMS and Beam-Shape using the weight matrix $\boldsymbol{W}$ as the design variable: (a) $K = M$ corresponding to a general MIMO radar, and (b) $K = 1$ which corresponds to a phased-array.

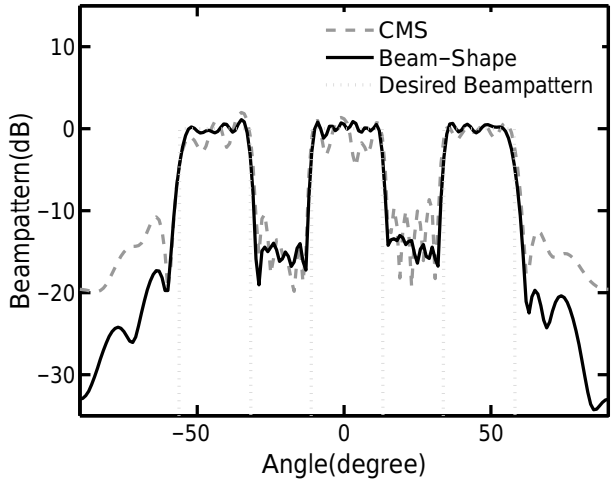

(a)

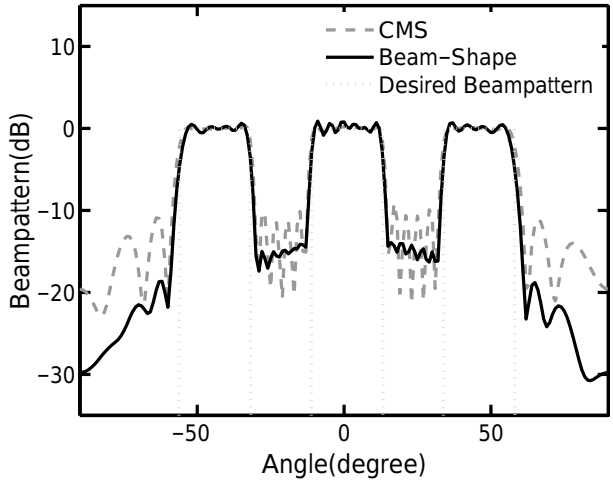

(b)

Figure 14.2. Comparison of MIMO radar beampattern matchings obtained by CMS and Beam-Shape using the signal matrix $\boldsymbol{S}$ as the design variable: (a) $N = 8$, (b) $N = 128$.

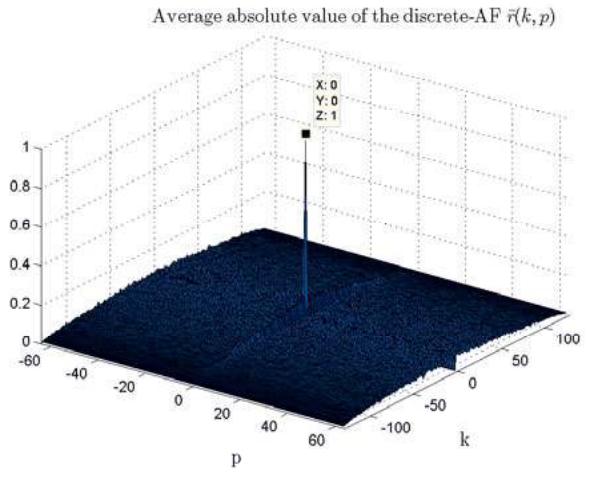

(a)

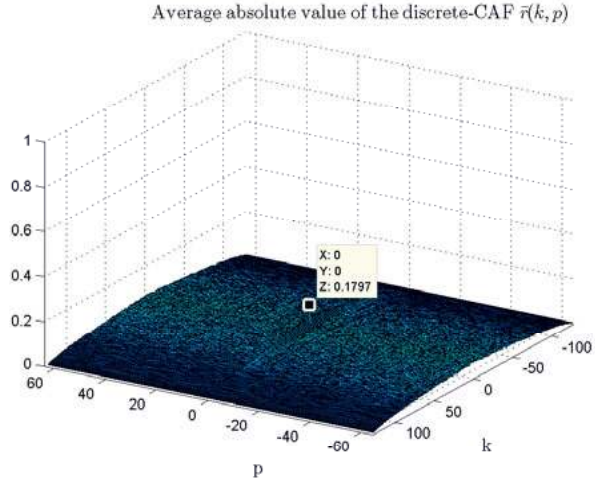

(b)

Figure 14.3. (a) normalized average absolute value of $M = 32$ discrete-AFs associated with the transmit signals in $\boldsymbol{S}$; (b) normalized average absolute value of $\binom{M}{2} = 496$ discrete-CAFs associated with $\boldsymbol{S}$.

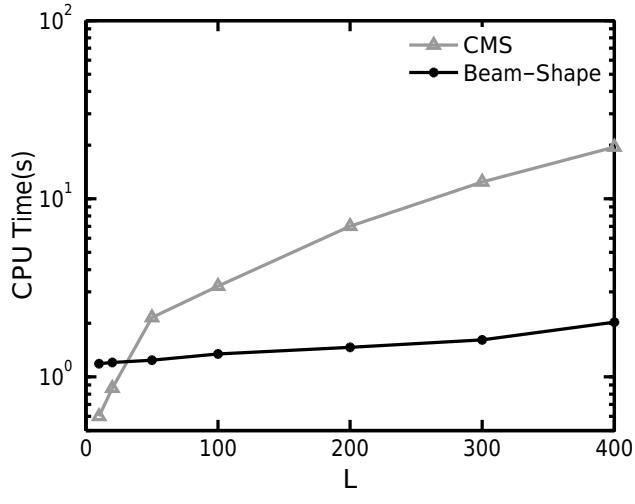

Figure 14.4. Comparison of computation times for Beam-Shape and CMS with different grid sizes L.

References

[1] S. Zhang and Y. Huang, "Complex quadratic optimization and semidefinite programming," *SIAM Journal on Optimization*, vol. 16, no. 3, pp. 871–890, 2006.

[2] Z.-Q. Luo, W.-k. Ma, A.-C. So, Y. Ye, and S. Zhang, "Semidefinite relaxation of quadratic optimization problems," *IEEE Signal Processing Magazine*, vol. 27, no. 3, pp. 20–34, 2010.

[3] S. W. Golomb and G. Gong, *Signal Design for Good Correlation: for Wireless Communication, Cryptography, and Radar*. Cambridge: Cambridge University Press, 2005.

[4] H. He, J. Li, and P. Stoica, *Waveform Design for Active Sensing Systems: A Computational Approach*. Cambridge, UK: Cambridge University Press, 2012.

[5] J. Ling, H. He, J. Li, W. Roberts, and P. Stoica, "Covert underwater acoustic communications," *Journal of the Acoustical Society of America*, vol. 128, no. 5, pp. 2898–2909, November 2010.

[6] P. Stoica, H. He, and J. Li, "New algorithms for designing unimodular sequences with good correlation properties," *IEEE Transactions on Signal Processing*, vol. 57, no. 4, pp. 1415–1425, Apr. 2009.

[7] H. He, P. Stoica, and J. Li, "Designing unimodular sequence sets with good correlations -including an application to MIMO radar," *IEEE Transactions on Signal Processing*, vol. 57, no. 11, pp. 4391–4405, November 2009.

[8] P. Stoica, H. He, and J. Li, "On designing sequences with impulse-like periodic correlation," *IEEE Signal Processing Letters*, vol. 16, no. 8, pp. 703–706, Aug. 2009.

[9] J. Jedwab, "A survey of the merit factor problem for binary sequences," in *Sequences and Their Applications - SETA 2004*, ser. Lecture Notes in Computer Science, T. Helleseth, D. Sarwate, H.-Y. Song, and K. Yang, Eds. Springer Berlin / Heidelberg, 2005, vol. 3486, pp. 19–21.

[10] H. Luke, "Sequences and arrays with perfect periodic correlation," *IEEE Transactions on Aerospace and Electronic Systems*, vol. 24, no. 3, pp. 287–294, May 1988.

[11] S. Kocabas and A. Atalar, "Binary sequences with low aperiodic autocorrelation for synchronization purposes," *IEEE Communications Letters*, vol. 7, no. 1, pp. 36–38, January 2003.

[12] X. Tang and W. H. Mow, "A new systematic construction of zero correlation zone sequences based on interleaved perfect sequences," *IEEE Transactions on Information Theory*, vol. 54, no. 12, pp. 5729–5734, December 2008.

[13] R. Frank, "Polyphase complementary codes," *IEEE Transactions on Information Theory*, vol. 26, no. 6, pp. 641–647, November 1980.

[14] S. M. Tseng and M. Bell, "Asynchronous multicarrier DS-CDMA using mutually orthogonal complementary sets of sequences," *IEEE Transactions on Communications*, vol. 48, no. 1, pp. 53–59, January 2000.
[15] Q. Liu, C. Khirallah, L. Stankovic, and V. Stankovic, "Image-in-image hiding using complete complementary sequences," in *IEEE International Conference on Multimedia and Expo*, April 2008, pp. 249–252.
[16] P. Cristea, R. Tuduce, and J. Cornelis, "Complementary sequences for coded aperture imaging," in *50th International ELMAR Symposium*, vol. 1, September 2008, pp. 53–56.
[17] P. Spasojevic and C. Georghiades, "Complementary sequences for ISI channel estimation," *IEEE Transactions on Information Theory*, vol. 47, no. 3, pp. 1145–1152, March 2001.
[18] E. Garcia, J. Garcia, J. Urena, M. Perez, and D. Ruiz, "Multilevel complementary sets of sequences and their application in UWB," in *International Conference on Indoor Positioning and Indoor Navigation (IPIN)*, September 2010, pp. 1–5.
[19] Z. Zhang, F. Zeng, and G. Xuan, "Design of complementary sequence sets based on orthogonal matrixes," in *International Conference on Communications, Circuits and Systems (ICCCAS)*, July 2010, pp. 383–387.
[20] M. J. E. Golay, "Multi-slit spectrometry," *Journal of the Optical Society of America*, vol. 39, no. 6, p. 437, 1949.
[21] ——, "Complementary series," *IRE Transactions on Information Theory*, vol. 7, no. 2, pp. 82–87, April 1961.
[22] J. Davis and J. Jedwab, "Peak-to-mean power control in OFDM, Golay complementary sequences, and Reed-Muller codes," *IEEE Transactions on Information Theory*, vol. 45, no. 7, pp. 2397–2417, November 1999.
[23] S. Eliahou, M. Kervaire, and B. Saffari, "A new restriction on the lengths of Golay complementary sequences," *Journal of Combinatorial Theory, Series A*, vol. 55, no. 1, pp. 49–59, 1990.
[24] R. Turyn, "Ambiguity functions of complementary sequences (corresp.)," *IEEE Transactions on Information Theory*, vol. 9, no. 1, pp. 46–47, January 1963.
[25] A. Dax, "Orthogonalization via deflation: a minimum norm approach for low-rank approximations of a matrix," *SIAM Journal on Matrix Analysis and Applications*, vol. 30, no. 1, pp. 236–260, January 2008.
[26] J. Tropp, I. Dhillon, R. Heath, and T. Strohmer, "Designing structured tight frames via an alternating projection method," *IEEE Transactions on Information Theory*, vol. 51, no. 1, pp. 188–209, January 2005.
[27] C. R. Rao, "Matrix approximations and reduction of dimensionality in multivariate statistical analysis," in *Multivariate Analysis*, P. R. Krishnaiah, Ed., North-Holland, Amsterdam, 1980, pp. 3–22.
[28] P. W. Day, "Rearrangement inequalities," *Canadian Journal of Mathematics*, vol. 24, pp. 930–943, 1972.
[29] G. Salinetti and R. J.-B. Wets, "On the convergence of sequences of convex sets in finite dimensions," *SIAM Review*, vol. 21, no. 1, pp. 18–33, 1979.
[30] J. Cadzow, "Signal enhancement-a composite property mapping algorithm," *IEEE Transactions on Acoustics, Speech and Signal Processing*, vol. 36, no. 1,

pp. 49–62, January 1988.
[31] P. L. Combettes and H. J. Trussell, "Method of successive projections for finding a common point of sets in metric spaces," *Journal of Optimization Theory and Applications*, vol. 67, pp. 487–507, 1990.
[32] Y. Tanada, "Synthesis of a set of real-valued shift-orthogonal finite-length PN sequences," in *IEEE 4th International Symposium on Spread Spectrum Techniques and Applications Proceedings*, vol. 1, September 1996, pp. 58–62.
[33] M. Soltanalian and P. Stoica, "Perfect root-of-unity codes with prime-size alphabet," in *IEEE International Conference on Acoustics, Speech and Signal Processing (ICASSP)*, May 2011, pp. 3136–3139.
[34] M. Parker, "Even length binary sequence families with low negaperiodic autocorrelation," in *Applied Algebra, Algebraic Algorithms and Error-Correcting Codes*, ser. Lecture Notes in Computer Science, S. Boztas and I. Shparlinski, Eds. Springer Berlin / Heidelberg, 2001, vol. 2227, pp. 200–209.
[35] L. Bomer and M. Antweiler, "Binary and biphase sequences and arrays with low periodic autocorrelation sidelobes," in *International Conference on Acoustics, Speech, and Signal Processing (ICASSP)*, vol. 3, April 1990, pp. 1663–1666.
[36] K. Arasu, C. Ding, T. Helleseth, P. Kumar, and H. Martinsen, "Almost difference sets and their sequences with optimal autocorrelation," *IEEE Transactions on Information Theory*, vol. 47, no. 7, pp. 2934–2943, November 2001.
[37] J. W. Moon and L. Moser, "On the correlation function of random binary sequences," *SIAM Journal on Applied Mathematics*, vol. 16, no. 2, pp. 340–343, 1968.
[38] J. Jedwab and K. Yoshida, "The peak sidelobe level of families of binary sequences," *IEEE Transactions on Information Theory*, vol. 52, no. 5, pp. 2247–2254, May 2006.
[39] N. Levanon and E. Mozeson, *Radar Signals*. New York: Wiley, 2004.
[40] S. Wang, "Efficient heuristic method of search for binary sequences with good aperiodic autocorrelations," *Electronics Letters*, vol. 44, no. 12, pp. 731–732, 2008.
[41] B. Dang, J. Li, and G. Liao, "Taylor polynomial expansion based waveform correlation cancellation for bistatic MIMO radar localization," *Signal Processing*, vol. 92, no. 6, pp. 1404–1410, 2012.
[42] C. De Marziani, J. Ureña, Á. Hernández, J. J. García, F. J. Álvarez, A. Jiménez, and M. C. Pérez, "Recursive algorithm to directly obtain the sum of correlations in a css," *Signal Processing*, vol. 91, no. 5, pp. 1343–1346, 2011.
[43] N. Levanon, "Noncoherent radar pulse compression based on complementary sequences," *Aerospace and Electronic Systems, IEEE Transactions on*, vol. 45, no. 2, pp. 742 –747, april 2009.
[44] S. Searle, S. Howard, and B. Moran, "The use of complementary sets in MIMO radar," in *Asilomar Conference on Signals, Systems and Computers*, oct. 2008, pp. 510 –514.
[45] M. Soltanalian and P. Stoica, "Computational design of sequences with good correlation properties," *IEEE Transactions on Signal Processing*, vol. 60,

no. 5, pp. 2180–2193, May 2012.
[46] I. Trots, A. Nowicki, W. Secomski, and J. Litniewski, "Golay sequences-sidelobe-cancelling codes for ultrasonography," *Archive of acoustics*, vol. 29, no. 1, pp. 87–97, 2004.
[47] K. U. Schmidt, "Complementary sets, generalized Reed-Muller codes, and power control for OFDM," *IEEE Transactions on Information Theory*, vol. 53, no. 2, pp. 808–814, Feb. 2007.
[48] T. Kojima, N. Ohtani, T. Matsumoto, and U. Parampalli, "On multiple information embedding by digital watermarking based on complete complementary codes," in *Signal Design and its Applications in Communications (IWSDA)*, Oct. 2011, pp. 100–103.
[49] R. Turyn, "Hadamard matrices, Baumert-Hall, four symbol sequences, pulse compression, and surface wave encodings," *J. Comb. Theory Ser. A*, vol. 16, pp. 313–333, 1974.
[50] L. Bomer and M. Antweiler, "Periodic complementary binary sequences," *IEEE Transactions on Information Theory*, vol. 36, no. 6, pp. 1487 –1494, Nov. 1990.
[51] M. Parker, K. G. Paterson, and Tellambura, *Golay Complementray Sequences*, 1st ed. Wiley Encyclopedia of Telecommunications, 2003.
[52] P. Borwein and R. Ferguson, "A complete description of Golay pairs for lengths up to 100," *Mathematics of Computation*, vol. 73, no. 246, pp. 967–986, 2004.
[53] A. T. Fam and I. Sarkar, "A new class of interlaced complementary codes based on components with unity peak sidelobes," *Signal Processing*, vol. 88, no. 2, pp. 307–314, 2008.
[54] P. Stoica and R. L. Moses, *Spectral Analysis of Signals*. Upper Saddle River, NJ: Prentice Hall, 2005.
[55] J. Loubes and S. Van De Geer, "Adaptive estimation with soft thresholding penalties," *Statistica Neerlandica*, vol. 56, no. 4, pp. 453–478, 2002.
[56] D. V. Sarwate, "Meeting the welch bound with equality," in *Sequences and their Applications (SETA)*. New York: Springer, 1999, pp. 79–102.
[57] L. Welch, "Lower bounds on the maximum cross correlation of signals," *IEEE Transactions on Information Theory*, vol. 20, no. 3, pp. 397–399, 1974.
[58] H. Rauhut, "Compressive sensing and structured random matrices," in *Theoretical foundations and numerical methods for sparse recovery*, ser. Radon Series on Computational and Applied Mathematics, M. Fornasier, Ed., vol. 9. De Gruyter, 2010, pp. 1–92.
[59] P. Xia, S. Zhou, and G. Giannakis, "Achieving the Welch bound with difference sets," *IEEE Transactions on Information Theory*, vol. 51, no. 5, pp. 1900–1907, 2005.
[60] C. Ding and T. Feng, "A generic construction of complex codebooks meeting the Welch bound," *IEEE Transactions on Information Theory*, vol. 53, no. 11, pp. 4245–4250, Nov. 2007.
[61] A. Zhang and K. Feng, "Two classes of codebooks nearly meeting the Welch bound," *IEEE Transactions on Information Theory*, vol. 58, no. 4, pp. 2507–2511, April 2012.
[62] T. Strohmer and R. W. Heath, "Grassmannian frames with applications to

coding and communication," *Applied and Computational Harmonic Analysis*, vol. 14, no. 3, pp. 257–275, 2003.
[63] T. Strohmer, R. W. Heath, and A. J. Paulraj, "On the design of optimal spreading sequences for CDMA systems," in *Asilomar Conference on Signals, Systems and Computers*, vol. 2. CA, USA: IEEE, 2002, pp. 1434–1438.
[64] S. Datta, S. Howard, and D. Cochran, "Geometry of the Welch bounds," *Linear Algebra and its Applications*, vol. 437, pp. 2455–2470, 2012.
[65] J. Marcus, S. Imtel, and P. Spasojevic, "On the size of binary MWBE sequence sets," in *International Symposium on Modeling and Optimization in Mobile, Ad Hoc and Wireless Networks (WiOpt)*. Princeton, NJ, USA: IEEE, 2011, pp. 374–374.
[66] V. Levenshtein, "Bounds on the maximal cardinality of a code with bounded modulus of the inner product," in *Soviet Math. Dokl*, vol. 25, no. 2, 1982, pp. 526–531.
[67] C. Ding and J. Yin, "Signal sets from functions with optimum nonlinearity," *IEEE Transactions on Communications*, vol. 55, no. 5, pp. 936–940, 2007.
[68] J. Kovacevic and A. Chebira, "Life beyond bases: The advent of frames (part II)," *IEEE Signal Processing Magazine*, vol. 24, no. 5, pp. 115–125, 2007.
[69] P. Pad, M. Faraji, and F. Marvasti, "Constructing and decoding GWBE codes using Kronecker products," *IEEE Communications Letters*, vol. 14, no. 1, pp. 1–3, 2010.
[70] P. Stoica, H. He, and J. Li, "Sequence sets with optimal integrated periodic correlation level," *IEEE Signal Processing Letters*, vol. 17, no. 1, pp. 63–66, 2010.
[71] H. He, P. Stoica, and J. Li, "On aperiodic-correlation bounds," *IEEE Signal Processing Letters*, vol. 17, no. 3, pp. 253–256, March 2010.
[72] V. Sidelnikov, "On mutual correlation of sequences," *Soviet Math. Dokl*, vol. 12, no. 1, pp. 197–201, 1971.
[73] H. Ganapathy, D. A. Pados, and G. N. Karystinos, "New bounds and optimal binary signature sets-part I: periodic total squared correlation," *IEEE Transactions on Communications*, vol. 59, no. 4, pp. 1123–1132, 2011.
[74] ——, "New bounds and optimal binary signature sets-part II: Aperiodic total squared correlation," *IEEE Transactions on Communications*, vol. 59, no. 5, pp. 1411–1420, 2011.
[75] T. Kasami, "Weight distribution formula for some class of cyclic codes," Coordinated Science Laboratory, University of Illinois, Tech. Rep., April 1966.
[76] R. Gold, "Optimal binary sequences for spread spectrum multiplexing," *IEEE Transactions on Information Theory*, vol. 13, no. 4, pp. 619 –621, October 1967.
[77] J. Rushanan, "Weil sequences: A family of binary sequences with good correlation properties," in *IEEE International Symposium on Information Theory*, Seattle, Washington, USA, July 2006, pp. 1648–1652.
[78] G. Gong, "New designs for signal sets with low cross correlation, balance property, and large linear span: GF (p) case," *IEEE Transactions on Information Theory*, vol. 48, no. 11, pp. 2847–2867, 2002.
[79] P. Fan and M. Darnell, "Construction and comparison of periodic digital sequence sets," in *IEE Proceedings on Communications*, vol. 144, no. 6. IET,

1997, pp. 361–366.
[80] H. A. Khan, Y. Zhang, C. Ji, C. J. Stevens, D. J. Edwards, and D. O'Brien, "Optimizing polyphase sequences for orthogonal netted radar," *IEEE Signal Processing Letters*, vol. 13, no. 10, pp. 589–592, 2006.
[81] R. Wei, Z. Mao, and K. Yuan, "Aperiodic correlation of complex sequences from difference sets," in *IEEE International Conference on Communications (ICC)*. Beijing, China: IEEE, 2008, pp. 1190–1194.
[82] Y. Jitsumatsu and T. Kohda, "Chip-asynchronous version of Welch bound: Gaussian pulse improves BER performance," in *Sequences and their Applications (SETA)*. New York: Springer, 2006, pp. 351–363.
[83] M. Soltanalian and P. Stoica, "Computational design of sequences with good correlation properties," *IEEE Transactions on Signal Processing*, vol. 60, no. 5, pp. 2180–2193, 2012.
[84] ——, "Designing unimodular codes via quadratic optimization," *IEEE Transactions on Signal Processing*, vol. 62, no. 5, pp. 1221–1234, 2014.
[85] M. Soltanalian, B. Tang, J. Li, and P. Stoica, "Joint design of the receive filter and transmit sequence for active sensing," *IEEE Signal Processing Letters*, vol. 20, no. 5, pp. 423–426, 2013.
[86] L. Bomer and M. Antweiler, "Perfect N-phase sequences and arrays [spread spectrum communication]," *IEEE Journal on Selected Areas in Communications*, vol. 10, no. 4, pp. 782–789, May. 1992.
[87] S. Ma and W. Ng, "On non-existence of perfect and nearly perfect sequences," *International Journal of Information and Coding Theory*, vol. 1, no. 1, pp. 15–38, 2009.
[88] E. Gabidulin, "Partial classification of sequences with perfect auto-correlation and bent functions," in *IEEE International Symposium on Information Theory*, Whistler, B.C. Canada, Sept. 1995, p. 467.
[89] H. He, J. Li, and P. Stoica, *Waveform design for active sensing systems: a computational approach*. Cambridge University Press, 2012.
[90] J. Benedetto, I. Konstantinidis, and M. Rangaswamy, "Phase-coded waveforms and their design," *IEEE Signal Processing Magazine*, vol. 26, no. 1, pp. 22–31, Jan. 2009.
[91] S. W. Golomb and G. Gong, *Signal design for good correlation: for wireless communication, cryptography, and radar*. Cambridge University Press, 2005.
[92] S. E. Kocabas and A. Atalar, "Binary sequences with low aperiodic autocorrelation for synchronization purposes," *IEEE Communications Letters*, vol. 7, no. 1, pp. 36–38, 2003.
[93] W. H. Mow, "A new unified construction of perfect root-of-unity sequences," in *IEEE 4th International Symposium on Spread Spectrum Techniques and Applications Proceedings*, vol. 3, Mainz, Germany, Sept. 1996, pp. 955–959.
[94] P. Fan and M. Darnell, "The synthesis of perfect sequences," in *Cryptography and Coding*, ser. Lecture Notes in Computer Science, C. Boyd, Ed. Springer Berlin / Heidelberg, 1995, vol. 1025, pp. 63–73.
[95] H. Luke, "Almost-perfect polyphase sequences with small phase alphabet," *IEEE Transactions on Information Theory*, vol. 43, no. 1, pp. 361–363, Jan. 1997.
[96] P. Fan and M. Darnell, *Sequence Design for Communications Applications*.

New York: Wiley, 1996.
[97] M. Soltanalian, M. M. Naghsh, and P. Stoica, "A fast algorithm for designing complementary sets of sequences," *Signal Processing*, vol. 93, no. 7, pp. 2096–2102, 2013.
[98] J. J. Benedetto and S. Datta, "Construction of infinite unimodular sequences with zero autocorrelation," *Advances in Computational Mathematics*, vol. 32, no. 2, pp. 191–207, 2010.
[99] E. Gabidulin and V. Shorin, "New families of unimodular perfect sequences of prime length based on gaussian periods," in *IEEE International Symposium on Information Theory*, Lausanne, Switzerland, 2002, p. 68.
[100] E. Gabidulin, "New perfect sequences of length $2p$," in *Proceedings of the ACCT-6*, Pskov, Russia, 1998, pp. 119–122.
[101] E. Gabidulin and V. Shorin, "Perfect sequences of length $3p$," in *IEEE International Symposium on Information Theory*, Yokohama, Japan, June 2003, p. 432.
[102] ——, "Perfect sequences of length $p_1 p_2$," in *Seventh International Symposium on Communication Theory and Applications*, Ambleside, Lake District, UK, July 2003.
[103] ——, "Unimodular perfect sequences of length p^s," *IEEE Transactions on Information Theory*, vol. 51, no. 3, pp. 1163–1166, Mar. 2005.
[104] H. Luke, "Sequences and arrays with perfect periodic correlation," *IEEE Transactions on Aerospace and Electronic Systems*, vol. 24, no. 3, pp. 287–294, May 1988.
[105] M. Soltanalian and P. Stoica, "Perfect root-of-unity codes with prime-size alphabet," in *IEEE International Conference on Acoustics, Speech and Signal Processing (ICASSP)*. Prague, Czech Republic: IEEE, 2011, pp. 3136–3139.
[106] T. Y. Lam and K. H. Leung, "On vanishing sums of roots of unity," *Journal of Algebra*, vol. 224, no. 1, pp. 91–109, 2000.
[107] T. Andreescu, D. Andrica, and I. Cucurezeanu, *An Introduction to Diophantine Equations: A Problem-based Approach*. Springer, 2010.
[108] A. Tripathi, "On a linear Diophantine problem of Frobenius," *Integers*, vol. 6, p. A14, 2006.
[109] J. L. R. Alfonsín, *The Diophantine Frobenius problem*. Oxford, UK: Oxford University Press, 2005.
[110] M. Buratti, "Old and new designs via difference multisets and strong difference families," *Journal of Combinatorial Designs*, vol. 7, no. 6, pp. 406–425, 1999.
[111] D. R. Stinson, *Combinatorial designs: constructions and analysis*. Springer, 2004.
[112] H. S. M. Coxeter, *Regular Polytopes*. MacMillan, 1963.
[113] H. D. Luke, L. Bomer, and M. Antweiler, "Perfect binary arrays," *Signal Processing*, vol. 17, no. 1, pp. 69–80, 1989.
[114] E. Szemerédi, "On sets of integers containing no k elements in arithmetic progression," *Acta Arithmetica*, vol. 27, pp. 299–345, 1975.
[115] W. Gowers, "A new proof of Szemerédi's theorem," *Geometric and Functional Analysis*, vol. 11, pp. 465–588, 2001.
[116] T. C. Brown and D. R. Hare, "Arithmetic progressions in sequences with bounded gaps," *Journal of Combinatorial Theory, Series A*, vol. 77, no. 2, pp.

222–227, 1997.
[117] W. Watkins and J. Zeitlin, "The minimal polynomial of $\cos(2\pi/n)$," *The American Mathematical Monthly*, vol. 100, no. 5, pp. pp. 471–474, 1993.
[118] I. Niven, *Irrational Numbers*. New York: Mathematical Association of America and Wiley, 1956.
[119] M. G. Parker, "Even length binary sequence families with low negaperiodic autocorrelation," in *Applied Algebra, Algebraic Algorithms and Error-Correcting Codes*. Springer, 2001, pp. 200–209.
[120] T. Jiang, X. Zhao, and L. Hou, "Perfect punctured binary sequence pairs," *Journal of Electronics (China)*, vol. 20, no. 4, pp. 285–288, 2003.
[121] Y. Manin and A. Panchishkin, *Introduction to Modern Number Theory, Encyclopaedia of Mathematical Sciences, vol.49 (2nd ed.)*. Springer-Verlag, 2005.
[122] G. Shimura, "The representation of integers as sums of squares," *American Journal of Mathematics*, vol. 124, no. 5, pp. pp. 1059–1081, 2002.
[123] S. Cooper, "Sums of five, seven and nine squares," *The Ramanujan Journal*, vol. 6, pp. 469–490, 2002.
[124] P. Barrucand and M. D. Hirschhorn, "Formulae associated with 5, 7, 9 and 11 squares," *Bulletin of the Australian Mathematical Society*, vol. 65, no. 03, pp. 503–510, 2002.
[125] S. Cooper, "On the number of representations of certain integers as sums of 11 or 13 squares," *Journal of Number Theory*, vol. 103, no. 2, pp. 135–162, 2003.
[126] J. J. Benedetto, I. Konstantinidis, and M. Rangaswamy, "Phase-coded waveforms and their design," *IEEE Signal Processing Magazine*, vol. 26, no. 1, pp. 22–31, 2009.
[127] A. De Maio, S. De Nicola, Y. Huang, Z.-Q. Luo, and S. Zhang, "Design of phase codes for radar performance optimization with a similarity constraint," *IEEE Transactions on Signal Processing*, vol. 57, no. 2, pp. 610–621, 2009.
[128] M. M. Naghsh, M. Soltanalian, P. Stoica, M. Modarres-Hashemi, A. De Maio, and A. Aubry, "A Doppler robust design of transmit sequence and receive filter in the presence of signal-dependent interference," *IEEE Transactions on Signal Processing*, vol. 62, no. 4, pp. 772–785, Feb. 2014.
[129] D. Petrolati, P. Angeletti, and G. Toso, "New piecewise linear polyphase sequences based on a spectral domain synthesis," *IEEE Transactions on Information Theory*, vol. 58, no. 7, pp. 4890–4898, 2012.
[130] F. Gini, A. De Maio, and L. Patton, Eds., *Waveform design and diversity for advanced radar systems*. The Institution of Engineering and Technology, 2012.
[131] A. De Maio, S. De Nicola, Y. Huang, S. Zhang, and A. Farina, "Code design to optimize radar detection performance under accuracy and similarity constraints," *IEEE Transactions on Signal Processing*, vol. 56, no. 11, pp. 5618 –5629, nov. 2008.
[132] A. De Maio and A. Farina, "Code selection for radar performance optimization," in *Waveform Diversity and Design Conference*, june 2007, pp. 219–223.
[133] H. He, P. Stoica, and J. Li, "On synthesizing cross ambiguity functions," in *IEEE International Conference on Acoustics, Speech and Signal Processing*

(ICASSP), Prague, Czech Republic, May 2011, pp. 3536–3539.
[134] J. Li and P. Stoica, *Robust Adaptive Beamforming*. NJ, USA.: John Wiley & Sons, Inc., 2005.
[135] K.-C. Tan, G.-L. Oh, and M. Er, "A study of the uniqueness of steering vectors in array processing," *Signal Processing*, vol. 34, no. 3, pp. 245–256, 1993.
[136] A. Khabbazibasmenj, S. Vorobyov, and A. Hassanien, "Robust adaptive beamforming via estimating steering vector based on semidefinite relaxation," in *Conference on Signals, Systems and Computers (ASILOMAR)*, nov. 2010, pp. 1102–1106.
[137] Z. Wen and W. Yin, "A feasible method for optimization with orthogonality constraints," *Mathematical Programming*, vol. 142, no. 1-2, pp. 397–434, 2013.
[138] J. Jalden, C. Martin, and B. Ottersten, "Semidefinite programming for detection in linear systems - optimality conditions and space-time decoding," in *IEEE International Conference on Acoustics, Speech, and Signal Processing (ICASSP)*, vol. 4, april 2003, pp. 9–12.
[139] S. Zhang and Y. Huang, "Complex quadratic optimization and semidefinite programming," *SIAM Journal on Optimization*, vol. 16, no. 3, pp. 871–890, 2006.
[140] A. T. Kyrillidis and G. N. Karystinos, "Rank-deficient quadratic-form maximization over m-phase alphabet: Polynomial-complexity solvability and algorithmic developments," in *IEEE International Conference on Acoustics, Speech and Signal Processing (ICASSP)*, may 2011, pp. 3856–3859.
[141] Z. Wen, D. Goldfarb, and K. Scheinberg, "Block coordinate descent methods for semidefinite programming," in *Handbook on Semidefinite, Conic and Polynomial Optimization*, ser. International Series in Operations Research & Management Science, M. F. Anjos and J. B. Lasserre, Eds. Springer US, 2012, vol. 166, pp. 533–564.
[142] S. Verdú, "Computational complexity of optimum multiuser detection," *Algorithmica*, vol. 4, pp. 303–312, 1989.
[143] W.-K. Ma, B.-N. Vo, T. Davidson, and P.-C. Ching, "Blind ML detection of orthogonal space-time block codes: efficient high-performance implementations," *IEEE Transactions on Signal Processing*, vol. 54, no. 2, pp. 738–751, feb. 2006.
[144] T. Cui and C. Tellambura, "Joint channel estimation and data detection for OFDM systems via sphere decoding," in *IEEE Global Telecommunications Conference (GLOBECOM)*, vol. 6, Texas, USA, Dec. 2004, pp. 3656–3660.
[145] S. Boyd and L. Vandenberghe, *Convex Optimization*. Cambridge University Press, 2004.
[146] M. X. Goemans and D. P. Williamson, "Improved approximation algorithms for maximum cut and satisfiability problems using semidefinite programming," *ACM Journal*, vol. 42, no. 6, pp. 1115–1145, Nov. 1995.
[147] A. De Maio, Y. Huang, M. Piezzo, S. Zhang, and A. Farina, "Design of optimized radar codes with a peak to average power ratio constraint," *IEEE Transactions on Signal Processing*, vol. 59, no. 6, pp. 2683–2697, june 2011.
[148] A. So, J. Zhang, and Y. Ye, "On approximating complex quadratic optimization problems via semidefinite programming relaxations,"

Mathematical Programming, vol. 110, pp. 93–110, 2007.
[149] M. Kisialiou and Z.-Q. Luo, "Performance analysis of quasi-maximum-likelihood detector based on semi-definite programming," in *IEEE International Conference on Acoustics, Speech, and Signal Processing (ICASSP)*, vol. 3. Pennsylvania, USA: IEEE, 2005, pp. iii–433.
[150] M. Soltanalian, B. Tang, J. Li, and P. Stoica, "Joint design of the receive filter and transmit sequence for active sensing," *IEEE Signal Processing Letters*, vol. 20, no. 5, pp. 423–426, 2013.
[151] R. Horn and C. Johnson, *Matrix Analysis*. Cambridge, UK: Cambridge University Press, 1990.
[152] G. Karystinos and A. Liavas, "Efficient computation of the binary vector that maximizes a rank-deficient quadratic form," *IEEE Transactions on Information Theory*, vol. 56, no. 7, pp. 3581–3593, july 2010.
[153] A. De Maio, Y. Huang, and M. Piezzo, "A Doppler robust max-min approach to radar code design," *IEEE Transactions on Signal Processing*, vol. 58, no. 9, pp. 4943–4947, sept. 2010.
[154] M. Soltanalian and P. Stoica, "Computational design of sequences with good correlation properties," *IEEE Transactions on Signal Processing, DOI: 10.1109/TSP.2012.2186134*.
[155] W. D. Rummler, "A technique for improving the clutter performance of coherent pulse trains," *IEEE Transactions on Aerospace and Electronic Systems*, vol. 3, pp. 898–906, Nov. 1967.
[156] D. F. Delong and E. M. Hofstteter, "On the design of optimum radar waveforms for clutter rejection," *IEEE Transactions on Information Theory*, vol. 13, pp. 454–463, Jul. 1967.
[157] ——, "The design of clutter-resistant radar waveforms with limited dynamic range," *IEEE Transactions on Information Theory*, vol. 15, pp. 376–385, May 1969.
[158] L. J. Spafford, "Optimum radar signal processing in clutter," *IEEE Transactions on Information Theory*, vol. 14, pp. 734–743, Sep. 1968.
[159] A. V. Balakrishnan, "Signal design for a class of clutter channels," *IEEE Transactions on Information Theory*, vol. 14, pp. 170–173, Jan. 1968.
[160] S. M. Kay, "Optimal signal design for detection of Gaussian point targets in stationary Gaussian clutter/reverberation," *IEEE Journal of Selected Topics in Signal Processing*, vol. 1, pp. 31–41, Jun. 2007.
[161] P. Stoica, H. He, and J. Li, "Optimization of the receive filter and transmit sequence for active sensing," *IEEE Transactions on Aerospace and Electronic Systems*, vol. 60, no. 4, pp. 1730 –1740, Apr. 2012.
[162] A. Aubry, A. De Maio, M. Piezzo, A. Farina, and M. Wicks, "Cognitive design of the receive filter and transmitted phase code in reverberating environment," *IET Journal on Radar, Sonar, and Navigation*, vol. 6, no. 9, pp. 822–833, 2012.
[163] A. Aubry, A. De Maio, B. Jiang, and S. Zhang, "Ambiguity function shaping for cognitive radar via complex quartic optimization," *IEEE Transactions on Aerospace and Electronic Systems*, vol. 61, pp. 5603–5619, 2013.
[164] R. A. Romero, J. Bae, and N. A. Goodman, "Theory and application of SNR and mutual information matched illumination waveforms," *IEEE Transactions on Aerospace and Electronic Systems*, vol. 47, pp. 912–927, Apr. 2011.

[165] B. Friedlander, "Waveform design for MIMO radars," *IEEE Transactions on Aerospace and Electronic Systems*, vol. 43, pp. 1227–1238, Jul. 2007.
[166] C. Y. Chen and P. P. Vaidyanathan, "MIMO radar waveform optimization with prior information of the extended target and clutter," *IEEE Transactions on Aerospace and Electronic Systems*, vol. 57, pp. 3533–3544, Sep. 2009.
[167] T. Naghibi and F. Behnia, "MIMO radar waveform design in the presence of clutter," *IEEE Transactions on Aerospace and Electronic Systems*, vol. 47, pp. 770–781, Apr. 2011.
[168] R. S. Blum and Y. Yang, "MIMO radar waveform design based on mutual information and minimum mean-square error estimation," *IEEE Transactions on Aerospace and Electronic Systems*, vol. 43, pp. 330–343, Jan. 2007.
[169] B. Tang, J. Tang, and Y. Peng, "MIMO radar waveform design in colored noise based on information theory," *IEEE Transactions on Aerospace and Electronic Systems*, vol. 58, pp. 4684–4697, Sep. 2010.
[170] X. Song, P. Willett, S. Zhou, and P. Luh, "The MIMO radar and jammer games," *IEEE Transactions on Aerospace and Electronic Systems*, vol. 60, no. 2, pp. 687–699, Feb. 2012.
[171] A. De Maio, M. Lops, and L. Venturino, "Diversity integration trade-off in MIMO detection," *IEEE Transactions on Aerospace and Electronic Systems*, vol. 56, pp. 5051–5061, Oct. 2008.
[172] A. De Maio, Y. Huang, and M. Piezzo, "A Doppler robust max-min approach to radar code design," *IEEE Transactions on Aerospace and Electronic Systems*, vol. 58, pp. 4943–4947, Sep. 2010.
[173] A. De Maio, Y. Huang, M. Piezzo, S. Zhang, and A. Farina, "Design of optimized radar codes with a peak to average power ratio constraint," *IEEE Transactions on Aerospace and Electronic Systems*, vol. 59, pp. 2683–2697, Jun. 2011.
[174] H. L. Van Trees, "Optimum signal design and processing for reverberation-limited environments," *IEEE Transactions on Military Electronics*, vol. 9, no. 3, pp. 212–229, 1965.
[175] J. Li and P. Stoica, *MIMO Radar Signal Processing*, 1st ed. Wiley, 2008.
[176] A. Aubry, A. De Maio, A. Farina, and M. Wicks, "Knowledge-aided (potentially cognitive) transmit signal and receive filter design in signal-dependent clutter," *IEEE Transactions on Aerospace and Electronic Systems*, vol. 49, pp. 93–117, Jan. 2013.
[177] S. Haykin, "Cognitive radars," *IEEE Signal Processing Magazine*, vol. 23, no. 1, pp. 30–40, Jan. 2006.
[178] S. M. Kay, *Fundamentals of Statistical Signal Processing-Volume II: Detection Theory*, 1st ed. New Jersey: Prentice Hall, 1998.
[179] M. M. Naghsh, M. Soltanalian, P. Stoica, and M. Modarres-Hashemi, "Radar code optimization for moving target detection," in *21st European Signal Processing Conference*, Marrakech, Morocco, 2013.
[180] P. Stoica, J. Li, and M. Xue, "Transmit codes and receive filters for radar," *IEEE Signal Processing Magazine*, vol. 25, no. 6, pp. 94 –109, Nov. 2008.
[181] M. M. Naghsh, M. Modarres-Hashemi, S. ShahbazPanahi, M. Soltanalian, and P. Stoica, "Unified optimization framework for multi-static radar code design using information-theoretic criteria," *IEEE Transactions on Aerospace and*

Electronic Systems, vol. 61, pp. 5401–5416, 2013.
[182] M. M. Naghsh and M. Modarres-Hashemi, "Exact theoretical performance analysis of optimum detector for statistical MIMO radars," *IET Journal on Radar, Sonar, and Navigation*, vol. 6, pp. 99–111, 2012.
[183] T. Kailath, "The divergence and Bhattacharyya distance measures in signal selection," *IEEE Transactions on Communications*, vol. 15, pp. 52–60, Feb. 1967.
[184] S. M. Kay, "Waveform design for multistatic radar detection," *IEEE Transactions on Aerospace and Electronic Systems*, vol. 45, pp. 1153–1165, Jul. 2009.
[185] A. Ben-Tal and A. Nemirovski, *Lectures on Modern Convex Optimization*. Philadelphia: SIAM, 2001.
[186] P. Stoica, J. Li, and X. Zhu, "Waveform synthesis for diversity-based transmit beampattern design," *IEEE Transactions on Aerospace and Electronic Systems*, vol. 56, no. 6, pp. 2593 –2598, Jun. 2008.
[187] P. Stoica and R. Moses, *Spectral Analysis of Signals*. New Jersey: Prentice Hall, 2005. [Online]. Available: http://user.it.uu.se/ ps/ref.html
[188] S. Boyd and L. Vanderberghe, *Convex Optimization*. Cambridge University Press, 2004.
[189] T. Roh and L. Vandenberghe, "Discrete transforms, semidefinite programming, and sum-of-squares representation of nonnegative polynomials," *SIAM Journal on Optimization*, vol. 16, no. 4, pp. 939–964, 2006.
[190] M. Soltanalian, B. Tang, J. Li, and P. Stoica, "Joint design of the receive filter and transmit sequence for active sensing," *IEEE Transactions on Aerospace and Electronic Systems*.
[191] J. A. Tropp, I. S. Dhillon, R. W. Heath, and T. Strohmer, "Designing structured tight frames via an alternating projection method," *IEEE Transactions on Information Theory*, vol. 51, no. 1, pp. 188–208, Jan. 2005.
[192] M. Skolnik, *Radar Handbook*, 3rd ed. New York: McGraw-Hill, 2008.
[193] M. Grant and S. Boyd, "CVX package," February 2012. [Online]. Available: http://www.cvxr.com/cvx
[194] M. Nayebi, M. Aref, and M. Bastani, "Detection of coherent radar signals with unknown doppler shift," *IEE Proceedings-Radar, Sonar and Navigation*, vol. 143, no. 2, pp. 79–86, 1996.
[195] J. Li, P. Stoica, and Z. Wang, "Doubly constrained robust Capon beamformer," *IEEE Transactions on Aerospace and Electronic Systems*, vol. 52, no. 9, pp. 2407 – 2423, Sep. 2004.
[196] P. Stoica, H. He, and J. Li, "Optimization of the receive filter and transmit sequence for active sensing," *IEEE Transactions on Signal Processing*, vol. 60, no. 4, pp. 1730–1740, April 2012.
[197] S. Haykin, "Cognitive radar: a way of the future," *IEEE Signal Processing Magazine*, vol. 23, no. 1, pp. 30–40, jan. 2006.
[198] W. Dinkelbach, "On nonlinear fractional programming," *Management Science*, vol. 13, no. 7, pp. 492–498, 1967.
[199] C. Chen and P. Vaidyanathan, "MIMO radar waveform optimization with prior information of the extended target and clutter," *IEEE Transactions on Aerospace and Electronic Systems*, vol. 57, no. 9, pp. 3533–3544, 2009.

[200] P. Stoica, J. Li, and Y. Xie, "On probing signal design for MIMO radar," *IEEE Transactions on Aerospace and Electronic Systems*, vol. 55, no. 8, pp. 4151–4161, 2007.
[201] F. Gini, A. De Maio, and L. Patton, *Waveform design and diversity for advanced radar systems*. London: Institution of Engineering and Technology, 2012, vol. 22.
[202] A. Aubry, A. De Maio, M. Piezzo, and A. Farina, "Radar waveform design in a spectrally crowded environment via nonconvex quadratic optimization," *IEEE Transactions on Aerospace and Electronic Systems*, vol. 50, no. 2, pp. 1138–1152, April 2014.
[203] A. De Maio, S. De Nicola, Y. Huang, S. Zhang, and A. Farina, "Code design to optimize radar detection performance under accuracy and similarity constraints," *IEEE Transactions on Aerospace and Electronic Systems*, vol. 56, pp. 5618–5629, Nov. 2008.
[204] J. Li, J. R. Guerci, and L. Xu, "Signal waveform's optimal-under-restriction design for active sensing," vol. 13, no. 2, pp. 565–568, Sep. 2006.
[205] A. De Maio, S. De Nicola, Y. Huang, Z.-Q. Luo, and S. Zhang, "Design of phase codes for radar performance optimization with a similarity constraint," *IEEE Transactions on Signal Processing*, vol. 57, no. 2, pp. 610–621, 2009.
[206] S. Schaible, "Parameter-free convex equivalent and dual programs of fractional programming problems," *Zeitschrift fur Operations Research*, vol. 18, pp. 187–196, 1974.
[207] D. Palomar and Y. Eldar, *Convex optimization in signal processing and communications*. Cambridge university press, 2010.
[208] A. d. Aspremont and S. Boyd, "Relaxations and randomized methods for nonconvex QCQPs," *EE392o Class Notes, Stanford University*, 2003.
[209] P. Stoica and Y. Selen, "Cyclic minimizers, majorization techniques, and the expectation-maximization algorithm: a refresher," *IEEE Signal Processing Magazine*, vol. 21, no. 1, pp. 112 – 114, Jan. 2004.
[210] A. Charnes and W. Cooper, "Programming with linear fractional functionals," *Naval Research logistics quarterly*, vol. 9, no. 3-4, pp. 181–186, 1962.
[211] R. A. Horn and C. A. Johnson, *Matrix analysis*. Cambridge University Press, 1985.
[212] Z. Q. Luo, W. K. Ma, A. M. C. So, Y. Ye, and S. Zhang, "Semidefinite relaxation of quadratic optimization problems," *IEEE Signal Processing Magazine*, vol. 27, no. 3, pp. 20 –34, May 2010.
[213] G. Pataki, "On the rank of extreme matrices in semidefinite programs and the multiplicity of optimal eigenvalues," *Mathematics of operations research*, vol. 23, pp. 339–358, 1998.
[214] Y. Huang and D. P. Palomar, "Rank-constrained separable semidefinite programming with applications to optimal beamforming," *IEEE Transactions on Aerospace and Electronic Systems*, vol. 58, no. 2, pp. 664–678, 2010.
[215] W. Ai, Y. Huang, and S. Zhang, "New results on hermitian matrix rank-one decomposition," *Mathematical programming*, vol. 128, no. 1, pp. 253–283, 2011.
[216] A. De Maio, Y. Huang, D. Palomar, S. Zhang, and A. Farina, "Fractional QCQP with applications in ML steering direction estimation for radar

detection," *IEEE Transactions on Aerospace and Electronic Systems*, vol. 59, no. 1, pp. 172–185, 2011.
[217] A. Aubry, A. De Maio, B. Jiang, and S. Zhang, "Ambiguity function shaping for cognitive radar via complex quartic optimization," *IEEE transactions on signal processing*, vol. 61, no. 21-24, pp. 5603–5619, 2013.
[218] M. Friese, "Polyphase Barker sequences up to length 36," *IEEE Transactions on Information Theory*, vol. 42, no. 4, pp. 1248–1250, 1996.
[219] F. R. Castella and J. R. Moore, "Improved target detection in littoral environment," in *Radar 97*, Oct. 1997, pp. 429–433.
[220] S. U. Pillai, H. S. Oh, D. C. Youla, and J. R. Guerci, "Optimum transmit-receiver design in the presence of signal-dependent interference and channel noise," *IEEE Transactions on Information Theory*, vol. 46, pp. 577–584, May 2000.
[221] M. R. Bell, "Information theory and radar waveform design," *IEEE Transactions on Information Theory*, vol. 39, no. 5, pp. 1578–1597, 1993.
[222] S. M. Sowelam and A. H. Tewfik, "Waveform selection in radar target classification," *IEEE Transactions on Information Theory*, vol. 46, no. 3, pp. 1014–1029, 2000.
[223] E. Grossi and M. Lops, "Space-time code design for MIMO detection based on Kullback-Leibler divergence," *IEEE Transactions on Information Theory*, vol. 58, no. 6, pp. 3989–4004, 2012.
[224] S. Sen and A. Nehorai, "OFDM MIMO radar with mutual-information waveform design for low-grazing angle tracking," *IEEE Transactions on Aerospace and Electronic Systems*, vol. 58, no. 6, pp. 3152–3162, Jun. 2010.
[225] R. Manasse, "The use of pulse coding to discriminate against clutter," *Technical report, MIT Lincoln Lab*, 1957.
[226] A. Sheikhi and A. Zamani, "Temporal coherent adaptive target detection for multi-input multi-output radars in clutter," *IET Journal on Radar, Sonar, and Navigation*, vol. 2, no. 2, pp. 86–96, 2008.
[227] F. Gini and M. Rangaswamy, *Knowledge based radar detection, tracking and classification*. Wiley-Interscience, 2008.
[228] J. R. Gureci, *Cognitive Radar: The Knowledge-aided Fully Adaptive Approach*. Artech House, 2010.
[229] A. Jain, P. Moulin, M. I. Miller, and K. Ramchandran, "Information-theoretic bounds on target recognition performance based on degraded image data," *IEEE Trans. Pattern Anal. Mach. Intell.*, vol. 24, pp. 1153–1166, Sep. 2002.
[230] S. Kullback, *Information theory and statistics*. New York: John Wiley and Sons, 1968.
[231] H. Kobayashi and J. B. Thomas, "Distance measures and related criteria," in *Proc. 5th Annu. Allerton Conf. Circuit and System Theory*, 1967, pp. 491–500.
[232] J. Tang, N. Li, Y. Wu, and Y. Peng, "On detection performance of MIMO radar: A relative entropy-based study," *IEEE Signal Processing Letters*, vol. 16, no. 3, pp. 184–187, 2009.
[233] T. Kadota and L. Shepp, "On the best finite set of linear observables for discriminating two Gaussian signals," *IEEE Transactions on Information Theory*, vol. 13, no. 2, pp. 278–284, 1967.
[234] T. Grettenberg, "Signal selection in communication and radar systems," *IEEE*

Transactions on Information Theory, vol. 9, no. 4, pp. 265–275, 1963.
[235] D. Guo, S. Shamai, and S. Verdú, "Mutual information and minimum mean-square error in Gaussian channels," *IEEE Transactions on Information Theory*, vol. 51, no. 4, pp. 1261–1282, 2005.
[236] F. Kanaya and K. Nakagawa, "On the practical implication of mutual information for statistical decision making," *IEEE Transactions on Information Theory*, vol. 37, no. 4, pp. 1151–1156, 1991.
[237] S. D. Briles, "Information-theoretic performance bounding of Bayesian identifiers," in *Optical Engineering and Photonics in Aerospace Sensing*. International Society for Optics and Photonics, 1993, pp. 255–266.
[238] T. M. Cover and J. A. Thomas, *Elements of Information Theory*, 2nd ed. Wiley, 2005.
[239] D. R. Hunter and K. Lange, "A toturial on MM algorithm," *The American Statistician*, vol. 58, pp. 30–37, February 2004.
[240] K. Lange, *Numerical Analysis for Statisticians*. New York: New York: Springer-Verlag, 1999.
[241] J. D. Leeuw and K. Lange, "Sharp quadratic majorization in one dimension," *Computational Statistics and Data Analysis*, vol. 53, pp. 2471–2484, May 2009.
[242] S. Rickard, "Open problems in Costas arrays," in *IMA International Conference on Mathematics in Signal Processing*, Cirencester, UK, 2006.
[243] K. Drakakis, "A review of Costas arrays," *Journal of Applied Mathematics*, vol. 2006, pp. 1–32, 2006.
[244] M. Sterling, E. L. Titlebaum, X. Dong, and M. F. Bocko, "An adaptive spread-spectrum data hiding technique for digital audio," in *IEEE International Conference on Acoustics, Speech, and Signal Processing (ICASSP)*. Philadelphia, PA, USA: IEEE, 2005, pp. 685–688.
[245] O. Moreno and S. Maric, "A new family of frequency-hop codes," *IEEE Transactions on Communications*, vol. 48, no. 8, pp. 1241–1244, 2000.
[246] S. Golomb and G. Gong, "The status of Costas arrays," *IEEE Transactions on Information Theory*, vol. 53, no. 11, pp. 4260–4265, 2007.
[247] K. Drakakis, F. Iorio, S. Rickard, and J. Walsh, "Results of the enumeration of Costas arrays of order 29," *Advances in Mathematics of Communications*, vol. 5, no. 3, pp. 547–553, 2011.
[248] L. Barker, K. Drakakis, and S. Rickard, "On the complexity of the verification of the Costas property," *Proceedings of the IEEE*, vol. 97, no. 3, pp. 586–593, 2009.
[249] M. Elad, *Sparse and redundant representations: from theory to applications in signal and image processing*. New York, NY: Springer, 2010.
[250] T. A. Davis, *Direct methods for sparse linear systems*. Philadelphia, PA: SIAM, 2006.
[251] P. Knee, "Sparse representations for radar with MATLAB examples," *Synthesis Lectures on Algorithms and Software in Engineering*, vol. 4, no. 1, pp. 1–85, 2012.
[252] E. J. Candès and M. B. Wakin, "An introduction to compressive sampling," *IEEE Signal Processing Magazine*, vol. 25, no. 2, pp. 21–30, 2008.
[253] E. J. Candès, M. B. Wakin, and S. P. Boyd, "Enhancing sparsity by reweighted

l_1 minimization," *Journal of Fourier Analysis and Applications*, vol. 14, no. 5-6, pp. 877–905, 2008.
[254] R. Chartrand and W. Yin, "Iteratively reweighted algorithms for compressive sensing," in *IEEE International Conference on Acoustics, Speech and Signal Processing (ICASSP)*, Las Vegas, NV, March 2008, pp. 3869–3872.
[255] E. J. Candès and T. Tao, "Decoding by linear programming," *IEEE Transactions on Information Theory*, vol. 51, no. 12, pp. 4203–4215, 2005.
[256] P. M. Pardalos and S. A. Vavasis, "Quadratic programming with one negative eigenvalue is NP-hard," *Journal of Global Optimization*, vol. 1, no. 1, pp. 15–22, 1991.
[257] S. Zhang, "Quadratic maximization and semidefinite relaxation," *Mathematical Programming*, vol. 87, no. 3, pp. 453–465, 2000.
[258] D. Donoho, "Compressed sensing," *IEEE Transactions on Information Theory*, vol. 52, no. 4, pp. 1289–1306, April 2006.
[259] E. Candès and M. Wakin, "An introduction to compressive sampling," *IEEE Signal Processing Magazine*, vol. 25, no. 2, pp. 21–30, March 2008.
[260] Y. He, X. Zhu, S. Zhuang, H. Li, and H. Hu, "Waveform optimization for compressive sensing radar imaging," in *IEEE CIE International Conference on Radar*, vol. 2. Chengdu, China: IEEE, 2011, pp. 1263–1266.
[261] Y. Yu, A. P. Petropulu, and H. V. Poor, "MIMO radar using compressive sampling," *IEEE Journal of Selected Topics in Signal Processing*, vol. 4, no. 1, pp. 146–163, 2010.
[262] W. Roberts, P. Stoica, J. Li, T. Yardibi, and F. A. Sadjadi, "Iterative adaptive approaches to MIMO radar imaging," *IEEE Journal of Selected Topics in Signal Processing*, vol. 4, no. 1, pp. 5–20, 2010.
[263] V. M. Patel, G. R. Easley, D. M. Healy Jr, and R. Chellappa, "Compressed synthetic aperture radar," *IEEE Journal of Selected Topics in Signal Processing*, vol. 4, no. 2, pp. 244–254, 2010.
[264] L. Zhang, M. Xing, C.-W. Qiu, J. Li, J. Sheng, Y. Li, and Z. Bao, "Resolution enhancement for inversed synthetic aperture radar imaging under low SNR via improved compressive sensing," *IEEE Transactions on Geoscience and Remote Sensing*, vol. 48, no. 10, pp. 3824–3838, October 2010.
[265] P. Stoica, J. Li, and M. Xue, "Transmit codes and receive filters for radar," *IEEE Signal Processing Magazine*, vol. 25, no. 6, pp. 94–109, 2008.
[266] M. Herman and T. Strohmer, "High-resolution radar via compressed sensing," *IEEE Transactions on Signal Processing*, vol. 57, no. 6, pp. 2275–2284, June 2009.
[267] J. Zhang, D. Zhu, and G. Zhang, "Adaptive compressed sensing radar oriented toward cognitive detection in dynamic sparse target scene," *IEEE Transactions on Signal Processing*, vol. 60, no. 4, pp. 1718–1729, 2012.
[268] M. Soltanalian, M. M. Naghsh, and P. Stoica, "On meeting the peak correlation bounds," *IEEE Transactions on Signal Processing*, vol. 62, no. 5, pp. 1210–1220, March 2014.
[269] M. Elad, *Sparse and redundant representations: from theory to applications in signal and image processing*. New York, NY: Springer, 2010.
[270] H. He, P. Stoica, and J. Li, "Designing unimodular sequence sets with good correlations—including an application to MIMO radar," *IEEE Transactions on*

Signal Processing, vol. 57, no. 11, pp. 4391–4405, 2009.
[271] M. Soltanalian, M. M. Naghsh, and P. Stoica, "A fast algorithm for designing complementary sets of sequences," *Signal Processing*, vol. 93, no. 7, pp. 2096–2102, 2013.
[272] M. Rossi, A. M. Haimovich, and Y. C. Eldar, "Spatial compressive sensing for MIMO radar," *IEEE Transactions on Signal Processing*, vol. 62, no. 2, pp. 419–430, January 2014.
[273] J. Li and P. Stoica, "MIMO radar with colocated antennas," *IEEE Signal Processing Magazine*, vol. 24, no. 5, pp. 106–114, 2007.
[274] A. M. Haimovich, R. S. Blum, and L. J. Cimini, "MIMO radar with widely separated antennas," *IEEE Signal Processing Magazine*, vol. 25, no. 1, pp. 116–129, 2008.
[275] P. Stoica, J. Li, and X. Yao, "On probing signal design for MIMO radar," *IEEE Transactions on Signal Processing*, vol. 55, no. 8, pp. 4151–4161, 2007.
[276] P. Stoica, J. Li, and X. Zhu, "Waveform synthesis for diversity-based transmit beampattern design," *IEEE Transactions on Signal Processing*, vol. 56, no. 6, pp. 2593–2598, 2008.
[277] P. Gong, Z. Shao, G. Tu, and Q. Chen, "Transmit beampattern design based on convex optimization for MIMO radar systems," *Signal Processing*, vol. 94, pp. 195–201, 2014.
[278] T. Aittomäki and V. Koivunen, "Signal covariance matrix optimization for transmit beamforming in MIMO radars," in *Asilomar Conference on Signals, Systems and Computers*, 2007, pp. 182–186.
[279] ——, "Low-complexity method for transmit beamforming in MIMO radars," in *IEEE International Conference on Acoustics, Speech and Signal Processing (ICASSP)*, vol. 2, 2007, pp. 305–308.
[280] D. R. Fuhrmann and G. San Antonio, "Transmit beamforming for MIMO radar systems using signal cross-correlation," *IEEE Transactions on Aerospace and Electronic Systems*, vol. 44, no. 1, pp. 171–186, 2008.
[281] G. Hua and S. Abeysekera, "MIMO radar transmit beampattern design with ripple and transition band control," *IEEE Transactions on Signal Processing*, vol. 61, no. 11, pp. 2963–2974, 2013.
[282] K. Shadi and F. Behnia, "MIMO radar beamforming using orthogonal decomposition of correlation matrix," *Circuits, Systems, and Signal Processing*, pp. 1–19, 2013.
[283] S. Ahmed, J. S. Thompson, Y. R. Petillot, and B. Mulgrew, "Unconstrained synthesis of covariance matrix for MIMO radar transmit beampattern," *IEEE Transactions on Signal Processing*, vol. 59, no. 8, pp. 3837–3849, 2011.
[284] H. Xu, J. Wang, J. Yuan, and X. Shan, "MIMO radar transmit beampattern synthesis via minimizing sidelobe level," *Progress In Electromagnetics Research B*, vol. 53, pp. 355–371, 2013.
[285] A. Khabbazibasmenj, S. A. Vorobyov, and A. Hassanien, "Robust adaptive beamforming via estimating steering vector based on semidefinite relaxation," in *Conference Record of the Forty Fourth Asilomar Conference on Signals, Systems and Computers (ASILOMAR)*. IEEE, 2010, pp. 1102–1106.
[286] A. Hassanien and S. A. Vorobyov, "Transmit energy focusing for DOA estimation in MIMO radar with colocated antennas," *IEEE Transactions on*

Signal Processing, vol. 59, no. 6, pp. 2669–2682, 2011.
[287] C. Xiang, D.-Z. Feng, H. Lv, J. He, and Y. Cao, "Robust adaptive beamforming for MIMO radar," *Signal Processing*, vol. 90, no. 12, pp. 3185–3196, 2010.
[288] A. Hassanien, M. W. Morency, A. Khabbazibasmenj, S. A. Vorobyov, J.-Y. Park, and S.-J. Kim, "Two-dimensional transmit beamforming for MIMO radar with sparse symmetric arrays," in *IEEE Radar Conference*, 2013.
[289] J. A. Tropp, I. S. Dhillon, R. W. Heath, and T. Strohmer, "Designing structured tight frames via an alternating projection method," *IEEE Transactions on Information Theory*, vol. 51, no. 1, pp. 188–209, 2005.
[290] J. Li, P. Stoica, and X. Zheng, "Signal synthesis and receiver design for MIMO radar imaging," *IEEE Transactions on Signal Processing*, vol. 56, no. 8, pp. 3959–3968, 2008.
[291] T. Aittomäki and V. Koivunen, "Beampattern optimization by minimization of quartic polynomial," in *IEEE/SP 15th Workshop on Statistical Signal Processing*. IEEE, 2009, pp. 437–440.
[292] J. Li and P. Stoica, Eds., *Robust adaptive beamforming*. New York: Wiley, 2006.
[293] B. Friedlander, "On transmit beamforming for MIMO radar," *IEEE Transactions on Aerospace and Electronic Systems*, vol. 48, no. 4, pp. 3376–3388, 2012.
[294] A. Srinivas and V. Reddy, "Transmit beamforming for colocated MIMO radar," in *International Conference on Signal Processing and Communications (SPCOM)*. Bangalore, India: IEEE, 2010, pp. 1–5.
[295] W. Rowe, M. Ström, J. Li, and P. Stoica, "Robust adaptive beamforming for MIMO monopulse radar," in *SPIE Defense, Security, and Sensing*. Baltimore, Maryland, USA: International Society for Optics and Photonics, 2013, pp. 1–15.

SAMMANFATTNING
Signaldesign för aktiv avkänning och kommunikation

Längtan efter interaktion med vår omgivning och andra av vår sort ligger i den mänskliga naturen— en viktig flaskhals som begränsar denna interaktion är vår informationsinsamlingsförmåga eller *avkänningskapacitet*. Genom historien har vi försökt att komma på smarta sätt att känna av vår miljö. Moderna sensorsystem kan kategoriseras som

- Aktiva system, dvs sensoriska system som fungerar genom att sondera miljön med självproducerad energi.
- Passiva system, dvs sensoriska system som förlitar sig på detektering av den naturligt förekommande energin inom miljön.

Aktiva sensorsystem som människan konstruerat, såsom aktiv radar och sonar, har varit en viktig del av vår civilisations framsteg inom navigation, försvar, meteorologi och utforskning av rymden. I djurriket används aktiva sensorsystem för positioneringsändamål av bland annat fladdermöss och delfiner. Intressant är att våra syntetiska sensorsystem använder en uppsättning tekniker som liknar de som används av fladdermöss och delfiner för att samla in information om målen (t.ex. läge och hastighet). En aktiv radar sänder ut radiovågor (kallade *radarsignaler*) mot målen. En del av den överförda energin reflekteras från målen och tas emot av antennen i radarmottagaren. Tack vare att hastigheten hos de elektromagnetiska vågorna är känd kan radarsystemet uppskatta placeringen av målen genom att mäta tidsskillnaden mellan utsändningen av radarsignalen och mottagningen av den reflekterade signalen.

Stående på giganters axlar så är utvecklingen av moderna aktiva sensorsystem starkt beroende av de betydande framsteg inom vetenskap och kommunikationsteknik som gjorts under det senaste århundradet. Men det är inte speciellt förvånande att det snabbväxande kommunikationsteknikfältet även har förändrat många aspekter av vår vardag. Denna avhandling handlar om signaldesign för att förbättra prestandan hos aktiva analys och kommunikationssystem: de aktiva sensorsystemens förmåga att upptäcka mål och skatta deras position och hastighet kan förbättras avsevärt genom noggrann design av de utsända signalerna. På liknande sätt har signaldesignen även en avgörande betydelse för konstruktionen av, och effektiviteten hos, kommunikationssystem.

Teoretiska och empiriska resultat inom signaldesign har under de senaste decennierna intresserat både ingenjörer och matematiker. Problemet att designa en signal inom aktiv avkänning eller kommunikation kokar oftast ner till optimering av ett signalkvalitetsmått. Faktum är att flera olika mått på kvaliteten används inom signaloptimering för aktiv avkänning och kommunikation, nämligen:

- *Korrelation och spektralt innehåll*
- *Signal-brus-förhållande (SNR) och Mean-Square-Error (MSE) medelkvadratfel*
- *Informationsteoretiska kriterier*
- *gleshetsrelaterade mått*
- *Matchning av Beam-Pattern (lobmönster)*

Denna avhandling är uppdelad i fem delar, var och en tillägnade en av ovanstående klasser av kvalitetsmått. Dessutom behandlas designproblem som inkluderar en uppsättning signalbegränsningar, en utmaning som uppstår i praktiska scenarier. Typiska exempel på sådana signalbegränsningar är begränsad energi, begränsat alfabet, och begränsningar på förhållandet mellan signalens topp- och medeleffekt. En sådan mångfald, både i mått på kvalitet och typer av problem, banar väg för många utmanande forskningsprojekt inom signaldesign— redan idag finns det en hel del öppna problem inom detta forskningsområde som är ganska lätt att beskriva, men bedöms som mycket svåra att ta itu med!

Avhandlingen är skriven inom ämnesområdet *elektroteknik med inriktning mot signalbehandling*.

Acta Universitatis Upsaliensis
Uppsala Dissertations from the Faculty of Science
Editor: The Dean of the Faculty of Science

1–11: 1970–1975

12. *Lars Thofelt*: Studies on leaf temperature recorded by direct measurement and by thermography. 1975.
13. *Monica Henricsson*: Nutritional studies on Chara globularis Thuill., Chara zeylanica Willd., and Chara haitensis Turpin. 1976.
14. *Göran Kloow*: Studies on Regenerated Cellulose by the Fluorescence Depolarization Technique. 1976.
15. *Carl-Magnus Backman*: A High Pressure Study of the Photolytic Decomposition of Azoethane and Propionyl Peroxide. 1976.
16. *Lennart Källströmer*: The significance of biotin and certain monosaccharides for the growth of Aspergillus niger on rhamnose medium at elevated temperature. 1977.
17. *Staffan Renlund*: Identification of Oxytocin and Vasopressin in the Bovine Adenohypophysis. 1978.
18. *Bengt Finnström*: Effects of pH, Ionic Strength and Light Intensity on the Flash Photolysis of L-tryptophan. 1978.
19. *Thomas C. Amu*: Diffusion in Dilute Solutions: An Experimental Study with Special Reference to the Effect of Size and Shape of Solute and Solvent Molecules. 1978.
20. *Lars Tegnér*: A Flash Photolysis Study of the Thermal Cis-Trans Isomerization of Some Aromatic Schiff Bases in Solution. 1979.
21. *Stig Tormod*: A High-Speed Stopped Flow Laser Light Scattering Apparatus and its Application in a Study of Conformational Changes in Bovine Serum Albumin. 1985.
22. *Björn Varnestig*: Coulomb Excitation of Rotational Nuclei. 1987.
23. *Frans Lettenström*: A study of nuclear effects in deep inelastic muon scattering. 1988.
24. *Göran Ericsson*: Production of Heavy Hypernuclei in Antiproton Annihilation. Study of their decay in the fission channel. 1988.
25. *Fang Peng*: The Geopotential: Modelling Techniques and Physical Implications with Case Studies in the South and East China Sea and Fennoscandia. 1989.
26. *Md. Anowar Hossain*: Seismic Refraction Studies in the Baltic Shield along the Fennolora Profile. 1989.
27. *Lars Erik Svensson*: Coulomb Excitation of Vibrational Nuclei. 1989.
28. *Bengt Carlsson*: Digital differentiating filters and model based fault detection. 1989.
29. *Alexander Edgar Kavka*: Coulomb Excitation. Analytical Methods and Experimental Results on even Selenium Nuclei. 1989.
30. *Christopher Juhlin*: Seismic Attenuation, Shear Wave Anisotropy and Some Aspects of Fracturing in the Crystalline Rock of the Siljan Ring Area, Central Sweden. 1990.

31. *Torbjörn Wigren*: Recursive Identification Based on the Nonlinear Wiener Model. 1990.
32. *Kjell Janson*: Experimental investigations of the proton and deuteron structure functions. 1991.
33. *Suzanne W. Harris*: Positive Muons in Crystalline and Amorphous Solids. 1991.
34. *Jan Blomgren*: Experimental Studies of Giant Resonances in Medium-Weight Spherical Nuclei. 1991.
35. *Jonas Lindgren*: Waveform Inversion of Seismic Reflection Data through Local Optimisation Methods. 1992.
36. *Liqi Fang*: Dynamic Light Scattering from Polymer Gels and Semidilute Solutions. 1992.
37. *Raymond Munier*: Segmentation, Fragmentation and Jostling of the Baltic Shield with Time. 1993.

Prior to January 1994, the series was called *Uppsala Dissertations from the Faculty of Science*.

Acta Universitatis Upsaliensis

Uppsala Dissertations from the Faculty of Science and Technology
Editor: The Dean of the Faculty of Science

1–14: 1994–1997. 15–21: 1998–1999. 22–35: 2000–2001. 36–51: 2002–2003.

52. *Erik Larsson*: Identification of Stochastic Continuous-time Systems. Algorithms, Irregular Sampling and Cramér-Rao Bounds. 2004.
53. *Per Åhgren*: On System Identification and Acoustic Echo Cancellation. 2004.
54. *Felix Wehrmann*: On Modelling Nonlinear Variation in Discrete Appearances of Objects. 2004.
55. *Peter S. Hammerstein*: Stochastic Resonance and Noise-Assisted Signal Transfer. On Coupling-Effects of Stochastic Resonators and Spectral Optimization of Fluctuations in Random Network Switches. 2004.
56. *Esteban Damián Avendaño Soto*: Electrochromism in Nickel-based Oxides. Coloration Mechanisms and Optimization of Sputter-deposited Thin Films. 2004.
57. *Jenny Öhman Persson*: The Obvious & The Essential. Interpreting Software Development & Organizational Change. 2004.
58. *Chariklia Rouki*: Experimental Studies of the Synthesis and the Survival Probability of Transactinides. 2004.
59. *Emad Abd-Elrady*: Nonlinear Approaches to Periodic Signal Modeling. 2005.
60. *Marcus Nilsson*: Regular Model Checking. 2005.
61. *Pritha Mahata*: Model Checking Parameterized Timed Systems. 2005.
62. *Anders Berglund*: Learning computer systems in a distributed project course: The what, why, how and where. 2005.
63. *Barbara Piechocinska*: Physics from Wholeness. Dynamical Totality as a Conceptual Foundation for Physical Theories. 2005.
64. *Pär Samuelsson*: Control of Nitrogen Removal in Activated Sludge Processes. 2005.

65. *Mats Ekman*: Modeling and Control of Bilinear Systems. Application to the Activated Sludge Process. 2005.
66. *Milena Ivanova*: Scalable Scientific Stream Query Processing. 2005.
67. *Zoran Radovic´*: Software Techniques for Distributed Shared Memory. 2005.
68. *Richard Abrahamsson*: Estimation Problems in Array Signal Processing, System Identification, and Radar Imagery. 2006.
69. *Fredrik Robelius*: Giant Oil Fields – The Highway to Oil. Giant Oil Fields and their Importance for Future Oil Production. 2007.
70. *Anna Davour*: Search for low mass WIMPs with the AMANDA neutrino telescope. 2007.
71. *Magnus Ågren*: Set Constraints for Local Search. 2007.
72. *Ahmed Rezine*: Parameterized Systems: Generalizing and Simplifying Automatic Verification. 2008.
73. *Linda Brus*: Nonlinear Identification and Control with Solar Energy Applications. 2008.
74. *Peter Nauclér*: Estimation and Control of Resonant Systems with Stochastic Disturbances. 2008.
75. *Johan Petrini*: Querying RDF Schema Views of Relational Databases. 2008.
76. *Noomene Ben Henda*: Infinite-state Stochastic and Parameterized Systems. 2008.
77. *Samson Keleta*: Double Pion Production in dd→αππ Reaction. 2008.
78. *Mei Hong*: Analysis of Some Methods for Identifying Dynamic Errors-invariables Systems. 2008.
79. *Robin Strand*: Distance Functions and Image Processing on Point-Lattices With Focus on the 3D Face-and Body-centered Cubic Grids. 2008.
80. *Ruslan Fomkin*: Optimization and Execution of Complex Scientific Queries. 2009.
81. *John Airey*: Science, Language and Literacy. Case Studies of Learning in Swedish University Physics. 2009.
82. *Arvid Pohl*: Search for Subrelativistic Particles with the AMANDA Neutrino Telescope. 2009.
83. *Anna Danielsson*: Doing Physics – Doing Gender. An Exploration of Physics Students' Identity Constitution in the Context of Laboratory Work. 2009.
84. *Karin Schönning*: Meson Production in pd Collisions. 2009.
85. *Henrik Petrén*: η Meson Production in Proton-Proton Collisions at Excess Energies of 40 and 72 MeV. 2009.
86. *Jan Henry Nyström*: Analysing Fault Tolerance for ERLANG Applications. 2009.
87. *John Håkansson*: Design and Verification of Component Based Real-Time Systems. 2009.
88. *Sophie Grape*: Studies of PWO Crystals and Simulations of the $\bar{p}p \to \bar{\Lambda}\Lambda, \bar{\Lambda}\Sigma^0$ Reactions for the PANDA Experiment. 2009.
90. *Agnes Rensfelt*. Viscoelastic Materials. Identification and Experiment Design. 2010.
91. *Erik Gudmundson*. Signal Processing for Spectroscopic Applications. 2010.
92. *Björn Halvarsson*. Interaction Analysis in Multivariable Control Systems. Applications to Bioreactors for Nitrogen Removal. 2010.
93. *Jesper Bengtson*. Formalising process calculi. 2010.
94. *Magnus Johansson*. Psi-calculi: a Framework for Mobile Process Calculi. Cook your own correct process calculus – just add data and logic. 2010.
95. *Karin Rathsman*. Modeling of Electron Cooling. Theory, Data and Applications. 2010.

96. *Liselott Dominicus van den Bussche*. Getting the Picture of University Physics. 2010.